CRANFIELD UNIVERSITY

College of Defence Technology

Department of Aerospace, Power & Sensors

PhD THESIS

Academic Year 2003-2004

MING FEI SIYAU

A Novel Training-Based MIMO Channel Estimation Scheme for Layered Space-Time Systems in Frequency Selective Wireless Channels

Supervisor:

Prof. Richard Ormondroyd

& Dr. Philip Nobles

April 2004

Abstract

New development in wireless technology using multiple antennas with appropriate space-time processing has recently become the new frontier of wireless communication systems due to the potential for providing very high spectral efficiency and enormous capacity improvement over the conventional wireless radio communications. The technical advances in using the multiple-input multiple-output (MIMO) wireless links present a promising breakthrough in resolving the bottleneck of current capacity limitation for future intensive wireless networks. The MIMO wireless systems utilize multiple antennas at both side of the transmitter and the receiver for enormous gains in spectral efficiency as well as system capacity in terms of higher data throughput by exploiting the multipath diversity in a rich scattering environment. A number of MIMO systems have been proposed to permit very high transmission rate, far exceeding the conventional communication technique. In particular, the Bell Laboratories layered space-time (BLAST) architecture has been presented that uses concept of spatial diversity and successive interference cancellation technique to improve the quality of signal reception over the flat-fading or the frequency selective fading channel.

However, in order to achieve the quoted capacity gains in MIMO systems, the channel information in terms of the multiple channel impulse responses (CIRs) and their fading coefficients must be known or estimated, which requires the design of a suitable channel estimator. Thus far, existing MIMO channel estimation schemes have been mostly limited to the flat-fading case or cater specifically for coded space-time systems such as space-time block code systems. In this thesis, the work is to consider the existing MIMO channel estimation techniques (used in the flat fading condition) and extend them to cater for a more realistic time-varying, frequency selective fading channel. The focus of this thesis has been the design and development of suitable training-based MIMO channel estimation scheme as well as the formulation of a new pilot code to enable effective estimation for the frequency selective channel. The novel channel estimator is also incorporated into the BLAST architecture to allow the practical assessment of using non-idealized channel to be studied and analysed for the performance of the MIMO systems. The driver for this work has been the recognition of the importance of channel knowledge for all the MIMO system to be used in practical application.

Acknowledgement

First of all, I would like to express my heartfelt gratitude to Prof. Richard Ormondroyd for his outstanding supervision and support for my work, especially for his sharpness in guidance and ideas towards the right direction, and his enormous valuable time spent on all the useful and fruitful discussions. He has also provided me numerous opportunities to attend worldwide technical conferences that have further enhanced my knowledge in the related field of research. I am also immensely indebted to my second supervisor, Dr. Nobles, for his indescribable patience, helpfulness and constructive suggestions and guidance, especially for his editorial efforts in many published papers. His supportive novel ideas of related research work have been a great encouragement to me.

I am thankful to the many people of the various organizations that have made this research possible during my years as a research student at the department of Aerospace, Power and Sensors (DAPS). My most special thanks to Heather, June and Jilly for their kindness and instantaneous helps related in the administrative work. I am also very grateful to all the fellow researchers: Dr. Samir Mezouari, Dr. Jonathan Loo, Dr. Georgios Pissanidis, Mr. Andrew Calkin, Dr. Lilian Bruyere, Dr. William Cheung, Dr. Victor Kueh and Mr. Soon Leh Ling for their fruitful discussions and suggestions in the related research areas as well as their valuable sharing of knowledge and enlightenments. I am also very grateful for the constant supports and encouragements from my fellow friends: Philip Phung, Amanda Yip, Dhanalakshmi, Dr. Immanuel Ashokaraj, Dr. Guray Acar, Carmen, Kar Ann and Ester Chew, C.K. Toh and Yoka Tang.

Also, my most heartfelt gratitude to my respected parents for their unfailing love and supports throughout the entire 'journey' of this research study. "Dad and Mum, you're the best gift that I have from God". Above all, I express my deepest gratitude to Sumiko Yuda, my adorable source of inspiration, for all her supports and encouragements during my struggles in overcoming the difficult times. Lastly, I would like to give thanks to my Lord Jesus Christ for His gift of wisdom and strength for completing this research.

Contents

List of Publications

1. **M.F. Siyau**, R.F. Ormondroyd, P. Nobles, "Performance of a Layered Space-Time Cellular System used with Fractionally-Spaced Channel Estimation Operated in a Time-Varying, Frequency-Selective Wireless Channel," *In Proc. IEEE conference on Vehicular Technology* (*VTC-fall'04*), Los Angeles, USA, September 2004.

2. **M.F. Siyau**, P. Nobles, R.F. Ormondroyd, "Channel estimation for layered space-time system in time-varying frequency selective wireless channels," *In Proc. IEEE conference on Vehicular Technology* (*VTC-fall'03*), Orlando, Florida, October 2003.

3. **M.F. Siyau**, P. Nobles, R.F. Ormondroyd, "Estimation of frequency selective wireless channels for layered space-time systems," *2003 IEEE International Antennas and Propagation Symposium and USNC/CNC/URSI North American Radio Science Meeting*, URSI session 29.8, Columbus, Ohio, United States of America, June 2003.

4. S.L. Ling, **M.F. Siyau**, R.F. Ormondroyd, "Comparison of space-time architecture performance for UMTS under time-varying Rayleigh fading channel," *IEE 3G conference'03*, Savoy Place, London, June 2003.

5. **M.F. Siyau**, P. Nobles, R.F. Ormondroyd, "Channel estimation for layered space-time systems," *IV IEEE Signal Processing Workshop on Signal Processing Advances in Wireless Communications* (SPAWC'03), W1.1, 615, Rome, Italy, June 2003.

6. S.L. Ling, **M.F. Siyau**, R.F. Ormondroyd, "Channel estimation of spatial-temporal UMTS uplink system for future generation mobile radio communication system," *In Proc. IEE 5th European Personal Mobile Communication Conference* (*EPMCC'03*), pp. 71-75, University of Strathclyde, Glasgow, April 2003.

7. **M.F. Siyau**, R.F. Ormondroyd, P. Nobles, "Estimation of time-varying channels for space-time system using a combined multi-element array pilot inversion (MEA-PI) and auto-tracking," *IEEE International Conference on Acoustic, Speech and Signal Processing* (*ICASSP'02*), student forum, Florida, USA, May 2002.

8. S.L. Ling, **M.F. Siyau**, R.F. Ormondroyd, "Space-time UMTS uplink system for future generation mobile radio communication system", *European Wireless conference'02*, vol.2, pp 865-869, Florence, Italy, February 2002.

9. **M.F. Siyau**, P. Nobles, R.F. Ormondroyd, "Nonlinear detection algorithm for space-time system using orthogonal triangularization by QR decomposition", *IEE Colloquium on MIMO system: Communication Systems - from concept to implementation*, pp 6/1-6/5, Savoy Place, London, December 2001.

10. **M.F. Siyau**, P. Nobles, R.F. Ormondroyd, "Channel estimation for space-time system using a multi-element array recursive least squares (MEA-RLS) algorithm", *4th International Symposium on Wireless Personal Multimedia Conference* (*WPMC'01*), vol. 3, pp 1451-1456, Aalborg, Denmark, September 2001.

Abbreviation

AOA	Angle of Arrival
AWGN	Additive White Gaussian Noise
BLAST	Bell Laboratories Layered Space-Time
D-BLAST	Diagonal-BLAST
DFE	Decision Feedback Equaliser
DOA	Direction of Arrival
CIR	Channel Impulse Response
CCI	Co-Channel Interference
FIR	Finite Impulse Response
ISI	Intersymbol Interference
LMS	Least Mean Squares
MEA	Multi Element Array
MISO	Multiple-Input Single-Output
MIMO	Multiple-Input Multiple-Output
MIMO-CE	MIMO Channel Estimation
ML	Maximum Likelihood
MSE	Mean Square Error
MMSE	Minimum Mean Square Error
OH	Ordinary Hadamard
OSIC	Ordered Successive Interference Cancellation
PH	Paley-Hadamard
PMI	Pilot Matrix Inversion
RLS	Recursive Least Squares
RMS	Root Mean Square
SIC	Successive Interference Cancellation
SISO	Single-Input Single-Output
SIMO	Single-Input Multiple-Output
SNR	Signal-to-Noise Ratio
STC	Space-Time Coding
STP	Space-Time Processing
SVD	Single Value Decomposition
QPSK	Quaternary Phase Shift Keying
V-BLAST	Vertical-BLAST
ZF	Zero-Forcing
LHS	Left-Hand-Side
RHS	Right-Hand-Side
w.r.t	with respect to

Chapter 1

Introduction

The works contained in this thesis focused on new development in wireless communication with the view to increase the capacity of cellular radio and wireless local area network that operate in severely dispersive channel. In particular, the thesis concentrates on the exploitation of the spatial domain as means of providing different types of diversity that can be used either to improve the overall data rate/capacity of the system or to provide improved quality of reception. During the preliminary research, many works assumed idealized channel. It was clear that significant degradation in the performance of this type of system is observed if the channel information is not known accurately. Consequently, one of the major contributions of the work presented in this thesis has been a detailed study of the impact of accurate channel estimation on the system performance and more importantly ways in which the MIMO channel could be estimated using algorithms which have minimal overhead, which can be found in [87, 144 – 148].

The original outcomes of the work in this thesis include the following:

a) The design of the novel MIMO channel estimation (MIMO-CE) method, which uses the concept of pilot matrix (derived from Hadamard matrix) that consists of orthogonal training sequences assigned to each transmit antenna in order to achieve optimum estimation of each channel path coefficient under both flat-fading and frequency-selective fading condition. These include all the MIMO-CE methods shown in Chapter 3 and 4.

b) The design of more efficient MIMO-CE scheme (derived from Paley-Hadamard matrix) with lesser pilot symbols required for each transmit antenna without affecting the original performance achieved in a). This is achieved by the exploitation in both orthogonal and Toeplitz-like structure, within the Paley's construction of the Hadamard matrix.

c) The extension of MIMO-CE scheme in b) to cater for fractionally-spaced model of the MIMO channel, in which paths existed within fraction of symbol period are allowed to be estimated. This allows more realistic consideration over the symbol-spaced model that has been initially considered in both a) and b).

1.1 An Overview of Wireless Communication Systems

Wireless transmission technology has evolved intensively over the last two decades since the early 1980s due to the tremendous growth in the need for mobile communication and mobile computing. With the growing demand in the current mobile communication market and the rapid growth of Internet users, future wireless systems are expected not only to provide faster, broadband, communication but also to provide a range of diverse wireless services, such as voice, data, image, video and multimedia services. In order to achieve the above objectives, very high capacity and more efficient use of the available frequency spectrum are needed. However, the physical limitations of the wireless channel pose a fundamental challenge for reliable communication due to the inherent limitations of multipath propagation loss, time variation of the channel characteristic, noise and other interferences, which effectively make the wireless channel a 'narrow pipe' that does not easily accommodate wideband data flow over the traditional "point-to-point" single-input single-output (SISO) wireless communication system.

The space-time (ST) architecture for wireless communication is of considerable current interest due to the needs for higher data rates to support future generation personal wireless multimedia systems. Recent research into multiple-input multiple-output (MIMO) systems (sometimes called a "volume-to-volume" wireless link) has provided significant technical breakthroughs in the feasibility of this type of wireless system and these developments promise considerable improvements in capacity. Basically, MIMO systems use multiple antennas at both the transmitter and receiver to permit very high transmission rate, far exceeding the conventional communication technique [1-4, 9, 10]. Together with intelligent space-time signal processing and detection techniques, higher traffic capacity and higher spectral efficiency are realisable.

At present, third-generation (3G) mobile wireless networks are designed to offer up to 2Mbit/sec data rates [5]. With MIMO technology, the data rates can be potentially increased up to 14.4Mbits/sec and higher [6]. In MIMO systems, it is believed that spectral efficiencies of 20 - 40 bits/sec/Hz can be achieved [4] as compared to traditional wireless modulation techniques in single-input single-output link where only order of 1-5 bits/sec/Hz is achieved. These potential advancements are made possible by adopting MIMO techniques that may solve the problem of capacity bottleneck in Internet-intensive wireless networks, which may become the necessary backbone technology in the upcoming advanced wireless local area network (WLAN) and broadband wireless access for the future generation of wireless communication systems [37].

1.1.1 Background of MIMO Systems

A good introduction to MIMO systems can be found in [7] and a comprehensive overview of MIMO wireless systems is presented in [8]. In brief, MIMO systems are capable of enormous

gains in spectral efficiency and system capacity. These gains are achieved by multiple parallel transmissions of *space-time* signals using the same frequency band and careful exploitation of the multipath information within a rich scattering MIMO wireless channel such as that found in an indoor wireless channel at a strongly scattered mobile radio channel. [1–4]. (Details are discussed in Chapter 2). Multipath scattering is traditionally viewed as a serious impairment to the conventional communication systems and the fundamental importance of the MIMO channel is that it exploits the fundamental propagation characteristics that provide poor performance when traditional communications systems are employed. Also, parallel transmissions using multiple antennas means that the effective transmission rate is increased in proportion to the number of transmit antennas used in the MIMO systems [9, 10] (although it must remember that not all the transmitted symbols will be delivered correctly). The signals arriving at the receive antennas are combined and processed by the space-time processing unit [11, 12], which is the essential element in MIMO systems. It is the combination of multiple antennas and the use of intelligent space-time signal processing algorithm that has given birth to the wireless MIMO communication systems.

The current state of MIMO research advancements owes a great deal to a number of key developments of signal processing and communication research in a number of seemingly unrelated areas. These include topics such as diversity combining, adaptive antenna arrays, smart antenna technology, adaptive beamforming, interference cancellation and channel estimation. Some related pioneering works are the use of *adaptive arrays* [13–17] and method of *optimum combining* by J. H. Winters [18-19]. The early concept of beamforming is also presented in [20, 21]. However, it should be realised that MIMO systems only rarely use traditional antenna arrays in which the element of the antenna are linked to a single receiver via beamforming network. Instead, the antenna 'arrays' in a space-time systems use receivers connected to each antenna which is capable of translating the signal to the IF prior to some form of processing.

In the 1990s, the joint concepts of above techniques became increasingly popular [22–33]. Researches were focused on the aspects of signal processing, capacity & performance analysis and the application of the adaptive antennas. Among the useful techniques was the use of adaptive antennas that led to the smart antenna technology which provided great improvement in the system performance of wireless cellular systems. [25]. Nevertheless, conventional *smart antenna* systems only used the antennas array at either the transmitter or receiver (typically at the base-station) as either the multiple-input single-output (MISO) or single-input multiple-output (SIMO) setup and the technology is used in combating (instead of exploiting) the multipath propagations by means of spatial diversity combining or beamforming where the signal transmission or reception energy is focused (or maximised) in the direction of the desired user while minimising other undesired signals like noise or co-channel interference [8].

Toward the late 1990s, the MIMO concept was revitalised. Multiple antennas at both the transmitter and receiver were utilised which opened up a whole new area of development in signal processing algorithms and detection techniques using the *space-time* concepts. [2–4, 11, 12, 24, 34, 45, 47]. Central to space-time techniques is the use of multiple antennas, which could be used in variety of ways to improve the system performance. Instead of mitigating the multipath effects, the multipath information is carefully exploited by using the scattering characteristic of the propagation environment to enhance rather than degrade the transmission accuracy by means of spatial diversity and space-time processing technique [8]. These techniques attempt to separate the corrupted signals (under the influence of co-channel interference) by treating the multiplicity of the scattering paths as separate parallel sub-channels and process the multiple received signals by means of combiner with appropriate weighting function that has an inverse response of the MIMO channel [4, 11]. Hence, *MIMO systems* can be viewed as the architectural and technological enhancement on top of the conventional smart antenna technology where utilisation of multiple antennas, adaptive arrays technique and space-time processing are effectively combined together to improve the wireless transmission quality as well as the link capacity.

Among the outstanding work in wireless MIMO systems was initially carried out by Bell laboratories, where the so-called Bell Labs Layered Space-Time (BLAST) architecture is proposed. Initially, the aim of BLAST system is to design a coding technique (known as Diagonal BLAST or D-BLAST coding system (by Foschini) [1], to efficiently make use of both the time and space entities. The encoded symbols are in turns fed into different transmit antennas for transmission at different time (cyclical coding) so that none of the individual transmitted sub-stream is totally subject to the worst channel paths at any time, which ultimately leads to higher spectral efficiencies. Although D-BLAST coding is attractive, the system suffered from high implementation complexity. Two years later, a simplified version of BLAST architecture known as vertical-BLAST (V-BLAST) was introduced [4]. The vector coding process in V-BLAST is simply a de-multiplex operation followed by the modulation mapping process of independent sub-streams. No cyclical coding (or coding of any kind) is required. The laboratory prototype of V-BLAST system was actually implemented for the purpose of demonstrating the feasibility of the BLAST approach [4] but became a useful technique in its own right.

The capability to cancel or reject the unwanted co-channel interference (ICI) is one of the crucial elements in V-BLAST systems to uplift the system performance where more resilient signal is to be detected first and its contribution is then cancelled out to assist the detection of a weaker signal. This technique has already proved to be very effective in the multiuser detection [43, 44]. A revised version of V-BLAST that further illustrates the successive interference cancellation (SIC) capability can be found in [34]. The so-called SIC scheme also offers the added advantage to the MIMO system in terms of improving bit error probability performance, which

complements the obvious benefit of increased data rate. Nonetheless, the analysis and computer simulation of the V-BLAST system presented in [4, 34] was restricted to frequency-flat fading MIMO channel. (The D-BLAST and V-BLAST algorithm will be further explained in Chapter 2).

In general, the MIMO system architectures can be extended to the frequency-selective fading MIMO channel by incorporating the appropriate signal processing to detect and resolve the signals in the presence of inter-symbol interference (ISI) arises from the delay spread of the multipath channel as well as the co-channel interference (CCI) from multiple transmission streams [47]. Two main approaches have been formulated to deal with ISI and CCI in the MIMO systems. The first method is carried out in the frequency domain based on the use of the orthogonal frequency division multiplexing (OFDM) method introduced in [2], where detection is performed over each 'narrowband' sub-carrier. This approach later known as the MIMO–OFDM system [35–39], has become increasingly vital as one of the potential candidate for the future generation wireless systems. It solves the problem of ISI by effectively slowing down the data rate by sending a single high-speed data channel as many slow-speed data channels on different orthogonally-spaced sub-carriers. The effect of the ISI is reduced because the data rate on each sub-carriers is low.

The second approach is based on time-domain equalisation structure with decision feedback (DFE) scheme, which is also known as MIMO-DFE. The MIMO-DFE considers the problem of ISI in the multiple transmissions signal model by using a bank of feedforward filters and the decision feedback filters where the corresponding tap-weights are obtained individually to resolve each transmitted symbol by using some criteria such as minimum mean square error (MMSE). In general, the feedforward equaliser unit tends to compensate the overall effect of the ISI whereas the decision feedback unit attempts to remove only the ISI contribution (or the postcursor ISI) due to the already recovered symbol to the future received symbols. Earlier works related to this concept were studied in the context of cross-coupled channels and dually polarised radio system where the problems of multiplexing subject to crosstalk were investigated [40, 41]. In later years, the concept of MIMO equaliser with the decision feedback unit was developed in [42, 45, 46]. Clearer illustration about the MIMO-DFE is provided in [47] and the implementation of MIMO-DFE receiver will be described in Chapter 2.

The main core of the system presented in [47] is however the extension model of the MIMO-DFE structure that incorporates the 'order successive interference cancellation' (OSIC) scheme, which is used to cancel both CCI and ISI inherent in this frequency-selective channel. Not surprisingly this system is named as MIMO-OSIC-DFE, which is also a natural extension from the V-BLAST systems from frequency-flat model to frequency-selective model. The difference between is that in MIMO-DFE, decisions on preceding symbols are fed back into the detection process of each streams and CCI from the undetected future and on-time symbols are not cancelled. However, for MIMO-OSIC-DFE, data streams are successively detected with prior

cancellation of the entire CCI contributions from the previously detected streams and this is far more effective in terms of interference cancellation [47]. A similar work on the MIMO-DFE V-BLAST based model can also be found in [48]. Note that the focus of this thesis will be based primarily on the work presented in [47] and its further developments.

1.1.2 Other Important Developments in MIMO Systems

From *circa* 2000 until the present, MIMO systems have received intensified attentions worldwide and wide range of new arenas in research related to MIMO systems are continuing to emerge. Among the popular areas of MIMO related researches are: space-time coding (STC), MIMO information theory, correlation in MIMO channel, space-time channel modelling, MIMO channel measurement and characterization, MIMO channel estimation and etc.

Space-time coding is of current emerging fields in MIMO systems. Good references regarding STC can be found in [49–54]. Among the prominent STCs are the space-time block code (STBC) and the space-time trellis code (STTC). The use of STC in the MIMO systems has brought forth several advantages that make it very attractive for high data rate wireless applications. First, STC makes use of transmit diversity [52] by providing coding at the multiple transmit antenna to improve the downlink performance with only a single receive antenna (MISO case), although multiple receive antennas can also be used. Secondly, STC combines spatial diversity with channel coding that provides additional coding gain in addition to diversity gain [49]. Thirdly, prior channel information is not required at the transmitter and this eradicates the need for an expensive reverse link. Lastly, due to the inherent coding structure (an orthogonal spatio-temporal structure), STC is found to be robust against non-ideal channel conditions such as channel correlation and Doppler effects [50]. (Good reviews of STC are also provided in [8, 49, 50]). A variety of other works related to STC; e.g. space-time auto-coding, unitary space-time modulation, differential Cayley coding, sphere decoding have also been considered and these can be found in [55].

The effect of *antenna correlation* in the MIMO systems has also been studied extensively [56–62]. Ideally, each path between a transmit antenna and receive antenna should be uncorrelated for maximum benefit. If the various paths become correlated the corresponding data streams are also faded coherently. It then becomes extremely difficult to remove the interference due to correlation and the system performance is significantly worsened. Spatial correlation may occur in the real world scenario mostly due to inadequate antenna spacing and insufficient scatterers [56], which may results in capacity reduction [56] and hence must be dealt carefully in order to prevent further capacity and performance degradation in the MIMO systems. However, recent research [60] has shown that correlated fading information can be utilised to advantage when channel knowledge is available at the transmitter, which may lead to a higher channel capacity than the uncorrelated fading channel would permit. This is a new concept that further exploits the use of a

priori channel information as well as new developments in coding scheme for the MIMO systems.

The success of MIMO technique is also dependent on the channel characteristic and in particular full exploitation of a priori channel information. Not surprisingly, current research work for MIMO system is focused on channel modelling, channel measurement and characterization and improved methods of MIMO channel estimation scheme. Due to the sensitivity of the space-time processing algorithms w.r.t the channel matrix properties, *MIMO channel modelling* is critical in accessing the performance of different MIMO architectures. A good review of MIMO channel modelling can be found in [63]. In [63], MIMO channel models can be categorised according to different analogy: 'wideband' versus 'narrowband' model (by considering the bandwidth of the system), field measurements versus scatterer models or non-physical models versus physical models. The 'narrowband' models [56, 58, 67] assume that the channel has frequency non-selective fading, and the channel has the same response over the entire system bandwidth whereas 'wideband' models [65, 66] are inherently frequency selective due to multipath propagation delay, and different frequency sub-bands have different channel response [63].

Field measurements method [65–69] involves direct measurement of the MIMO channel responses through collective points of a certain location whereas the scatterer models [56, 64] attempt to capture the channel characteristic based on parametering the scattering effects in the MIMO channel environment. The non-physical models are derived based on statistical characteristic of the MIMO channels while the physical models use some physical parameters of the surroundings to provide reasonable description of the MIMO channel characteristic; e.g. ray tracing technique.

MIMO channel measurement and *channel characterisation* are being actively carried out to gain more insight into the real propagation characteristic of the MIMO channels since the simulated channel modelling approach may not be able to effectively to represent the actual propagation scenario of the MIMO systems. By using detail measurements, the MIMO channel response can be properly identified and characterised. On the other hand, MIMO measurements can also serve as a good tool to verify how faithfully the MIMO channel model represents real life. Some of this crucial research can be found in [65–72].

1.1.3 Overview of Channel Estimation Techniques in MIMO Systems

A particularly important area of MIMO research is channel estimation. In order to achieve the quoted capacity gains for MIMO systems, the multiple channel impulse responses and their fading coefficients must be known or estimated. Any deviation from perfect channel estimates results in reduced system performance. Most of the capacity analyses have been based on the assumption of perfect channel knowledge at the receiver [1,2]. Moreover, for the majority of the space-time

signal processing algorithms such as MIMO-DFE or STC, accurate channel state information (CSI) of the each sub-channel link in the MIMO channel is needed at the receiver in order to carry out the respective detection and decoding process.

Many of the useful training-based MIMO channel estimation (MIMO-CE) schemes that have been developed can be found in [49, 73–90]. Most of the MIMO channel estimation research mostly catered for *coded* space-time systems; e.g. MIMO-CE for MIMO systems that utilise STC [73–77] or for the MIMO-OFDM systems [78–82]. These methods are designed to cope specifically with the nature of the coding such as space-time block codes or space-time multi-tone. Channel estimation research that related to the MIMO – BLAST systems is provided in [83–87]. In [83], it is shown that by using training signals from multiple antennas that are mutually orthogonal, produces best estimation accuracy (maximum likelihood estimate) for a given transmit power under most cases. It is also shown in [73, 83] that for the layered space-time system the required training sequence length grows approximately linearly with the number of transmit antennas when the transmit power for training is optimised provided that the transmit powers for data and training are allowed to vary. However, when both transmit powers are required to be equal, the number of pilot symbols may be larger than the number of antennas. (In this thesis equal transmit power on both data and training is used). Nevertheless, the optimum length is independent of both the number of receive antennas and signal-to-noise [73]. However, the discussion therein is restricted to the flat-fading MIMO channel.

Estimation of time-varying flat-fading MIMO channels was presented in [84], where trade-off between minimising the training sequence length and channel estimation error (caused by the noise and temporal variation of the channel) was demonstrated. This was one of the very first works that presented a MIMO channel estimation scheme for *uncoded* space-time systems; i.e. the BLAST system, although the work in [83] did cater for the more general MIMO case. A similar approach can also be found in [87]. The influence of the channel estimation error that leads to the new design of the V-BLAST architecture that cope with channel estimation error is shown in [85] and the impact of channel estimation error on the spectral efficiency of the MIMO systems was studied in [86]. Nevertheless, MIMO-CE research presented so far has been mostly restricted to the *frequency-flat fading* environment.

There are some other MIMO channel estimation techniques worthy of being pointed out. The work on joint channel estimation, decoding and detection in MIMO systems are presented in [88–90] for STC related systems. In these systems, as the name implies, channel estimation and data decoding are achieved simultaneously by using different algorithms such as expectation maximisation (EM) in [88], constant modulus algorithm (CMA) with STBC in [89] and iterative parallel cancellation detection with interleaver in [90]. Nonetheless, those methods exhibit high algorithm complexity.

Other significant research that is related to MIMO-CE is found in [91, 92] where concept of adaptive channel estimation and channel tracking is employed for multi-channel systems. Maximum likelihood sequence estimator has been considered in [91] and MMSE MIMO-DFE in [92] for equalisation that resolves both CCI and time dispersion effects of the MIMO channel. The key technique in both pieces of research is the use of a Kalman filter for adaptive tracking of the time varying Doppler channel. Nevertheless, the preliminary assumption is that perfect knowledge of the MIMO channel must avilable for the purpose of illustrating multi-channel tracking using the MIMO-Kalman filter in [92].

The MIMO-CE methods that have been discussed so far are based on pilot-assistance, which is also know as training-based approach. In contrast, non-training based, or 'blind' MIMO channel estimation is another active MIMO system research area. Some of the key work of blind MIMO channel estimation can be found in [93–99] and a very good introduction and review of blind space-time signal processing is presented in [93–95]. Blind channel estimation methods do not use any training signals to estimate the channel characteristic, but instead, it uses some kind of higher order statistic or take a subspace approach with oversampling technique to approximate the channel response though only the ordinary received data signals. Since no training is required, blind channel estimation appears to be very attractive since maximisation of the data throughput in the wireless application might now be possibly attainable.

1.2 Motivation and Aim of Research

The motivation of this research comes from the understanding that a good knowledge of the channel characteristic is vital for most of the space-time MIMO processes discussed above. Without proper and accurate channel information, the performance of MIMO systems is severely degraded and the practical performance is significantly worse than predicted. Theoretically, in order to assess the practicability of MIMO systems, all possible information about the MIMO channel must be obtained. This requires a suitable MIMO channel estimation scheme.

The main aim of the research reported in this thesis is to investigate and devise possible approaches to the problem of MIMO channel estimation for *uncoded* space-time MIMO systems. The focus is on the incorporation of a suitable MIMO-CE scheme for the V-BLAST-based MIMO-OSIC-DFE systems described in [47], with the specific requirement of extending the channel estimator from the frequency-flat fading MIMO channel to the more realistic frequency-selective fading MIMO channel. The research address the particular problem of co-channel interference (CCI) posed by the multiple antennas configuration and the inter-symbol interference (ISI) posed by the frequency selectivity of the channel in wideband MIMO systems. The overall aim is to design a universal and simplified time domain training-based method that could perform

MIMO channel estimation efficiently while effectively dealing with the joint CCI and ISI problem in the frequency-selective case of the MIMO channel.

Drawing on the works reported in [73, 83, 84] for the flat fading MIMO channel case a new training-based MIMO channel estimation and tracking algorithm has been developed using pilot matrix training for both frequency-flat fading and frequency-selective fading channel condition. The trade-off between the length of the training sequence and the channel estimation error is examined in detail for a number of different channel scenarios. The time-varying nature of the channel impulse response is also considered and the impact that this has on the quality of the channel estimate and subsequent MIMO system performance is considered in great detail for different channel scenarios.

Computer simulations have been carried out to assess the impact of the channel estimation error on the bit error probability–system performance of a 'pure' MIMO system without the influence of coding; i.e. channel coding or STC. These results are also compared with the case where perfect channel estimation is assumed. The performance of the proposed channel estimation scheme is also studied and analysed for different MIMO channel parameters of the frequency-selective fading MIMO channel. Although, the proposed MIMO-CE method is primarily designed for the class of BLAST-based receivers described in [47], the channel estimation scheme could be also employed in any general MIMO systems for training of channel information.

1.3 Thesis Outline and Contributions

The thesis consists of six chapters. The major contribution to the field by the author is mainly presented in Chapter 4 and the corresponding simulation results are offered in Chapter 5.

Chapter 1 provides a general overview of the key development in MIMO system and current MIMO research. The literature surveys of various MIMO research methods have been provided together with an overview of current MIMO channel estimation schemes.

Chapter 2 is an introductory chapter that provides all the necessary fundamentals of MIMO wireless systems. It begins with a description of the basic wireless propagation, pace-time channel characteristic and basic MIMO architecture. The concept of space-time processing (STP) is subsequently introduced in order to provide the necessary understanding of how STP has evolved and applied to MIMO systems. The related problem of CCI and ISI is also discussed. The BLAST-based systems in [1, 4, 47] will also be described, emphaising the importance of interference cancellation schemes. This description of MIMO–BLAST systems includes the D-BLAST and the V-BLAST versions that operate in the frequency flat fading conditions and its extended version, MIMO-DFE-OSIC receivers, which operates in the frequency-selective fading channel. The main contribution of the author in this chapter is the development of a modified version of V-BLAST

system that is based on QR decomposition of the MIMO channel, which has been published in [126]. In the proposed QR detection method, a computationally efficient sub-optimum successive interference cancellation technique is presented. The QR method has excellent performance and does not require the computationally intensive matrix inversion operation. The chapter concludes with a summary of the needs of channel estimation in the MIMO systems.

Chapter 3 presents three general approaches for the estimation of the flat-fading MIMO channel, namely the MIMO-LMS algorithm, the MIMO-RLS algorithm and the MIMO-PMI algorithm. The first two algorithms belong to the family of adaptive methods, which uses the conventional method of least mean squares (LMS) and recursive least squares (RLS) respectively. The last algorithm is a non-adaptive type where channel estimation is obtained by direct inversion of the pilot matrix sent. The difference between the adaptive and non-adaptive approach is that in the adaptive approaches, the pilot symbols are successively sent across the transmit antennas in a vector format and processed adaptively at the receiver's estimator so that the estimate can finally be converged to the actual value of the channel. Whereas in the non-adaptive approach, the pilot symbols are sent over the channel in a block of matrix (in burst), known as pilot matrix whereby the corresponding block received signals are jointly used to estimate the channel through a single matrix inversion process. Hence, the name pilot matrix inversion (PMI). Author's contributions to this work are the MIMO-RLS algorithm [87] and the MIMO-PMI algorithm [144].

Chapter 4 presents a novel MIMO channel estimation scheme for the class of MIMO-OSIC-DFE receivers described in Chapter 2. In this chapter, the development of MIMO-CE from the frequency-flat model to the frequency-selective model is considered together with the related problems of CCI and ISI effects. The development and implementation of the novel MIMO-CE scheme are demonstrated, where the design of training symbols and the construction of the pilot matrix is based on the use of set of orthogonal Hadamard sequence. Perhaps, the most important achievement of this work has been the discovery of a more efficient MIMO-CE method that employs the training sequences extracted from the Paley's construction of the Hadamard matrix instead of the ordinary Hadamard matrix. It is found that pilot matrix construction using ordinary Hadamard matrix results in unnecessary time-gaps and longer training sequences. However, through the unique matrix arrangement of *Paley-Hadamard* matrix (that combines the orthogonal and Toeplitz-like structure), the length of the pilot sequence is minimised. Examples are also given to illustrate this MIMO-CE method for different channel parameters.

Another important achievement is the attempt of utilising the fractionally-spaced channel model that enables the MIMO systems to be demonstrated under far more realistic channel conditions whereas the original MIMO-CE scheme assumes that the path delays are symbol-spaced. The extended MIMO-CE scheme incorporates a fractionally-spaced design to allow the path delays within a fraction of the symbol period to be estimated. The design and implementation

of the novel fractional MIMO-CE scheme is demonstrated by mean of an example case. The author's contribution in terms of the MIMO-CE works can be found in [145, 146, 147, 148].

Channel tracking that assists the proposed MIMO-CE scheme is also shown in the last section of Chapter 4. The method uses the recovered data blocks to perform tracking so that the channel estimate initially obtained by the proposed MIMO-CE method can be adaptively updated. The advantage of this approach is two fold. First, it allows the period between the transmissions of pilot symbols to be lengthened; thereby improving throughput since training of channel is allowed to be farther apart. Second, if throughput if not an issue channel tracking can be used to minimise the channel estimation error due to the time-variation of channel.

Chapter-5 presents the simulation results obtained from the works described in Chapter 2, 3 and 4. The chapter is divided in five major sections. Section 5.1 shows the performance of the layered space-time receiver in a frequency-flat fading MIMO channel with different MIMO configurations. Results are shown for various detection methods: linear ZF, linear MMSE, nonlinear ZF and nonlinear MMSE. Section 5.2 shows the performance of the layered space-time receiver using the QR detection methods for both linear and nonlinear detection. The results also demonstrate the importance of the need for re-arranging the channel matrix prior to QR detection. Section 5.3 presents the results related to all the MIMO-CE methods described in Chapter 3, where the performances of the respective estimator as well as the impact of channel estimation error on the layered space-time receiver's performance are shown. Same emphasis is placed on the proposed MIMO-RLS and MIMO-PMI algorithms where the results are obtained for different estimator parameters and different channel conditions.

Perhaps the major contributions to the results presented in Chapter 5 are provided in Sections 5.4 and 5.5, which correspond to the theoretical work in Chapter 4. Section 5.4 presents the performance of the novel MIMO channel estimator described for a range of different time-varying frequency-selective fading MIMO channel conditions. Results are shown for the symbol-spaced method as well as the fractionally-spaced method for different channel and system parameters. Section 5.5 presents the performance of the MIMO-OSIC-DFE layered space-time receiver in the frequency-selective multipath fading MIMO channel. The results are shown for different system configurations, equaliser settings and different numbers of channel paths within each sub-channel link. The results also compared with the case where perfect channel knowledge is assumed. The impact of the channel estimation error on the system performance of the layered space-time receiver is also shown. These results have applications to the practical design of space-time systems for high-capacity over frequency-selective fading MIMO channels.

Chapter-6 concludes the thesis with respect to each chapter. Recommendations for future areas of investigation related to this research work are also discussed.

Chapter 2

Multiple-Input Multiple-Output Wireless Communication Systems

This chapter focuses on the basic architecture of multiple-input multiple-output (MIMO) wireless communication systems, which requires the understanding of space-time signal processing. For this reason, the concepts of space-time signal processing and various detection techniques will be discussed initially before proceeding to a specific MIMO wireless architecture; the Bell Laboratories LAyered Space-time System (BLAST), which is believed to be one of the pioneering technique in using the multiple antenna array elements to enhance system capacity.

An understanding of different types of MIMO channels is also essential for the development of the BLAST architecture especially from frequency-flat to frequency-selective MIMO channels. The evolution of the BLAST system, particularly on the Vertical-BLAST (V-BLAST) architecture and its extended versions will be discussed accordingly in this chapter.

2.1 Basic Wireless Propagation

The mobile radio channel provides the physical medium that supports electromagnetic wave propagation between a transmitter and a receiver. A signal travel through the wireless channel arrives at the destination along a number of different paths as multipath. These paths arise from reflection, diffraction and scattering of the radiated energy by the objects or buildings around the vicinity of the receiver. These effects have a range of impacts on the received signal.

2.1.1 Signal Attenuation – Free Space Path Loss

Free-space loss is an overall variation in the signal's power that varies due to the distance of travel between the transmitter and the receiver. The reduction in power can be related to the inverse square law [112]. The received signal power (Friis equation) can be expressed as:

$$P_r = P_t\left(\frac{\lambda_c}{4\pi d}\right)^2 G_t G_r \qquad (2.1)$$

where P_t and P_r are the transmit and receive powers respectively. λ_c is the wave-length, G_t & G_r are the power gains of the transmit and receive antennas respectively and d is the distance between the transmit antenna and the receive antenna. The received signal power decreases as the distance of separation increases.

2.1.2 Macroscopic Fading – Shadowing

Shadowing arises due to the varying nature of the particular cluster of obstructions between the transmitter and the receiver. This type of fading is generally associated with an increase in signal absorption due to the environment. Different clusters along individual path at a given distance will results in variation with respect to the nominal value of the path loss model in (2.1). Some paths will suffer increased loss, while others will be less obstructed and have increased signal strength. Shadowing is normally associated with log-normal distribution. (Refer to [108] for further detailed explanation).

2.1.3 Microscopic Fading – Rapid Fading

Microscopic fading refers to rapid fluctuation of the received signal in space, time and frequency with variations on small-scale of ½ wave-lengths. The rapid fading results from the constructive and destructive signal between the multiple waves that are caused by the scattering effect of the arriving multipaths (which carries the copies of same signal with a different phase, amplitude and time of arrival). The superimposition of these signals produces variations in the signal envelope, which causes 'fading' in the received signal. Depending on whether a line of sight (LOS) path exists or not, the rapid fading condition gives rise to either Ricean or Rayleigh distribution of the received signal envelope respectively [111, 113]. The Rayleigh distribution is considered to be a good approximation to measured fading amplitude statistics for the mobile fading channels in the non line-of-sight (NLOS) situations, which is often the case in urban areas. Whereas, the Ricean distribution resembles the LOS situation, which is observed mostly in the open-spaced rural areas. The Ricean and Rayleigh p.d.f. may be given as follows:

$$p_{Ricean}(r) = \frac{r}{\sigma^2} e^{-r^2/(2\sigma^2)} e^{-K} I_0\left(\frac{r\sqrt{2K}}{\sigma}\right) \qquad (2.2)$$

where r is the amplitude of the received signal and σ^2 is the variance of the multipath. The function I_0 is the modified Bessel function of the first kind and zeroth order. The factor K gives a

measure of the ratio of the power received in the direct LOS to the total power received *via* other paths. Thus, in the NLOS situation, $K = 0$ and distribution of the received signal's amplitude becomes Rayleigh. On the other hand, as the K increases until infinity, which is the pure LOS with no indirect paths scenario, the distribution of r become Gaussian. This is similar to the situation where only additive white Gaussian noise (AWGN) condition is present in the channel.

2.1.4 Channel Classification

Signal propagation over the mobile radio channel is subject to spreading in both the time and frequency domains. Doppler frequency-spread is caused by the movement of the mobile unit and the different angles of arrival of the scattered signal at the receiver and the time-delay spread is caused by the multiple arrival of many signal echoes at the receiver in several 'beams' of multiple waves with large differences its arrival time. Doppler spreading gives rise to time-selective fading and frequency dispersion, whereas the time delay spread results in time-dispersion and hence frequency selective fading. Although all of the channel effects are almost always present, the classification of the channel is based on the transmitted signal's nature and the most dominant of these effects.

2.1.4.1 Delay Spread - Time Dispersive/Frequency Selective Channel

This kind of channel results from the presence of significant delays in each multipath which leads to stretching of the transmitted signal in the time domain. The previous symbol continues to arrive at the receiver as the initial energy of the next symbol arrives, thus creating ambiguity in the demodulation of the new symbol. This process manifests itself as *intersymbol interference* (ISI). The span of the path delays is called the delay spread. Time dispersive channels are also frequency selective fading because the superimpositions of two signals, one time-delayed from the other, can be modelled as a transversal filter that provides signal cancellation at certain frequencies around the reciprocal of the delay-spread.

Frequency selective fading can be characterised in terms of coherence bandwidth B_C, which is inversely proportional to the RMS delay spread τ_{rms} of the channel.

$$B_C \approx \frac{1}{\tau_{rms}}; \quad \text{where} \quad \tau_{rms} = \sqrt{\frac{1}{P_T}\sum_{i=1}^{L} P_i \tau_i^2 - \tau_0^2} \tag{2.3}$$

where P_T is the total power in the channel and L is the total number of significant paths. P_i is the power in the i^{th} path and τ_i is the time-delay of signals on the i^{th} path.

The RMS delay spread is a good indicator of system performance for the moderate delay spread. If τ_{rms} is less than the symbol duration T_s, no significant ISI is encountered and channel may assumed to be frequency flat. Conversely, when the coherence bandwidth B_C of the channel is comparable to or less than the signal bandwidth B_S, $B_S > B_C$, the channel is said to experience frequency selective fading, which is also known as wideband channels since the bandwidth of the signal is wider than bandwidth of the channel impulse response [113].

2.1.4.2 Doppler Spread - Frequency Dispersive/Time Selective Channel

The time-selective fading due to transmitter, receiver or scatterer motion results in a Doppler spread, B_D. In this case, a pure tone (frequency f_c in hertz) spreads over a finite spectral bandwidth ($f_c + f_d$) give rise to frequency dispersion [12]. The Doppler effect results in the change of apparent frequency (which is the Doppler shift f_d) of the arriving waves according to the mobile speed and direction of wave. The Doppler shift f_d is given as:

$$f_d = f_c \frac{v}{c} \cos\alpha = f_{d\max} \cos\alpha \tag{2.4}$$

where v is the speed of the transmitter, receiver or the scatterer, c is the light speed (3×10^8 m/s), α is angle of arrival, f_c is the carrier frequency and $f_{d\max}$ is the maximum Doppler shift at α=0. The reason why the received signal suffers from Doppler-spread is because the scattered signals may arrive over a wide range of angles, each having its own frequency shift. The Doppler power spectrum has the classical U-shaped form is approximated by the Jakes model [112].

Time-selective fading can be characterised by the coherence time, T_C of the channel, which is inversely proportional to the Doppler spread of the channel B_D:

$$T_C \approx \frac{1}{B_D} \quad or \quad \frac{1}{f_{d\max}} \tag{2.5}$$

A useful approximation by Steele [114], to T_C for the classical channel is:

$$T_C \approx \frac{9}{16\pi f_{d\max}} \tag{2.6}$$

Coherence time T_C is actually a statistical measure of the time duration over which the channel response is relatively invariant. If the reciprocal bandwidth of the signal (the maximum symbol duration) is greater than the coherence time; $T_S > T_C$, then the channel is considered time-varying with fast fading. On contrary, if the baseband signal bandwidth B_S is much greater than B_D then the effects of Doppler spread are negligible at the receiver, which can be classified as the slow fading invariant channel.

2.1.4.3 Non-Dispersive Channel

In the non-dispersive channel, signal does not fade with either time or frequency. It is also known as doubly-flat channel, where the signal bandwidth and its symbol duration is less than the coherence bandwidth and the coherence time of the channel, respectively.

2.1.4.4 Doubly Dispersive Channel

Doubly dispersive channel exhibit both frequency selective fading and time selective fading due to long propagation delays and rapid varying nature of the channel. In this case, the signal bandwidth and its symbol duration are greater than the coherence bandwidth and the coherence time of the channel respectively.

2.1.4.5 Summary of Channel Classification

1) Frequency Flat (no delay-spread) & Time-Flat (slow fading) Channel $B_S << B_C$ $T_S << T_C$ or or $T_S >> \tau_{rms}$ $B_S >> B_D$ (Doubly –flat fading channel)	2) Frequency Flat (no delay-spread) & Time-Selective (fast fading) Channel $B_S << B_C$ $T_S > T_C$ or or $T_S >> \tau_{rms}$ $B_S < B_D$ (Fast-varying flat fading channel)
3) Frequency Selective (Delay-spread) & Time-Flat (slow fading) Channel $B_S > B_C$ $T_S << T_C$ or or $T_S < \tau_{rms}$ $B_S >> B_D$ (Slow-varying frequency-selective channel)	4) Frequency Selective (Delay-spread) & Time-Selective (fast fading) Channel $B_S > B_C$ $T_S > T_C$ or or $T_S < \tau_{rms}$ $B_S < B_D$ (Doubly dispersive fading channel)

B_S = Bandwidth of the baseband signal — T_S = Symbol duration of the baseband signal

B_C = Coherence bandwidth of the channel — T_C = Coherence time of the channel

B_D = Doppler spread of the channel — τ_{rms} = RMS delay spread of the channel

Table A.1: Summary of different types of fading channel.

2.1.4.6 Angle Spread – Space Selective Fading [12]

Angle spread can be observed in the multiple array antennas at the receiver as the spread in angle-of-arrivals (AOAs) of the multipath component. Similarly, angle spread at the transmitter refers to the spread in angles of departure (AODs) of the multipath that reaches the receiver. Angle spread θ_{rms} causes space-selective fading which means that signal amplitude depends on the spatial location of the antenna. Space selective fading is characterised by the coherence distance D_C, which is the spatial separation for which the autocorrelation coefficient of the spatial fading drops to 0.7 [12]. The coherence distance is inversely proportional to angle spread.

2.1.5 Scattering Model

Two types of major scattering effects can be observed in both the uplink and downlink transmission. However, only the uplink will be discussed here since the scattering effects can be applied in both directions. First is the local to terminal scattering and second is the remote scattering. Local to terminal scattering is caused by buildings or other scatterers within the vicinity of the handset (near field effect). Terminal motion and local scattering give rise to Doppler spread. While local scatterers contribute to Doppler spread, the delay spread induced by local scatterers is usually insignificant because of the small scattering radius.

In the remote scattering, the emerging wavefront from the local scatterers may travel directly to the based-station or may be scattered towards the base-station by remote dominant scatterers, giving rise to a specular multipath. Remote scatterers can be either terrain features or high rise buildings. Remote scatterers can cause significant delay spread. Doppler spread is also experienced due to motion of the terminal as well as the scatterers.

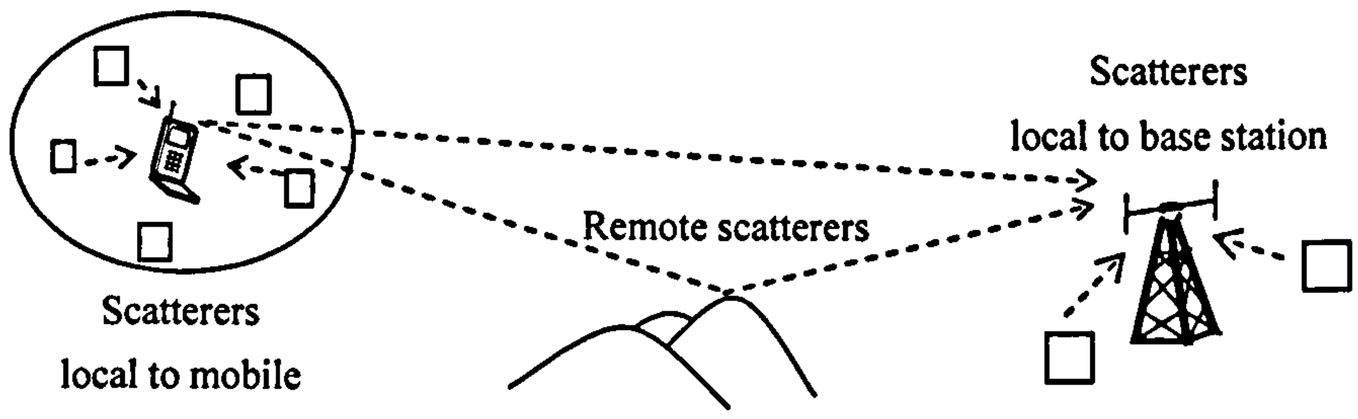

Figure 2.1: Classification of scatterers

2.2 Space-Time Propagation Characteristic and MIMO Channel

In this section, the propagation representation of the MIMO channel model is presented, in particular, for integration of spatial dimension (in MIMO sense) into its basic propagation model [12]. Some of these topics in [12, 110, 111] are worthy of being pointed out for the understanding of the MIMO channel model, which are mostly used in the works presented in this thesis.

2.2.1 Space-Time Random Field [12]

The space-time channel can be modelled as a linear time-varying system. The propagation impulse response between the transmitter and receiver can be generally denoted as $p(\tau, t, d)$, which can visualised in figure 2.2. The 'channel' can also defined as the response at receiver whose antenna is located as position d at time t to an impulse launched at time $(t-\tau)$ from the transmit antenna placed at origin, where t is the time-varying index.

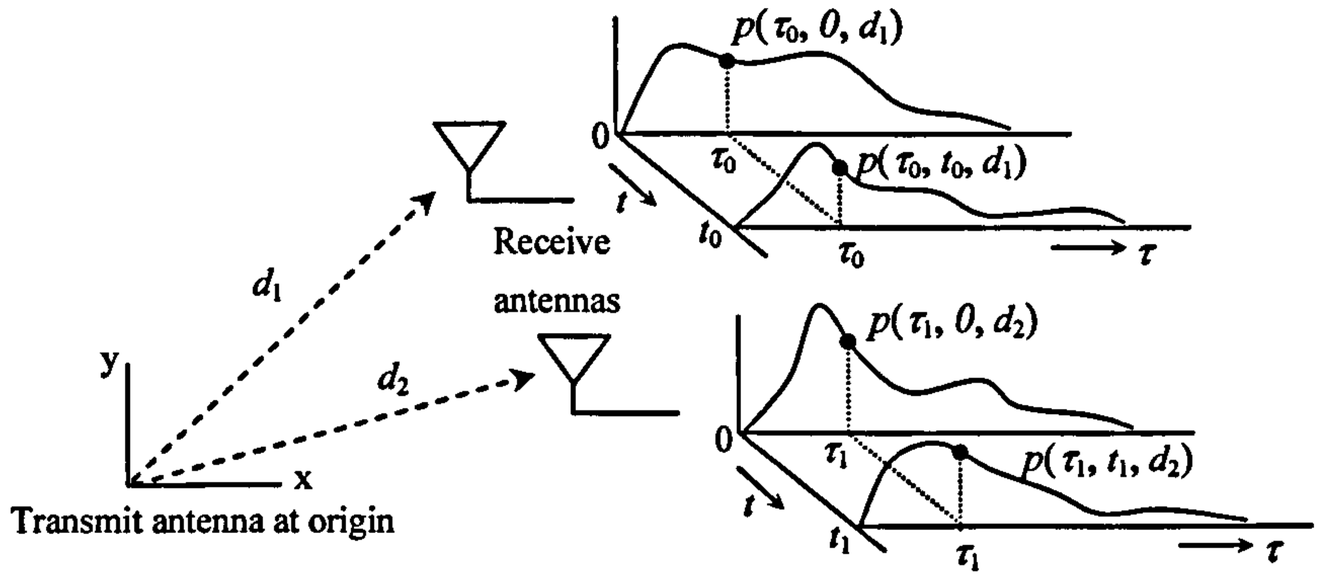

Figure 2.2: Space-time channel impulse response as a vector valued ST random field

Note that $p(\tau)$ sampled at the various delays (τ) can collectively be described by a vector and consequently $p(\tau, t, d)$ may be thought as a vector valued ST random field. [11]. The behaviour of $p(\tau, t, d)$ is generally very complicated though practical situations lend themselves to certain simplifying assumptions such as stationarity, which shall be pointed out next.

2.2.1.1 Wide Sense Stationarity (WSS)

WSS implies that the 2nd order time statistics of the channel are stationary (justified over short periods, T_u). For clarity, d of $p(\tau, t, d)$ is dropped temporarily and WWS implies:

$$E\left\{p(\tau,t)\,p^*(\tau,t+\Delta t)\right\} = R_t(\tau,\Delta t) \tag{2.7}$$

where $R_t(\tau,\Delta t)$ is called the lagged time correlation function. Note that the autocorrelation in time depends only on the lag Δt and not on t. In the frequency domain, as $T_u \rightarrow \infty$, we have

$$E\left\{U(\tau,f_1)U(\tau,f_2)\right\} = 0 \quad \text{if } f_1 \neq f_2 \tag{2.8}$$

where U(τ, f) is the channel description in delay(τ) of the Doppler frequency(f) domain. (2.8) implying that the channel at different Doppler frequency is uncorrelated [100].

2.2.1.2 Uncorrelated Scattering (US)

In US model the scatterers contributing to delay spread in the channel is assumed to have independent fading, i.e.:

$$E\left\{p(\tau_1,t)\,p^*(\tau_2,t)\right\} = 0 \quad \text{if } \tau_1 \neq \tau_2 \tag{2.9}$$

The US model also assumes stationarity in the transmission frequency domain as:

$$E\left\{P(f,t)\,P^*(f+\Delta f,t)\right\} = R_f(\Delta f,t) \tag{2.10}$$

where $R_f(\Delta f,t)$ is called the lagged-transmission frequency correlation function. The combination of the WWS and US assumptions leads to what is called the wide sense stationary

uncorrelated scattering (WSSUS) model, which is stationary in time and frequency domains and conversely has independent components in Doppler frequency (f) and delay (τ) dimensions.

2.2.1.3 Homogeneous Channels (HO) [12]

In the HO model, the space dimension d is introduced. The model assume that the statistical behaviour of $p(\tau, t, d)$ is locally stationary in space over several tens of the coherence distance.

$$E\left\{p(\tau,t,d)\,p^{*}(\tau,t,d+\Delta d)\right\} = R_d(\tau,t,\Delta d) \tag{2.11}$$

where $R_d(\tau,t,\Delta d)$ is called the lagged space correlation function. The space dimension d is also related to the angle θ and the angular transformation of the channel response, $S(\tau, t, \theta)$ as:

$$p(\tau,t,d) = \int_{-\pi}^{\pi} S(\tau,t,\theta)\, e^{-j2\pi\sin(\theta)\frac{d}{\lambda_c}t}\, d\theta \tag{2.12}$$

where $S(\tau, t, \theta)$ is the channel description in the delay(τ), time(t), angle(θ) domain. Assuming a discrete scattering model, with scatterers located at different path delays and AOAs, $S(\tau_l,\theta_l)$ (dropping t) can be interpreted as the scattering amplitude of the scatterer located at τ_l and θ_l. For homogenous model in $p(\tau, t, d)$, leads to the following:

$$E\left\{S(\tau,t,\theta_1)S^{*}(\tau,t,\theta_2)\right\} = 0 \quad \text{if } \theta_1 \neq \theta_2 \tag{2.13}$$

(2.13) implies that signal arriving from scatterers at different angles are uncorrelated. The WSSUS and the HO model can be combined to form the WSSUS-HO channel. Homogeneity requires scatterers to have statistically omnidirectional scattering and linear uniformity.

2.2.2 Space-Time Channel and Signal Model [12]

In this part, the MIMO channel model is illustrated using the physical scattering model for both flat fading and frequency selective fading channel, which is used throughout the works presented in this thesis where the non line-of-sight (NLOS) Rayleigh fading with WSSUS-HO model is assumed for each path between the transmit-receive antenna pair in the MIMO systems.

2.2.2.1 MIMO channel model [12]

Let $h(\tau, t)$ be the overall time-varying channel impulse response (CIR) from the input of the pulse-shaping filter $g(\tau)$ at the transmitter, through the propagation channel $p(\tau, t)$, to the output of the receiver matched filter. For convenience, $h_{j,i}(\tau, t)$ is referred as the individual CIR from the i^{th} transmit antenna to j^{th} receive antenna. Hence, within this sub-channel, the received signal $y(t)$ as a SISO model can be viewed as:

$$y(t) = \int_0^{\tau_{total}} h(\tau,t)s(t-\tau)d\tau = h(\tau,t) * s(t) \tag{2.14}$$

where * denotes the convolution operator. Note that the received signal $y(t)$ is produced by the integration of same signal $s(t)$ that arrived in different scattering paths within the duration τ_{total}.

However, in the MIMO scenario, the signal model involves more that one sub-channel and multiple signals from different sources. Consider a MIMO system with M transmit antennas and N receive antennas. The $(N\times M)$ MIMO channel matrix $\mathbf{H}(\tau, t)$ can be defined as:

$$\mathbf{H}(\tau,t) = \begin{bmatrix} h_{1,1}(\tau,t) & h_{1,2}(\tau,t) & \cdots & h_{1,M}(\tau,t) \\ h_{2,1}(\tau,t) & h_{2,2}(\tau,t) & \cdots & h_{2,M}(\tau,t) \\ \vdots & \vdots & \ddots & \vdots \\ h_{N,1}(\tau,t) & h_{N,2}(\tau,t) & \cdots & h_{N,M}(\tau,t) \end{bmatrix} \tag{2.15}$$

The column vector $\left[h_{1,i}(\tau,t) \;\; h_{2,i}(\tau,t) \cdots h_{N,i}(\tau,t)\right]^{\mathsf{T}}$ is the spatio-temporal signature or sub-channel link from i^{th} transmit antenna to all N receive antenna. The signal received at the j^{th} receive antenna at time t, can be expressed in the following single input-output relationship as:

$$y_j(t) = \sum_{i=1}^{M} h_{j,i}(\tau,t) * s_i(t); \quad j = 1,2,\ldots,N \tag{2.16}$$

where $s_i(t)$ is the signal sent from i^{th} transmit antenna at time t. The input-output relationship (in MIMO sense) can be further expressed as:

$$\mathbf{y}(t) \;=\; \mathbf{H}(\tau,t) * \mathbf{s}(t) \tag{2.17}$$

where $\mathbf{s}(t) = \left[s_1(t) \;\; s_2(t) \cdots s_M(t)\right]^{\mathsf{T}}$ is an $(M\times 1)$ input (transmit) vector and the $(N\times 1)$ output (receive) vector is denoted by $\mathbf{y}(t) = \left[y_1(t) \;\; y_2(t) \cdots y_N(t)\right]^{\mathsf{T}}$.

2.2.2.2 Physical Scattering Model for Space-Time Channel [12]

The $(N\times M)$ MIMO channel matrix $\mathbf{H}(\tau, t)$ in (2.15) can be related to the physical scattering model of the channel. A single scatterer is assumed where $S(\theta_i, \tau_i)$ is the complex scatterer amplitude of the scatterer located at angle θ_i and delay τ_i. The transmitted signal is scattered and arrives at the receiver at different angles and delays. $S(\theta_i, \tau_i)$ is an independent identically distributed (IID) complex Gaussian random variable (US assumption). Dropping the time-varying dependence, t, the $(N\times M)$ MIMO channel matrix $\mathbf{H}(\tau)$ can be constructed as:

$$\mathbf{H}(\tau) = \int_{-\pi}^{\pi} \int_{0}^{\tau_{max}} S(\theta,\tau')\,\mathbf{a}(\theta)\,\mathbf{b}(\phi)^{\mathsf{T}}\, g(\tau-\tau')\, d\tau'\, d\theta \tag{2.18}$$

where τ_{max} is the maximum delay spread of the physical channel. $\mathbf{b}(\phi)$ and $\mathbf{a}(\theta)$ are the array

response vector at the transmit and receive antenna array respectively, which defines the spatial signature across the respective antenna array, representing the phase difference induced at the antennas at angle θ. (The spatial signature is a function of array geometry, antenna element pattern and AOA). $g(\tau)$ is the combined effect of the pulse-shaping at the transmitter and matched-filtering at the receiver. The scattering effects in (2.18) implies that a scatterer located at angle θ and delay τ w.r.t the receive antenna array now appears to be located at angle ϕ w.r.t the transmit antenna array. No difference is made for the scattering amplitude resulted from the receive and transmit antenna array; $S(\theta,\tau) = S(\phi,\tau)$ since the scatterers being the same.

Nevertheless, the physical scattering ST channel described in (2.18) is based on a single scatterer for illustration purpose, which cannot adequately model all the channel effects. Usually, there are more scatterers which create the multiple scattering effects in the channel, where signal uses more than one scatterer to reach the receiver. θ, ϕ and τ become independent when multiple scattering effects are assumed. According to [12], with suitable choice of scatterer location, antenna element patterns and the use of multiple scattering model, the elements of **H** are found be independent zero mean complex Gaussian (ZMCG) random variables, which can be described as $Z = X+jY$ where X and Y are independent real Gaussian variables with zero mean and equal variance (which represents the NLOS Rayleigh fading distribution). If the delay spread in the channel is negligible; i.e. $\tau_{max} \approx 0$, (18) can be rewritten as:

$$\mathbf{H}(\tau) = \left(\int_{-\pi}^{\pi} \int_{0}^{\tau_{max}} S(\theta,\tau')\mathbf{a}(\theta)\mathbf{b}(\phi)^{\mathsf{T}} d\tau' d\theta \right) g(\tau) = \mathbf{H}\, g(\tau) \qquad (2.19)$$

where **H** becomes $\mathbf{H}_w$, the IID (spatial white) MIMO channel is with the following properties:

$$\begin{aligned} &E\left\{ [\mathbf{H}_w]_{j,i} \right\} = 0, \quad \& \quad E\left\{ \left| [\mathbf{H}_w]_{j,i} \right|^2 \right\} = 1, \\ &E\left\{ [\mathbf{H}_w]_{j,i} [\mathbf{H}_w]^*_{n,m} \right\} = 0 \quad if\ j \neq n\ or\ i \neq m \end{aligned} \qquad (2.20)$$

Hence, **H** or $\mathbf{H}_w$ in the subsequent discussion is of non-physical models since they do not incorporate the actual physical path structure. Since it is ZMCG model, each coefficient or elements in **H** can now be independently generated according to Rayleigh fading as follows:

$$h_{j,i} = a + jb \doteq Normal\left(0, \frac{1}{\sqrt{2}}\right) + j\, Normal\left(0, \frac{1}{\sqrt{2}}\right) \qquad (2.21)$$

The complex coefficient $h_{j,i}$ generated in (2.21) has zero mean, unit variance and has the normalised condition as: $E\left\{ |h_{j,i}|^2 \right\} = 1$. The complex entities in (2.21) will be used for the MIMO channel model throughout the thesis.

2.2.2.3 MIMO Sampled Signal Model

For a *frequency flat* fading condition, the MIMO channel is modelled by a ($N\times M$) matrix **H** [12, 83] and the received signal vector $\mathbf{y}(k)$ can be expressed as:

$$\mathbf{y}(k) = \sqrt{\frac{P_T}{M}}\mathbf{H}\mathbf{s}(k)+\mathbf{n}(k) \tag{2.22}$$

where P_T is the total transmit power, $\mathbf{s}(k)$ is the transmit vector that consists of all signals sent from M transmit antenna as $\mathbf{s}(k)=\left[s_1(k) \;\; s_2(k) \cdots s_M(k)\right]^{\mathsf{T}}$. $\mathbf{n}(k)$ is the ($N\times 1$) AWGN noise vector with variance N_0. Next, for the *frequency selective fading* channel, the MIMO signal model [12, 47] can be related as follows:

$$\mathbf{y}(k) = \sqrt{\frac{P_T}{M}}\begin{bmatrix}\mathbf{h}_{1,1} & \cdots & \mathbf{h}_{1,M}\\ \vdots & \ddots & \vdots \\ \mathbf{h}_{N,1} & \cdots & \mathbf{h}_{N,M}\end{bmatrix}\begin{bmatrix}\mathbf{s}_1(k)\\ \vdots \\ \mathbf{s}_M(k)\end{bmatrix}+\mathbf{n}(k), \tag{2.23}$$

where $\mathbf{h}_{j,i}=\left[h_{j,i}(0)\ldots h_{j,i}(L-1)\right]$ is the ($1\times M$) CIR (with length L specifying the delay spread of the channel) from i^{th} transmit antenna to j^{th} receive antenna. $\mathbf{s}_i(k)=\left[s_i(k)\ldots s_i(k-L+1)\right]^{\mathsf{T}}$ is the transmit vector representing consecutive L past and present signals sent from i^{th} transmit antenna. $\mathbf{n}(k)$ is the same ($N\times 1$) AWGN noise vector. (2.23) can also be re-written as:

$$\mathbf{y}(k) = \sqrt{\frac{P_T}{M}}\sum_{i=1}^{M}\mathbf{H}_i\mathbf{s}_i(k)+\mathbf{n}(k) \tag{2.24}$$

where $\mathbf{H}_i=\left[\mathbf{h}_{1,i}\ldots\mathbf{h}_{N,i}\right]^{\mathsf{T}}$ is the dedicated channel matrix that contains all the CIRs from i^{th} transmit antenna to all receive antenna. The usefulness of having such expression will be revealed in the MIMO equalisation process shown in later section.

2.3 Basic Wireless MIMO Architecture

The Multiple-input multiple-output (MIMO) wireless communication system, which is also named as multiple antenna system [109], uses multiple antenna arrays or multiple transmit-receive antennas to permit data transmission rates far in excess of those using conventional single-input single-output approaches. This is made possible by simultaneous data transmission in parallel using the same frequency band through multiple spatially separated antennas at the transmitter. The receiver employs the spatial diversity that exists over wireless channel together with the space-time signal processing to handle the multipath propagation and the resulting co-

channel interferences in order to improve signal reception for simultaneous data detection.

A general block diagram of a MIMO wireless communication system that comprises of the transmitter and the receiver is shown in figure 2.3 below.

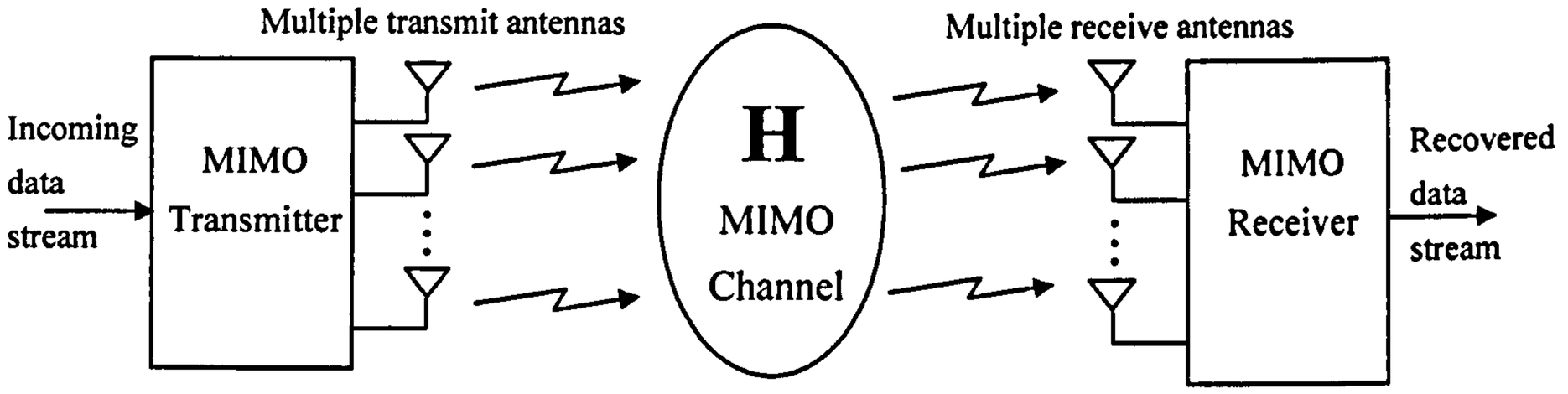

Figure 2.3: General block diagram of a MIMO wireless communication system

The multiple antenna set-up at both the transmitter and receiver results in a MIMO communication channel. Depending on the nature of the environment (either frequency-flat fading or frequency-selective fading), the MIMO channel and its multipath scattering can be properly exploited in order to provide useful spatial diversity where the scattering characteristics of the propagation environment is used to enhance rather than to degrade transmission accuracy by treating the multiplicity of the scattering path as separate parallel sub-channels.

At the transmitter, an incoming single user's data stream is split into multiple parallel sub-streams and an array of transmit antennas is used to simultaneously launch these parallel sub-streams. Since all sub-streams are sent using the same carrier frequency band (for each transmit antenna), the spectrum is used very efficiently. Through parallel data transmission, the effective data rate is also increased nearly in proportion to the number of transmit antennas used.

The MIMO wireless channel can be fundamentally described by a channel matrix, **H**, which comprises the random complex component, that describes the radio path from a specific transmit antenna to the specific antenna. Hence, **H** contains all the sub-channels that exist between the multiple antennas at both sides of the transmitter and receiver. Nevertheless, these coefficients are described by the basic propagation characteristic addressed previously in the section 2.2.

The receiver's structure acts as the central processing unit for the MIMO system. It is here that contains all the sophisticated algorithms, which process the received signals that are distorted over the channel. The receivers unit are capable of handling most types interferences that are encountered in the MIMO system such as co-channel interference (CCI) and the inter-symbol interference (ISI). Clever signal processing methods such as temporal equalisation process and array beamforming are employed. These methods can be referred as the 'space-time' processing which will be addressed in the next section.

2.4 Space-Time Signal Processing

The use of multiple antennas and array signal processing has become increasingly popular due to the demand to support more users in the existing wireless communication systems and to improve the economics and performance of the networks. This technology is sometimes referred as smart antennas or space-time processing (STP) [11, 24], where the received signals is processed in space and time to maximise signal reception. In general, STP technique provides three processing leverages [11]. First is the *array gain*. Multiple antennas capture more signal energy, which can be combined to improve the signal-to-noise ratio (SNR). Second is the *spatial diversity gain* to combat space-selective fading. Finally, STP can simultaneously reduce *co-channel* and *adjacent channel interference*. These potentials in STP have indeed improved the coverage, link quality, data transmission rate and system capacity of the wireless network.

STP extends earlier techniques to incorporate rich structure of communication signals and improve resistance to fading and interference. In the following discussions, the evolution of STP from the conventional equalisation in time to the array signal processing (adaptive beamforming) in space and the combination of both space-time processing will be discussed systematically to provide more insightful understanding for the purpose of utilising the multiple antennas architecture. Here, the context of STP in [11] will be followed through and further analyses about the STP will be provided to illustrate the necessary concept of using space and time processing.

2.4.1 Time-Only Processing [11]

Time-only processing corresponds to *equalisation* process to counteract the inter-symbol interference (ISI) of the channel. (See [118, 119] for a review of channel equalisation). Figure 2.4 depicts the standard baseband temporal equalizer set-up for the single-input single-output model:

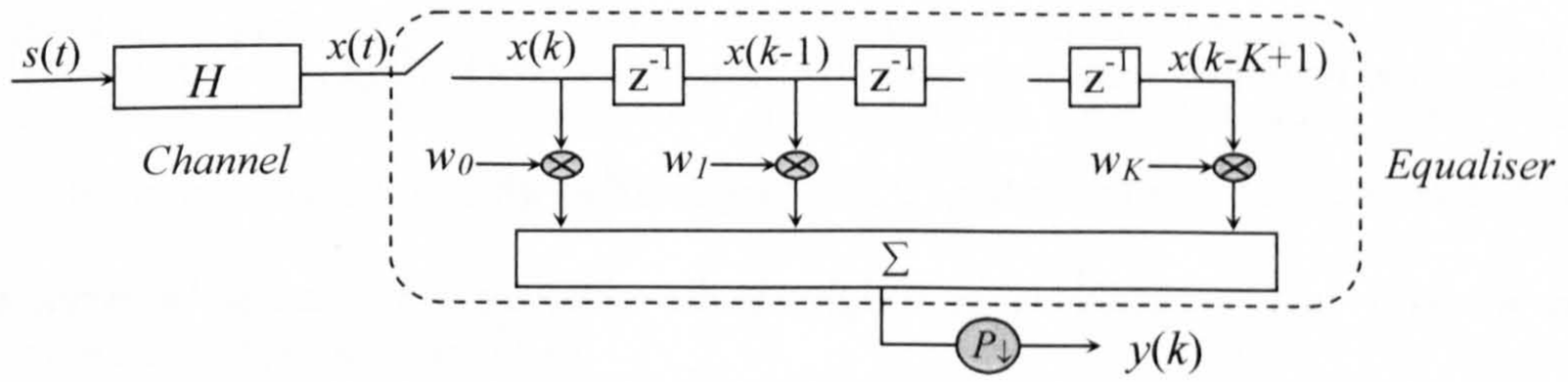

Figure 2.4: Baseband equaliser for SISO model. (Horizontal processing structure)

The received signal, $x(t)$, is sampled (at baud or higher rate) and discrete-time input, $x(k)$, is then filtered through a linear equaliser which is usually implemented as a tapped delay line, finite impulse response (FIR) filter. The FIR structure allows the collection of present and past received signals to be processed by the equaliser in time, which has $K+1$ taps that corresponds to

respective weights, w_k. The discrete output, $y(k)$, is produced by the sum of the weighted past and present input of the FIR filter. Depending on the sampling rate, $y(k)$ may be down-sampled (for the over-sampling case) before the symbol decision (slicing) process.

The equalisation process can be applied either to the single-user case, which is the single-input single-output (SISO) model or to the multi-users scenario, which is the multiple-input single-output (MISO) model. In the SISO model, ISI is the only problem therefore the equalisation can be carried out effectively using time-only processing provided the channel state information is known. However, in the MISO model, besides ISI, the co-channel interference (CCI) becomes an additional problem if all users are transmitting in the same frequency band. In the following illustration, the time-only processing is used to deal with both ISI and CCI.

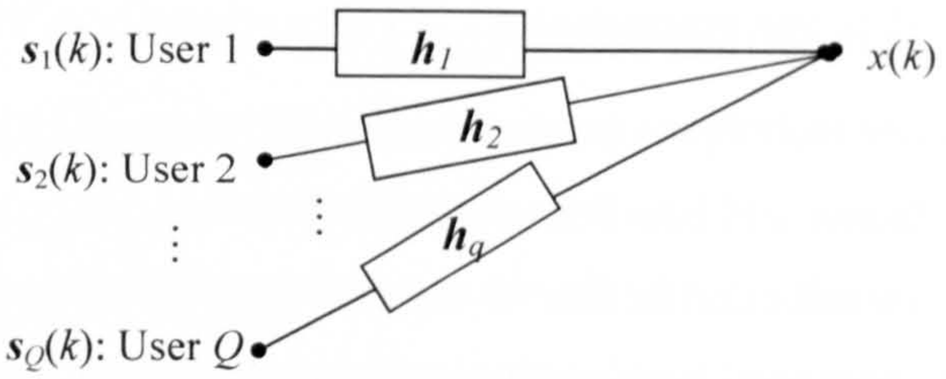

Figure 2.5: MISO model of multi-users scenario with single received antenna.

Consider the MISO model above with Q users in a noiseless case. With the sampling rate at baud, the discrete input to the equaliser (the individual received signal) can be represented as:

$$x(k) = \sum_{q=1}^{Q} \boldsymbol{h}_q \boldsymbol{s}_q(k) = \boldsymbol{h}_1 \boldsymbol{s}_1(k) + \ldots + \boldsymbol{h}_Q \boldsymbol{s}_Q(k) \tag{2.25}$$

where $\boldsymbol{h}_q = \begin{bmatrix} h_q(1) & h_q(2) & \cdots & h_q(L) \end{bmatrix}$ is the FIR channel of the q^{th} user which is a $(1\times L)$ row vector and $\boldsymbol{s}_q(k) = \begin{bmatrix} s_q(k) & \cdots & s_q(k-L+1) \end{bmatrix}^{\mathsf{T}}$ is the transmit vector from the current $(k)^{\text{th}}$ symbol back to the previous $(k–L+1)^{\text{th}}$ symbol by the q^{th} user. As mentioned, the equaliser output is obtained by the weighted sum of present and past inputs, $\boldsymbol{x}(k) = \begin{bmatrix} x(k) & \cdots & x(k-K) \end{bmatrix}^{\mathsf{T}}$ as:

$$y(k) = \boldsymbol{w}^{\mathsf{H}} \boldsymbol{x}(k) \tag{2.26}$$

where $\boldsymbol{w} = \begin{bmatrix} w(0) & w(1) & \cdots & w(K) \end{bmatrix}^{\mathsf{T}}$ is the weights in the equaliser. $\boldsymbol{x}(k)$ can also be expressed as:

$$\boldsymbol{x}(k) = \sum_{q=1}^{Q} \boldsymbol{H}_q \, \bar{\boldsymbol{s}}_q(k) \tag{2.27}$$

where $\bar{\boldsymbol{s}}_q(k) = \begin{bmatrix} s_q(k) & \cdots & s_q(k-L-K+1) \end{bmatrix}^{\mathsf{T}}$ is the new $(K+L)\times 1$ transmit vector that consists current $(k)^{\text{th}}$ symbol back to the previous $(k–L–K+1)^{\text{th}}$ symbol of the q^{th} user and $\boldsymbol{H}_q$ is the $(K+1)\times(K+L)$ block-Toeplitz channel matrix of the q^{th} user expressed as:

$$\boldsymbol{H}_q = \begin{bmatrix} \boldsymbol{h}_q & 0 & \cdots & 0 \\ 0 & \boldsymbol{h}_q & \ddots & \vdots \\ \vdots & \ddots & \ddots & 0 \\ 0 & \cdots & 0 & \boldsymbol{h}_q \end{bmatrix} \tag{2.28}$$

Substituting (2.27) into (2.26), the equaliser's output, $y(k)$ can be re-expressed as:

$$y(k) = \boldsymbol{w}^{\mathsf{H}}\, \boldsymbol{H}_{1:Q}\, \bar{\boldsymbol{s}}_{1:Q}(k) \tag{2.29}$$

where $\boldsymbol{H}_{1:Q} = \begin{bmatrix} \boldsymbol{H}_1 & \cdots & \boldsymbol{H}_Q \end{bmatrix}$ is the concatenated channel matrix and $\bar{\boldsymbol{s}}_{1:Q}(k) = \begin{bmatrix} \bar{\boldsymbol{s}}_1^{\mathsf{T}} & \cdots & \bar{\boldsymbol{s}}_Q^{\mathsf{T}} \end{bmatrix}^{\mathsf{T}}$ is a $Q(K+L)\times 1$ long column vector that consists of all transmitted symbols by all users. In order to find the weights in $\boldsymbol{w}$ (for the MISO case) that can completely cancel the ISI and all CCI during the demodulation process, the zero-forcing (ZF) condition must be satisfied as:

$$\boldsymbol{w}^{\mathsf{H}}\, \boldsymbol{H}_{1:Q} = [0...010...0] \tag{2.30}$$

This requires that $\boldsymbol{H}_{1:Q}$ be full-column rank. Since $\boldsymbol{H}_{1:Q}$ is always a wide matrix (with more columns than rows; $(K+1)\times Q(K+L)$), $\boldsymbol{H}_{1:Q}$ cannot be full-column rank, which implies that joint linear ISI and CCI cancellation is impossible with time-only processing when the received signal is sampled at the symbol rate. With P-rate over-sampling, $\boldsymbol{H}_{1:Q}$ will now be block-Toeplitz matrix of size $P(K+1) \times Q(K+L)$, and will be full rank if the following condition holds [116]:

$$(K+1)P \;\geq\; Q\,(K+L) \qquad \text{or} \qquad (K+1)(P-Q) \;\geq\; Q\,(L-1) \tag{2.31}$$

The nomenclature of (2.31) implies that number of rows in $\boldsymbol{H}_{1:Q}$ must be greater than the number of columns. From (2.31), it follows that ZF equalisation is not possible when no over-sampling is used. (i.e. $P = 1$), even with no CCI (Q=1) present in time-only processing. However, with $P \geq 2$, it should theoretically be possible to achieve perfect ZF equalisation and cancel both ISI and CCI with the time-only processing. Hence, over-sampling plays a vital role in time-only processing. However, in practice, for symbol waveforms with small excess bandwidth, the temporal channel for signal and CCI will not be well separated and the channel matrix, $\boldsymbol{H}_{1:Q}$ will be ill conditioned. Therefore, CCI cancellation might lead to excessive noise enhancement. Hence, time-only processing offers only small degree of CCI reduction in a MISO model [11].

2.4.2 Space-Only Processing [11]

Space-only processing is a technique, which uses multiple antennas to exploit spatial diversity that is available through multipath and signals received at different point in space. It is also referred as *array beamforming* method [20, 21] with array of weighted taps separated in space and a combiner [18] to effectively suppress the unwanted interferences such as CCI. Joint cancellation of ISI and CCI can also be achieved when sufficient antennas are used. The

following is the multiple-input multiple-output (MIMO) model, which represents the multi-users scenario with multiple receiving antennas at the base-station. First, the MIMO channel with 'single-tap' in each link is used to demonstrate for the case of CCI-only cancellation. Secondly, a MIMO channel with 'multiple-taps' is used to demonstrate for the case of joint ISI and CCI suppression. The limitation of using space-only processing will be discussed.

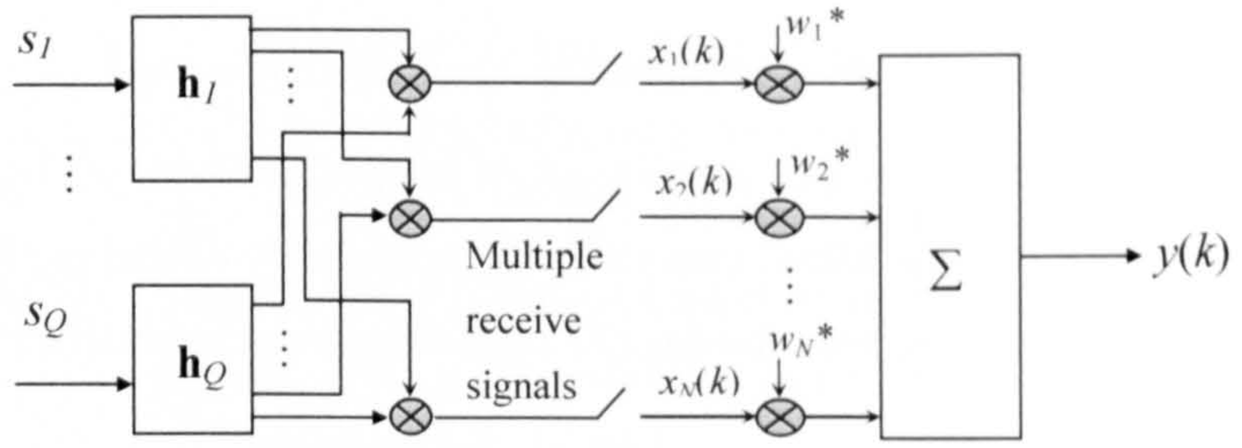

Figure 2.6: Space-only processing (beamforming) – vertical structure

Figure 2.6 depicts an array beamforming structure (with vertical spatial input). Assuming Q users are present with single path (flat-fading channel), the beamformer's input is a set of received signals x_j, grouped as vector $\boldsymbol{x}(k) = \left[x_1(k) \quad \cdots \quad x_N(k)\right]^{\mathsf{T}}$ and can be expressed as:

$$\boldsymbol{x}(k) = \sum_{q=1}^{Q} \mathbf{h}_q \; s_q(k) \tag{2.32}$$

where now $\mathbf{h}_q = \left[h_{1q} \quad \cdots \quad h_{Nq}\right]^{\mathsf{T}}$ specifying fading coefficient h_{ij} between q^{th} user and j^{th} receive antenna and $s_q(k)$ is the signal sent by the q^{th} user. Different set of weights w_j in the beamformer can be obtained to determine which q^{th} user is to be detected at its output. For instance, let the 1st user, $s_1(k)$ be the desired signal. The corresponding beamformer's output can be expressed as:

$$y(k) = \boldsymbol{w}^{\mathsf{H}} \; \boldsymbol{x}(k) \tag{2.33}$$

where $\boldsymbol{w} = \left[w_1 \quad \cdots \quad w_N\right]^{\mathsf{T}}$ is the weight vector. Hence, combining (2.32) and (2.33), leads to:

$$y(k) = \sum_{q=1}^{Q} \boldsymbol{w}^{\mathsf{H}} \; \mathbf{h}_q \; s_q(k) \tag{2.34}$$

or equivalently as:

$$y(k) = \boldsymbol{w}^{\mathsf{H}} \; \mathbf{H}_{1:Q} \; \boldsymbol{s}_{1:Q}(k)$$

where $\mathbf{H}_{1:Q} = \left[\mathbf{h}_1 \quad \cdots \quad \mathbf{h}_Q\right]$ is a $N \times Q$ MIMO channel matrix and $\boldsymbol{s}_{1:Q}(k) = \left[s_1(k) \quad \cdots \quad s_Q(k)\right]^{\mathsf{T}}$ is the transmit vector that consists of the signals sent by all users. Hence, the ZF condition to receive the *first* user and cancel all CCI contributions from other users will then be:

$$\boldsymbol{w}^{\mathsf{H}} \; \mathbf{H}_{1:Q} = \left[10 \ldots 0\right] \tag{2.35}$$

This indeed requires $\mathbf{H}_{1:Q}$ to be full-column rank where the following condition must hold:

$$N \quad \geq \quad Q \tag{2.36}$$

This implies that the number of receive antennas must be greater than the number of users, where (rows) ≥ (columns), to effectively cancel CCI contributed by other users in a non-delay spread channel. Also note that the position for '1' in (2.35) is critical in determining which user's signal to be detected. By placing the '1' into different position, the respective $\mathbf{h}_q$ from $\mathbf{H}_{1:Q}$ can be "inverted" accordingly so that different set of $\boldsymbol{w}$ can be produced for the detection of that particular user. In fact, all users can be detected at once by obtaining individual weight vector $\boldsymbol{w}$ according to (2.35) first and then placed them together in a weighting matrix $\mathbf{W}$ as follows:

$$\mathbf{W} = \begin{bmatrix} \boldsymbol{w}_1 & \boldsymbol{w}_2 & \cdots & \boldsymbol{w}_Q \end{bmatrix} \tag{2.37}$$

Replacing the weight vector $\boldsymbol{w}$ in (2.33) with the weighting matrix $\mathbf{W}$ in (2.37) allows all user signals to be detected simultaneously in $y_q(k)$ where $q = 1$ to M.

For frequency-selective fading environment, the delay spread is introduced with L multipath for each user. Hence, it is a joint ISI and CCI problem using the space-only processing. Figure 2.7 shows the beamformer applied to multi-users case in the delay spread channel.

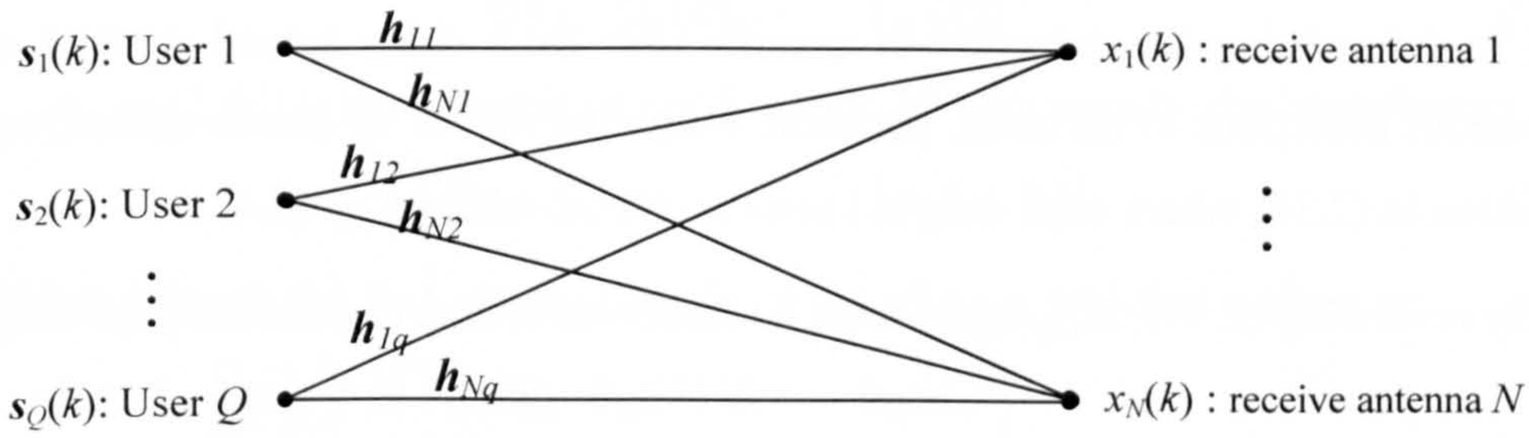

Figure 2.7: Space-Only Processing in delay-spread channel for multi-users MIMO model.

Assuming noiseless case is applied, the input of the beamformer, which is the $N\times1$ received signal vector $\boldsymbol{x}(k)$, under the delay-spread channel can be expressed as:

$$\boldsymbol{x}(k) = \sum_{q=1}^{Q} \mathbf{H}_q \, \boldsymbol{s}_q(k) \tag{2.38}$$

where $\boldsymbol{s}_q(k) = \begin{bmatrix} s_q(k) & \cdots & s_q(k-L+1) \end{bmatrix}^{\mathsf{T}}$ is the $(L\times1)$ transmit vector of the q^{th} user that consists the current $(k)^{\text{th}}$ symbol back to the previous $(k–L+1)^{\text{th}}$ symbol. $\mathbf{H}_q$ in (2.38) is the channel matrix that consists all the channel impulse response (CIR), $\boldsymbol{h}$ from the q^{th} user expressed as:

$$\mathbf{H}_q = \begin{bmatrix} \boldsymbol{h}_{1q}^{\mathsf{T}} \\ \boldsymbol{h}_{2q}^{\mathsf{T}} \\ \vdots \\ \boldsymbol{h}_{Nq}^{\mathsf{T}} \end{bmatrix}, \qquad q = 1,2,\ldots,Q \tag{2.39}$$

where $\boldsymbol{h}_{jq} = \begin{bmatrix} h_{jq}(1) & h_{jq}(2) & \cdots & h_{jq}(L) \end{bmatrix}^{\mathsf{T}}$ is the CIR with L length with $j = 1$ to N. The input to the

beamformer, $x(k)=[x_1(k) \ \cdots \ x_N(k)]^T$ is also the received signal vector, re-written as:

$$x(k) = H_{1:Q}\, s_{1:Q}(k) \tag{2.40}$$

where $H_{1:Q}=[\mathbf{H}_1 \ \cdots \ \mathbf{H}_Q]$ is the $N\times QL$ concatenated channel matrix seen by the beamformer, which comprises all channel matrices w.r.t each user. $s_{1:Q}(k)=[s_1^T(k) \ \cdots \ s_Q^T(k)]^T$ is a ($QL\times 1$) long column vector that consists of all transmitted symbols by all users. Similarly, the beamformer output for any user's signal detection can be again generally expressed as:

$$y(k) = w^H\, x(k) \tag{2.41}$$

which is equivalently expressed as:

$$y(k) = w^H\, H_{1:Q}\, s_{1:Q}(k) \tag{2.42}$$

Again, the ZF condition to receive the first user and cancel both CCI and ISI will be:

$$w^H\, H_{1Q} = [10...0] \tag{2.43}$$

where $w=[w_1 \ \cdots \ w_N]^T$ is still the $N\times 1$ weight vector. Similarly, the position for '1' is also critical in determining the detection of specific user for a delay spread channel case. For the simultaneous detections of all users, the same weighting matrix **W** can be utilised with the same formulation in (2.37) where each weight vector w can be obtained by (2.43).

By reviewing (2.43), $H_{1:Q}$ again must be full-column rank and satisfied the following:

$$N \quad \geq \quad QL \tag{2.44}$$

Comparing to previous condition in (2.36), the number of antennas required in this case has been increased. Hence, space-only processing can also perform joint cancellation of ISI and CCI provided that sufficient antennas are used. However, it might require too many antennas at the beamformer to deal with rich multipaths channel. Moreover, if either the multipath angle spread is small or the CCI and desired signal DOAs are not well separated, the columns of $H_{1:Q}$ become again nearly linearly dependent, making $H_{1:Q}$ ill conditioned and resulting in excessive noise enhancement. Unlike time-only processing, space-only processing can be quite effective against CCI, whereas it effectiveness against ISI depends upon the angle spread of the multipath.

2.4.3 Space-Time Processing [11, 24]

This section combines the strengths of space-only processing and time-only processing and integrates them to become the space-time processing. In the time-only processing, the equalisation process that deals well with ISI can only be effective against CCI simultaneously provided that the oversampling is sufficiently applied. On the other hand, space-only processing with the beamforming structure not only counteracts CCI well but is also able to perform both

CCI and ISI cancellation provided that sufficient receive antennas are used. Therefore, by combining these two processing techniques, allowing the task of handling the CCI and ISI to be allocated accordingly to each processing's capability while simultaneously compensating the drawbacks and shortcoming that oppositely encountered by each technique when used separately.

In the following, the space-time processing is applied for the MIMO model shown previously in figure 2.7 with the multi-users scenario in delay-spread channel. Consider again for the case with Q users presents and N receive antennas is applied. Assuming channel length is L, the CIR, $\mathbf{h}_{jq}$, from the q^{th} user to the j^{th} receive antenna can be expressed as:

$$\mathbf{h}_{nq} = \left[h_{nq}(1) \quad h_{nq}(2) \quad \cdots \quad h_{nq}(L)\right]^{\mathsf{T}} \tag{2.45}$$

The input to the beamformer or the received signal vector (in noiseless case) can be expressed as:

$$\mathbf{x}(k) = \sum_{q=1}^{Q} \mathbf{H}_q \, s_q(k) \tag{2.46}$$

where $\mathbf{x}(k)$ is also the $(N\times 1)$ received signal vector in the space dimension, expressed as:

$$\mathbf{x}(k) = \left[x_1(k) \quad \cdots \quad x_N(k)\right]^{\mathsf{T}} \tag{2.47}$$

Note that the s_q(k) in (2.46) is the transmit vector from the q^{th} user seen by the beamformer as:

$$s_q(k) = \left[s_q(k) \quad \cdots \quad s_q(k-L+1)\right]^{\mathsf{T}} \tag{2.48}$$

and $\mathbf{H}_q$ in (2.46) represents the $N\times L$ channel matrix of the q^{th} user, which is written as:

$$\mathbf{H}_q = \begin{bmatrix} \mathbf{h}_{1q}^{\mathsf{T}} \\ \mathbf{h}_{2q}^{\mathsf{T}} \\ \vdots \\ \mathbf{h}_{Nq}^{\mathsf{T}} \end{bmatrix} = \begin{bmatrix} h_{1q}(1) & h_{1q}(2) & \cdots & h_{1q}(L) \\ h_{2q}(1) & h_{2q}(2) & \cdots & h_{2q}(L) \\ \vdots & \vdots & \cdots & \vdots \\ h_{Nq}(1) & h_{Nq}(2) & \cdots & h_{Nq}(L) \end{bmatrix}, \qquad q = 1,2,...,Q \tag{2.49}$$

Note that $\mathbf{H}_q$ in (2.49) contains the spatial elements (expressed vertically in the columns) and the temporal elements (expressed horizontally in the rows) that specify the impulse response due to the frequency-selective fading characteristic. The incorporation of time dimension into space-domain is presented when $(K+1)$ inputs to the beamformer that is received at different time are taken into consideration for the equalisation process. The so-called space-time *beamformer-equaliser* structure has $(K+1)$ number of equaliser taps in each receiving element, forming the space-time weighting matrix with size of $N\times(K+1)$ for each designated output as:

$$\mathbf{W}_q = \begin{bmatrix} w_{1q}(0) & w_{1q}(1) & \cdots & w_{1q}(K) \\ w_{2q}(0) & w_{2q}(1) & \cdots & w_{2q}(K) \\ \vdots & \vdots & \vdots & \vdots \\ w_{Nq}(0) & w_{Nq}(1) & \cdots & w_{Nq}(K) \end{bmatrix}; \quad q = 1 \ldots Q \tag{2.50}$$

The space-time weighting matrix **W** in (2.50) and the beamformer-equaliser structure is depicted in figure 2.8. Note that, weights in **W** is now distributed horizontally in time dimension (equaliser) and vertically in space dimension (beamformer) where the output of the beamformer-equaliser is the sum of weighted present and past inputs combined in time and space together.

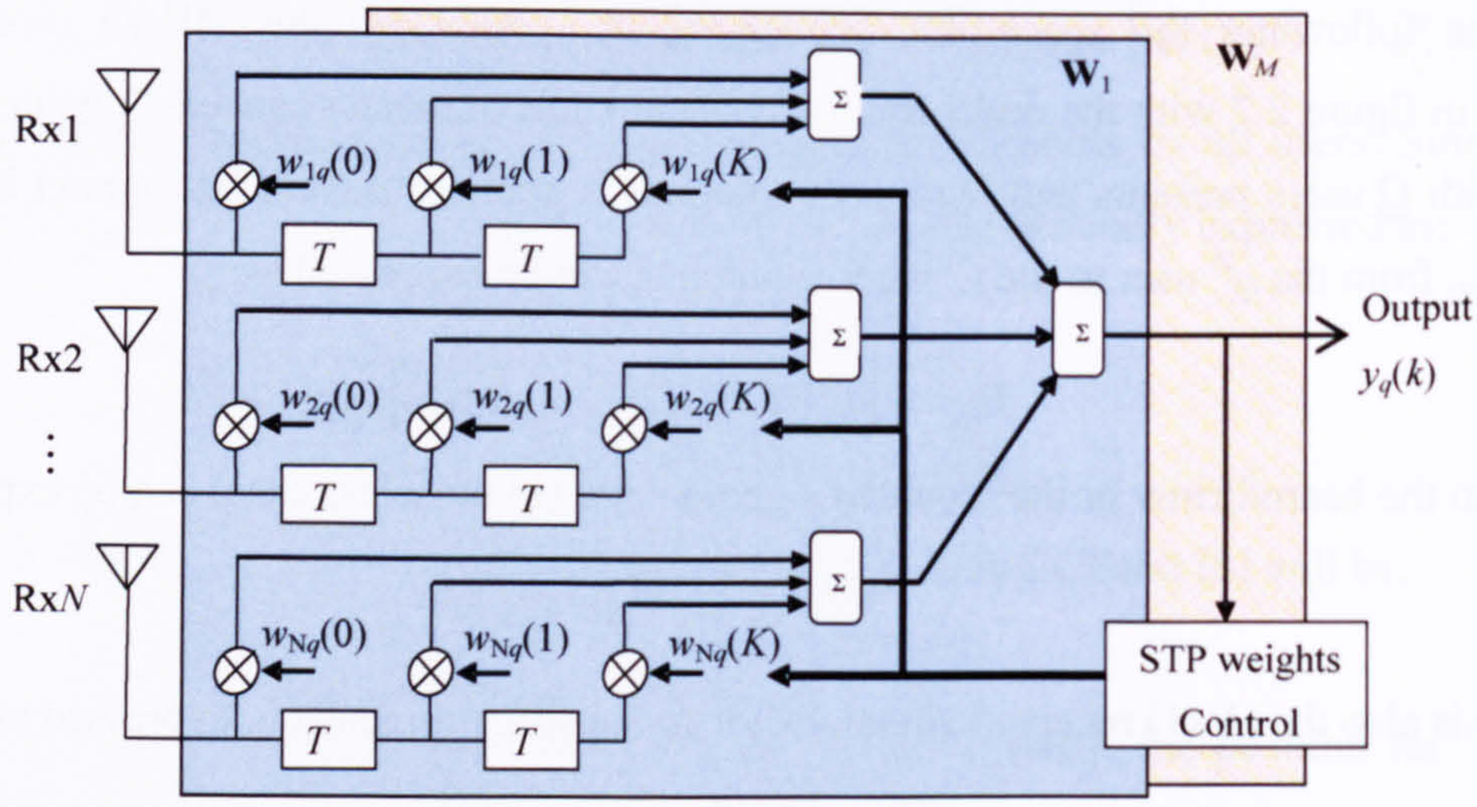

Figure 2.8: Space-Time Processing (Beamformer-Equaliser)

Since there are K+1 taps in the equaliser, K+1 received signal vectors are also required for the equalisation process in time, which can be grouped into a received signal matrix as:

$$\mathbf{X}(k) = \begin{bmatrix} \mathbf{x}(k) & \mathbf{x}(k-1) & \cdots & \mathbf{x}(k-K) \end{bmatrix} \tag{2.51}$$

The output of the beamformer-equaliser for q^{th} user's bit stream, can be deduced as:

$$y_q(k) = trace\left\{ \mathbf{W}_q^{\mathsf{H}}\, \mathbf{X}(k) \right\} \tag{2.52}$$

$$= trace\left\{ \begin{bmatrix} w_{1q}^*(0) & w_{2q}^*(0) & \cdots & w_{Nq}^*(0) \\ w_{1q}^*(1) & w_{2q}^*(1) & \cdots & w_{Nq}^*(1) \\ \vdots & \vdots & \cdots & \vdots \\ w_{1q}^*(K) & w_{2q}^*(K) & \cdots & w_{Nq}^*(K) \end{bmatrix} \begin{bmatrix} x_1(k) & x_1(k-1) & \cdots & x_1(k-K) \\ x_2(k) & x_2(k-1) & \cdots & x_2(k-K) \\ \vdots & \vdots & \vdots & \vdots \\ x_N(k) & x_N(k-1) & \cdots & x_N(k-K) \end{bmatrix} \right\}$$

where $(.)^*$ denotes the complex conjugation of elements in $\mathbf{W}_q$.

In order to compute for the weighting matrix and to proceed the formulation in the space-time processing, the *vec*(.) operator [120] is introduced here as:

$$vec\left(\begin{bmatrix} \mathbf{v}_1 & \cdots & \mathbf{v}_K \end{bmatrix} \right) = \begin{bmatrix} \mathbf{v}_1 \\ \vdots \\ \mathbf{v}_K \end{bmatrix} \tag{2.53}$$

Applying the *vec*(.) operator to (2.51) as *vec*(**X**(k)), producing a long column vector that consists of all the past and present received signal vector, **x**, across all antennas as:

$$\bar{\boldsymbol{x}}(k) \;=\; vec\big(\mathbf{X}(k)\big) \;=\; \begin{bmatrix} \mathbf{x}(k) \\ \mathbf{x}(k-1) \\ \vdots \\ \mathbf{x}(k-K) \end{bmatrix} \tag{2.54}$$

Note that (2.54) can also be conveniently expressed as:

$$\bar{\boldsymbol{x}}(k) = \sum_{q=1}^{Q} \overline{\mathbf{H}}_q \; \bar{\boldsymbol{s}}_q(k) \tag{2.55}$$

where $\bar{\boldsymbol{s}}_q(k)$ is the new transmit vector that consists of L+K transmitted symbols (i.e. from the current $(k)^{\text{th}}$ symbol back to the previous $(k–L–K+1)^{\text{th}}$ symbol) sent by the q^{th} user as:

$$\bar{\boldsymbol{s}}_q(k) = \begin{bmatrix} s_q(k) & \cdots & s_q(k-L-K+1) \end{bmatrix}^{\mathsf{T}} \tag{2.56}$$

whereas $\overline{\mathbf{H}}_q$ in (2.55) is the $N(K+1)\times(L+K)$ block Toeplitz channel matrix of the q^{th} user as:

$$\overline{\mathbf{H}}_q = \begin{bmatrix} \mathbf{H}_q & 0 & \cdots & 0 \\ 0 & \mathbf{H}_q & \ddots & \vdots \\ \vdots & \ddots & \ddots & 0 \\ 0 & \cdots & 0 & \mathbf{H}_q \end{bmatrix} \tag{2.57}$$

$\overline{\mathbf{H}}_q$ now contains both the space and time entites where the basic channel matrix $\mathbf{H}_q$ in (2.49), are echoed in time as seen in the block Toeplitz structure of $\overline{\mathbf{H}}_q$ in (2.57) above. To proceed with the weight finding in the space-time processing, (2.55) can be re-written as:

$$\bar{\boldsymbol{x}}(k) = \boldsymbol{H}_{1:Q} \; \boldsymbol{s}_{1:Q}(k) \tag{2.58}$$

where $\boldsymbol{H}_{1:Q} = \begin{bmatrix} \overline{\mathbf{H}}_1 & \cdots & \overline{\mathbf{H}}_Q \end{bmatrix}$ is a $N(K+1)\times Q(L+K)$ concatenated channel matrix that comprises all channel matrices w.r.t each user and $\boldsymbol{s}_{1:Q}(k) = vec\left(\begin{bmatrix} \bar{\boldsymbol{s}}_1 & \cdots & \bar{\boldsymbol{s}}_Q \end{bmatrix}\right)$ is a $Q(L+K)\times 1$ long column vector that consists of all transmitted symbols by all users. The derivation of (2.52) and its weights finding are obtained according to some criteria such as ZF condition. Using $\boldsymbol{w}_q = vec\big(\mathbf{W}_q\big)$, the output of the beamformer-equaliser can be similarly expressed as:

$$y_q(k) = \boldsymbol{w}_q^{\mathsf{H}} \; \bar{\boldsymbol{x}}(k) \tag{2.59}$$

$$y_q(k) = \Big[\underbrace{\big[w_{1q}^*(0) \quad \cdots \quad w_{Nq}^*(0)\big]}_{\text{space}} \quad \cdots \quad \underbrace{\big[w_{1q}^*(K) \quad \cdots \quad w_{Nq}^*(K)\big]}_{\text{space}}\Big]_{\text{time}} \begin{bmatrix} \begin{bmatrix} x_1(k) \\ \vdots \\ x_N(k) \end{bmatrix} \\ \vdots \\ \begin{bmatrix} x_1(k-K) \\ \vdots \\ x_N(k-K) \end{bmatrix} \end{bmatrix}$$

Note that (2.59) has managed to combine the space and time processing together in a single equation to obtain the estimate of the q^{th} user's bit stream. Each estimate will have specific $\boldsymbol{w}_q$ associated to each user. Substituting (2.58) into (2.59), leads to the following:

$$y_q(k) = \boldsymbol{w}_q^{\mathsf{H}}\, \boldsymbol{H}_{1:Q}\, \boldsymbol{s}_{1:Q}(k) \tag{2.60}$$

Again, the ZF condition to receive the first user and cancel both CCI and ISI will be:

$$\boldsymbol{w}_q^{\mathsf{H}}\, \boldsymbol{H}_{1:Q} = \Big[\big[\overbrace{0\ldots0\ \ 1\ \ 0\ldots0}^{(L+K)\text{ of }1^{st}\text{ user}}\big]\ \underbrace{[0\ \ \ldots\ \ 0]}_{(L+K)\text{ of }2^{nd}\text{ user}}\ \cdots\ \underbrace{[0\ \ \ldots\ \ 0]}_{(L+K)\text{ of }Q^{th}\text{ user}}\Big]_{\in 1\times Q(K+L)} \tag{2.61}$$

Note that the insertion of '1' among the '0' determines the estimate $\hat{s}_q(k-\tau)$ to be obtained in time, where 'τ' is a delay chosen to 'centre' the estimator's function. The choice of 'τ' is vital since it affects the performance of the beamformer-equaliser.

Again, by reviewing (2.61), $\boldsymbol{H}_{1:Q}$ must be full-column rank to fulfil the ZF condition and carry out joint cancellation for CCI and ISI together. Since $\boldsymbol{H}_{1:Q}$ is the block-Toeplitz matrix of size $N(K+1)\times Q(L+K)$, full-column rank condition is satisfied when (rows) ≥ (columns) as:

$$(K+1)N \ \geq\ Q(K+L) \qquad \text{or} \qquad (K+1)(N-Q) \ \geq\ Q\,(L-1) \tag{2.62}$$

Several observations can be made from (2.62). First, when K is set to zero ($K = 0$), the condition returns to (2.44) for the case of using space-only processing by the beamforming array for joint ISI and CCI cancellation with no temporal process (or equalisation). (K indicates the additional number of taps extended from the initial single-tap structure). Also, when no multipath is present (single path frequency-flat condition), L is set to '1' in (2.62), leading to exactly the same condition in (2.36) for the pure CCI cancellation in space-only processing. This confirms that the beamformer-equaliser structure in space-time processing is exactly the extension of the beamformer structure in space-only processing.

Secondly, (2.62) is very similar to the condition of time-only processing in (2.31) for MISO model with oversampling, except that the multiple antennas N is used to replace the oversampling P. In fact, effective cancellation of ISI and CCI should be achieved with the space-time processing in the MIMO model through the beamformer-equaliser structure instead of using oversampling in time-only processing. Lastly, (2.62) also implies that the number of multiple antennas (N) used for spatial processing must be greater than the number of users (Q) even for no CCI case (L=1). Hence, the space-time processing has demonstrated the powerful structure in counteracting both CCI and ISI problem in a frequency-selective fading MIMO channel.

2.5 Bell Laboratory Layered Space-Time Architecture

Recent information theory research has demonstrated the enormous potential of MIMO wireless communication systems with multiple antennas (or antenna arrays) at both the transmitter and receiver [1, 4]. Bell Laboratories (or Bell Labs) were one of the first to exploit this potential and propose the so-called Bell Labs layered space-time (BLAST) architecture. In the following, two versions of BLAST structure will be introduced; namely the diagonal BLAST (D-BLAST) system [1] and the vertical BLAST (V-BLAST) system [4]. This will be followed by the BLAST's main feature, the interference cancellation scheme along with the symbol detection process, which provides significant improvement in system performance. The development of the V-BLAST from the flat-fading to frequency selective fading environment will also be presented.

2.5.1 Diagonal BLAST System – D-BLAST

The D-BLAST architecture was initially developed by Foschini [1]. The D-BLAST system utilizes multi-element antenna arrays at both transmitter and receiver and an elegant diagonally layered coding structure in which codes are dispersed across diagonally in space domain and virtually in time domain – cyclical assignment. (Time domain here is of different proposition from aspect of the time-only processing). It is this complex coding that leads to D-BLAST's higher spectral efficiencies for a given number of transmitters and receivers [1, 121].

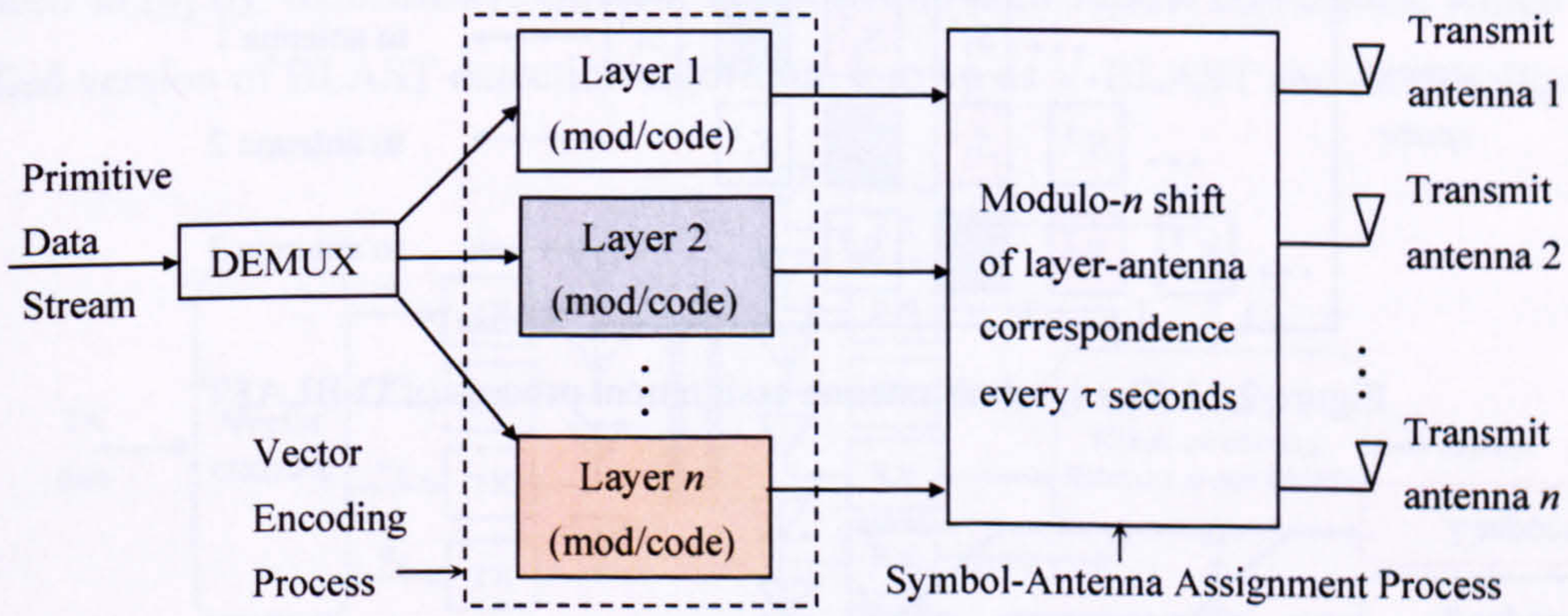

Figure 2.9: Transmission process using space-time layering in D-BLAST

The figure above illustrates the D-BLAST's transmission process. The entire diagonally layered coding comprises of both the vector encoding and the symbol-antenna assignment. First, a primitive data stream is demultiplexed into n layers of data substreams (space). The diagonally layered coding structure means that rather than committing each of the n-encoded substreams to the specific antenna, the bit-stream/symbol & antenna association is periodically cycled (virtually time), so that none of the individual substreams is hostage to the worst channel paths. This

provides a balanced occurrence over all n-path to the receiver (assuming flat-fading environment) and each subchannel has virtually the same capacity. Each substream is essentially the same as regard to the opportunity for coding since the balance make it possible to use the same constellation for each sub-channel with the lowest number of constellation point per subchannel.

The following shows the vector encoding process of the D-BLAST. During encoding, each subsequence is encoded by a 1-D encoder. The output of each 1-D encoder is a sequence of symbols denoted as s_κ^τ where $(.)_\kappa$ specifies the codes from κ^{th} encoder w.r.t space and $(.)^\tau$ specifies the τ^{th} symbol of the encoded sequence in time, as illustrate in figure 2.10 below.

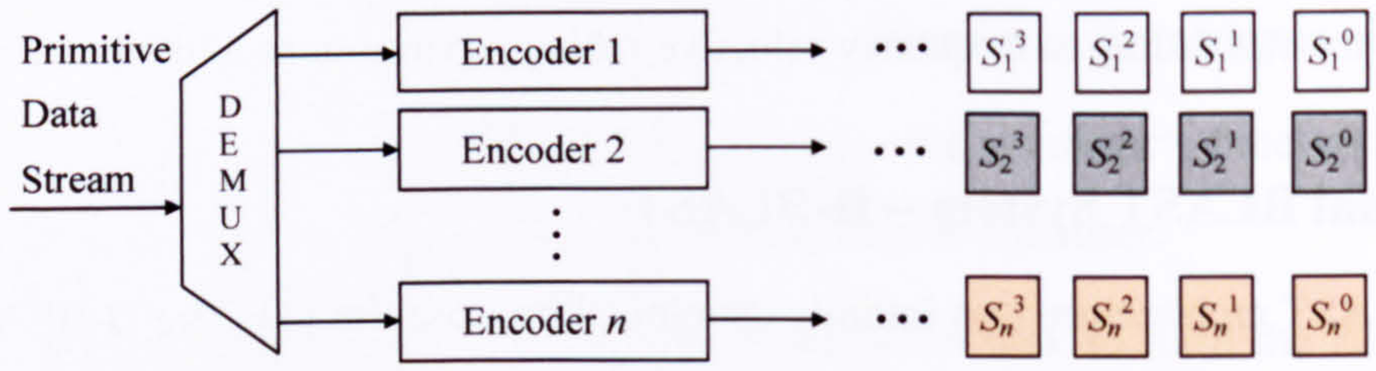

Figure 2.10: The vector encoding process of D-BLAST

During the symbol-antenna assignment, instead of sending the encoded symbols to a particular transmit antenna, they are fed to all the n transmit antenna in turns [121]. For example if n=3, then the periodically cycled symbol-antenna assignment is illustrated as follows:

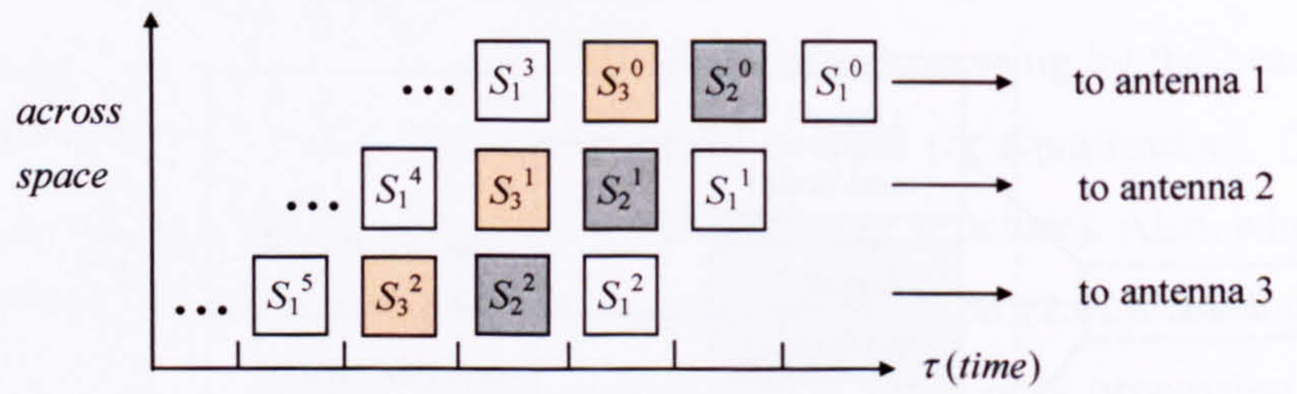

Figure 2.11:The symbol-antenna assignment process of D-BLAST

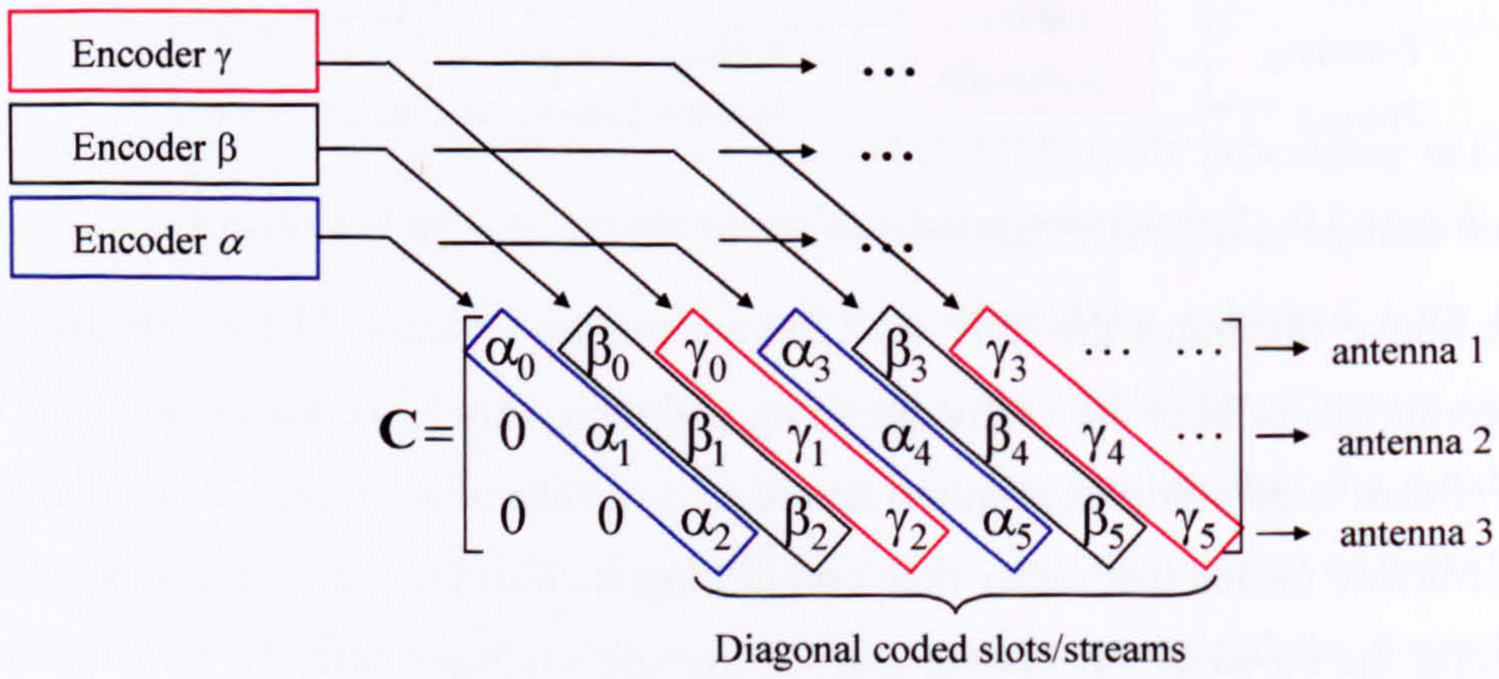

Figure 2.12: Codeword matrix of D-BLAST

A codeword matrix **C** can be formed to represent the n constituents of transmitted bit-streams [121]. Consider the diagonal slots where the encoded symbols are properly indexed to follow the coded sequence from each encoder. The symbols in **C** are subsequently clocked out (column by column) to individual antenna where the cyclical symbol-antenna assignment can be achieved for each encoder. **C** for the case of n=3 is illustrated in figure 2.12.

The decoding of D-BLAST is carried out diagonal by diagonal for each coded slots/streams [121]. Consider again the codeword matrix, **C** in figure 2.12. The receiver first generates the decision variables [1] for the symbols of the first diagonal slot of **C**, namely α_0, α_1 and α_2. Based on the decision variables, this diagonal slot is decoded and the detected symbols (within this slot) are then fed back to remove its contributions to the received signals. This process is referred as interference cancellation. Upon completed the first slot, the receiver then continues to decode the next diagonal slot. Since the whole decoding process in D-BLAST can be complex and tedious, the actual decoding/detection (nulling process) and interference cancellation will be explained in the V-BLAST system that has employed much straightforward encoding and decoding strategy.

2.5.2 Vertical BLAST System – V-BLAST

The D-BLAST system suffers from certain implementation complexities that make it inappropriate for initial implementation. For this reason, the vertical approach was later introduced in [4] by Wolniansky, Golden, Foschini and their fellow colleagues, which describe a simplified version of BLAST detection algorithm, known as V-BLAST shown as follows:

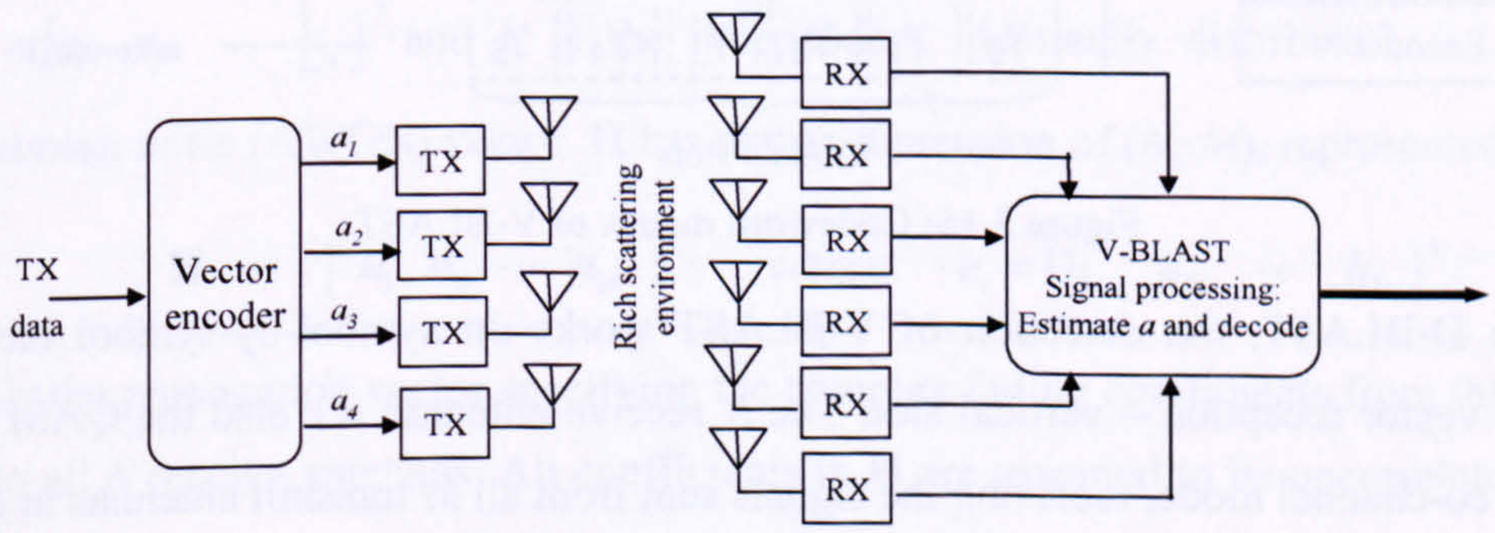

Figure 2.13: V-BLAST high-level system diagram.

The essential difference between D-BLAST and V-BLAST lies in the vector encoding process. In D-BLAST, redundancy between the substreams is introduced through the use diagonal coding. However, the vector coding process in V-BLAST is simply a demultiplex

[1] Decision variable is essential the output of the slicing operation appropriate to the constellation in use.

operation followed by independent bit-to-symbol mapping of each substream. No inter-substream coding or coding of any kind is required, though conventional coding of individual substreams may certainly be applied. However, in the subsequent discussion, it is assumed that uncoded substreams with independent data symbols were used to explain the V-BLAST system.

An example for M=3 case is illustrated in figure 2.14 for the V-BLAST system. a_m^τ is the *uncoded* symbol assigned to m^{th} transmit antenna with the symbol rate of $1/\tau$ symbol/sec. All M transmit antennas in V-BLAST operate in co-channel using the same frequency band. Each transmit antenna is itself an ordinary QAM transmitter, utilising the same constellation scheme for all substreams. The power launched by each transmit antenna is proportional to $1/M$ so that the total radiated power is kept constant and independent of M.

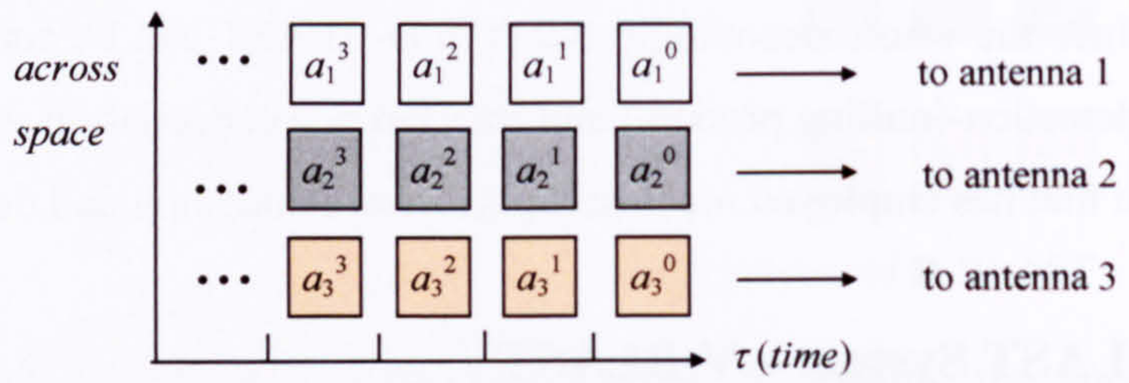

Figure 2.14: The symbol-antenna assignment process of V-BLAST

Example of codeword matrix **C** for V-BLAST system with M=3 is shown as follows:

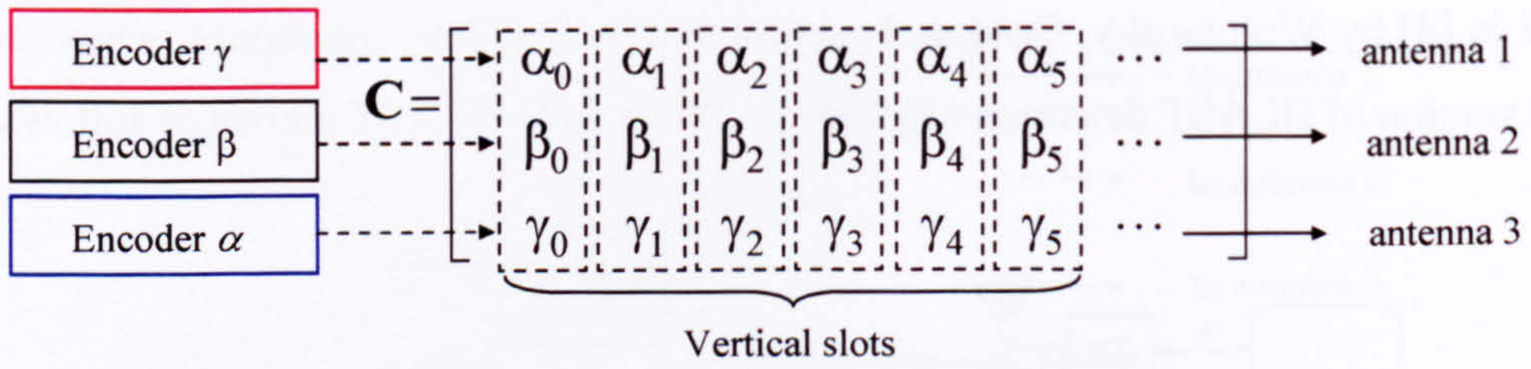

Figure 2.15: Codeword matrix of V-BLAST

Unlike D-BLAST, the detection of V-BLAST works on symbol-by-symbol basis upon every single vector reception – vertical slot. The N receive antennas are also the QAM receiver operating in co-channel mode, receiving the signals sent from all M transmit antennas in the same frequency band. The received signals are fed into the signal processing unit for symbol detection with iterative decoding that involves nulling (detection) and interference cancellation. The nulling process intends to perform symbol recovery as well as signal segregations whereas the interference cancellation process aims to improve the performance by removing the contribution from the already-detected symbols and modifying the received vector (in each vertical slot) so that 'cleaner' version of received signals can be achieved (with fewer interferers present) and successively used for the next detection and nulling process.

2.5.2.1 System and Channel Model for V-BLAST system

For simplicity in sequel of V-BLAST's detection algorithm, flat-fading channel is initially assumed with only single propagation path for each transmit-receive antenna pair and each path is also assumed to be time-invariant. The channel matrix, **H**, specifies the MIMO transfer function that contains h_{ji} complex coefficients from i^{th} transmit antenna to j^{th} receive antenna. Also, the channel is assumed to be known or perfectly estimated. No distinction is made between **H** and its estimates at this point. Perfect synchronisation with symbol-spaced sampling is also assumed [4].

A V-BLAST system consists of M parallel transmit antennas and N parallel receive antennas operated at co-channel mode. The single transmit vector, $\boldsymbol{a}$ (which contains individual transmit symbols a_i from each i^{th} transmit antenna) can be denoted as:

$$\boldsymbol{a} = \begin{bmatrix} a_1 & a_2 & \cdots & a_M \end{bmatrix}^{\mathsf{T}} \tag{2.63}$$

Each transmit symbol 'a' is a complex component mapped from the QPSK modulation scheme. Each substream is pre-multiplied with a factor of $\sqrt{\rho / M}$, where ρ is the expected signal to noise ratio at the receiver and the total power radiated by each transmit antenna is proportional to $1/M$ in order to provide a constant power to the receiver regardless of the changes in number of transmit antenna. The symbols are sent over a Rayleigh flat-fading MIMO channel, **H**, where signals are distorted and superimposed at each receive antenna. The corresponding received signal vector, $\boldsymbol{r}$, (contains N received signal r_j at each j^{th} receive antenna) can be expressed as:

$$\boldsymbol{r} \;=\; \mathbf{H}\boldsymbol{a} \;+\; \boldsymbol{n} \tag{2.64}$$

where $\boldsymbol{r} = \begin{bmatrix} r_1 & r_2 & \cdots & r_N \end{bmatrix}^{\mathsf{T}}$ and $\boldsymbol{n}$ is the independent identically distributed, (i.i.d.) additive white Gaussian noise (AWGN) vector. **H** has matrix dimension of ($N \times M$), represented as:

$$\mathbf{H} \;=\; \begin{bmatrix} \boldsymbol{u}_1 & \boldsymbol{u}_2 & \cdots & \boldsymbol{u}_M \end{bmatrix} \qquad \text{where} \qquad \boldsymbol{u}_i = \begin{bmatrix} h_{1i} & h_{2i} & \cdots & h_{Ni} \end{bmatrix}^{\mathsf{T}} \tag{2.65}$$

where $\boldsymbol{u}_i$ is the propagation vector specifying the complex fading coefficients from the i^{th} transmit antenna to all N receive antennas. All coefficients in **H** are assumed to be uncorrelated with zero mean and unit variance, which can be represented by random complex components whose real and imaginary parts are normally distributed:

$$h_{ji} \;=\; Normal\left(0, \frac{1}{\sqrt{2}}\right) \;+\; j.\,Normal\left(0, \frac{1}{\sqrt{2}}\right) \tag{2.66}$$

where $|h_{ji}|^2$ is a chi-squared χ^2 variate. Next, the V-BLAST detection process or the "nulling" process is illustrated in the following figure 2.16.

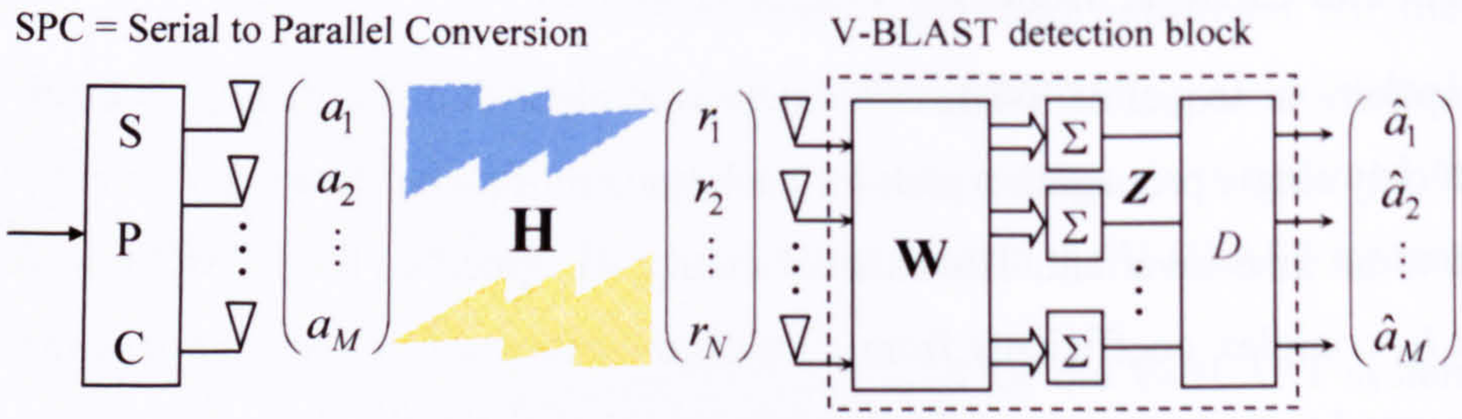

Figure 2.16: V-BLAST system model with symbol detection block

The received signals are processed by weighting $\boldsymbol{r}$ with ω_{ij} of the weighting matrix $\mathbf{W}$:

$$\mathbf{W} = \begin{bmatrix} \omega_{11} & \omega_{12} & \cdots & \omega_{1N} \\ \omega_{21} & \omega_{22} & \cdots & \omega_{2N} \\ \vdots & \vdots & \vdots & \vdots \\ \omega_{M1} & \omega_{M2} & \cdots & \omega_{MN} \end{bmatrix} = \begin{bmatrix} \boldsymbol{w}_1 \\ \boldsymbol{w}_2 \\ \vdots \\ \boldsymbol{w}_M \end{bmatrix} \tag{2.67}$$

Note that $\boldsymbol{w}_m$ is the nulling vector. The weighted signals are combined to form vector $\boldsymbol{Z} = [z_1, z_2, \cdots, z_M]^{\mathsf{T}}$ and each element in $\boldsymbol{Z}$ can be expressed as:

$$z_i = \sum_{j=1}^{N} \omega_{ij} r_j \quad \text{or} \quad z_i = \boldsymbol{w}_i^{\mathsf{T}} \boldsymbol{r} \tag{2.68}$$

Each element z_i is referred as the decision variable or decision statistic and is then 'quantised' or 'sliced' according to the chosen modulation scheme in order to yield the estimates of the individual transmitted symbols. Hence, the estimated transmit vector can be expressed as:

$$\hat{\boldsymbol{a}} = D(\boldsymbol{Z}) \tag{2.69}$$

where 'D' is the slicing operator according to QPSK modulation scheme.

2.5.2.2 Symbol Detection –The Nulling Process [4]

The method to perform detection for this MIMO system is to use the conventional adaptive array antenna (AAA) technique i.e. linear combinatorial nulling [122]. This is similar to the beamforming technique in space-only processing previously discussed for the flat-fading case. Nulling is performed by linearly weighting the received signals so as to satisfy some performance-related criteria such as zero-forcing (ZF) and minimum mean squared error (MMSE). An example of ZF nulling can be shown by choosing $\boldsymbol{w}_i$ in the following:

$$\boldsymbol{w}_i^{\mathsf{T}} (\mathbf{H})_j = \delta_{ij} \tag{2.70}$$

where $(\mathbf{H})_j$ is the j^{th} column of $\mathbf{H}$ and δ is the Kronecker delta. Hence, nulling process is essentially the process of obtaining the right value of the weights in $\mathbf{W}$ to detect the symbol at the receiver. Note that the zero-forcing condition in (2.70) is basically an inverse operation of $\mathbf{H}$.

Ideally, the weighting matrix, **W** should have the impulse response inversely proportional to the channel matrix, **H**. However, under the influence of the additive white Gaussian noise and interferences in the environment, the weights in **W** must be obtained according to certain criteria mentioned earlier in which the symbols can be detected correctly. The weights findings and nulling process using either the ZF or MMSE criterion, are shown in the following respectively:

a) ZF:

$$\boxed{\begin{aligned} \mathbf{W}_{ZF} &= \mathbf{H}^{+}; \\ \hat{\boldsymbol{a}}_{ZF} &= D\left(\mathbf{W}_{ZF}\boldsymbol{r}\right) \end{aligned}} \tag{2.71}$$

b) MMSE:

$$\boxed{\begin{aligned} \boldsymbol{w}_{\mathrm{d}} &= \mathbf{R}_{\boldsymbol{uu}}^{-1}\boldsymbol{u}_{\mathrm{d}} \quad \text{for } 1 \le d \le M \\ \mathbf{B} &= \left[\boldsymbol{w}_1 \;\; \boldsymbol{w}_2 \;\; \cdots \;\; \boldsymbol{w}_M\right] \\ \mathbf{W}_{\mathrm{MSE}} &= \mathbf{B}^{\mathrm{H}} \\ \hat{\boldsymbol{a}}_{\mathrm{MSE}} &= D\left(\mathbf{W}_{\mathrm{MSE}}\boldsymbol{r}\right) \end{aligned}} \tag{2.72}$$

where 'D' is the same slicing operator, $(.)^{+}$ denotes the Moore-Penrose pseudo-inverse [116] and $(.)^{\mathrm{H}}$ is the Hermitian operator. $\mathbf{R}_{\boldsymbol{uu}}^{-1}$ is the inverse of the covariance matrix of the channel and $\boldsymbol{u}_d$ is the desired propagation vector for the d^{th} transmit antenna and $\mathbf{R}_{\boldsymbol{uu}}$ is expressed as follows:

$$\mathbf{R}_{\boldsymbol{uu}} = \sum_{i=1}^{M} \boldsymbol{u}_i \boldsymbol{u}_i^{\mathsf{T}} + \sigma^2 \mathbf{I} \tag{2.73}$$

where σ^2 is the noise variance and **I** is the identity matrix. Every $\boldsymbol{u}$ in **H** is assumed to be uncorrelated. Ultimately, the corresponding symbol estimates, $\hat{\boldsymbol{a}}$, for each criterion can then be obtained linearly through nulling as shown in (2.71) and (2.72).

2.5.2.3 Linear and Non-linear Detection

The nulling process using the ZF or MMSE criterion shown respectively in (2.71) and (2.72) may be implemented either linearly or non-linearly. For the linear method (or pure nulling), the detection process is accomplished in a single-step for all symbols arriving at the receiver at a particular time and all symbols are resolved simultaneously where (2.71) and (2.72) can be applied directly. Consider the following ZF-nulling:

$$\hat{\boldsymbol{a}} \;=\; D(\mathbf{W}_{\mathrm{ZF}}\boldsymbol{r}) \;=\; \begin{bmatrix} \hat{a}_1 \\ \hat{a}_2 \\ \vdots \\ \hat{a}_M \end{bmatrix} \;=\; D\left(\begin{bmatrix} \omega_{11} & \omega_{12} & \cdots & \omega_{1N} \\ \omega_{21} & \omega_{22} & \cdots & \omega_{2N} \\ \vdots & \vdots & \vdots & \vdots \\ \omega_{M1} & \omega_{M2} & \cdots & \omega_{MN} \end{bmatrix} \begin{bmatrix} r_1 \\ r_2 \\ \vdots \\ r_N \end{bmatrix} \right) \begin{matrix} \\ \leftarrow \boldsymbol{w}_1 \\ \leftarrow \boldsymbol{w}_2 \\ \\ \leftarrow \boldsymbol{w}_M \end{matrix} \tag{2.74}$$

where $\mathbf{W}_{\mathrm{ZF}} = \mathbf{H}^{+}$ is the pseudo-inverse of **H** and D is the slicing operator. Each symbol estimate $\hat{a}_i$ has an associated nulling vector $\boldsymbol{w}_i$ and all nulling vectors are contained in $\mathbf{W}_{\mathrm{ZF}}$ as in (2.67).

However, non-linear detection resolves each symbol sequentially in an iterative manner using *symbol interference cancellation* technique. This is done by treating the already-detected symbols in vector $\boldsymbol{a}$ as interference and subsequently eliminated them from $\boldsymbol{r}$ one at a time, according to the "*optimum detection ordering*" [4] explained later in the V-BLAST algorithm. Another word, the most reliable recovered symbol is first cancelled out, to remove the interference of that symbol, which cleans up $\boldsymbol{r}$ in order to aid the recovery of other symbols with poorer SNR value. Hence, the order in which symbols are detected also becomes very important. The non-linear detection offers better system performance than the linear detection provided that the propagation error incurred during the symbol cancellation is considered insignificant compared to the effect of AWGN and interference at a particular instant of measurement.

2.5.2.4 Successive Interference Cancellation (SIC) Scheme

The SIC approach is widely known in the multi-user case [43, 124, 125] where the "best first" concept is used. In V-BLAST detection, SIC is carried out on symbol basis (instead of user) according the "strongest stream" over the transmitted path. Assuming that z obtained for the desired symbol in (2.69), is correctly detected as:

$$\hat{a}_i = D(z_i) = a_i \tag{2.75}$$

Next, the interference (symbol) cancellation operation can be carried out as follows:

$$\boldsymbol{r}_{i+1} = \boldsymbol{r}_i - \hat{a}_{v_i} (\mathbf{H})_{v_i} \tag{2.76}$$

where i is the recursion index of $\boldsymbol{r}$ and v_i is the appointed index in accordance to the optimum detection ordering set. $(\mathbf{H})_{v_i}$ denotes the v_i^{th} column of $\mathbf{H}$ which is the propagation vector, $\boldsymbol{u}_{v_i}$, associated with the desired symbol $\hat{a}_{v_i}$ that applied for the cancellation process. For instant, if the desired symbol a_2 is to be cancelled out from $\boldsymbol{r}$ using the interference cancellation as:

$$\boldsymbol{r}_{i+1} = \boldsymbol{r}_i - \hat{a}_2 (\mathbf{H})_2 \quad \text{or} \quad \boldsymbol{r}_{i+1} = \boldsymbol{r}_i - \hat{a}_2 \boldsymbol{u}_2 \tag{2.77}$$

This can be further illustrated as:

$$\underbrace{\begin{bmatrix} r_1 \\ r_2 \\ \vdots \\ r_N \end{bmatrix}}_{\boldsymbol{r}_{i+1}} = \underbrace{\begin{bmatrix} h_{11}a_1 + h_{12}a_2 + \ldots + h_{1M}a_M + n_1 \\ h_{21}a_1 + h_{22}a_2 + \ldots + h_{2M}a_M + n_1 \\ \vdots \\ h_{N1}a_1 + h_{N2}a_2 + \ldots + h_{NM}a_M + n_N \end{bmatrix}}_{\boldsymbol{r}_i = \mathbf{H}\boldsymbol{a} + \boldsymbol{n}} - \underbrace{\hat{a}_2 \begin{bmatrix} h_{12} \\ h_{22} \\ \vdots \\ h_{N2} \end{bmatrix}}_{\hat{a}_2 (\mathbf{H})_2} \tag{2.78}$$

Symbol Cancellation

Note that the symbol estimate $\hat{a}_2$ is cancelled out from the original received signal vector, $\boldsymbol{r}_i$ (together with its propagation vector $\boldsymbol{u}_2$ which contains each transmitted path) in order to form the new received vector, $\boldsymbol{r}_{i+1}$ that is 'interference-free' from symbol a_2.

2.5.2.5 Optimum Detection Ordering [4, 34]

When symbol cancellation is used, the system performance is affected by the order in which the symbol in $\boldsymbol{a}$ is detected first, whereas it does not matter in the pure nulling [4]. The ordering of detection is determined by the post-detection SNR value, denoted as ρ, which can be obtained by substituting (2.64) and (2.70) into (2.68) and taking the expected value:

$$\rho_{v_i} = \frac{< \left| a_{v_i} \right|^2 >}{\sigma^2 \left\| \boldsymbol{w}_{v_i} \right\|^2} \tag{2.86}$$

Note that (2.86) also implies that the smaller the norm square of the nulling vector, $\boldsymbol{w}_{v_i}$, the higher the post-detection SNR value, ρ_{v_i}. σ^2 is the noise variance and v_i is the index for the ordering set which can be arbitrary defined to specify the order in which components of $\boldsymbol{a}$ are extracted:

$$S_{\text{V-BLAST}} = \{v_1, v_2, \ldots, v_M\} \tag{2.87}$$

The important of ordering is simply that it permits (during the detection of i^{th} component) a choice as to which subset of M-i rows that $\boldsymbol{w}_{v_i}$ should be constrained since different choices lead to different ρ_{v_i}. For instance, in an M=3 system, detecting component 1 first (in the present of 2 and 3) will, in general result in a different ρ_{v_i} than if component 2 was detected first (in the presence of 1 and 3). With pure nulling, each component is always detected in the presence of all the others, so ordering does not matter. Assuming that all components of $\boldsymbol{a}$ utilise same constellation in non-linear nulling, the component with the smallest ρ_{v_i} will dominate the error performance. The incorrect detection of the current component might result in error propagation, which will affect the detection of next component. Therefore, choosing the best ρ_{v_i} at each stage in the detection process leads to globally optimum ordering [34].

2.5.2.6 V-BLAST Detection Algorithm [4]

The V-BLAST detection algorithm consists of two operations; 1) the determination of index v_i in detection ordering set as in (2.80) and 2) the nulling and symbol cancellation of each component as in (2.68) & (2.76) respectively. These two operations are integrated together into a single flow of algorithm shown in the following table as:

initialisation :	
$i \leftarrow 1$	(a) Assign '1' into counter i
$\mathbf{G}_1 = \mathbf{H}^+$	(b) Obtain 1st $\mathbf{G}$ by Pseudo-inverse of $\mathbf{H}$ – ZF criterion
$v_i = \arg\min_j \left\|(\mathbf{G}_1)_j\right\|^2$	(c) Determine ordering index v_i by taking the value of which (j^{th}) row vector in $\mathbf{G}_1^{\mathsf{T}}$ that gives the minimum norm square value.
recursion :	
$\boldsymbol{w}_{v_i} = (\mathbf{G}_i)_{v_i}$	(d) Obtain nulling vector $\boldsymbol{w}$ from $\mathbf{G}_i$ according to (c)
$\hat{a}_{v_i} = D\left(\boldsymbol{w}_{v_i}^{\mathsf{T}} \boldsymbol{r}_i\right)$	(e) Detecting symbol $\hat{a}_{v_i}$ with index from (c)
$\boldsymbol{r}_{i+1} = \boldsymbol{r}_i - \hat{a}_{v_i} (\mathbf{H})_{v_i}$	(f) Symbol cancellation process to find new $\boldsymbol{r}$
$\mathbf{G}_{i+1} = \mathbf{H}_{v_i}^{+}$	(g) Obtain new $\mathbf{G}$ by from the "deflated" $\mathbf{H}_{v_i}^{-}$
$v_{i+1} = \arg\min_{j \notin \{v_1 \cdots v_i\}} \left\|(\mathbf{G}_{i+1})_j\right\|^2$	(h) Determine next ordering index v_{i+1} as (c) from new $\mathbf{G}_{i+1}$
$i \leftarrow i+1$	(i) Increment counter i

Table 2.1: The V-BLAST detection algorithm with optimum ordering process.

During initialisation, the first ordering index can be determined in (c) by looking at which j^{th} row vector of $\mathbf{G}_1$, produce the minimum norm square value i.e. highest post-detection SNR using (2.79). $(\mathbf{G}_1)_j$ denotes the j^{th} row of $\mathbf{G}_1$. The ordering index is vital in order to decide which symbol to be detected first. The $\mathbf{G}$ matrix in (b) is obtained from the inversion of $\mathbf{H}$. (The ZF criterion is used in (b) to ease the explanation although MMSE can also be applied).

The recursion consists of the two processes: 1) nulling process in (d) and (e) and 2) symbol cancellation in (f). First, the nulling vector $\boldsymbol{w}_{v_i}$ is obtained in (d) for the detection of the chosen symbol according to the current ordering index found in (c). Then, the nulling (detection) of the chosen symbol is obtained in (e) by weighting $\boldsymbol{r}_i$ with $\boldsymbol{w}_{v_i}$. Next, the symbol cancellation is carried out in (f) where new $\boldsymbol{r}_{i+1}$ is generated by subtracting the contribution of the detected symbol and its path from the current $\boldsymbol{r}$ so that $\boldsymbol{r}_{i+1}$ is 'interference-free' from that detected symbol. Next, (g) computes the new pseudo-inverse, i.e. matrix $\mathbf{G}_{i+1}$ for the next iteration. The next ordering index is also computed in (h) in order to determine which symbol is to be detected next. The recursion process, from (d) to (i) steps, is then repeated until all symbols have been detected completely.

Note that the pseudo-inverse in (g) is performed onto the deflated version of $\mathbf{H}$ in which respective columns $v_1, v_2, \ldots, v_i$, that correspond to detected components of the transmit vector, $\boldsymbol{a}$ (which has already cancelled), is 'zeroed' and the corresponding transmit antenna have been removed accordingly. The "zeroing columns" operation of the original $\mathbf{H}$ is denoted by $\mathbf{H}_{v_i}^{-}$ and it

is always performed prior to the pseudo-inverse operation denoted by the '$^+$', on top of the '-' sign in $\mathbf{H}_{v_i}^{+}$. The columns in $\mathbf{H}$ that have been previously "deflated" will remain zeroed for the subsequent pseudo-inverse operation. The 'zeroing' also means that the respective paths (that undergone by the chosen symbol) have been deliberately cancelled so that $\boldsymbol{w}_{v_i}$ obtained in (d) during next iteration, can also be "interference-free" from those paths. The V-BLAST detection algorithm will be illustrated in table 2.2 below where (3×3) system is used.

Step	Optimum Ordering & Weight finding: $\mathbf{H}=\mathbf{G}^{+}$		Ordering Index	Nulling & Symbol Cancellation
1	$\mathbf{H}=\begin{bmatrix} h_{11} & h_{12} & h_{13} \\ h_{21} & h_{22} & h_{23} \\ h_{31} & h_{32} & h_{33} \end{bmatrix}$	$\mathbf{G}_1=\begin{bmatrix} g_{11} & g_{12} & g_{13} \\ \boxed{g_{21} \quad g_{22} \quad g_{23}} \\ g_{31} & g_{32} & g_{33} \end{bmatrix}=\boldsymbol{w}_2$	2	$\hat{a}_2=D\left(\boldsymbol{w}_2^{\mathsf{T}}\boldsymbol{r}_1\right)$ $\boldsymbol{r}_2=\boldsymbol{r}_1-\hat{a}_2(\mathbf{H})_2$
2	$\mathbf{H}_2^{-}=\begin{bmatrix} h_{11} & 0 & h_{13} \\ h_{21} & 0 & h_{23} \\ h_{31} & 0 & h_{33} \end{bmatrix}$	$\mathbf{G}_2=\begin{bmatrix} \boxed{g_{11} \quad g_{12} \quad g_{13}} \\ 0 \quad 0 \quad 0 \\ g_{31} & g_{32} & g_{33} \end{bmatrix}=\boldsymbol{w}_1$	1	$\hat{a}_1=D\left(\boldsymbol{w}_1^{\mathsf{T}}\boldsymbol{r}_2\right)$ $\boldsymbol{r}_3=\boldsymbol{r}_2-\hat{a}_1(\mathbf{H})_1$
3	$\mathbf{H}_1^{-}=\begin{bmatrix} 0 & 0 & h_{13} \\ 0 & 0 & h_{23} \\ 0 & 0 & h_{33} \end{bmatrix}$	$\mathbf{G}_3=\begin{bmatrix} 0 & 0 & 0 \\ 0 & 0 & 0 \\ \boxed{g_{31} \quad g_{32} \quad g_{33}} \end{bmatrix}=\boldsymbol{w}_3$	3	$\hat{a}_3=D\left(\boldsymbol{w}_3^{\mathsf{T}}\boldsymbol{r}_3\right)$

Table 2.2: Illustration example for the V-BLAST algorithm with SIC feature.

The V-BLAST algorithm is illustrated in 3 steps. Since $M=3$, there are only 3 components to be detected in $\boldsymbol{a}$. The channel matrix $\mathbf{H}$ consists of (3×3) path coefficients. The boxes in $\mathbf{G}$ indicate the row vector in $\mathbf{G}$ that has the local minimum norm square, determined according to either (c) or (h) to compute the current ordering index. The nulling vector is also obtained.

For example, in step-1, symbol a_2 is to be detected first where $\boldsymbol{w}_2$ is used in the 1st nulling process of $\hat{a}_2$. The symbol cancellation is performed next to produce the new received signal vector, $\boldsymbol{r}_2$. In step-2, the 2nd column of $\mathbf{H}$ is zeroed to remove the related paths before computing the new $\mathbf{G}_2$. It can be noticed that 2nd of $\mathbf{G}_2$ has also been zeroed after the pseudo-inverse of $\mathbf{H}_2^{-}$. This time, the 1st row of $\mathbf{G}_2$ has the lower norm square value as compared to the 3rd row. (Note that, only non-zeroed rows of $\mathbf{G}$ will be considered in each iteration). Hence, symbol a_1 is detected in the 2nd nulling process where $\boldsymbol{w}_1$ and $\boldsymbol{r}_2$ are used. Subsequently, $\hat{a}_1$ is cancelled out to produce another new received signal vector, $\boldsymbol{r}_3$. Finally, after the zeroing and pseudo-inverse process, the last nulling vector $\boldsymbol{w}_3$ was obtained to detect symbol a_3 with $\boldsymbol{r}_3$. Thus, it can be seen clearly that the detection ordering set is expressed as:

$$S=\{2,1,3\} \tag{2.81}$$

2.5.3 Novel QR Detection Algorithm [126].

The conventional V-BLAST detection described previously is a single flow algorithm that consists of the two major operations: 1) the finding of the ordering index and 2) the nulling and symbol cancellation process. This section focuses on the second operation and provides an alternative way for the nulling and symbol cancellation process using the QR decomposition to modify the V-BLAST algorithm for alternative way of effective detection. [127, 128] partially adopted the concept of QR decomposition of the space-time channel matrix, while [129] applied the Gram-Schmitt Orthogonalisation (GSO) to propose a low complexity V-BLAST architecture.

The concept of using QR decomposition to explain the iterative cancellation and detection algorithm is also reported in [83] where the decomposition of the channel matrix into the orthonormal matrix **Q** and the triangular matrix **R** have created a way of achieving symbol cancellation by means of backward substitution. Nevertheless, the concept of incorporating the optimum detection ordering in a pre-arranged channel matrix to achieve the sub-optimum performance of the BLAST receiver was reported initially in [126], which will be explained here.

2.5.3.1 Basic principal in QR detection method

QR decomposition achieves the orthogonal triangularization through GSO or Householder [116, 123]. The idea is to decompose the channel matrix **H** into an orthonormal matrix **Q** and a upper-triangular matrix **R** such that the orthogonal property of **Q** and the triangular structure of **R** can be utilised to carry out the symbol detection. The orthogonal properties are shown as:

$$\mathbf{Q}^{-1} = \mathbf{Q}^{\mathsf{T}} \quad \& \quad \mathbf{Q}^{\mathsf{T}}\mathbf{Q} = \mathbf{I} \tag{2.82}$$

Assuming noiseless case, the received signal vector, $\boldsymbol{r}$ can be re-written as:

$$\boldsymbol{r} \;=\; \mathbf{H}\,\boldsymbol{a} \;=\; \mathbf{Q}\begin{bmatrix}\mathbf{R}\\ \boldsymbol{0}\end{bmatrix}\boldsymbol{a} \tag{2.83}$$

where $\boldsymbol{0}$ is the zero matrix with dimension $(N\text{-}M)\times M$. Using the orthogonal properties in (2.82), and left multiply (2.83) with $\mathbf{Q}^{\mathsf{T}}$, produce the "orthogonalised" received signal vector, $\boldsymbol{x}$ as:

$$\mathbf{Q}^{\mathsf{T}}\boldsymbol{r} \;=\; \boldsymbol{x} \;=\; \begin{bmatrix}\mathbf{R}\\ \boldsymbol{0}\end{bmatrix}\boldsymbol{a} \tag{2.84}$$

It can be noticed in (2.84) that the resulting triangular structure in **R** allows the detection of the components in $\boldsymbol{a}$ to be carried out using backward substitution, in which symbol cancellation has already been incorporated without particular order. The non-linear QR detection that gives similar performance as V-BLAST can only be achieved when the correct detection ordering is also incorporated, where stronger component is detected first, which is explained in next section.

2.5.3.2 Channel Matrix Re-arrangement – Incorporation of Detection Ordering

The novelty of the QR detection is the incorporation of the optimum detection ordering by means of the channel matrix re-arrangement process. Assuming that the detection ordering set S in (2.80) is already obtained by some other methods (optimum or sub-optimum) shown as:

$$S = \{v_1, v_2, \ldots, v_M\} \tag{2.85}$$

The incorporation of the ordering is simply achieved by re-arranging the columns of $\mathbf{H}$ such that stronger propagation vector $\boldsymbol{u}$ associated with the order index in (2.85) is placed at right-most column of the new "re-arranged" channel matrix $\mathbf{H}_{\text{new}}$, using the following procedure:

initialisation :

$$i \leftarrow 1 \tag{2.86a}$$

$$i \leftarrow M \tag{2.86b}$$

recursion :

$$(\mathbf{H}_{new})_b = (\mathbf{H})_{v_i} \tag{2.86c}$$

$$i \leftarrow i+1 \tag{2.86d}$$

$$b \leftarrow b\text{-}1 \tag{2.86e}$$

Corresponding to (2.85), (2.86c) means that the v_i^{th} column of $\mathbf{H}$ is chosen and placed into the b^{th} column of $\mathbf{H}_{new}$ until i reaches M. For example, consider the same detection ordering set in (2.81) which is in the order of 2, 1, 3, $\mathbf{H}$ is re-arranged into $\mathbf{H}_{new}$ as:

$\boldsymbol{r} = \mathbf{H}\,\boldsymbol{a}$ $\qquad\qquad$ $\boldsymbol{r} = \mathbf{H}_{new}\,\boldsymbol{a}_{new}$

$$\begin{bmatrix} r_1 \\ r_2 \\ r_3 \end{bmatrix} = \begin{bmatrix} : & : & : \\ \boldsymbol{u}_1 & \boldsymbol{u}_2 & \boldsymbol{u}_3 \\ : & : & : \end{bmatrix} \begin{bmatrix} a_1 \\ a_2 \\ a_3 \end{bmatrix} \quad \text{is rearranged to} \rightarrow \quad \begin{bmatrix} r_1 \\ r_2 \\ r_3 \end{bmatrix} = \begin{bmatrix} : & : & : \\ \boldsymbol{u}_3 & \boldsymbol{u}_1 & \boldsymbol{u}_2 \\ : & : & : \end{bmatrix} \begin{bmatrix} a_3 \\ a_1 \\ a_2 \end{bmatrix}$$

Note that $\boldsymbol{r}$ remains the same since $\boldsymbol{a}$ is also been "re-arranged" into $\boldsymbol{a}_{\text{new}}$ to detect the stronger component first in the backward manner. In this case, a_2 followed by a_1 and then a_3.

2.5.3.3 Orthogonal Triangularisation by QR Decomposition.

Having rearranged $\mathbf{H}$ into $\mathbf{H}_{new}$, the QR decomposition is applied to $\mathbf{H}_{new}$, to obtain the new set of the $(N \times N)$ orthonormal matrix, $\mathbf{Q}_{new}$, and the $(M \times M)$ upper triangular matrix, $\mathbf{R}_{new}$, as:

$$\mathbf{H}_{new} = \mathbf{Q}_{new} \begin{bmatrix} \mathbf{R}_{new} \\ \boldsymbol{O} \end{bmatrix} \tag{2.87}$$

where $\boldsymbol{O}$ is the zero matrix. $\mathbf{R}_{new}$ having the triangular structure can be expressed as:

$$\mathbf{R}_{\text{new}} = \begin{bmatrix} \boldsymbol{\Gamma}_1 & \boldsymbol{\Gamma}_2 & \cdots & \boldsymbol{\Gamma}_M \end{bmatrix} = \begin{bmatrix} \gamma_{11} & \gamma_{12} & \cdots & \gamma_{1M} \\ 0 & \gamma_{22} & \cdots & \gamma_{2M} \\ \vdots & 0 & \ddots & \vdots \\ 0 & \cdots & 0 & \gamma_{MM} \end{bmatrix} \tag{2.88}$$

where Γ_i is the i^{th} column vector in $\mathbf{R}_{new}$ and γ_{nm} are the elements in $\mathbf{R}_{new}$. Under the noise free condition, the received signal vector $\boldsymbol{r}$ can be written as:

$$\boldsymbol{r} = \mathbf{Q}_{new} \begin{bmatrix} \mathbf{R}_{new} \\ \boldsymbol{O} \end{bmatrix} \boldsymbol{a}_{new} \tag{2.89}$$

Note that the new $\mathbf{Q}_{new}$ and $\mathbf{R}_{new}$ produced from the $\mathbf{H}_{new}$ will be different from the $\mathbf{Q}$ and $\mathbf{R}$ produced from the original $\mathbf{H}$ (without channel matrix re-arrangement). Hence the resulting 'orthogonalised' receive signal vector $\boldsymbol{x}$ will also be different. The new 'orthogonalised' $\boldsymbol{x}_{new}$ is obtained by left multiplying (2.89) with $\mathbf{Q}_{new}^{\mathsf{T}}$ and applying the orthogonal properties in (2.82); leaving only the matrix $\mathbf{R}_{new}$ on the right hand side (*RHS*) of (2.89), as shown in the following:

$$\underset{RHS}{\boxed{\boldsymbol{x}_{\text{new}} = \mathbf{Q}_{\text{new}}^{\mathsf{T}} \boldsymbol{r}}} = \underset{LHS}{\boxed{\begin{bmatrix} \mathbf{R}_{\text{new}} \\ \boldsymbol{O} \end{bmatrix} \boldsymbol{a}_{new}}} \tag{2.90}$$

where elements of $\boldsymbol{x}$ can be expressed as:

$$\boldsymbol{x} = [q_1, q_2, \cdots, q_N]^{\mathsf{T}} \tag{2.91}$$

The advantages of having the orthonormal matrix $\mathbf{Q}_{new}$ is that, it allows the inversion of matrix to be carried out simply by matrix transposition or the Hermitian operation which in turn removes $\mathbf{Q}_{new}$ from the *RHS* of (2.90) while retaining the statistical property of the initial $\boldsymbol{r}$ vector on the *LHS* of (2.90). The triangular structure of $\mathbf{R}_{new}$ in (2.90) allows recovery of the components in $\boldsymbol{a}_{\text{new}}$ to be carried out by backward substitution and symbol cancellation with the correct order of detection through channel matrix re-arrangement in (2.86).

2.5.3.4 Non-linear QR detection algorithm

Using (2.88), (2.90) and (2.91), the nonlinear QR detection is accomplished as follows:

initialisation :

$$j \leftarrow M \tag{2.92a}$$

$$k = 1 \tag{2.92b}$$

recursion :

$$\hat{a}_j = D\left(\frac{q_j^k}{\gamma_{jj}}\right) \tag{2.92c}$$

$$\boldsymbol{x}_{k+1} = \boldsymbol{x}_k - \hat{a}_j \boldsymbol{\Gamma}_j \tag{2.92d}$$

$$j \leftarrow j-1 \tag{2.92e}$$

$$k \leftarrow k+1 \tag{2.92f}$$

where 'D' is the same decision operator and 'k' is the recursion index. It can be noticed that (2.92c) resolves each symbol estimate sequentially in a backward manner and (2.92d) performs the symbol cancellation of the already detected component $\hat{a}_j$ from the "orthogonalised" received vector $\boldsymbol{x}$. The nonlinear QR detection algorithm can be illustrated using the same example case for a (3×3) system with the detection ordering set is $S = \{2,1,3\}$, as shown in the following table:

Step	Vector $\boldsymbol{x}$ & backward substitution with symbol cancellation.	Detecting Symbol
1	$\boldsymbol{x}_1 = \mathbf{R}_{new}\,\boldsymbol{a}_{new} + \boldsymbol{n}$ $= \begin{bmatrix} q_1^1 \\ q_2^1 \\ q_3^1 \end{bmatrix} = \begin{bmatrix} \gamma_{11}a_3 + \gamma_{12}a_1 + \gamma_{13}a_2 + \tilde{n}_1 \\ 0 + \gamma_{22}a_1 + \gamma_{23}a_2 + \tilde{n}_2 \\ 0 + 0 + \gamma_{33}a_2 + \tilde{n}_3 \end{bmatrix}$	$\hat{a}_2 = D\left(\dfrac{q_3^1}{\gamma_{33}}\right)$
2	$\boldsymbol{x}_2 = \boldsymbol{x}_1 - \hat{a}_2\boldsymbol{\Gamma}_3$ (cancel) $= \begin{bmatrix} q_1^2 \\ q_2^2 \\ q_3^2 \end{bmatrix} = \begin{bmatrix} \gamma_{11}a_3 + \gamma_{12}a_1 + \gamma_{13}a_2 + \tilde{n}_1 \\ 0 + \gamma_{22}a_1 + \gamma_{23}a_2 + \tilde{n}_2 \\ 0 + 0 + \gamma_{33}a_2 + \tilde{n}_3 \end{bmatrix} - \begin{bmatrix} \hat{a}_2\gamma_{13} \\ \hat{a}_2\gamma_{23} \\ \hat{a}_2\gamma_{33} \end{bmatrix}$	$\hat{a}_1 = D\left(\dfrac{q_2^2}{\gamma_{22}}\right)$
3	$\boldsymbol{x}_3 = \boldsymbol{x}_2 - \hat{a}_1\boldsymbol{\Gamma}_2$ (cancel) $= \begin{bmatrix} q_1^1 \\ q_2^1 \\ q_3^1 \end{bmatrix} = \begin{bmatrix} \gamma_{11}a_3 + \gamma_{12}a_1 + \tilde{n}_1 \\ 0 + \gamma_{22}a_1 + \tilde{n}_2 \\ 0 + 0 + \tilde{n}_3 \end{bmatrix} - \begin{bmatrix} \hat{a}_1\gamma_{12} \\ \hat{a}_1\gamma_{22} \\ 0 \end{bmatrix}$	$\hat{a}_3 = D\left(\dfrac{q_1^3}{\gamma_{11}}\right)$

Table 2.3: Illustration example for the nonlinear QR detection algorithm.

It can be seen that the triangular structure in step-1 allows component a_2 to be detected first, according to the detection ordering set. The estimate $\hat{a}_2$ can be obtained by dividing q_3^1 in $\boldsymbol{x}_1$ with γ_{33} in $\mathbf{R}_{new}$, by a single division process. The purpose of this single division is the same as the nulling process in (2.68). The only difference is that the channel information can be used directly in the nonlinear QR method rather than going through the pseudo-inverse of $\mathbf{H}$ by $\mathbf{G}$ to obtain the required nulling vector $\boldsymbol{w}$ in the conventional V-BLAST nulling process shown in table 2.1.

Under the pure backward substitution method, the already detected symbol is subtracted (together with the corresponding paths) to detect the subsequent signal component; e.g. estimate $\hat{a}_2$ is then feedback to detect the 2nd component, a_1. The subtraction and backward substitution process are repeated until the all symbols are detected. Nevertheless, this process is also equivalent with the symbol cancellation process (shown in the red box) that replaces the subtraction of individual product term $\gamma_{ij}\,a_i$, to allow the symbol detection in each step to be obtained through just a single division process as shown in table 2.3.

The nonlinear QR method provides a way to dissolve the detection ordering and symbol cancellation into backward substitution process just by re-arranging the columns of $\mathbf{H}$ according to the correct order of detection required. Hence, the success of nonlinear QR detection depends on the finding of correct detection ordering set, which is vital for the symbol cancellation scheme. It is worth noting that QR decomposition applied to $\mathbf{H}_{new}$ is only carried out once in the nonlinear QR method to achieve the sub-optimum performance of the layered space-time systems.

2.6 V-BLAST: Extension to Frequency-Selective fading Model

The V-BLAST technique explained earlier is catered for frequency flat-fading MIMO channel case. However, in order to enable high-data-rate application, it is necessary to utilise signal whose bandwidth exceeds the coherence bandwidth of the channel. MIMO equaliser is one of the methods that use space-time processing to resolve signals in frequency-selective fading channel. MIMO equalisation presents a significant challenge because of the need to detect signals buried in both the co-channel interference (CCI) as well as inter-symbol interference (ISI), in addition to noise. In the following, the concept of MIMO equaliser [45, 47] will be introduced systematically followed by the incorporation of decision feedback unit – MIMO-DFE. The incorporation of the Order Successive Interference Cancellation (OSIC) scheme (extended from the V-BLAST) in the MIMO-DFE receiver (generally referred as the MIMO-OSIC-DFE receivers [47] throughout this thesis) will also be illustrated in order to provide necessary background and understanding of more complex receiver structure for the MIMO system.

2.6.1 System and Channel Models

The basic MIMO system and the frequency selective fading MIMO channel model are outlined below which followed the details in [47]. A discrete-time complex baseband model is considered for a single-user link. Perfect channel estimation and synchronisation are assumed. Figure 2.17 shows the typical frequency-selective fading characteristic of a MIMO communication channel.

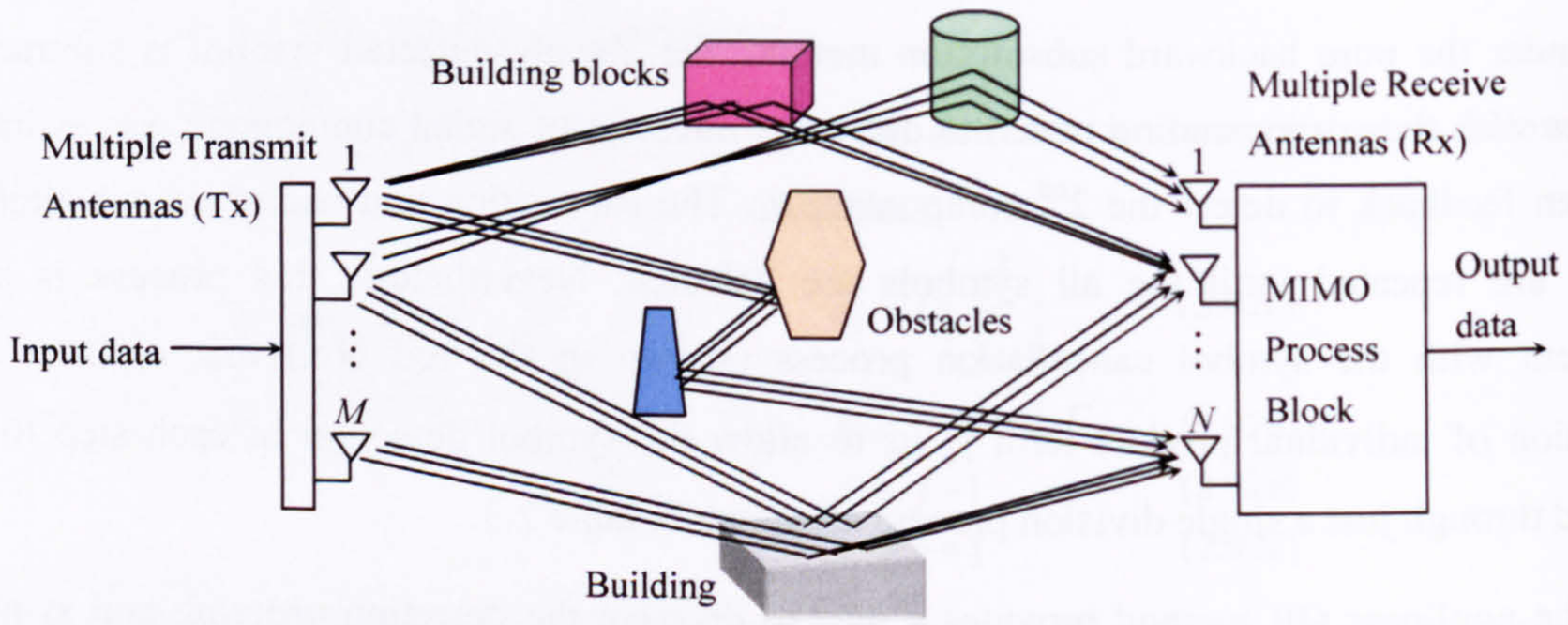

Figure 2.17: The frequency selective fading MIMO channel

There are M transmit and N receive antenna where $(N \times M)$ is system configuration. $(L+1)$ indicates the number of symbol-spaced FIR taps used for the simulated channel that corresponds to the delayed paths in a frequency selective fading environment. Thus, the sampled channel impulse response (CIR) from the m^{th} transmit antenna to n^{th} receive antenna can be expressed as:

$$\mathbf{h}_{nm} = \begin{bmatrix} h_{nm}(0) & h_{nm}(1) & \cdots & h_{nm}(L) \end{bmatrix}^{\mathsf{T}} \tag{2.93}$$

where $\mathbf{h}_{nm}$ can be grouped into M separate channel matrices $\mathbf{H}_m$, w.r.t each m^{th} transmit antenna. Hence, $\mathbf{H}_m$ consists of multiple $\mathbf{h}_{nm}$ between the m^{th} transmit antenna to all N receive antennas as:

$$\mathbf{H}_m = \begin{bmatrix} \mathbf{h}_{1m}^{\mathsf{T}} \\ \mathbf{h}_{2m}^{\mathsf{T}} \\ \vdots \\ \mathbf{h}_{Nm}^{\mathsf{T}} \end{bmatrix} = \begin{bmatrix} h_{1m}(0) & h_{1m}(1) & \cdots & h_{1m}(L) \\ h_{2m}(0) & h_{2m}(1) & \cdots & h_{2m}(L) \\ \vdots & \vdots & \vdots & \vdots \\ h_{Nm}(0) & h_{Nm}(1) & \cdots & h_{Nm}(L) \end{bmatrix}, \quad m = 1, 2, \ldots, M. \tag{2.94}$$

Each coefficient, h_{nm} in (2.94) is generated as random complex components and all h_{nm} are assumed to be uncorrelated. The (M×1) transmit vector $\boldsymbol{s}(k)$ at time k has spatial covariance as:

$$E\left[\boldsymbol{s}(k)\,\boldsymbol{s}^{\mathsf{H}}(k)\right] = \frac{P_T}{M}\mathbf{I}_M \tag{2.95}$$

where P_T is the total average transmit power, which is held constant irrespective of the number of transmit antennas or M. The receiver's additive white Gaussian noise (AWGN) vector can be in turn expressed, as (N×1) vector with spatial covariance:

$$E\left[\mathbf{n}(k)\,\mathbf{n}^{\mathsf{H}}(k)\right] = \sigma^2\mathbf{I}_N \tag{2.96}$$

Next, the (N×1) received signal vector, $\mathbf{x}(k)$ at time k can be expressed as:

$$\mathbf{x}(k) = \sum_{m=1}^{M} \mathbf{H}_m\mathbf{s}_m(k) + \mathbf{n}(k) \tag{2.97}$$

where $\mathbf{n}(k)$ is AWGN vector. $\mathbf{s}_m(k)$ is the transmit vector sent by the m^{th} transmit antenna as:

$$\mathbf{s}_m(k) = \begin{bmatrix} s_m(k) & s_m(k-1) & \cdots & s_m(k-L) \end{bmatrix}^{\mathsf{T}} \tag{2.98}$$

Note that each transmit vector $\mathbf{s}_m(k)$ consists of a sequence of L+1 symbols (i.e. from the current $(k)^{\text{th}}$ symbol back to previous $(k–L)^{\text{th}}$ symbol). $\mathbf{x}(k)$ in (2.97) can be further expanded as:

$$\mathbf{x}(k) = \mathbf{H}_1\mathbf{s}_1(k) + \ldots + \mathbf{H}_M\mathbf{s}_M(k) + \mathbf{n}(k) \tag{2.99}$$

$$\begin{bmatrix} x_1(k) \\ \vdots \\ x_N(k) \end{bmatrix} = \begin{bmatrix} h_{11}(0) \cdots h_{11}(L) \\ \vdots \\ h_{N1}(0) \cdots h_{N1}(L) \end{bmatrix}\begin{bmatrix} s_1(k) \\ \vdots \\ s_1(k-L) \end{bmatrix} + \cdots + \begin{bmatrix} h_{1M}(0) \cdots h_{1M}(L) \\ \vdots \\ h_{NM}(0) \cdots h_{NM}(L) \end{bmatrix}\begin{bmatrix} s_M(k) \\ \vdots \\ s_M(k-L) \end{bmatrix} + \begin{bmatrix} n_1(k) \\ \vdots \\ n_N(k) \end{bmatrix}$$

Note that the ISI contribution is shown through the interaction of each CIR $\mathbf{h}_{nm}$ and their respective transmit vector $\mathbf{s}_m$. whereas, the CCI contribution is shown through the summation of all the product $\mathbf{H}_m\mathbf{s}_m$. Thus, it can be seen that each received signal $\mathbf{x}(k)$ is a complex entity of the CCI and ISI contributions as well as noise. Therefore, it requires a method to separate all these mixed terms in order to resolve for each symbol individually. MIMO equaliser is one of the advance methods that can be used to resolve this problem.

2.6.2 MIMO Equalisation [42, 47]

The MIMO equaliser is similar to the beamformer-equaliser described earlier except that Q users being altered to become M transmit antennas for a single-user case. Traditionally, equaliser is used to counteract the ISI in a SISO model, which can be found in [118, 119]. However, equalisation in MIMO model becames more complex since the multi-stream signals have to be resolved in the presence of both ISI as well as CCI, making the equalisation process more difficult to be achieved. In this section, the MIMO equaliser (with only feed-forward part) will be described, followed by the MIMO decision feedback equaliser (MIMO-DFE). Consider the MIMO equaliser with feedforward filter structure and temporal span of K_f+ 1 taps per input as:

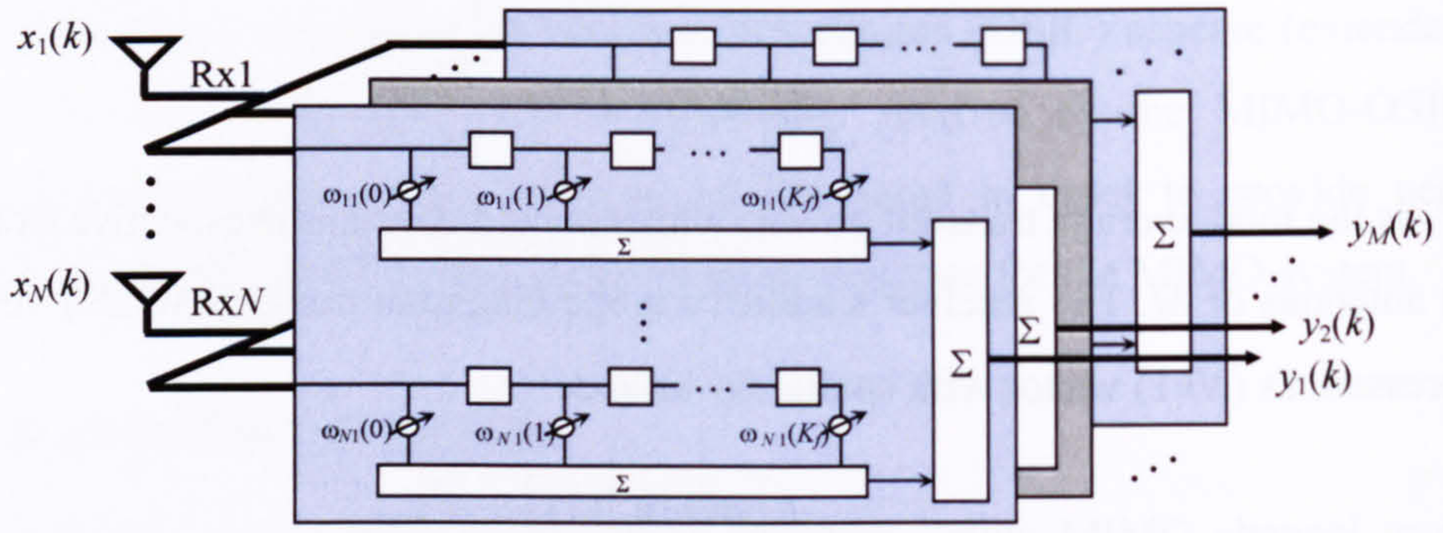

Figure 2.18: MIMO equaliser's structure

The MIMO equaliser can be viewed as a 3-dimensional filter structure with dimension of $(K_f+1)\times N\times M$ consisting of M stages of weighting matrix, $\mathbf{W}_m$. Each $\mathbf{W}_m$ is in turn a 2-D, with N multiple-link equaliser structure with (K_f+1) taps. Its spatial and temporal weights are placed respectively across the vertical and horizontal fields (similar to $\mathbf{W}_q$ in (2.50)), expressed as:

$$\mathbf{W}_m = \begin{bmatrix} \boldsymbol{\omega}_m(0) & \boldsymbol{\omega}_m(1) & \cdots & \boldsymbol{\omega}_m(K_f) \end{bmatrix} = \begin{bmatrix} \omega_{1m}(0) & \omega_{1m}(1) & \cdots & \omega_{1m}(K_f) \\ \omega_{2m}(0) & \omega_{2m}(1) & \cdots & \omega_{2m}(K_f) \\ \vdots & \vdots & \vdots & \vdots \\ \omega_{Nm}(0) & \omega_{Nm}(1) & \cdots & \omega_{Nm}(K_f) \end{bmatrix} \tag{2.100}$$

Note that $(K_f + 1)$ taps are needed so that enough temporal samples are collected to consider for the ISI effects in the temporal domain. Therefore, the K_f+1 N-dimensional received signals can be grouped into the received signals matrix $\mathbf{X}(k)$ as:

$$\mathbf{X}(k) = \begin{bmatrix} \mathbf{x}(k) & \mathbf{x}(k-1) & \cdots & \mathbf{x}(k-K_f) \end{bmatrix} = \begin{bmatrix} x_1(k) & x_1(k-1) & & x_1(k-K_f) \\ x_2(k) & x_2(k-1) & \cdots & x_2(k-K_f) \\ \vdots & \vdots & & \vdots \\ x_N(k) & x_N(k-1) & & x_N(k-K_f) \end{bmatrix} \tag{2.101}$$

which in turn served as the input to the M stages MIMO equaliser at time $(k\text{-}n)$. The number of

weights in each $\mathbf{W}_m$ must be equivalent to the number of elements in $\mathbf{X}(k)$, which is $N(K_f+1)$, in order to allow the equalisation process to be carried out for each symbol in the transmit vector. Each $\mathbf{W}_m$ has the role of projecting one of the incoming data streams away from its own un-cancelled (pre-cursor) ISI as well as the un-cancelled CCI from all other streams.

Next, the output of each m^{th} stage equalisation process, $y_m(k)$, can be expressed as follows:

$$y_m(k) = \text{trace}\left\{ \mathbf{W}_m^{\mathsf{H}} \ \mathbf{X}(k) \right\} \tag{2.102}$$

$$= \text{trace}\left\{ \begin{bmatrix} \omega_{1m}^*(0) & \omega_{2m}^*(0) & \cdots & \omega_{Nm}^*(0) \\ \omega_{1m}^*(1) & \omega_{2m}^*(1) & \cdots & \mathrm{w}_{Nm}^*(1) \\ \vdots & \vdots & \cdots & \vdots \\ \omega_{1m}^*(K_f) & \omega_{2m}^*(K_f) & \cdots & \omega_{Nm}^*(K_f) \end{bmatrix} \begin{bmatrix} x_1(k) & x_1(k-1) & \cdots & x_1(k-K_f) \\ x_2(k) & x_2(k-1) & \cdots & x_2(k-K_f) \\ \vdots & \vdots & \vdots & \vdots \\ x_N(k) & x_N(k-1) & \cdots & x_N(k-K_f) \end{bmatrix} \right\}$$

Note that $y_m(k)$ is also the estimate for stream m at time k. (2.102) is equivalent to (2.52) in STP. To further proceed the formulation, the $vec(.)$ operator is introduced as:

$$vec\left(\begin{bmatrix} \mathbf{v}_1 & \mathbf{v}_2 & \cdots & \mathbf{v}_K \end{bmatrix}\right) = \begin{bmatrix} \mathbf{v}_1 \\ \mathbf{v}_2 \\ \vdots \\ \mathbf{v}_K \end{bmatrix} \tag{2.103}$$

where $\mathbf{v}_1,\ldots,\mathbf{v}_K$ are equal size column vectors. The $vec(.)$ operator is used to re-defined (2.101) as:

$$\boldsymbol{x}(k) \quad = \quad vec(\mathbf{X}(k)) \quad = \quad \begin{bmatrix} \mathbf{x}(k) \\ \mathbf{x}(k\text{-}1) \\ \vdots \\ \mathbf{x}(k-K_f) \end{bmatrix} \quad = \quad \begin{bmatrix} \begin{bmatrix} x_1(k) \\ \vdots \\ x_N(k) \end{bmatrix} \\ \begin{bmatrix} x_1(k\text{-}1) \\ \vdots \\ x_N(k\text{-}1) \end{bmatrix} \\ \vdots \\ \begin{bmatrix} x_1(k-K_f) \\ \vdots \\ x_N(k-K_f) \end{bmatrix} \end{bmatrix}_{\in N(K_f+1)\times 1} \tag{2.104}$$

which can also be conveniently expressed as:

$$\boldsymbol{x}(k) = \sum_{m=1}^{M} \bar{\mathbf{H}}_m \bar{\mathbf{s}}_m(k) + \boldsymbol{n}(k) \tag{2.105}$$

where the extended sequence of symbols from the m^{th} transmitter is expressed as:

$$\bar{\mathbf{s}}_m(k) = \begin{bmatrix} s_m(k) \\ s_m(k\text{-}1) \\ \vdots \\ s_m(k-L-K_f) \end{bmatrix} \tag{2.106}$$

and the block Toeplitz channel matrix with $N(K_f+1)$ rows and $L+K_f+1$ columns is expressed as:

$$\bar{\mathbf{H}}_m = \begin{bmatrix} \mathbf{H}_m & \cdots & 0 \\ & \ddots & \\ 0 & \cdots & \mathbf{H}_m \end{bmatrix} \tag{2.107}$$

Also, the noise vector in (2.75) can be viewed as:

$$n(k) \;=\; vec\Big(\big[\mathbf{n}(k) \quad \mathbf{n}(k-1) \quad \cdots \quad \mathbf{n}(k-K_f)\big]\Big) \tag{2.108}$$

In order to show the finding of weights in $\mathbf{W}_m$ (according to some performance criteria, e.g. MMSE), the *vec*(.) operator is used on $\mathbf{W}_m$ such that $w_m = vec\,(\mathbf{W}_m)$ as:

$$w_m(k) \;=\; vec(\mathbf{W}_m(k)) \;=\; \begin{bmatrix} \omega_m(0) \\ \omega_m(1) \\ \vdots \\ \omega_m(K_f) \end{bmatrix} \;=\; \begin{bmatrix} \begin{bmatrix} \omega_{1m}(0) \\ \vdots \\ \omega_{Nm}(0) \end{bmatrix} \\ \begin{bmatrix} \omega_{1m}(1) \\ \vdots \\ \omega_{Nm}(1) \end{bmatrix} \\ \vdots \\ \begin{bmatrix} \omega_{1m}(K_f) \\ \vdots \\ \omega_{Nm}(K_f) \end{bmatrix} \end{bmatrix}_{\in N(K_f+1)\times 1} \tag{2.109}$$

Using $x(k)$ in (2.104) and w_m in (2.109), the output in (2.102) can be re-written as:

$$y_m(k) \;=\; w_m^{\mathsf{H}}\; x(k) \tag{2.110}$$

Note that the elements in $x(k)$ are also serve as the input to the feedforward filter of the MIMO equaliser. Next, the weights in w_m can be obtained by using the MMSE Wiener-Hopf solution [107] (refer to section 3.2.1 for MMSE Wiener solution), which minimise the following:

$$E\left|y_m(k) - s_m(k-d)\right|^2 \tag{2.111}$$

where 'd' is the decision delay parameter. Subsequently, w_m can be determined as:

$$w_m = R^{-1} p_m \tag{2.112}$$

where $\boldsymbol{R}$ is the auto-correlation matrix of the MIMO equaliser's tap-input, $x(k)$, as:

$$\boldsymbol{R} \;=\; E\Big[x(k)\, x^{\mathsf{H}}(k)\Big] \;=\; \frac{P_T}{M}\left[\sum_{i=1}^{M} \bar{\mathbf{H}}_i\, \bar{\mathbf{H}}_i^{\mathsf{H}} + \sigma^2 \mathbf{I}\right] \tag{2.113}$$

and p_m is the cross-correlation matrix between the tap-input $x(k)$ and the m^{th} stage desired data stream, $s_m(k\text{-}d)$, which is defined as:

$$p_m \;=\; E\Big[x(k)\, s_m^{*}(k-d)\Big] \;=\; \frac{P_T}{M}\Big[\big(\bar{\mathbf{H}}_m\big)_{d+1}\Big] \tag{2.114}$$

where $(.)_{d+1}$ indicates the $(d+1)^{th}$ column of the corresponding matrix. The decision delay 'd' is vital that determines the 'delay' in decision taken during the detection before a detected symbol (from the m^{th} detected data stream) can be considered valid, thus affecting the overall system performance. It is normally set to 'half' of the column size of $\bar{\mathbf{H}}_m$ in (2.107) and assumed to be identical for all stages. Also note that both (2.113) and (2.114) eventually resort to utilize $\bar{\mathbf{H}}$.

2.6.3 MIMO-Decision Feedback Equalisation – MIMO-DFE [45, 47]

The decision feedback unit can be incorporated with the MIMO equaliser to become the so-called MIMO-decision feedback equaliser (MIMO-DFE), which attempts to eliminate the post-cursor ISI of the previous detected symbols [45] in order to further improve the performance of the MIMO system. The fully connected MIMO-DFE filter is shown in figure 2.19 below:

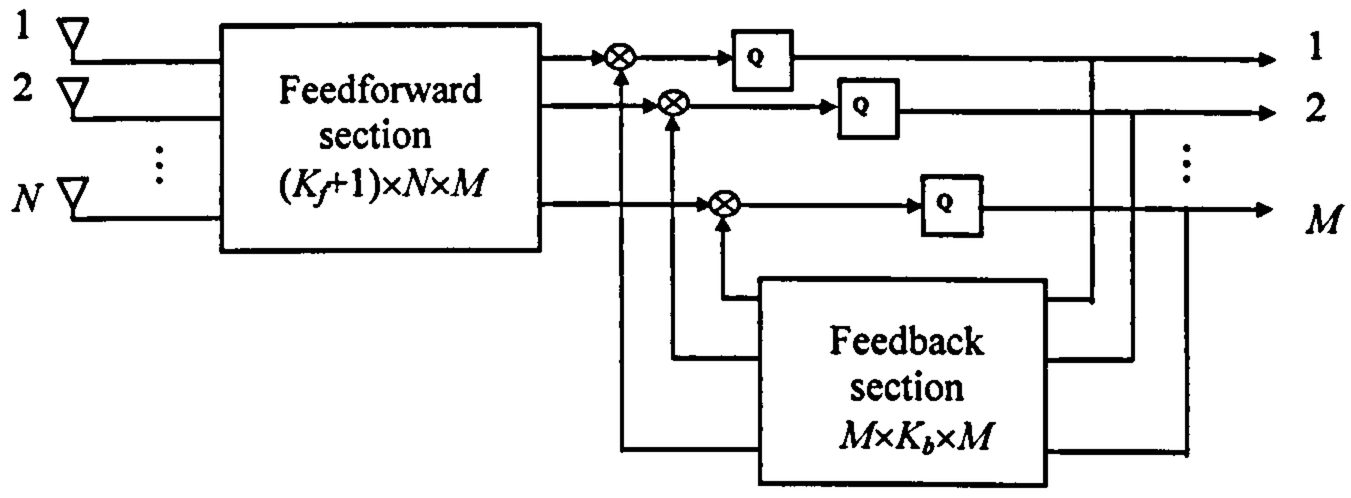

Figure 2.19: Fully connected MIMO-DFE structure

The MIMO-DFE contains the M stages of feedback weighting matrices, denoted as $\mathbf{B}_m$, and each feedback path has K_b feedback taps. For each $\mathbf{B}_m$, the past decisions on all M stages detect the data stream that is fed back to subtract itself from the feedforward detection process for each stream. Each feedback weighting matrix, $\mathbf{B}_m$ with the size of $K_b \times M$, can be expressed as:

$$\begin{aligned}\mathbf{B}_m &= \begin{bmatrix} \beta_{1m} & \cdots & \beta_{Mm} \end{bmatrix} \\ &= \begin{bmatrix} b_{1m}(1) & \cdots & b_{Mm}(1) \\ \vdots & \cdots & \vdots \\ b_{1m}(K_b) & \cdots & b_{Mm}(K_b) \end{bmatrix}\end{aligned} \tag{2.115}$$

Note that K_b taps are needed so that sufficient past detected symbols is considered for cancellation of the entire previous ISI span. To facilitate the MIMO-DFE, the following terms are introduced. The sequence of K_b most recent decisions on every stream is labelled as:

$$\hat{\mathbf{s}}_m(k-d-1) = \begin{bmatrix} \hat{s}_m(k-d-1) \\ \vdots \\ \hat{s}_m(k-d-K_b) \end{bmatrix}; \quad m = 1 \text{ to } M \tag{2.116}$$

where d is the same decision delay parameter. Similarly, $\hat{\mathbf{s}}_m$ in (2.116) can be grouped as:

$$\begin{aligned}\hat{\mathbf{S}}(k-d-1) &= \begin{bmatrix} \hat{\mathbf{s}}_1(k-d-1) & \cdots & \hat{\mathbf{s}}_M(k-d-1) \end{bmatrix} \\ &= \begin{bmatrix}\begin{bmatrix} \hat{s}_1(k-d-1) \\ \vdots \\ \hat{s}_1(k-d-K_b) \end{bmatrix} & \cdots & \begin{bmatrix} \hat{s}_M(k-d-1) \\ \vdots \\ \hat{s}_M(k-d-K_b) \end{bmatrix}\end{bmatrix}\end{aligned} \tag{2.117}$$

Now, with both the feedforward matrix $\mathbf{W}_m$ from (2.107) and the feedback matrix $\mathbf{B}_m$ from (2.115), together with $\mathbf{X}(k)$ from (2.101) and $\hat{\mathbf{S}}(k\text{-}d\text{-}1)$ from (2.117), the output of each m^{th} stage decision feedback equalisation process, $y_m(k)$, can be re-expressed as follows:

$$y_m(k) = \text{trace}\left\{ \mathbf{W}_m^{\mathsf{H}} \ \mathbf{X}(k) \right\} - \text{trace}\left\{ \mathbf{B}_m^{\mathsf{H}} \ \hat{\mathbf{S}}(k-d-1) \right\} \tag{2.118}$$

$$=\text{tr}\left\{\begin{bmatrix} \omega_{1m}^*(0) & \cdots & \omega_{Nm}^*(0) \\ \vdots & \vdots & \vdots \\ \omega_{1m}^*(K_f) & \cdots & \omega_{Nm}^*(K_f) \end{bmatrix}\begin{bmatrix} x_1(k) & \cdots & x_1(k-K_f) \\ \vdots & \cdots & \vdots \\ x_N(k) & \cdots & x_N(k-K_f) \end{bmatrix}\right\} - \text{tr}\left\{\begin{bmatrix} b_{1m}^*(1) & \cdots & b_{1m}^*(K_b) \\ \vdots & \vdots & \vdots \\ b_{Mm}^*(1) & \cdots & b_{Mm}^*(K_b) \end{bmatrix}\begin{bmatrix} \hat{s}_1(k-d-1) & \cdots & \hat{s}_M(k-d-1) \\ \vdots & \cdots & \vdots \\ \hat{s}_1(k-d-K_b) & \cdots & \hat{s}_M(k-d-K_b) \end{bmatrix}\right\}$$

The $vec(.)$ operator is used on (2.115) and (2.117) to produce the equivalent expressions that facilitate weights finding for a MIMO-DFE. First, the long vector $\boldsymbol{b}_m$ is produced from $\mathbf{B}_m$ as:

$$\boldsymbol{b}_m = vec(\mathbf{B}_m) = \begin{bmatrix} \boldsymbol{\beta}_{1m} \\ \vdots \\ \boldsymbol{\beta}_{Mm} \end{bmatrix} = \begin{bmatrix}\begin{bmatrix} b_{1m}(1) \\ \vdots \\ b_{1m}(K_b) \end{bmatrix} \\ \vdots \\ \begin{bmatrix} b_{Mm}(1) \\ \vdots \\ b_{Mm}(K_b) \end{bmatrix}\end{bmatrix}_{\in M(K_b)\times 1} \tag{2.119}$$

Secondly, the long vector $\hat{\boldsymbol{s}}(k-d-1)$ is produced from $\hat{\mathbf{S}}(k-d-1)$ as follows:

$$\hat{\boldsymbol{s}}(k-d-1) = vec(\hat{\mathbf{S}}(k-d-1)) = \begin{bmatrix} \hat{\mathbf{s}}_1(k-d-1) \\ \vdots \\ \hat{\mathbf{s}}_M(k-d-1) \end{bmatrix} = \begin{bmatrix}\begin{bmatrix} \hat{s}_1(k-d-1) \\ \vdots \\ \hat{s}_1(k-d-K_b) \end{bmatrix} \\ \vdots \\ \begin{bmatrix} \hat{s}_M(k-d-1) \\ \vdots \\ \hat{s}_M(k-d-K_b) \end{bmatrix}\end{bmatrix}_{\in M(K_b)\times 1} \tag{2.120}$$

Therefore, using the input $\boldsymbol{x}(k)$ in (2.104) and feedforward $\boldsymbol{w}_m$ in (2.109) together with the long vectors $\boldsymbol{w}_m$ and $\hat{\boldsymbol{s}}(k-d-1)$ in both (2.119) and (2.120) respectively, the m^{th} stage output of the MIMO-DFE in (2.118) can be re-written as:

$$
\begin{aligned}
y_m(k) &= w_m^{\mathsf{H}}\, x(k) - b_m^{\mathsf{H}}\, \hat{s}_m(k-d-1) \\
&= \begin{bmatrix} w_m \\ b_m \end{bmatrix}^{\mathsf{H}} \begin{bmatrix} x(k) \\ -\hat{s}_m(k-d-1) \end{bmatrix}
\end{aligned} \tag{2.121}
$$

where the feedforward and feedback filter's weights in the MIMO-DFE can be achieved by using the MMSE Wiener-Hopf solution as:

$$
\begin{bmatrix} w_m \\ b_m \end{bmatrix} = R^{-1} p_m \tag{2.122}
$$

Note that the MMSE is used in the same way as in (2.112) except that now the feedback weights are provided. Hence, the resulting R and p_m also become slightly altered as:

$$
R = E\left(\begin{bmatrix} x(k) \\ -\hat{s}_m(k-d-1) \end{bmatrix} \begin{bmatrix} x(k) \\ -\hat{s}_m(k-d-1) \end{bmatrix}^{\mathsf{H}} \right) \tag{2.123}
$$

$$
= \frac{P_T}{M} \begin{bmatrix}
\sum_{i=1}^{M} \bar{\mathbf{H}}_i \bar{\mathbf{H}}_i^{\mathsf{H}} + \sigma^2 \mathbf{I} & -\left(\bar{\mathbf{H}}_1\right)_{d+2\ldots d+K_b+1} & \cdots & -\left(\bar{\mathbf{H}}_M\right)_{d+2\ldots d+K_b+1} \\
-\left(\bar{\mathbf{H}}_1\right)^{\mathsf{H}}_{d+2\ldots d+K_b+1} & \mathbf{I} & \cdots & \mathbf{0} \\
\vdots & \vdots & \ddots & \vdots \\
-\left(\bar{\mathbf{H}}_M\right)^{\mathsf{H}}_{d+2\ldots d+K_b+1} & \mathbf{0} & \cdots & \mathbf{I}
\end{bmatrix}
$$

and $$p_m = E\begin{bmatrix} x(k) \\ -\hat{s}_m(k-d-1) \end{bmatrix} s_m^*(k-d) = \frac{P_T}{M} \begin{bmatrix} \left(\bar{\mathbf{H}}_m\right)_{d+1} \\ \mathbf{0} \end{bmatrix} \tag{2.124}$$

where $(.)_{d+1\ldots\, d+K_b+1}$ in (2.123) indicates columns d+1 to d+K_b+1 and $(.)_{d+1}$ in (2.124) indicate the $(d+1)^{\text{th}}$ column of the corresponding matrix. Note that both (2.123) and (2.124) also eventually resort to utilize the block Toeplitz channel matrix, $\bar{\mathbf{H}}$.

Although the solutions in (2.110) and (2.121) show only single output detection for a symbol, the entire data stream will be detected using the same weighting matrix w_m and b_m obtained under the assumption that the channel stays constantly throughout the burst. (Further discussions for the time-varying channels will be given in the results part of Chapter 5 later). Also, it must be stressed that the analysis of DFEs is difficult due to their inherent nonlinear nature. In order to 'linearise' the above formulation for the MIMO-DFE, the past decisions in detection of $\hat{s}(k-d-1)$ are assumed to be correct, in which MMSE solution may be formulated [47]. Since the impact of error propagation might be important, computer simulations are used to access the relative behaviour of the MIMO-DFE and the OSIC receivers for performance evaluation.

2.6.4 Order Successive Interference Cancellation (OSIC) [47]

The MIMO-DFE can be extended to incorporate the 'ordered successive interference cancellation' (OSIC) scheme to become a MIMO-OSIC-DFE receiver in order to further improve the performance of the MIMO systems. Unlike MIMO-DFE, the OSIC-DFE structure detects each data stream on an ordered basis where the detections are divided into M successive stages instead of a single 'one-go' detection process for all the M data streams. Depending on which version of OSIC-DFE, the weighting matrices, w_m and b_m. are obtained at each stage for the chosen data stream [47]. Figure 2.20 shows the difference between MIMO-DFE (on the left) and OSIC-DFE (on the right) where the detection is assumed to start in an ascending order of the data stream in space. The example depicts the detection process at the time of extracting the symbol marked with 'O'. Symbols marked with '×' have already been detected and cancelled.

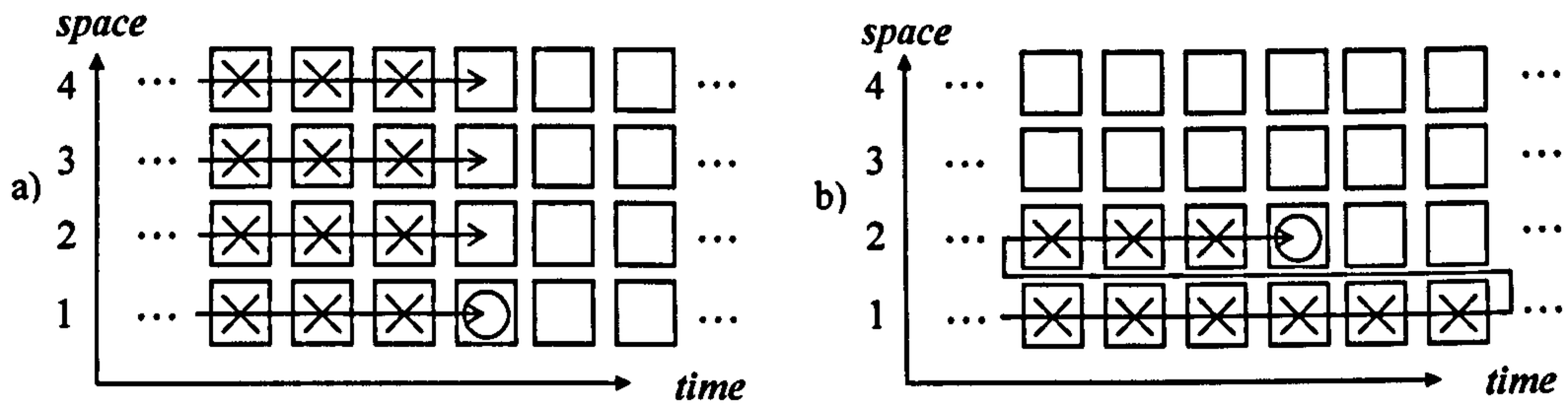

Figure 2.20: Detection strategy in space-time plane.

In MIMO-DFE, only decisions on temporally preceding symbols are fed back into the detection process of each stream. Therefore, CCI contribution from undetected future and on-time symbols are not cancelled. Only the ISI contribution from the detected symbols is removed by the DFE. However, in the OSIC-DFE, the data streams are successively detected and each stream is detected with the entire CCI contribution from every previously detected stream already cancelled out. The detection ordering is organised so that stronger streams, which is more resilient to interference, are detected earlier in the process in order to assist the weaker streams to be detected more reliably later. As a result, the overall performance may improve remarkably. Next, two different structures of OSIC-DFE are introduced here as 1) the partially connected OSIC-DFE and 2) the fully connected OSIC-DFE, which are natural extension of the V-BLAST.

2.6.4.1 Partially Connected MIMO-OSIC-DFE [47]

The partially connected MIMO-OSIC-DFE consists of M successive stages, each having a feedforward filter **W** with temporal span of $K_f + 1$ taps per receive antenna and a feedback filter **b** with temporal span of K_b taps. Hence, every $(K_f + 1, K_b)$ stage resembles a multiple-input single-output (MISO) DFE. The 'partially connected' structure means that only the chosen detected data

stream is fed back into the interference cancellation process at each stage. The first two stages of the partially connected MIMO-OSIC-DFE structure are shown in figure 2.21.

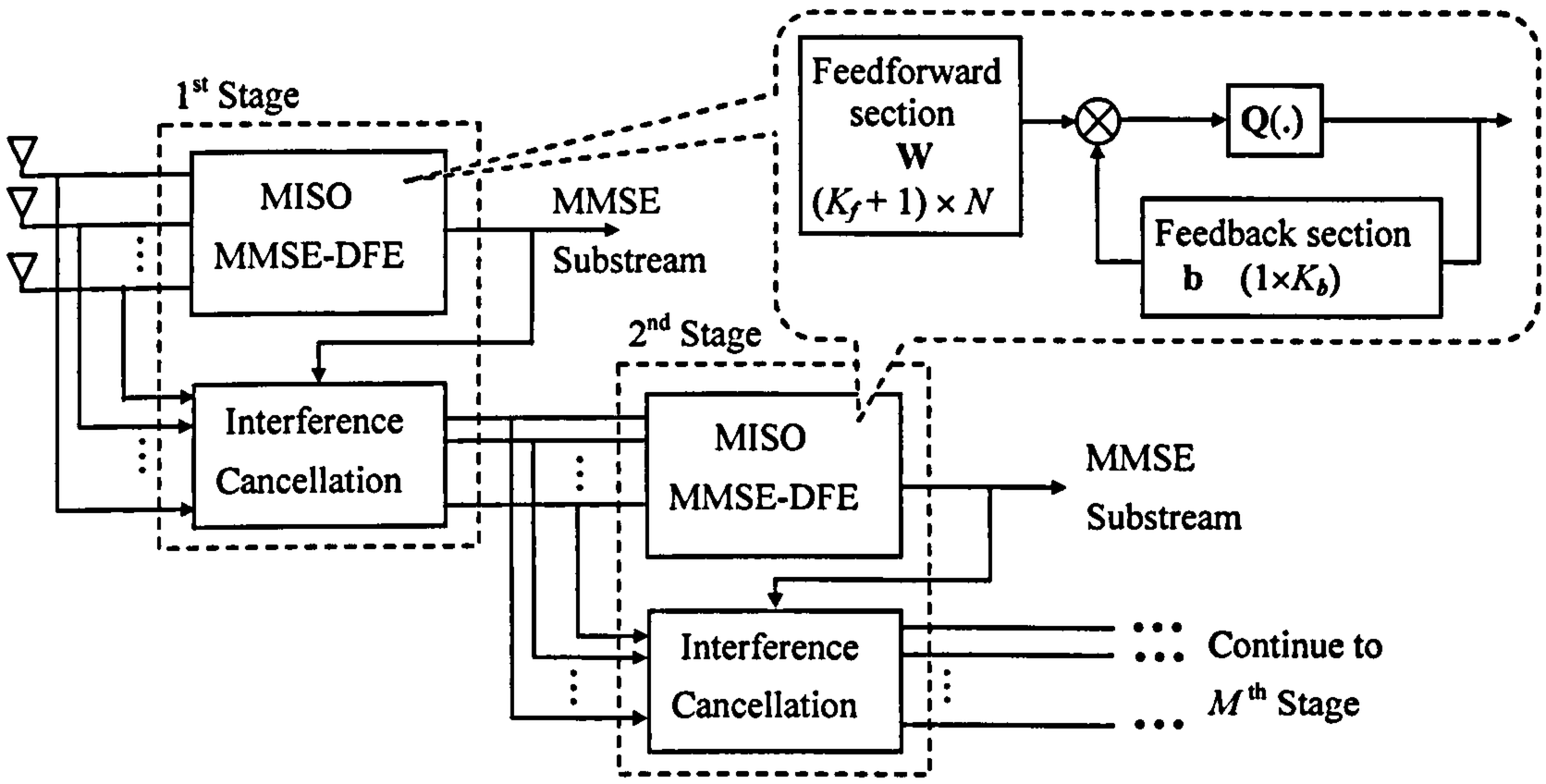

Figure 2.21: Partially connected MIMO-OSIC-DFE structure

At each stage, the 'best' data stream (in the MMSE sense) is detected and cancelled out. Since the receiver only needs to deal with a single data stream at each stage, the MISO-DFE structure consists only a *single set* of feedforward **W** and feedback **b**, with lower computational complexity compared to the fully connected MIMO-OSIC-DFE (discuss later). The formulation of partially connected MIMO-OSIC-DFE together with the OSIC feature will be explained next.

The input signals to the MISO-DFE is $x(k) = vec\,(\mathbf{X}(k))$ as stated in (2.104) earlier. Since the DFE's structure is only partially connected, the sequence of K_b most recently decisions produced by that stage are similar to (2.116) as:

$$\hat{\mathbf{s}}_m(k-d-1) = \begin{bmatrix} \hat{s}_m(k-d-1) \\ \vdots \\ \hat{s}_m(k-d-K_b) \end{bmatrix}; \quad m = 1 \text{ to } M \tag{2.125}$$

which constitutes the input to the corresponding feedback filter.

The feedforward filter $\mathbf{W}_m$ at each stage will have the same setting as (2.100), whereas the feedback filter $\mathbf{b}_m$ is now one of the column vector $\boldsymbol{\beta}$ extracted from (2.115), according to the chosen stream. Thus, the output at each stage for stream m can be re-expressed as:

$$y_m(k) = \text{trace}\left\{ \mathbf{W}_m^{\mathsf{H}}\ \mathbf{X}(k) \right\} \ - \ \mathbf{b}_m^{\mathsf{H}}\ \hat{\mathbf{s}}_m(k-d-1) \tag{2.126}$$

$$= \text{trace}\left\{ \begin{bmatrix} \omega_{1m}^*(0) & \cdots & \omega_{Nm}^*(0) \\ \vdots & \vdots & \vdots \\ \omega_{1m}^*(K_f) & \cdots & \omega_{Nm}^*(K_f) \end{bmatrix} \begin{bmatrix} x_1(k) & \cdots & x_1(k-K_f) \\ \vdots & \cdots & \vdots \\ x_N(k) & \cdots & x_N(k-K_f) \end{bmatrix} \right\} - \begin{bmatrix} b_m^*(1) & \cdots & b_m^*(K_b) \end{bmatrix} \begin{bmatrix} \hat{s}_m(k-d-1) \\ \vdots \\ \hat{s}_m(k-d-K_b) \end{bmatrix}$$

Note that there is only one feedback path at each stage and its input is the selected data stream. Every undetected stream is a candidate for selection. Using the same operation as $w_m = vec(\mathbf{W}_m)$, the output in (2.126) is equivalent to the following expression as:

$$\begin{aligned} y_m(k) &= w_m^{\mathsf{H}}\, x(k) - \mathbf{b}_m^{\mathsf{H}}\, \hat{\mathbf{s}}_m(k-d-1) \\ &= \begin{bmatrix} w_m \\ \mathbf{b}_m \end{bmatrix}^{\mathsf{H}} \begin{bmatrix} x(k) \\ -\hat{\mathbf{s}}_m(k-d-1) \end{bmatrix} \end{aligned} \tag{2.127}$$

Assuming correct decisions at all stages, the MMSE Wiener-Hopf solution for w_m and $\mathbf{b}_m$ is:

$$\begin{bmatrix} w_m \\ b_m \end{bmatrix} = R_m^{-1} p_m \tag{2.128}$$

with the m^{th} stage auto-correlation matrix R_m given as:

$$R_m = E\left(\begin{bmatrix} x(k) \\ -\mathbf{s}_m(k-d-1) \end{bmatrix} \begin{bmatrix} x(k) \\ -\mathbf{s}_m(k-d-1) \end{bmatrix}^{\mathsf{H}} \right) \tag{2.129}$$

$$= \frac{P_T}{M} \begin{bmatrix} \sum_{i=1}^{M} \bar{\mathbf{H}}_i \bar{\mathbf{H}}_i^{\mathsf{H}} + \sigma^2 \mathbf{I} & -\left(\bar{\mathbf{H}}_m\right)_{d+2\ldots d+K_b+1} \\ -\left(\bar{\mathbf{H}}_m\right)^{\mathsf{H}}_{d+2\ldots d+K_b+1} & \mathbf{I} \end{bmatrix}$$

and the m^{th} stage cross-correlation matrix p_m given as:

$$p_m = E\begin{bmatrix} x(k) \\ -\mathbf{s}_m(k-d-1) \end{bmatrix} s_m^*(k-d) = \frac{P_T}{M} \begin{bmatrix} \left(\bar{\mathbf{H}}_m\right)_{d+1} \\ \mathbf{0} \end{bmatrix} \tag{2.130}$$

where $(.)_{d+1}$ also indicates the $(d+1)^{\text{th}}$ column of the corresponding $\bar{\mathbf{H}}_m$. The resulting R_m in (2.129) is less complex compared to R in (2.123) since it is required only to deal with one stage at a time in the partially connected OSIC-DFE whereas all the M stages are required in the MIMO-DFE. Nevertheless, R_m needs to be computed M times in the OSIC-DFE in order to carry out the detections for all the M stages. However, the resulting p_m in (2.130) is equivalent to the one in (2.124) due only to the cross-correlation between the tap-input $x(k)$ and the m^{th} stage desired data stream, $s_m(k-d)$, that leads both equations to become identical eventually.

2.6.4.2 The Interference Cancellation Scheme [47]

The OSIC-DFE receiver is more powerful algorithm due to its SIC feature, which is capable of not only removing the ISI contribution due to the frequency-selective nature but also removing the CCI contribution from each multiple transmit antenna. The arrangement of M stages in OSIC-DFE structure now becomes useful since the removal of both interferences can be viewed clearly at each stage where ISI is internally removed by the DFE at each stage and CCI from the detected data stream is externally cancelled out by the OSIC feature at each stage.

The selection criterion for which data stream to be detected and subsequently cancelled out is according to the MMSE criteria where the MSE for each stream m can be found as:

$$E\left|y_m(k)-s_m(k-d)\right|^2 \;=\; 1-p_m^{\mathsf{H}}R_m^{-1}p_m \tag{2.131}$$

where R_m and p_m can be obtained from (2.129) and (2.130) respectively. The undetected stream with the *smallest* MSE will be selected at every stage and extracted using the w_m and $\mathbf{b}_m$ settings defined by (2.128). Once the stream has been detected, its interference contribution can be removed from the input signal $x(k)$ as follows:

$$\begin{aligned}
\mathbf{x}(k) &\leftarrow \mathbf{x}(k)-(\mathbf{H}_m)_1\,\hat{s}_m(k)\\
\mathbf{x}(k+1) &\leftarrow \mathbf{x}(k+1)-(\mathbf{H}_m)_2\,\hat{s}_m(k)\\
&\vdots\\
\mathbf{x}(k+L) &\leftarrow \mathbf{x}(k+L)-(\mathbf{H}_m)_{L+1}\,\hat{s}_m(k)
\end{aligned} \tag{2.132}$$

where $(.)_g$ indicates the g^{th} column of $\mathbf{H}_m$. Notice that, since the channel response spans for $(L+1)$ symbols, the interference arising from $s_m(k)$ has to be cancelled from $(L+1)$ consecutive entries. For illustration, consider the basic m channel matrix with CIR of $(L+1)=3$ as:

$$\begin{aligned}
\mathbf{H}_m &= \begin{bmatrix} (\mathbf{H}_m)_1 & (\mathbf{H}_m)_2 & (\mathbf{H}_m)_3 \end{bmatrix}\\
&= \begin{bmatrix} \begin{bmatrix} h_{1m}(0)\\ \vdots\\ h_{Nm}(0)\end{bmatrix} & \begin{bmatrix} h_{1m}(1)\\ \vdots\\ h_{Nm}(1)\end{bmatrix} & \begin{bmatrix} h_{1m}(2)\\ \vdots\\ h_{Nm}(2)\end{bmatrix}\end{bmatrix}, \quad m=1,2,\ldots,M.
\end{aligned} \tag{2.133}$$

Note that again, $(\mathbf{H}_m)_g$ signifies the g^{th} column vector of the channel matrix $\mathbf{H}_m$.

Given the corresponding data streams: $s_m(a)$, $s_m(b)$, $s_m(c)$, $s_m(d)$, $s_m(e)$, $s_m(f)$, $s_m(g)$, where $s_m(a)$ being the first symbol; the transmit vectors $\mathbf{s}_m(t)$ at time t can be collected as follows:

$$\begin{aligned}
\mathfrak{I}_m(\tau) &= \begin{bmatrix} \mathbf{s}_m(0) & \mathbf{s}_m(1) & \mathbf{s}_m(2) & \mathbf{s}_m(3) & \mathbf{s}_m(4) & \cdots \end{bmatrix}\\
&= \begin{bmatrix} \begin{bmatrix} s_m(c)\\ s_m(b)\\ s_m(a)\end{bmatrix} & \begin{bmatrix} s_m(d)\\ s_m(c)\\ s_m(b)\end{bmatrix} & \begin{bmatrix} s_m(e)\\ s_m(d)\\ s_m(c)\end{bmatrix} & \begin{bmatrix} s_m(f)\\ s_m(e)\\ s_m(d)\end{bmatrix} & \begin{bmatrix} s_m(g)\\ s_m(f)\\ s_m(e)\end{bmatrix} & \cdots \end{bmatrix}
\end{aligned} \tag{2.134}$$

Thus, from (2.133) and (2.134), the so-called 'forward grouped received signal matrix' as:

$$\begin{aligned}
\aleph(\tau) &= \sum_{m=1}^{M}\mathbf{H}_m\,\mathfrak{I}_m(\tau)\\
&= \begin{bmatrix} \mathbf{x}(k) & \mathbf{x}(k+1) & \mathbf{x}(k+2) & \mathbf{x}(k+3) & \mathbf{x}(k+4) & \cdots \end{bmatrix}
\end{aligned} \tag{2.135}$$

Now, suppose that $s_m(c)$ has been detected correctly and it is now going through the interference cancellation in (2.132). It can be noticed that the symbol $s_m(c)$ only existed in the first 3 columns of (2.135), which is in $\mathbf{x}(k)$, $\mathbf{x}(k+1)$ and $\mathbf{x}(k+2)$ respectively. Their detailed interaction with each column vector of the basic channel matrix is shown in the following:

$$\left[\mathbf{x}(k) \quad \mathbf{x}(k+1) \quad \mathbf{x}(k+2)\right] = \left[(\mathbf{H}_m)_1 \quad (\mathbf{H}_m)_2 \quad (\mathbf{H}_m)_3\right]\left[\mathbf{s}_m(0) \quad \mathbf{s}_m(1) \quad \mathbf{s}_m(2)\right] \tag{2.136}$$

$$= \begin{bmatrix} \begin{bmatrix} h_{1m}(0) \\ \vdots \\ h_{Nm}(0) \end{bmatrix} & \begin{bmatrix} h_{1m}(1) \\ \vdots \\ h_{Nm}(1) \end{bmatrix} & \begin{bmatrix} h_{1m}(2) \\ \vdots \\ h_{Nm}(2) \end{bmatrix} \end{bmatrix} \begin{bmatrix} \begin{bmatrix} s_m(c) \\ s_m(b) \\ s_m(a) \end{bmatrix} & \begin{bmatrix} s_m(d) \\ s_m(c) \\ s_m(b) \end{bmatrix} & \begin{bmatrix} s_m(e) \\ s_m(d) \\ s_m(c) \end{bmatrix} \end{bmatrix}$$

It can be seen that, due to the characteristic of frequency selectivity, $s_m(c)$ has been echoed in $\mathbf{s}_m(0)$, $\mathbf{s}_m(1)$, $\mathbf{s}_m(2)$, in the positions that successively interact with each column vectors $(\mathbf{H}_m)_1$, $(\mathbf{H}_m)_2$, $(\mathbf{H}_m)_3$, of the channel matrix $\mathbf{H}_m$. The 'interference' of $s_m(c)$ is cancelled out accordingly from the respective $\mathbf{x}(k)$, $\mathbf{x}(k+1)$ and $\mathbf{x}(k+2)$ in an order using (2.132). Note in (2.132) that the increments of the both vector $\mathbf{x}(k)$ and $(\mathbf{H}_m)$ in each line, are only attained until $(L+1)$.

It is important to realise that having the incorrect estimate in (2.132) might leads to another error propagation problem that arises from the OSIC feature, which might worsen the performance. This resembles another nonlinear issue, which resorts to computer simulation for performance evaluation. Lastly, take note that the OSIC scheme in (2.132) also requires the knowledge of the basic channel matrix, $\mathbf{H}_m$.

2.6.4.3 Fully Connected MIMO-OSIC-DFE [47]

The fully connected MIMO-OSIC-DFE is similar to the partially connected version except that MIMO-DFE is used at each M stages instead of MISO-DFE. The first two stages of the fully connected MIMO-OSIC-DFE's structure are shown in figure 2.22 below.

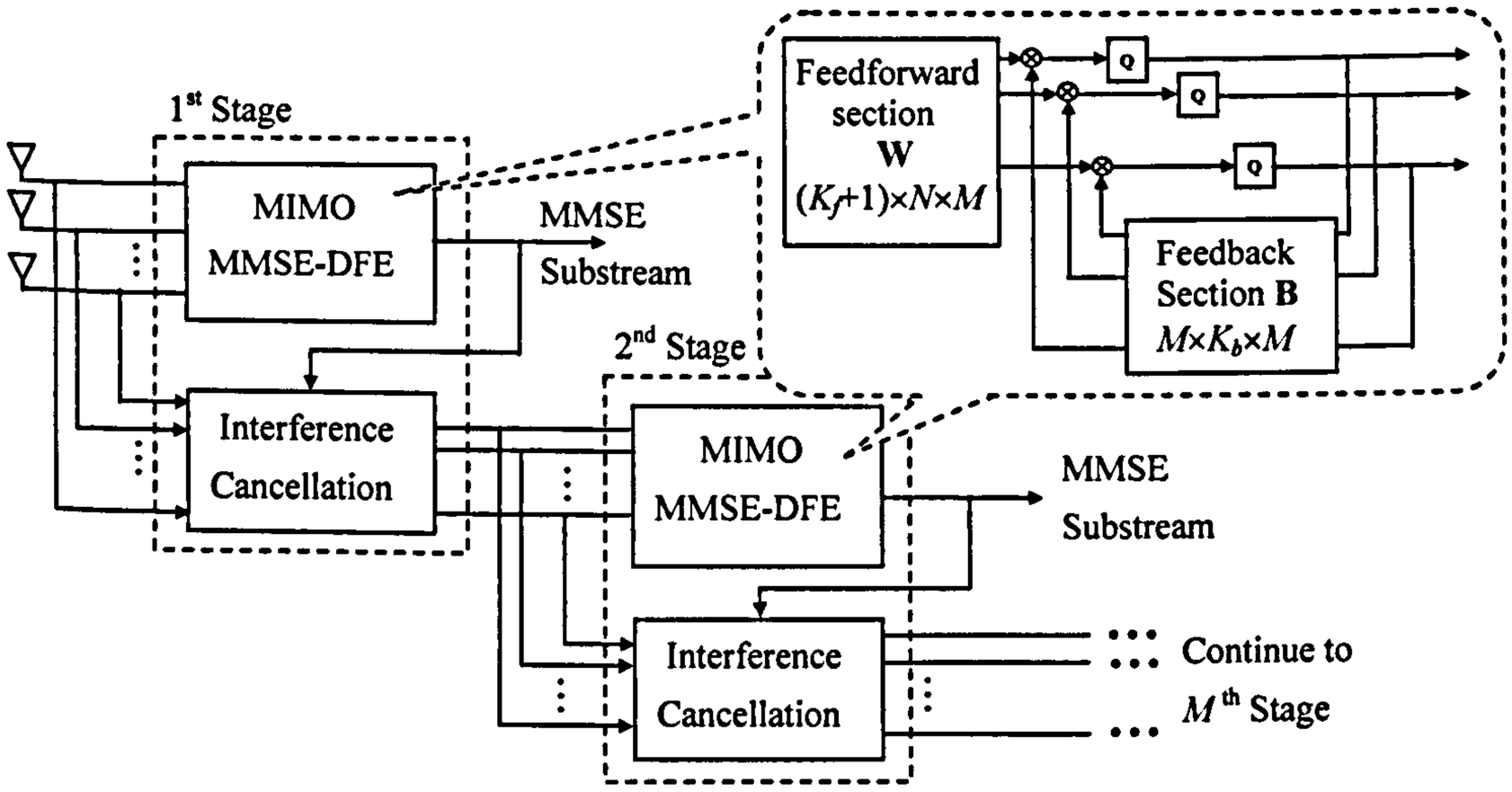

Figure 2.22: Fully connected MIMO-OSIC-DFE's structure

Using the same $(K_f + 1, K_b)$ configuration for its feedforward and feedback filter, every stage consists of $(K_f + 1) \times N \times M$ feedforward taps and $M \times K_b \times M$ feedback taps. Same as the

partially connected case, the M stages are ordered so that the data streams are extracted and decoded in sequence of decreasing MSE. However, unlike the partially connected receiver, all M streams (instead of only one stream) are implicitly decoded within every stage and their symbol decisions fed back internally. Only the stream selected by the ordering algorithm at every stage is retained while others are discarded and decoded again in a later stage.

Thus, the potential advantage of the fully connected receiver arises from having more powerful feedback section within every stage. At the same time, this enhancement is also a potential drawback because it makes the receiver more vulnerable to error propagation, in particular given that potentially unreliable decisions of weaker streams are utilised to estimate the symbols of stronger streams. Since the MIMO-DFE was formulated and shown previously, it will not be repeated here. The extension to the fully-connected OSIC-DFE is straightforward cascade of M such identical structures.

2.7 The Importance of Channel Estimation

Channel estimation plays a vital role in any wireless communication systems in order to reliably recover all the transmission data. Without this feature, the entire communication might collapse if the channel, in which the transmitted data had travelled through, has not been known. It has been demonstrated that the MIMO algorithms described in the previously in this chapter, (especially the BLAST version and the MIMO-OSIC-DFE receivers) have assumed perfect knowledge of the channel to carry out the respective signal detection process via the successive interference cancellation (SIC) scheme and the MIMO equalisation process. All these processing connected to the necessity of channel information are shown in the following:

In the V-BLAST receiver model, the ZF detection algorithm shown in (2.71) requires the channel matrix **H** to obtain its weighting matrix **W** by means of inverting **H**. Whereas, the MMSE detection shown in (2.72) and (2.73) uses the auto-correlation of the channel matrix as well as its cross-correlation to process the signals. The SIC feature shown in (2.76) also acquire the corresponding channel path to perform the interference cancellation process.

In the proposed QR detection technique, channel information is required for a) channel matrix re-arrangement process in (2.86), b) QR decomposition of the re-arranged channel matrix in (2.87) where the corresponding triangular matrix $\mathbf{R}_{new}$ is obtained in (2.88) and c) the QR detection process for linear case in (2.92) where $\mathbf{R}_{new}$ (that relates to the channel) is used in the backward substitution process.

In the frequency-selective case, the entire channel matrix that contains all CIRs is required to perform the MIMO equalisation process in (2.112), (2.113) and (2.114). Likewise for the MIMO-DFE case shown in (2.122), (2.123), (2.124). The need of accurate channel information in the MIMO-OSIC-DFE receivers is inevitably necessary a) for the recovery of each data stream shown in (2.128), (2.129) and (2.130) as well as b) the order successive interference cancellation – OSIC scheme in (2.131) & (2.132) for both the partially-connected and fully connected version.

Having appreciated the needs of the channel information in all the MIMO processes mentioned the channel must be known or estimated before these respective processes can be carried out. This can be done by incorporating suitable channel estimation scheme that could effectively estimate all path coefficients within each CIR of the MIMO channel. Therefore, the channel estimation scheme is an important component that obtains all necessary information of the MIMO channel characteristic, which necessitates all related processes in the MIMO systems.

2.8 Summary

In Chapter 2, the basic MIMO systems and the MIMO channel model have been introduced. The fundamentals and usefulness the space-time processing have been shown for its application in equalisation (space-only), beamforming (time-only) and the combination of both techniques (space-time). More specific MIMO systems, e.g. the BLAST architecture with the SIC feature has also been introduced to illustrate the MIMO processing capabilities. The modified version of the V-BLAST receiver with QR detection technique has also been presented for alternative solution of MIMO process. As a result, sub-optimum SIC-based MIMO detectors were successfully modelled and implemented, which incorporated proper detection ordering by the re-arrangement of the channel matrix prior to the QR decomposition process. By using this special feature of channel matrix rearrangement, the proposed QR detection method was found to approximate the performance of the conventional V-BLAST receiver.

The extended version of V-BLAST receiver into frequency-selective MIMO channel model, which is known as the MIMO-OSIC-DFE receivers, has also been discussed. Nevertheless, it is realised that channel information is essential for most of the MIMO processing algorithms and it must be acquired accurately for the practical use of MIMO systems, which can be accomplished by incorporating a suitable estimation scheme in the exiting MIMO receivers. In the next two chapters, various channel estimation schemes will be introduced and discussed for the application in the frequency-flat fading MIMO channel model (in Chapter 3) as well as the frequency-selective multipath fading MIMO channel model (in Chapter 4).

Chapter 3

Basic MIMO Channel Estimation

This chapter focuses on the basic MIMO channel estimation (MIMO-CE) methods for space-time communication systems operated in the frequency-flat fading channel. The incorporation of a suitable channel estimation scheme is essential since most of the space-time processors need the "best" knowledge of the MIMO channel to carry-out signal detections and processing. (e.g. the Successive Interference Cancellation scheme and MIMO Equalisation in Chapter 2). Conventional adaptive methods that have been commonly used in a SISO or SIMO system are extended to cater for channel estimation in the MIMO system. The Least Mean Squares (LMS) and Recursive Least Squares (RLS) algorithm will be discussed and developed for channel estimation scheme in the MIMO system, followed by the non-adaptive method, which uses the matrix inversion and orthogonal property. The Hadamard matrix structure will also be studied and utilised for designing the pilot matrix of the MIMO channel estimation.

3.1 Type of Channel Estimation Schemes

In general, the channel estimation can be categorized into two groups namely a) the data aided – training-based approach and b) the non-data aided – blind-estimation approach.

3.1.1 The Data Aided – Training-Based Channel Estimation

The data aided method make use of the 'pilot symbols' known *a priori* by the receiver to 'train' the channel by means of error measurement and weights adjustment based on "Least Squares" method. (Least Mean Square (LMS) and the Recursive Least Squares (RLS) [102–104] are the popular adaptively methods). Another type of data aided method uses non-adaptive approach, where block of pilot signals (in a matrix form) and the respective received pilot signals block are utilised to perform the channel estimation by means of matrix inversion. This is often referred as the maximum likelihood (ML) or linear minimum mean square error (LMMSE) estimator when orthogonal pilot sequences are used. (Details can be found in [11, 73, 83]).

3.1.2 The Non-data Aided – Blind Channel Estimation

The non-data aided approach trains the channel without the assistance of any pilot symbols or any codes, which usually known as the 'blind' algorithm. The blind methods make use of the knowledge of statistical signal's properties and structure to perform channel estimation. Among the famous blind algorithms is called "Constant Modulus Algorithm (CMA)" [105], which seeks to minimize error cost function. More sophisticated blind methods like higher order statistic method, second order statistic or subspace approach are becoming increasingly popular in the current research of the MIMO systems. [95, 96, 99, 106]. Nevertheless, the discussion of MIMO-CE methods in this thesis will only be focused on the non-blind channel estimation techniques rather than the blind methods.

3.2 Basic Adaptive Filtering Process

Before proceeding to the actual channel estimation algorithm, it is important to understand the concept of adaptive filtering. In this Section, the Wiener filtering process that leads to optimum solution is described, followed by the two general adaptive approaches, the least mean squares (LMS) algorithm and the recursive least squares (RLS) algorithm. Both methods eventually arrive or lead to the optimum Wiener solution. [104, 107].

The conventional adaptive method can be categorised into two basic discrete-time filter structures. The first structure is the transversal structure (or serial combiner), which is applied to the SISO model. The second structure is parallel combiner, which is applied to the SIMO model. Both structures will be shown in the following figure 3.1.

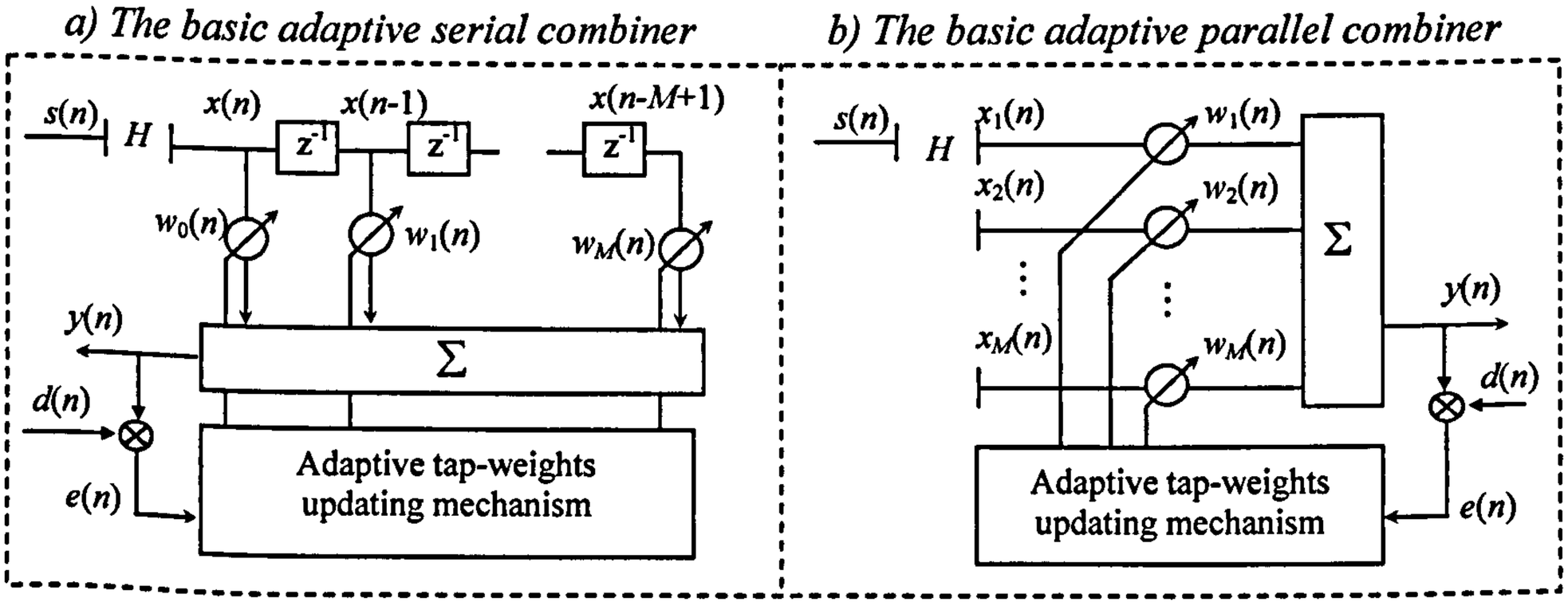

Figure 3.1: The basic adaptive filter structure a) The serial combiner & b) the parallel combiner

Both structures consist of a) adjustable tap weights denoted as $w_1(n)$, $w_2(n)$, ... $w_M(n)$ and b) a mechanism to adjust these taps weights adaptively. During the filtering process, the desired response $d(n)$ is supplied along with the inputs $\mathbf{x}(n)$ at time n, and the filter output is denoted as

$y(n)$. The error response $e(n)$ to adjust these taps weights with some criteria such as the minimum mean squared error–MMSE. $s(n)$ is the training bits sent and H is the channel.

3.2.1 The Wiener Filtering [104]

To understand the adaptive filtering process, the Wiener filtering will be initially discussed. The second order statistical properties of the filter's input are used here. Two assumptions are made here: First, the discrete-time *stochastic* process represented by each tap inputs is weakly stationary and secondly, the mean value of the process is zero.

From figure 3.1, the output of the filter, $y(n)$, in both structure can be expressed as:

$$y(n) = \mathbf{w}^{\mathsf{H}}(n)\,\mathbf{x}(n) \tag{3.2}$$

where the tap-weight vector $\mathbf{w}(n)$ consists of M individual weights, expressed as follows:

$$\mathbf{w}(n) = \begin{bmatrix} w_1(n) & w_2(n) & \cdots & w_M(n) \end{bmatrix}^{\mathsf{T}} \tag{3.3}$$

Depending on the structure, the tap-input vector $\mathbf{x}(n)$ can be termed differently. For the transversal structure (shown in figure 3.1a), the input to the filter $\mathbf{x}(n)$ can be expressed as:

$$\mathbf{x}(n) = \begin{bmatrix} x(n) & x(n-1) & \cdots & x(n-M+1) \end{bmatrix}^{\mathsf{T}} \tag{3.4}$$

whereas $\mathbf{x}(n)$ for the parallel structure (shown in figure 3.1b) can be expressed as:

$$\mathbf{x}(n) = \begin{bmatrix} x_1(n) & x_2(n) & \cdots & x_M(n) \end{bmatrix}^{\mathsf{T}} \tag{3.5}$$

Note that both input vectors in (3.4) and (3.5) contain M entries.

Next, the adaptive approach starts by designing the filter such that the *difference* between the desired response $d(n)$ and the output of the filter $y(n)$ (which is referred as the estimation error $e(n)$) is at minimal as follows:

$$e(n) \;=\; d(n) - y(n) \;=\; d(n) - \mathbf{w}^{\mathsf{H}}(n)\,\mathbf{x}(n) \tag{3.6}$$

In the Wiener theory, the MMSE solution for finding the optimum tap-weight vector is obtained by minimising the cost function of $e(n)$. The cost function can be defined as:

$$J(n) = E\left[e(n)^2\right] \tag{3.7}$$

where $E[.]$ is the expectation operator. Note that the cost function $J(n)$ defined in (3.7) is also the mean squares error (MSE) of $e(n)$, which can also be defined as:

$$E\left[e(n)^2\right] \;=\; E\left[\left\{d(n) - \mathbf{w}^{\mathsf{H}}(n)\,\mathbf{x}(n)\right\}^2\right] \tag{3.8}$$

In order to appreciate the use of MMSE criterion, (3.8) can be expanded as follows:

$$J(n) = E\left[d(n)^2\right] + \mathbf{w}^{\mathsf{H}}(n)E\left[\mathbf{x}(n)\mathbf{x}(n)^{\mathsf{H}}\right]\mathbf{w}(n) - 2E\left[d(n)\mathbf{x}(n)^{\mathsf{H}}\right]\mathbf{w}(n) \tag{3.9}$$

Let **R** be the auto-correlation matrix of the tap-input vector $\mathbf{x}(n)$ that is defined as:

$$\mathbf{R} = E\left[\mathbf{x}(n)\mathbf{x}^{\mathsf{H}}(n)\right] \tag{3.10}$$

and **p** be the cross-correlation vector between $\mathbf{x}(n)$ and $d(n)$ defined as:

$$\mathbf{p}^{\mathsf{H}} = E\left[d(n)\mathbf{x}^{\mathsf{H}}(n)\right] \tag{3.11}$$

Therefore, (3.9) can be further expressed as:

$$J(n) = E\left[d(n)^2\right] + \mathbf{w}^{\mathsf{H}}(n)\mathbf{R}\mathbf{w}(n) - 2\mathbf{p}^{\mathsf{H}}\mathbf{w}(n) \tag{3.12}$$

Assuming that $d(n)$ has zero mean, $E\left[d(n)^2\right]$ is the *variance* of $d(n)$, expressed as:

$$\sigma_d^2 = E\left[d(n)^2\right] \tag{3.13}$$

By eliminating the time-dependent index n, (3.12) can be re-expressed as:

$$J = \sigma_d^2 + \mathbf{w}^{\mathsf{H}}\mathbf{R}\mathbf{w} - 2\mathbf{p}^{\mathsf{H}}\mathbf{w} \tag{3.14}$$

(3.12) and (3.14) state that, when $\mathbf{x}(n)$ and $d(n)$ are jointly stationary, $J(n)$ is precisely a second-order function of $\mathbf{w}(n)$. The dependency of $J(n)$ on the tap-weight elements, w_1, w_2, … w_M, can be visualised as a bowl shaped surface with a unique minimum shown in the following figure 3.2. The bowl shaped surface is also referred as the error-performance surface of the adaptive filter. The requirement is to design the filter such that it operates at the minimum point of the error-performance surface, where the optimum value of tap-weight vector $\mathbf{w}_0$ is obtained.

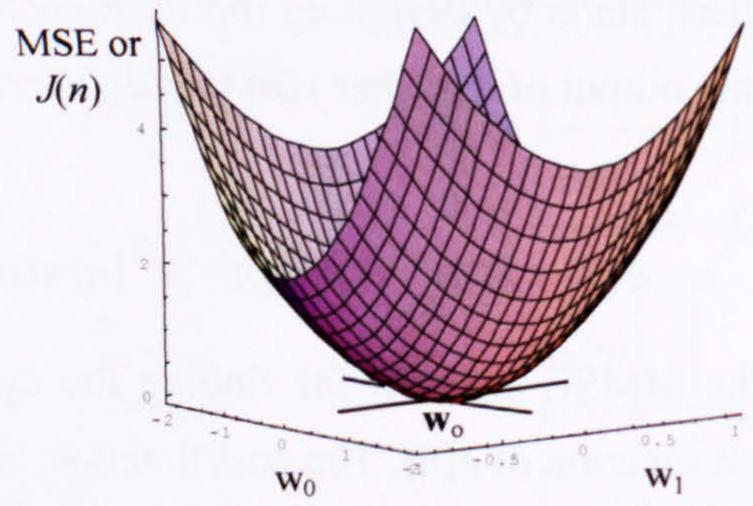

Figure 3.2: The error-performance surface of the cost-function J(n)

In a stationary environment, the error-performance surface has the constant shape as well as orientation. However, when it operates in a non-stationary environment, the bottom of the error-performance surface continually moves, while its orientation and curvature of the surface may be changing too. Hence, when the inputs are non-stationary, the adaptive filter has the task to search the bottom of the error-performance surface while continuingly tracking it [104].

The adaptive method seeks to find the minimum point in the error-performance surface by applying the MMSE criterion. To determine the optimum tap-weight vector $\mathbf{w}_o$, differentiation function is applied to (3.14) and the derivative of the cost function is set to zero. This produces the minimum MSE for the cost function. The process of differentiating the cost-function $J(n)$ w.r.t its tap-weight elements in $\mathbf{w}(n)$, can be shown as follows:

$$\nabla = \frac{\partial J}{\partial \mathbf{w}} = 2\mathbf{R}\mathbf{w} - 2\mathbf{p} \tag{3.15}$$

where ∇ is the gradient vector, which is the derivative of MSE (or cost function) w.r.t the tap weight vector. Subsequently, the ∇ is set to zero to obtain the minimum MSE:

$$\mathbf{R}\mathbf{w}_o = \mathbf{p} \tag{3.16}$$

(3.16) is the discrete form of Wiener-Hopf equation, yielding the optimum $\mathbf{w}_o$ as:

$$\mathbf{w}_o = \mathbf{R}^{-1}\mathbf{p} \tag{3.17}$$

where $\mathbf{R}^{-1}$ is the inverse of correlation matrix. Thus, the true value of MMSE or the minimum cost function J_{min}, can be obtained by substituting (3.17) into (3.14) as:

$$J_{min} = \sigma_d^2 - \mathbf{p}^{\mathrm{H}}\mathbf{w}_o \tag{3.18}$$

The cost function J can be modified (with the additional bracket terms shown below) and re-written to include the optimum weight value $\mathbf{w}_o$ and J_{min}, as follows:

$$\begin{aligned} J &= \underbrace{\sigma_d^2 \left(-\mathbf{p}^{\mathrm{H}}\mathbf{w}_o\right)} + \mathbf{w}^{\mathrm{H}}\mathbf{R}\mathbf{w} - 2\mathbf{p}^{\mathrm{H}}\mathbf{w} \left(+\mathbf{p}^{\mathrm{H}}\mathbf{w}_o\right) \\ &= J_{min} + \mathbf{w}^{\mathrm{H}}\mathbf{R}\mathbf{w} - 2\mathbf{w}^{\mathrm{H}}(\mathbf{R}\underbrace{\mathbf{R}^{-1})\mathbf{p}} + \underbrace{\mathbf{p}^{\mathrm{H}}(\mathbf{R}^{-1}}\mathbf{R})\mathbf{w}_o \\ &= J_{min} + \mathbf{w}^{\mathrm{H}}\mathbf{R}\mathbf{w} - 2\mathbf{w}^{\mathrm{H}}\mathbf{R}\,\mathbf{w}_o^{\mathrm{H}} + \mathbf{w}_o^{\mathrm{H}}\,\mathbf{R}\mathbf{w}_o \\ &= J_{min} + (\mathbf{w}-\mathbf{w}_o)^{\mathrm{H}}\mathbf{R}\,(\mathbf{w}-\mathbf{w}_o) \end{aligned} \tag{3.19}$$

where (3.19) shows that when the tap-weight vector is operating at the optimum value as $\mathbf{w} = \mathbf{w}_o$, $J = J_{min}$ or the MMSE can be achieved. It is vital to note that the computation of $\mathbf{w}_o$ requires knowledge of: a) the correlation matrix $\mathbf{R}$ of $\mathbf{x}(n)$ and b) the cross-correlation vector $\mathbf{p}$ between $\mathbf{x}(n)$ and $d(n)$. Although (3.17) leads to the optimum solution, it present a serious computational difficulties since the matrix inversion for $\mathbf{R}$ needs to be obtained each time for each set of tap-weight vector $\mathbf{w}(n)$. This can be very unpractical and time-consuming especially when the filter contains large number of tap-weights and the input data rate is high. Hence, more practical real-time approaches are needed, which involve automatic adjustment of the tap weights (in a updating fashion), to avoid the extensive computations of $\mathbf{R}$ and $\mathbf{p}$. These involve recursive solutions introduced later by LMS and RLS algorithm discussed in next Sections.

3.2.2 Least Mean Squares (LMS) Algorithm

The first recursive approach is the *least mean squares* (LMS) algorithm [102–104, 107]. The LMS algorithm is simple and does not require measurement of the pertinent correlation functions, **R** and **p**, nor does it require any matrix inversion [107], where its simplicity has become the benchmark against other adaptive filtering techniques. It is developed based on the method of steepest descent, which recursively performs gradient search for the minimum point of the error-performance surface without the knowledge of the error-performance surface itself.

In the steepest descent method, successive corrections to the tap-weight vector in the direction of the negative gradient vector should finally lead to J_{min}, at optimum $\mathbf{w}_o$. Again, let ∇ denote the value of the gradient vector at time n and $\mathbf{w}(n)$ denote the value of the tap-weight vector at time n. According to the method of steepest descent, the updated value of the tap-weight vector at time n+1 is computed by using the simple recursion relation as follows:

$$\mathbf{w}(n+1) = \mathbf{w}(n) + \frac{1}{2}\mu[-\nabla(n)] \tag{3.20}$$

where μ is a constant. By substituting (3.15) into (3.20), the adaptive algorithm is formulated as:

$$\mathbf{w}(n+1) = \mathbf{w}(n) + \mu[\mathbf{p}-\mathbf{R}\mathbf{w}(n)] \tag{3.21}$$

where μ is the step-size parameter that controls the size of the incremental correction applied to the tap-weight vector, from one iteration cycle to next. In (3.21), it is necessary that **R** and **p** are known so that ∇ can be computed, for a given value of $\mathbf{w}(n)$. In reality, however, exact measurements of ∇ are not always possible and it must be estimated from the available data. However, LMS modifies (3.21) so that $\mathbf{w}(n)$ is updated in accordance with an algorithm that estimate the gradient vector instead of measuring, which adapts to the incoming data as real-time approach. (LMS algorithm can be applied to both basic structures in figure 3.1.) To develop an estimate of gradient vector, the most obvious strategy is to substitute **R** and **p** in (3.21) with the *instantaneous* estimates that are based on the sample values of $\mathbf{x}(n)$ and $d(n)$, defined as follows:

$$\hat{\mathbf{R}} = \mathbf{x}(n)\mathbf{x}^{H}(n) \tag{3.22}$$

$$\hat{\mathbf{p}} = \mathbf{x}(n)d^{*}(n) \tag{3.23}$$

Hence, the corresponding instantaneous estimate of the gradient vector can be obtained as:

$$\hat{\nabla}(n) = -2\mathbf{x}(n)d^{*}(n) + 2\mathbf{x}(n)\mathbf{x}^{H}(n)\hat{\mathbf{w}}(n) \tag{3.24}$$

Substituting (3.24) in (3.20), a new recursive relation for updating $\mathbf{w}(n)$ can be obtained as:

$$\hat{\mathbf{w}}(n+1) = \hat{\mathbf{w}}(n) + \mu\mathbf{x}(n)\left[d^{*}(n)-\mathbf{x}^{H}(n)\hat{\mathbf{w}}(n)\right] \tag{3.25}$$

where $\left[d^{*}(n)-\mathbf{x}^{H}(n)\hat{\mathbf{w}}(n)\right]$ is exactly the difference between $d(n)$ and $y(n)$, which is $e(n)$ in

(3.6). Note that only the instantaneous input value $\mathbf{x}(n)$ is required here instead of obtaining $\mathbf{R}$ and $\mathbf{p}$ *a priory* as shown in (3.21) for each iteration.

Equivalently, (3.25) can be re-written in the form of a pair of recursive relations as follows:

$$e(n) = d(n) - \hat{\mathbf{w}}^{H}(n)\mathbf{x}(n) \tag{3.26}$$

$$\hat{\mathbf{w}}(n+1) = \hat{\mathbf{w}}(n) + \mu\,\mathbf{x}(n)e^{*}(n) \tag{3.27}$$

Both (3.26) and (3.27) describe the adaptive *least mean squares* (LMS) algorithm. The second term, $\mu\,\mathbf{x}(n)e^{*}(n)$ in (3.27) represents the *innovation* that allows correction applied to the estimate of $\hat{\mathbf{w}}(n)$ in each recursion, so that $\hat{\mathbf{w}}(n)$ can converge toward the optimum point. However, the amount of correction as well as the convergence rate are controlled by the step size parameter μ. If μ is too small, the filter will take longer time to converge and if μ is too large, it may cause stability problem. [103, 104], that results in a larger steady-state error (which is the MMSE or J_{min}) as illustrated in the following figure 3.3.

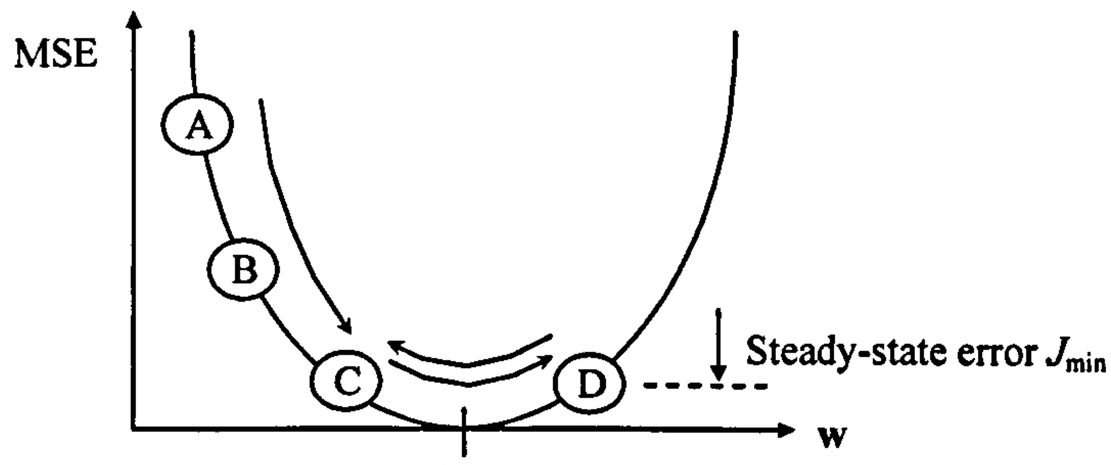

$\mathbf{w}_o$ – Optimum point

Figure 3.3: Convergence of the LMS algorithm

At initial guess, coefficient at point A usually has a larger error and successive iteration in LMS algorithm causing the coefficient to move towards the optimum value via point B and C. After C, the coefficient overshoots the optimum point towards D. Subsequent iterations cause the coefficient to oscillate between point C and D, resulting in a steady-state error, which may be reduced by decreasing μ so that the overshoot is smaller. The trade-off is the slower convergence rate, which requires more points between A and C. Typical values of μ are bounded between:

$$0 < \mu < \frac{1}{\lambda_{max}} \tag{3.28}$$

where λ_{max} is the maximum eigenvalue of $\mathbf{R}$. Although the LMS algorithm has low-complexity for computing the optimum weights, the convergence time is too long for many applications such as fast-changing mobiles communications. The channel coherence time may be shorter than the LMS convergence time, which prevents the weights get closer to their optimum values. Another algorithm that has faster convergence but with more complex computations, is the recursive least square (RLS) algorithm, which is discussed next section.

3.2.3 Recursive Least Squares (RLS) Algorithm [102–104, 130]

Recursive Least Squares (RLS) algorithm is a more advance recursive approach than the LMS algorithm, since RLS algorithm utilise all the present and past inputs that extend to the time when the algorithm is initiated. The convergence attribute in the RLS algorithm is based on a *deterministic* least squares approach, as opposed to the statistical approach used in the LMS algorithm [104]. The resulting rate of convergence is therefore much faster, but more computational intensive. The rapid convergence can be achieved by taking on error measurement as a *time average* of the actual received signal instead of a statistical average.

The RLS algorithm can also be applied to both basic structures in figure 3.1. To understand the derivation of RLS algorithm, the least square error based on the time average is defined:

$$J(n) = \sum_{i}^{n} \gamma^{n-i} \left| e(i,n) \right|^2 \tag{3.29}$$

where γ is the forgetting factor. $e(i,n)$ is the error response using the new tap weight vector $\mathbf{w}(n)$ at time n to test the old data at time i and is expressed as follows:

$$e(i,n) = d(i) - \mathbf{w}^{\mathsf{H}}(n)\,\mathbf{x}(i) \qquad 0 \le i \le n \tag{3.30}$$

where $\mathbf{w}(n)$ is the tap-weight vector, $d(i)$ is desired and $\mathbf{x}(i)$ is the filter input at time i expressed for both the transversal structure and parallel structure in figure 3.1 respectively as:

$$\mathbf{x}(i) = \left[x(i) \quad x(i-1) \quad \cdots \quad x(i-M+1) \right]^{\mathsf{T}} \quad \text{or} \quad \mathbf{x}(i) = \left[x_1(i) \quad x_2(i) \quad \cdots \quad x_M(i) \right]^{\mathsf{T}} \tag{3.31}$$

In RLS, $\mathbf{w}(n)$ is obtained such that the cumulative squared error $J(n)$ in (3.29) is minimised. γ tends to weight recent data more heavily in the computations so that $J(n)$ tends to 'forget' the old data in a non-stationary environment. If the environment is stationary, γ=1, representing the ordinary method of least squares. In practice, γ is set closed to 1 to retain some finite weighted 'memory' of the past data for updating the tap-weights recursively with time average process.

For minimum value of the least squares error $J(n)$, the gradient of $J(n)$ is set to zero as:

$$\frac{\partial J(n)}{\partial \mathbf{w}(n)} = 0 \tag{3.32}$$

which leads to the optimum solution as:

$$\mathbf{R}(n)\,\hat{\mathbf{w}}(n) = \mathbf{p}(n) \tag{3.33}$$

where $\mathbf{R}(n)$ is the $(M \times M)$ deterministic correlation matrix of input data $\mathbf{x}(i)$ defined as:

$$\mathbf{R}(n) = \sum_{i}^{n} \gamma^{n-i}\, \mathbf{x}(i)\, \mathbf{x}^{\mathsf{H}}(i) \tag{3.34}$$

and $\mathbf{p}(n)$ is the $(M \times 1)$ deterministic cross-correlation vector between $\mathbf{x}(i)$ and $d(i)$ defined as:

$$\mathbf{p}(n) = \sum_{i}^{n} \gamma^{n-i}\, \mathbf{x}(i)\, d^{*}(i) \tag{3.35}$$

From (3.34) and (3.35), the present term can be separated from the past terms by isolating the term with $i = n$ from the rest. For example, $\mathbf{R}(n)$ can be re-expressed as:

$$\mathbf{R}(n) = \underbrace{\gamma\left[\sum_{i}^{n-1}\gamma^{n-1-i}\,\mathbf{x}(i)\,\mathbf{x}^{H}(i)\right]}_{\text{past terms}} + \underbrace{\mathbf{x}(n)\,\mathbf{x}^{H}(n)}_{\text{present term}} \tag{3.36}$$

Hence, it is possible to formulate the present $\mathbf{R}(n)$ in terms of the past $\mathbf{R}(n\text{-}1)$ as:

$$\mathbf{R}(n) = \gamma\,\mathbf{R}(n\text{-}1) + \mathbf{x}(n)\,\mathbf{x}^{H}(n) \tag{3.37}$$

Similarly, $\mathbf{p}(n)$ can also be expressed in terms of its past values as:

$$\mathbf{p}(n) = \gamma\,\mathbf{p}(n\text{-}1) + \mathbf{x}(n)\,d^{*}(n) \tag{3.38}$$

However, it is still tedious to recursively update compute $\mathbf{R}^{-1}(n)$ for $\hat{\mathbf{w}}(n)$ in (3.33). Thus, the *matrix inversion lemma* [104] is used to derive $\mathbf{R}^{-1}(n)$ as a recursive update in terms of previous $\mathbf{R}^{-1}(n\text{-}1)$. The *matrix inversion lemma* is also used to generate the recursive formulation for updating the $\hat{\mathbf{w}}(n)$. The *matrix inversion lemma* states the following:

$$\mathbf{A} = \mathbf{B}^{-1} + \mathbf{C}\mathbf{D}^{-1}\mathbf{C}^{H} \tag{3.39}$$

$$\mathbf{A}^{-1} = \mathbf{B} - \mathbf{B}\mathbf{C}(\mathbf{D} + \mathbf{C}^{H}\mathbf{B}\mathbf{C})^{-1}\mathbf{C}^{H}\mathbf{B} \tag{3.40}$$

where $\mathbf{A}$ and $\mathbf{B}$ are the two positive-definite ($M\times M$) matrices and $\mathbf{D}$ is another positive-definite ($N\times N$) matrix, whereas $\mathbf{C}$ is an ($M\times N$) matrix. With $\mathbf{R}(n)$ assumed to be positive-definite, the *matrix inversion lemma* can be applied with the following identifications:

$$\mathbf{A} = \mathbf{R}(n) \;;\; \mathbf{B}^{-1} = \gamma\,\mathbf{R}(n-1) \;;\; \mathbf{C} = \mathbf{x}(n) \;;\; \mathbf{D} = 1 \tag{3.41}$$

Let $\mathbf{\Phi}(n) = \mathbf{R}^{-1}(n)$, substitute (3.41) into (3.40), to obtain the following the recursion as:

$$\mathbf{\Phi}(n) = \gamma^{-1}\mathbf{\Phi}(n\text{-}1) - \frac{\gamma^{-1}\mathbf{\Phi}(n\text{-}1)\,\mathbf{x}(n)\,\mathbf{x}^{H}(n)\,\gamma^{-1}\mathbf{\Phi}(n\text{-}1)}{1 + \mathbf{x}^{H}(n)\,\gamma^{-1}\mathbf{\Phi}(n\text{-}1)\,\mathbf{x}(n)} \tag{3.42}$$

which can be simplified by the insertion of gain vector $\mathbf{k}(n)$ in the following:

$$\mathbf{\Phi}(n) = \frac{1}{\gamma}\left[\mathbf{\Phi}(n\text{-}1) - \mathbf{k}(n)\,\mathbf{x}^{H}(n)\,\mathbf{\Phi}(n\text{-}1)\right] \tag{3.43}$$

where the gain vector $\mathbf{k}(n)$ is define as:

$$\mathbf{k}(n) = \frac{\gamma^{-1}\mathbf{\Phi}(n\text{-}1)\,\mathbf{x}(n)}{\left[1 + \gamma^{-1}\mathbf{x}^{H}(n)\,\mathbf{\Phi}(n\text{-}1)\,\mathbf{x}(n)\right]} \tag{3.44}$$

which interestingly leads to the following:

$$\mathbf{k}(n) = \underbrace{\left[\gamma^{-1}\mathbf{\Phi}(n\text{-}1) - \gamma^{-1}\mathbf{k}(n)\,\mathbf{x}^{H}(n)\,\mathbf{\Phi}(n\text{-}1)\right]}\,\mathbf{x}(n) \tag{3.45}$$

$$\mathbf{k}(n) = \mathbf{\Phi}(n)\,\mathbf{x}(n) \tag{3.46}$$

Next, the recursion for the estimate of the tap-weight vector can be obtained by utilising (3.42), (3.46) and (3.38) into the formulation optimum tap-weight vector in (3.33) as:

$$\begin{aligned}\hat{\mathbf{w}}(n) &= \mathbf{R}^{-1}(n)\,\mathbf{p}(n) \\ &= \boldsymbol{\Phi}(n)\left[\gamma\,\mathbf{p}(n-1) + \mathbf{x}(n)\,d^{*}(n)\right] \\ &= \underbrace{\boldsymbol{\Phi}(n)\,\gamma\,\mathbf{p}(n-1)}_{1^{st}\text{ term}} + \underbrace{\boldsymbol{\Phi}(n)\mathbf{x}(n)\,d^{*}(n)}_{2^{nd}\text{ term}} \end{aligned} \tag{3.47}$$

It can seen that the 1st term can be expanded using (3.43) as follows:

$$\begin{aligned}\boldsymbol{\Phi}(n)\,\gamma\,\mathbf{p}(n-1) &= \frac{1}{\gamma}\left[\boldsymbol{\Phi}(n-1) - \mathbf{k}(n)\,\mathbf{x}^{H}(n)\,\boldsymbol{\Phi}(n-1)\right]\gamma\,\mathbf{p}(n-1) \\ &= \boldsymbol{\Phi}(n-1)\,\mathbf{p}(n-1) - \mathbf{k}(n)\,\mathbf{x}^{H}(n)\,\boldsymbol{\Phi}(n-1)\,\mathbf{p}(n-1) \\ &= \hat{\mathbf{w}}(n-1) - \mathbf{k}(n)\,\mathbf{x}^{H}(n)\,\hat{\mathbf{w}}(n-1) \end{aligned} \tag{3.48}$$

where $\boldsymbol{\Phi}(n-1)\,\mathbf{p}(n-1)$ is the previous estimate, $\hat{\mathbf{w}}(n-1)$. The 2nd term in (3.47) also contains the gain vector in (3.46). Using (3.48) and (3.46) into (3.47), $\hat{\mathbf{w}}(n)$ can be recursively expressed as:

$$\begin{aligned}\hat{\mathbf{w}}(n) &= \hat{\mathbf{w}}(n-1) - \mathbf{k}(n)\,\mathbf{x}^{H}(n)\,\hat{\mathbf{w}}(n-1) + \mathbf{k}(n)d^{*}(n) \\ &= \hat{\mathbf{w}}(n-1) - \mathbf{k}(n)\left[\mathbf{x}^{H}(n)\,\hat{\mathbf{w}}(n-1) - d^{*}(n)\right] \\ &= \hat{\mathbf{w}}(n-1) + \mathbf{k}(n)\left[d^{*}(n) - \mathbf{x}^{H}(n)\,\hat{\mathbf{w}}(n-1)\right] \end{aligned} \tag{3.49}$$

Note that $\mathbf{x}^{H}(n)\,\hat{\mathbf{w}}(n-1)$ in (3.49) represents an estimate of $d(n)$, based on the old least-squares estimate of tap-weight vector at time n-1. The bracket term at the *RHS* of (3.49) is called the *a priori* estimation error, which is referred as the *innovation* to the RLS algorithm defined as:

$$\alpha(n) = d(n) - \hat{\mathbf{w}}^{H}(n-1)\,\mathbf{x}(n) \tag{3.50}$$

Hence, $\hat{\mathbf{w}}(n)$ can be updated in the following recursion as:

$$\hat{\mathbf{w}}(n) = \hat{\mathbf{w}}(n-1) + \mathbf{k}(n)\,\alpha^{*}(n) \tag{3.51}$$

Equations (3.44), (3.50), (3.51) and (3.43) collectively constitute the RLS algorithm. In particular, (3.50) describes the filtering operation of the algorithm, whereby the adaptive filter is excited to compute the a priori estimation error $\alpha(n)$. (3.51) describes the adaptive operation of the RLS algorithm whereby the tap-weight vector is updated by incrementing its old value by $\alpha(n)$ and $\mathbf{k}(n)$. (3.44) & (3.43) enable the update of $\mathbf{k}(n)$ and the inverse of the correlation matrix $\boldsymbol{\Phi}(n)$ respectively. An important feature of the RLS algorithm described by these equations is that the inversion matrix $\boldsymbol{\Phi}(n)$ is replaced at each step by a simple scalar division.

The forgetting factor γ in (3.43) and (3.44) is the weighting coefficients that can change the performance of the adaptive filter. Usually $0.8 < \gamma < 1$ is used. When $\gamma = 1$, the filter has an infinite memory. All previous data will have equal weights. However, setting $\gamma < 1$, it assigns lesser weight to older data, which leads to a finite memory. Note that the value of γ has no

influence on the convergence rate but it does determine the tracking ability of the equaliser. [102, 104]. The smaller the γ, the better the tracking ability of the adaptive filter. However, if γ is too small, the filter will be unstable. The convergence analysis is provided in [104] for full details.

3.2.4 Summary of the LMS and RLS Algorithms

The LMS algorithm can be summarised in the following table 3.1:

Initialise parameters	
a) $n = 0$	- Initialise recursion-index $n = 0$.
b) $0 < \mu < \frac{1}{\lambda_{max}}$	- Compute the step-size parameter μ.
c) $\hat{\mathbf{w}}(0) = [0 \quad 0 \quad \cdots \quad 0]^T$	- Set all tap-weights to zero
Recursion	
a) $y(n) = \hat{\mathbf{w}}^H(n)\mathbf{x}(n)$	- Compute the adaptive filter's output
b) $e(n) = d(n) - y(n)$	- Compute the error response as innovation
c) $\hat{\mathbf{w}}(n+1) = \hat{\mathbf{w}}(n) + \mu\mathbf{x}(n)e^*(n)$	- Updating the tap-weight vector with correction term
d) $n = n + 1$	- Increment the recursion-index.

Table 3.1 Summary of LMS algorithm.

The RLS algorithm can be summarised in the following table-3.2:

Initialise parameters	
a) $n = 0$ b) $\hat{\mathbf{w}}(0) = [0 \quad 0 \quad \cdots \quad 0]^T$ c) $0.8 < \gamma < 0.98$ d) $\Phi(0) = \mathbf{I}$	- Initialise recursion-index $n = 0$ - Set all tap-weights to zero - Set the value of the forgetting factor γ. - Set the inverse correlation matrix equal to the identity matrix
Recursion	
a) $y(n) = \hat{\mathbf{w}}^H(n)\mathbf{x}(n)$	- Compute the filter's output
b) $\alpha(n) = d(n) - y(n)$	- Compute the *a priori* estimation error
c) $\mathbf{k}(n) = \frac{\Phi(n)\mathbf{x}(n)}{\left[\gamma + \mathbf{x}^H(n)\Phi(n)\mathbf{x}(n)\right]}$	- Compute the gain vector with $\mathbf{x}(n)$, $\Phi(n)$ and the forgetting factor γ.
c) $\hat{\mathbf{w}}(n+1) = \hat{\mathbf{w}}(n) + \mathbf{k}(n)\alpha^*(n)$	- Updating the tap-weight vector
d) $\Phi(n+1) = \frac{1}{\gamma}\left[\Phi(n) - \mathbf{k}(n)\mathbf{x}^H(n)\Phi(n)\right]$	- Update the inverse correlation matrix
e) $n = n + 1$	- Increment the recursion-index.

Table 3.2 Summary of RLS algorithm.

3.3 General MIMO Channel Estimation Algorithms (for Frequency-Flat Fading Channel)

In this section, two general types of MIMO channel estimation algorithms (adaptive and non-adaptive method) for frequency-flat fading channel are introduced. First, for the adaptive method, a) the MIMO Least Mean Squares (MIMO-LMS) algorithm and b) the MIMO Recursive Least Squares (MIMO-RLS) algorithm that extended from LMS and RLS algorithms are presented. This is followed by the non-adaptive method called MIMO "pilot matrix inversion" (MIMO-PMI) where orthogonal training sequences are utilised, which only requires non-recursive solution by performing matrix inversion onto the "pilot matrix" sent for training. The necessary concepts behind and system model used for these algorithms are also presented in order to show how the channel estimation is developed in the MIMO configuration.

3.3.1 Channel Matrix Definition and System Model

The MIMO transfer function that describes the frequency-flat fading channel propagation for a basic ($N\times M$) MIMO wireless system can be defined in a channel matrix as follows:

$$\mathbf{H} = \begin{bmatrix} \mathbf{u}_1 & \mathbf{u}_2 & \cdots & \mathbf{u}_M \end{bmatrix} \tag{3.52}$$
$$= \begin{bmatrix} h_{11} & h_{12} & & h_{1M} \\ h_{21} & h_{22} & \cdots & h_{2M} \\ \vdots & \vdots & & \vdots \\ h_{N1} & h_{N2} & & h_{NM} \end{bmatrix}$$

where each $\mathbf{u}_i$ in (3.52) is the individual propagation vector that is contains the complex NLOS Rayleigh fading coefficients h_{ji} between the i^{th} transmit antenna to all N receive antennas. The basic MIMO signal model can be illustrated in following:

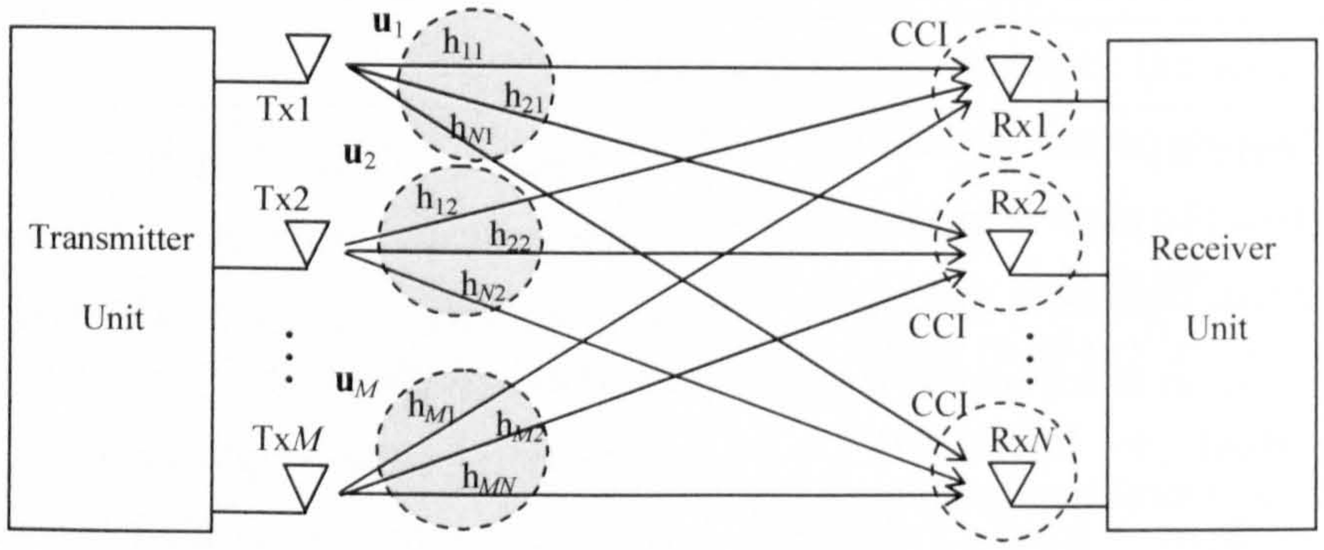

Figure 3.4: The basic signal model for the frequency-flat MIMO channel.

Note that each link from i^{th} transmit antenna to j^{th} receive antenna consists only a single path represented by the respective fading coefficient h_{ji}. Each link in effect is a source of CCI

contribution to the others as they superimposed at the respective receive antenna. All h_{ji} are assumed to be time-invariant and uncorrelated. The MIMO-CE methods described later aim to estimate all coefficients by data-aided approach, using both adaptive and non-adaptive solutions.

In order to appreciate the training-based MIMO-CE, the signal model must be studied to understand the interaction between the transmitted signals and the MIMO channel. The $N\times1$ received signal vector $\boldsymbol{r}(n)$ can be again expressed in the following:

$$\boldsymbol{r}(n) \;=\; \mathbf{H}\,\boldsymbol{s}(n) \;+\; \boldsymbol{n}(n) \tag{3.53}$$

where n is the time-instant. $\boldsymbol{r}(n) = [r_1(n),\ \ldots,\ r_N(n)]^{\mathsf{T}}$, $\boldsymbol{s}(n) = [s_1(n),\ \ldots,\ s_M(n)]^{\mathsf{T}}$ and $\boldsymbol{n}(n)$ is the noise vector. This can be relating to the space-time channel model described in section 2.2.2. Assuming $\mathbf{H}$ is time-invariant, $\boldsymbol{s}(n)$ at time n can be recovered as:

$$\hat{\boldsymbol{s}}(n) \;=\; D\big[\mathbf{W}\,\boldsymbol{r}(n)\big] \tag{3.54}$$

where D is the slicing-decision operator and $\mathbf{W}$ can be obtained as:

$$\mathbf{W} = \mathbf{H}^{+} \tag{3.55}$$

Note that the $(.)^{+}$ is the pseudo-inverse operation. The relationship between $\mathbf{H}$ and $\mathbf{W}$ are closely related in an inverse manner where columns of $\mathbf{H}$ corresponds to the row of $\mathbf{W}$. The propagation vector $\mathbf{u}_m$ contained in $\mathbf{H}$ shown in (3.52) is inversely proportional to the respective weighting vector $\mathbf{w}_m$ contained in the $\mathbf{W}$ matrix shown in the following:

$$\mathbf{W} \;=\; \begin{bmatrix} \boldsymbol{w}_1 \\ \boldsymbol{w}_2 \\ \vdots \\ \boldsymbol{w}_M \end{bmatrix} ;\quad \mathbf{H} \;=\; \begin{bmatrix} \boldsymbol{u}_1 & \boldsymbol{u}_2 & \cdots & \boldsymbol{u}_M \end{bmatrix} \tag{3.56}$$

where $i = 1$ to M, $\boldsymbol{u}_i = \begin{bmatrix} h_{1i} & h_{2i} & \cdots & h_{Ni} \end{bmatrix}^{\mathsf{T}}$ and $\boldsymbol{w}_i = \begin{bmatrix} \omega_{i1} & \omega_{i2} & \cdots & \omega_{iN} \end{bmatrix}$.

The implicit relationship in (3.56) also reveals that the individual weighting vector $\boldsymbol{w}_i$ which is the *inverse response* of individual $\boldsymbol{u}_i$, can be obtained through either adaptive or non-adaptive algorithm. Reciprocally, it also means that the estimate of channel matrix $\hat{\mathbf{H}}$ can also be obtained in terms of each individual $\hat{\boldsymbol{u}}_i$ by jointly estimating the respective $\boldsymbol{w}_i$ in $\mathbf{W}$ first and then perform the matrix inversion onto the corresponding $\hat{\mathbf{W}}$.

Note that transmit vector $\boldsymbol{s}(n)$ has become the 'training' vector which is known *a priori* at the receiver. For channel estimation, a series of $\mathbf{s}(n)$ is sent across the channel for training of the channel, where $n = 1$ to V, assuming that $\mathbf{H}$ remains relatively constant throughout the 'training' period. In the adaptive method, V is the number of iterations required for the channel estimates to reach a convergence solution. In non-adaptive method, V represents the number of $\mathbf{s}(n)$ required to be transmitted in burst of block to form a 'pilot matrix' in order to estimate the channel.

3.3.2 Adaptive Training-Based approach

To adaptively estimate the **H** in the frequency-flat channel, the parallel combiner from figure 3.1b can be extended into a *multiple array beamformer* for the ($N\times M$) system as follows:

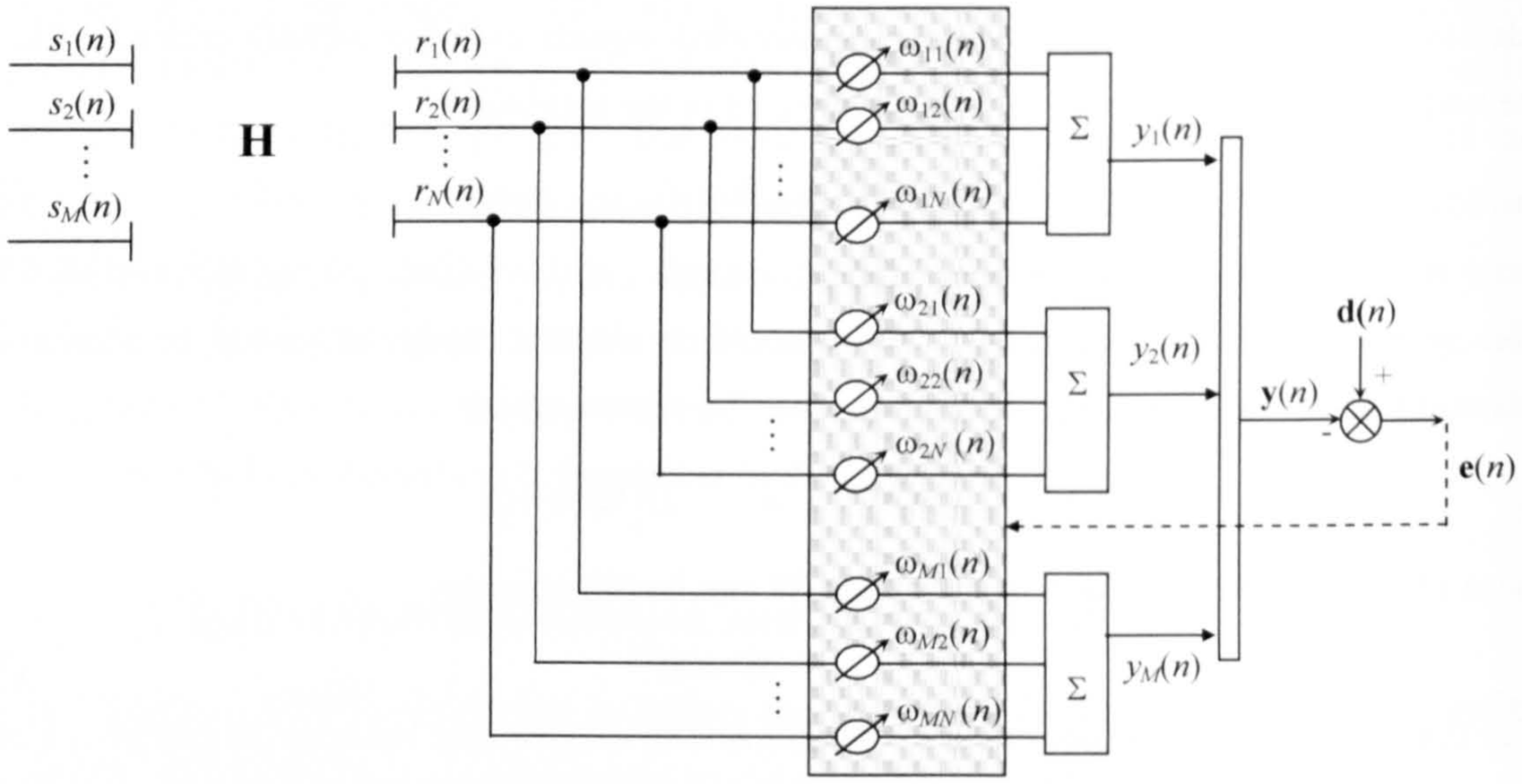

Figure 3.5: Multiple Array Beamformer for adaptive MIMO channel estimation

It can be seen that the parallel combiner structure from figure 3.1b is duplicated M times in the above multiple array beamformer structure. The individual output $y_i(n)$ of each parallel combiner is produced by the weighted sum of the received signals and can be expressed as:

$$\mathbf{y}(n) = \mathbf{W}(n)\,\mathbf{r}(n) \tag{3.59}$$

$$\begin{bmatrix} y_1(n) \\ \vdots \\ y_M(n) \end{bmatrix} = \begin{bmatrix} \omega_{11}(n) & \cdots & \omega_{1N}(n) \\ \vdots & \ddots & \vdots \\ \omega_{M1}(n) & \cdots & \omega_{MN}(n) \end{bmatrix} \begin{bmatrix} r_1(n) \\ \vdots \\ r_N(n) \end{bmatrix}$$

where $\mathbf{r}(n)$ is the input received signal vector and $\mathbf{y}(n)$ is the output vector. $\mathbf{W}(n)$ is the weighting matrix at time n, consist of individual tap-weight coefficients, ω_{ij}. In the recursion, the tap-weight coefficients are updated with the aim to jointly minimise the MSE of the error response vector $\mathbf{e}(n)$, which can be obtained by subtracting $\mathbf{y}(n)$ from the desired response vector $\mathbf{d}(n)$ as:

$$\mathbf{e}(n) = \mathbf{d}(n) - \mathbf{y}(n) \qquad \text{where} \qquad \mathbf{d}(n) = \mathbf{s}(n) \tag{3.61}$$

$$\begin{bmatrix} e_1(n) \\ \vdots \\ e_M(n) \end{bmatrix} = \begin{bmatrix} d_1(n) \\ \vdots \\ d_M(n) \end{bmatrix} - \begin{bmatrix} y_1(n) \\ \vdots \\ y_M(n) \end{bmatrix} \qquad \begin{bmatrix} d_1(n) \\ \vdots \\ d_M(n) \end{bmatrix} = \begin{bmatrix} s_1(n) \\ \vdots \\ s_M(n) \end{bmatrix}$$

where $\mathbf{d}(n)$ is usually the transmit training vector $\mathbf{s}(n)$. Instead of using individual $e(n)$ for recursion, all $e_i(n)$ are jointly computed as $\mathbf{e}(n)$ that serves as the innovation to jointly update each ω_{ij} in the adaptive process for the MIMO system. As mentioned, two adaptive MIMO-CE

algorithms can be subsequently developed: a) the MIMO-LMS algorithm and b) the MIMO-RLS algorithm. Upon completing the recursive process, all tap-weight coefficients in **W** eventually reach its optimum value, which have also converged into the inverse response of **H**. Finally, the estimate of the MIMO channel can be obtained by inverting the final value of **W** matrix.

3.3.2.1 Adaptive MIMO Least Mean Squares Algorithm (MIMO-LMS)

The MIMO-LMS algorithm can be summarised in the following table 3.3:

Initialise parameters	
a) $n = 0$ b) $0 < \mu < \frac{1}{\lambda_{max}}$ c) $\hat{\mathbf{W}}_{LMS}(0) = \mathbf{0}$	- Initialise recursion-index $n = 0$. - Compute the step-size parameter μ. - Initialise all tap-weights in $\hat{\mathbf{W}}(0)$ to zero
Recursion	
a) $\mathbf{y}(n) = \hat{\mathbf{W}}_{LMS}(n)\mathbf{r}(n)$ b) $\mathbf{e}(n) = \mathbf{d}(n) - \mathbf{y}(n)$ c) $\hat{\mathbf{W}}_{LMS}(n+1) = \hat{\mathbf{W}}_{LMS}(n) + \mu\mathbf{e}(n)\mathbf{r}^{H}(n)$ d) $n = n + 1$	- Compute the output vector - Compute the error vector - Updating the weighting matrix with correction term - Increment the recursion-index.

Table 3.3 Summary of MIMO-LMS algorithm.

During initialisation, **W** and its tap-weight coefficients are set to zero as follows:

$$\mathbf{W}_{LMS} = \begin{bmatrix} \omega_{11}(0) & \cdots & \omega_{1N}(0) \\ \vdots & \ddots & \vdots \\ \omega_{M1}(0) & \cdots & \omega_{MN}(0) \end{bmatrix} = \begin{bmatrix} 0 & \cdots & 0 \\ \vdots & \ddots & \vdots \\ 0 & \cdots & 0 \end{bmatrix} \tag{3.62}$$

During estimation, a series of training vectors $\mathbf{s}(n)$ containing pilot symbols s_i is sent across the MIMO channel. The 'pilot' received signals form the input vector $\mathbf{r}(n)$ to the adaptive filter, and its output vector $\mathbf{y}(n)$ and error vector $\mathbf{e}(n)$ are then computed. With the appropriate step-size parameter μ, the entire weighting matrix $\mathbf{W}_{LMS}$ can be updated using the recursion as follows:

$$\hat{\mathbf{W}}_{LMS}(n+1) = \hat{\mathbf{W}}_{LMS}(n) + \mu\mathbf{e}(n)\mathbf{r}^{H}(n) \tag{3.63}$$

$$\begin{bmatrix} \hat{\omega}_{11}(n+1) & \cdots & \hat{\omega}_{1N}(n+1) \\ \vdots & \ddots & \vdots \\ \hat{\omega}_{M1}(n+1) & \cdots & \hat{\omega}_{MN}(n+1) \end{bmatrix} = \begin{bmatrix} \hat{\omega}_{11}(n) & \cdots & \hat{\omega}_{1N}(n) \\ \vdots & \ddots & \vdots \\ \hat{\omega}_{M1}(n) & \cdots & \hat{\omega}_{MN}(n) \end{bmatrix} + \mu \begin{bmatrix} e_1(n) \\ \vdots \\ e_M(n) \end{bmatrix} \begin{bmatrix} r_1^*(n) & \cdots & r_N^*(n) \end{bmatrix}$$

Note that (.)* is the complex conjugation and n is the recursion-index.

The recursion in (3.63) basically constitutes the MIMO-LMS adaptive algorithm, which is slightly different from the basic LMS algorithm, shown in (3.27). First, the entire weighting matrix **W** is being updated instead of individual tap-weight vector $\boldsymbol{w}$ in (3.57). Secondly, joint

error vector $\mathbf{e}(n)$ is used instead of individual error response $e_i(n)$ to allow simultaneous correction on $\mathbf{W}$. Note the position and the conjugation of the error vector $\mathbf{e}(n)$ and the input vector $\mathbf{r}(n)$ in (3.63) has been swapped as compared to (3.27), to facilitate the formulation of the MIMO-LMS algorithm. Finally, upon completing the iteration process, the MIMO channel estimate $\hat{\mathbf{H}}$ can be obtained by inverting the final value of $\mathbf{W}_{LMS}$.

3.3.2.2 Adaptive MIMO Recursive Least Squares Algorithm (MIMO-RLS)

The idea of MIMO-RLS algorithm is similar to MIMO-LMS except that the update of weighting matrix $\mathbf{W}$ is of complexity. The MIMO-RLS algorithm is also referred as the multi element array RLS (MEA-RLS) channel estimation technique in [87].

The MIMO-RLS algorithm can be summarised in the following table-3.4:

Initialise parameters	
a) $n = 0$ b) $\hat{\mathbf{W}}_{RLS}(0) = \mathbf{0}$ c) $0.8 < \gamma < 0.98$ d) $\mathbf{\Phi}(0) = \mathbf{I}$	- Initialise recursion-index $n = 0$ - Initialise all tap-weights in $\hat{\mathbf{W}}(0)$ to zero - Set the value of the forgetting factor γ. - Set the inverse correlation matrix equal to the identity matrix
Recursion	
a) $\mathbf{y}(n) = \hat{\mathbf{W}}_{RLS}(n)\mathbf{r}(n)$ b) $\mathbf{e}(n) = \mathbf{d}(n) - \mathbf{y}(n)$ c) $\mathbf{k}(n) = \dfrac{\mathbf{\Phi}(n)\mathbf{r}(n)}{\left[\gamma + \mathbf{r}^H(n)\mathbf{\Phi}(n)\mathbf{r}(n)\right]}$ c) $\hat{\mathbf{W}}_{RLS}(n+1) = \hat{\mathbf{W}}_{RLS}(n) + \mathbf{e}(n)\mathbf{k}^H(n)$ d) $\mathbf{\Phi}(n+1) = \frac{1}{\gamma}\left[\mathbf{\Phi}(n) - \mathbf{k}(n)\mathbf{r}^H(n)\mathbf{\Phi}(n)\right]$ e) $n = n+1$	- Compute the output vector - Compute the error vector - Compute the gain vector with $\mathbf{r}(n)$, $\mathbf{\Phi}(n)$ and the forgetting factor γ. - Updating the tap-weight vector - Update the inverse correlation matrix - Increment the recursion-index.

Table 3.4 Summary of MIMO-RLS algorithm.

During initialisation, besides $\mathbf{W}_{RLS}$ and its tap-weight coefficients is set to zero, same as (3.62), additional initialisation is needed on the inverse of correlation matrix shown as follows:

$$\mathbf{\Phi}(0) = \delta^{-1}\mathbf{I} \tag{3.64}$$

$$\begin{bmatrix} \phi_{11}(0) & \cdots & \phi_{1N}(0) \\ \vdots & \ddots & \vdots \\ \phi_{N1}(0) & \cdots & \phi_{NN}(0) \end{bmatrix} = \delta^{-1}\begin{bmatrix} 1 & 0 & 0 \\ 0 & \ddots & 0 \\ 0 & 0 & 1 \end{bmatrix}$$

where δ is a small constant and $\mathbf{I}$ is the identity matrix. The forgetting factor γ is typically set closer to unity as $\gamma = 0.98$. During the recursion, $\mathbf{y}(n)$ and $\mathbf{e}(n)$ are computed. However, for the MIMO-RLS algorithm, each $e_i(n)$ in the $\mathbf{e}(n)$ is slightly different from the definition in the basic

RLS algorithm in (3.50). Each error response $e_i(n)$ for the MIMO-RLS algorithm, is obtained based on *present* estimate of tap-weight vector $\hat{\mathbf{w}}(n)$ (instead of *previous* $\hat{\mathbf{w}}(n-1)$) shown as:

$$e(n) = d(n) - \hat{\mathbf{w}}(n)\,\mathbf{r}(n) \tag{3.66}$$

Next, the ultimate difference between the basic LMS and RLS lies at the additional computation of the gain vector, $\mathbf{k}(n)$ in RLS algorithm, which is computed as follows:

$$\mathbf{k}(n) = \frac{\boldsymbol{\Phi}(n)\,\mathbf{r}(n)}{\left[\gamma + \mathbf{r}^{H}(n)\,\boldsymbol{\Phi}(n)\,\mathbf{r}(n)\right]} = \begin{bmatrix} g_1(n) \\ \vdots \\ g_N(n) \end{bmatrix} \tag{3.67}$$

Finally, the weighting matrix $\mathbf{W}_{RLS}$ can be updated as follows:

$$\hat{\mathbf{W}}_{RLS}(n+1) = \hat{\mathbf{W}}_{RLS}(n) + \mathbf{e}(n)\mathbf{k}^{H}(n) \tag{3.68}$$

$$\begin{bmatrix} \hat{\omega}_{11}(n+1) & \cdots & \hat{\omega}_{1N}(n+1) \\ \vdots & \ddots & \vdots \\ \hat{\omega}_{M1}(n+1) & \cdots & \hat{\omega}_{MN}(n+1) \end{bmatrix} = \begin{bmatrix} \hat{\omega}_{11}(n) & \cdots & \hat{\omega}_{1N}(n) \\ \vdots & \ddots & \vdots \\ \hat{\omega}_{M1}(n) & \cdots & \hat{\omega}_{MN}(n) \end{bmatrix} + \begin{bmatrix} e_1(n) \\ \vdots \\ e_M(n) \end{bmatrix} \begin{bmatrix} g_1^*(n) & \cdots & g_N^*(n) \end{bmatrix}$$

Similar to the basic RLS algorithm, the inverse of correlation matrix $\boldsymbol{\Phi}(n)$ in the recursion can be subsequently updated as:

$$\boldsymbol{\Phi}(n+1) = \frac{1}{\gamma}\left[\boldsymbol{\Phi}(n) - \mathbf{k}(n)\,\mathbf{r}^{H}(n)\,\boldsymbol{\Phi}(n)\right] \tag{3.69}$$

Note that the ultimate difference between the basic RLS algorithm and the MIMO-RLS algorithm lies within the recursive formulation for updating the tap-weights shown respectively in (3.51) and (3.68), using different form of error response. In the MIMO-RLS algorithm, the error vector $\mathbf{e}(n)$ is used instead of using only single error response $e(n)$ in the basic RLS algorithm. Consequently, the MIMO channel estimate $\hat{\mathbf{H}}$ can be obtained by inverting the final value of $\hat{\mathbf{W}}_{RLS}$ matrix upon completing the iteration process in (3.68).

3.3.2.3 Comparison between MIMO-LMS and MIMO-RLS Algorithm

Interestingly, when comparing the two MIMO adaptive algorithms for updating the weighting matrix $\mathbf{W}$, in (3.63) and (3.68) respectively, the MIMO-RLS algorithm appears to be very alike with the MIMO-LMS algorithm in the basic structure defined as follows:

$$\hat{\mathbf{W}}(n+1) = \hat{\mathbf{W}}(n) + \mathbf{C}(n) \tag{3.70}$$

where $\mathbf{C}(n)$ denotes as the correction matrix. Obviously, the correction matrix is different in both MIMO-LMS and MIMO-RLS algorithms. The reason that MIMO-RLS being a faster convergence algorithm is that the gain vector $\mathbf{k}(n)$ computed in the correction matrix $\mathbf{C}(n)$

provides more powerful adaptation in (3.70), which is depending on the past value of the inverse of correlation matrix $\mathbf{\Phi}(n)$ in the deterministic manner that always leads to the Wiener-Hopf optimum solution. This has been shown in section 3.2.3 for the derivation of basic RLS algorithm. On the other hand, correction matrix in MIMO-LMS algorithm provides less powerful adaptation, which requires larger input samples $\mathbf{r}(n)$ to reach the optimum solution (even the step-size parameter has set to optimum value), using the statistical approach shown in section 3.2.2.

3.3.3 Non-Adaptive Training-Based Approach

In the non-adaptive training-based approach, V number of training vectors $\mathbf{s}(n)$ are sent in burst of data-block, which form the necessary "pilot matrix" $\mathbf{S}$ as follows:

$$\mathbf{S} = [\,\mathbf{s}(1) \quad \mathbf{s}(2) \quad \cdots \quad \mathbf{s}(V)\,] = \left[\begin{bmatrix} s_1(1) \\ \vdots \\ s_M(1) \end{bmatrix} \begin{bmatrix} s_1(2) \\ \vdots \\ s_M(2) \end{bmatrix} \cdots \begin{bmatrix} s_1(V) \\ \vdots \\ s_M(V) \end{bmatrix}\right] \tag{3.71}$$

The formulation in (3.71) can also be viewed as each m^{th} transmit antenna sending their respective training sequence that consists of pilot symbol $s_m(1)$ to $s_m(V)$. Hence, $\mathbf{S}$ sent over the flat fading MIMO channel $\mathbf{H}$ can be related to its corresponding received signal matrix $\mathbf{R}$ as:

$$\mathbf{R} = \mathbf{H}\mathbf{S} + \mathbf{N} \tag{3.72}$$

where $\mathbf{N}$ is the corresponding noise matrix that consists the collective AWGN noise vectors $\mathbf{n}(n)$. The corresponding received signal matrix $\mathbf{R}$ consists of respective received signal vectors as:

$$\mathbf{R} = [\,\mathbf{r}(1) \quad \mathbf{r}(2) \quad \cdots \quad \mathbf{r}(V)\,] = \left[\begin{bmatrix} r_1(1) \\ \vdots \\ r_N(1) \end{bmatrix} \begin{bmatrix} r_1(2) \\ \vdots \\ r_N(2) \end{bmatrix} \cdots \begin{bmatrix} r_1(V) \\ \vdots \\ r_N(V) \end{bmatrix}\right] \tag{3.73}$$

In the adaptive method, the estimation started as soon as the first received signal vector $\mathbf{r}(1)$ arrives. However, in the non-adaptive method, the receiver needs to wait until all V received signal vectors $\mathbf{r}(n)$ have arrived first, to form the corresponding received signal matrix $\mathbf{R}$, so that channel estimation can be performed with the use of *a priori* known pilot matrix $\mathbf{S}$ as:

$$\hat{\mathbf{H}} = \mathbf{R}\,\mathbf{S}^{+} \tag{3.74}$$

where $(.)^{+}$ is the pseudo-inverse operation which can be achieved through different ways, e.g. Moore-Penrose or SVD [116, 123]. Obviously, the accuracy of the channel estimation in (3.74) depends on the success of matrix inversion process on $\mathbf{S}$ as well as the noise condition.

Although the formulation in (3.74) appears to be simpler as compared to the adaptive algorithms, it requires time-consuming computation to perform the matrix inversion on $\mathbf{S}$. (e.g. if $\mathbf{S}$ is a wide matrix with dimension of $(M \times V)$ where $V >> M$, where the pseudo-inverse operation

which is tedious to be performed). An alternative way is to slightly modify (3.74) such that direct matrix inversion $(.)^{-1}$ is performed as follows instead of using pseudo-inversion:

$$\hat{\mathbf{H}} = \mathbf{R}\mathbf{S}^{H}\left(\mathbf{S}\mathbf{S}^{H}\right)^{-1} \tag{3.75}$$

where $(.)^{H}$ is the Hermitian operation. Note that the product term $\mathbf{S}\mathbf{S}^{H}$ now becomes a square matrix that allows direct matrix inversion to be applied. The method used in (3.75) for MIMO channel estimation can be referred as the maximum-likelihood (ML) estimator, which can be found in [11, 73, 83, 84]. This concept has been studied for the flat fading channel and it is also learned that the optimum training sequence that minimises the MSE is made of orthogonal sequences, which can be used to construct **S** to achieve the best estimation accuracy. The use of orthogonal sequence and its property are presented next.

3.3.3.1 Matrix Inversion and Orthonormal Properties

The matrix inversion is a vital process in the non-adaptive channel estimation technique, which usually requires high computational power depending on the size of the matrix to be inverted. Also, whether a matrix is invertible or not depends on the condition of the matrix itself [116]. If the matrix is ill-conditioned, the inversion process may become invalid since the matrix is close to singular case. [116, 117].

It is however, possible to utilise the orthogonal properties in order to assist the matrix inversion process where matrix inversion can simply be replaced by the matrix transposition [117, 123]. The following orthonormal property shows the inverse-transpose relationship:

$$\mathbf{Q}^{\mathsf{T}}\mathbf{Q} = \mathbf{I} \quad \text{and} \quad \mathbf{Q}^{\mathsf{T}} = \mathbf{Q}^{-1} \tag{3.76}$$

$$\mathbf{Q}^{\mathsf{T}}\mathbf{Q} = \begin{bmatrix} — q_1^{\mathsf{T}} — \\ \vdots \\ — q_n^{\mathsf{T}} — \end{bmatrix} \begin{bmatrix} | & & | \\ q_1 & \cdots & q_n \\ | & & | \end{bmatrix} = \begin{bmatrix} 1 & 0 & 0 \\ 0 & \ddots & 0 \\ 0 & 0 & 1 \end{bmatrix}$$

where

$$q_i^{\mathsf{T}} q_j = 0 \quad \text{and} \quad q_i^{\mathsf{T}} q_i = 1 \tag{3.77}$$

q is the orthonormal column vector obtained by the Gram-Schmidt orthogonalisation (GSO) [116, 123]. **I** is the identity matrix. (3.76) simply states that **I** can be produced if the columns of **Q** matrix are orthonormal and left-multiplying **Q** with its matrix transpose $\mathbf{Q}^{\mathsf{T}}$. This also means that if **Q** is an orthogonal matrix, then its matrix inversion $\mathbf{Q}^{-1}$ is equivalent to its matrix transposition $\mathbf{Q}^{\mathsf{T}}$. If **Q** is a square matrix with orthonormal columns, then the following is also true:

$$\mathbf{Q}\,\mathbf{Q}^{\mathsf{T}} = \mathbf{I} \tag{3.78}$$

Note that (3.78) is written differently from (3.76) where **Q** is now right-multiplied by the transpose matrix $\mathbf{Q}^{\mathsf{T}}$. However, when **Q** is a tall matrix with lesser columns or more rows that consists of only orthonormal column vectors q, then only the orthogonal properties shown in

(3.76) are true whereas the property in (3.78) becomes invalid, which can be easily verified. The orthogonal properties for the rectangular tall matrix are shown in the following:

$$\mathbf{Q}^{\mathsf{T}}\mathbf{Q} = \begin{bmatrix} \text{——} & q_1^{\mathsf{T}} & \text{——} \\ & \vdots & \\ \text{——} & q_m^{\mathsf{T}} & \text{——} \end{bmatrix} \begin{bmatrix} | & & | \\ q_1 & \cdots & q_m \\ | & & | \end{bmatrix} = \mathbf{I} \tag{3.79}$$

On the other hand, if **Q** matrix is a wide matrix with orthonormal row vectors q (instead of orthonormal column vectors), then, only orthogonal property in (3.78) is valid as:

$$\mathbf{Q}\,\mathbf{Q}^{\mathsf{T}} = \begin{bmatrix} \text{——} & q_1 & \text{——} \\ & \vdots & \\ \text{——} & q_m & \text{——} \end{bmatrix} \begin{bmatrix} | & & | \\ q_1^{\mathsf{T}} & \cdots & q_m^{\mathsf{T}} \\ | & & | \end{bmatrix} = \mathbf{I} \tag{3.80}$$

Note that in both (3.79) and (3.80), the wide-rectangular matrix is always placed on the left side of the tall-rectangular matrix in order to make the orthogonal properties valid. This is because the multiplication of inner product must be performed on the corresponding 'orthonormal' vector, but not on the non-orthonormal vector, for the respective structure of **Q**.

Hence, the properties from (3.76) to (3.80) can be utilised to replace the task of matrix inversion by the matrix transposition that requires lesser computations. However, the orthonormal vectors must be obtained first before these orthogonal properties can be applied and the methods of achieving these orthonormal sequences can be found in [116, 117, 123], which will not be discussed here. Instead, its application will be focused to design specific pilot sequences for the non-adaptive channel estimation approach in a MIMO flat-fading channel.

3.3.3.2 Hadamard Matrix – The Structure and Orthogonal Properties [132, 133]

The Hadamard matrix is a square matrix that consists of orthogonal rows or columns with uniform amplitude of ±1. (Unlike the orthonormal vector where each element is normalised). An example of Hadamard matrix **Z** of order of 4 with (4×4) entries, is presented as follows:

$$\mathbf{Z} = \begin{bmatrix} 1 & 1 & 1 & 1 \\ 1 & -1 & 1 & -1 \\ 1 & 1 & -1 & -1 \\ 1 & -1 & -1 & 1 \end{bmatrix} \tag{3.81}$$

It can be seen that the Hadamard matrix has the symmetrical structure with orthogonal entries in each row or column. Therefore, the following orthogonal properties can be applied:

$$\mathbf{Z}^{\mathsf{T}}\mathbf{Z} = v\mathbf{I} \quad \text{or} \quad \mathbf{Z}\mathbf{Z}^{\mathsf{T}} = v\mathbf{I}; \qquad \mathbf{Z}^{\mathsf{T}} = v\mathbf{Z}^{-1} \tag{3.82}$$

where 'v' is the Hadamard matrix order. (3.82) implies that the inversion of the Hadamard matrix is equivalent to its matrix transposition and (3.82) is only different from (3.76) by a factor of v.

3.3.3.3 Non-adaptive MIMO-Pilot Matrix Inversion Algorithm (MIMO-PMI)

In the following, the non-adaptive MIMO-PMI channel estimation technique for the flat-fading MIMO channel will be illustrated for a (4×4) system. First, the Hadamard matrix is generated with suitable order v based on following criterion:

$$v = \min(2^{\ell}) \geq M \tag{3.83}$$

where ℓ is an integer and M is the number of transmit antenna. Here, the (4×4) Hadamard matrix with minimum order $v = 4$ is generated since $M = 4$ in this case. Next, the pilot matrix **S** is designed such that M row orthogonal sequence of the Hadamard matrix is extracted and assigned to **S** where **S** is constructed into its real and imaginary matrices, **A** and **B** shown as follows:

$$\mathbf{S} = \mathbf{A} + j\mathbf{B} = \begin{bmatrix} 1 & 1 & 1 & 1 \\ 1 & -1 & 1 & -1 \\ 1 & 1 & -1 & -1 \\ 1 & -1 & -1 & 1 \end{bmatrix} + j\begin{bmatrix} 1 & 1 & 1 & 1 \\ 1 & -1 & 1 & -1 \\ 1 & 1 & -1 & -1 \\ 1 & -1 & -1 & 1 \end{bmatrix} \tag{3.84}$$

where **A** and **B** are each constructed from the Hadamard matrix in (3.81). For simplicity, matrix **A** and **B** are chosen to be the same, although other combinations of **A** and **B** are possible to achieve the same objective. To illustrate the MIMO-PMI algorithm in the complex form, the channel matrix **H** is split into its real and imaginary matrices, **X** and **Y** respectively as:

$$\mathbf{H} = \mathbf{X} + j\mathbf{Y} \tag{3.85}$$

Hence the corresponding received signal matrix **R** (in noiseless case) can be expressed as:

$$\mathbf{R} = \mathbf{HS} = (\mathbf{X}+j\mathbf{Y})(\mathbf{A}+j\mathbf{B}) = (\mathbf{XA}-\mathbf{YB}) + j(\mathbf{XB}+\mathbf{YA}) \tag{3.86}$$

Next, to obtain the estimate of the MIMO channel, **R** is right-multiply by the Hermitian of **S** instead of the pseudo-inversion of **S** shown in (3.74), which is demonstrated in the following:

$$\hat{\mathbf{H}} = f\{\mathbf{R}\mathbf{S}^{\mathsf{H}}\} = f\left[(\mathbf{XA}-\mathbf{YB}) + j(\mathbf{XB}+\mathbf{YA})\right]\left[\mathbf{A}^{\mathsf{T}}-j\mathbf{B}^{\mathsf{T}}\right] \tag{3.87}$$

$$= f\left[\left(\mathbf{XAA}^{\mathsf{T}}\underbrace{-\mathbf{YBA}^{\mathsf{T}}+\mathbf{YAB}^{\mathsf{T}}}_{\text{middle terms}}+\mathbf{XBB}^{\mathsf{T}}\right)+j\left(\mathbf{YAA}^{\mathsf{T}}\underbrace{+\mathbf{XBA}^{\mathsf{T}}-\mathbf{XAB}^{\mathsf{T}}}_{\text{middle terms}}+\mathbf{YBB}^{\mathsf{T}}\right)\right]$$

where f is the correction factor. Through proper design in **A** and **B**, leads to the following:

$$\mathbf{BA}^{\mathsf{T}} = \mathbf{AB}^{\mathsf{T}} \tag{3.88}$$

By setting **A** = **B** in (3.87), the condition in (3.88) is guaranteed. Thus, the middle terms in (3.87) can be effectively cancelled out, leading to the following final expression:

$$\hat{\mathbf{H}} = f\left(\mathbf{X} + j\mathbf{Y}\right)\left(\mathbf{A}\mathbf{A}^{\mathsf{T}} + \mathbf{B}\mathbf{B}^{\mathsf{T}}\right) = f\left(\mathbf{H}\mathbf{S}\right)\mathbf{S}^{\mathsf{H}} \tag{3.89}$$

When **A** = **B** are both the orthogonal matrices, which lead to simplified term as:

$$\left(\mathbf{S}\,\mathbf{S}^{\mathsf{H}}\right) = \left(\mathbf{A}\mathbf{A}^{\mathsf{T}} + \mathbf{B}\mathbf{B}^{\mathsf{T}}\right) = 2\mathbf{A}\mathbf{A}^{\mathsf{T}} = 2v\mathbf{I} \tag{3.90}$$

Therefore, the resulting expression in (3.89) can be re-written as:

$$\hat{\mathbf{H}} = f\left(\mathbf{X} + j\mathbf{Y}\right)\left(2v\mathbf{I}\right) = f\left(\mathbf{H}\right)\left(2v\mathbf{I}\right) \tag{3.91}$$

where **I** is the identity matrix. Note that (3.91) consists **X** and **Y** of the channel matrix **H** in (3.85). Finally, $\hat{\mathbf{H}}$ can be obtained with appropriate f to compensate the '$2v$' term as follows:

$$f = 1/2v \tag{3.92}$$

Note that the pilot matrix **S** contains pilot symbols with uniform amplitude of ±1 within **A** and **B** as shown in (3.84). However, the value of this uniform amplitude can be changed accordingly to the required magnitude ±s required by the MIMO system as follows:

$$\mathbf{S} = \mathbf{A} + j\mathbf{B} = \begin{bmatrix} +s & +s & +s & +s \\ +s & -s & +s & -s \\ +s & +s & -s & -s \\ +s & -s & -s & +s \end{bmatrix} + j\begin{bmatrix} +s & +s & +s & +s \\ +s & -s & +s & -s \\ +s & +s & -s & -s \\ +s & -s & -s & +s \end{bmatrix} \tag{3.93}$$

As a result, the estimation equation in (3.91) is also changed accordingly as follows:

$$\hat{\mathbf{H}} = f\left(\mathbf{X} + j\mathbf{Y}\right)\left(2vs^2\mathbf{I}\right) \tag{3.94}$$

Now, the correction factor f has to compensate the term $2vs^2$ as:

$$f = 1/\left(2vs^2\right) \tag{3.95}$$

where s^2 is the energy per pilot symbol. Now, s can be set to any arbitrary number.

An alternative way to include the transmit-power into the expression of **R** while retaining uniform amplitude of ±1 in **A** and **B** of **S** as in (3.84) is re-expressed as follows:

$$\mathbf{R} = \sqrt{\frac{\rho}{M}}\mathbf{H}\mathbf{S} + \mathbf{N} \tag{3.96}$$

where ρ denotes the expected SNR. The $\sqrt{\rho/M}$ term is the power control that keep the total transmit power constant at the receiver regardless of the number of transmit antennas M. According to [73], the channel estimate $\hat{\mathbf{H}}$ can then be obtained as follows:

$$\hat{\mathbf{H}} = f\,\mathbf{R}\,\mathbf{S}^{\mathsf{H}}\left(\mathbf{S}\,\mathbf{S}^{\mathsf{H}}\right)^{-1} = f\left(\sqrt{\frac{\rho}{M}}\mathbf{H}\mathbf{S}\right)\mathbf{S}^{\mathsf{H}}\left(\mathbf{S}\,\mathbf{S}^{\mathsf{H}}\right)^{-1} \tag{3.97}$$

It is obvious that the correction factor f above is set to $\sqrt{M/\rho}$. Although (3.97) allows **S** to constitute any structure, the best estimation result is obtained when **S** is constructed by the

orthogonal matrices in both its **A** and **B** and the channel estimate $\hat{\mathbf{H}}$ can be obtained as:

$$\hat{\mathbf{H}} = f\,\mathbf{R}\,\mathbf{S}^{\mathsf{H}} = f\left(\sqrt{\frac{\rho}{M}}\,\mathbf{H}\mathbf{S}\right)\mathbf{S}^{\mathsf{H}} \tag{3.98}$$

Since $\mathbf{S}\mathbf{S}^{\mathsf{H}} = 2v\mathbf{I}$ as obtained in (3.90), the correction factor f for (3.98) is set to $\sqrt{M/\rho} \times 1/2v$.

Therefore, it can be seen that with the use of orthogonal matrix, the term $\left(\mathbf{S}\,\mathbf{S}^{\mathsf{H}}\right)^{-1}$ in (3.97) is now eliminated and substituted by just the extra constant value of '1/2v' in the setting of f. The formulations from (3.83) to (3.98) in effect constitute the basic of the MIMO-PMI algorithm for the non-adaptive channel estimation method in a MIMO system. The importance of using the orthogonal sequences in forming the pilot matrix has been shown; not only avoiding the need of matrix inversion but also providing a way for virtual segregation of each collective transmission that enables effective CCI mitigation at the receiver during the training of the channel.

3.3.3.4 The Pilot Matrix Design Consideration for Different System Configuration

The formulations from (3.83) to (3.98) are explained using the (4×4) system, where the number of transmit antenna M equals to the number of receive antenna N. Also, M is the same value as the order v used to generate the Hadamard matrix to form the subsequent pilot matrix **S**.

To generalise the MIMO-PMI channel estimation method for any (N×M) system for the flat fading channel, the following procedure must be followed:

First the value of M is crucial in determining the order v that is needed to generate the Hadamard matrix with the correct size. The condition in (3.83) can be still used here

$$\left[v = \min\left(2^{\ell}\right)\right] \geq M \tag{3.99}$$

Equation (3.99) means that v is assigned with the value that fulfils two conditions: First, v must be assigned with the valid order of the Hadamard matrix. Secondly, the order v must be at least equal or greater than the number of transmit antenna M. This produces a range of possible values where v can be increased accordingly to next levels of Hadamard's order. However, the minimum value of v that fulfils (3.99) will be used here. Once the value of v is determined, the Hadamard matrix is generated using the order of v with the matrix dimension of (v×v).

Next, the pilot matrix **S** can be constructed from this (v×v) Hadamard matrix whereby each row of **S** is assigned with an orthogonal row sequence extracted from the Hadamard matrix. Each orthogonal row sequence must contain v symbols in full length. Depending on the value of M, any M non-repetitive consecutive rows of the Hadamard matrix can be extracted. Therefore, the (M×v) size pilot matrix **S** can be acquired directly from the (v×v) Hadamard matrix previously

generated. The (M×v) size pilot matrix **S** is defined in the following:

$$\mathbf{S} = \begin{bmatrix} \boldsymbol{s}_1 \\ \boldsymbol{s}_2 \\ \vdots \\ \boldsymbol{s}_M \end{bmatrix} = \begin{bmatrix} \mathrm{s}_1(1) & \mathrm{s}_1(2) & \cdots & \mathrm{s}_1(v) \\ \mathrm{s}_2(1) & \mathrm{s}_2(2) & \cdots & \mathrm{s}_2(v) \\ & & \vdots & \\ \mathrm{s}_M(1) & \mathrm{s}_M(2) & \cdots & \mathrm{s}_M(v) \end{bmatrix} \tag{3.100}$$

where $\mathrm{s}_i(t)$ denotes the complex pilot symbol sent from i^{th} transmit antenna at time t. The pilot matrix **S** in (3.100) can also be expressed in terms of each row sequence $\boldsymbol{s}_i$ sent by i^{th} transmit antenna, which is orthogonal to one another. The basic formulation of **S** in (3.71) can still be applied except that the number of vectors V is now replaced to the value of v.

One of the vital rules in creating **S** is that its matrix size must be attained according to the basic dimension of (M×v). This rule can generally be applied for any (N×M) system configuration for N=M as well as N>M case. Note that the generation **S** is totally independent of the value of N. Two other (N×M) systems will be used next to explain the case of $(N \geq M) \neq v$:

a) *Example using* (3×3) *system for* $(N=M) \neq v$ *case*

In a (3×3) system, the MIMO-PMI algorithm is required to estimate the channel matrix with (3×3) entries. Following the criterion in (3.99), the minimum order that required to generate the right size Hadamard matrix is v = 4 in order to fulfil the condition of v>M since M=3. Therefore, the Hadamard matrix with order of 4 is first generated. Next, for the construction of the pilot matrix **S**, only three orthogonal rows sequences are selected from this (4×4) Hadamard matrix. For simplicity, any three consecutive rows can be chosen. This forms a (3×4) pilot matrix **S**. Subsequently, for the estimation of the (3×3) channel matrix, the formulations from (3.89) to (3.98) can still be applied and can be easily verified. Note that the length of the pilot matrix must always constitute the full-length of the orthogonal sequence (which is the value of v used for generating the Hadamard matrix), in order to fulfil the orthogonal properties shown in (3.82). Since the pilot matrix is a wide-rectangular matrix, the property in (3.80) will be applied.

b) *Example using* (5×3) *system for* $(N > M) \neq v$ *case*

For the case of $N > M$, in a (5×3) system, the MIMO-PMI algorithm is required to estimate the channel matrix with (5×3) entries. Nevertheless, since the value of N has no effect in the procedure of constructing the pilot matrix, the resulting pilot matrix **S** will be same as the previous case. Similarly, for the estimation of the (5×3) channel matrix, the formulations from (3.89) to (3.98) can still be applied. One can easily verify this condition by using method of dimension matching for matrix representation in those formulations.

3.3.3.5 The Pilot Matrix Expansion

This basic dimension ($M \times v$) of the pilot matrix used in MIMO-PMI algorithm previously can be further expanded (in columns) to improve the performance of the channel estimator. However, the expansion of the basic pilot matrix must be accomplished such that each row of training sequence in the expanded pilot matrix is still orthogonal to one another so that the fundamental orthogonal properties can still be applied for the MIMO-PMI algorithm.

There are two ways to expand the basic pilot matrix. First, according to (3.99), v can be increased to the next valid order to generate a bigger size of Hadamard matrix. For example, the previous v=4 can be increased to v=8 or v=16. The size of expanded pilot matrix $\mathbf{S}_{exp}$ will now be a wider ($M \times 8$) or ($M \times 16$) rectangular matrix instead of ($M \times 4$) matrix. The newly generated (8×8) Hadamard matrix provides more choices of row sequences to be selected for the construction of pilot matrix. To further expand the size of the pilot matrix, its length can be further increased by extracting the orthogonal sequences from the next higher order of Hadamard matrix.

The second method is less tedious, since only the basic pilot matrix constructed from the minimum v ordered Hadamard matrix is needed. Using same example, the basic pilot matrix $\mathbf{S}_{int}$ will have minimum size of ($M \times v$) where $v \geq M$ and v is of minimum according to (3.83). The expansion can be accomplished by duplicating this $\mathbf{S}_{int}$ and cascading them together so that the length of the expanded pilot matrix $\mathbf{S}_{exp}$ can be further increased. This is shown in the following:

$$\mathbf{S}_{exp} = \left[\mathbf{S}_{int}(1) \quad \mathbf{S}_{int}(2) \quad \cdots \quad \mathbf{S}_{int}(P) \right] \tag{3.101}$$

Note that the expanded pilot matrix $\mathbf{S}_{exp}$ comprises multiple P set of basic $\mathbf{S}_{int}$. Depending on the size required, the length of the pilot matrix can be increased in the multiple of ($P \times v$), forming the $\mathbf{S}_{exp}$ with matrix dimension of $M \times (P \times v)$. The expansion still preserves the orthogonal structure of the training sequence (since basic $\mathbf{S}_{int}$ is orthogonal), thereby allowing the orthogonal properties to be applied for the same procedure of channel estimation from (3.87) to (3.98).

Thus, the estimate of the channel using the expanded pilot matrix $\mathbf{S}_{exp}$ shown by the two methods can be obtained with the modified version of the MIMO-PMI algorithm as follows:

$$\hat{\mathbf{H}} = f\left\{\mathbf{R}\,\mathbf{S}_{exp}{}^{H}\right\} \tag{3.102}$$

where f is the same compensation factor. In the 1st method of expansion in $\mathbf{S}_{exp}$, f is set exactly as in (3.95), according to the increased order v used to generate the 'higher-ordered' Hadamard matrix. However, for the 2nd expansion method in $\mathbf{S}_{exp}$, f is set to include the 'P' factor as follows:

$$f = \frac{1}{2vPs^2} \tag{3.103}$$

3.4 Comparison in Implementation Complexity

It is useful to access the computational complexity of each MIMO-CE algorithm; i.e. MIMO-LMS, MIMO-RLS and MIMO-PMI, in order to know how costly in terms of computational power for obtaining the required channel estimates. In this part, the computation will be carried out by counting the number of floating point operations as number of "*flops*", that each algorithm requires. Each addition, subtraction, multiplication, division operation will be counted as one *flop*. However, to show clearly for the counting, the operation counts will be displayed along each equation used by the respective estimation algorithm. The following abbreviations for respective operation are used as follows: '*add*' for addition, '*sub*' for subtraction, '*mul*' for multiplication and '*div*' for division. Appropriate parameter; e.g. N, M, v, n will be used along to denote the number of *flops* for respective operations in each equation.

First, the computational complexity of the adaptive approach; the MIMO-LMS and the MIMO-RLS channel estimation will be accessed. (Refer to section 3.3.3 for the summary of both MIMO-LMS and MIMO-RLS algorithms).

a) MIMO-LMS channel estimation process algorithm	
a) $\mathbf{y}(n) = \hat{\mathbf{W}}_{\text{LMS}}(n)\mathbf{r}(n)$	a) NM *muls* $+ M(N-1)$ *adds*
b) $\mathbf{e}(n) = \mathbf{d}(n) - \mathbf{y}(n)$	b) M *subs*
c) $\hat{\mathbf{W}}_{\text{LMS}}(n+1) = \hat{\mathbf{W}}_{\text{LMS}}(n) + \mu\mathbf{e}(n)\mathbf{r}^{\text{H}}(n)$	c) NM *adds* $+ 2N^2$ *muls*

Table 3.5: Computational complexity of the MIMO-LMS algorithm

Therefore, the number of flops needed to complete 1 iteration in MIMO-RLS algorithm:

$$\cong 3MN + 2N^2 + M \text{ flops} \quad (\text{where } N\text{–}1 \text{ is treated as} \sim N)$$

b) MIMO-RLS channel estimation process algorithm	
a) $\mathbf{y}(n) = \hat{\mathbf{W}}_{\text{RLS}}(n)\mathbf{r}(n)$	a) NM *muls* $+ M(N-1)$ *adds*
b) $\mathbf{e}(n) = \mathbf{d}(n) - \mathbf{y}(n)$	b) M *subs*
c) $\mathbf{k}(n) = \dfrac{\boldsymbol{\Phi}(n)\mathbf{r}(n)}{\left[\gamma + \mathbf{r}^{\text{H}}(n)\boldsymbol{\Phi}(n)\mathbf{r}(n)\right]}$	c) N^2 *muls* $+ N(N-1)$ *adds* $+$ (N^2+N) *muls* $+ N^2$ *adds*
c) $\hat{\mathbf{W}}_{\text{RLS}}(n+1) = \hat{\mathbf{W}}_{\text{RLS}}(n) + \mathbf{e}(n)\mathbf{k}^{\text{H}}(n)$	d) NM *adds* $+ 2N^2$ *muls*
d) $\boldsymbol{\Phi}(n+1) = \dfrac{1}{\gamma}\left[\boldsymbol{\Phi}(n) - \mathbf{k}(n)\mathbf{r}^{\text{H}}(n)\boldsymbol{\Phi}(n)\right]$	e) N^2 *subs* $+ N^2$ *muls* $+$ $N(N-1)$ *adds* $+ N^2$ *divs*

Table 3.6: Computational complexity of the MIMO-RLS algorithm

Therefore, the number of flops needed to complete 1 iteration in MIMO-RLS algorithm:

$$\cong 3MN + 10N^2 + M + 2N \textit{ flops} \text{ (where } N\text{–}1 \text{ is treated as} \sim N)$$

Hence, if total n training vectors that corresponds to n iterations are used in both adaptive approaches to arrive at the converged solution of the channel estimates, then, the total number of *flops* required for each case is obtained as follows:

For MIMO-LMS: $n(3MN+2N^2+M)$ *flops* &

For MIMO-RLS: $n(3MN+10N^2+M+2N)$ *flops*

Next, the computational complexity of the non-adaptive MIMO-PMI channel estimation algorithm is accessed. Recall that MIMO-PMI algorithm in equation (3.83) only requires a single equation to obtain the channel estimate, which is shown again as follows:

$\hat{\mathbf{H}} = f\left\{\mathbf{R}\,\mathbf{S}^{\mathsf{H}}\right\}$: Total *flops* = Nv *muls* + $M(v-1)$ *adds* + NM *muls* (for correction factor f) and Mv *flops* (for Hermitian-transposition operation).

Hence, the number or flops needed in the MIMO-PMI algorithm:

$\cong v(N+2M)+NM$ *flops* (where $v-1$ is treated as $\sim v$)

Note that v is the pilot length of the training sequence in the pilot matrix **S**, which is also the total number of pilot (column) vectors needed to be sent in the MIMO-PMI algorithm. Therefore, it can be viewed as the same entity as the n iterations needed in MIMO-RLS algorithm, since n pilot (column) vectors is also needed.

We can generalise these two parameters as $v = n = k$ if the same number of pilot vectors are used in each approach, which allow us to make direct comparison of the computation complexity between MIMO-RLS and MIMO-PMI channel estimation algorithm.

a) MIMO-RLS: $k(3MN+10N^2+M+2N)$ *flops* &

b) MIMO-PMI: $k(N+2M)+NM$ *flops*

It is found that although both methods achieved similar BER performance (shown later in result section), the MIMO-PMI approach has less computational complexity as compared to the MIMO-RLS algorithm.

3.5 Summary

In Chapter 3, three training-based MIMO channel estimation schemes namely the MIMO-LMS, MIMO-RLS and MIMO-PMI algorithms, have been introduced and demonstrated. The first two approaches are the adaptive MIMO channel estimation schemes whereas the MIMO-PMI is the non-adaptive channel estimation method. The fundamentals of the adaptive approaches such as Wiener filtering, the basic of LMS and RLS derivations have been shown and

adaptive method devised for MIMO systems have been illustrated. Comparisons between the MIMO-LMS algorithm and MIMO-RLS algorithm have been pointed out. This is followed by the illustration of non-adaptive MIMO-PMI algorithm, which uses concept of pilot matrix to perform channel estimation by a single matrix inversion operation. The design and criteria of the pilot matrix construction with different parameter configurations and the need for orthogonal training sequences have also been shown where the Hadamard structure and its orthogonal properties were used to assist the channel estimation in the MIMO systems. Scenario for possible extension of pilot matrix to achieve better system performance, has also been demonstrated. Lastly, comparison in terms of computational complexity between MIMO-RLS and MIMO-PMI algorithms has also been carried where MIMO-PMI algorithm is found to have less implementation complexity than the MIMO-RLS algorithm.

Although various channel estimation schemes have been successfully implemented in the MIMO systems to estimate the $N \times M$ fading coefficients, the methods used in this chapter are solely catered for the frequency-flat fading MIMO channel condition where only single path link exists between each transmit-receive antennas pair. In the next chapter, the MIMO channel estimation schemes are extended to the frequency-selective fading channel to cater more complicated scenario where $(L+1)$ multipath fading within each channel impulse response of each link is considered. The novel MIMO channel estimation scheme presented in Chapter 4 attempts to estimate all the $N \times M \times (L+1)$ fading coefficients while resolving the co-channel interference and the inter-symbol interference posed by the frequency-selective fading MIMO channel. The design criteria and all other related issues of the proposed frequency-selective MIMO channel estimation scheme will be demonstrated in the next chapter.

Chapter 4

Novel MIMO Channel Estimation Scheme (Design and Implementation)

This chapter presents a novel training-based MIMO channel estimation (MIMO-CE) scheme for the class of layered space-time receivers described in Chapter 2. The development of the proposed MIMO-CE scheme from the frequency-flat fading channel to the frequency selective fading channel is presented. This includes the extension from the MIMO-PMI method (described in Chapter 3) to include the consideration of (L+1) frequency-selective paths and the problem of CCI and ISI interferences in a MIMO channel. The use of both ordinary and Paley-Hadamard matrix for the construction of the pilot matrix is also presented. The MIMO-CE scheme is also extended from the symbol-spaced model to the fractionally-spaced model to allow mulitpath that arrives within a fraction of a symbol period to be considered and estimated accordingly. Finally, this novel MIMO-CE method is further extended to include channel tracking in order to cater for the time-varying channel model with different Doppler velocities.

4.1 Development of MIMO Channel Estimation from Frequency-Flat Fading Model to Frequency-Selective Fading Model

The MIMO-CE methods presented in Chapter 3 are restricted for flat fading channel where each sub-channel (from m^{th} Tx to n^{th} Rx) contains only a single path. However, in the frequency selective channel, multiple paths are present in each sub-channel. Due to the delay spread, each path may arrive at different time, causing the inter-symbol interference (ISI) event when the RMS delays spread of the channel is greater than the symbol duration itself [113]. In addition, co-channel interference (CCI) also exists when the multiple received signals are superimposed at each receive antenna. The joint CCI and ISI effect creates more complicated scenario for the channel estimation process since the received signals buried under these interferences must be amply segregated. Hence, issue of interference needs to be considered carefully when designing the MIMO-CE scheme for frequency selective channel. This is addressed in next section.

4.1.1 Recap of MIMO-CE methods for Flat-Fading MIMO channel

In order to demonstrate the development of the proposed MIMO-CE scheme from the flat fading channel to frequency-selective fading channel, the previous MIMO-PMI algorithm (for non-adaptive case) is again illustrated using a (2×2) configuration shown below:

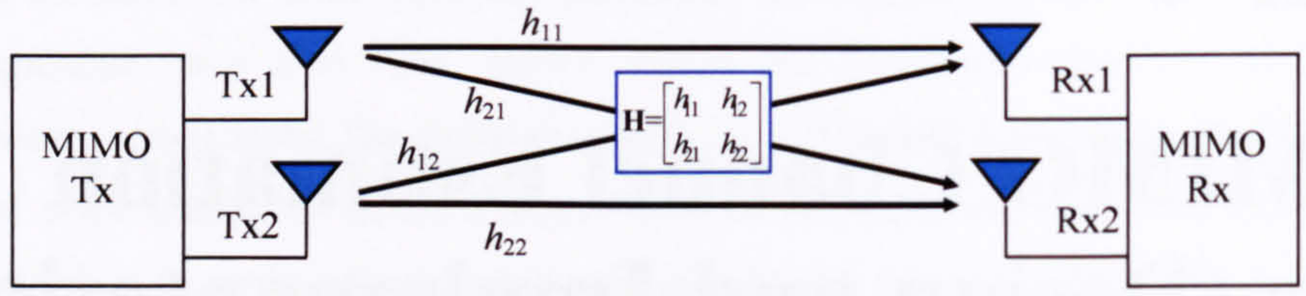

Figure 4.1: A (2×2) system in a flat-fading MIMO channel

The (2×1) receive signal vector **r** can be related to the transmit signal vector **s** as:

$$\mathbf{r}(k) = \sqrt{\rho/M}\,\mathbf{H}\mathbf{s}(k)+\mathbf{n}(k) \tag{4.1}$$

$$\begin{bmatrix} x_k \\ y_k \end{bmatrix} = \sqrt{\frac{\rho}{M}}\begin{bmatrix} h_{11} & h_{12} \\ h_{21} & h_{22} \end{bmatrix}\begin{bmatrix} a_k \\ b_k \end{bmatrix}+\mathbf{n}(k) \tag{4.2}$$

where **H** is the flat-fading channel matrix that describes individual complex path coefficients, h_{ji}, from Tx-i to Rx-j. $\sqrt{\rho/M}$ is the transmit power as described in (3.96) and $\mathbf{n}(k)$ is the AWGN noise vector. For illustration, the pilot symbols sent respectively from antenna Tx1 and Tx2 are denoted as 'a_k' and 'b_k' whereas signals received at antenna Rx1 and Rx2 are denoted as 'x_k' and 'y_k' at time-instant k. Using the MIMO-PMI algorithm with the pilot length of $v = 4$, the corresponding transmitted pilot matrix **S** and the received signal matrix **R** can be related as:

$$\mathbf{R} = \sqrt{\rho/M}\,(\mathbf{H}\,\mathbf{S}) + \mathbf{N} \tag{4.3a}$$

where

$$\mathbf{S} = [\mathbf{s}(1)\ \ \mathbf{s}(2)\ \ \mathbf{s}(3)\ \ \mathbf{s}(4)] = \begin{bmatrix} a_1 & a_2 & a_3 & a_4 \\ b_1 & b_2 & b_3 & b_4 \end{bmatrix} \tag{4.3b}$$

$$\mathbf{R} = [\mathbf{r}(1)\ \ \mathbf{r}(2)\ \ \mathbf{r}(3)\ \ \mathbf{r}(4)] = \begin{bmatrix} \Updownarrow & \Updownarrow & \Updownarrow & \Updownarrow \\ x_1 & x_2 & x_3 & x_4 \\ y_1 & y_2 & y_3 & y_4 \end{bmatrix} \tag{4.3c}$$

and **N** is the corresponding AWGN noise matrix. According to the description of the non-adaptive approach in Chapter 3, $\hat{\mathbf{H}}$ can be obtained by any of the following equations:

a) $\hat{\mathbf{H}} = \sqrt{M/\rho}\,\mathbf{R}\,\mathbf{S}^{+}$, *where* $(.)^{+}$ *is the pseudo-inverse operation* (4.4)

b) $\hat{\mathbf{H}} = \sqrt{M/\rho}\,\mathbf{R}\,\mathbf{S}^{\mathsf{H}}\left(\mathbf{S}\,\mathbf{S}^{\mathsf{H}}\right)^{-1}$, *where* $(.)^{\mathsf{H}}$ *is the Hermitian operation* (4.5)

c) $\hat{\mathbf{H}} = 1/2v\times\sqrt{M/\rho}\,\mathbf{R}\,\mathbf{S}^{\mathsf{H}}$, *where* **S** *is an orthogonal complex matrix* (4.6)

These solutions have different implications. In a), solution of $\hat{\mathbf{H}}$ is possible only if the pseudo-inverse of the pilot matrix, $\mathbf{S}^{+}$, can be obtained. To avoid the problem of unattainable pseudo-inverse operation (e.g. due to ill-conditioning – high singularity case), solution b) can be applied, where $\mathbf{S}\mathbf{S}^{\mathsf{H}}$ results in a square matrix that makes the matrix inversion more likely to be obtained. Lastly, solution c) appears to be more favourable since it allows the matrix inversion,

$(.)^{+}$ in (4.4), to be effectively replaced by the Hermitian of **S**, $\mathbf{S}^{H}$ in (4.6) when the pilot matrix **S** is designed using the orthogonal matrix. Therefore, if the training sequence $[a_1\ a_2\ a_3\ a_4]$ from Tx1 and $[b_1\ b_2\ b_3\ b_4]$ from Tx2 are mutually orthogonal, then $\hat{\mathbf{H}}$ can be obtained by using (4.6). However, the respective received signals $[x_1\ x_2\ x_3\ x_4]$ from Rx1 and $[y_1\ y_2\ y_3\ y_4]$ from Rx2 must be collected first to form proper sequence of **R** matrix before $\mathbf{S}^{H}$ can be applied in (4.6).

4.1.2 Channel Estimation in Frequency Selective MIMO Channel

An example is shown in order illustrate the vital concept behind the proposed MIMO-CE scheme designed for the frequency selective fading channel and the consideration of joint ISI and CCI problem. The same (2×2) system is used with $(L+1)= 2$ delay paths model shown as follows:

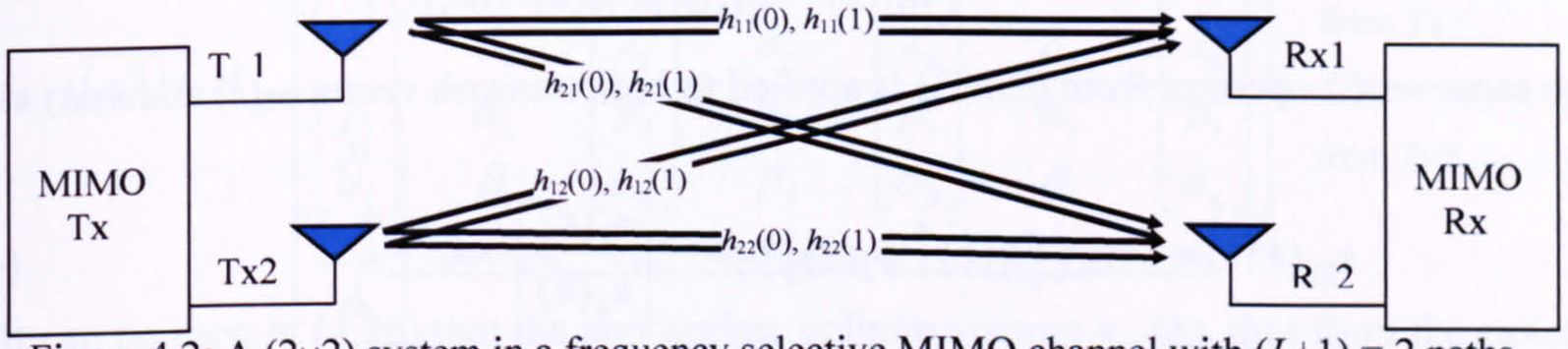

Figure 4.2: A (2×2) system in a frequency selective MIMO channel with $(L+1) = 2$ paths

For illustration, straight paths are drawn, although multipath may arrives *via* different routes either by LOS or NLOS in practice. The delay between the paths is assumed to be symbol-spaced. The corresponding channel matrices using same format in (2.94), can be represented as:

$$\mathbf{H}_1 = \begin{bmatrix} h_{11}(0) & h_{11}(1) \\ h_{21}(0) & h_{21}(1) \end{bmatrix} \quad and \quad \mathbf{H}_2 = \begin{bmatrix} h_{12}(0) & h_{12}(1) \\ h_{22}(0) & h_{22}(1) \end{bmatrix} \tag{4.7}$$

where $\mathbf{H}_i$ denotes the channel matrix w.r.t i^{th} transmit antenna, Tx-i, each containing the fading coefficients $h_{nm}(t)$ w.r.t time t. Hence, the corresponding (2×1) receive signal vector **r** is:

$$\mathbf{r}(k) = \sqrt{\rho/M}\left(\mathbf{H}_1\,\mathbf{s}_1(k)+\mathbf{H}_2\,\mathbf{s}_2(k)\right)+\mathbf{n}(k) \tag{4.8}$$

$$\begin{bmatrix} x_k \\ y_k \end{bmatrix} = \sqrt{\frac{\rho}{M}}\left(\begin{bmatrix} h_{11}(0) & h_{11}(1) \\ h_{21}(0) & h_{21}(1) \end{bmatrix}\begin{bmatrix} a_k \\ a_{k-1} \end{bmatrix}+\begin{bmatrix} h_{12}(0) & h_{12}(1) \\ h_{22}(0) & h_{22}(1) \end{bmatrix}\begin{bmatrix} b_k \\ b_{k-1} \end{bmatrix}\right)+\mathbf{n}(k) \tag{4.9}$$

where $\mathbf{s}_m(k)$ is the respective transmit vector from m^{th} transmit antenna at k time-instant. Note that for the noiseless condition, the respective received signal x_k & y_k at each antenna is the sum of the current k^{th} and previous $(k-1)^{th}$ transmitted symbols from each transmit antenna as:

$$x_k = \sqrt{\rho/M}\,(\,h_{11}(0)\,a_k + h_{11}(1)\,a_{k-1} + h_{12}(0)\,b_k + h_{12}(1)\,b_{k-1}\,) \tag{4.10}$$

$$y_k = \sqrt{\rho/M}\,(\,h_{21}(0)\,a_k + h_{21}(1)\,a_{k-1} + h_{22}(0)\,b_k + h_{22}(1)\,b_{k-1}\,) \tag{4.11}$$

Note that x_k & y_k consists of superimposition of multiple signals that give rise to not only to CCI but also to ISI since the previous $(k-1)^{th}$ paths are involved. The objective is to estimate all eight fading coefficients in (4.7) for both k^{th} and $(k-1)^{th}$ paths under the influence of CCI and ISI.

This can be achieved by providing sufficient path segregation for each pilot symbol whereby orthogonal pilot sequences can be utilised and assigned to each transmit antenna as well as to individual path. To do this, (4.10) and (4.11) are examined carefully in order to re-express both (4.8) and (4.9) into suitable matrix format for channel estimation process shown in the following:

$$\mathbf{r}(k) = \begin{bmatrix} x_k \\ y_k \end{bmatrix} = \sqrt{\frac{\rho}{M}} \left(\left[\begin{array}{cc|cc} h_{11}(0) & h_{11}(1) & h_{12}(0) & h_{12}(1) \\ h_{21}(0) & h_{21}(1) & h_{22}(0) & h_{22}(1) \end{array}\right] \left[\begin{array}{c} a_k \\ a_{k-1} \\ \hline b_k \\ b_{k-1} \end{array}\right] \right) = \sqrt{\frac{\rho}{M}} \left(\left[\mathbf{H}_1 \middle| \mathbf{H}_2\right] \begin{bmatrix} \mathbf{s}_1(k) \\ \mathbf{s}_2(k) \end{bmatrix} \right) \tag{4.12}$$

where the channel matrices $\mathbf{H}_1$ and $\mathbf{H}_2$ are concatenated together as:

$$\mathbf{H}_{1|2} = \left[\mathbf{H}_1 \mid \mathbf{H}_2 \right] = \left[\begin{array}{cc|cc} h_{11}(0) & h_{11}(1) & h_{12}(0) & h_{12}(1) \\ h_{21}(0) & h_{21}(1) & h_{22}(0) & h_{22}(1) \end{array}\right] \tag{4.13}$$

and the same *vec*(.) operator from (2.103) is applied to both transmit vector $\mathbf{s}_1(k)$ and $\mathbf{s}_2(k)$ as:

$$s_{1|2}(k) = vec\left(\left[\mathbf{s}_1(k) \quad \mathbf{s}_2(k) \right] \right) = \begin{bmatrix} \mathbf{s}_1(k) \\ \mathbf{s}_2(k) \end{bmatrix} = \left[\begin{array}{c} a_{\mathrm{k}} \\ a_{\mathrm{k-1}} \\ \hline b_{\mathrm{k}} \\ b_{\mathrm{k-1}} \end{array}\right] \tag{4.14}$$

Note that each transmit vector $\mathbf{s}$ in $\mathbf{s}_{1|2}(k)$ now contains the present and previous symbols at time-instant k and k-1 respectively. Alternatively, equation (4.12) to (4.14) can be re-written as:

$$\mathbf{r}(k) = \sqrt{\rho/M} \left(\mathbf{H}_{1|2} \, \mathbf{s}_{1|2}(k) \right) + \mathbf{n}(k) \tag{4.15}$$

Note that the format in (4.15) is the simplified version of (4.12), which has grouped all the channel coefficients into a single matrix $\mathbf{H}_{1|2}$ and combined both transmit vectors into a single vector $\mathbf{s}_{1|2}(k)$. Such arrangement permits pilot symbols in $\mathbf{s}_{1|2}(k)$ to be collectively assigned to each transmit antenna and their individual associated path (both previous and present) at different time-instant k in order to form a so-called "pilot matrix" suitable for channel estimation.

Suppose the pilot matrix $\mathbf{S}_F$ is composed by four different column of $\mathbf{s}_{1|2}(k)$, each containing different pilot symbols shown in the following, (since $M = 2$ and $(L+1) = 2$):

$$\mathbf{S}_F = \left[\mathbf{s}_{1|2}(a) \quad \mathbf{s}_{1|2}(b) \quad \mathbf{s}_{1|2}(c) \quad \mathbf{s}_{1|2}(d) \right] = \left[\begin{array}{cccc} \delta_1 & \delta_2 & \delta_3 & \delta_3 \\ \lambda_1 & \lambda_2 & \lambda_3 & \lambda_4 \\ \hdashline \beta_1 & \beta_2 & \beta_3 & \beta_4 \\ \alpha_1 & \alpha_2 & \alpha_3 & \alpha_4 \end{array}\right] \begin{array}{l} \} \text{ for Tx1} \\ \\ \} \text{ for Tx2} \end{array} \tag{4.16}$$

where respective time-instances a, b, c, d in (4.16) have not yet been determined. δ_i, λ_i, β_i & α_i present different sets of pilot sequences that are deliberately designed to cater for individual path that may exist within each sub-channel. However, the actual corresponding training sequences sent from respective transmit antenna in time-domain are represented as:

$$\text{Tx1} \Leftarrow [\ \boxed{\lambda_1 \quad \delta_1}\ \lambda_2 \quad \delta_2 \quad \lambda_3 \quad \delta_3 \quad \lambda_4 \quad \delta_4\ ] \rightarrow \text{sliding window} \tag{4.17}$$

$$\text{Tx2} \Leftarrow [\ \boxed{\alpha_1 \quad \beta_1}\ \alpha_2 \quad \beta_2 \quad \alpha_3 \quad \beta_3 \quad \alpha_4 \quad \beta_4\ ] \tag{4.18}$$

These pilot symbols are later received into consecutive received signal vectors **r**, which forms the corresponding signal matrix **R**. Using the above sliding window to show the effect of delay spread, **r** in (4.15) can be jointly illustrated in accordance to the respective pilot symbols as:

$$\mathbf{R} = [\mathbf{r}(1) \quad \mathbf{r}(2) \quad \mathbf{r}(3) \quad \mathbf{r}(4) \quad \mathbf{r}(5) \quad \mathbf{r}(6) \quad \mathbf{r}(7)] \tag{4.19}$$

$$= \left[\begin{bmatrix} x_1 \\ y_1 \end{bmatrix} \quad \begin{matrix} x_2 \\ y_2 \end{matrix} \quad \begin{bmatrix} x_3 \\ y_3 \end{bmatrix} \quad \begin{matrix} x_4 \\ y_4 \end{matrix} \quad \begin{bmatrix} x_5 \\ y_5 \end{bmatrix} \quad \begin{matrix} x_6 \\ y_6 \end{matrix} \quad \begin{bmatrix} x_7 \\ y_7 \end{bmatrix}\right]$$

$$= \sqrt{\rho/M}\ \mathbf{H}_{1|2} \left[\mathbf{s}_{1|2}(1) \quad \mathbf{s}_{1|2}(2) \quad \mathbf{s}_{1|2}(3) \quad \mathbf{s}_{1|2}(4) \quad \mathbf{s}_{1|2}(5) \quad \mathbf{s}_{1|2}(6) \quad \mathbf{s}_{1|2}(7)\right] \tag{4.20}$$

$$= \sqrt{\rho/M}\ \mathbf{H}_{1|2} \left[\begin{bmatrix} \delta_1 \\ \lambda_1 \end{bmatrix} \quad \begin{matrix} \lambda_2 \\ \delta_1 \end{matrix} \quad \begin{bmatrix} \delta_2 \\ \lambda_2 \end{bmatrix} \quad \begin{matrix} \lambda_3 \\ \delta_2 \end{matrix} \quad \begin{bmatrix} \delta_3 \\ \lambda_3 \end{bmatrix} \quad \begin{matrix} \lambda_3 \\ \delta_2 \end{matrix} \quad \begin{bmatrix} \delta_4 \\ \lambda_4 \end{bmatrix}\right] \text{ from Tx1}$$

$$\left[\begin{bmatrix} \beta_1 \\ \alpha_1 \end{bmatrix} \quad \begin{matrix} \alpha_2 \\ \beta_1 \end{matrix} \quad \begin{bmatrix} \beta_2 \\ \alpha_2 \end{bmatrix} \quad \begin{matrix} \alpha_3 \\ \beta_2 \end{matrix} \quad \begin{bmatrix} \beta_3 \\ \alpha_3 \end{bmatrix} \quad \begin{matrix} \alpha_3 \\ \beta_2 \end{matrix} \quad \begin{bmatrix} \beta_4 \\ \alpha_4 \end{bmatrix}\right] \text{ from Tx2}$$

$$\leftarrow \text{time-gap} \rightarrow \quad \leftarrow \text{time-gap} \rightarrow \quad \leftarrow \text{time-gap} \rightarrow$$

It can be seen in (4.20) that the appropriate column vectors $\mathbf{s}_{1|2}(k)$ that form the exact pilot matrix $\mathbf{S}_F$ in (4.16), only corresponding to those with time-instance k = 1, 3, 5 & 7 in this case. Those 'in-between' $\mathbf{s}_{1|2}(k)$ with k = 2, 4, 6 & 8 are regarded as 'redundant' since they do not constitute the exact format of $\mathbf{S}_F$ in (4.16) in the correct order of the pilot symbols. Hence, successive **r** cannot be used since the respective 'time-gaps' must be considered by the channel estimation process to acquire the exact format of $\mathbf{S}_F$ at the receiver in order to establish the useful relationship shown in (4.22) later. The appropriate **r** must be collected at proper interval (discussed later), to form the 'required' receive signal matrix **X**, which is shown for this case as:

$$\mathbf{X} = [\mathbf{r}(1) \quad \mathbf{r}(3) \quad \mathbf{r}(5) \quad \mathbf{r}(7)] = \begin{bmatrix} x_1 & x_3 & x_5 & x_7 \\ y_1 & y_3 & y_5 & y_7 \end{bmatrix} \tag{4.21}$$

Now, **X** in (4.21) 'contains' the exact pilot matrix **S** in (4.16) that has been sent over the frequency-selective MIMO channel. The relationship between **X** and **S** can be written as:

$$\mathbf{X} = \sqrt{\rho/M}\ \mathbf{H}_{1|2}\ \mathbf{S}_F + \mathbf{n}(k) \tag{4.22}$$

Thus, the MIMO channel can now be estimated in the single format of $\mathbf{H}_{1|2}$ by using (4.6) where **R** is replaced by **X** and applying the *a priori* known $\mathbf{S}^H$ to **X** at the receiver. Obviously, ideal choice is to choose those pilot symbols in **S** to constitute the orthogonal structure, which requires $[\delta_1\ \delta_2\ \delta_3\ \delta_4]$, $[\lambda_1\ \lambda_2\ \lambda_3\ \lambda_4]$, $[\beta_1\ \beta_2\ \beta_3\ \beta_4]$ and $[\alpha_1\ \alpha_2\ \alpha_3\ \alpha_4]$ to be mutually orthogonal to one another in this case. This ensures sufficient segregation between each path in the frequency selective fading channel while retaining the MIMO-PMI method used in flat-fading channel, where the use of orthogonal transmission across the multiple transmit antennas is still preserved.

4.2 Novel MIMO-CE Scheme for frequency selective channel

Having seen the example in Section 4.1.2, the proposed MIMO-CE scheme for frequency selective channel is presented here for general model of a (N×M) MIMO configuration with (L+1) symbol-spaced paths that exist within each channel impulse response of the sub-channel.

4.2.1 Basic Channel and Signal Model

In the frequency selective MIMO channel, the sampled channel impulse response (CIR) for each sub-channel (from m^{th} transmit antenna to n^{th} receive antenna) can be expressed as:

$$\mathbf{h}_{nm} = \begin{bmatrix} h_{nm}(0) & h_{nm}(1) & \cdots & h_{nm}(L) \end{bmatrix}^{\mathsf{T}} \tag{4.23}$$

where $[.]^{\mathsf{T}}$ is the transpose operation. Note that each CIR contains (L+1) number of multiple path coefficients, $h_{nm}(l)$, which are assumed to be evenly spaced by one symbol period. Consequently, the respective channel matrix, $\mathbf{H}_m$, can be defined with respect to each m^{th} transmit antenna as:

$$\mathbf{H}_m = \begin{bmatrix} \mathbf{h}_{1m}^{\mathsf{T}} \\ \mathbf{h}_{2m}^{\mathsf{T}} \\ \vdots \\ \mathbf{h}_{Nm}^{\mathsf{T}} \end{bmatrix} = \begin{bmatrix} h_{1m}(0) & h_{1m}(1) & \cdots & h_{1m}(L) \\ h_{2m}(0) & h_{2m}(1) & \cdots & h_{2m}(L) \\ \vdots & \vdots & \vdots & \vdots \\ h_{Nm}(0) & h_{Nm}(1) & \cdots & h_{Nm}(L) \end{bmatrix}, \quad m = 1,2,\ldots,M. \tag{4.24}$$

Note that each $\mathbf{H}_m$ has matrix size of N×(L+1) and comprises of multiple CIRs, $\mathbf{h}_{nm}$, from m^{th} transmit antenna to all (n = 1 to N) receive antennas. Each coefficient, h_{nm}, is generated as random Rayleigh complex components and all coefficients are assumed to be uncorrelated.

Subsequently, the received signal vector, $\mathbf{r}(k)$ at time-instant k can be written as:

$$\mathbf{r}(k) = \sum_{m=1}^{M} \mathbf{H}_m \, \mathbf{s}_m(k) + \mathbf{n}(k) \tag{4.25}$$

where $\mathbf{n}(k)$ is the AWGN noise vector and $\mathbf{s}_m(k)$ is the transmit vector w.r.t m^{th} transmit antenna that consists of L+1 symbols (i.e. from current $(k)^{th}$ symbol back to previous $(k\text{-}L)^{th}$ symbol) as:

$$\mathbf{s}_m(k) = \begin{bmatrix} s_m(k) & s_m(k-1) & \cdots & s_m(k-L) \end{bmatrix}^{\mathsf{T}} \tag{4.26}$$

In order to facilitate the formulation of the proposed MIMO-CE scheme, (4.25) is carefully examined and its representation is modified with the use of the following operators: First, $[\boldsymbol{Y} \mid \boldsymbol{Z}]$ is used to denote the matrix concatenation for $\boldsymbol{Y}$ and $\boldsymbol{Z}$. By concatenating the channel matrices from $\mathbf{H}_1$ to $\mathbf{H}_M$ in (4.25), the concatenated channel matrix $\mathbf{H}_{1|M}$ can be expressed as:

$$\mathbf{H}_{1|M} = \begin{bmatrix} \mathbf{H}_1 \mid \cdots \mid \mathbf{H}_M \end{bmatrix} \tag{4.27}$$

Secondly, the same *vec*(.) operator in (2.103) is employed and applied to all the transmit vectors from $\mathbf{s}_1(k)$ to $\mathbf{s}_M(k)$, to form the concatenated transmit vector $\boldsymbol{s}_{1|M}(k)$ as follows:

$$\boldsymbol{s}_{1|M}(k) = vec\left(\begin{bmatrix} \mathbf{s}_1(k) & \cdots & \mathbf{s}_M(k) \end{bmatrix} \right) \tag{4.28}$$

Consequently, utilising both expressions in (4.27) and (4.28), the representation of received signal vector $\mathbf{r}(k)$ in (4.25) can be alternatively re-written as:

$$\mathbf{r}(k) = \mathbf{H}_{1|M} \cdot s_{1|M}(k) + \mathbf{n}(k) \tag{4.29}$$

$$\mathbf{r}(k) = \left[\mathbf{H}_1 | \cdots | \mathbf{H}_M \right] \cdot \begin{bmatrix} \underline{\mathbf{s}_1(\mathrm{k})} \\ \vdots \\ \underline{\mathbf{s}_M(\mathrm{k})} \end{bmatrix} + \mathbf{n}(\mathrm{k}) \tag{4.30}$$

The expressions in (4.29) & (4.30) do not alter the original result of $\mathbf{r}$ in (4.25) but instead, it provide an alternative structure that allows proper partitioning of the respective channel matrices, (from $\mathbf{H}_1$ to $\mathbf{H}_M$ in $\mathbf{H}_{1|M}$) and the associated transmit vectors (from $\mathbf{s}_1(k)$ to $\mathbf{s}_M(k)$ in $s_{1|M}(k)$). This has two advantages. First, the format of $\mathbf{H}_{1|M}$ allows '*joint*' estimation of all fading coefficients in each channel matrix, $\mathbf{H}_m$ to be obtained simultaneously in a single matrix structure. Secondly, the format of $s_{1|M}(k)$ in (4.28) and their respective $\mathbf{s}_m(k)$ in (4.26), allows the assignment of pilot symbols to be considered for each associated path w.r.t each antenna.

To perform channel estimation for frequency selective MIMO channel (following the exampled in section 4.1.2), (F+1) non-adjacent received signal vectors $\mathbf{r}$, must be collected at the proper interval of p, to form the necessary received signal matrix $\mathbf{X}$, as follows:

$$\mathbf{X} = \left[\mathbf{r}(k) \quad \mathbf{r}(k+p) \quad \mathbf{r}(k+2p) \quad \cdots \quad \mathbf{r}(k+Fp) \right] \tag{4.31}$$

Assuming $\mathbf{H}_{1|M}$ stays relatively constant, the required $\mathbf{X}$ in (4.31) also corresponds to:

$$\mathbf{X} = \sqrt{\rho/M}\, \mathbf{H}_{1|M} . \mathbf{S}_F + \mathbf{N} \tag{4.32}$$

where $\sqrt{\rho/M}$ is the transmit power as described in (3.96) and $\mathbf{N}$ is a grouped matrix of $\mathbf{n}$(k). The corresponding pilot matrix $\mathbf{S}_F$ can also be expressed as:

$$\mathbf{S}_F = \left[s_{1|M}(k) \mid s_{1|M}(k+p) \mid s_{1|M}(k+2p) \mid \cdots \mid s_{1|M}(k+Fp) \right] \tag{4.33}$$

Note that the interval p is crucial and must be considered carefully during the collection of the received signal vectors $\mathbf{r}$ so that $\mathbf{X}$ comprises just the signal components that constitute the exact intended format of $\mathbf{S}_F$ sent for channel estimation. The expression in (4.33) suggests that $s_{1|M}(k)$ can be grouped together to form the necessary pilot matrix $\mathbf{S}_F$. The structure in (4.33) allows the MIMO-PMI algorithm used in the flat fading channel to be extended for frequency-selective fading channel such that extra (L+1) delay paths are taken into consideration during the channel estimation process. The objective is to design a suitable pilot matrix $\mathbf{S}_F$ with suitable assignment of pilot symbols in each $s_{1|M}(k)$ so that $\mathbf{H}_{1|M}$ can be jointly estimated accordingly.

4.2.2 The Implementation of the Novel MIMO Channel Estimator

The proposed MIMO-CE scheme combines the following concepts to perform channel estimation in frequency-selective MIMO channel: 1) A pilot matrix sent as joint multiple sequences of pilot symbols is used to jointly estimate the CIRs, as opposed to using the adaptive algorithm [87] with pilot symbols sent individually in series. 2) The orthogonal property of the Hadamard matrix is utilised to resolve the problem of ISI and CCI in the channel. 3) The Toeplitz-like structure of the Paley-Hadamard matrix [132, 133] is exploited to reduce the number of pilot symbols that must be transmitted without sacrificing the original performance.

One key assumption in the proposed MIMO-CE method is that the total number of $(L+1)$ paths (in the symbol-spaced model) or the total delay-spread of the channel φ (in the fractionally-spaced model discussed later) must be known *a priori* or predicted by both the transmitter and the receiver. This is to ensure that the transmitter know the exact minimum size of the pilot matrix $\mathbf{S}_F$ to be sent (although longer pilot length improves the accuracy of estimation, discussed later in the result section). The receiver too must know about this information in order to collect $\mathbf{r}$ into $\mathbf{X}$ at appropriate instance so that estimate of the delay paths and its fading coefficient can be obtained.

4.2.2.1 Utilising Orthogonal Properties and Hadamard Matrix Structure

The orthogonal property in (3.82) is again employed for the frequency-selective case as:

$$\mathbf{G}(v).\mathbf{G}(v)^{\mathsf{T}} = v.\mathbf{I} \quad \& \quad \mathbf{G}(v)^{\mathsf{T}} = v.\mathbf{G}(v)^{-1} \tag{4.34}$$

where $\mathbf{G}(v)$ is a real Hadamard matrix of order v and $\mathbf{I}$ is the identity matrix. If $\mathbf{G}$ is a complex matrix, then v becomes $2v$ and Hermitian transposition $(.)^{\mathsf{H}}$ replaces $(.)^{\mathsf{T}}$.

First, the Hadamard matrix is generated with suitable order v based on following criterion:

$$\left[v = (2^{\ell})\right] \geq M \times (L+1) \tag{4.35}$$

where ℓ is an integer. The valid order v obtained must be either equal or greater than the product of the number of transmit antenna M and the number of $(L+1)$ paths existing within each CIR for frequency-selective case. (Both parameters are assumed to be known *a priori* by the transmitter).

4.2.2.2 Pilot Matrix Construction Using Ordinary Hadamard Matrix

Next, the suitable pilot matrix $\mathbf{S}_F$ in (4.33) is constructed such that the orthogonal property in (4.34) is satisfied. This can be accomplished by directly extracting $M\times(L+1)$ number of the orthogonal rows from the Hadamard matrix with order v obtained in (4.35). Any non-repeated orthogonal rows can be chosen arbitrarily. For example, if $M = 2$ & $(L+1) = 3$, then $M\times(L+1)=6$. First, Hadamard matrix is constructed with minimum order $v = 8$ according to (4.35) and six row sequences (from 2^{nd} row to 7^{th} row) directly extracted to form the required pilot matrix as:

$$\mathbf{S}_F = \mathbf{A} + j\mathbf{B} \tag{4.36}$$

where $\mathbf{A} = \mathbf{B} =$

$$\left[\begin{array}{cccccccc} \begin{bmatrix}+1\\+1\\+1\end{bmatrix} & \begin{bmatrix}-1\\+1\\-1\end{bmatrix} & \begin{bmatrix}+1\\-1\\-1\end{bmatrix} & \begin{bmatrix}-1\\-1\\+1\end{bmatrix} & \begin{bmatrix}+1\\+1\\+1\end{bmatrix} & \begin{bmatrix}-1\\+1\\-1\end{bmatrix} & \begin{bmatrix}+1\\-1\\-1\end{bmatrix} & \begin{bmatrix}-1\\-1\\+1\end{bmatrix} \\ \hline \begin{bmatrix}+1\\+1\\+1\end{bmatrix} & \begin{bmatrix}+1\\-1\\+1\end{bmatrix} & \begin{bmatrix}+1\\+1\\-1\end{bmatrix} & \begin{bmatrix}+1\\-1\\+1\end{bmatrix} & \begin{bmatrix}-1\\-1\\-1\end{bmatrix} & \begin{bmatrix}-1\\+1\\-1\end{bmatrix} & \begin{bmatrix}-1\\-1\\+1\end{bmatrix} & \begin{bmatrix}-1\\+1\\+1\end{bmatrix} \end{array}\right] \begin{array}{l}\} \text{Tx1} \\ \\ \} \text{Tx2}\end{array}$$

Note that **A** and **B** are its real and imaginary matrices. (Full length of orthogonal sequence with v pilot symbols is required in each row of $\mathbf{S}_F$). Note that the middle partition virtually divides $\mathbf{S}_F$ into its respective upper and lower regions for antenna Tx1 & Tx2 such that pilot symbols can also be assigned to the associated $(L+1)$ paths existed in the channel. Once the pilot matrix $\mathbf{S}_F$ has been constructed, the pilot symbols are sent from each Tx in sequence of consecutive (3×1) column vectors (from left to right) in the order shown by the arrows in (4.36).

4.2.2.3 Transmission of the Training Sequence from each Transmit Antenna

For the purpose of illustration (using $M = 2$ & $(L+1) = 3$), each row of orthogonal pilot sequence of $\mathbf{S}_F$ in (4.36) is replaced by the respective row of different sets of symbols as:

$$\left[\begin{array}{cccccccc} \theta_1 & \theta_2 & \theta_3 & \theta_4 & \theta_5 & \theta_6 & \theta_7 & \theta_8 \\ \lambda_1 & \lambda_2 & \lambda_3 & \lambda_4 & \lambda_5 & \lambda_6 & \lambda_7 & \lambda_8 \\ \delta_1 & \delta_2 & \delta_3 & \delta_4 & \delta_5 & \delta_6 & \delta_7 & \delta_8 \\ \hline \alpha_1 & \alpha_2 & \alpha_3 & \alpha_4 & \alpha_5 & \alpha_6 & \alpha_7 & \alpha_8 \\ \beta_1 & \beta_2 & \beta_3 & \beta_4 & \beta_5 & \beta_6 & \beta_7 & \beta_8 \\ \mu_1 & \mu_2 & \mu_3 & \mu_4 & \mu_5 & \mu_6 & \mu_7 & \mu_8 \end{array}\right] \begin{array}{l}\} \text{Tx1} \\ \\ \\ \\ \} \text{Tx2}\end{array} \tag{4.37}$$

Thus, the actual training sequence sent from Tx1 and Tx2 in time can be viewed as:

$$\begin{aligned} \text{Tx1} \Leftarrow\ & [\delta_1\ \lambda_1\ \theta_1 \quad \delta_2\ \lambda_2\ \theta_2 \quad \delta_3\ \lambda_3\ \theta_3 \quad \delta_4\ \lambda_4\ \theta_4 \quad \delta_5\ \lambda_5\ \theta_5 \quad \delta_6\ \lambda_6\ \theta_6 \quad \delta_7\ \lambda_7\ \theta_7 \quad \delta_8\ \lambda_8\ \theta_8\ ] \quad \text{time} \rightarrow \\ \text{Tx2} \Leftarrow\ & [\mu_1\ \beta_1\ \alpha_1 \quad \mu_2\ \beta_2\ \alpha_2 \quad \mu_3\ \beta_3\ \alpha_3 \quad \mu_4\ \beta_4\ \alpha_4 \quad \mu_5\ \beta_5\ \alpha_5 \quad \mu_6\ \beta_6\ \alpha_6 \quad \mu_7\ \beta_7\ \alpha_7 \quad \mu_8\ \beta_8\ \alpha_8] \end{aligned} \tag{4.38}$$

Note that each training sequence in (4.38) consists of 24 'interleaved' pilot symbols from (4.37). The use of the pilot matrix $\mathbf{S}_F$ thus allows the pilot symbols to be serially transmitted from each antenna that may then be reconstructed at the receiver for the channel estimation process.

4.2.2.4 Proper Collection of the Wanted Received Signal Vectors

At the receiver, collection of **r** into **X** with proper interval p is a crucial step such that the component of previous pilot symbols is not duplicated within any other entries of **X** in the frequency selective case. Using the same case of $M = 2$ & $(L+1) = 3$ for illustration, suppose the consecutive **r** is collected at $p = 1$ to form **R**, the corresponding matrix **S** can be shown as:

$$\mathbf{R} = \left[\mathbf{r}(k) \quad \mathbf{r}(k+1) \quad \mathbf{r}(k+2) \quad \cdots \quad \mathbf{r}(k+21)\right] = \sqrt{\rho/M}\,\mathbf{H}_{1|2}\,.\,\mathbf{S} + \mathbf{N} \tag{4.39}$$

where $$\mathbf{S} = \left[\, \boldsymbol{s}_{1|2}(k) \mid \boldsymbol{s}_{1|2}(k+1) \mid \boldsymbol{s}_{1|2}(k+2) \mid \boldsymbol{s}_{1|2}(k+3) \mid \cdots \mid \boldsymbol{s}_{1|2}(k+21) \,\right] \tag{4.40}$$

$$= \left[\begin{array}{c|c|c|c|c|c} \theta_1 & \delta_2 & \lambda_2 & \theta_2 & & \theta_8 \\ \lambda_1 & \theta_1 & \delta_2 & \lambda_2 & & \lambda_8 \\ \delta_1 & \lambda_1 & \theta_1 & \delta_2 & \cdots & \delta_8 \\ \hline \alpha_1 & \mu_2 & \beta_2 & \alpha_2 & & \alpha_8 \\ \beta_1 & \alpha_1 & \mu_2 & \beta_2 & & \beta_8 \\ \mu_1 & \beta_1 & \alpha_1 & \mu_2 & & \mu_8 \end{array}\right]$$

It can be seen in (4.40) that due to the delay spread of the channel, the pilot symbols are echoed into the adjacent $\boldsymbol{s}_{1|2}$, resulting in the duplications of the pilot symbols. Thus, the intended orthogonal structure of the pilot matrix $\mathbf{S}_F$ in (4.37) is no longer preserved if the adjacent $\mathbf{r}$ is used to form the 'required' received signal matrix $\mathbf{X}$. In this case, the new non-repetitive pilot symbols only appeared at every $p = (L+1) = 3$ intervals, corresponding to the exact format of $\mathbf{S}_F$ in (4.37). For the case of $M = 2$ & $(L+1) = 3$, the collection of $\mathbf{r}$ into $\mathbf{X}$ with $p = 3$ is shown as:

$$\mathbf{X} = \left[\mathbf{r}(k) \quad \mathbf{r}(k+3) \quad \mathbf{r}(k+6) \quad \mathbf{r}(k+9) \quad \mathbf{r}(k+12) \quad \mathbf{r}(k+15) \quad \mathbf{r}(k+18) \quad \mathbf{r}(k+21)\right] \tag{4.41}$$

Thus, in general, in order to restore the orthogonality of the pilot matrix $\mathbf{S}_F$ and avoid duplication of pilot symbols (due to the delay-spread of the channel) at the receiver, non-adjacent $\mathbf{r}$ must be collected at proper interval of $p = (L+1)$ to form the 'required' received matrix $\mathbf{X}$ as:

$$\mathbf{X} = \left[\mathbf{r}(k) \quad \mathbf{r}(k+p) \quad \mathbf{r}(k+2p) \quad \cdots \quad \mathbf{r}(k+Fp)\right] \tag{4.42}$$

where F is obtained based on the Hadamard matrix order v (obtained according to (4.35)) as:

$$F = v - 1 \tag{4.43}$$

Note that the collection of $\mathbf{r}$ into $\mathbf{X}$ in (4.42) ensures the preservation of the orthogonal structure of the pilot matrix $\mathbf{S}_F$ at the receiver when proper interval p is considered. The key to the proposed MIMO-CE method lies within the ability to extract the orthogonal information carried by the received signals at the appropriate interval p corresponding to the pilot symbols sent.

4.2.2.5 Obtaining the MIMO Channel Estimate

Once both the appropriate $\mathbf{X}$ and $\mathbf{S}_F$ are ready (where $\mathbf{S}_F$ is known by the receiver prior to the estimation), the estimate of the concatenated channel matrix $\hat{\mathbf{H}}_{1|M}$ can be obtained as:

$$\hat{\mathbf{H}}_{1|M} = \frac{1}{2v}\sqrt{M/\rho}\,\mathbf{X}\,\mathbf{S}_F{}^{\mathsf{H}} \tag{4.44}$$

Note that (4.44) requires $\mathbf{S}_F$ to be an orthogonal matrix so that properties in (4.34) can be applied where $\hat{\mathbf{H}}_{1|M}$ can be estimated using single matrix operation. (Refer to section 3.3.3.3 for the mathematics). Consequently, $\hat{\mathbf{H}}_{1|M}$ contains the estimates of each fading coefficients in each respective estimated channel matrix $\hat{\mathbf{H}}_m$ in $\hat{\mathbf{H}}_{1|M}$ (where $m = 1$ to M), which can be expressed as:

$$\hat{\mathbf{H}}_{1|M} = \left[\, \hat{\mathbf{H}}_1 \,\middle|\, \cdots \,\middle|\, \hat{\mathbf{H}}_M \,\right] \tag{4.45}$$

Once (4.45) is obtained, $\hat{\mathbf{H}}_{1|M}$ is then disintegrated into its individual estimate: $\hat{\mathbf{H}}_1$ to $\hat{\mathbf{H}}_M$, for the subsequent use in the MIMO equalisation and OSIC process described in Chapter 2. The discussions and procedures from section 4.2.2.1 to 4.2.2.5 in general constitute the proposed MIMO-CE method that caters for the channel estimation in frequency-selective MIMO channel.

4.2.3 Minimisation in Length of the Training Sequence

With reference to section 4.2.2.3, the expansion in **X** in (4.41) leads to the following:

$$\mathbf{X} = \sqrt{\rho/M}\ \mathbf{H}_{1|2}\,\mathbf{S}_F + \mathbf{N} \tag{4.46}$$

$$= \sqrt{\rho/M}\ \mathbf{H}_{1|2}\ \Big[\underbrace{\mathbf{s}_{1|2}(k)}_{\Phi}\cdots\underbrace{\mathbf{s}_{1|2}(k+3)}_{\Phi}\cdots\underbrace{\mathbf{s}_{1|2}(k+6)}_{\Phi}\cdots\underbrace{\mathbf{s}_{1|2}(k+9)}_{\Phi}\cdots\cdots\cdots\underbrace{\mathbf{s}_{1|2}(k+21)}_{\Phi}\Big] + \mathbf{N}$$

$$= \sqrt{\rho/M}\ \mathbf{H}_{1|2}\left[\begin{bmatrix}\theta_1\\ \lambda_1\\ \delta_1\\ \alpha_1\\ \beta_1\\ \mu_1\end{bmatrix} \underset{\text{gap}}{\overset{\text{time-}}{\leftarrow\rightarrow}} \cdots \begin{bmatrix}\theta_2\\ \lambda_2\\ \delta_2\\ \alpha_2\\ \beta_2\\ \mu_2\end{bmatrix} \underset{\text{gap}}{\overset{\text{time-}}{\leftarrow\rightarrow}} \cdots \begin{bmatrix}\theta_3\\ \lambda_3\\ \delta_3\\ \alpha_3\\ \beta_3\\ \mu_3\end{bmatrix} \underset{\text{gap}}{\overset{\text{time-}}{\leftarrow\rightarrow}} \cdots \begin{bmatrix}\theta_4\\ \lambda_4\\ \delta_4\\ \alpha_4\\ \beta_4\\ \mu_4\end{bmatrix} \cdots\cdots\cdots \begin{bmatrix}\theta_8\\ \lambda_8\\ \delta_8\\ \alpha_8\\ \beta_8\\ \mu_8\end{bmatrix}\right] + \mathbf{N}$$

With the interval $p = 3$, the respective $\boldsymbol{s}_{1|2}$ above constitutes to exactly the appointed pilot symbols shown in (4.37) for the $\mathbf{S}_F$. However, this also requires the channel estimator to wait for every $p = 3$ intervals in order to collect each 'wanted' **r** into **X**. The 'wasted' time-gaps exist in between the 'unwanted' $\mathbf{r}(k+t)$ at $t = 1,2,4,5,\ldots,19,20$, resulting in slow estimation process time [2].

4.2.3.1 Exploitation on the repetition of Pilot Symbols

It is however, possible to exploit these 'in-between' time-gaps and the duplications of pilot symbols in the successive **r**, in order to minimise the length of training sequence and the estimation process time without sacrificing the achievable performance. This can be achieved by re-considering the collection of successive **r** into **X** at interval $p = 1$, rather than $p = (L+1)$, where the components in pilot matrix $\mathbf{S}_F$ are intentionally designed in such a way that the pilot symbols are repeated in a 'Toeplitz-like' fashion (to cater for repetition of symbols shown in (4.40) due to the delay spread of the channel), whilst maintaining the orthogonal property in (4.34).

This is fulfilled by selecting pilot symbols in a particular order from a Hadamard matrix based on Paley's construction or the Paley-Hadamard matrix [132, 133]. For illustration, same case of $M = 2$ and $(L+1) = 3$ is used. Suppose a new pilot matrix $\mathbf{S}_F$ is designed with different arrangement of pilot symbols from (4.37) and with a 'Toeplitz-like' format shown as:

---

[2] The duration from the start of collection of **r** into **X** until the actual channel estimation is fully carried out.

$$\left[\begin{array}{cccccccc}
\theta_1 & \delta_2 & \lambda_2 & \theta_2 & \delta_3 & \lambda_3 & \theta_3 & \theta_4 \\
\lambda_1 & \theta_1 & \delta_2 & \lambda_2 & \theta_2 & \delta_3 & \lambda_3 & \lambda_4 \\
\delta_1 & \lambda_1 & \theta_1 & \delta_2 & \lambda_2 & \theta_2 & \delta_3 & \delta_4 \\
\hline
\alpha_1 & \mu_2 & \beta_2 & \alpha_2 & \mu_3 & \beta_3 & \alpha_3 & \alpha_4 \\
\beta_1 & \alpha_1 & \mu_2 & \beta_2 & \alpha_2 & \mu_3 & \beta_3 & \beta_4 \\
\mu_1 & \beta_1 & \alpha_1 & \mu_2 & \beta_2 & \alpha_2 & \mu_3 & \mu_4
\end{array}\right] \begin{array}{l} \} \text{Tx1} \\ \\ \\ \} \text{Tx2} \end{array} \tag{4.47}$$

$\mathbf{S}_F$ in (4.47) is purposely designed such that those pilot symbols (duplicated diagonally in the shaded regions) do not required to be transmitted. Thus, the actual training sequence sent from respective Tx1 & Tx2, is of those non-shaded symbols in the time-domain sequence as:

$$\begin{aligned} \text{Tx1} \Leftarrow [\ & \delta_1\ \lambda_1\ \theta_1 \mid \delta_2\ \lambda_2\ \theta_2 \quad \delta_3\ \lambda_3\ \theta_3 \quad \delta_4\ \lambda_4\ \theta_4 \ ] \\ \text{Tx2} \Leftarrow [\ & \mu_1\ \beta_1\ \alpha_1 \mid \mu_2\ \beta_2\ \alpha_2 \quad \mu_3\ \beta_3\ \alpha_3 \quad \mu_4\ \beta_4\ \alpha_4 \ ] \end{aligned} \tag{4.48}$$

sliding window → ; time →

Consider the following diagram for the frequency selective fading MIMO channel model with its time-domain representation in the respective channel matrix $\mathbf{H}_1$ & $\mathbf{H}_2$ with each CIR $\mathbf{h}_{nm}^{\mathsf{T}}$ and their corresponding fading coefficient $h_{nm}(k)$ into $\mathbf{H}_{1|2}$:

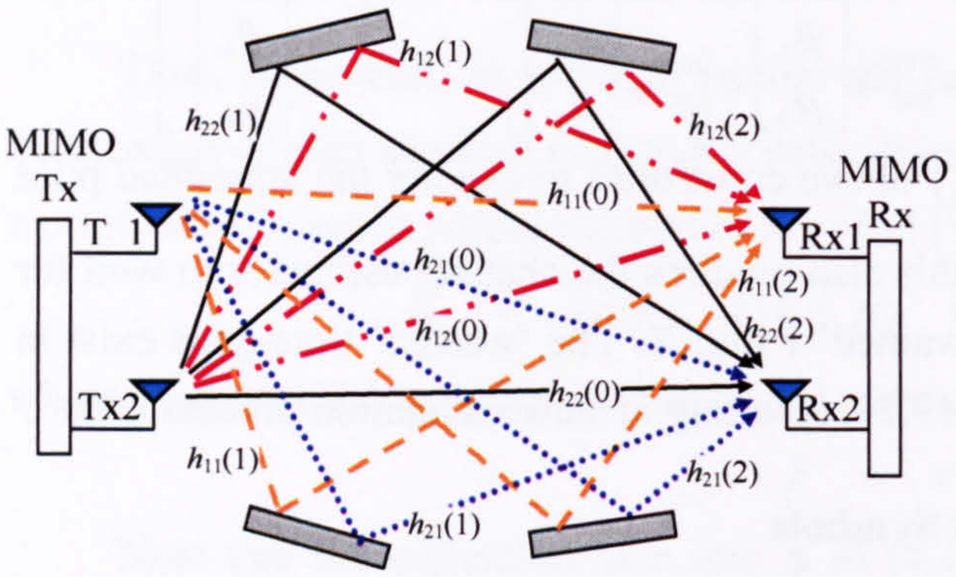

$$\mathbf{H}_1 = \begin{bmatrix} \mathbf{h}_{11}^{\mathsf{T}} \\ \mathbf{h}_{21}^{\mathsf{T}} \end{bmatrix} = \begin{bmatrix} h_{11}(0) & h_{11}(1) & h_{11}(2) \\ h_{21}(0) & h_{21}(1) & h_{21}(2) \end{bmatrix} \quad \text{(- - - →)(·····→)}$$

$$\mathbf{H}_2 = \begin{bmatrix} \mathbf{h}_{12}^{\mathsf{T}} \\ \mathbf{h}_{22}^{\mathsf{T}} \end{bmatrix} = \begin{bmatrix} h_{12}(0) & h_{12}(1) & h_{12}(2) \\ h_{22}(0) & h_{22}(1) & h_{22}(2) \end{bmatrix} \quad \text{(— · —→)(——→)}$$

$$\mathbf{H}_{1|2} = \left[\mathbf{H}_1 \middle| \mathbf{H}_2\right] = \left[\begin{array}{ccc|ccc} h_{11}(0) & h_{11}(1) & h_{11}(2) & h_{12}(0) & h_{12}(1) & h_{12}(2) \\ h_{21}(0) & h_{21}(1) & h_{21}(2) & h_{22}(0) & h_{22}(1) & h_{22}(2) \end{array}\right]$$

First, respective pilot symbols within each training sequence in (4.48) are sent from each transmit antenna (Tx1 & Tx2) to estimate all 12 fading coefficients $h_{nm}(k)$ above. Under the frequency selective channel with symbol-spaced delay, the scenario become very complicated; the transmitted pilot symbols at current instant ($k = 0$) and two previous instants ($k = 1$ & 2) are superimposed at each receive antenna (Rx1 & Rx2) together with their associated path. The resultant $\mathbf{r}(k)$ at k-instant and its interaction of respective path and pilot symbols can be described using (4.25). The effect of channel delay spread can be shown through 'sliding' the window (containing 3 symbols at one time) by one symbol period for each k-instant. Alternatively, this can be viewed using the FIR tap-delay-line (TDL) model in its time-domain representation as:

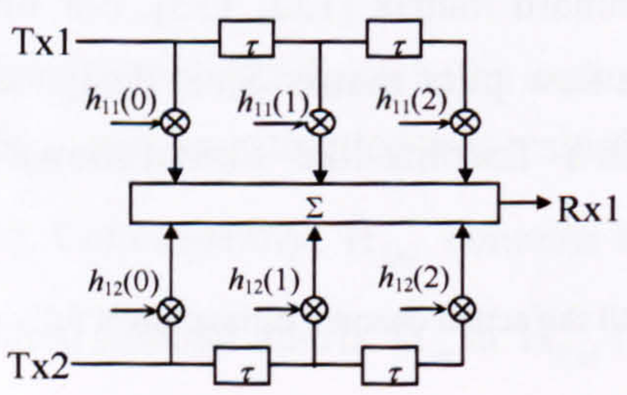

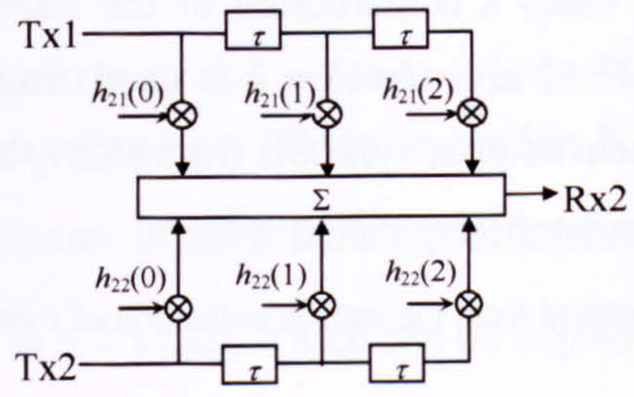

where τ = spacing between taps signifying symbol-spaced delay and $1/\tau$ is the symbol rate. The pilot symbols (at Tx1 & Tx2) in (4.48) are sequentially fed and shifted into the respective TDL model above and interact with the associated path at different time. They are then summed at respective output (Rx1 & Rx2) to produce the received signal vector $\mathbf{r}(k)$ at respective k-instant.

At the receiver, successive $\mathbf{r}$ (with p=1) are initially collected into $\mathbf{R}$ and the corresponding expansion in term of respective pilot symbols (in the time-sequence representation) is shown as:

$$\mathbf{R}=\begin{bmatrix} \mathbf{r}(k) & \mathbf{r}(k+1) & \mathbf{r}(k+2) & \mathbf{r}(k+3) & \mathbf{r}(k+4) & \mathbf{r}(k+5) & \mathbf{r}(k+6) & \mathbf{r}(k+7) & \mathbf{r}(k+8) & \mathbf{r}(k+9) \end{bmatrix} \quad (4.49)$$

$$= \sqrt{\frac{\rho}{M}}\mathbf{H}_{1|2} \begin{bmatrix} \begin{bmatrix} \theta_1 \\ \lambda_1 \\ \delta_1 \\ \hdashline \alpha_1 \\ \beta_1 \\ \mu_1 \end{bmatrix} & \begin{bmatrix} \delta_2 \\ \theta_1 \\ \lambda_1 \\ \hdashline \mu_2 \\ \alpha_1 \\ \beta_1 \end{bmatrix} & \begin{bmatrix} \lambda_2 \\ \delta_2 \\ \theta_1 \\ \hdashline \beta_2 \\ \mu_2 \\ \alpha_1 \end{bmatrix} & \begin{bmatrix} \theta_2 \\ \lambda_2 \\ \delta_2 \\ \hdashline \alpha_2 \\ \beta_2 \\ \mu_2 \end{bmatrix} & \begin{bmatrix} \delta_3 \\ \theta_2 \\ \lambda_2 \\ \hdashline \mu_3 \\ \alpha_2 \\ \beta_2 \end{bmatrix} & \begin{bmatrix} \lambda_3 \\ \delta_3 \\ \theta_2 \\ \hdashline \beta_3 \\ \mu_3 \\ \alpha_2 \end{bmatrix} & \begin{bmatrix} \theta_3 \\ \lambda_3 \\ \delta_3 \\ \hdashline \alpha_3 \\ \beta_3 \\ \mu_3 \end{bmatrix} & \begin{bmatrix} \delta_4 \\ \theta_3 \\ \lambda_3 \\ \hdashline \mu_4 \\ \alpha_3 \\ \beta_3 \end{bmatrix} & \begin{bmatrix} \lambda_4 \\ \delta_4 \\ \theta_3 \\ \hdashline \beta_4 \\ \mu_4 \\ \alpha_3 \end{bmatrix} & \begin{bmatrix} \theta_4 \\ \lambda_4 \\ \delta_4 \\ \hdashline \alpha_4 \\ \beta_4 \\ \mu_4 \end{bmatrix} \end{bmatrix}$$

Due to the delay-spread of the channel, the pilot symbols are duplicated 'diagonally' in the adjacent columns of (4.49). The arrangement of the pilot symbols in (4.49) almost resemble the format of $\mathbf{S}_F$ designed in (4.47), except of those marked with the '×'. Thus, to acquire exact $\mathbf{S}_F$ in (4.47), successive $\mathbf{r}$ (except for the last $\mathbf{r}$) can be collected to form the required $\mathbf{X}$ as:

$$\mathbf{X} = \begin{bmatrix} \mathbf{r}(k) & \mathbf{r}(k+1) & \mathbf{r}(k+2) & \mathbf{r}(k+3) & \mathbf{r}(k+4) & \mathbf{r}(k+5) & \mathbf{r}(k+6) & \mathbf{r}(k+9) \end{bmatrix} \quad (4.50)$$

Hence, by choosing pilot matrix that assimilates the 'Toeplitz-like' structure shown in (4.47), provide a way to minimise the pilot symbols sent for channel estimation. The objective is to design a new pilot matrix that contains the combination of both 'Toeplitz-like' and orthogonal structures such that the characteristic of delay spread in frequency selective channel is exploited (for duplication of pilot symbols) while allowing the orthogonal property in (4.34) to be applied concurrently. Such unique structure can be found in the Paley-Hadamard matrix [132, 133]. An example of the Paley-Hadamard matrix $\mathbf{P}$ with matrix order v = 8 is shown in the following:

$$\mathbf{P} = \begin{bmatrix} +1 & +1 & +1 & +1 & +1 & +1 & +1 & +1 \\ +1 & -1 & +1 & +1 & -1 & +1 & -1 & -1 \\ +1 & -1 & -1 & +1 & +1 & -1 & +1 & -1 \\ +1 & -1 & -1 & -1 & +1 & +1 & -1 & +1 \\ +1 & +1 & -1 & -1 & -1 & +1 & +1 & -1 \\ +1 & -1 & +1 & -1 & -1 & -1 & +1 & +1 \\ +1 & +1 & -1 & +1 & -1 & -1 & -1 & +1 \\ +1 & +1 & +1 & -1 & +1 & -1 & -1 & -1 \end{bmatrix} \quad (4.51)$$

The formulation of Paley's construction of Hadamard matrix (using Paley's 2nd lemma [132]) is presented in Appendix C1. (Please refer Appendix C1 for detailed procedure of Paley-Hamard matrix generation for matrix order v=8 used in above example).

4.2.3.2 Construction of Pilot Matrix using Paley-Hadamard Matrix

The Paley-Hadamard matrix $\mathbf{P}(v)$ also has the orthogonal property shown as follows:

$$\mathbf{P}(v).\mathbf{P}(v)^{\mathsf{T}} = v.\mathbf{I} \qquad \& \qquad \mathbf{P}(v)^{\mathsf{T}} = v.\mathbf{P}(v)^{-1} \tag{4.52}$$

where $(.)^{\mathsf{T}}$ is the transposition. Note that properties in (4.52) are similar to (4.34) for ordinary Hadamard case. If $\mathbf{P}$ in (4.52) is a complex matrix, then v becomes $2v$ and $(.)^{\mathsf{H}}$ replaces $(.)^{\mathsf{T}}$.

In the case of Paley-Hadamard matrix $\mathbf{P}$, its suitable matrix order v must be determined first such that v is divisible by 4, $(v-1)$ is prime (using Paley's 2nd lemma) and follows the criterion as:

$$v > M \times (L+1) \tag{4.53}$$

where v must be 'only' greater than the product of M and $(L+1)$, which is different from the criteria in (4.35) where '>' sign is used instead of '≥' sign. Once the suitable order v is obtained, the Paley-Hadamard matrix $\mathbf{P}$ is generated (refer to Appendix C1). However, prior to the actual formulation of the new pilot matrix $\mathbf{S}_F$, $\mathbf{P}$ is slightly modified from (4.51) where the original 1st column of +1s is moved from the front to the back at the last column of $\mathbf{P}$, shown as:

$$\mathbf{P} = \underbrace{\left[\begin{array}{ccccccc|c} +1 & +1 & +1 & +1 & +1 & +1 & +1 & +1 \\ -1 & +1 & +1 & -1 & +1 & -1 & -1 & +1 \\ -1 & -1 & +1 & +1 & -1 & +1 & -1 & +1 \\ -1 & -1 & -1 & +1 & +1 & -1 & +1 & +1 \\ +1 & -1 & -1 & -1 & +1 & +1 & -1 & +1 \\ -1 & +1 & -1 & -1 & -1 & +1 & +1 & +1 \\ +1 & -1 & +1 & -1 & -1 & -1 & +1 & +1 \\ +1 & +1 & -1 & +1 & -1 & -1 & -1 & +1 \end{array}\right]}_{\text{1st column moved to last}} \quad \begin{array}{l} \text{2nd row to 7th row} \end{array} \tag{4.54}$$

The modified format in $\mathbf{P}$ still preserves the orthogonal structure and the Toeplitz structure, which makes the required format of $\mathbf{S}_F$ in (4.47) immediately available. This can be attained from 2nd row to 7th row sequence above. Note that the first row sequence of $\mathbf{P}$ with all '+1s' will not be considered as pilot symbols since they do not constitute the format of the Toeplitz-like structure.

Next, the pilot matrix $\mathbf{S}_F$ can be formed by directly extracting the *successive* orthogonal rows sequences from $\mathbf{P}$ in (4.54) and assigned them to both $\mathbf{A}$ and $\mathbf{B}$, based on the value of $M\times(L+1)$. This can be shown by using the same example of $M = 2$ and $(L+1) = 3$ as:

$$\mathbf{S}_F = \mathbf{A} + j\mathbf{B} \tag{4.55}$$

where

$$\mathbf{A} = \mathbf{B} = \left[\begin{array}{cccccccc} -1 & +1 & +1 & -1 & +1 & -1 & -1 & +1 \\ -1 & -1 & +1 & +1 & -1 & +1 & -1 & +1 \\ -1 & -1 & -1 & +1 & +1 & -1 & +1 & +1 \\ \hline +1 & -1 & -1 & -1 & +1 & +1 & -1 & +1 \\ -1 & +1 & -1 & -1 & -1 & +1 & +1 & +1 \\ +1 & -1 & +1 & -1 & -1 & -1 & +1 & +1 \end{array}\right] \begin{array}{l} \left.\begin{array}{l} \\ \\ \\ \end{array}\right\} \text{Tx1} \\ \left.\begin{array}{l} \\ \\ \\ \end{array}\right\} \text{Tx2} \end{array}$$

The Toeplitz-like structure is effectively utilised so that duplications of pilot components shown in those shaded areas in (4.55) are not required to be sent, while retaining the orthogonal

structure. Only those 'un-shaded' symbols are required to be sent for channel estimation. The corresponding training sequence sent from each transmit antenna is shown in the following:

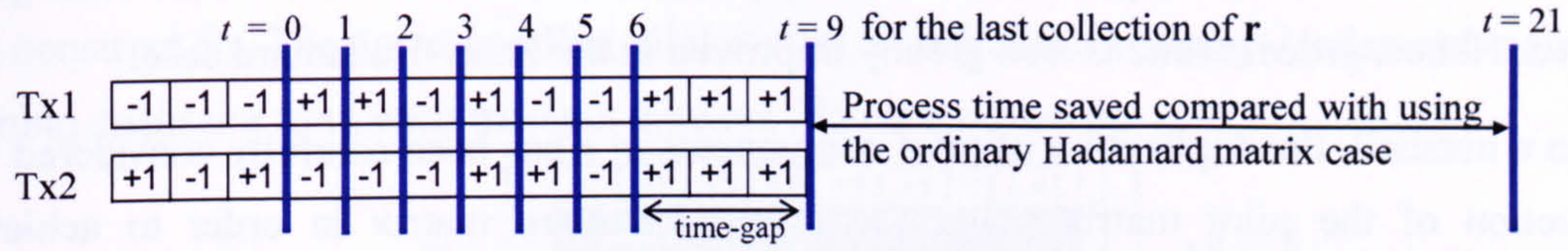

Figure 4.3: Training sequence based on Paley-Hadamard matrix for $M = 2$ and $(L+1) = 3$ case

For comparison, the training sequence obtained from previous case using the ordinary Hadamard matrix case is shown as:

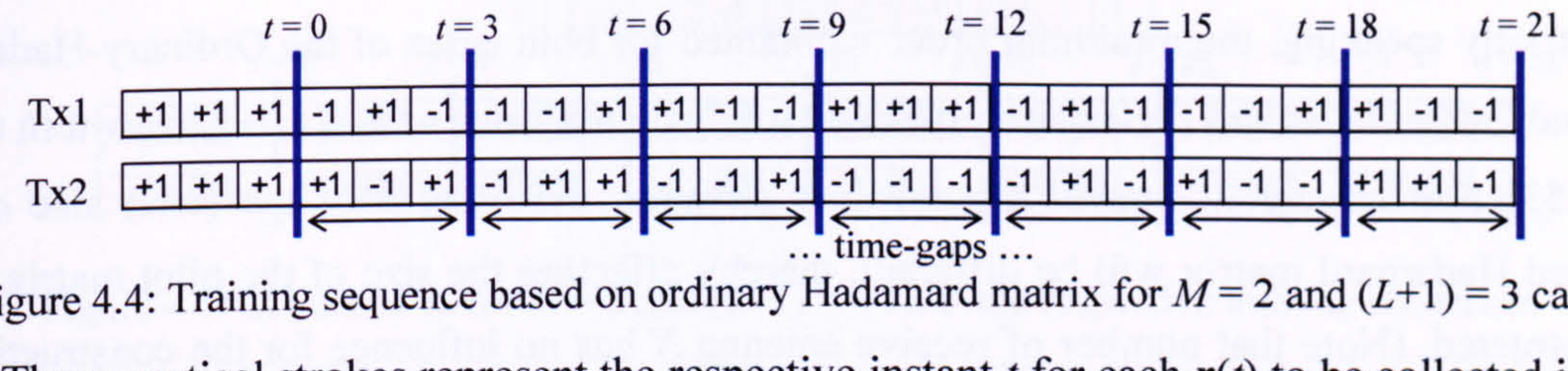

Figure 4.4: Training sequence based on ordinary Hadamard matrix for $M = 2$ and $(L+1) = 3$ case

Those vertical strokes represent the respective instant t for each $\mathbf{r}(t)$ to be collected into the required matrix $\mathbf{X}$ in each case. Only a small time-gap is noticed in the first case since adjacent $\mathbf{r}$ (except the last one) is collected at interval $p = 1$. Each stroke in later case is noticed to be further apart (with multiple time-gaps) due to collection of $\mathbf{r}$ at non-adjacent $p = (L+1)$ interval for the reason explained in section 4.2.2.4, which results in extra process time for channel estimation.

By utilising the Toeplitz-like structure obtained from the modified Paley-Hadamard matrix, the length of the training sequence (only 12 symbols) for each transmit antenna is minimised, as compared to the case for the ordinary Hadamard matrix (24 symbols). The length of the training sequence for *each* transmit antenna for Paley-Hadamard case can be computed as:

$$v + 2L \tag{4.56}$$

Consequently, the minimum number of pilot symbols that must be sent in total (from all transmit antennas) has been reduced from $M \times (L+1) \times v$ for the ordinary Hadamard matrix case, to $M \times (v + 2L)$ for the Paley-Hadamard matrix case.

4.2.3.3 Proper collection of r into X for the Paley-Hadamard case

For the general Paley-Hadamard case, in order to restore the exact 'Toeplitz-like' and orthogonal format of the pilot matrix $\mathbf{S}_F$ sent for channel estimation in the frequency selective channel, successive $\mathbf{r}$ at p=1 can be collected at the receiver in order to form the require $\mathbf{X}$ as:

$$\mathbf{X} = \left[\mathbf{r}(k) \;\; \mathbf{r}(k+p) \;\; \mathbf{r}(k+2p) \;\; \cdots \;\; \mathbf{r}(k+q) \;\vdots\; \mathbf{r}(k+(L+1)+q)\right] \tag{4.57}$$

time-gaps

where parameter 'q' is set to the following:

$$q = v - 2 \tag{4.58}$$

Note that only small time-gap of $(L+1)$ interval is needed between the second last $\mathbf{r}$ and the

last **r**, which is between **r**(k+q) & **r**(k+(L+1)+q) respectively during the formation of **X** for the Paley-Hadamard case as compared to the ordinary Hadamard case where multiple time-gaps are observed. Hence, process time is also greatly improved in the Paley-Hadamard case.

In a nutshell, the duplication of pilot components in **r** has been carefully considered for the construction of the pilot matrix using the Paley-Hadamard matrix in order to achieve the minimisation in the length of training sequence as well as the improvement in the process time.

4.2.3.4 Consideration for Different (N×M) system and (L+1) delay paths

Strictly speaking, the minimum order v obtained for both cases of the Ordinary-Hadamard (OH) and Paley-Hadamard (PH) matrix depends solely on the value of $M \times (L+1)$ shown in (4.35) and (4.53) respectively. If one of these values changes, the order v or the (v×v) size of the generated Hadamard matrix will be different, thereby affecting the size of the pilot matrix $\mathbf{S}_F$ to be constructed. (Note that number of receive antenna N has no influence for the construction of pilot matrix in both cases). To generalise the novel MIMO-CE algorithm for any (N×M) system with any (L+1) delay path condition, the pilot matrix $\mathbf{S}_F$ can be formulated as:

$$\mathbf{S}_F = \mathbf{A} + j\mathbf{B}; \tag{4.59}$$

$$\text{where} \quad \mathbf{A} = \mathbf{B} = \begin{bmatrix} \boldsymbol{C}_1 \\ \hline \vdots \\ \hline \boldsymbol{C}_M \end{bmatrix} \quad \& \quad \boldsymbol{C}_m = \begin{bmatrix} s_{m1}(1) & s_{m1}(2) & \cdots & s_{m1}(v) \\ s_{m2}(1) & s_{m2}(2) & \cdots & s_{m2}(v) \\ & \vdots & & \\ s_{m(L+1)}(1) & s_{m(L+1)}(2) & \cdots & s_{m(L+1)}(v) \end{bmatrix} \tag{4.60}$$

Note that there are (L+1) orthogonal sequences in $\boldsymbol{C}_m$, each extracted from the respective row of the Hadamard matrix and consists of full-length (v-ordered) pilot symbols. Depending on the value of M, $\mathbf{S}_F$ may consist of M block of $\boldsymbol{C}_m$ in each **A** & **B** matrices where each $\boldsymbol{C}_m$ consists of pilot symbols with respect to each m^{th} transmit antenna.

For illustration, two examples are shown for different values of M and (L+1) with reference to the previous case of M = 2 and (L+1) = 3. Either one of these values, M or (L+1) is increased to illustrate the change in the construction of the pilot matrix and corresponding training sequence w.r.t each antenna for both cases of OH and PH.

1) 1st Example using (N×M) = (2×2) system for (L+1) = 4 case with $M \times (L+1) = 8$

The corresponding the concatenated channel matrix with 16 entries of fading coefficients is shown as:

$$\mathbf{H}_{1|2} = \left[\mathbf{H}_1 \,|\, \mathbf{H}_2\right] = \left[\begin{array}{cccc|cccc} h_{11}(0) & h_{11}(1) & h_{11}(2) & h_{11}(3) & h_{12}(0) & h_{12}(1) & h_{12}(2) & h_{12}(3) \\ h_{21}(0) & h_{21}(1) & h_{21}(2) & h_{21}(3) & h_{22}(0) & h_{22}(1) & h_{22}(2) & h_{22}(3) \end{array}\right] \tag{4.61}$$

a) Pilot matrix and order v by the ordinary Hadamard matrix.

Since $M \times (L+1) = 8$ and according to (4.35) the full size OH matrix of order $v = 8$ can be used to construct $\mathbf{S}_F$. The corresponding pilot matrix $\mathbf{S}_F$ using the ordinary-Hadamard matrix and the training sequence from each transmit antenna (Tx) are shown as:

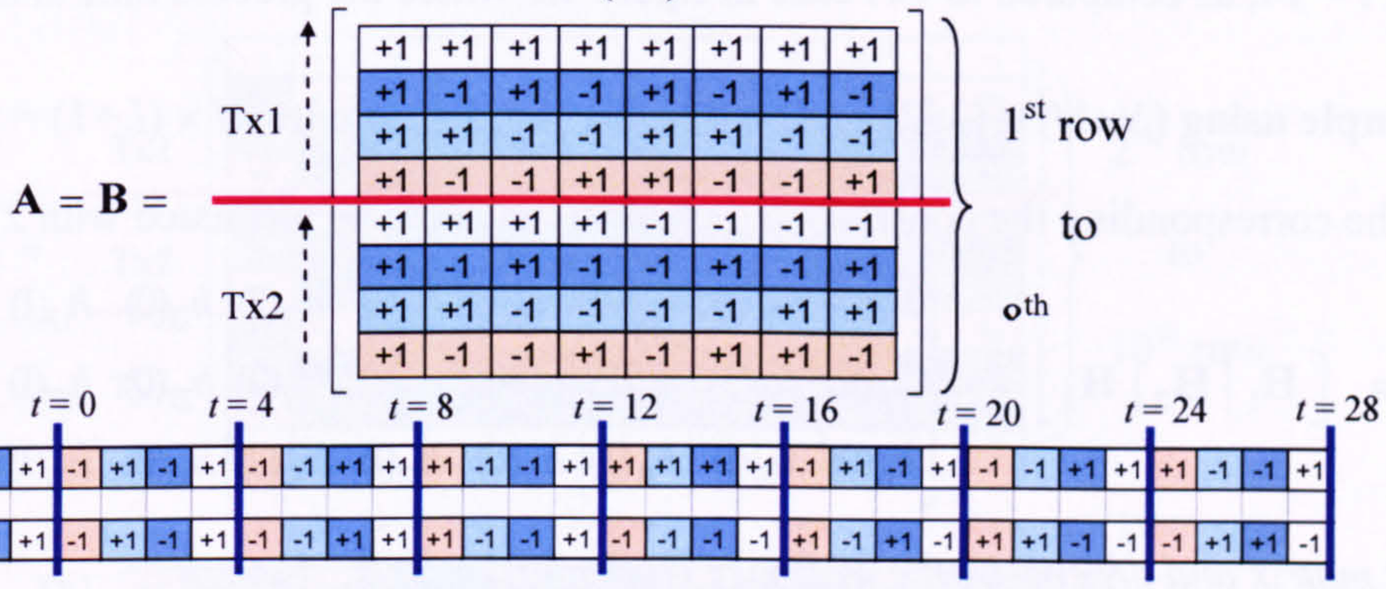

Figure 4.5: OH based $\mathbf{S}_F$ for $M = 2$ and $(L+1) = 4$ case and respective training sequences

Note that each training sequence (per Tx) consists of 32 symbols and only 8 extra symbols are observed as compared to figure 4.4 when $(L+1)$ is increased from 3 to 4. However, for fixed $M = 2$, any further increase in $(L+1)$, requires v to be increased to the next or higher valid order of the OH matrix so that (4.35) is fulfilled, causing further increase in the length of the training sequence. Also, the estimator has to wait until $t = 28$ before carrying out the channel estimation.

b) Pilot matrix and order v by the Paley-Hadamard matrix

For PH case, $M \times (L+1) = 8$ according to (4.53). However, $v = 8$ is no longer valid in this case since $(v > 8)$. Hence, the next valid order is $v = 12$, where PH matrix with size of (12×12) is generated and only eight rows of orthogonal sequences are extracted from this PH matrix to form the required $\mathbf{S}_F$. The corresponding $\mathbf{S}_F$ using the Paley-Hadamard matrix and the training sequences from each transmit antenna is shown as:

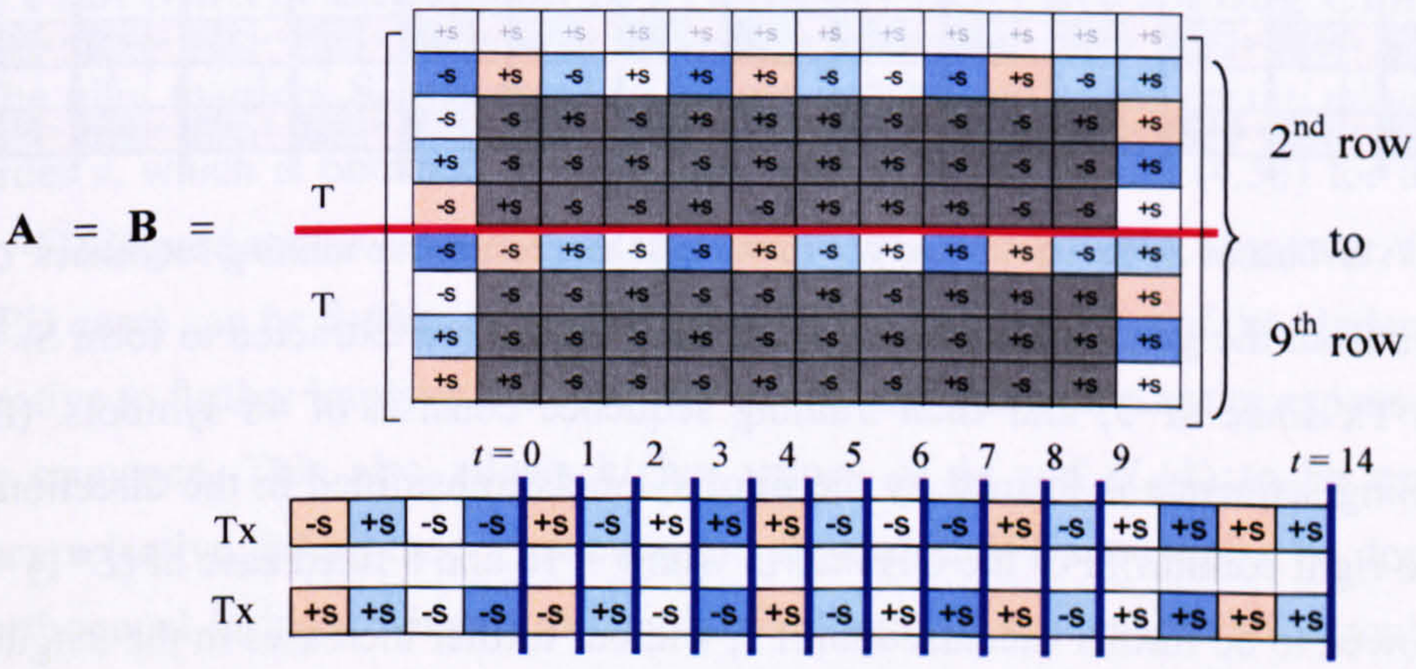

Figure 4.6: PH based $\mathbf{S}_F$ for $M = 2$ and $(L+1) = 4$ case and respective training sequences.

Although larger size of PH matrix with higher order (v=12) is used, each training sequence (per Tx) only consists of 18 symbols as compared to previous case of OH in figure 4.5. As

compared to figure 4.3, only 6 extra symbols per training sequence (per Tx) is needed to cover the extra path from $(L+1) = 3$ to 4 for fixed case of $M = 2$. With v=12 PH matrix, additional paths are allowed to be increased until $(L+1) = 5$ according to (4.60). Also, the estimator only has to wait for $t = 14$, as compared to OH case in figure 4.5 where the process time is improved by 50%.

2) Example using $(N\times M) = (3\times3)$ system for $(L+1) = 3$ case with $M \times (L+1) = 9$

The corresponding the concatenated channel matrix to be estimated with 27 entries as:

$$\mathbf{H}_{1|3} = \left[\mathbf{H}_1 \,\middle|\, \mathbf{H}_2 \,\middle|\, \mathbf{H}_3\right] = \left[\begin{array}{ccc|ccc|ccc} h_{11}(0) & h_{11}(1) & h_{11}(2) & h_{12}(0) & h_{12}(1) & h_{12}(2) & h_{13}(0) & h_{13}(1) & h_{13}(2) \\ h_{21}(0) & h_{21}(1) & h_{21}(2) & h_{22}(0) & h_{22}(1) & h_{22}(2) & h_{23}(0) & h_{23}(1) & h_{23}(2) \\ h_{31}(0) & h_{31}(1) & h_{31}(2) & h_{32}(0) & h_{32}(1) & h_{32}(2) & h_{33}(0) & h_{33}(1) & h_{33}(2) \end{array}\right] \quad (4.62)$$

a) Pilot matrix and order v by the ordinary Hadamard matrix.

For the OH case, since $M \times (L+1) = 9$ according to (4.35), the next valid order for generating the Hadamard matrix is $v = 16$. (Please refer to [132] for reference of library class of Hadamard matrix). The corresponding pilot matrix $\mathbf{S}_F$ (with dimension of 9×16) using the ordinary-Hadamard matrix and the training sequence from each transmit antenna are shown as:

Figure 4.7: OH based $\mathbf{S}_F$ for $M = 3$ and $(L+1) = 3$ case and respective training sequences

First 9 rows from the generated ordinary Hadamard matrix are extracted to form $\mathbf{S}_F$ (into 3 regions for each Tx since M=3) and each training sequence consists of 48 symbols. (In each region, each training sequence is formed by the pilot symbols transmitted in the direction of the arrow from left to right column). For the OH matrix with $v = 16$ and a fixed case of $(L+1) = 3$, the value of M is allowed to be further increased until 5, without further increases in the length of the training sequence. However, longer estimation process-time (with $t = 45$) is needed as compared to figure 4.5 where M is increased from 2 to 3 in this case.

b) Pilot matrix and order v by the Paley-Hadamard matrix.

Since $M\times(L+1)=9$ and according to (4.53), the previous generated PH matrix with $v=12$ can still be used to form the required $\mathbf{S}_F$ but 9 orthogonal row sequences are extracted this time. The corresponding (9×12) $\mathbf{S}_F$ using the PH matrix and the training sequences from each Tx are:

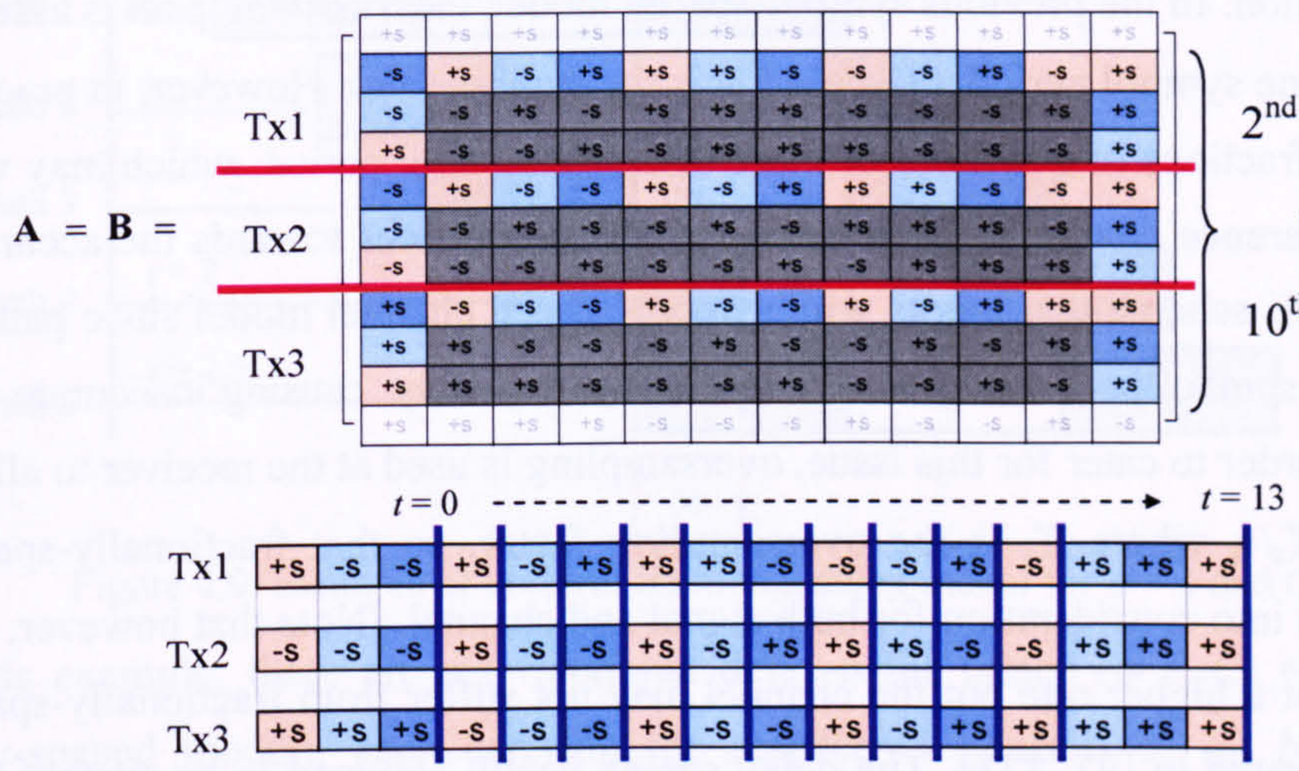

Figure 4.8: PH based $\mathbf{S}_F$ for $M=3$ and $(L+1)=3$ case and respective training sequences.

It can be seen that each training sequence (per Tx) in figure 4.8 only consists of 16 pilot symbols, as compared to the OH case in figure 4.7. Using the PH-based matrix, the pilot length is significantly reduced and the process time (with t=13) is also greatly improved, although an extra row of training sequence is needed (since $M=3$) to cater for the additional transmit antenna. In fact, the improvement is more than 50% in terms of pilot length and process time, demonstrating the significant achievement in using PH-based pilot matrix (instead of OH-based pilot matrix) for the purpose of channel estimation in the frequency selective fading MIMO channel.

4.2.4 Pilot Matrix Expansion in Frequency Selective Fading Channel

The pilot matrices $\mathbf{S}_F$ presented so far are constructed based on the minimum size of the valid order v, which is obtained through the criterion in (4.35) and (4.53) for the both cases of ordinary-Hadamard matrix and Paley-Hadamard matrix respectively. However, the size of $\mathbf{S}_F$ (in OH or PH case) can be further expanded using higher valid order v of the Hadamard matrix with the objective to further improve the accuracy of channel estimation at the expense of using longer training sequence. This also allows higher values of M and $(L+1)$ to be catered for in the frequency selective fading case. However, the expansion of $\mathbf{S}_F$ must also be done in accordance to the orthogonal fashion; where full-length of orthogonal sequence with v symbols in each row must be adopted. The impact of using longer training sequence to achieve better performance of the proposed channel estimation scheme is presented in Chapter 5 for results section.

4.3 Fractionally-Spaced Delay Model Consideration

This section examines the fractionally-spaced delay model of the frequency-selective MIMO channel and extends the proposed MIMO-CE scheme to cater for the fractionally-spaced delay spread condition. In the previous symbol-spaced model, each arriving path is assumed to be evenly spaced by one symbol period τ (where $1/\tau$ is the symbol rate). However, in practice, paths may arrive within fractions of a symbol or more than one symbol period, which may worsen the inter-symbol interference condition. This has serious consequences towards the accuracy of the proposed MIMO-CE scheme that works with symbol-spaced channel model since paths arriving within fractions of symbol period may not be resolved completely; causing inaccurate estimation of the channel. In order to cater for this issue, oversampling is used at the receiver to allow higher sampling rate of K_s/τ, where K_s is the oversampling factor, so that fractionally-spaced delay model can be taken into consideration for both signal and channel. (Note that however, one might sample the signal at a higher rate but the channel may not suffer from fractionally-spaced delay spread, as demonstrated in [97, 131]. The delay spread is still assumed to be symbol-spaced for the multi-channel model and the fractionally-spaced equaliser therein).

In the following, 'φ' is defined as the total span of the delay spread in terms of symbol period (which is equivalent to (L+1) in the previous symbol-spaced model) and 'C' is defined as the fractional sampling rate. In general, the total number of fractional delay-paths can be found as ($\varphi \times C$). These parameters must be known to both transmitter and receiver in order to carry out the fractionally-spaced MIMO-CE method. This is explained later in the formation of pilot matrix and the collection into appropriate receive matrix **X'** respectively at transmitter and receiver.

Thus, the fractionally-sampled CIR (between m^{th} transmit antenna and n^{th} receive antenna), $\mathbf{h}'_{nm}$, that consists of fractionally-spaced delay path can be generally re-expressed as:

$$\mathbf{h}'_{nm} = \left[\; h^1_{nm}(0) \ldots h^C_{nm}(0) \quad \cdots \quad h^1_{nm}(L) \ldots h^C_{nm}(L) \; \right]^{\mathsf{T}} \tag{4.63}$$

where $h^k_{nm}(r)$ specifies the k^{th} fractionally-sampled channel coefficient within r^{th} symbol period and the overall duration of the CIR is equivalent to $\varphi = (L+1)$ symbols. The little apostrophe sign denotes the fractionally-spaced model of the CIR.

Next, the fractional delay model is systematically illustrated using single CIR of a sub-channel link. In the following, 3 examples are demonstrated to provide different scenario of fractionally-spaced channel model. For the uniform fractionally-spaced model (shown in example *a)* and *b)* later), the actual number of fractional delay-paths is equivalent to the product of φ and C. However, in the non-uniform fractionally-spaced model, the actual number of fractional delay-paths could be lesser with 'non-evenly' spacing between the paths (shown in example *c)* later).

a) Example of uniform fractionally-spaced model for $C = 2$ and $\varphi = 3$

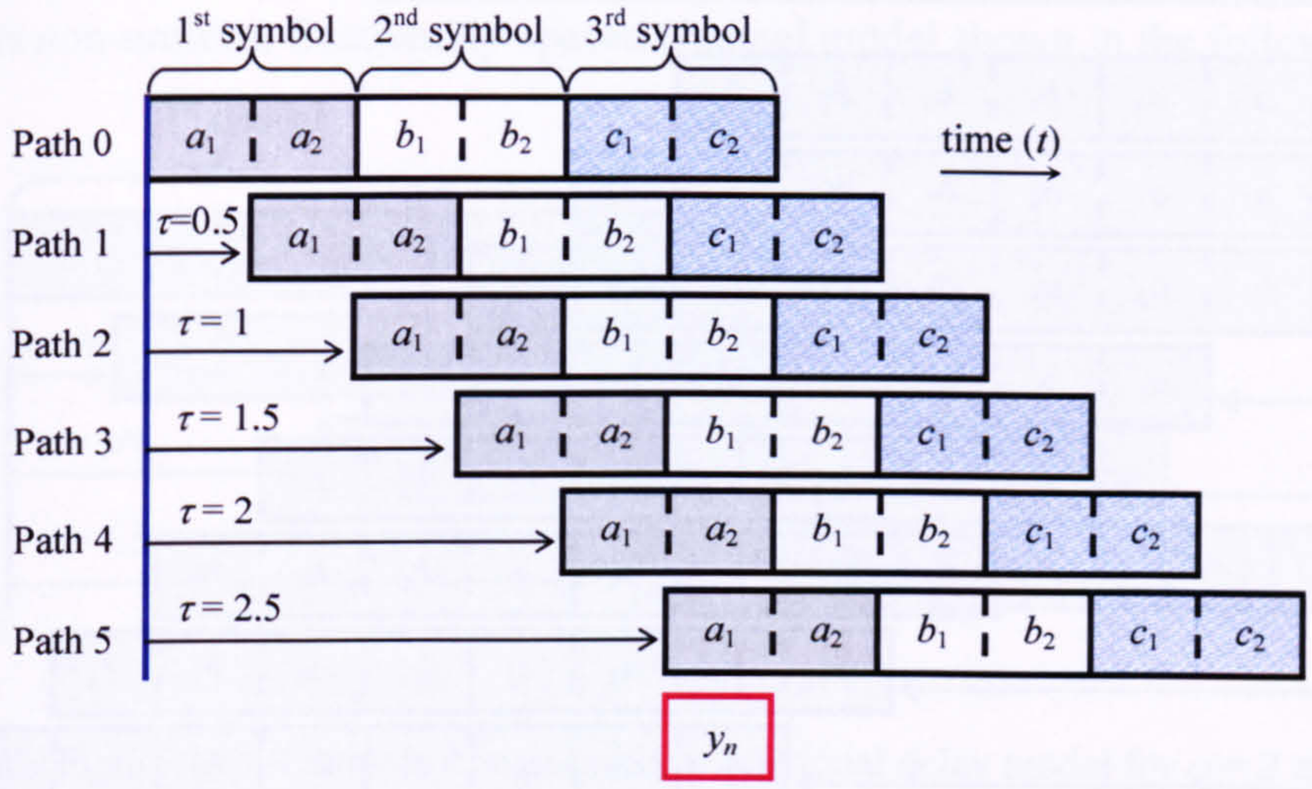

Figure 4.9: Example of uniform fractional delay model for $\varphi = 3$ and $C = 2$

In this example, there are six fractional delay-paths (since $(\varphi \times C) = 6$ in the uniform fractionally-spaced model), each carrying the respective symbols as a_k, b_k and c_k with the subscript 'k' indicating k^{th} half of the respective symbol. Each path is evenly spaced by ½ symbol period. Therefore, the total delay span is $\varphi = 3$ symbols period. Note that y_n at the bottom of figure 4.9 represents the ISI effect resulting from the sum of these 6 delay paths due to delay spread condition. This can also be illustrated using the FIR tap-delay-line (TDL) as follows:

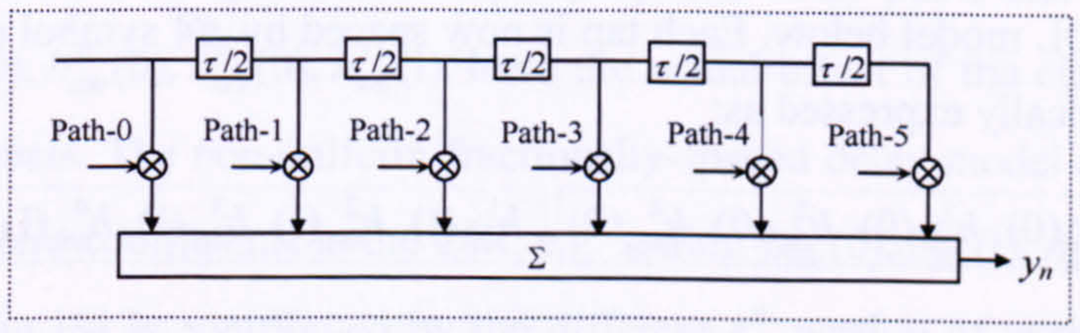

Figure 4.10: FIR-TDL model for uniform $C = 2$ and $\varphi = 3$ case

Note that each tap is spaced by $\tau/2$ symbol period and the sum at y_n can be expressed as:

$$y_n = \begin{bmatrix} h_{nm}^1(0) & h_{nm}^2(0) & h_{nm}^1(1) & h_{nm}^2(1) & h_{nm}^1(2) & h_{nm}^2(2) \end{bmatrix} \begin{bmatrix} c_2 \\ c_1 \\ b_2 \\ b_1 \\ a_2 \\ a_1 \end{bmatrix} \tag{4.64}$$

The expression in (4.64) means that each respective symbol a, b and c is duplicated according to the value of fractional sampling rate, C and interact respectively with each associated fractional sample of the channel coefficients $h_{nm}^k(r)$, which is generated using independent identical distributed (i.i.d) process with Rayleigh fading assumption.

b) Example of uniform fractionally-spaced model for $C = 4$ and $\varphi = 2$

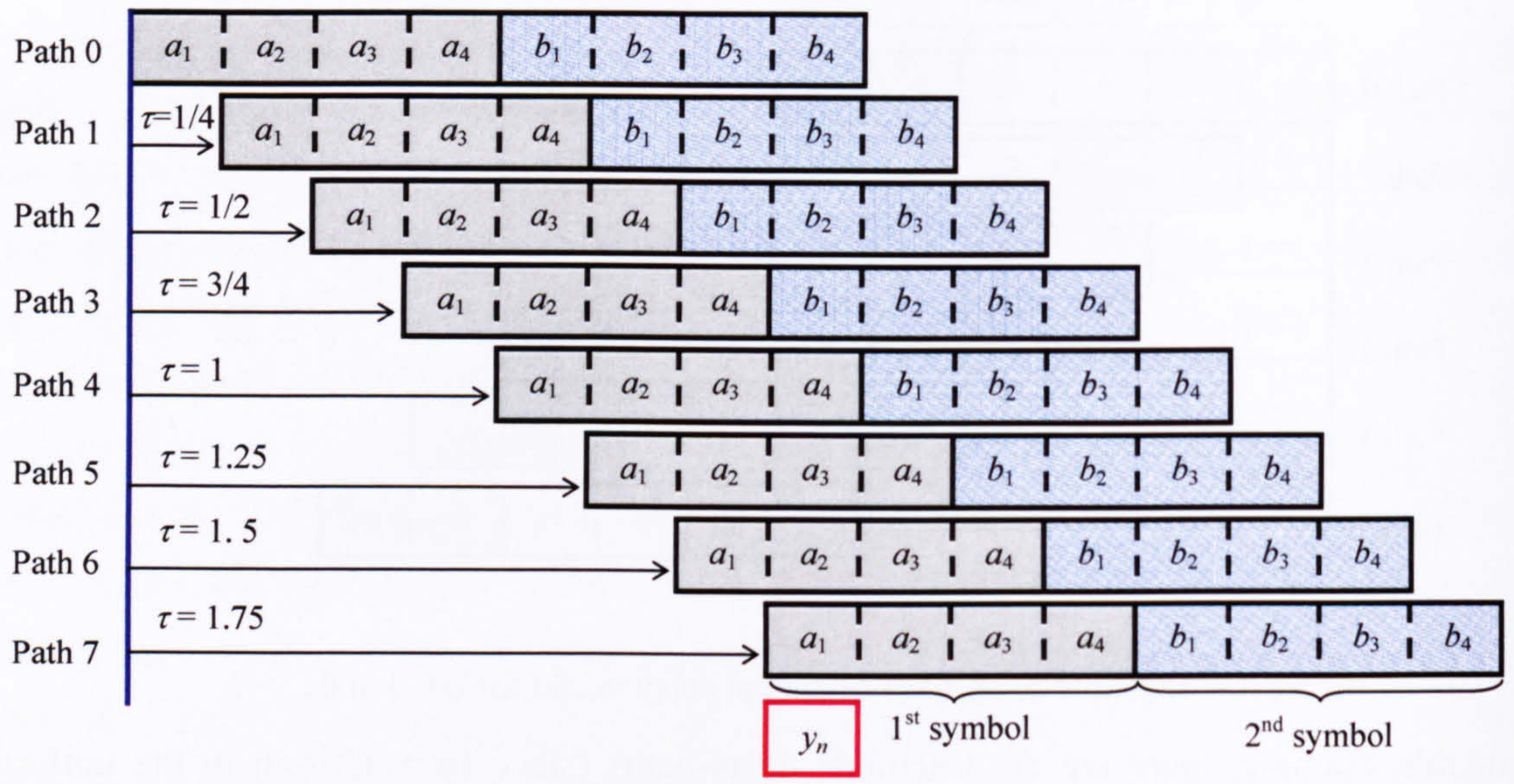

Figure 4.11: Example of uniform fractional delay model for $\varphi = 2$ and $C = 4$

In this example, higher fractional sampling rate, $C = 4$ is used with total delay span of $\varphi = 2$ symbols period. There are 8 uniform delay-paths, each evenly spaced by ¼ symbol periods. Here, only 2 corresponding full-symbols denoted as a_k, and b_k are involved. Similarly, y_n represents the ISI effect resulting from the sum of the 8 paths and the k^{th} quarter of the respective symbol, as illustrated in the TDL model below. Each tap is now spaced by $\tau/4$ symbol period and the sum at y_n can be mathematically expressed as:

$$y_n = \left[h_{nm}^1(0)\ h_{nm}^2(0)\ h_{nm}^3(0)\ h_{nm}^4(0)\ \middle|\ h_{nm}^1(1)\ h_{nm}^2(1)\ h_{nm}^3(1)\ h_{nm}^4(1) \right] \begin{bmatrix} b_4 \\ b_3 \\ b_2 \\ b_1 \\ \hline a_4 \\ a_3 \\ a_2 \\ a_1 \end{bmatrix} \tag{4.65}$$

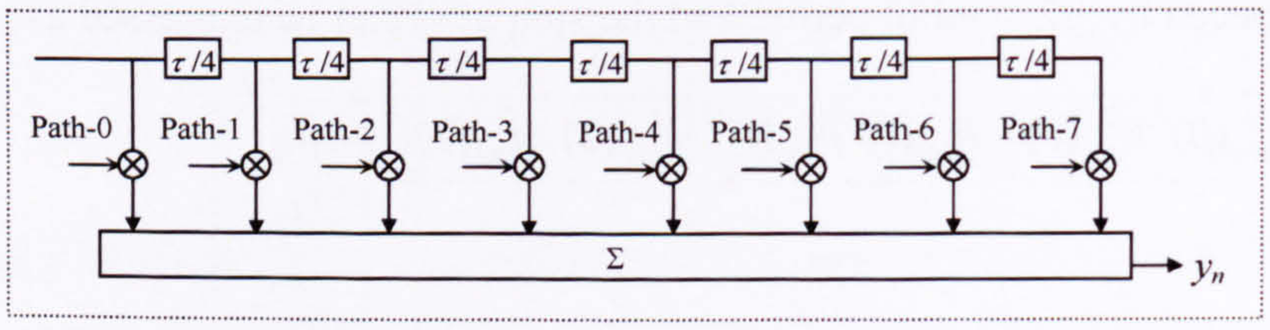

Figure 4.12: FIR-TDL model for uniform $C = 2$ and $\varphi = 3$ case

Each respective symbol a or b is duplicated according to C and interacts respectively with each $h_{nm}^k(r)$ that is independent to one another, where $k = 1$ to 4 in this case.

c) Example of non-uniform fractionally-spaced model for $C = 4$ and $\varphi = 2$

In the two previous examples, the delay-paths are uniformly spaced within each symbol period. Here, non-uniform model with unequal spacing between delay-paths is shown using the

same parameter of $C = 4$ & $\varphi = 2$. Path 2, 4, 5 and 7 of figure 4.11 are absent and the remainder represents non-uniform fractionally-spaced channel model shown in the following:

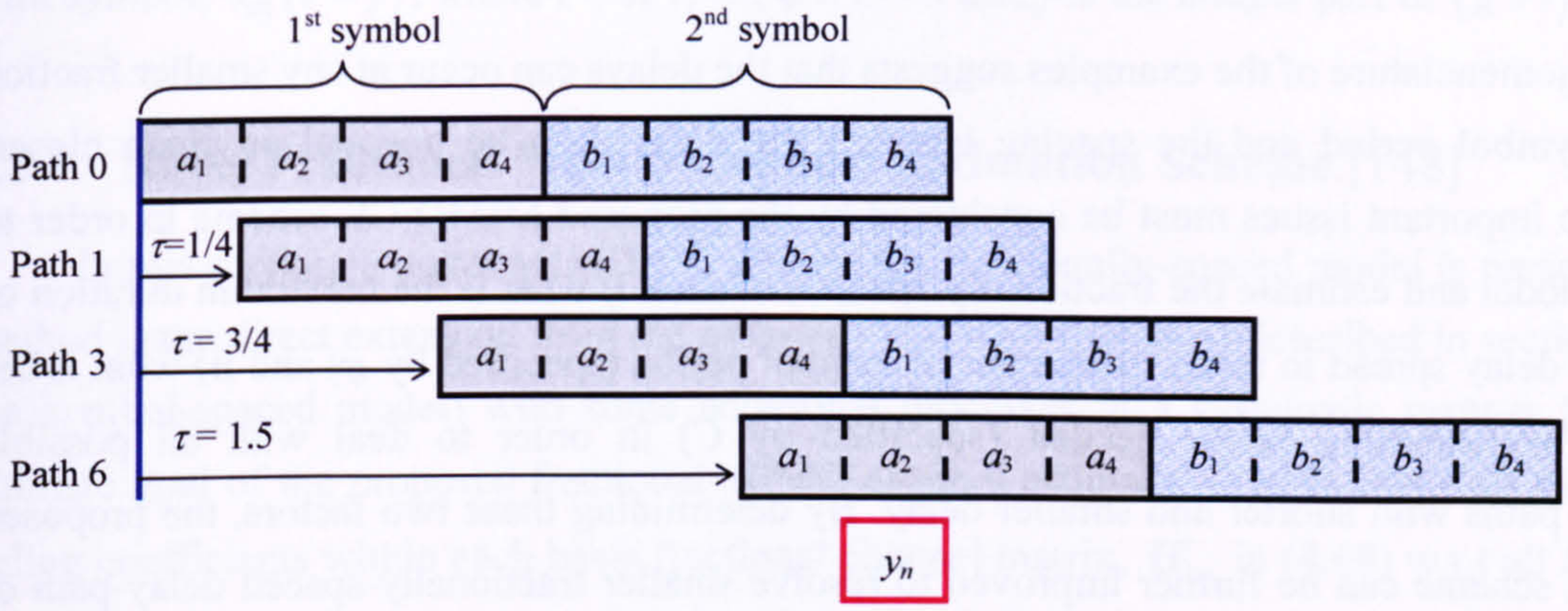

Figure 4.13: Example of non-uniform fractional delay model for $\varphi = 2$ and $C = 4$

Note that only 4 paths exist in this case and arrive at different time. Path-1 arrives at ¼ symbol period later with reference to path-0, path-3 arrives at ¾ symbol period later and lastly, path-6 arrives at 1.5 symbol period later, illustrating a fractionally-spaced channel model that is more realistic to be assumed. Thus, the sampled CIR for this case can be written as:

$$\mathbf{h}'_{nm} = \begin{bmatrix} h^1_{nm}(0) & h^2_{nm}(0) & 0 & h^4_{nm}(0) & 0 & 0 & h^3_{nm}(1) & 0 \end{bmatrix} \tag{4.66}$$

It can be seen that, although up to 8 equally spaced delay-paths can be accommodated originally, only $h^1_{nm}(0), h^2_{nm}(0), h^4_{nm}(0), h^3_{nm}(1)$ have the actual effect of the channel delay spread on the transmitted signals. The non-uniform fractionally-spaced delay model can be obtained by inserting appropriate zero coefficients in the CIR, e.g. setting $h^3_{nm}(0), h^1_{nm}(1), h^2_{nm}(1), h^4_{nm}(1)$ to zero in (4.66). The resulting ISI is contributed by the different k^{th} portion of each symbol a_k and b_k along with their associated path as illustrated and expressed in the following TDL model:

$$y_n = \begin{bmatrix} h^1_{nm}(0) & h^2_{nm}(0) & 0 & h^4_{nm}(0) & 0 & 0 & h^3_{nm}(1) & 0 \end{bmatrix} \begin{bmatrix} b_4 \\ b_3 \\ b_2 \\ b_1 \\ a_4 \\ a_3 \\ a_2 \\ a_1 \end{bmatrix} \tag{4.67}$$

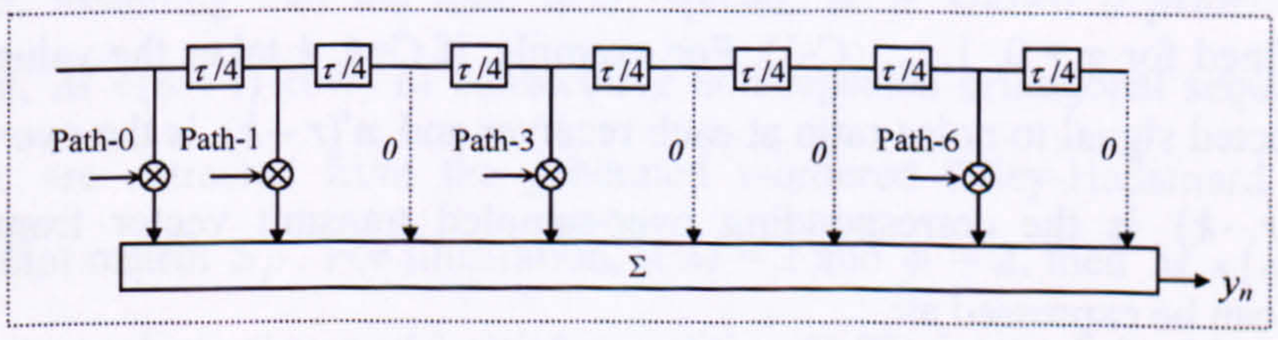

Figure 4.14: FIR-TDL model for uneven $c = 2$ and $\varphi = 3$ case

Note that the ISI effect on y_n (at that instant) constitutes the sum of one-quarter of symbol a and three-quarter of symbol b with their associated delay-path (Path-0, Path-1, Path-3, Path-6). Therefore, the ISI effect might constitute the uneven portion of each respective symbol,

depending on the actual delay between each fractional path. Hence, with oversampling at rate of $4/\tau$, we can choose to estimate these 4 paths effectively in a more refined version of channel.

The nomenclature of the examples suggests that the delays can occur at any smaller fraction within a symbol period and the spacing between the delays can be unequal or much closer. Hence, two important issues must be considered by the proposed MIMO-CE scheme in order to correctly model and estimate the fractionally-spaced channel: i) what is the maximum duration of the overall delay spread in terms of number of symbol period (specified by φ) and ii) what is the minimum oversampling factor needed (specified by C) in order to deal with all possible significant paths with shorter and smaller delay. By determining these two factors, the proposed MIMO-CE scheme can be further improved to resolve smaller fractionally-spaced delay-path of the frequency-selective fading MIMO channel. It must be stressed that, although oversampling is used here, we do not deal with blind channel estimation [93–97]; but instead, exploits the oversampling concept to perform channel estimation for the fractionally-spaced model.

4.3.1 Signal and Channel Model in Fractionally-Spaced Model

Having defined the fractional CIR $\mathbf{h}'_{nm}$ in (4.63), the basic fractional channel matrix $\mathbf{H}'_m$ w.r.t m^{th} transmit antenna (with matrix dimension of $N\times(L+1)C$) can be expressed as:

$$\mathbf{H}'_m = \begin{bmatrix} \mathbf{h}'^{\mathsf{T}}_{1m} \\ \vdots \\ \mathbf{h}'^{\mathsf{T}}_{Nm} \end{bmatrix} = \begin{bmatrix} h^1_{1m}(0)\ldots h^C_{1m}(0) & \cdots & h^1_{1m}(L)\ldots h^C_{1m}(L) \\ & \vdots & \\ h^1_{Nm}(0)\ldots h^C_{Nm}(0) & \cdots & h^1_{Nm}(L)\ldots h^C_{Nm}(L) \end{bmatrix} \tag{4.68}$$

At some fractions of a symbol, k within the r^{th} symbol, the received signal vector $\boldsymbol{x}'(r-k)$ (with dimension of $(N\times 1)$ containing signal samples at each of the N receive antenna from all M transmit antennas) can be expressed as:

$$\boldsymbol{x}'(r-k) = \sqrt{\rho/M} \sum_{m=1}^{M} \mathbf{H}'_m \mathbf{s}'_m(r-k) + \mathbf{n}'(r-k) \tag{4.69}$$

where $k = g/C$, is defined for $g = 0, 1,\ldots, (C\text{-}1)$. For example, if C=4, k takes the values, 0, 1/4, 1/2, 3/4. ρ is the expected signal to noise ratio at each receiver and $\mathbf{n}'(r-k)$ is the over-sampled AWGN vector. $\mathbf{s}'_m(r-k)$ is the corresponding over-sampled transmit vector from the m^{th} transmit antenna that can be expressed as:

$$\mathbf{s}'_m(r-k) = \left[s_m\left(r-\frac{g}{C}\right) \; s_m\left(r-\frac{g+1}{C}\right) \; \cdots \; s_m\left(r-\frac{g+\varphi\times C-1}{C}\right) \right]^{\mathsf{T}} \tag{4.70}$$

In order to correctly model the effect of fractionally-spaced channel on the transmitted signal, it is vital to realise that the received samples are fractionally-spaced but the transmitted symbols are

symbol-spaced. Hence, $s_m\left(r-(g+i)/C\right)$ are the duplicated samples of the same transmitted pilot symbol, $s_m(r-j)$, where $i = 0, 1, \ldots, \varphi \times C - 1$ and j is the integer part of $(g+i)/C$.

4.3.2 Novel Fractional MIMO Channel Estimation Scheme [148]

In this section, a novel MIMO-CE scheme for fractionally-spaced model is presented. This method is the direct extension from the proposed MIMO-CE method described in section 4.2 (for the symbol-spaced model) with some additional processes in a systematic manner [148]. The ultimate goal of the proposed fractional MIMO channel estimator is to estimate all the complex fading coefficients within each basic fractional channel matrix, $\mathbf{H}'_m$ in (4.68) w.r.t all M transmit antennas. The basic concatenated fractional channel matrix can be expressed as:

$$\mathbf{H}'_{1|M} = \left[\ \mathbf{H}'_1 \ \middle|\ \cdots \ \middle|\ \mathbf{H}'_M\ \right] \tag{4.71}$$

4.3.2.1 Construction of the pilot matrix $\mathbf{S}_F$ at the transmitter

At the transmitter, a pilot matrix, $\mathbf{S}_F$ (for the fractional case) is initially constructed based on the Paley-Hadamard matrix of order v which is obtained according to the following criteria:

$$v \ > \ M \times (\varphi + 1) \tag{4.72}$$

where v must be divisible by 4 and (v-1) is prime. M is the number of transmit antenna and φ is the total span of the delay spread in terms of symbol period.

It is vital to note that the criterion in (4.72) is slightly different from the one in (4.35) and (4.53) for the symbol-spaced model where L is replaced by φ. Note that φ itself is already equivalent to (L+1). The extra '+1' term in (4.72) is needed to include an *additional row* of training sequences per transmit antenna in order to provide the essential format of the block-Toeplitz channel matrix $\bar{\mathbf{H}}'_m$ shown later in (4.77) and the formulation of $\bar{\mathbf{H}}'_{1|M}$ shown in (4.76).

Next, assuming that the total delay-spread, φ, is known *a priori* or predicted by the transmitter, $M \times (\varphi + 1)$ rows of consecutive non-repeated orthogonal sequences (except for the first row), are extracted from the generated v-ordered Paley-Hadamard matrix to form the required pilot matrix $\mathbf{S}_F$. For illustration, if $M = 2$ and $\varphi = 2$, then $M \times (\varphi + 1) = 6$. Therefore, the minimum order v that could satisfy condition (4.72) is $v = 8$ in this case. Subsequently, a (8×8) Paley-Hadamard matrix is first generated with 6 successive orthogonal row sequences from 2nd row to 7th row (except the 1st row) extracted to construct the 'required' (6×8) pilot matrix $\mathbf{S}_F$ with the uniform amplitude of '±s' shown as:

$$\mathbf{S}_F = \mathbf{A} + j\mathbf{B} \tag{4.73}$$

where

$$\mathbf{A} = \mathbf{B} = \left[\begin{array}{cccccccc} -s & +s & +s & -s & +s & -s & -s & +s \\ -s & -s & +s & +s & -s & +s & -s & +s \\ -s & -s & -s & +s & +s & -s & +s & +s \\ \hline +s & -s & -s & -s & +s & +s & -s & +s \\ -s & +s & -s & -s & -s & +s & +s & +s \\ +s & -s & +s & -s & -s & -s & +s & +s \end{array}\right] \begin{array}{l} \left.\begin{array}{c} \\ \\ \\ \end{array}\right\} \text{Tx1} \\ \left.\begin{array}{c} \\ \\ \\ \end{array}\right\} \text{Tx2} \end{array} \tag{4.74}$$

Note that the additional row sequence at the 'last row' is needed in each region according to (4.72) for the reason previously mentioned and will be explained later. Once $\mathbf{S}_F$ is constructed, the 'non-shaded pilot' symbols in (4.74) are then assigned to each transmit antenna and launched sequentially in the same manner described previously in the symbol spaced model. (Refer to Section 4.2.3.2 for the transmission of training sequence in Paley-Hadamard case).

4.3.2.2 Essential matrix expressions and format for fractionally-spaced MIMO-CE scheme

In order to perform the MIMO-CE for the fractional case, each fractional $x'(r-k)$ obtained in (4.69) has to be grouped appropriately at the receiver so that the received signal matrix $\mathbf{X}'$ contains the following necessary matrices (that is vital to allow the channel estimation to take place in a similar way described in symbol-spaced method in section 4.2) as:

$$\mathbf{X}' = \sqrt{\rho/M}\,\bar{\mathbf{H}}'_{1|M} \,.\, \mathbf{S}'_F + \mathbf{N}' \tag{4.75}$$

where $\mathbf{N}'$ is the AWGN matrix in fractional case. $\mathbf{S}'_F$ is the 're-constructed' pilot matrix at the receiver described in Section 4.3.2.4. $\bar{\mathbf{H}}'_{1|M}$ is the fractional version of the concatenated channel matrix that cascades all the associated 'block-Toeplitz' channel matrices from $\bar{\mathbf{H}}'_1$ to $\bar{\mathbf{H}}'_M$ as:

$$\bar{\mathbf{H}}'_{1|M} = \left[\ \bar{\mathbf{H}}'_1 \mid \cdots \mid \bar{\mathbf{H}}'_M\ \right] \tag{4.76}$$

where the individual $\bar{\mathbf{H}}'_m$ in (4.76) has dimension of $N(K_s+1)$ rows and $c\times\varphi+K_s$ columns and is constructed by the basic fractional channel matrix $\mathbf{H}'_m$ from (4.68) as:

$$\bar{\mathbf{H}}'_m = \begin{bmatrix} \mathbf{H}'_m & 0 \ldots & 0 \\ 0\ \mathbf{H}'_m & 0 \ldots & 0 \\ \vdots & \ddots & \vdots \\ 0 & \ldots 0 & \mathbf{H}'_m \end{bmatrix} \tag{4.77}$$

Note that respective 'block-Toeplitz' channel matrix, $\bar{\mathbf{H}}'_m$ in (4.77) contains both the basic fractional channel matrices $\mathbf{H}'_m$ in (4.68), and the appropriate entry of zeros as shown above, forming the vital structure of $\bar{\mathbf{H}}'_{1|M}$ that is essential for the development of the fractional channel estimation which will be explained in the next section.

4.3.2.3 The proper grouping of the received signal vector samples

Upon receiving each fractionally-sampled signal at the receiver, each received signal vector $\boldsymbol{x}'(r-k)$ in (4.69) is buffered and grouped into the 'required' received signal matrix $\mathbf{X}'$ (based on oversampling rate C), so that the necessary format of $\bar{\mathbf{H}}'_{1|M}$ in (4.76) and $\mathbf{S}'_F$ in (4.92) later in accordance to (4.75) can be acquired and restored accordingly with the following procedure:

First, received signal vectors $\boldsymbol{x}'(r-k)$ from the previous $(r-1)^{\text{th}}$ sample to the next $(r)^{\text{th}}$ sample are gathered to form the temporally matrix $\boldsymbol{Z}(r)$ as:

$$\boldsymbol{Z}(r) = \left[\boldsymbol{x}'(r) \quad \cdots \quad \boldsymbol{x}'\left(r - \frac{t}{C}\right) \quad \cdots \quad \boldsymbol{x}'(r-1) \right]; \quad 1 \le t \le C-1 \tag{4.78}$$

Note that $\boldsymbol{Z}(r)$ has matrix dimension of $(C+1)\times N$, which contains all the 'in-between' fractional received signal samples taken at $(r-t/C)$ where t is an integer taking values from 1 to $(C-1)$ and $C \ge 2$. Next, the *vec*(.) operator in (2.103) is used on $\boldsymbol{Z}(r)$ as:

$$\mathbf{z}(r) = vec(\boldsymbol{Z}(r)) \tag{4.79}$$

Subsequently, the required fractionally-spaced received signal matrix $\mathbf{X}'$ can be obtained by grouping the corresponding $\mathbf{z}(r)$ with $p = 1$ at different appropriate time instants as:

$$\mathbf{X}' = \left[\mathbf{z}(k) \quad \mathbf{z}(k+p) \quad \mathbf{z}(k+2p) \quad \cdots \quad \mathbf{z}(k+q) \quad \mathbf{r}(k+\varphi+q) \right] \tag{4.80}$$

where parameter q can be obtained from the value of matrix order v in (4.72) as follows:

$$q = v - 2 \tag{4.81}$$

4.3.2.4 Reconstruction of pilot matrix

In the symbol-spaced model, the reconstruction of the pilot matrix at the receiver is the same as the construction of the pilot matrix at the transmitter. Therefore, no distinction is made previously between them for the proposed MIMO-CE scheme in the symbol-spaced model. However, in the fractionally-spaced model, the reconstruction of pilot matrix at the receiver is different from the pilot matrix constructed at the transmitter, in order to take into consideration of the interaction between those pilot symbols and the fractionally-spaced delay paths that exist within the channel. The pilot matrix needs to be reconstructed carefully in the format shown in (4.82) so that it can be applied later to $\mathbf{X}'$ in (4.80), in order to carry out channel estimation in the fractionally-spaced frequency selective fading MIMO channel.

The reconstruction of pilot matrix, $\mathbf{S}'_F$ is carried out at the channel estimator such that each row of the original orthogonal sequence of pilot symbols in $\mathbf{S}_F$ (from the transmitter) is

duplicated according to the value of over-sampling, C, in the format expected by the receiver (using fractional samples of the pilot symbols) in order to cater for those fractionally-spaced delay paths that already exist within the period of φ in the fractionally-spaced delayed channel.

Mathematically, $\mathbf{S}_F$ can be expressed using a set of individual fractional concatenated transmit vectors $\vec{s}_{1|M}(r)$ cascaded at adjacent interval $p = 1$ with q obtained in (4.81) as:

$$\mathbf{S}'_F = \left[\vec{s}_{1|M}(r) \mid \vec{s}_{1|M}(r+p) \mid \vec{s}_{1|M}(r+2p) \mid \cdots \mid \vec{s}_{1|M}(r+q) \mid \vec{s}_{1|M}(r+\varphi+q) \right] \quad (4.82)$$

Using the *vec*(.) operator, the individual $\vec{s}_{1|M}(r)$ in (4.82) is equivalent to:

$$\vec{s}_{1|M}(r-k) = vec\left(\left[\vec{s}_1(r-k) \quad \cdots \quad \vec{s}_M(r-k) \right] \right) \quad (4.83)$$

where each $\vec{s}_m(r-k)$ in (4.83) is the extended version of the transmit vector in (4.70) with only minor difference by having additional φ samples, that can be expressed as:

$$\vec{s}_m(r-k) = \left[s_m\left(r-\frac{g}{C}\right) \; s_m\left(r-\frac{g+1}{C}\right) \; \cdots \; s_m\left(r-\frac{g+\varphi\times C-1+(\varphi)}{C}\right) \right]^{\mathsf{T}} \quad (4.84)$$

Recall that $s_m\left(r-(g+i)/C\right)$ are the duplicated samples of the same transmitted pilot symbol, $s_m(r-j)$, where $i = 0, 1, \ldots, \varphi \times C - 1 + \varphi$ and j is the integer part of $(g+i)/C$.

An example of pilot matrix reconstruction at the receiver (using previous case of $M = 2$ and $\varphi = 2$, hence, $M \times (\varphi+1) = 6$) with the oversampling rate of C=2 is shown in the following:

$$\mathbf{S}'_F = \mathbf{A}' + j\,\mathbf{B}' \quad (4.85)$$

where

$$\mathbf{A}' = \mathbf{B}' = \left[\begin{array}{cccccccc} -S & +S & +S & -S & +S & -S & -S & +S \\ -S & +S & +S & -S & +S & -S & -S & +S \\ -S & -S & +S & +S & -S & +S & -S & +S \\ -S & -S & +S & +S & -S & +S & -S & +S \\ -S & -S & -S & +S & +S & -S & +S & +S \\ -S & -S & -S & +S & +S & -S & +S & +S \\ \hline +S & -S & -S & -S & +S & +S & -S & +S \\ +S & -S & -S & -S & +S & +S & -S & +S \\ -S & +S & -S & -S & -S & +S & +S & +S \\ -S & +S & -S & -S & -S & +S & +S & +S \\ +S & -S & +S & -S & -S & -S & +S & +S \\ +S & -S & +S & -S & -S & -S & +S & +S \end{array}\right] \quad (4.86)$$

Since C=2, each row sequence in the original $\mathbf{S}_F$ in (4.73) is duplicated as shown above in the shaded parts, forming the reconstructed pilot matrix $\mathbf{S}'_F$ in (4.85) and (4.86). If C increases, the number of duplication for each row sequence is also increased with additional 'C–1' row.

Using same setting of $M = 2$ and $\varphi = 2$; if C increases to 3 (due to the needs of higher sampling), the matrices $\mathbf{A}'$ and $\mathbf{B}'$ in $\mathbf{S}'_F$ are reconstructed as follows:

$$\mathbf{A}' = \mathbf{B}' = \left[\begin{array}{cccccccc} -s & +s & +s & -s & +s & -s & -s & +s \\ -s & +s & +s & -s & +s & -s & -s & +s \\ -s & +s & +s & -s & +s & -s & -s & +s \end{array}\right] \left[\begin{array}{cccccccc} -s & -s & +s & +s & -s & +s & -s & +s \\ -s & -s & +s & +s & -s & +s & -s & +s \\ -s & -s & +s & +s & -s & +s & -s & +s \end{array}\right] \left[\begin{array}{cccccccc} -s & -s & -s & +s & +s & -s & +s & +s \\ -s & -s & -s & +s & +s & -s & +s & +s \\ -s & -s & -s & +s & +s & -s & +s & +s \end{array}\right] \left[\begin{array}{cccccccc} +s & -s & -s & -s & +s & +s & -s & +s \\ +s & -s & -s & -s & +s & +s & -s & +s \\ +s & -s & -s & -s & +s & +s & -s & +s \end{array}\right] \left[\begin{array}{cccccccc} -s & +s & -s & -s & -s & +s & +s & +s \\ -s & +s & -s & -s & -s & +s & +s & +s \\ -s & +s & -s & -s & -s & +s & +s & +s \end{array}\right] \left[\begin{array}{cccccccc} +s & -s & +s & -s & -s & -s & +s & +s \\ +s & -s & +s & -s & -s & -s & +s & +s \\ +s & -s & +s & -s & -s & -s & +s & +s \end{array}\right] \tag{4.87}$$

Each original row sequence in (4.87) is duplicated twice (since C–1 = 2) in the successive rows of $\mathbf{S}'_F$, instead of just once in (4.86). Hence, the receiver only needs to decide the value of C based on the characteristic of the multipath channel for the purpose of channel estimation.

4.3.2.5 Obtaining the channel estimate in fractionally-spaced model

Once $\mathbf{X}'$ in (4.80) and $\mathbf{S}'_F$ in (4.82) have been obtained, the proposed fractional MIMO-CE scheme can be carried out accordingly with the following procedures:

First, the partial estimated channel matrix $\mathbf{J}$ is obtained by applying the Hermitian of reconstructed channel matrix, $\mathbf{S}'_F$ to the 'required' received signal matrix, $\mathbf{X}'$ as follows:

$$\mathbf{J} = f\left\{\mathbf{X}' \cdot \mathbf{S}'^{\mathsf{H}}_F\right\} = f\left\{\left(\bar{\mathbf{H}}'_{1|M} \cdot \underbrace{\mathbf{S}'_F}\right)\mathbf{S}'^{\mathsf{H}}_F\right\} \tag{4.88}$$

where f is the correction factor with the following value:

$$f = \frac{1}{2v}\sqrt{M/\rho} \tag{4.89}$$

The partial estimated channel matrix **J** obtained (4.88) is the crucial step to partially unwrap the information of the fractional delay-paths 'once for all', shown by the inherent product of $\mathbf{S}'_F$ and its Hermitian, producing a so-called weighted block-identity matrix $\breve{\mathbf{I}}$ with the unique structure, illustrated in the following:

$$\mathbf{S}'_F . \mathbf{S}'^{\mathsf{H}}_F = 2v\,\breve{\mathbf{I}} \tag{4.90}$$

$$\text{where} \quad \breve{\mathbf{I}} = \begin{bmatrix} \mathbf{A} & \mathbf{0} & \cdots & \mathbf{0} \\ \mathbf{0} & \mathbf{A} & \mathbf{0} & \vdots \\ \vdots & \mathbf{0} & \ddots & \mathbf{0} \\ \mathbf{0} & \cdots & \mathbf{0} & \mathbf{A} \end{bmatrix} \quad \text{and} \quad \mathbf{A} = \begin{bmatrix} 1 & \cdots & 1 \\ \vdots & \ddots & \vdots \\ 1 & \cdots & 1 \end{bmatrix} \quad \text{and} \quad \mathbf{0} = \begin{bmatrix} 0 & \cdots & 0 \\ \vdots & \ddots & \vdots \\ 0 & \cdots & 0 \end{bmatrix} \tag{4.91}$$

A is the ($C\times C$) all-ones square matrix that is diagonally placed along with the ($C\times C$) all-zeros square matrix, **0**, in $\breve{\mathbf{I}}$. Again, v is the PH's matrix order known *a priori* at the receiver. The size of $\breve{\mathbf{I}}$ depends on the value of $M\times(\varphi+1)$ and C. For instance, if $M\times(\varphi+1)=4$ and $C=2$, $\breve{\mathbf{I}}$ contains 4 sets of **A**, each has matrix size of (2×2). Similarly, if $M\times(\varphi+1)$ increases to 6 and C increases to 3, $\breve{\mathbf{I}}$ contains 6 sets of **A**, each has matrix size of (3×3). The structure in $\breve{\mathbf{I}}$ is uniquely planned to contain appropriate all-zero matrices, **0**, so that it can be used effectively in conjunction with $\bar{\mathbf{H}}'_{1|M}$. (Recall also the block Toeplitz structure of $\bar{\mathbf{H}}'_{1|M}$ in (4.76), which also consists of zero matrices **0**). Therefore, substituting (4.90) into (4.88) leads to the following:

$$\mathbf{J} = f\left\{ \bar{\mathbf{H}}'_{1|M} . 2v . \breve{\mathbf{I}} \right\} \tag{4.92}$$

Next, it can be seen in (4.92) that **J** comprises of $\breve{\mathbf{I}}$ and $\bar{\mathbf{H}}'_{1|M}$ that ultimately containing all the information of the basic fractional channel matrix, $\mathbf{H}'_m$. However, since $\breve{\mathbf{I}}$ is non-invertible, the channel estimates cannot be obtained directly by matrix inversion. Providentially, both $\bar{\mathbf{H}}'_{1|M}$ and $\breve{\mathbf{I}}$ have a unique matrix structure that contains necessary zeros shown in (4.77) and (4.91) respectively, allowing each individual $\mathbf{H}'_m$ contained in $\bar{\mathbf{H}}'_{1|M}$ to be conveniently extracted through a linear arithmetic operation. This is illustrated using an example with φ=2, $M\times(\varphi+1)$=3 and C=2 for a (2×2) system. The basic fractional channel matrices are shown as:

$$\mathbf{H}'_1 = \begin{bmatrix} \mathbf{h}'_{11} \\ \mathbf{h}'_{21} \end{bmatrix} = \begin{bmatrix} a & c & e & g \\ b & d & f & h \end{bmatrix} \quad \text{and} \quad \mathbf{H}'_2 = \begin{bmatrix} \mathbf{h}'_{12} \\ \mathbf{h}'_{22} \end{bmatrix} = \begin{bmatrix} i & k & m & o \\ j & l & n & p \end{bmatrix} \tag{4.93}$$

Assuming that the correct Hermitian of the reconstructed pilot matrix, $\mathbf{S}'^{\mathsf{H}}_F$ has been applied to the corresponding $\mathbf{X}'$ according to (4.88), leading to the following expressions as:

$$\mathbf{J} = \bar{\mathbf{H}}'_{1|2}.\breve{\mathbf{I}} = \begin{bmatrix} \bar{\mathbf{H}}'_1 & \bar{\mathbf{H}}'_2 \end{bmatrix} \begin{bmatrix} \breve{\mathbf{I}}_1 & \breve{\mathbf{I}}_2 \\ \breve{\mathbf{I}}_3 & \breve{\mathbf{I}}_4 \end{bmatrix} \tag{4.94}$$

$$= \begin{bmatrix} \mathbf{J}_1 & \mathbf{J}_2 \end{bmatrix} = \begin{bmatrix} \bar{\mathbf{H}}'_1 \breve{\mathbf{I}}_1 + \bar{\mathbf{H}}'_2 \breve{\mathbf{I}}_3 & \bar{\mathbf{H}}'_1 \breve{\mathbf{I}}_2 + \bar{\mathbf{H}}'_2 \breve{\mathbf{I}}_4 \end{bmatrix} \tag{4.95}$$

where

$$\breve{\mathbf{I}} = \begin{bmatrix} \breve{\mathbf{I}}_1 & \breve{\mathbf{I}}_2 \\ \breve{\mathbf{I}}_3 & \breve{\mathbf{I}}_4 \end{bmatrix} = \left[\begin{array}{ccc:ccc} \mathbf{A} & \mathbf{0} & \mathbf{0} & \mathbf{0} & \mathbf{0} & \mathbf{0} \\ \mathbf{0} & \mathbf{A} & \mathbf{0} & \mathbf{0} & \mathbf{0} & \mathbf{0} \\ \mathbf{0} & \mathbf{0} & \mathbf{A} & \mathbf{0} & \mathbf{0} & \mathbf{0} \\ \hdashline \mathbf{0} & \mathbf{0} & \mathbf{0} & \mathbf{A} & \mathbf{0} & \mathbf{0} \\ \mathbf{0} & \mathbf{0} & \mathbf{0} & \mathbf{0} & \mathbf{A} & \mathbf{0} \\ \mathbf{0} & \mathbf{0} & \mathbf{0} & \mathbf{0} & \mathbf{0} & \mathbf{A} \end{array}\right] ; \quad \mathbf{A} = \begin{bmatrix} 1 & 1 \\ 1 & 1 \end{bmatrix} \quad \mathbf{0} = \begin{bmatrix} 0 & 0 \\ 0 & 0 \end{bmatrix} \tag{4.96}$$

For simplicity, factor f and $2v$ are omitted. Note that $\breve{\mathbf{I}}$ is divided into 4 quadrants where quadrants $\breve{\mathbf{I}}_2$ and $\breve{\mathbf{I}}_3$ contains only the zeros matrix and quadrants $\breve{\mathbf{I}}_1$ and $\breve{\mathbf{I}}_4$ contains matrix **A**. Since $\breve{\mathbf{I}}_2 = \breve{\mathbf{I}}_3 = 0$, ultimately, $\mathbf{J} = \begin{bmatrix} \bar{\mathbf{H}}'_1 \breve{\mathbf{I}}_1 & \bar{\mathbf{H}}'_2 \breve{\mathbf{I}}_4 \end{bmatrix}$, which can be individually expressed as:

$$\mathbf{J}_1 = \bar{\mathbf{H}}'_1.\breve{\mathbf{I}}_1 = \begin{bmatrix} a & c & e & g & 0 & 0 \\ b & d & f & h & 0 & 0 \\ 0 & a & c & e & g & 0 \\ 0 & b & d & f & h & 0 \\ 0 & 0 & a & c & e & g \\ 0 & 0 & b & d & f & h \end{bmatrix} \begin{bmatrix} 1 & 1 & 0 & 0 & 0 & 0 \\ 1 & 1 & 0 & 0 & 0 & 0 \\ 0 & 0 & 1 & 1 & 0 & 0 \\ 0 & 0 & 1 & 1 & 0 & 0 \\ 0 & 0 & 0 & 0 & 1 & 1 \\ 0 & 0 & 0 & 0 & 1 & 1 \end{bmatrix} \tag{4.97}$$

$$\mathbf{J}_2 = \bar{\mathbf{H}}'_2.\breve{\mathbf{I}}_4 = \begin{bmatrix} i & k & m & o & 0 & 0 \\ j & l & n & p & 0 & 0 \\ 0 & i & k & m & o & 0 \\ 0 & j & l & n & p & 0 \\ 0 & 0 & i & k & m & o \\ 0 & 0 & j & l & n & p \end{bmatrix} \begin{bmatrix} 1 & 1 & 0 & 0 & 0 & 0 \\ 1 & 1 & 0 & 0 & 0 & 0 \\ 0 & 0 & 1 & 1 & 0 & 0 \\ 0 & 0 & 1 & 1 & 0 & 0 \\ 0 & 0 & 0 & 0 & 1 & 1 \\ 0 & 0 & 0 & 0 & 1 & 1 \end{bmatrix} \tag{4.98}$$

Consequently, the expansion of $\mathbf{J}_1$ and $\mathbf{J}_2$ and its linear algebra operation and resultant can be conveniently solved in either ascending or descending order of the alphabets as:

$$\mathbf{J}_1 = \begin{array}{c} \text{Ascending process} \\ \uparrow \\ \left[\begin{array}{cccccc} a+c & a+c & e+g & e+g & 0 & 0 \\ b+d & b+d & f+h & f+h & 0 & 0 \\ a & a & c+e & c+e & g & g \\ b & b & d+f & d+f & h & h \\ 0 & 0 & a+c & a+c & e+g & e+g \\ 0 & 0 & b+d & b+d & f+h & f+h \end{array}\right] \\ \downarrow \\ \text{Descending process} \end{array} \tag{4.99}$$

$$\mathbf{J}_2 = \begin{array}{c} \text{Ascending process} \\ \left[\begin{array}{cccccc} i+k & i+k & m+o & m+o & 0 & 0 \\ j+l & j+l & n+p & n+p & 0 & 0 \\ i & i & k+m & k+m & o & o \\ j & j & l+n & l+n & p & p \\ 0 & 0 & i+k & i+k & m+o & m+o \\ 0 & 0 & j+l & j+l & n+p & n+p \end{array}\right] \\ \text{Descending process} \end{array} \tag{4.100}$$

Our aim is to estimate all the fading coefficients from '*a*' to '*p*' in each basic fractional channel matrix, $\mathbf{H}'_m$. Once all the coefficients have been estimated, the estimated basic fractional channel matrix, $\hat{\mathbf{H}}'_m$ for $m = 1$ to M, can be cascaded as follows:

$$\hat{\mathbf{H}}'_{1|M} = \left[\, \hat{\mathbf{H}}'_1 \,\middle|\, \cdots \,\middle|\, \hat{\mathbf{H}}'_M \,\right] \tag{4.101}$$

This information will be used by the OSIC receiver for MIMO-equalisation process.

4.3.2.6 Summary of Fractional MIMO Channel Estimation Scheme

Assuming the following are known a priori:
(i) The total span of the delay spread, φ, in terms of symbol periods within each CIR and
(ii) The over-sampling rate, C, required to model the fractional delay paths.

<u>At transmitter:</u>

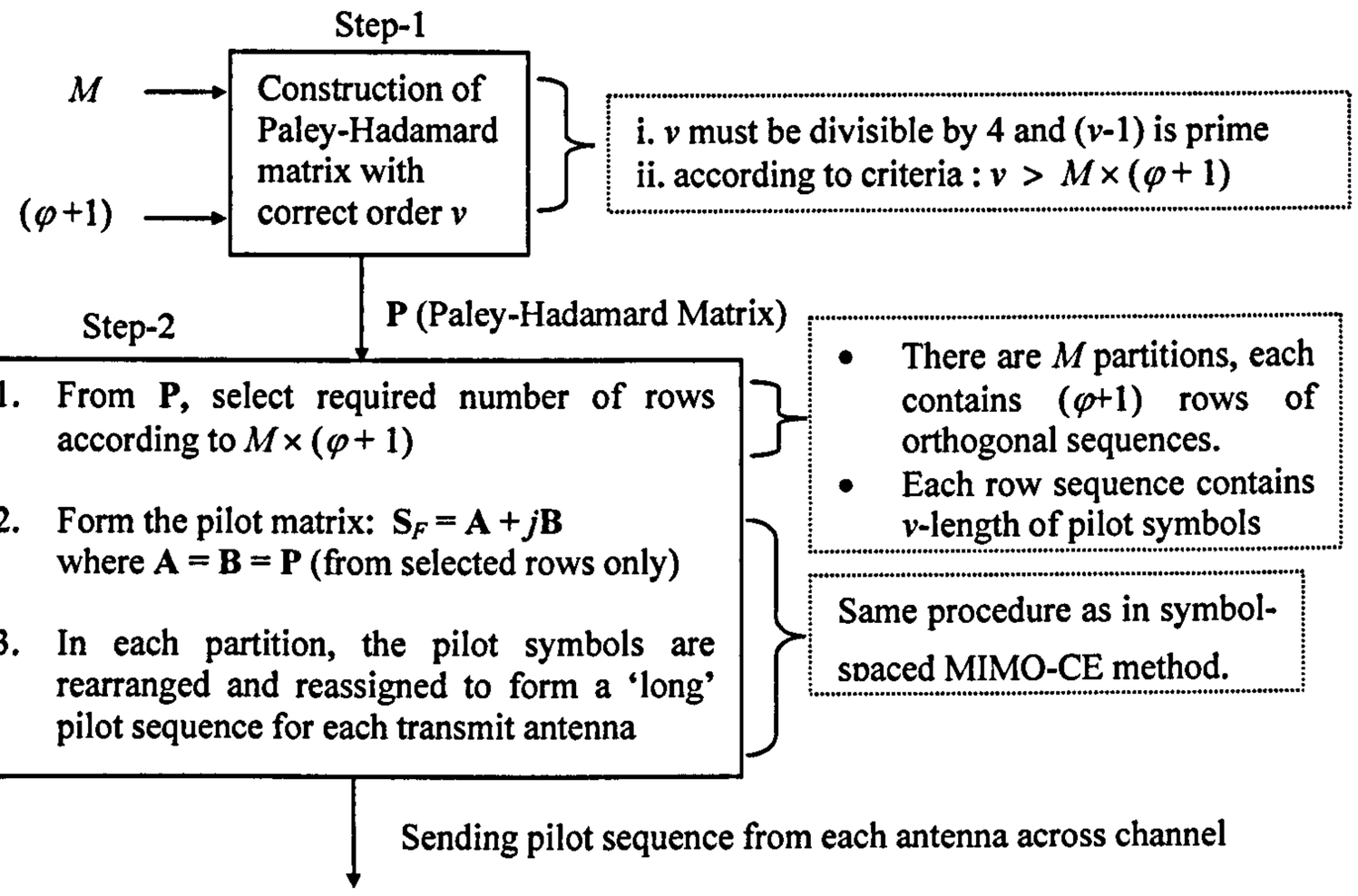

Note: A 'long' pilot sequence contains a series of pilot symbols.

Each transmit antenna sends an appointed pilot sequence for channel training purpose.

At receiver:

1) Over-sampling mechanism with rate C is used to receive fractionally-spaced received samples expressed in signal vector $x'(r\text{-}k)$; where r = symbol instant and k = fractional instant.
2) First, these fractional samples are grouped with respect to each symbol period as $Z(r)$, $Z(r+1)$, ..., $Z(r+p)$, where each $Z(r+p)$ can be generally expressed as:

$$Z(r+p) = \left[\mathbf{x}'(r+p) \quad \cdots \quad \mathbf{x}'\left(r+p-\frac{t}{C}\right) \quad \cdots \quad \mathbf{x}'(r+p-1) \right]; \quad 1 \le t \le C\text{-}1$$

3) To facilitate the next formulation, each $Z(r+p)$ is then vectorised using *vec*(.) operator as:

$$\mathbf{z}(r+p) \;=\; vec\left(Z(r+p)\right) \;=\; \begin{bmatrix} \mathbf{x}'(r+p) \\ \vdots \\ \mathbf{x}'\left(r+p-\frac{t}{C}\right) \\ \vdots \\ \mathbf{x}'(r+p-1) \end{bmatrix}$$

4) Subsequently, the appropriate $\mathbf{z}(r+p)$ vectors are further grouped to form the received signal matrix $\mathbf{X}'$ as follows:

$$\mathbf{X}' \;=\; \left[\mathbf{z}(r) \quad \mathbf{z}(r+1) \quad \mathbf{z}(r+2) \quad \cdots \quad \mathbf{z}(r+q) \quad \mathbf{z}(r+\varphi+q) \right]$$

where parameter q can be obtained as: $q = v - 2$.

5) Simultaneously, reconstruction of pilot matrix $\mathbf{S'}_F$ is carried out at the receiver given the prior knowledge of the transmitted $\mathbf{S}_F$ and value of C. This is accomplished by duplicating each row sequence of the original $\mathbf{S}_F$ in a successive manner according to the value of C. (Refer to section.4.3.2.4).

Block diagram of fractionally-spaced MIMO-CE scheme at the receiver:

4.4 Channel Tracking in Time-Varying Mode

The novel MIMO channel estimator presented (for both the symbol-spaced model as well as the fractionally-spaced model) in the previous sections assumes that the channel remains constant during the period over which the pilot matrix (or training sequence) is received, which is characterised as the block-invariant time-varying MIMO channel. In a time-varying channel, however, the MIMO channel will be varying continuously with time, dependent on the Doppler velocity. This might affect the accuracy of the channel estimation process during reception of the pilot sequence, i.e. during the "training" periods, and subsequently the performance of the MIMO OSIC equalisation process during the "data delivery" periods. (The later process is more significantly affected). The reason will be pointed as follows:

During the 'training' period, the channel might have changed from the reception of first pilot symbol to the last pilot symbol since the non-adaptive method required to buffer all the necessary received signals (that are related to all the transmitted pilot symbols) before carrying out the actual estimation process. Fortunately, the variation of the channel within this training period is so minor that it can be regarded as insignificant since the number of pilot symbols required by the proposed method is normally at minimal, (though the size of the pilot matrix can be increased to improve the channel estimation accuracy). Nevertheless, the accuracy of channel estimation also depends on the length of the training sequence that is sent in a way that if the training sequence is too short, it might not reach the 'best' performance of the estimator, but if it is too long, accuracy of estimation might drop since the estimator might not be able to cope efficiently with the larger variation of the channel.

During the 'data-delivery' period, the channel estimate obtained (through the 'training') is used for the MIMO equalisation process. However, the actual channel might have changed from the beginning of data to the end of the data received for that frame, depending on how long the entire data frame might be. This variation of channel is more significant as the data frame is usually about 90% longer than the total length of the training sequence. Therefore, the channel estimate that is used for the MIMO equalisation process might only be valid for the start but becomes erroneous at the end (due to the deviation from the actual channel), which might results in incorrect data detection, thereby affecting the performance of the MIMO equalisation process.

It is possible, however, to utilise the available data recovery information to perform channel tracking using a decision feedback algorithm during data delivery periods, since the received data is the only available information. The entire data frame can be divided into smaller blocks of transmitted data denoted as $\mathbf{D}_k$ and the corresponding received data matrix $\mathbf{R}(k)$ at time-block k can be related to $\mathbf{D}_k$ as follows:

$$\mathbf{R}(k) \quad = \quad \mathbf{H}_{1|\mathrm{M}}(k)\ \mathbf{D}_k + \mathbf{N}(k) \tag{4.102}$$

where $\mathbf{H}_{1|\mathrm{M}}(k)$ is the concatenated MIMO channel matrix as expressed in (4.24) with the inclusion of time-block k and $\mathbf{N}(k)$ is the respective AWGN noise matrix. For simplicity, the $\mathbf{H}_{1|\mathrm{M}}(k)$ of the symbol-spaced model is used here to illustrate the channel tracking, although the concatenated channel matrix $\mathbf{H}_{1|\mathrm{M}}(k)$ can be extended to the fractionally-spaced model with the alteration in its corresponding $\mathbf{R}(k)$ and data-block $\mathbf{D}_k$. Note that the format in (4.102) is similar to the expression in (4.32), whereby time-block k is incorporated to show the time-varying characteristic model. Meantime, $\mathbf{D}_k$ has the similar format as $\mathbf{S}_F$ and $\mathbf{R}(k)$ has the similar format as $\mathbf{X}$. Instead of having matrix size of $M(L+1)\times v$, each data-block $\mathbf{D}_k$ has matrix size of $M(L+1)\times T$ where $T \geq v$ that is set to suitable size in order to allow effective channel tracking process to take place. Also, there are B numbers of data-blocks $\mathbf{D}_k$ in the entire frame. The basic data structure is shown in the following figure:

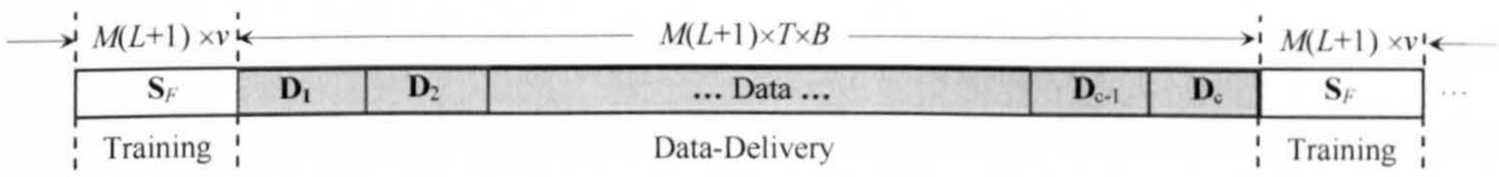

Figure 4.15: Data structure for i) channel training & ii) data delivery

The overview of channel estimation and channel tracking process for a time-varying channel can be illustrated in the following figure:

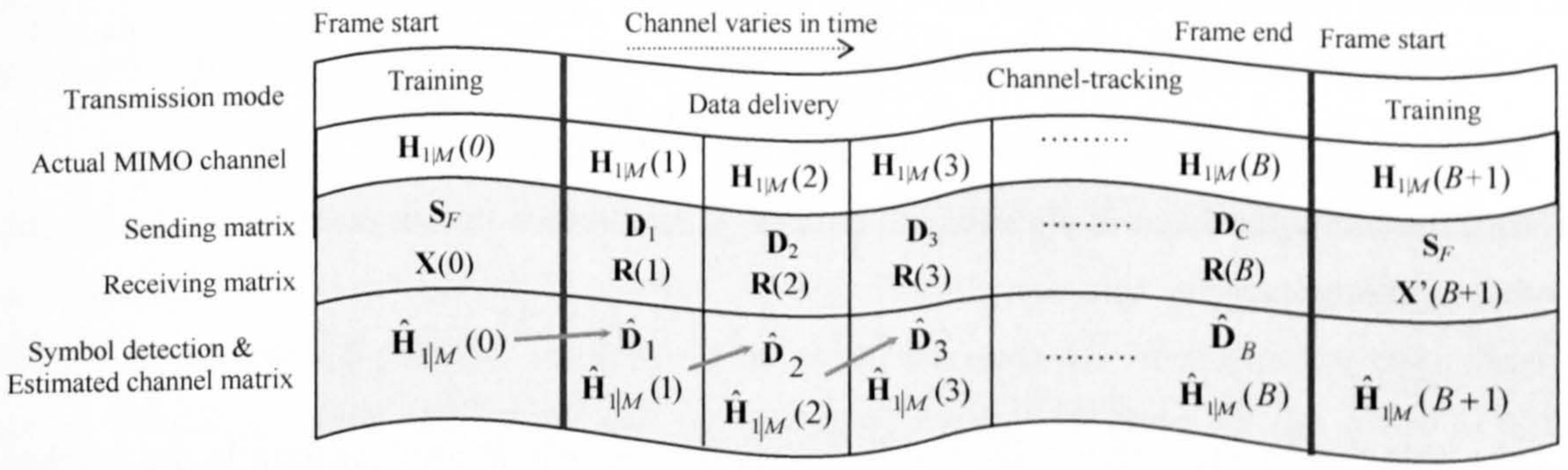

Figure 4.16: Overview of MIMO channel estimation and channel tracking process.

There are two transmission modes as mentioned earlier, the 'training' and the 'data-delivery', with the respective actual MIMO channel $\mathbf{H}_{1|\mathrm{M}}(k)$ presented from the start of the data frame to the end of the data frame. Note that the actual MIMO channel matrix $\mathbf{H}_{1|\mathrm{M}}(k)$ are categorized by time-block k that corresponds to the pilot matrix $\mathbf{S}_F$ and the respective data-block $\mathbf{D}_k$ to characterize time-varying scenario where $k = 1$ to B during the data delivery period. During the training period, a pilot matrix $\mathbf{S}_F$ is transmitted to obtain an initial estimate of the MIMO

channel $\hat{\mathbf{H}}_{1|M}(0)$ from the corresponding $\mathbf{X}(0)$. This channel estimate is normally used in the subsequent data delivery period for the data detection in the MIMO equalization process, which has been described in Chapter 2.

For each received data matrix $\mathbf{R}(k)$, the previous channel estimate $\hat{\mathbf{H}}_{1|M}(k-1)$ is used for the data detection process to give the current detected data matrix, $\hat{\mathbf{D}}_k$ (shown by the arrows in figure). Hence it is important to realize the individual block of channel estimate $\hat{\mathbf{H}}_{1|M}(k-1)$, since the initial channel estimate $\hat{\mathbf{H}}_{1|M}(0)$ might no longer represent the valid estimate of $\hat{\mathbf{H}}_{1|M}(k-1)$ later in time as the MIMO channel continues to vary. The following channel tracking process allows the individual block of channel estimate $\hat{\mathbf{H}}_{1|M}(k)$ to be tracked so that the data can be detected based on the latest 'estimated' or tracked channel instead of the initial channel estimate $\hat{\mathbf{H}}_{1|M}(0)$.

Because of the individual 'detected' data-block is applied to perform the channel tracking, it is also referred as the decision feedback channel tracking process. In the decision feedback tracking process, the received data matrix $\mathbf{R}(k)$ and the detected data matrix, $\hat{\mathbf{D}}_k$ of each time-block k are then employed to generate a new channel estimate, $\hat{\mathbf{H}}_{1|M}(k)$, as follows:

First the partial channel estimate, $\mathbf{F}_k$ is obtained by applying the Hermitian of the current detected data matrix, $\hat{\mathbf{D}}_k^{\mathsf{H}}$, to the corresponding received data matrix, $\mathbf{R}(k)$ as follows:

$$\begin{aligned} \mathbf{F}_k &= \mathbf{R}(k)\,\hat{\mathbf{D}}_k^{\mathsf{H}} \\ &= \left[\mathbf{H}_{1|M}(k)\;\; \mathbf{D}_k\right]\hat{\mathbf{D}}_k^{\mathsf{H}} \;+\; \mathbf{N}\hat{\mathbf{D}}_k^{\mathsf{H}} \end{aligned} \tag{4.103}$$

Next, the individual current channel estimate $\hat{\mathbf{H}}_{1|M}(k)$ can then be obtained as:

$$\hat{\mathbf{H}}_{1|M}(k) = \mathbf{F}_k\left[\hat{\mathbf{D}}_k\hat{\mathbf{D}}_k^{\mathsf{H}}\right]^{-1} \tag{4.104}$$

Take note that by multiplying $\hat{\mathbf{D}}_k$ and $\hat{\mathbf{D}}_k^{\mathsf{H}}$ together, the whole product term in the bracket of (4.104) can be reduced to a $M(L+1) \times M(L+1)$ square matrix that is suitable for the matrix inversion process shown in (4.104). It is important to note that the product of $\hat{\mathbf{D}}_k\hat{\mathbf{D}}_k^{\mathsf{H}}$ must be non-singular in order for the matrix inversion to be successfully obtained. One might extend the dimension of $\hat{\mathbf{D}}_k$ by adjusting the value of T as shown in figure 4.15 in order to avoid the problem of singularity. A pre-check for ill-conditioning of $\hat{\mathbf{D}}_k\hat{\mathbf{D}}_k^{\mathsf{H}}$ can be performed to ensure that this term is always invertible.

4.5 Summary

In Chapter 4, the novel training-based MIMO channel estimation scheme that makes use of pilot matrix concept has been presented and successfully implemented in the MIMO-OSIC-DFE receivers described in Chapter 2. The development of the proposed channel estimator from the frequency-flat model to the frequency-selective model has been discussed with thorough consideration of the corresponding co-channel interference and inter-symbol interference problem in the frequency-selective channel. The concept and usefulness of utilising orthogonal pilot sequences extracted from the Hadamard matrix in order to obtain the channel estimation as well as counteracting both CCI and ISI effects simultaneously have also been presented. The design of pilot sequences and the construction of the pilot matrix have also been illustrated with different parameter and system configurations.

Comparison of using either the ordinary Hadamard matrix or the Paley-Hadamard matrix to construct the pilot matrix has also been demonstrated. It has been found that minimisation in pilot length could be achieved by using the Paley-Hadamard matrix instead of the ordinary one with no loss in its initial estimator's performance. The Paley-Hadamard matrix is found to have unique combination in its orthogonal and Toeplitz-like structure, which could shorten the unnecessary time-gaps, introduced by the ordinary Hadamard matrix, while effectively performing the estimation process and resolving the frequency-selective effects simultaneously. As a result, shorter training sequence of minimum pilot symbols was required by each transmit antenna to provide necessary channel estimate for the MIMO systems, which in effect also to allow higher data throughput. Channel tracking method has also been presented to further assist the channel estimation process by recursive update of the variation in channel due to the Doppler velocity.

Extension of the novel MIMO-CE scheme from the symbol-spaced model to the fractionally-spaced model has also been presented to consider the arriving paths with delay that could occur within a fraction of symbol period. The design and implementation of the novel fractional MIMO-CE scheme have also been demonstrated. The performance evaluation of the novel MIMO channel estimators and its impact of estimation error on the MIMO-OSIC-DFE receivers will be shown in the next chapter.

Chapter 5

Results and Performance Evaluation

In this chapter, results are mainly presented in two categories: i) the system performance of the various layered space-time receivers in Chapter-2 (i.e. V-BLAST, MIMO-OSIC receiver) for different system configuration and ii) the performance of the proposed MIMO-CE schemes in Chapter-3 & 4. Both symbol-spaced and fractionally-spaced models are considered. These results are systematically evaluated for the performances under the influence of both the frequency-flat fading as well as frequency-selective fading channel by means of detailed computer simulation in Matlab. For consistency, the ***QPSK** modulation scheme* is employed throughout this chapter for all performance results and discussion.

In the simulation, no particular actual physical channel is being employed but instead the channel model in this work assumes worst-case fading scenario where non line-of-sight Rayleigh condition is assumed for each path coefficient. This applies to both flat-fading and frequency-selective MIMO channels with respective models shown in Appendix-C. (Its physical scattering characteristics are also described in section 2.2.2). Uncorrelated path and uniform delay are also assumed between each path for both the symbol-spaced & fractionally-spaced models in frequency-selective MIMO channel (Refers to Chapter 4). Time-varying characteristic is also considered for each path, which will be described in respective sections.

5.1 Performance Evaluation of the Layered Space-Time Receiver in Frequency-Flat Fading MIMO Channel

In the following, the basic V-BLAST receiver (described in Chapter 2) with different ($N\times M$) MIMO configurations will be initially assessed for its system performance under the flat fading channel condition. (Recall that M denotes the number for transmit antennas and N denote the number of receive antennas used). Each sub-channel from each transmit-receive antenna pair consists of a single path that is represented by a complex coefficient. The system performance of the V-BLAST receiver will be evaluated using four means of symbol-

detection algorithms as: a) the linear zero-forcing (ZF) algorithm, b) the linear minimum mean square error (MMSE) algorithm, c) the nonlinear ZF algorithm and d) the nonlinear MMSE algorithm. The results are plotted using the performance metric as the bit error probability (*Pe*) against the mean signal-to-noise ratio (SNR) value for different ($N \times M$) configurations. The mean SNR is the overall average of all the SNR values measured at each receive antenna. *Perfect channel knowledge at the receiver is assumed here*.

Before results are presented for the general MIMO case, perhaps it is useful examine the basic spatial diversity scheme from a single-input multiple-output (SIMO) model where single transmit antenna and multiple receive antennas are used. The linear ZF algorithm is used with the setting of $M = 1$ and $N = 1, 2$ & 4 respectively to demonstrate the performance achieved by the reception diversity. (The diversity gain or order is defined as N/M).

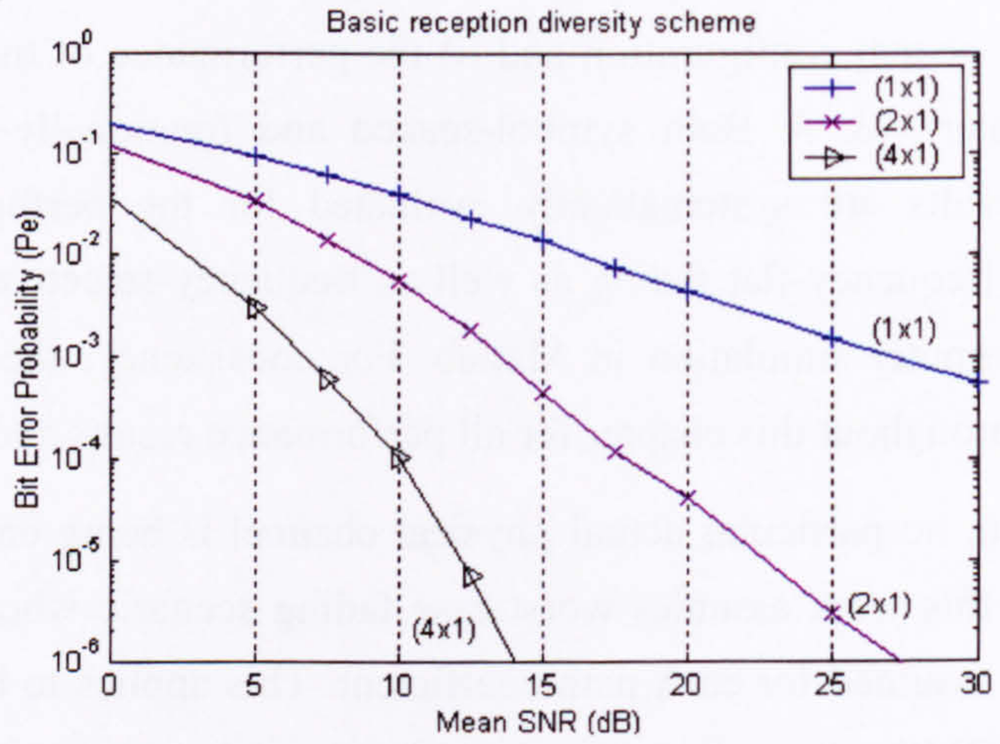

Figure 5.1.1: Performance of diversity scheme using linear ZF algorithm in a SIMO system

Figure 5.1.1 demonstrates the performance of the basic diversity scheme for a SIMO system. The results demonstrate that reception diversity does improve the overall performance of the wireless system. This is similar to the equal-gain combining method used in the antenna arrays technique where same results are exhibited. [18-19].

Next, the performance of MIMO system is assessed over a flat-fading ***Rayleigh*** channel where multiple transmit-receive antennas are used. First, equal number of receive antennas N and transmit antennas M is employed with no diversity gain since $N = M$. The immediate question from this test is that can we achieve better bit error probability performance while achieving increased data rate simultaneously. It can be observed in figure 5.1.2 that, the performance of the MIMO system with no diversity gain becomes deteriorated in a flat-fading MIMO channel condition as M and N increase simultaneously. Although, the data rate has been improved by M-fold, having multiple links with no diversity will not be beneficial in this case or even worsen the system performance when the linear ZF detection algorithm is used.

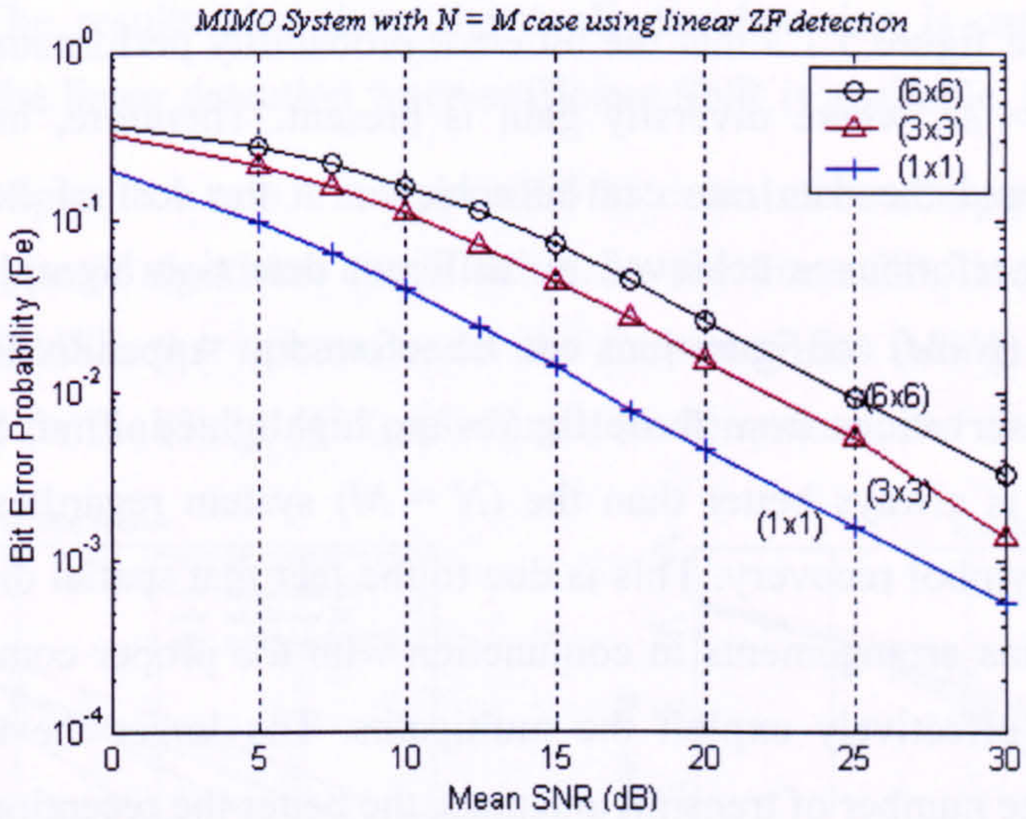

Figure 5.1.2: Performance of $N = M$ system with linear ZF algorithm

This makes sense because the performance of the (1×1) system has already reached the state of "as good as it gets" under typical Rayleigh condition. Having more links with no diversity (in linear ZF detection) simply means further deterioration in the overall channel condition thereby worsening the system performance. Also, each antenna in the MIMO case is now transmitting power in reduced proportion of $1/M$ in order to maintain the same transmitting power as in the single antenna case of SISO system. The degradation in performance is expected when the ZF algorithm is used. This is mainly due to the noise enhancement during the matrix inversion, which worsens the system performance of the MIMO system as the matrix's size grows when M and N increases simultaneously. [10, 11]. However, when added diversity order is presented in the MIMO systems (where $N > M$ case), the system performance can be improved accordingly as shown in the following figure.

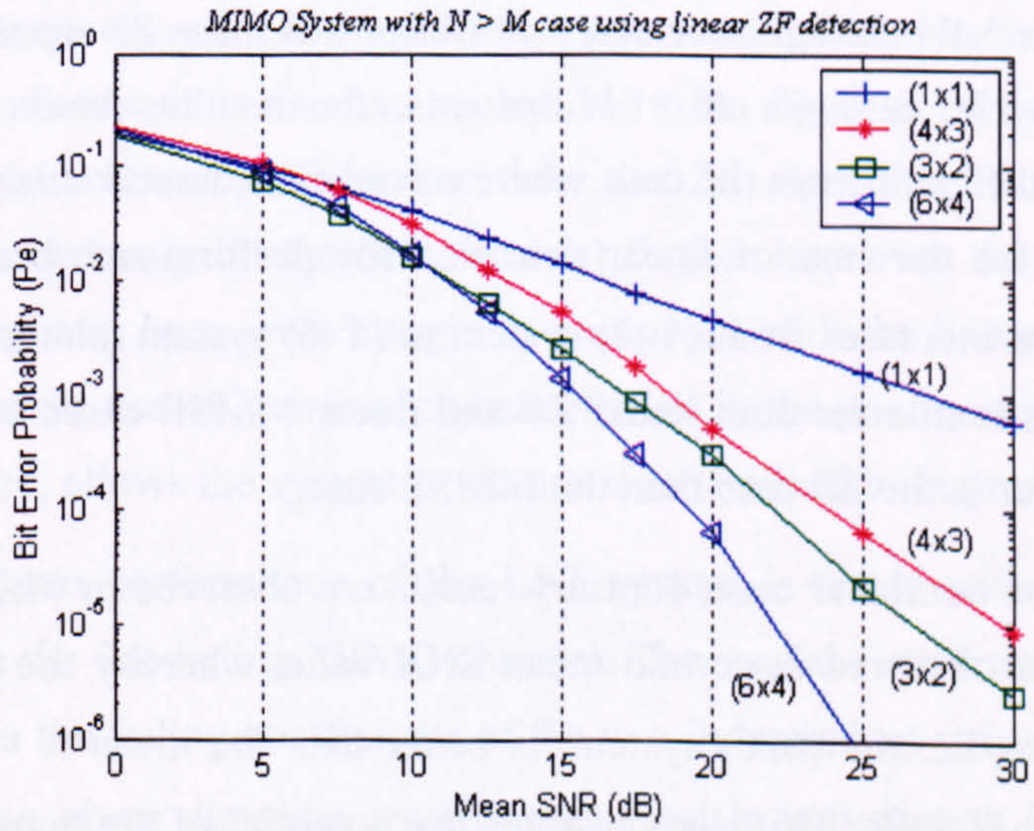

Figure 5.1.3: Performance of $N > M$ system with linear ZF algorithm

It can be seen in figure 5.1.3 that the bit error probability performance is improved for any system with $N > M$, where diversity gain is present. Therefore, improvement in the system performance and the data rate can be achieved at the cost of extra hardware. The results showing the performance achieved by different detection algorithms in the MIMO systems for different ($N \times M$) configurations can be referred at Appendix-B1 for extra results section. Important observations from those figures are highlighted. First, the performance of the ($N > M$) system is always better than the ($N = M$) system regardless of the detection algorithms used for symbol recovery. This is due to the fact that spatial diversity is achieved by the multiple antenna arrangements in conjunction with the proper combiner by means of weighting matrix to effectively exploit the multipaths. The larger the number of receive antennas relative to the number of transmit antennas, the better the reception diversity.

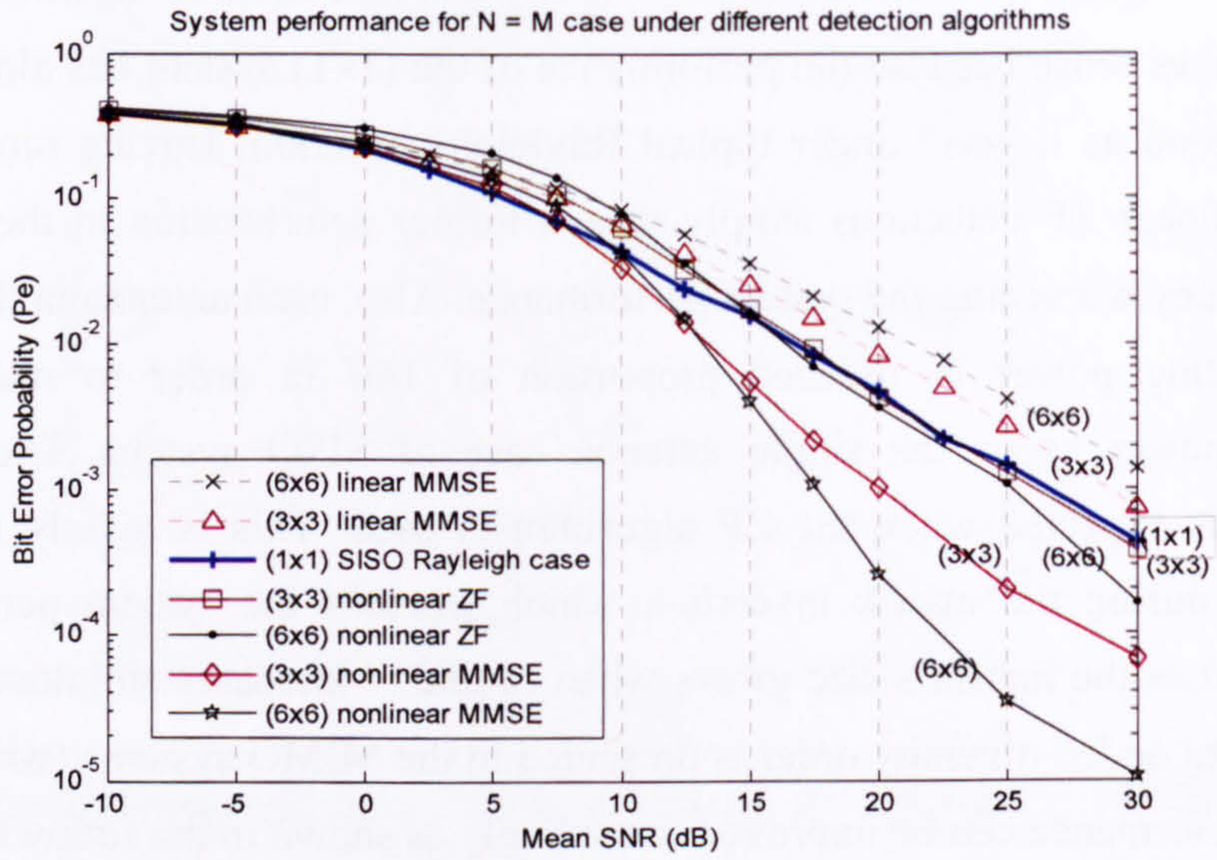

Figure 5.1.4: Performance of $N > M$ system with linear ZF algorithm

Next, back to the case for $N = M$ systems, the results obtained using the linear detections are quite different from the case where a nonlinear detection is used. It can be seen in figure 5.1.4 that for the case of linear detection the performance become poorer as the antenna configuration increases from (1×1) system to (6×6) system (similar to the earlier case in figure 5.1.2.) This is true for both linear ZF and linear MMSE cases but the distinction in performance is greater in the ZF case than the MMSE case.

However, in the nonlinear case, contrary results are observed in which a 'switch' in the performance curve is observed at certain mean SNR value whereby the performance of the higher $N = M$ system, i.e. the (6×6) system, is better than the lower $N = M$ system, i.e. the (3×3) system, at higher SNR. This demonstrates the potential of the nonlinear detection that uses successive interference cancellation scheme, which improves the BER performance of

the LST system. The results also show the nonlinear detection is capable of providing a breakthrough over the linear detection when sufficient SNR is available. [10, 11].

Results from figure b.1 to b.4 in Appendix-B1 can also be compared in order to assess the effect of each type of algorithm combination; i.e the linear ZF, linear MMSE, nonlinear ZF and nonlinear MMSE, that operate under the frequency-flat fading MIMO channel. The results are extracted for the (3×3), (4×3), (3×2) and (6×4) systems and shown as follows:

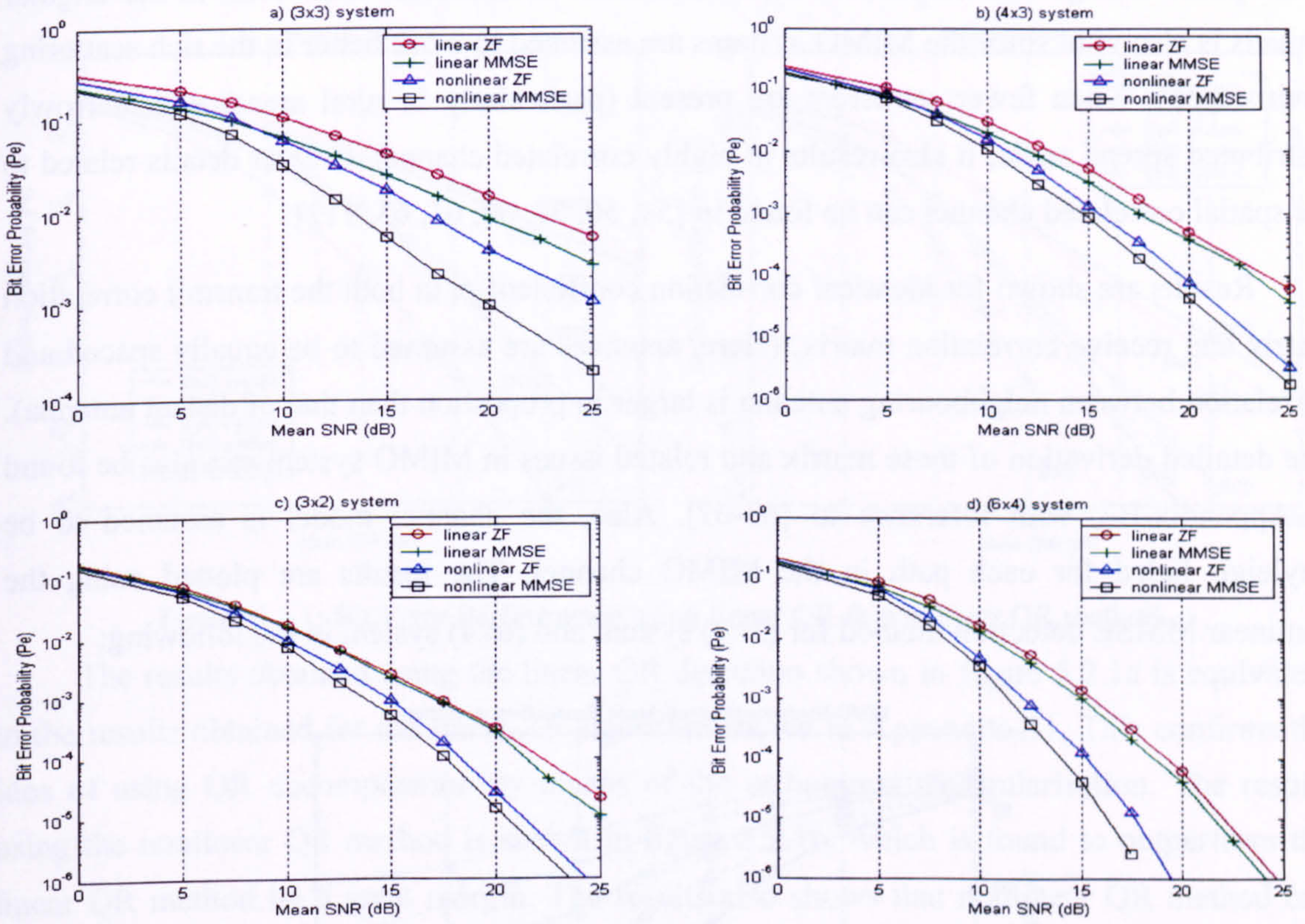

Figure 5.1.5: Performance comparison using different detection algorithm for various (N×M) systems

The two main observations that can be deduced from figure 5.1.5 are that a) the MMSE algorithm always gives better performance than the ZF algorithm and b) the use of the nonlinear symbol detection (with the SIC scheme) further improves the performance of the layered space-time system by a great margin as compared with the linear detection methods. The results show that the use of interference cancellation in the nonlinear detection techniques on top of the diversity, allows the system performance to be further improved [4, 6, 8, 47, 48].

Next, the system performance of the LST system is tested with different degree of spatial correlation in the flat-fading MIMO channel. The spatial correlation defines the degree of similarity between the fading coefficients of the two independent streams being received at antennas spaced by a given distance, usually measured in wavelength λ of the transmitted signal [60]. In general, the mechanisms that give rise to spatial correlation are based on

several factors: the distance between each antenna's spacing in the multiple antenna setting, the number & distribution of the scatterers and the angular spreads of the incoming waves to the receiver [61]. Lower correlation is expected when the antenna's spacing is large and wider angular spread of received signals is assumed when scatterers are largely distributed around the receiver. In contrast, two independent paths are said to be highly correlated when antenna's spacing is very small, causing the two paths to fade almost in the same way in term of its phase change and amplitude. The distribution of scatterers that result in the angular spreads is also vital since the MIMO systems are assumed to work better in the rich scattering environment. When fewer scatterers are present (particularly in rural areas) with narrowly distributed spread angle, it also results in highly correlated channel. Greater details related to the spatial correlated channel can be found in [54, 56, 57, 60, 61, 63, 112].

Results are shown for identical correlation coefficient ρ, in both the transmit correlation matrix and receive correlation matrix. (Here, antennas are assumed to be equally spaced and correlation between neighbouring antenna is larger in proportion than that of distant antenna). The detailed derivation of these matrix and related issues in MIMO system can also be found in Appendix-B2, with reference to [63-67]. Also, the channel model is assumed to be Rayleigh faded for each path in the MIMO channel. The results are plotted using the nonlinear MMSE detection method for (3×3) system and (6×4) system in the following:

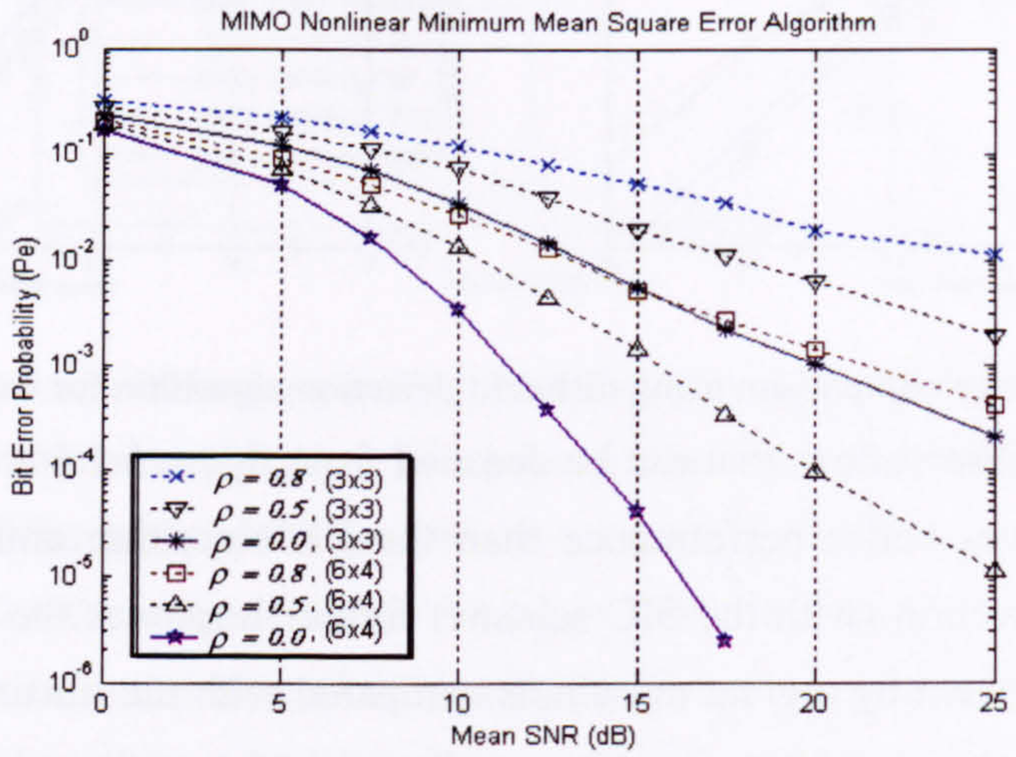

Figure 5.1.6: Effect of spatial channel correlation on performance.

It can be seen clearly from figure 5.1.6 that the spatial correlation in the frequency-flat MIMO channel has severe effect on the system performance of the layered space-time system. The performance becomes degraded as the spatial correlation coefficient of the MIMO channel increases. Clearly only the antenna arrangement with zero or no spatial correlation provides the best performance for MIMO systems.

5.2 Performance Evaluation of the Layered Space-Time Receiver Using the QR Detection Method

In this section, the BER performance of the LST system using the QR detection algorithm (for both the linear and nonlinear detection) described in section 2.5.3 is presented for various ($N \times M$) systems under flat fading MIMO channel condition. *Perfect channel knowledge at the receiver is also assumed here.*

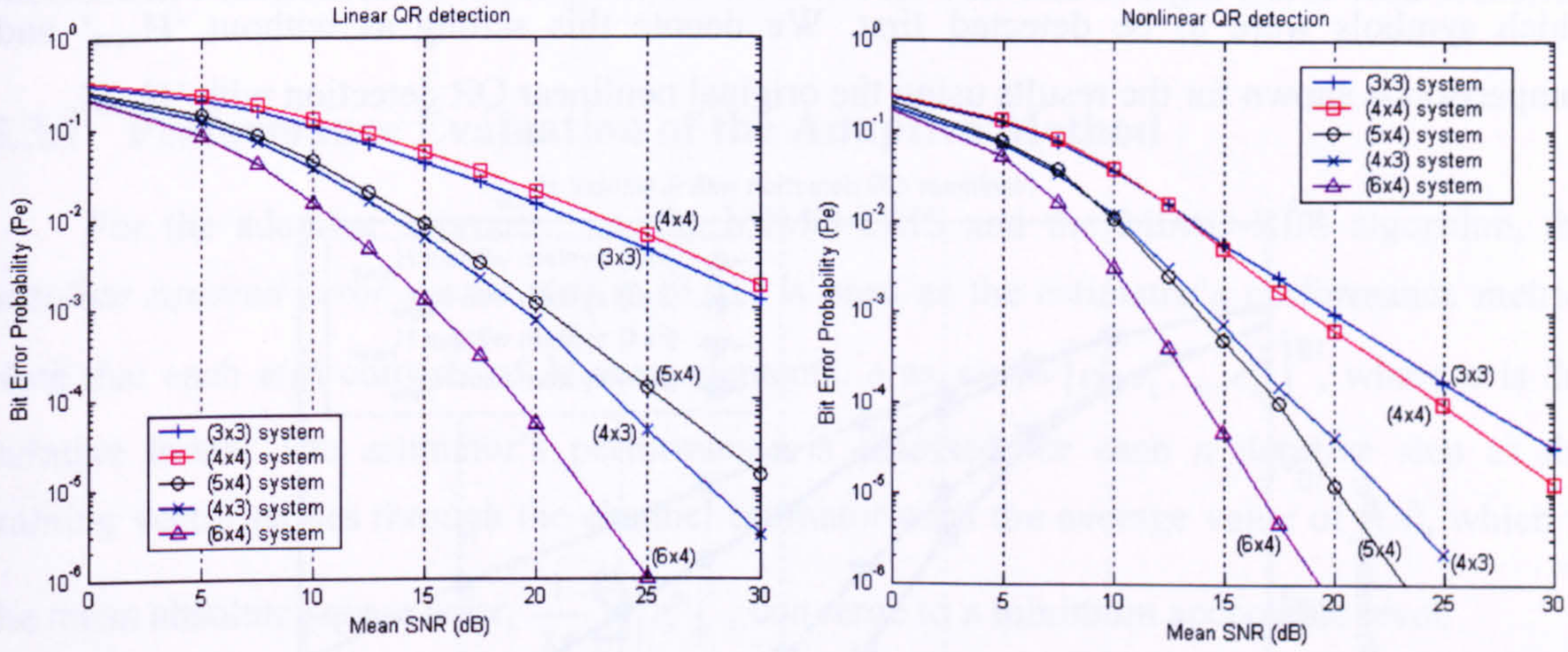

Figure 5.2.1: Bit Error Performance using linear QR & nonlinear QR method.

The results obtained using the linear QR detection shown in figure 5.2.1a is equivalent to the results obtained for the linear ZF algorithm shown in Appendix-B1. This confirms the idea of using QR decomposition by means of the orthogonal triangularisation. The results using the nonlinear QR method is shown in figure 5.2.1b, which is found to outperform the linear QR method by a great margin. The results also shows that nonlinear QR method can perform equally well with the nonlinear V-BLAST detection when the SIC feature is applied. The results are also compared in the following figure:

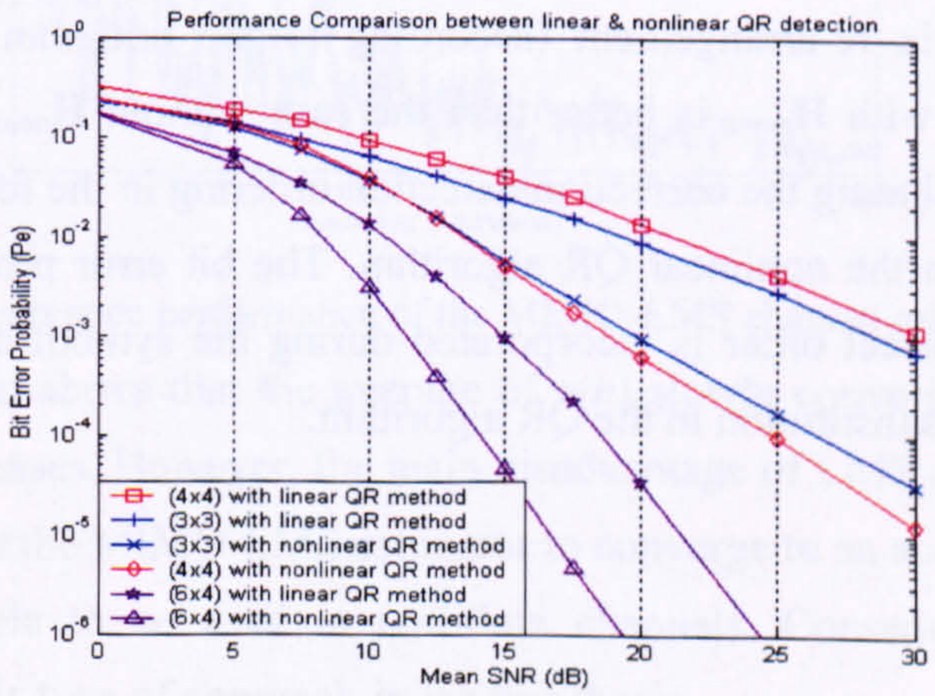

Figure 5.2.2: Performance comparison between linear & nonlinear QR detection

Next, in order to assess the performance due to the effect of correct detection ordering, we deliberately conceal the process of channel matrix re-arrangement in the nonlinear QR detection. This is equivalent by either freezing this feature (no re-arrangement made prior to the QR decomposition of **H** – QR decomposition is performed on the original **H**) or by allowing random re-arrangement (meaning that re-arrangement not according to the optimum detection ordering set). The reason to perform this channel matrix re-arrangement process is to effectively incorporate the detection ordering required by the SIC feature in determining which symbols were to be detected first. We denote this setting as without '$\mathbf{H}_{new}$' and comparison is shown for the results using the original nonlinear QR detection with '$\mathbf{H}_{new}$'.

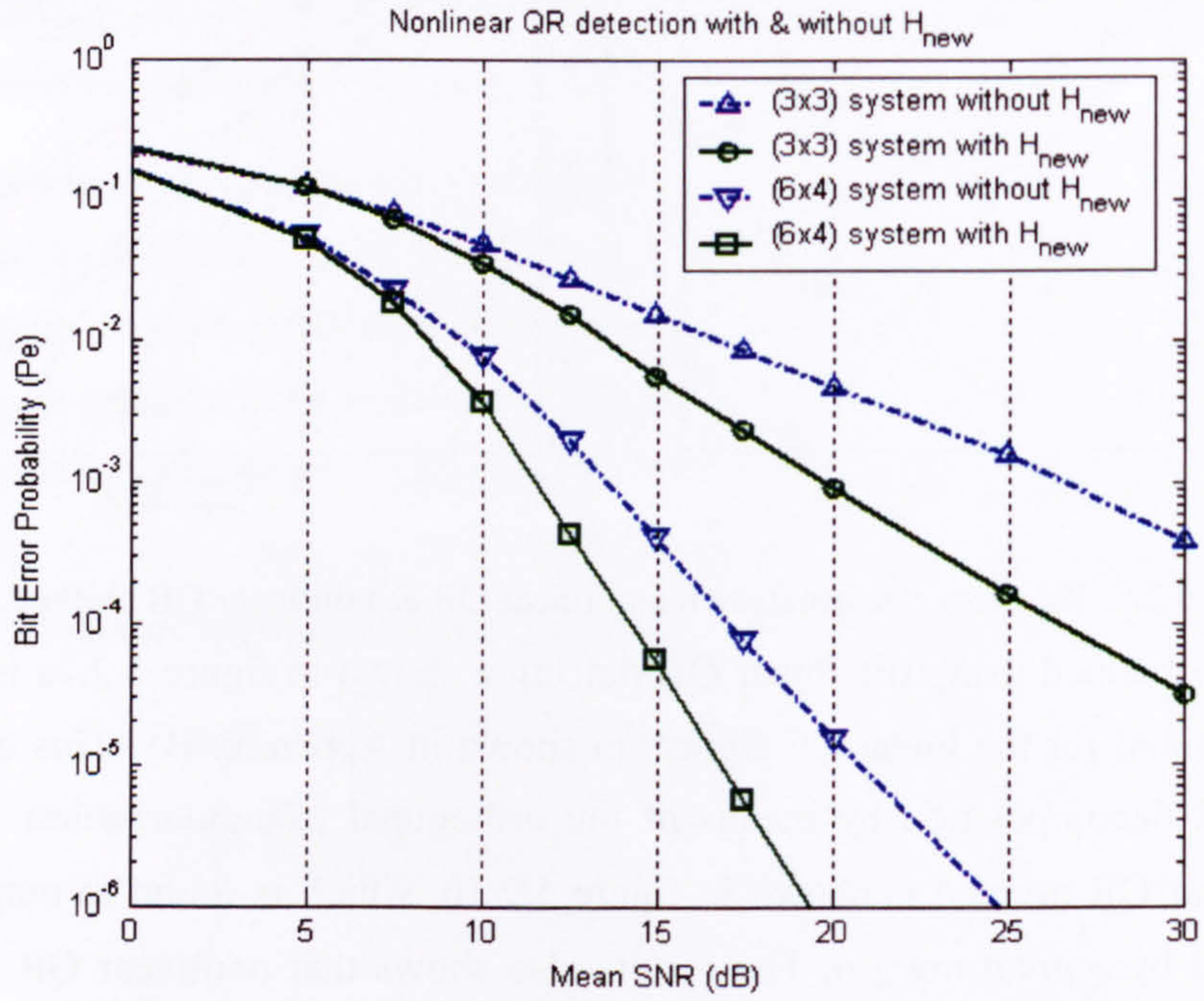

Figure 5.2.3: System performance using nonlinear QR detection a) with $\mathbf{H}_{new}$ & b) without $\mathbf{H}_{new}$

It can be seen clearly in figure 5.2.4 that the system performance of the case with the proper channel matrix re-arrangement (according to the optimum detection ordering set obtained *a priori*) – with $\mathbf{H}_{new}$, is better than the case without $\mathbf{H}_{new}$. This demonstrates the importance of the including the correction detection ordering in the feature that rearranges the original **H** to $\mathbf{H}_{new}$ in the nonlinear QR algorithm. The bit error probability is considerably reduced when the correct order is incorporated during the symbol detection process by the method of backward substitution in the QR algorithm.

5.3 Performance of MIMO Channel Estimation Methods in Frequency-Flat Fading MIMO Channel

The performance of various MIMO channel estimation methods used in the flat-fading channel (either adaptive or non-adaptive) described in Chapter 3; i.e. MIMO-LMS, MIMO-RLS & MIMO-PMI are presented here. In the simulation model for the ($N\times M$) flat-fading MIMO channel, each sub-channel consists of a single path represented by a complex coefficient, which assumes Rayleigh channel model for non-line of sight worse-case scenario.

5.3.1 Performance Evaluation of the Adaptive Method

For the adaptive approach; i.e. the MIMO-LMS and the MIMO-RLS algorithm, the *absolute squared error vector* $\mathbf{e}(n)$ in (3.61) is used as the estimator's performance metric. Note that each $\mathbf{e}(n)$ consists of M error elements, e as $\mathbf{e}(n)=\left[e_1^n, e_2^n, \ldots, e_M^n\right]^{\mathrm{T}}$, where n is the iterative index. The estimator's performance is assessed for each n iterative step as the training vector passes through the channel estimator until the average value of $\mathbf{e}(n)$, which is the mean absolute square error, $\frac{1}{M}\sum_{i=1}^{M}\left|e_i^n\right|^2$, converge to a minimum acceptable level.

First, the performance of the MIMO-LMS algorithm is shown in figure 5.3.1 below for a (3×3) system with mean SNR of 20dB in a stationary flat fading MIMO channel.

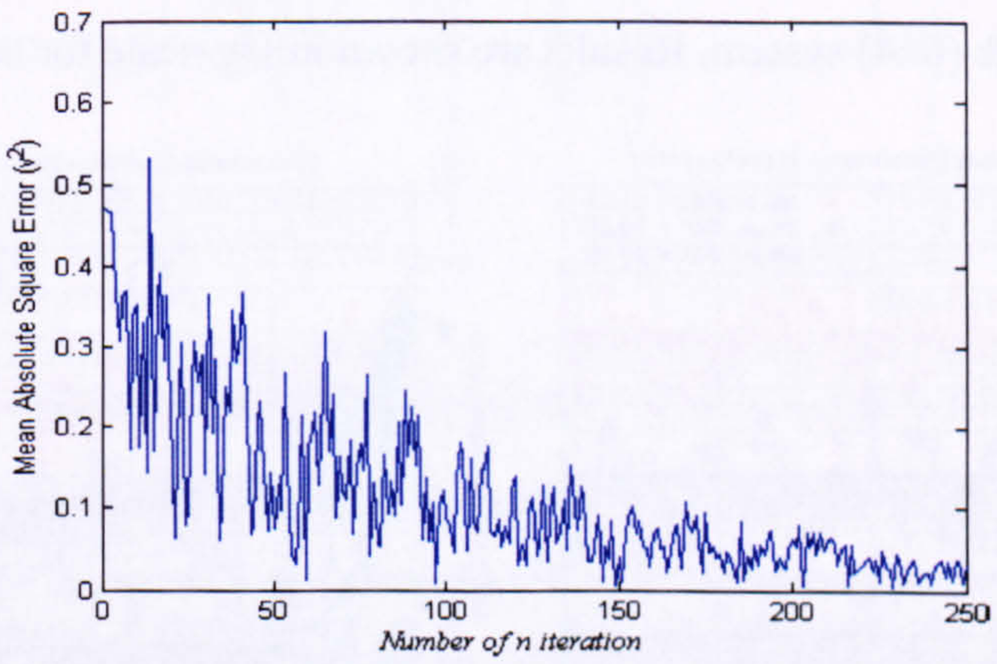

Figure 5.3.1: The convergence performance of the MIMO-LMS channel estimation algorithm

It can be seen from above that the average of $\mathbf{e}(n)$ slowly converges as the number of adaptive iteration n increases. However, the main disadvantage of LMS algorithm is the huge length of time needed for the MIMO-LMS estimator to converge to an acceptable level, which often makes it unsuitable to be used in real-time channels. Consequently, relative little emphasis is placed on this type of approach in the this thesis

Next, the performance of the MIMO-RLS algorithm is presented. Results are shown for a fixed (4×4) system operating over a stationary flat-fading channel for mean SNR = 20dB & 10dB with the forgetting factor of $\gamma = 0.98$. (All M error elements in that $\mathbf{e}(n)$ are shown).

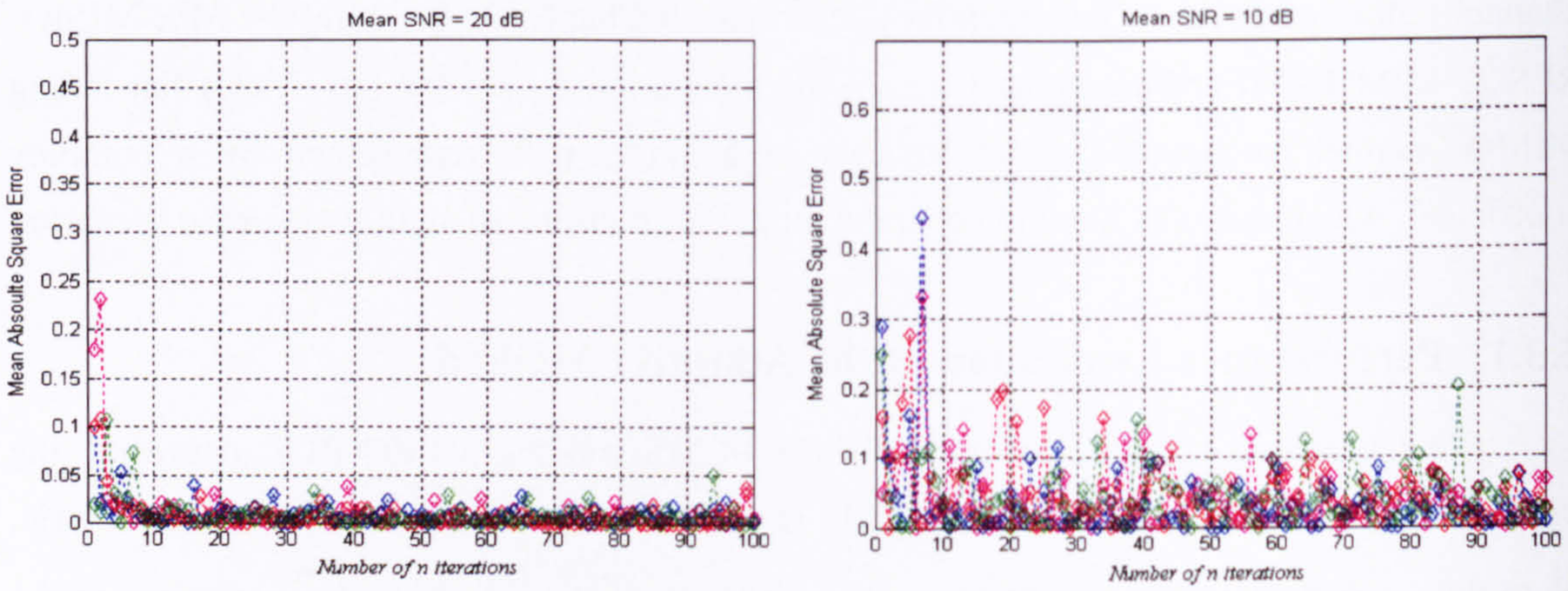

Figure 5.3.2: Performance of MIMO-RLS algorithm in mean SNR = 20dB

It can be seen from figure 5.3.2 that the performance of the MIMO-RLS algorithm shows much faster convergence compared to the MIMO-LMS algorithm (within about $n = 20$ iterations) at SNR=20dB, demonstrating the superiority of the MIMO-RLS over the MIMO-LMS algorithm. However, the performance deteriorates as the mean SNR decreases to 10dB. (Refer to Appendix-B3 for more individual results with various SNR values).

Next, the performance of the MIMO-RLS algorithm is compared for different mean SNR values for (4×4) & (6×4) system. Results are shown in log-scale for better visualisation.

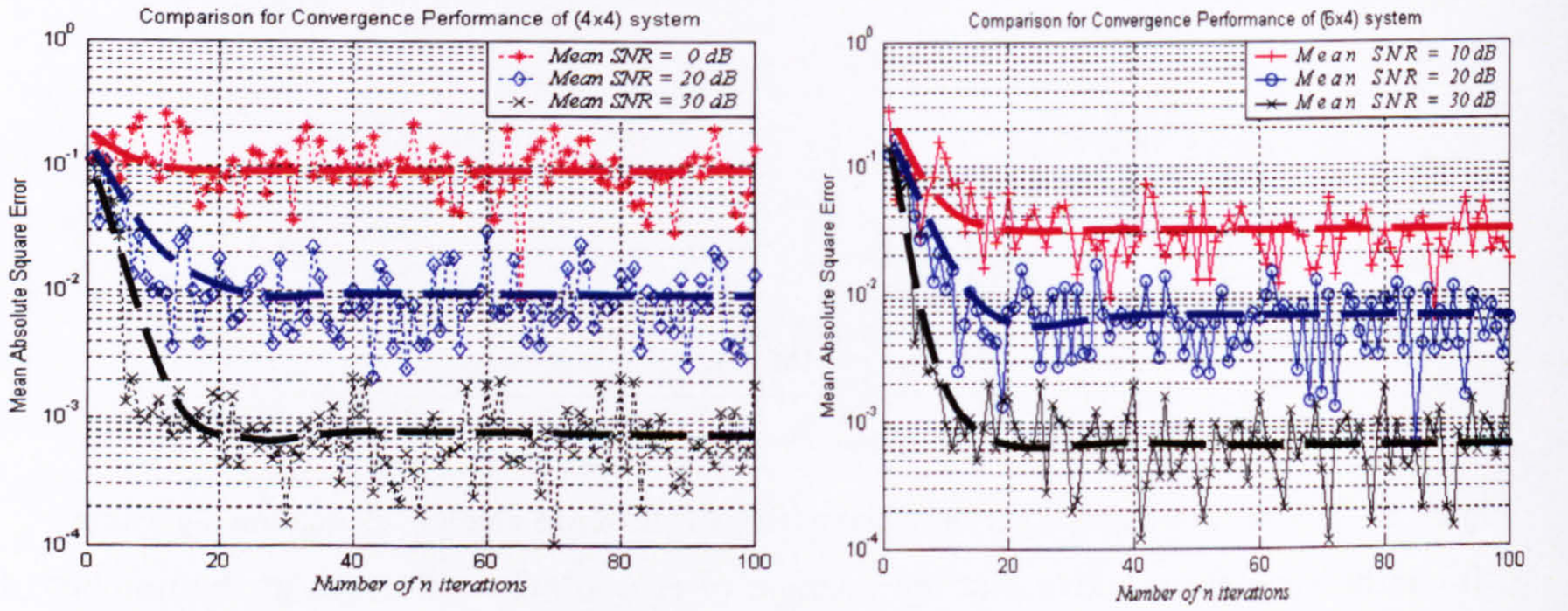

Figure 5.3.3: Performance Comparison for different mean SNR in (4×4) & (6×4) system

It can be seen in both figures of 5.3.3 that the mean absolute square error falls to an error 'floor' within about 20 to 30 iterations, depending on the mean SNR value. The fluctuation in performance is due to the noise in the system. Using further training vectors

achieves no further accuracy in the channel estimate. For a mean SNR of 30dB, the error 'floor' is about 1×10^{-3} but as the mean SNR reduces, the error 'floor' also rises accordingly.

Next, the performance of the MIMO-RLS estimator also depends on the forgetting factor. So far, fixed value of $\gamma = 0.98$ is used. In the following, the effect of changing the value of forgetting factor are shown for the (6×4) system using mean SNR = 20dB.

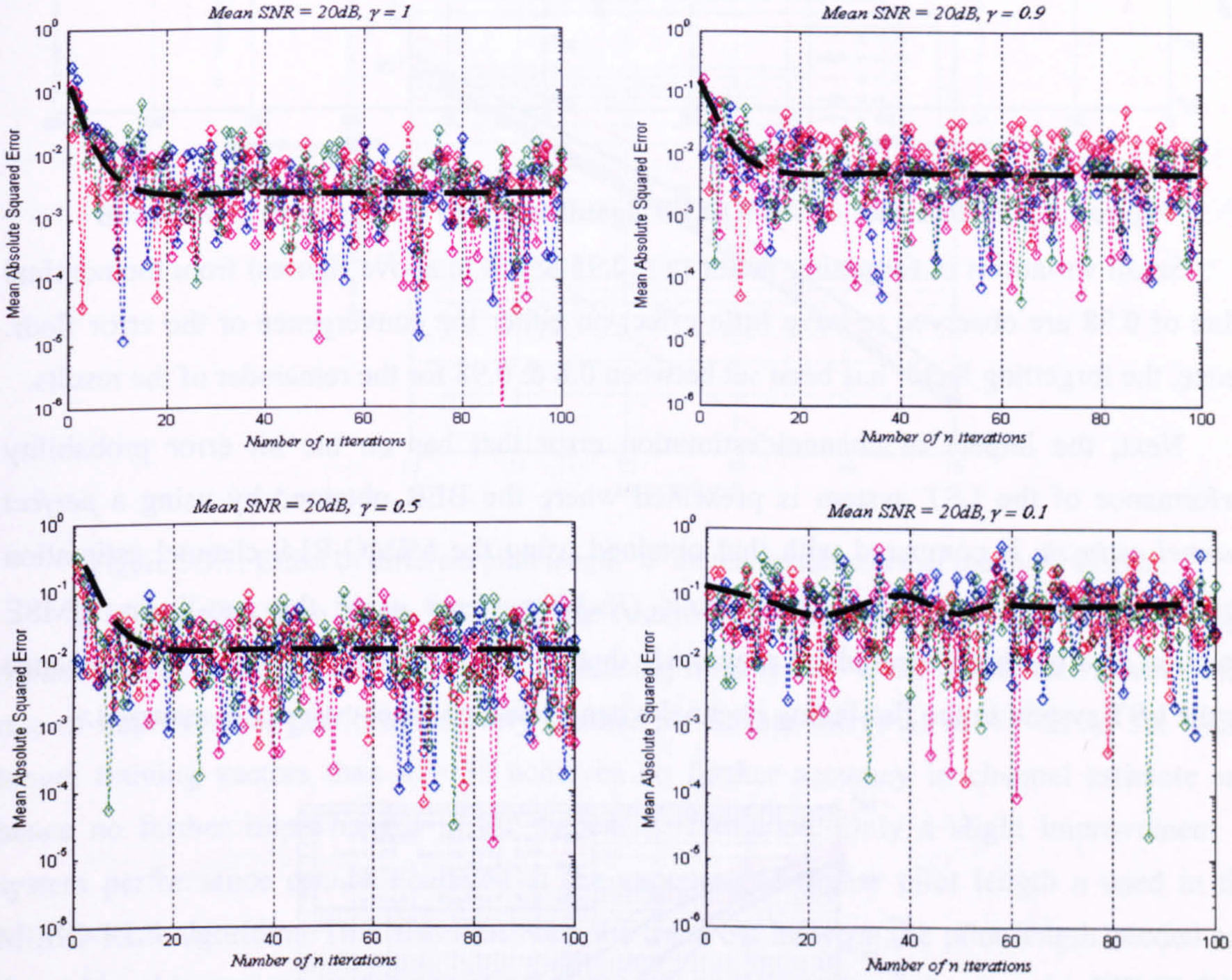

Figure 5.3.4: Performance of MIMO-RLS using $\gamma = 1, 0.9, 0.5$ & 0.1 for mean SNR = 20dB

Several observations can be made in figures of 5.3.4. The performance of the MIMO-RLS estimator is still acceptable as γ decreases to 0.9. However, the performance deteriorates as γ decreases to 0.5 and becomes highly unstable as γ set to 0.1. The stability issues of using the RLS algorithm in general are discussed in [104] and Cioffi [130] has discussed the applicability of the RLS algorithm at the high and low SNR cases. It is also seen from the results that, the error performance converges within about 15~20 iterations.

Next, results are also plotted for $\gamma = 0.95$ & $\gamma = 0.8$ in figure 5.3.5 in order to demonstrate the nominal value of the forgetting factor in the (6×4) system.

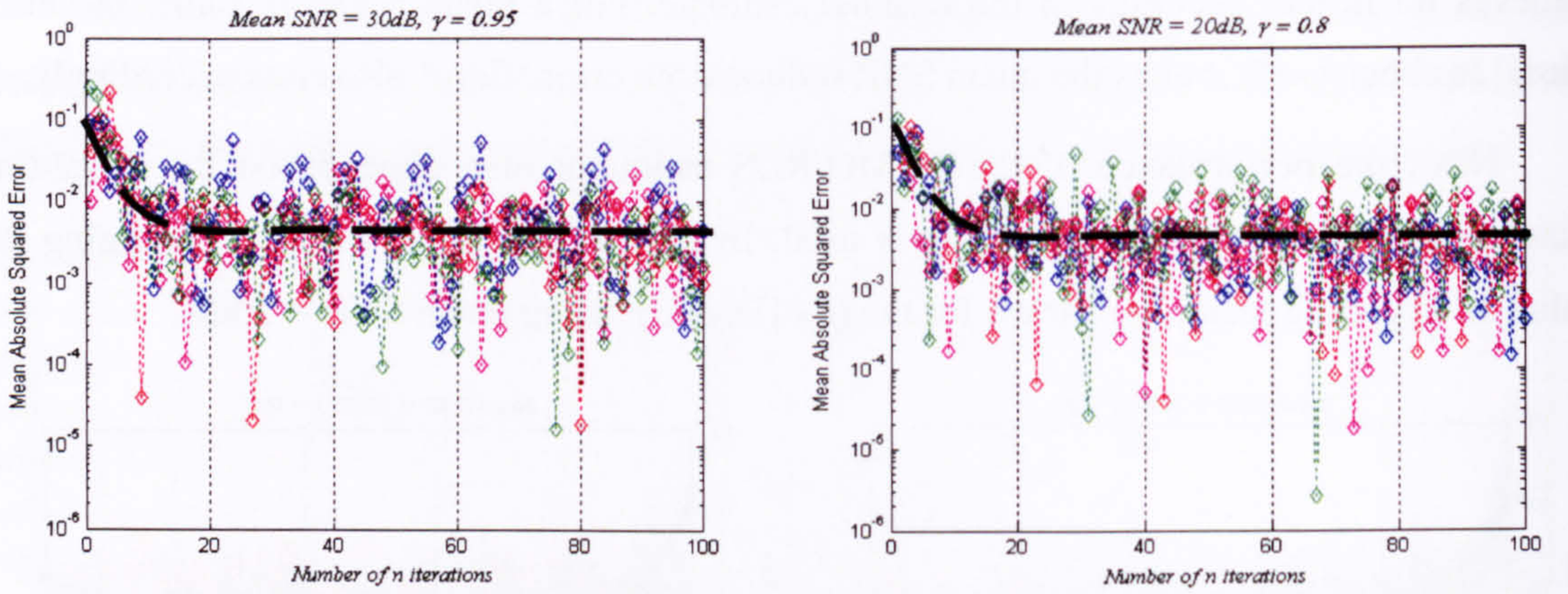

Figure 5.3.5: Performance of MIMO-RLS algorithm using $\gamma = 0.8$ in mean SNR = 20dB

Small variations in forgetting factor ($\gamma = 0.95$ & 0.8 in above figures) from the nominal value of 0.98 are observed to have little effect on either the convergence or the error floor. Hence, the forgetting factor has been set between 0.8 & 0.98 for the remainder of the results.

Next, the impact of channel estimation error that has on the bit error probability performance of the LST system is presented where the BER obtained by using a *perfect channel estimate* is compared with that obtained using the MIMO-RLS channel estimation algorithm. Results are plotted for various ($N \times M$) systems using the non-linear MMSE detection as it has been ascertained previously that the method provides the best performance for the LST system in the flat-fading channel when perfect channel estimate is assumed.

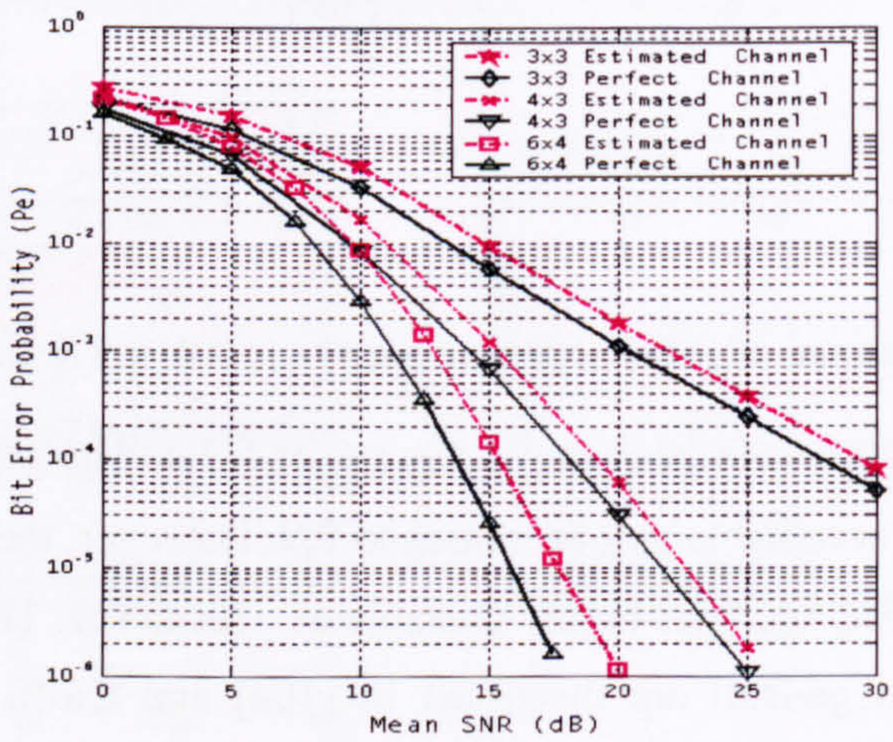

Figure 5.3.6: Performance comparison of various ($N \times M$) non-linear MMSE configurations for a) perfect channel case & b) estimated channel case using the MIMO-RLS channel estimation method

The results show quite clearly that the MIMO-RLS estimator displayed only a small degradation in the bit error probability performance as compared to the perfect channel estimate case for all systems tested.

The previous results for the estimated channel are obtained using pilot vectors with minimum length of n = 25 iterations as ascertained from figure 5.3.3. In the following, the effect of varying the pilot vector length (from n=10 to n=30) is examined for the MIMO-RLS estimator to assess its impact on the system performance. Results are compared with the case where perfect channel estimate are used in the (6×4) system.

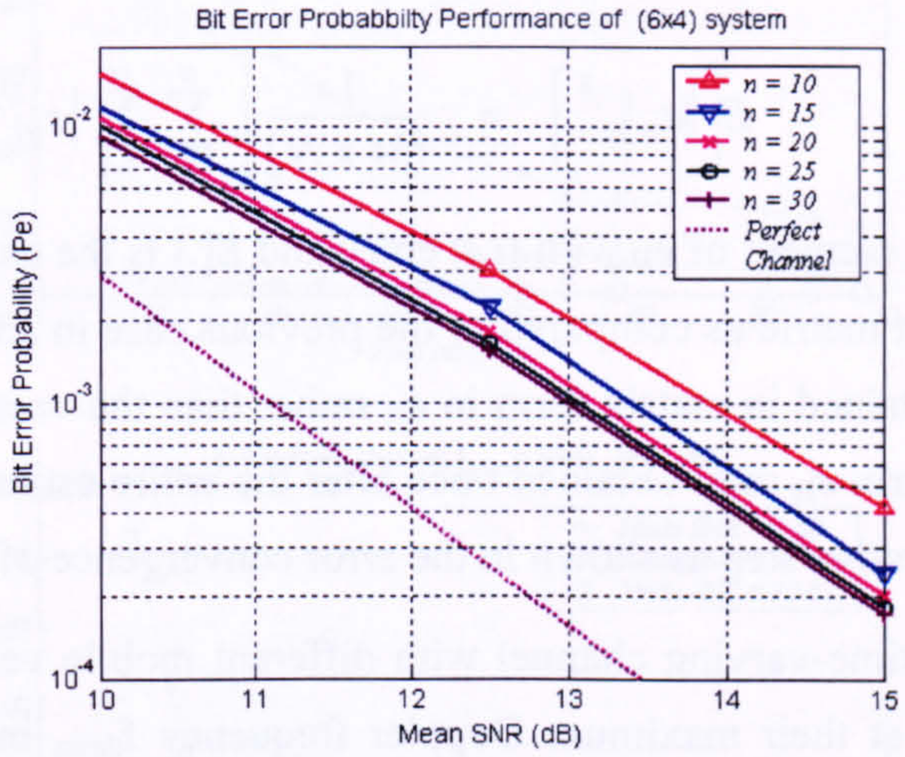

Figure 5.3.7: Effect of different pilot length 'n' on the performance of the (6×4) system.

It is observed from figure 5.3.7 that the system performance improves as the pilot length n increases. This can be seen in case of increasing from n = 10 to 20 iterations. However, the rate of improvement gets progressively smaller for further increases of n = 25 to 30. Using longer training vectors than n = 30 achieves no further accuracy in channel estimate and hence no further improvement in the system performance. Only a slight improvement in system performance can be achieved at the expenses of higher pilot length n used in the MIMO-RLS algorithm. This also illustrates the trade-off between the pilot length needed and the achievable system performance when the channel is estimated using the MIMO-RLS estimator. This also justifies the used of n = 25 pilot vectors used in the previous figure.

5.3.2 Performance Evaluation of the Non-adaptive Method

Next, the performance of the non-adaptive MIMO-PMI channel estimator that described in section 3.3.3 is presented here. In the following, the performance of the MIMO-PMI estimator is tested under various time-varying frequency-flat MIMO channels for different (N×M) system configurations and different mean SNR values. The performance of the MIMO-PMI channel estimator will be demonstrated using the mean square error (MSE) (or the mean Frobenius norm squared error) as the performance metric, which is a scalar measurement of the of the error matrix $\boldsymbol{e}_{\mathrm{H}}$ that can be obtained as follows:

First, the error matrix of the channel estimation e_H is obtained by taking the estimated MIMO channel matrix $\hat{\mathbf{H}}$ and subtract from the actual MIMO channel matrix $\mathbf{H}$ as follows:

$$e_H = \mathbf{H} - \hat{\mathbf{H}} \tag{5.1}$$

Subsequently, the MSE or the mean Frobenius norm squared error of e_H can be obtained as:

$$E\left[\|e_H\|_F^2\right] = \frac{1}{(M \times N)}\left[\sum_{i=1}^{N}\sum_{j=1}^{M}|\varepsilon_{ij}|^2\right] \tag{5.2}$$

where ε_{ij} is the matrix element of e_H with (i,j) entry and $E[.]$ is the expectation operator. Note that (5.2) is a different metric as compared to the previous case in adaptive methods since the estimation error is obtained in matrix form in e_H rather than the vector form of $\mathbf{e}(n)$ in (3.61) and also the error matrix e_H only obtained once after the entire estimation process rather than obtained at each n-iterative step as shown in the error convergence of the adaptive methods.

Three types of time-varying channel with different mobile velocities are used and the results are simulated at their maximum Doppler frequency f_{dmax} in each case using carrier frequency of $f_c = 2.11$GHz with the end-to-end data rate of $D_{total} = 480$Kbps. The data rate of individual transmit antenna D_{single} depends on the value of M where $D_{single} = D_{total}/M$. The respective travel velocities Λ of the 3 different time-varying channels, together with their respective Doppler frequency are stated in the following:

a) The pedestrian channel: $f_{dmax} = 6$ Hz, $\Lambda = 3$ km/hr $\cong 0.833$m/s.
b) The city/town channel: $f_{dmax} = 88$ Hz, $\Lambda = 45$ km/hr $\cong 28$ mph.
c) The motorway/highway channel: $f_{dmax} = 176$ Hz, $\Lambda = 90$ km/hr $\cong 56$ mph.

In the simulation model, each complex channel coefficient in the time-varying MIMO channel is individually filtered by two Doppler filters (for real and imaginary coefficient) according to their respective Doppler velocities. The detail of how the Doppler effect is added into the simulated channel model and its mathematics are presented in Appendix-B4.

In the following, the MSE is plotted against the pilot length v, expressed using the available valid order v of the Hadamard matrix (as discussed in Chapter 3), where $v = 8$, 12, 20, 24, 32, 44, 48, 60, 68 are shown. The construction of the pilot matrix and its criterion can be referred in section 3.3.3.

First, the performance of the proposed estimator is tested under the three different types of mobile time-varying channels listed above, for a fixed (2×2) system with three different mean SNR values: 5dB, 10dB and 20dB respectively. Results are plotted for increasing pilot length expressed in terms of the matrix order v ranging from 8 to 68.

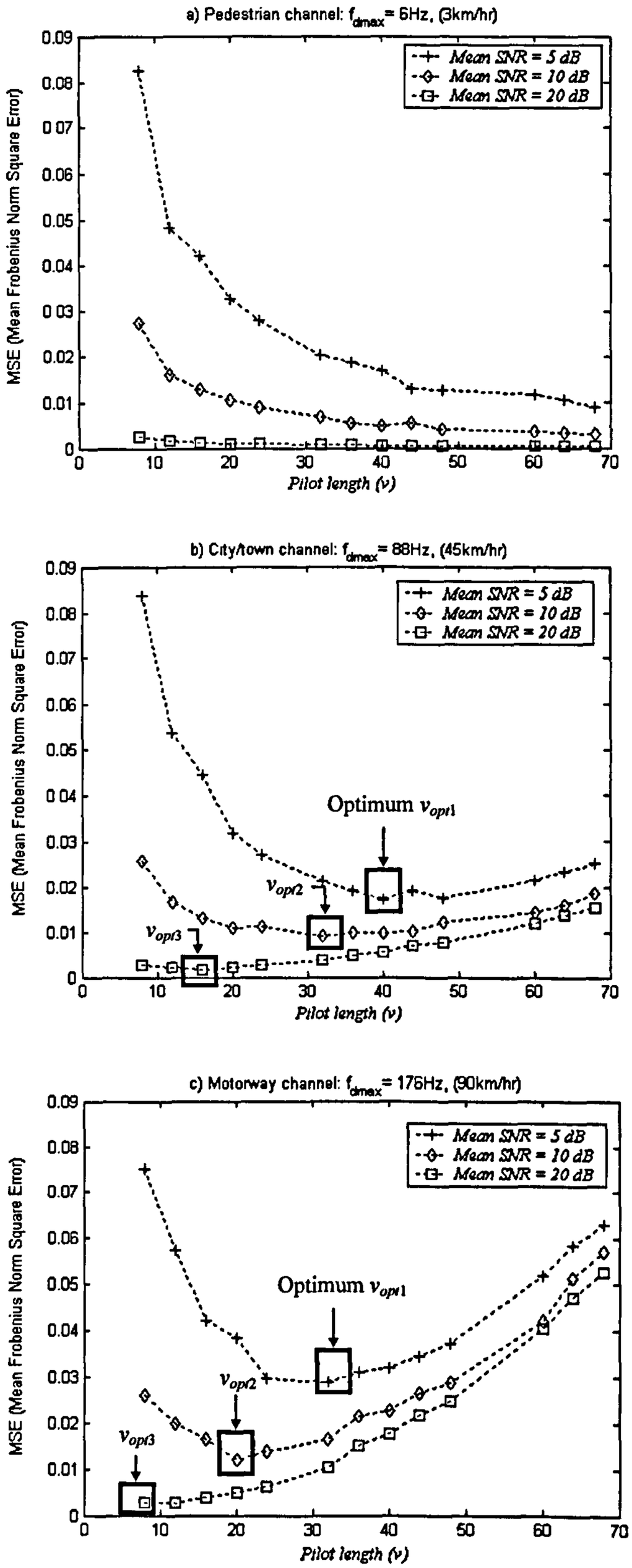

Figure 5.3.8: Performance of MIMO-PMI estimator for a (2×2) system in different time-varying channels

Several observations can be made from figure 5.3.8. In the slow-varying pedestrian channel, the MSE performance improves as the pilot length v increases. The slow-varying pedestrian can be treated as static channel virtually since the channel varies very slowly compared to the coherence-time of the channel. The result demonstrates the basic trade-off between the pilot length and the estimation error.

However, as the channel varies faster, different trend of results are observed. Depending on the mean SNR, the estimator's performance improves as pilot length v is increases initially for the short period of v, until at a critical pilot length, then, the estimator's performance becomes poorer again for any further increases of v. The 'U' curves can be observed (in the 5dB & 10dB case) and the optimum pilot length, v_{opt} for each case produces the minimum MSE. This is because the estimator can only cope with small amount of variation in the channel to provide a good estimation when reasonable pilot length is used. Longer pilot length means larger channel variation is involved, where the obtained channel estimates might be deviated in greater proportion from its actual value. In contrary, the performance for the 20 dB case degraded almost immediately for any increases in v. This is because, minimum MSE has been already achieved at minimum v = 8 (for sufficient pilot length) and any further increases in v will only degrade the performance since longer channel variation is involved.

The results of figure 5.3.8 can be compared for different mobile velocity for fixed values of mean SNR = 5dB and 10dB, shown in the following:

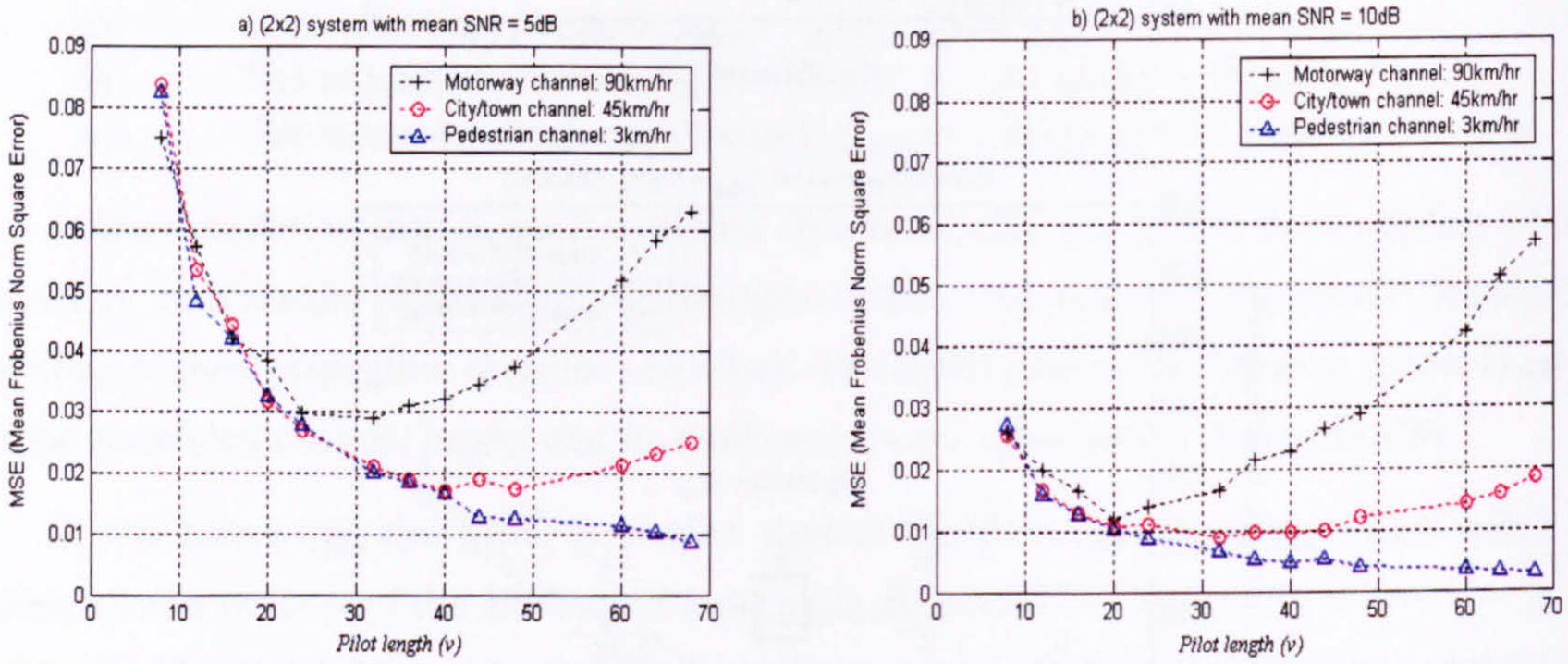

Figure 5.3.9: MIMO-PMI Performance for different mobile channels in a (2×2) system.

The effect of increasing pilot length under various time-varying channels for different mean SNR can be observed in figure 5.3.9. The trade-off between the needs of sufficient pilot lengths and the MSE concludes where the worsening of the channel estimate (the 'U' point) begins to take place for shorter values of v as the channel changes more rapidly. Faster time-varying channel; i.e. the motorway channel produces more obvious 'U' shaped curve.

The same test in figure 5.3.8 & figure 5.3.9 is repeated for the (3×3) system and the results are presented in Appendix-B4. The similar results trend in figure 5.3.8 & figure 5.3.9 can also be observed therein, demonstrating the trade-off between the pilot lengths and MSE under various time-varying channels with different mobile speeds at different mean SNR.

Next, the performance of MIMO-PMI estimator for both (2×2) & (3×3) system can be compared directly to assess the impact of increasing (N×M) value. Results are shown for the city/town channel and the motorway channel for mean SNR of 5dB & 10dB in the following:

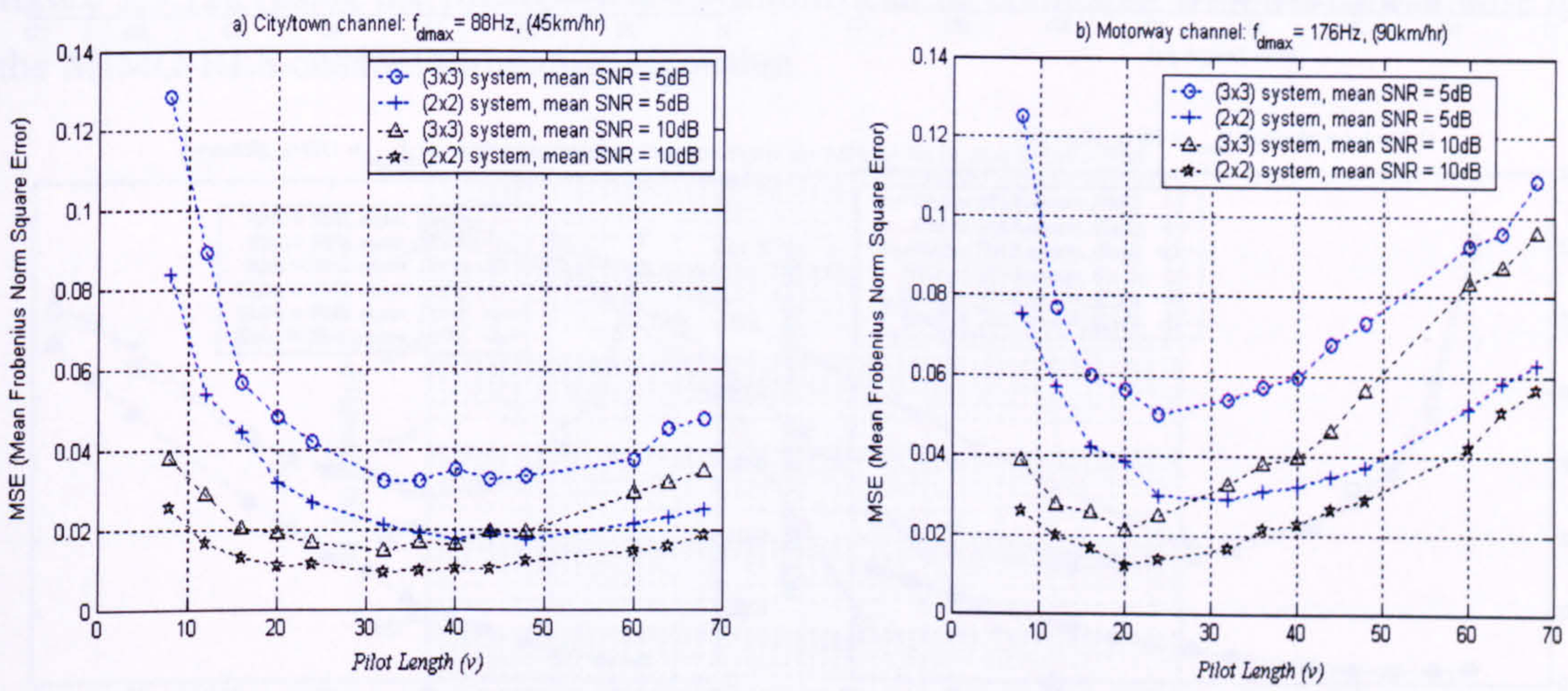

Figure 5.3.10: Impact of increasing (N×M) configuration on MIMO-PMI estimator's performance

It can be seen that the (2×2) system always performs better than the (3×3) system at the respective mean SNR values, for the two types of channels shown above. For the same value of v, the MSE for the $M = 3$ system is higher compared with the $M = 2$ system, although same diversity ratio, $N/M = 1$ is kept. This is because the total transmit power have to be kept constant (to achieve the expected mean SNR) by controlling the transmit power of each transmit antenna using a multiplier of $\sqrt{1/M}$ prior to symbol transmission. Therefore, the pilot symbols (transmitted from each transmit antenna) of the higher M system; i.e. the (3×3) system, are having a lower power than the pilot symbols of the lower M system; i.e. the (2×2).

Next, we assess the impact of different reception diversity order for the $N \geq M$ systems by increasing the value of N for fixed $M = 2$ and 3 systems. Results are plotted for different mean SNR at 5dB and 20dB for both city/town channel and motorway channel. It can be seen in figure 5.3.11 that the reception diversity gain achieved in the $N>M$ system has no significant influence on the MIMO-PMI estimator's performance. The results are independent of N for both the mean SNR values, demonstrating that reception diversity did not contribute to any improvement in the MIMO-PMI estimator's performance.

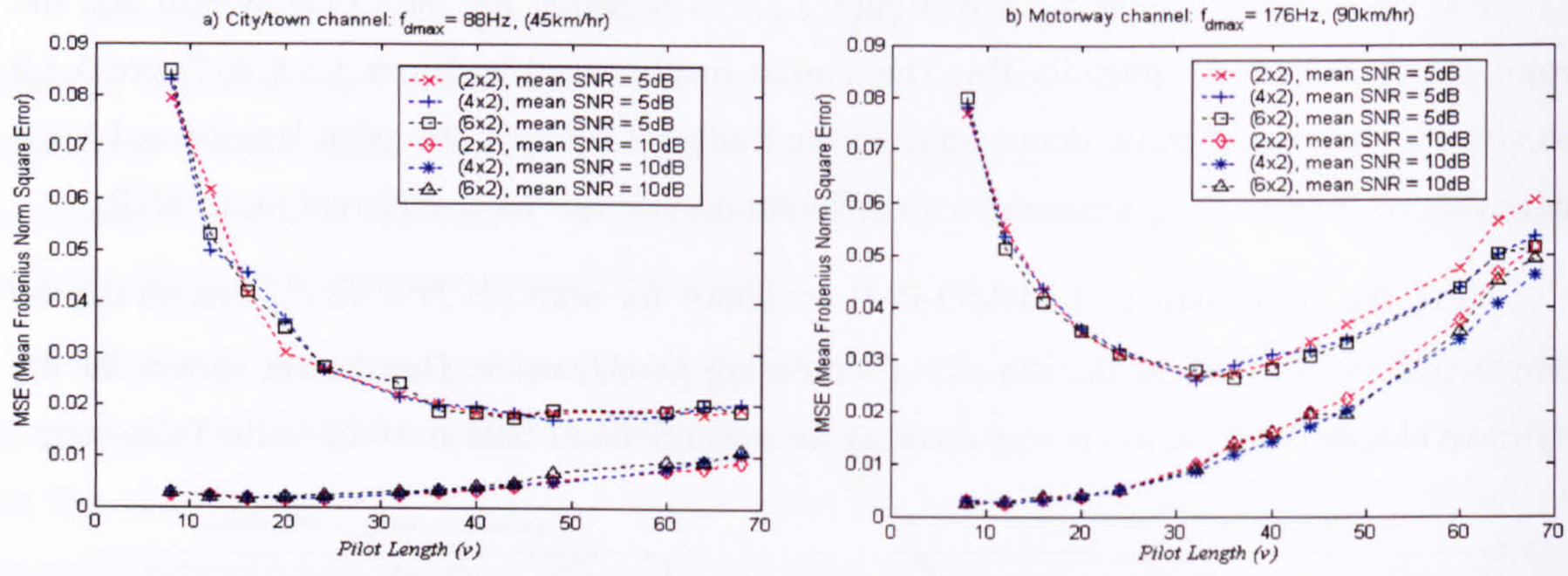

Figure 5.3.11: Impact of reception diversity on MIMO-PMI estimator's performance

Next, the bit error probability performance of the layered space-time system is assessed using the nonlinear MMSE detection process under the two frequency-flat time-varying channels. The results are shown for the case using perfect channel estimate and estimated channel obtained by the MIMO-PMI estimator. The optimum pilot length $v_{opt} = 24$ is used in the MIMO-PMI estimator for each ($N \times M$) system shown.

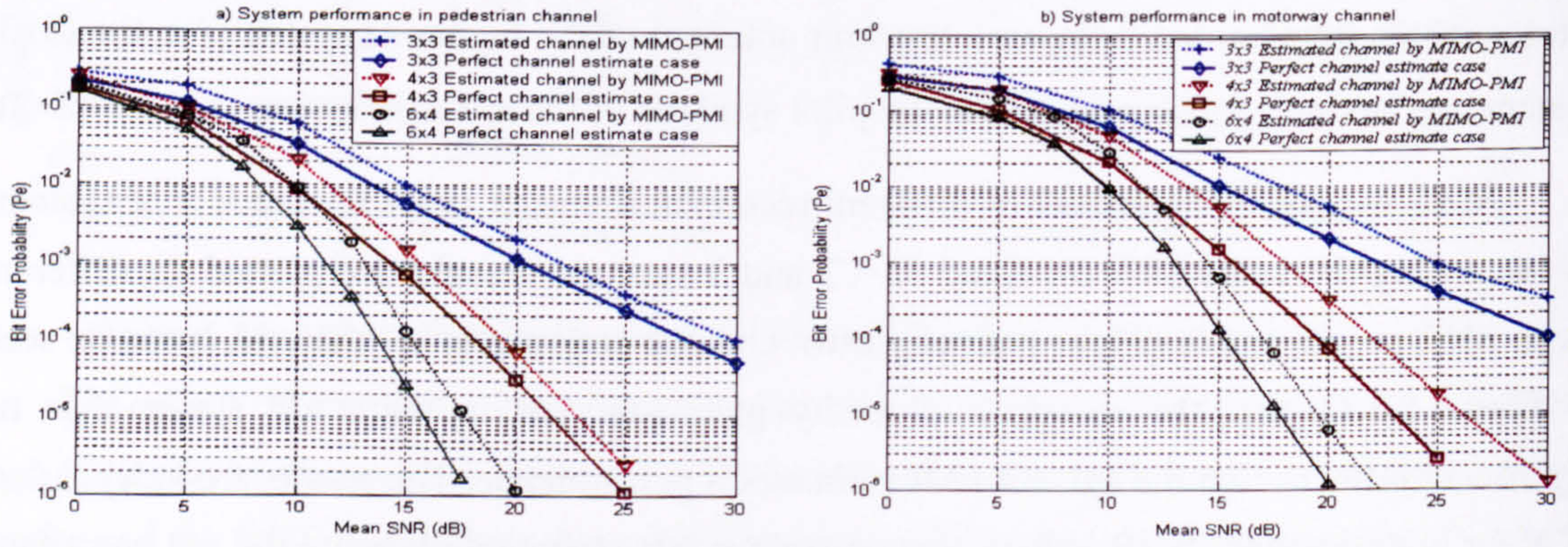

Figure 5.3.12: Performance comparison of various ($N \times M$) non-linear MMSE configurations for a) perfect channel case & b) estimated channel case using the MIMO-PMI channel estimation method

The results in figure 5.3.12 show the impact of channel estimation error that has on the system performance (using the MIMO-PMI algorithm) under the slowly varying pedestrian channel and the fast varying motorway channel. It can be seen that consistent performance is achieved in the estimated channel case as compared to the perfect channel estimate case. The bit error probability performance is poorer in the motorway channel as compared to the pedestrian channel for both perfect and estimated channel case.

In fact, since the channel is slowly varying, the pedestrian estimated channel case in figure 5.3.12a (using the MIMO-PMI algorithm) can be compared with the similar case using the MIMO-RLS channel estimation algorithm.

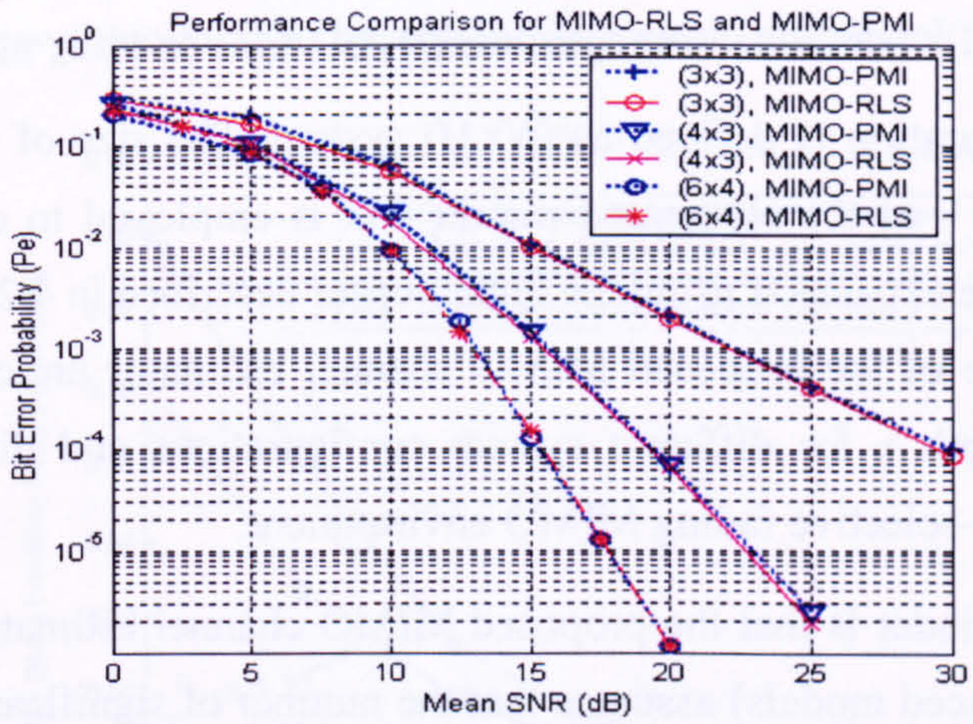

Figure 5.3.13: Comparison of system performance using a) MIMO-RLS & b) MIMO-PMI algorithm

It is found that the results are very close to one another with the optimum pilot length used in each channel estimation method. In the MIMO-PMI estimation, the optimum pilot length for each training sequence at each transmit antenna is $v_{opt} = 24$, whereas in the MIMO-RLS estimation, the pilot length for each training sequence at each transmit antenna is $n = 25$.

5.4 Performance of the Novel MIMO Channel Estimator in the frequency-selective MIMO Channel Condition

In this section, the performances of the of the proposed MIMO channel estimator that operate in the frequency-selective fading channel are demonstrated using two types of model (described in Chapter 4): a) the symbol-spaced model (where each delay is assumed to be equally spaced by one symbol period) and b) the fractionally-spaced model (where delays are assumed to be occurred within fractions of symbol period for several symbols period) of the proposed MIMO channel estimator. For each case, two types of channel models are employed: a) the block-invariant channel where its propagation coefficients are assumed to be

constant (throughout the entire channel estimation process and for every short block of T = 200 symbols period, after which they change to a new independent random values which they maintain for another T symbol periods, and so on) and b) the time-varying channel where coefficients are varied in time (for each pilot symbol and data symbol sent) according to the pre-selected Doppler velocities and related parameters, which will be described accordingly.

The simulated results will be categorised systematically to illustrate the influence of those main parameters involved for the MIMO channel estimation as follows:

i) M – the number of transmit antennas. ii) N – the number of receive antennas.
iii) v – the size of the pilot length.
iv) Number of paths (depending either symbol-spaced or fractionally-spaced models)

The MIMO configuration is defined as ($N\times M$) system. The size of the pilot length is represented by the order v of the Hadamard matrix that is employed to construct the pilot matrix $\mathbf{S}_F$ with its possible expansion using the higher order described in 4.2.3.5. The aim is to compare the performance of the proposed MIMO channel estimator under the influence of using different pilot length v for different system configurations and different models of channels in the frequency-selective fading MIMO environment.

Also, one vital reminder is that the proposed MIMO channel estimator (either symbol-spaced or fractionally-spaced models) assumes that the number of significant paths as well as the total delay spread are known *a priori* to the receiver in order to be able to carry out channel estimation for the frequency selective MIMO channel. (Refer Chapter 4 for details).

5.4.1 Performance of MIMO-CE in Symbol-Spaced Channel Model

For the symbol-spaced model, the MSE in (5.1) and (5.2) is again used as the performance metric with slight modification where the ordinary MIMO channel matrix $\mathbf{H}$ in (5.1) is replaced by the concatenated channel matrix $\mathbf{H}_{1|M}$ from (4.27) as well as its estimated value $\hat{\mathbf{H}}_{1|M}$ from (4.45). Similarly, the error matrix of the MIMO channel estimation, $\boldsymbol{e}_{\mathrm{H}}$ is obtained by subtracting the estimated $\hat{\mathbf{H}}_{1|M}$ from the actual $\mathbf{H}_{1|M}$ as follows:

$$\boldsymbol{e}_{\mathrm{H}} = \mathbf{H}_{1|M} - \hat{\mathbf{H}}_{1|M} \tag{5.3}$$

and the corresponding mean Frobenius norm squared error of $\boldsymbol{e}_{\mathrm{H}}$ can be obtained as:

$$E\left[\left\|\boldsymbol{e}_{\mathrm{H}}\right\|_F^2\right] = \frac{1}{(M\times(L+1)\times N)}\left[\sum_{i=1}^{N}\sum_{j=1}^{M\times(L+1)}\left|\varepsilon_{ij}\right|^2\right] \tag{5.4}$$

where ε_{ij} is the matrix element of $\boldsymbol{e}_{\mathrm{H}}$ with (i,j) entry and $E[.]$ is the expectation operator.

For reminder, there are (L+1) number of significant paths for each CIR of the "transmit-receive" sub-channel in symbol-spaced model. If the (L+1) number of significant paths increases, the pilot length v must also be expended to the next valid order according to the criterion in (4.35), so that the estimation can be sufficiently catered for all significant paths.

5.4.1.1 Performance in Block-Invariant Symbol-Spaced Channel Model

In this section, the symbol-spaced, block-invariant channel model is used. First, the performance of the proposed estimator with pilot matrix $\mathbf{S}_F$ constructed from either the ordinary Hadamard (OH) matrix or Paley-Hadamard (PH) matrix is shown. Two pilot length, v=24 and v=32 are used for both OH & PH matrix for a fixed (2×2) MIMO system with fixed (L+1) = 3 significant paths in each CIR of the frequency selective MIMO channel.

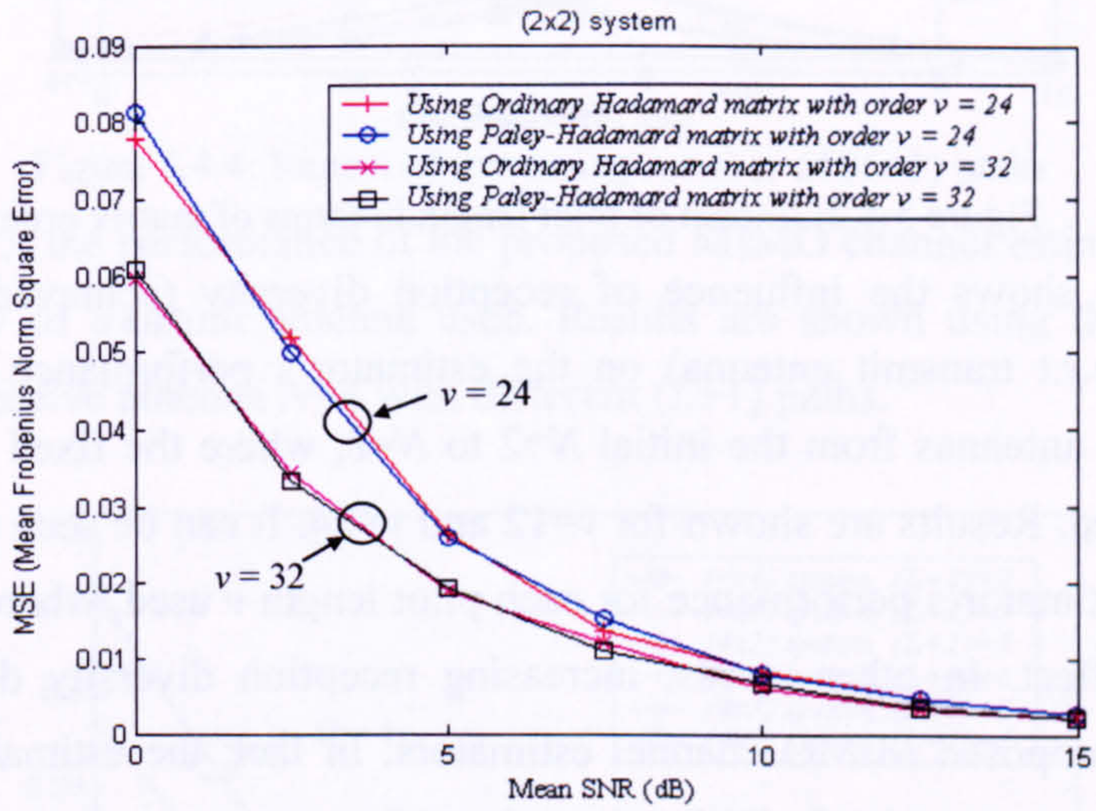

Figure 5.4.1: Performance comparison using OH and PH matrix with order v=24 and 32

It can be seen that the performance of the estimator improves as the mean SNR increases. Also, the performance for both case OH and PH pilot matrix appears to be almost identical for each v shown. This also demonstrates that the construction of pilot matrix using the Paley's method (described in Chapter 4) to achieve significant reduction in pilot length (for the same v value) results in no loss in the estimator's performance. Therefore, the PH type of pilot matrix will be consequently used throughout the rest of the results sections.

In figure 5.4.2, the impact of the pilot length v on the estimator's performance is shown. MSE is plotted against mean SNR with increasing v, for a fixed (N×M) = (2×2) system and (L+1) = 3. Results for different v = 12, 20, 24 and 32 are only presented here, although the result for minimum v = 8 may also be used (not shown in the result). The corresponding number of pilot symbols sent per transmit antenna is also stated. It can be observed that as v increases, the number of pilot symbols sent also increases, which in turn reduces the MSE,

thereby improving the performance of the proposed channel estimator. The results demonstrate the consistency of the channel estimation performance and the trade-off between the pilot length and the channel estimation error.

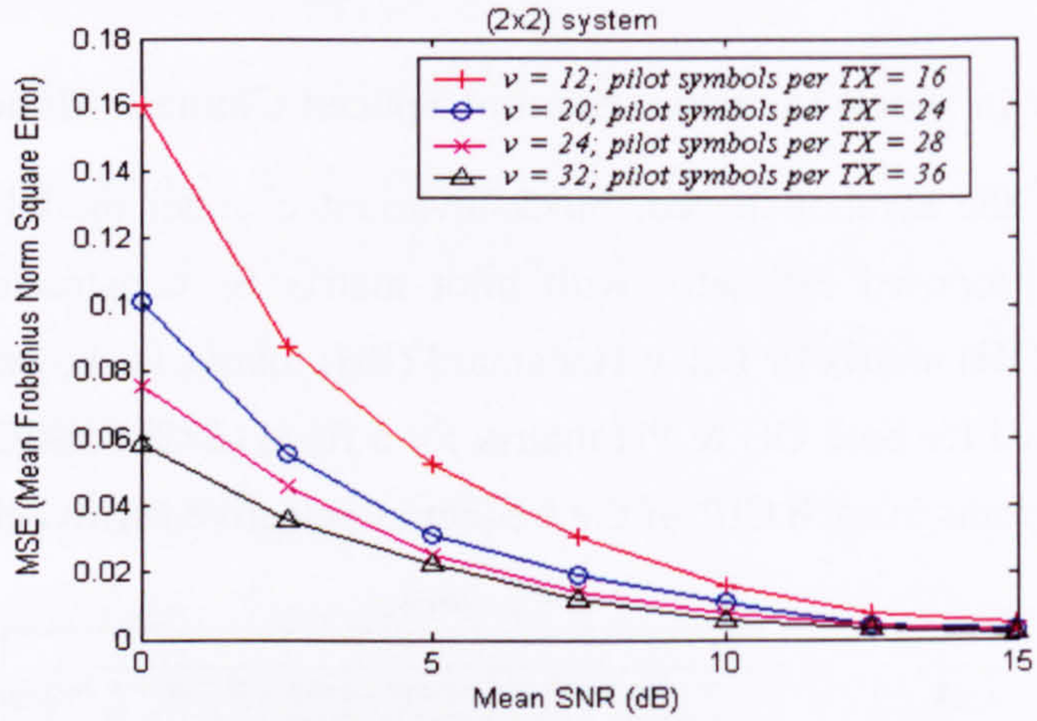

Figure 5.4.2: Impact of pilot length in terms of matrix order v

Figure 5.4.3 shows the influence of reception diversity (achieved by having more receive antenna w.r.t transmit antenna) on the estimator's performance by increasing the number of receive antennas from the initial N=2 to N=8, where the fixed value of M=2 and $(L+1) = 3$ is applied. Results are shown for v=12 and v=24. It can be seen that N has literally no effect on the estimator's performance for each pilot length v used, whereas changing v has a very obvious effect. In other words, increasing reception diversity does not offer any advantage to the proposed MIMO channel estimators. In fact, the estimator has to actually estimate more paths as a result of additional number of receive antennas.

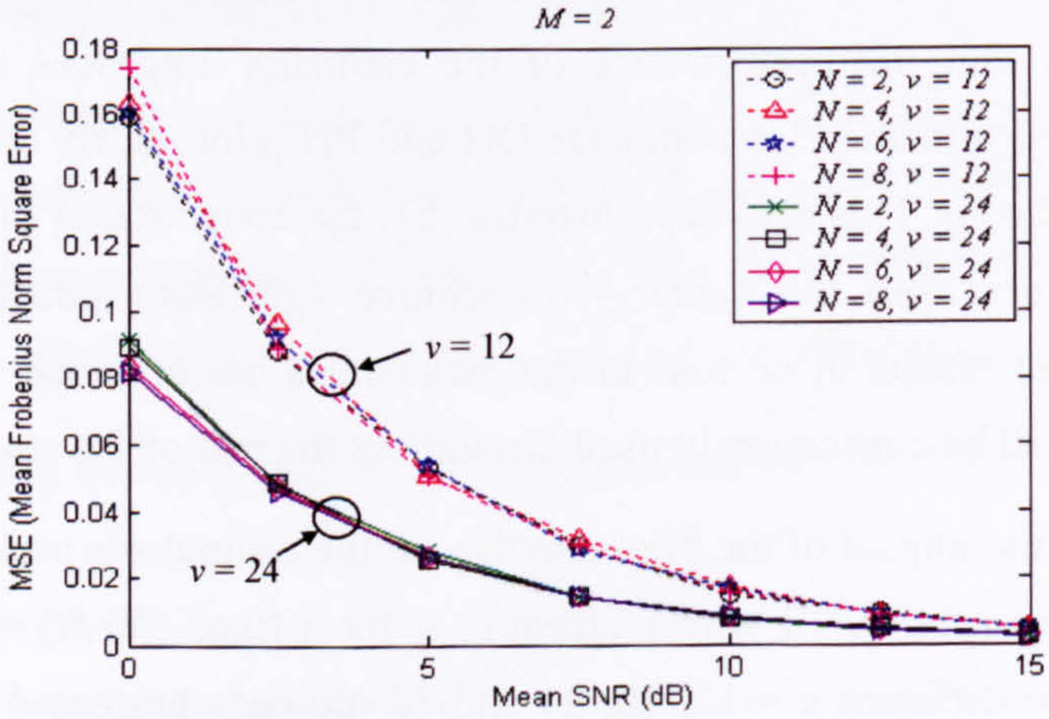

Figure 5.4.3: Impact of increasing number of receive antenna N

In figure 5.4.4, the estimator's performance is tested for increasing the number of $(L+1)$ paths from 3 to 8 in each CIR of the MIMO channel for a fixed (3×2) system. Results are

shown for two pilot matrix orders v=20 and v=32. It can be seen that, increasing the number of (L+1) paths also has no influence on the performance of the proposed channel estimator for either value of pilot matrix order in the block-invariant channel condition.

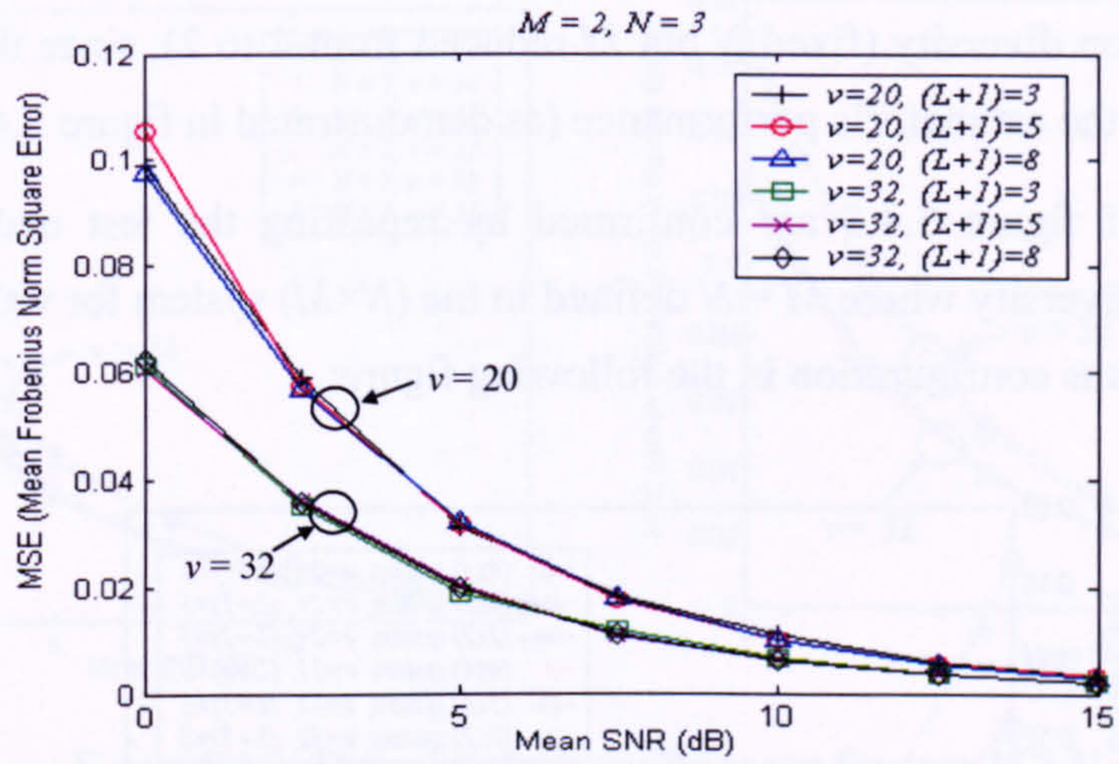

Figure 5.4.4: Impact of increasing number of (L+1) paths

In figure 5.4.5, the performance of the proposed MIMO channel estimation is examined against the number of transmit antenna used. Results are shown using the fixed v=32 and fixed number for receive antenna N=4 with different (L+1) paths.

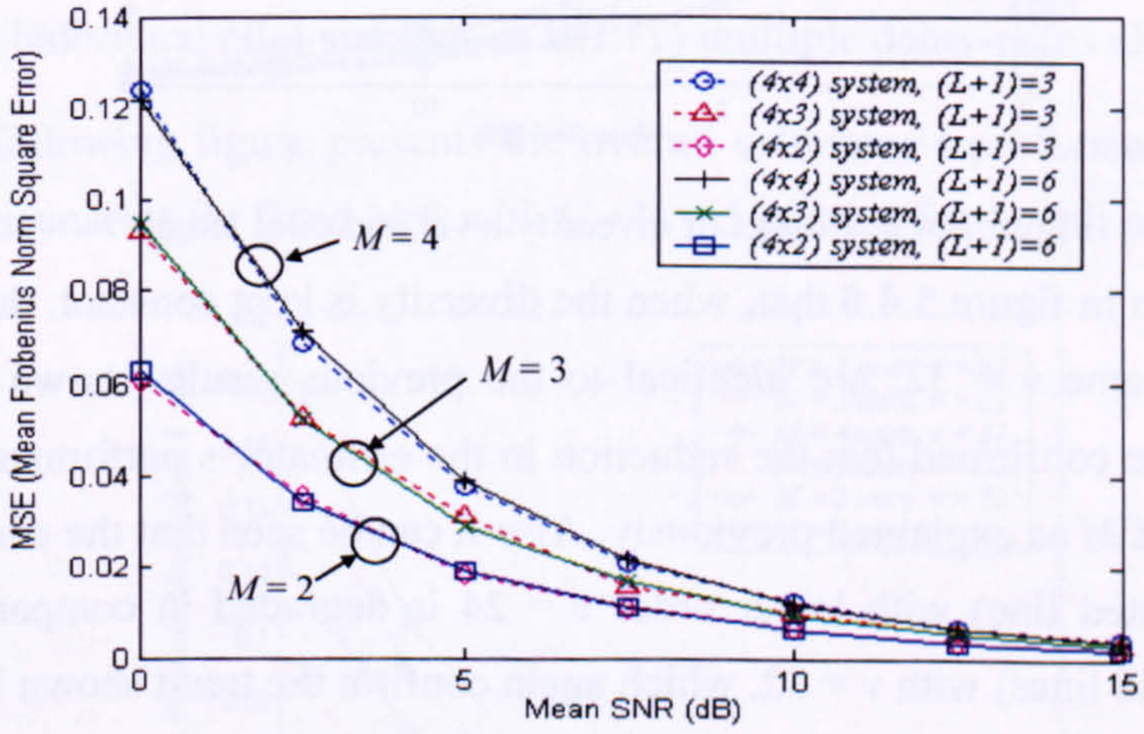

Figure 5.4.5: Impact of number of M transmit antenna used

It can be seen that as the number of transmit antennas increases from M = 2 to M = 4, the estimator's performance degrades accordingly for different mean SNR. Firstly, this is because as M increases, the transmit power for each antenna must also be reduced accordingly by a factor of M in order to maintain constant total transmit power to the receiver (to achieve the expected mean SNR value as described in section 2.3.2.1). Hence, the effective SNR is also reduced. Second reason is that the estimator has to deal with additional co-channel interferences (from other transmit antennas) as the number of transmit antennas increases.

However, it can also be seen that the variation in the number of (L+1) paths does not affect the estimator's performance, which confirm the trend shown in figure 5.4.4. Nevertheless, it must be stressed that the drop in estimator's performance is not due to the reduction in reception diversity (fixed N but M reduced from 4 to 2), since the diversity gain has no influence on the estimator's performance (as demonstrated in figure 5.4.3).

The results of figure 5.4.5 are confirmed by repeating the test under condition of constant degree of diversity where $M = N$ defined in the ($N \times M$) system for v=24 and v=32 and a fixed (L+1) = 5 paths configuration in the following figure:

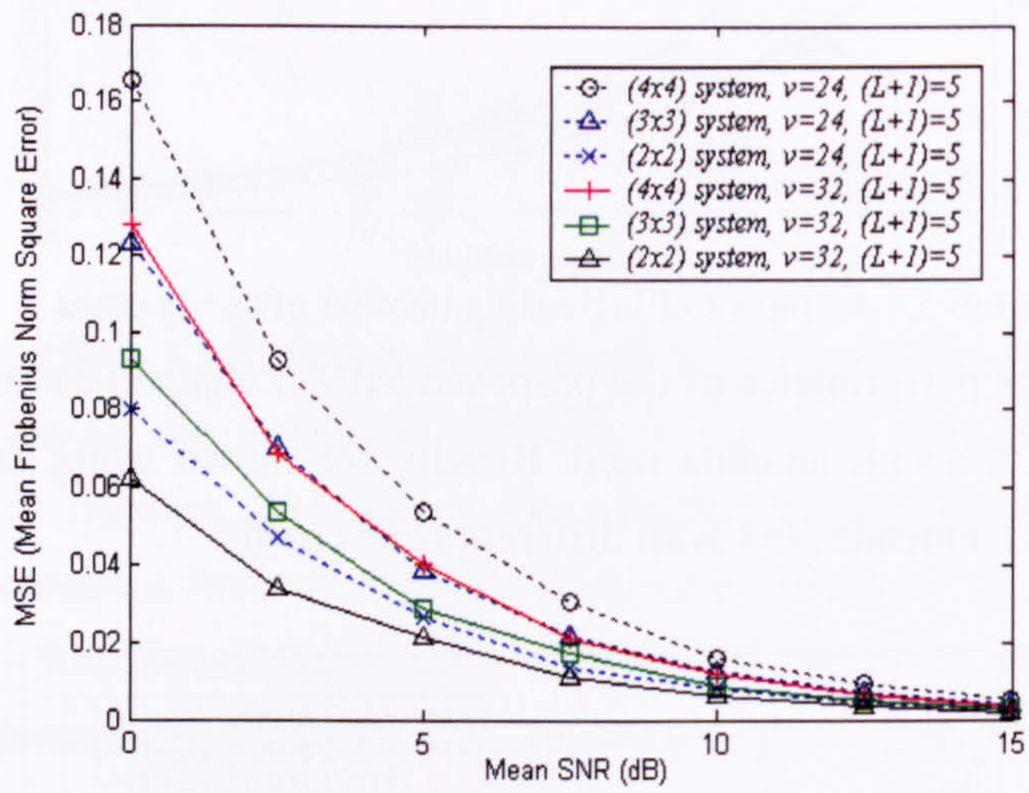

Figure 5.4.6: Impact of diversity level and pilot length v

It can be seen in figure 5.4.6 that, when the diversity is kept constant, the 3 results (with solid lines) with same v = 32, are identical to the previous results shown in figure 5.4.5. Therefore, it can be confirmed that the reduction in the estimator's performance is due to the increase in value of M as explained previously. Also it can be seen that the performance of the 3 results (with dotted line) with lower order v = 24 is degraded in comparison with the 3 bottom results (solid lines) with v = 32, which again confirm the trend shown in figure 5.4.2.

All the previous results from figure 5.4.1 to 5.4.6 are obtained based on the system configuration where $N \geq M$; i.e. the number of receive antennas N is either equal or greater than the number of transmit antennas M. This is the conventional setting for the OSIC MIMO equaliser described in Chapter 2. However, the proposed MIMO channel estimation method is also found to have an additional advantage, which is capable to perform under any setting of N and M for any number of (L+1) paths in the MIMO channel, even including the case where $M > N$. (Although symbol detection in $M>N$ case is only attainable by methods of space-time coding and transmit diversity mentioned in [49–54]; not discussed in this thesis).

In the following, the proposed estimator's performance is tested for $M \geq N$ case for both a) M=3 system and b) M=4 system with fixed $(L+1) = 3$ paths.

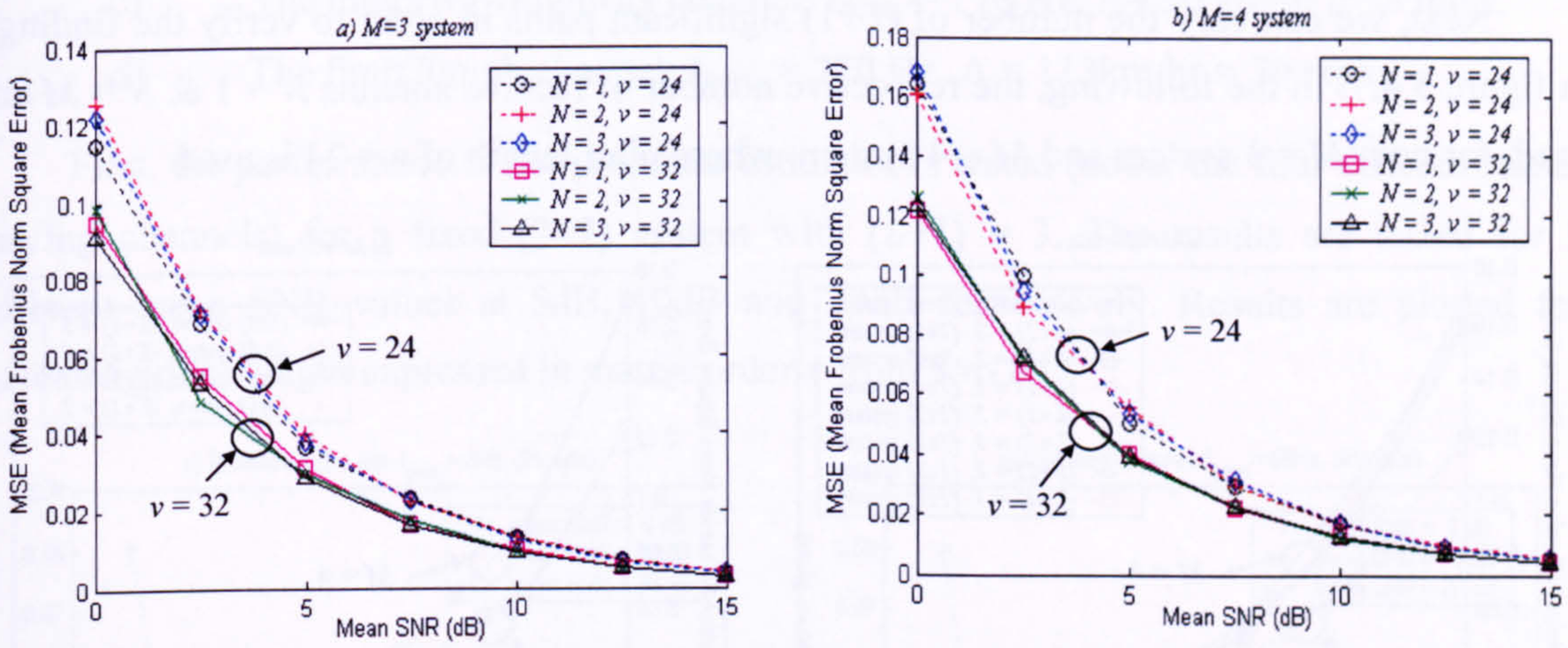

Figure 5.4.7: The estimator's performance for case $M \geq N$

It can be seen in figure 5.4.7 that the estimator's performance is again independent of N for each of the pilot matrix length used. This demonstrate the ability of the proposed MIMO channel estimator to perform in the system where $M \geq N$, which can also resemble the case of multi-user system where M can be viewed as the number of multi-users having a single antenna, sending individual pilot symbols in a $(L+1)$ multiple delay-paths channel.

Next, the following figure presents the overall estimator's performance of the $M \geq N$ case (multi-user scenario) for fixed N=3 with $(L+1) = 5$ paths. Pilot length of $v = 32$ is used.

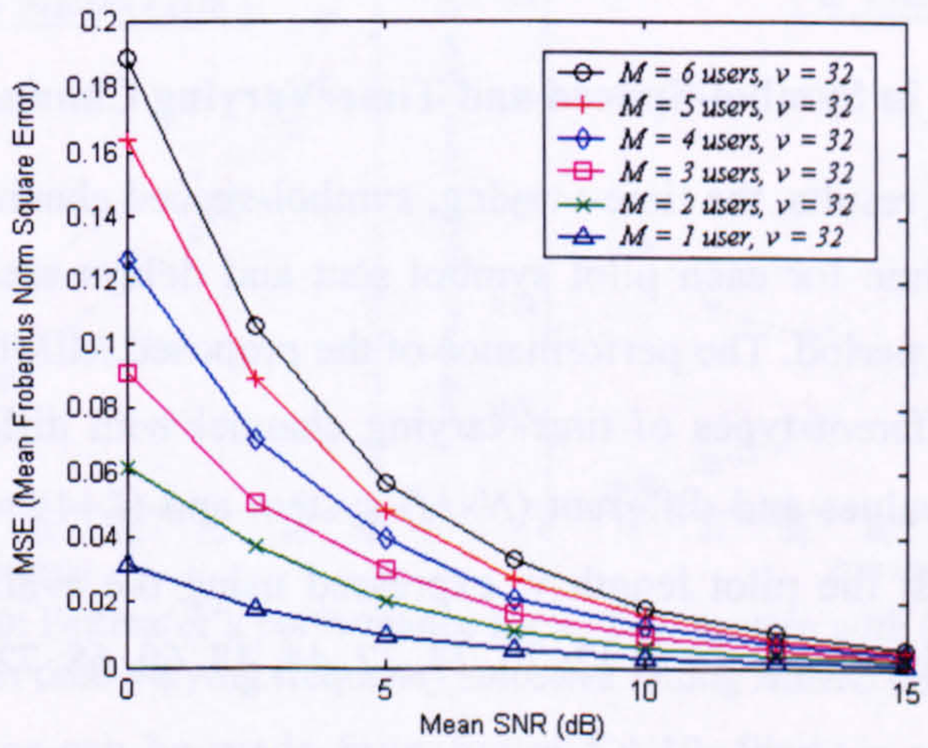

Figure 5.4.8: Estimator's performance for multi-user case with $v = 32$.

It can be seen in figure 5.4.8 that the estimator's performance degraded gradually as the value of M increases. Nevertheless, the performance depends on the order v that is employed in constructing the 'localised' pilot matrix for each user. (Recall the criteria in (4.60) for

obtaining v). Similarly, if the number of $(L+1)$ significant paths increase, v must also be increased to the next order to sufficiently cater the channel estimation for all users.

Next, we can vary the number of $(L+1)$ significant paths in order to verify the findings in figure 5.4.7. In the following, the respective number of receive antenna $N = 1$ & $N = M$ are used, for both $M = 3$ system and $M = 4$ system, where pilot length of $v = 24$ is used.

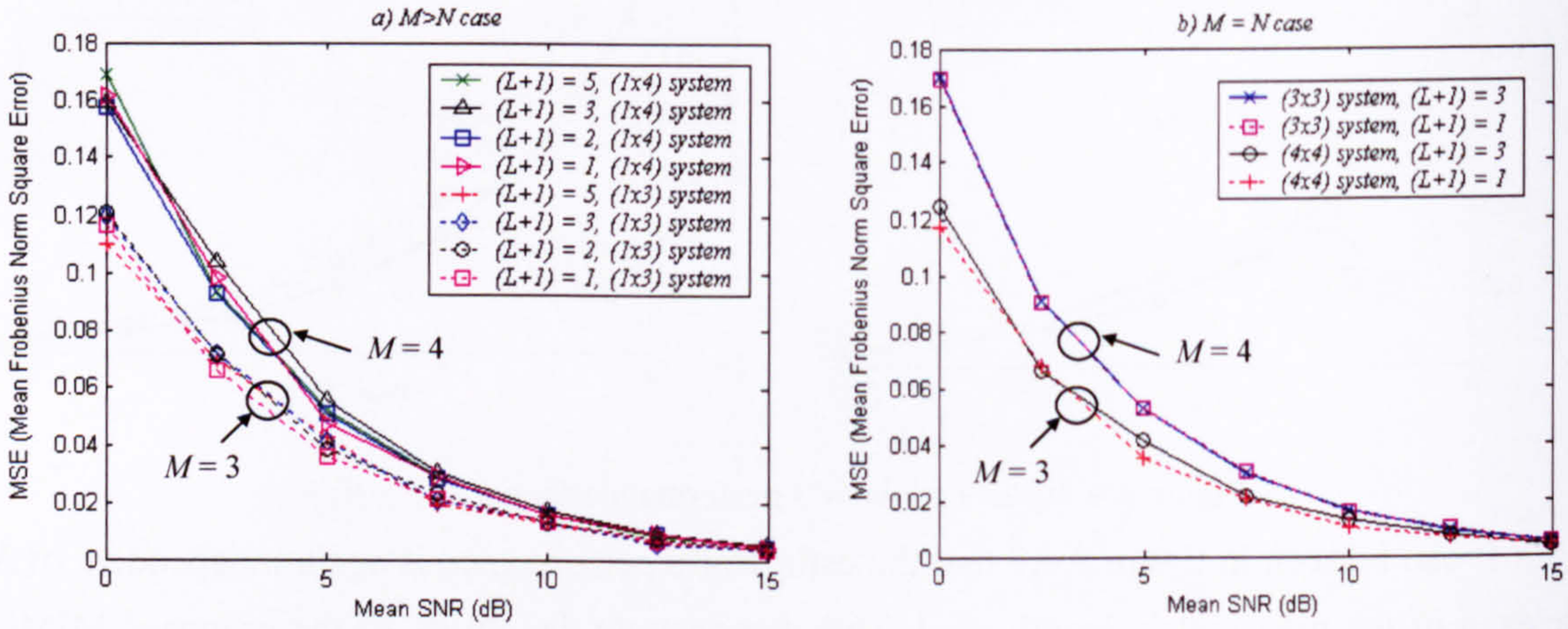

Figure 5.4.9: Impact of $(L+1)$ paths for a) $M > N$ case and b) $M = N$ case

In can be seen in figure 5.4.9a that the results are identical for different $(L+1)$ paths, confirming the trend seen in figure 5.4.7 and they remain consistent in each $(N \times M)$ system even only one receive antenna is used. On the other hand, the results in figure 5.4.9b demonstrate the frequency-flat MIMO channel scenario when $(L+1)$ reduces from 3 to 1. Again the results are identical in each $(N \times M)$ system for the $M = N$ case.

5.4.1.2 Performance in Symbol-Spaced and Time-Varying Channel Model

In the following results, the time-varying, symbol-spaced channel model is used, where channel varies with time for each pilot symbol sent and delays are assumed to be equally spaced by one symbol period. The performance of the proposed MIMO channel estimator will be shown using 4 different types of time-varying channel with different mobile velocities, different mean SNR values and different $(N \times M)$ system and $(L+1)$ paths configuration. The MSE is plotted against the pilot length v, expressed using the available valid order of the Paley-Hadamard matrix, where $v = 8, 12, 20, 24, 32, 44, 48, 60, 68, 72, 80, 84$ are shown.

The results are simulated at their maximum Doppler frequency f_{dmax} in each case using carrier frequency of $f_c = 2.11$GHz with the end-to-end data rate of $D_{total} = 480$Kbps. The data rate of individual transmit antenna D_{single} depends on the value of M where $D_{single} = D_{total} / M$.

The respective travel velocities Λ of the four different time-varying channels, together with their respective Doppler frequencies are given below:

a) The pedestrian channel: f_{dmax} = 6 Hz, Λ = 3 km/hr $\cong$ 0.833m/s.

b) The city/town channel: f_{dmax} = 88 Hz, Λ = 45 km/hr $\cong$ 28 mph.

c) The motorway/highway channel: f_{dmax} = 176 Hz, Λ= 90 km/hr $\cong$ 56 mph.

d) The limit70mph channel: f_{dmax} = 220 Hz, Λ = 113km/hr $\cong$ 70 mph.

First, the performance of the proposed estimator is tested (under the four different time-varying channels) for a fixed (2×2) system with (L+1) = 3. The results are tested for 3 different mean SNR values at 5dB, 10dB and 20dB respectively. Results are plotted for increasing pilot length expressed in matrix order v from 8 to 84.

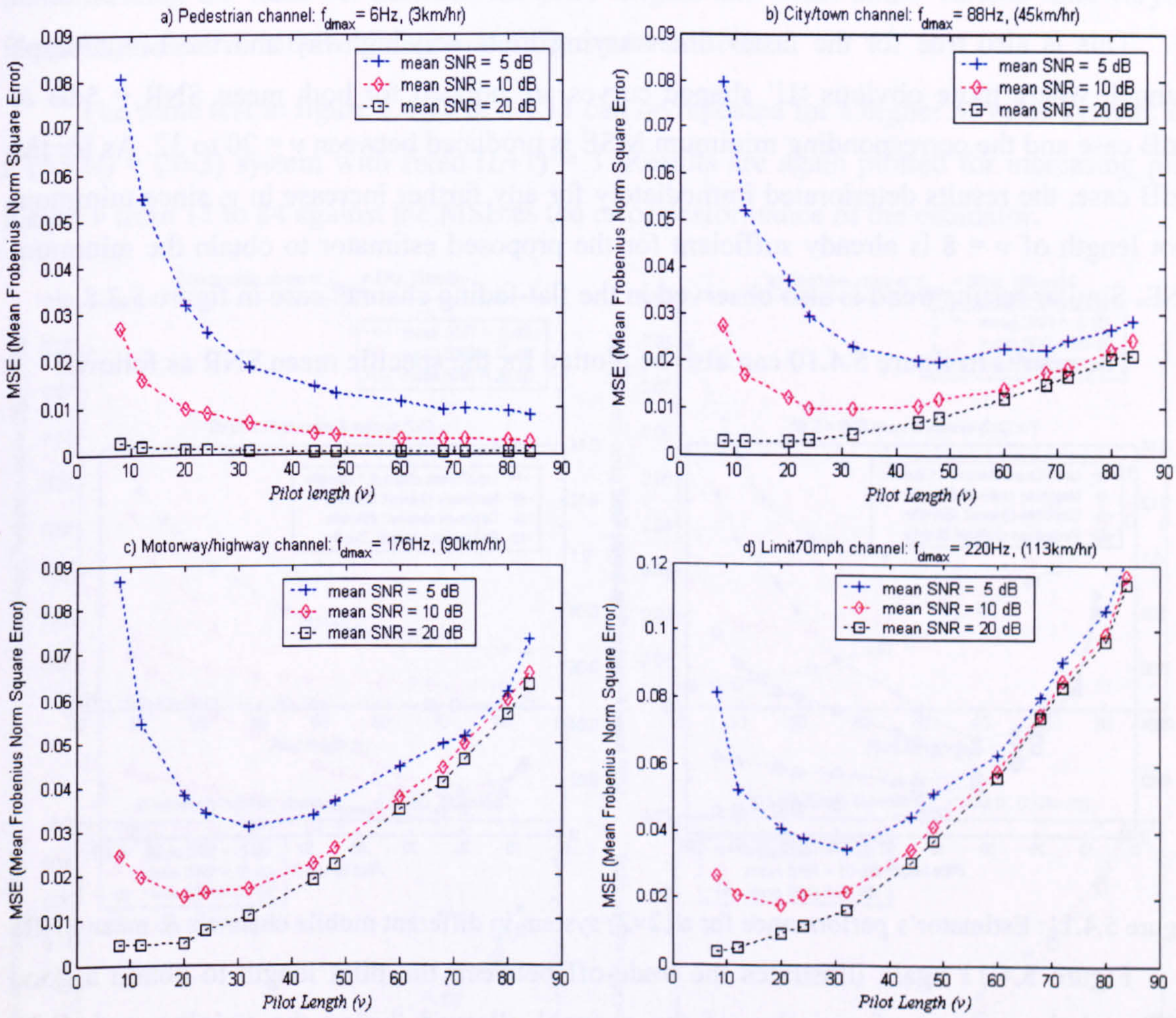

Figure 5.4.10: Estimator's performance for a (2×2) system with (L+1) = 3 in different time-varying frequency selective fading MIMO channels

Several observations can be made from figure 5.4.10. First, in a slower time-varying pedestrian channel, the results resemble the previous block-invariant case, where the error performance of the proposed estimator improves as the pilot length v increases. The figure shows that the convergence of the estimate becomes better as the SNR improves. In the 20dB case, the estimator converges within minimum v=8 and achieve a very low value of MSE.

As the mobile speed increases to higher time-varying city/town channel, it can be observed initially that the channel estimate improves as the pilot length v increases from $v = 8$ until a particular length (depending on the mean SNR values) where the MSE deteriorates afterward for further increases of v. The reason for this behaviour is due to variation of the channel during the training period. Initially, for short pilot lengths, the MSE of the estimator is dominated by inadequate training and the estimate improves v increases. However, while the training bits are being sent the time-varying channel characteristics are changing. Consequently, when the length of the pilot bits exceeds the channel coherence time the quality of the estimate worsen quite significantly.

This is also true for the faster time-varying motorway/highway and the Limit70mph channel, where more obvious 'U' shaped curves are noticed for both mean SNR = 5dB & 10dB case and the corresponding minimum MSE is produced between $v = 20$ to 32. As for the 20dB case, the results deteriorated immediately for any further increase in v, since minimum pilot length of $v = 8$ is already sufficient for the proposed estimator to obtain the minimum MSE. Similar results trend is also observed in the flat-fading channel case in figure 5.3.8.

The results in figure 5.4.10 can also be plotted for the specific mean SNR as follows:

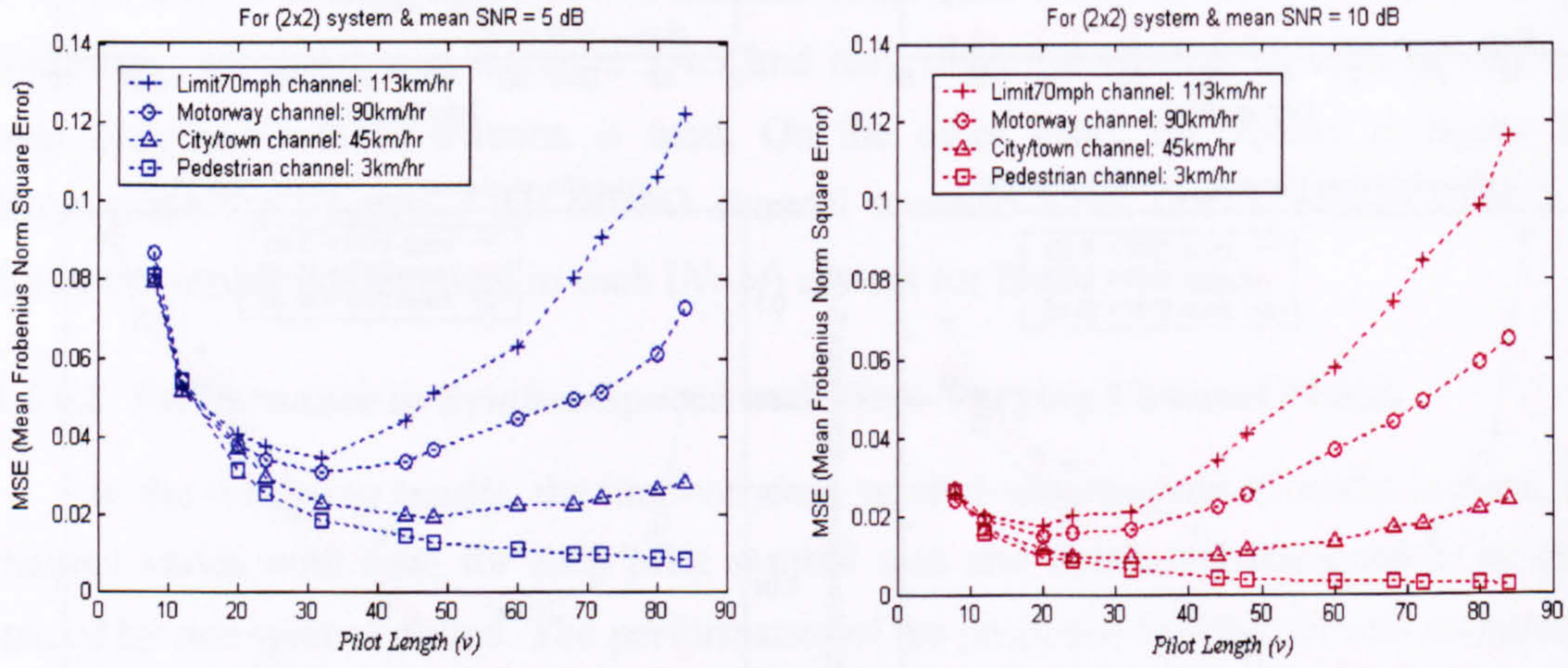

Figure 5.4.11: Estimator's performance for a (2×2) system in different mobile channels & mean SNR.

Figure 5.4.11 again illustrates the trade-off between the pilot length to obtain a good MSE and the amount of variation of the channel allowed during the training period for estimation over the frequency selective channel. The above results in figure 5.4.11 can be compared with results in figure 5.3.9 (for flat-fading channel). It is observed under the same velocity that although the channel suffers from frequency selectivity with $(L+1) = 3$ delay paths, the MSE results are still very much identical as compared to the frequency-flat case. This demonstrates the ability of the proposed MIMO-CE method also working efficiently in frequency selective MIMO channel. (In fact, more channel coefficients are to be estimated).

The proposed MIMO-CE technique and the use of Paley-Hadamard matrix for the pilot matrix not only permit minimum pilot symbols sent but also allow the channel estimation to be completed within shorter possible time with minimum variation in channel. Nevertheless, such comparison is trivial since consideration of relative channel variation within the delays of the frequency-selective paths is difficult to be analysed. The MSE performance under different (L+1) paths are expected to be slightly worsen (shown later in figure 5.4.16).

The same test in figure 5.3.10 & figure 5.3.11 is repeated for the (3×3) system and the results are presented in Appendix-B5. The similar results trend can also be observed therein, demonstrating the trade-off between the pilot lengths and MSE under various time-varying frequency selective MIMO channels at different mean SNR.

The same test in figure 5.4.10 & 5.4.11 can be repeated for a higher M value system; i.e. a (N×M) = (3×3) system with fixed (L+1) = 3. Results are again plotted for increasing pilot length v from 12 to 84 against the MSE as the error performance of the estimator.

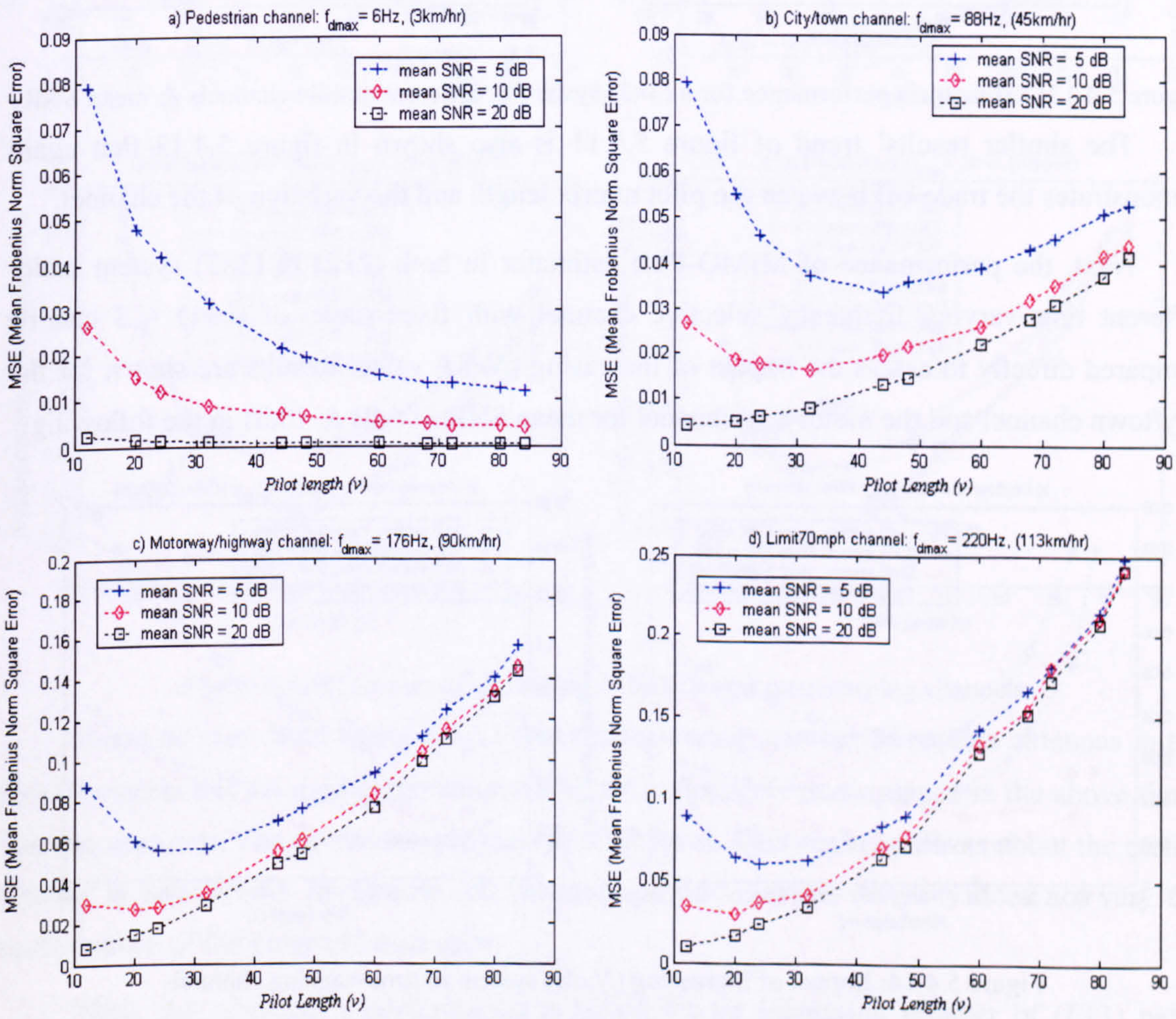

Figure 5.4.12: Estimator's performance for a (3×3) system with (L+1) = 3 in different time-varying channels

Similar trends in the results of figure 5.4.10 can also be observed in figure 5.4.12. However, note that all results are started from pilot length of $v = 12$ instead of $v = 8$ since this is the minimum required matrix order for the pilot matrix construction (using Paley's method) for the (3×3) system with $(L+1) = 3$. Subsequently, the results of different mobile channels in figure 5.4.12 can also be plotted for the specific mean SNR values as follows:

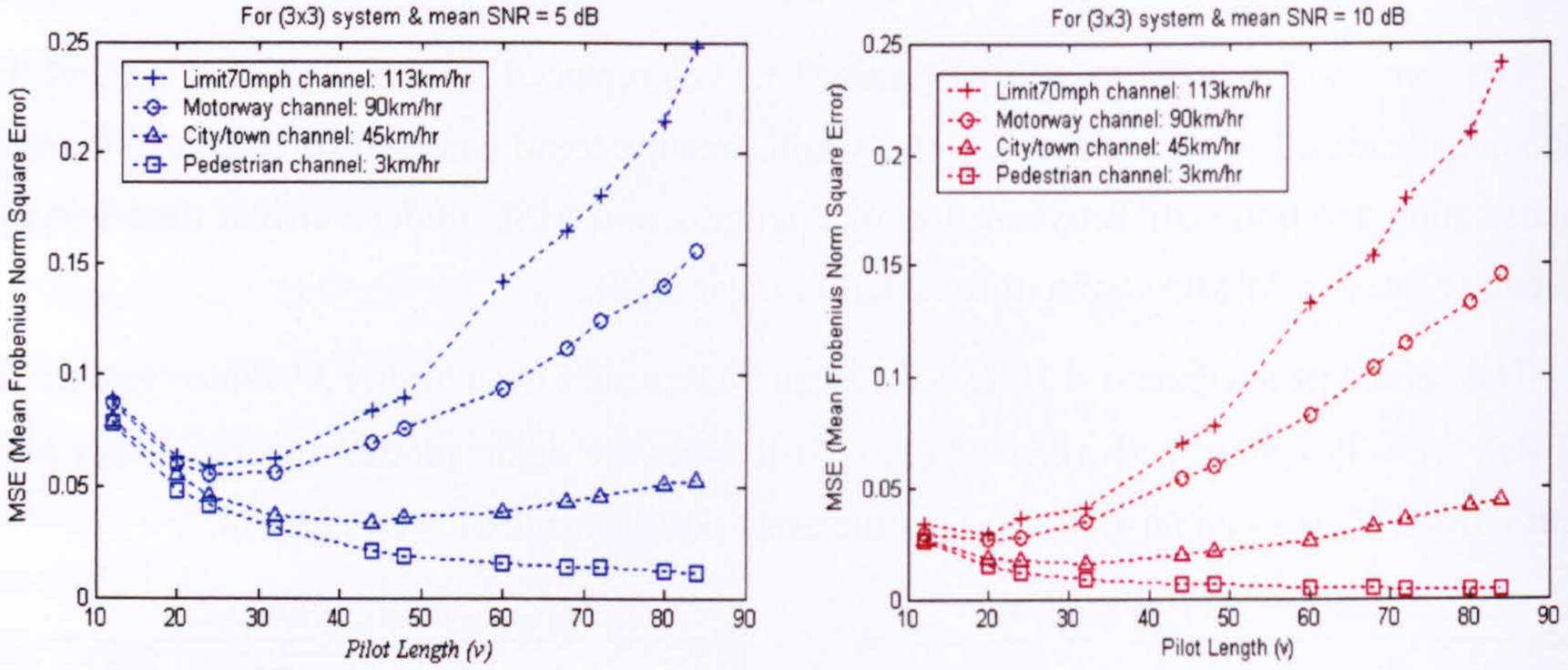

Figure 5.4.13: Estimator's performance for a (3×3) system in different mobile channels & mean SNR.

The similar results' trend of figure 5.4.11 is also shown in figure 5.4.13 that again demonstrates the trade-off between the pilot matrix length and the variation of the channel.

Next, the performance of MIMO-PMI estimator in both (2×2) & (3×3) system under different time-varying frequency selective channel with fixed paths of $(L+1) = 3$ can be compared directly to assess the impact of increasing $(N \times M)$ value. Results are shown for the city/town channel and the motorway channel for mean SNR of 5dB & 10dB in the following:

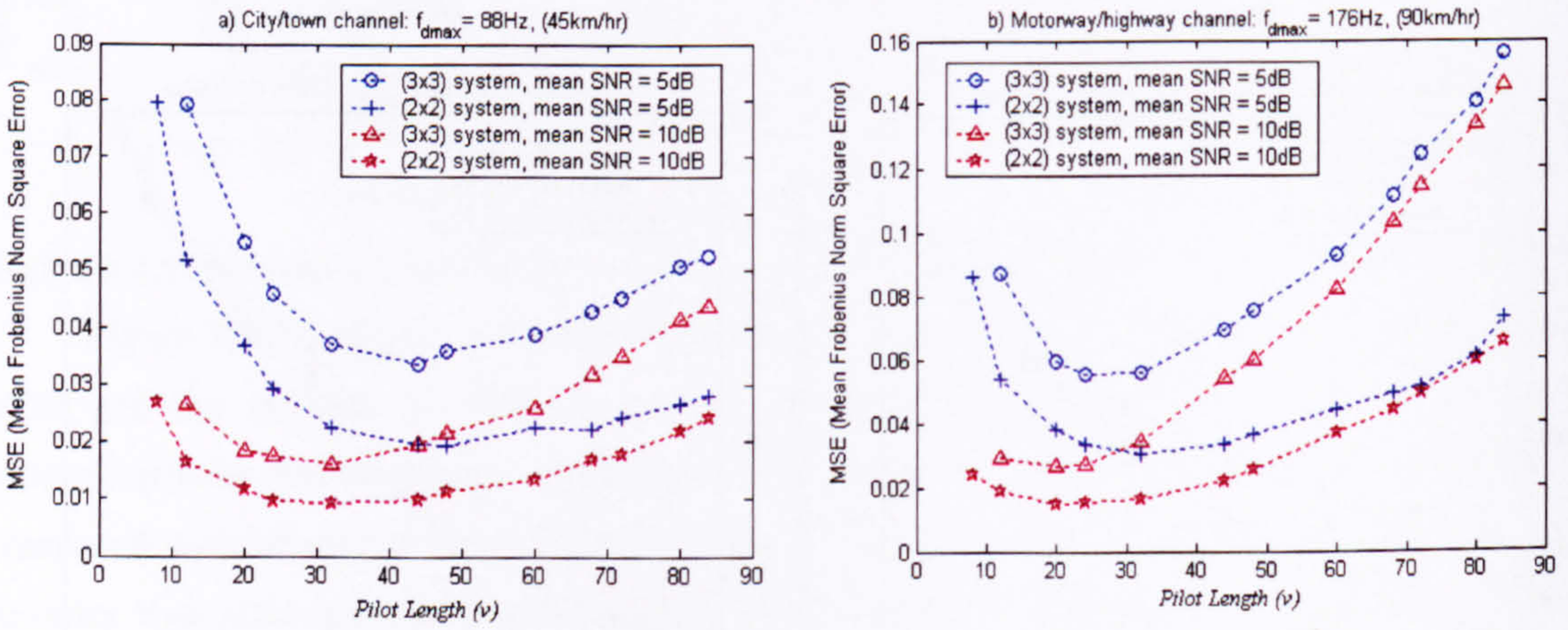

Figure 5.4.14: Impact of increasing $(N \times M)$ system in time-varying channel

It can be seen that the (2×2) system always performs better than the (3×3) system at the respective mean SNR values, for the two types of channels shown above. For the same value

of v, the MSE for the $M = 3$ system is higher compared with the $M = 2$ system. The reason for this has been explained in figure 5.4.5 for the same test in the block-invariant channel.

Next, results are presented to assess the impact of reception diversity that has on the estimator's performance for increasing number of receive antennas, N, for a fixed M=2 system and $(L+1) = 3$. Results are plotted for two different mean SNR level at 5dB and 20dB, for all the four different time-varying channels in the following figures:

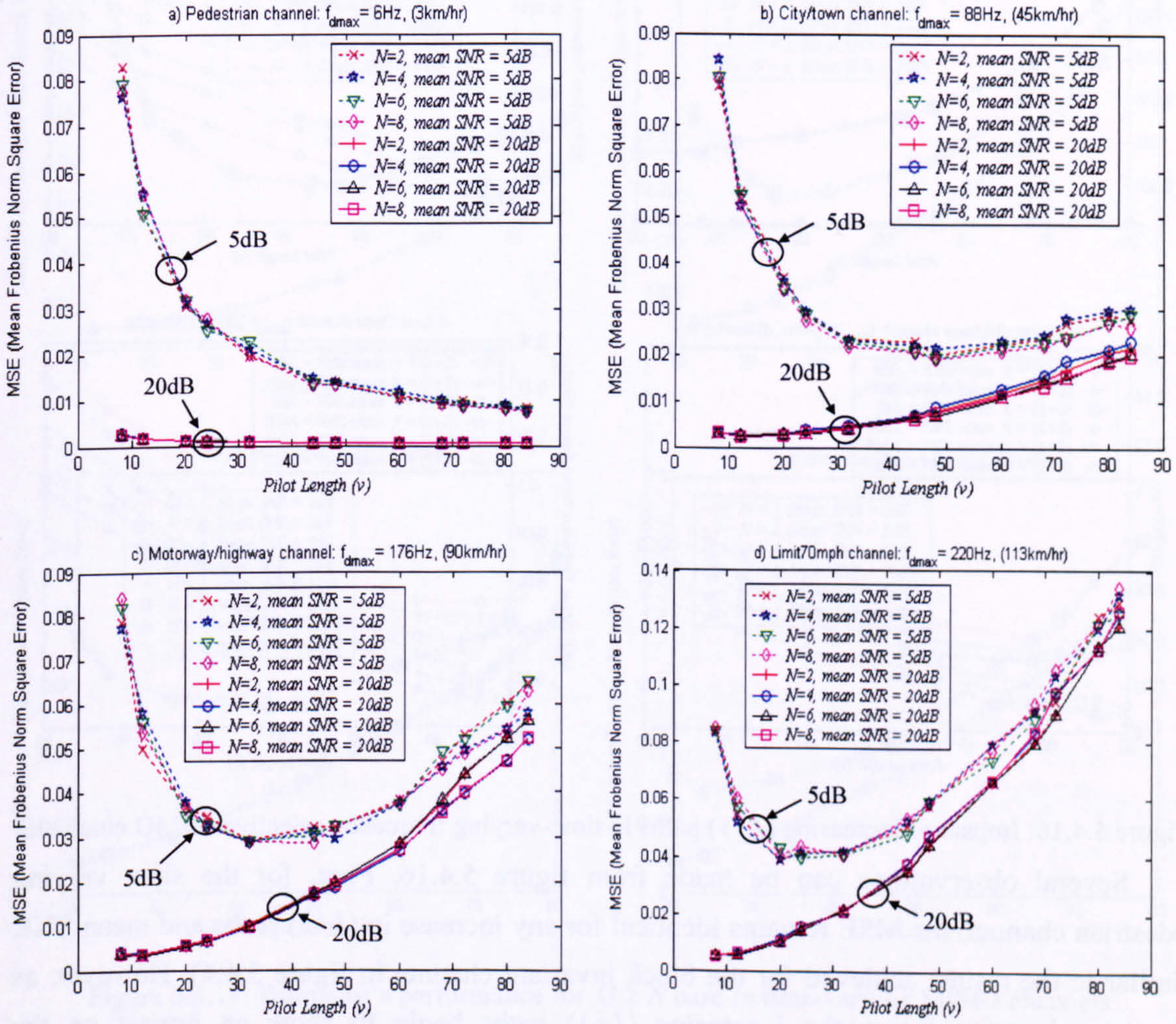

Figure 5.4.15: Impact of increasing N in different time-varying channels

It can be seen from figure 5.4.15 that the increasing number of receive antennas in the $(N\times M)$ system has no significant influence on the estimator's performance in the above time-varying channels. The results are identical at SNR level. This again confirms about the earlier finding in figure 5.4.3 & figure 5.4.7 concluding that reception diversity does not vary the performance of the proposed estimator.

Next, the estimator's performance is tested for an increasing number of $(L+1)$ paths (from 3 to 9 paths in each CIR) for a fixed (2×2) system for the four different time-varying

frequency selective MIMO channels. The results are shown for two different mean SNR values at 5dB and 20dB, for increasing pilot matrix lengths v from 20 to 80.

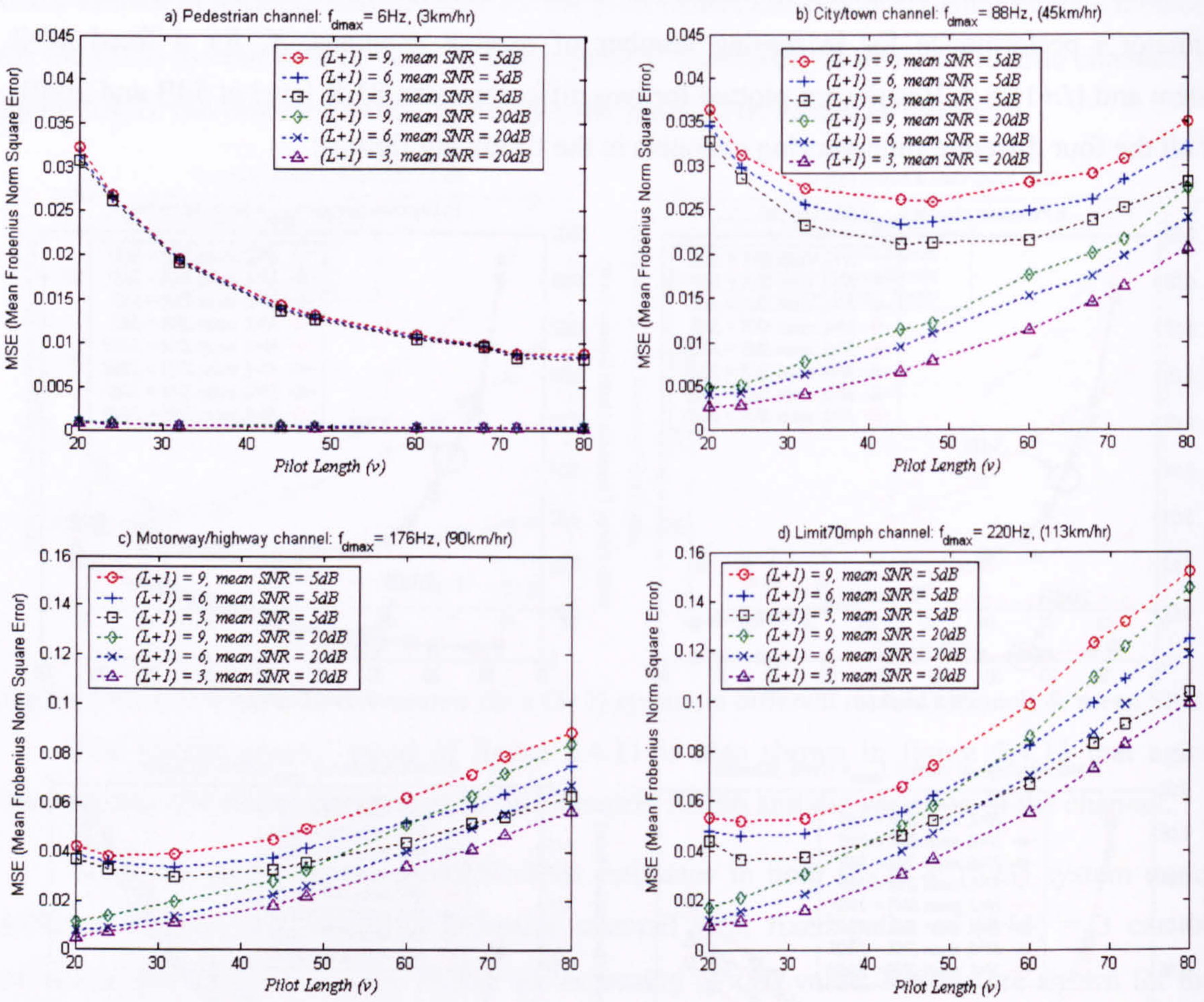

Figure 5.4.16: Impact of increasing (L+1) paths in time-varying frequency selective MIMO channels

Several observations can be made from figure 5.4.16. First, for the slow varying pedestrian channel, the MSE remains identical for any increase in (L+1) paths and mean SNR (similar to the results achieved for the block invariant channel in figure 5.4.4). However, as the channel varies faster, the increasing (L+1) paths begin to show an impact on the estimator's performance. Higher number of (L+1) paths would cause the MSE performance to deteriorate accordingly. This could be due to the fact that increasing number of (L+1) paths increases the estimator's process time for dealing with the extra frequency selectivity which in turn causes further deviation in the channel variation within the delays itself, results in poorer estimation. The (L+1) = 3 paths case has better error performance since the deviation of the channel variation is smaller compared to the (L+1) = 9 paths case. The results also demonstrate that having severe time variation either in the frequency selective MIMO channel itself or within its delay paths could greatly affect the estimator's accuracy and further degrade the MSE performance of the proposed channel estimator.

In the following four figures, the results are presented for the case where the number of transmit antennas is greater or equal to the number of receive antennas, (the $M \geq N$ case), using a fixed $(L+1) = 3$ paths for the both time-varying city/town & motorway channels. Results are plotted for both the $M = 3$ system and $M = 4$ system.

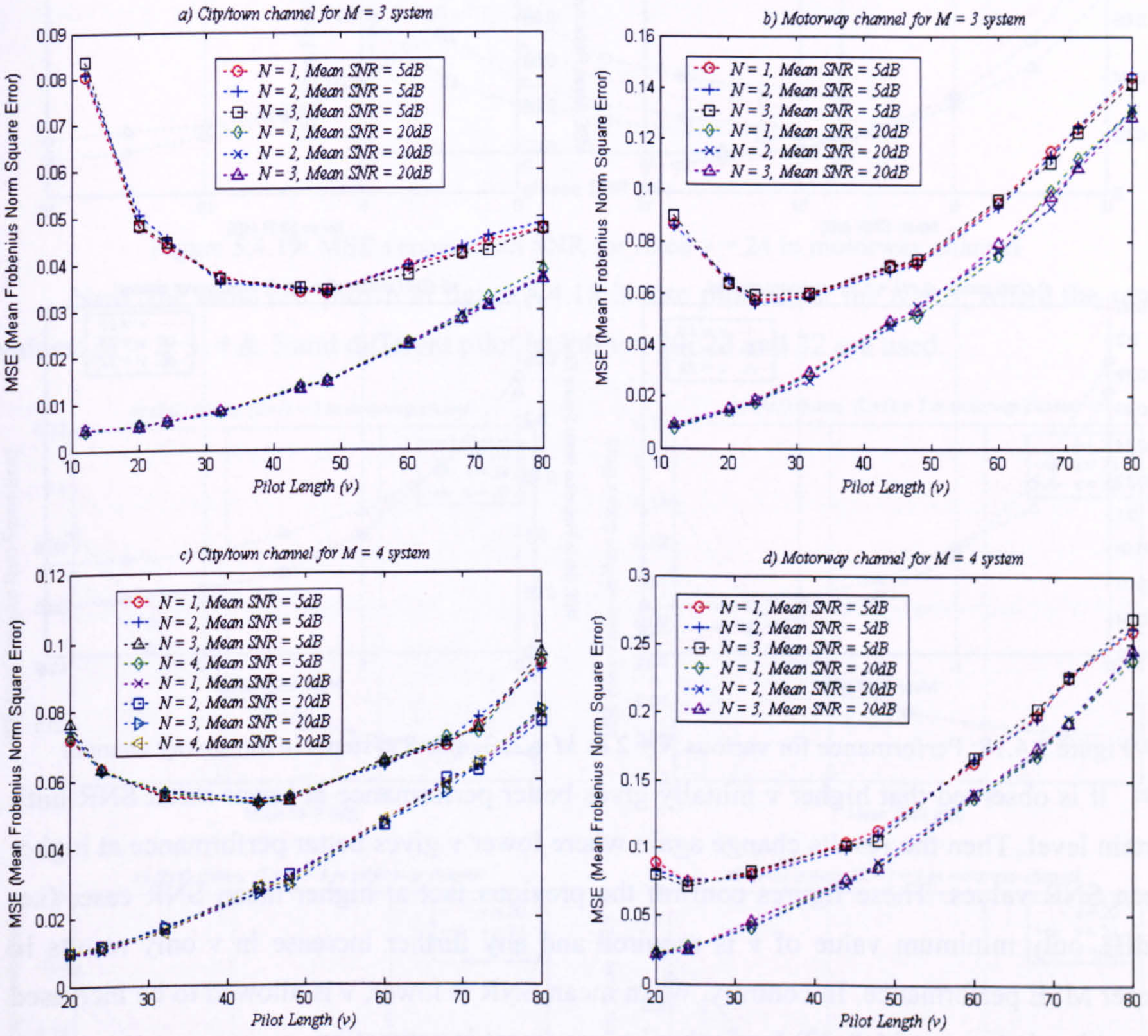

Figure 5.4.17: Estimator's performance for $M \geq N$ case in time-varying MIMO channels

First, it can be seen that the results are independent of N for both mean SNRs, thus confirming again the results seen earlier in figure 5.4.7. Secondly, the results also show the ability of the proposed estimator to perform under various time-varying frequency-selective fading channel for $M \geq N$ case.

Next, figure 5.4.18 shows the MSE performance of the proposed estimator as a function of SNR, for a fixed $N = 2$ system with $M = 2$, 3, 4 & 5 and also for different pilot matrix lengths of $v = 20$, 24 and 32. These results are obtained for the time-varying frequency selective motorway channel with fixed $(L+1) = 3$ paths.

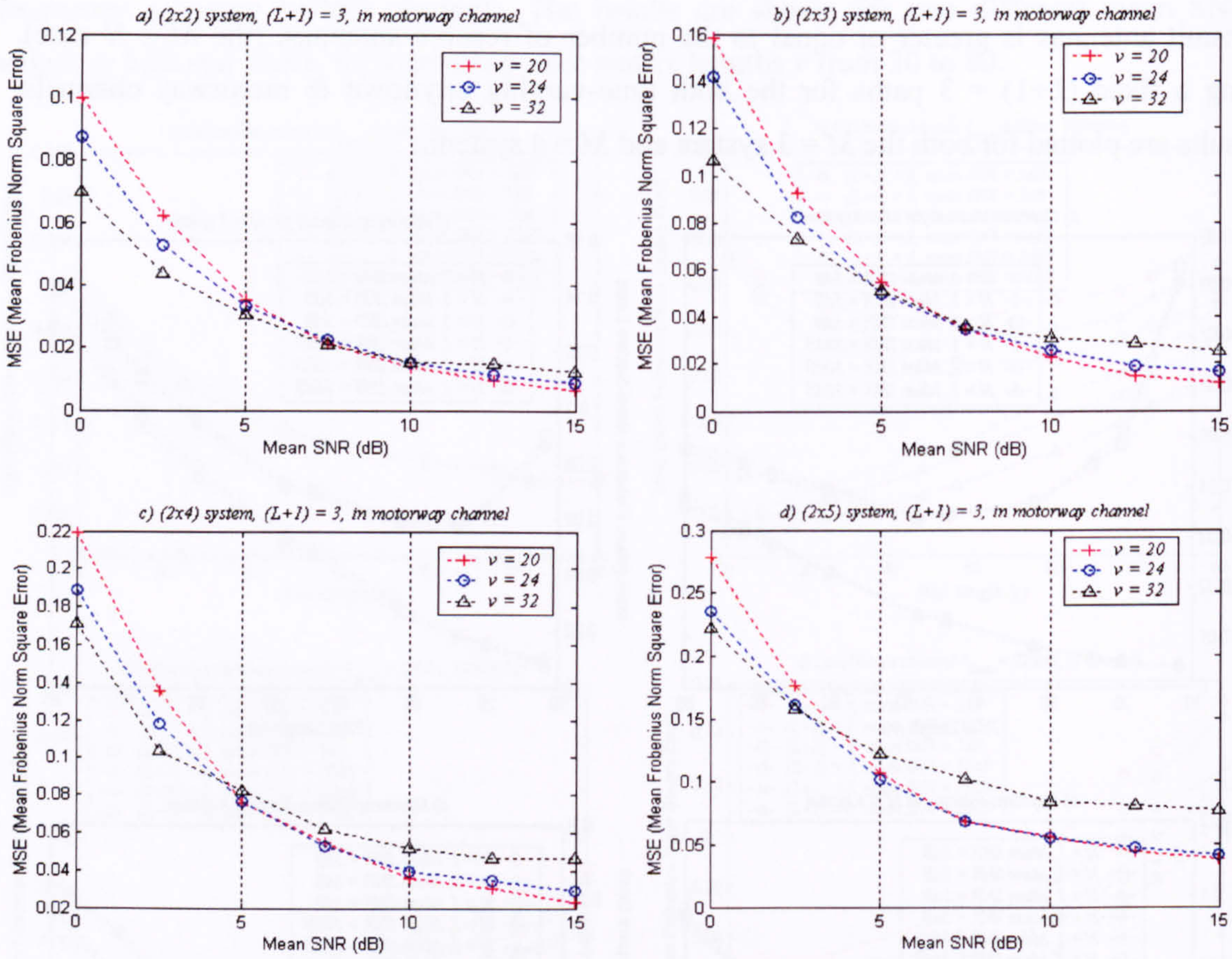

Figure 5.4.18: Performance for various $N = 2$ & $M = 2, 3, 4$ & 5 systems in motorway channel

It is observed that higher v initially gives better performance at lower mean SNR until certain level. Then the results change again where lower v gives better performance at higher mean SNR values. These figures confirm the previous fact at higher mean SNR case; (i.e. 15dB), only minimum value of v is required and any further increase in v only results in poorer MSE performance. In contrary, when mean SNR is lower, v is allowed to be increased to next levels (i.e. $v = 24$ & 32) for further improvement in estimation.

However, if v is too high, the performance deteriorates again due to the variation in the respective time-varying channels during the training period. In addition, for each ($N \times M$) system, the 'switching' level moves backward in mean SNR as M increases because overall MSE value also increases with M. (This trend is only obvious in the more rapid channel; i.e. the motorway and the limit70mph channels. The slower pedestrian and city/town channels exhibit similar results to those shown previously for the block-invariant MIMO channel)

It can also be noticed that different error floor existed for each value of v in each case of M and the error floor gets higher as M increases from 2 to 5. The error floor also represents the best performance of the estimator for different pilot length v used. As M increases, the MSE gets poorer, which can be shown by comparing the above results for $v = 24$ as follows:

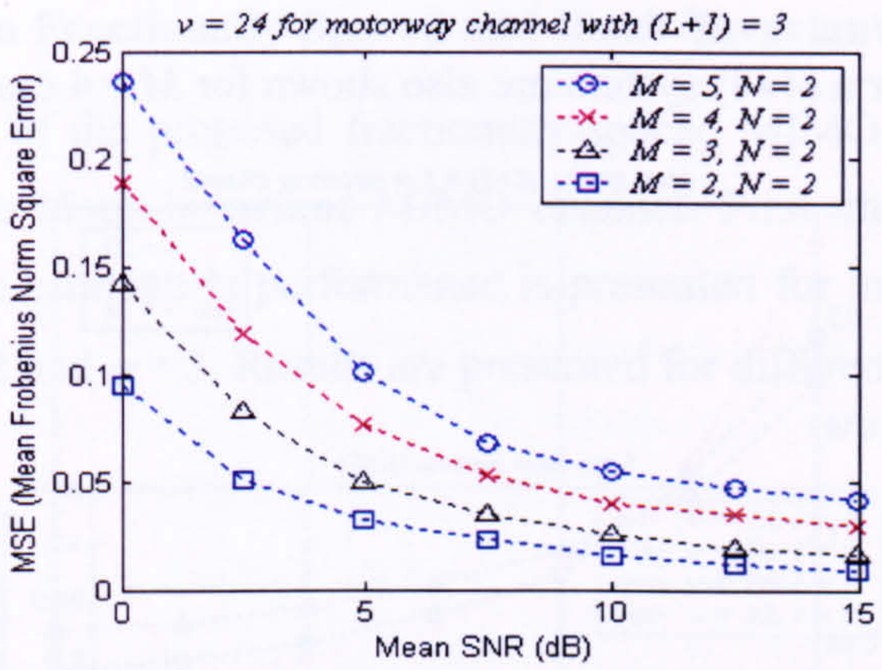

Figure 5.4.19: MSE versus mean SNR for fixed $v = 24$ in motorway channel

Next, the same test shown in figure 5.4.18 is also plotted for the $N = 3$, where the same values: $M = 2$, 3, 4 & 5 and different pilot length $v = 20$, 24 and 32 are used.

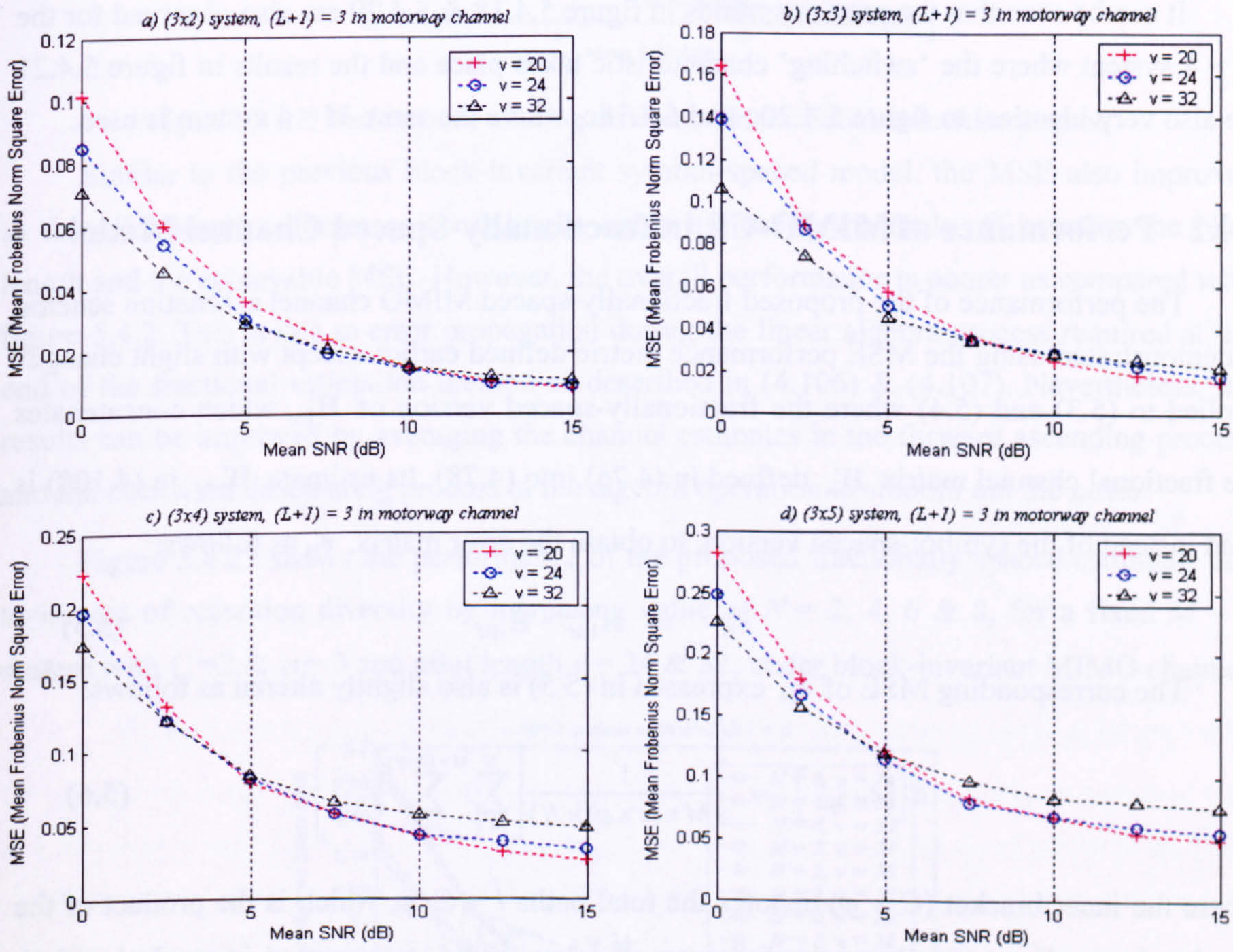

Figure 5.4.20: Performance for various $N = 3$ & $M = 2$, 3, 4 & 5 systems in motorway channel

It can be observed from figure 5.4.20 that the results are similar to the results in figure 5.4.18 and this also confirms the finding in figure 5.4.17 where changing N does not have any influence on the estimator's performance. The similar trends from figure 5.4.19 can also be seen in figure 5.4.20 where the error floor gets poorer as the value of M increases.

Lastly, the results for a (4×4) system are also shown for $M = 4$ case.

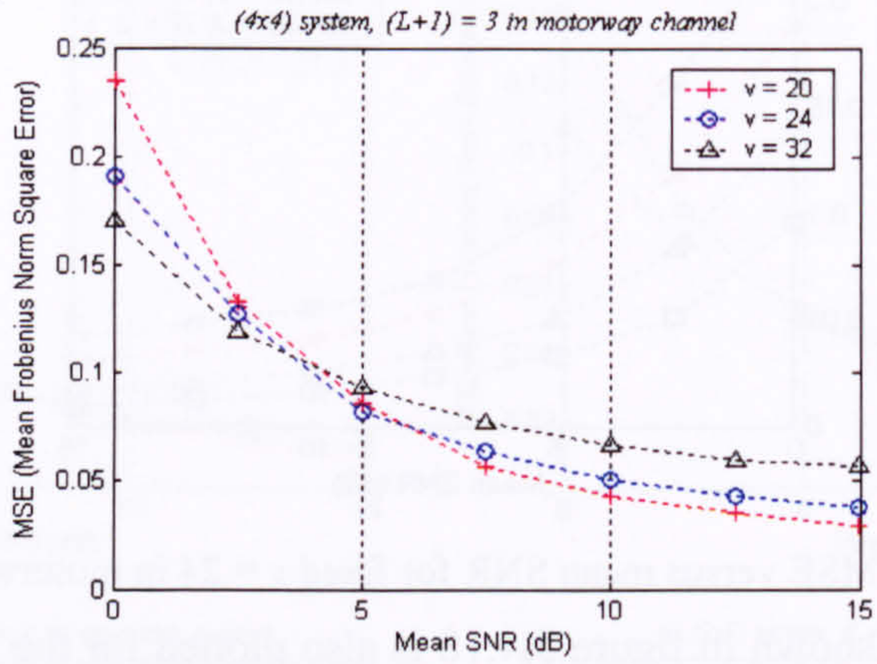

Figure 5.4.21: Performance for (4×4) system in motorway channel

It can be seen that the previous trends in figure 5.4.18 & 5.4.20 are also observed for the $M = 4$ system where the 'switching' characteristic takes place and the results in figure 5.4.21 are also very identical to figure 5.4.20c and 5.4.18c, where the same $M = 4$ system is used.

5.4.2 Performance of MIMO-CE in fractionally-Spaced Channel Model

The performance of the proposed fractionally-spaced MIMO channel estimation scheme is demonstrated using the MSE performance metric defined earlier except with slight changes applied to (5.3) and (5.4) where the fractionally-spaced version of $\mathbf{H}'_{1|M}$ which concatenates the fractional channel matrix $\mathbf{H}'_m$ defined in (4.75) into (4.78). Its estimate $\hat{\mathbf{H}}'_{1|M}$ in (4.108) is used instead of the symbol-spaced version, to obtain the error matrix, $\boldsymbol{e}'_{\mathrm{H}}$ as follows:

$$\boldsymbol{e}'_{\mathrm{H}} = \mathbf{H}'_{1|M} - \hat{\mathbf{H}}'_{1|M} \tag{5.5}$$

The corresponding MSE of $\boldsymbol{e}'_{\mathrm{H}}$ expressed in (5.5) is also slightly altered as follows:

$$E\left[\left\|\boldsymbol{e}_{\mathrm{H}}\right\|_F^2\right] = \frac{1}{(M\times(c\times\varphi)\times N)}\left[\sum_{i=1}^{N}\sum_{j=1}^{M\times(c\times\varphi)}\left|\varepsilon_{ij}\right|^2\right] \tag{5.6}$$

where the inner bracket ($C \times \varphi$) denotes the total paths $l = C\times\varphi$, which is the product of the fractional sampling rate, C and the full-span of delay spread φ expressed in symbol period. Uniform fractionally-spaced model in section 4.3 is considered here for maximum number of paths setting in the simulation. Note that in the case of the proposed fractionally-spaced MIMO channel estimator, the total delay spread φ is assumed to be known *a priori* to both the transmitter & receiver in order to carry out channel estimation in the fractionally-spaced delay model for frequency selective MIMO channel. (Refer section 4.3.2.6 for details).

5.4.2.1 Performance in Fractionally-Spaced and Block-Invariant Channel Model

The performance of the proposed fractionally-spaced MIMO-CE scheme is shown in the following using the **block-invariant** MIMO channel. First, the impact of pilot matrix length v that has on the estimator's performance is presented for increasing value of v for a (2×2) system with $C = 2$ and $\varphi = 3$. Results are presented for different v = 12, 20, 24 & 32 as:

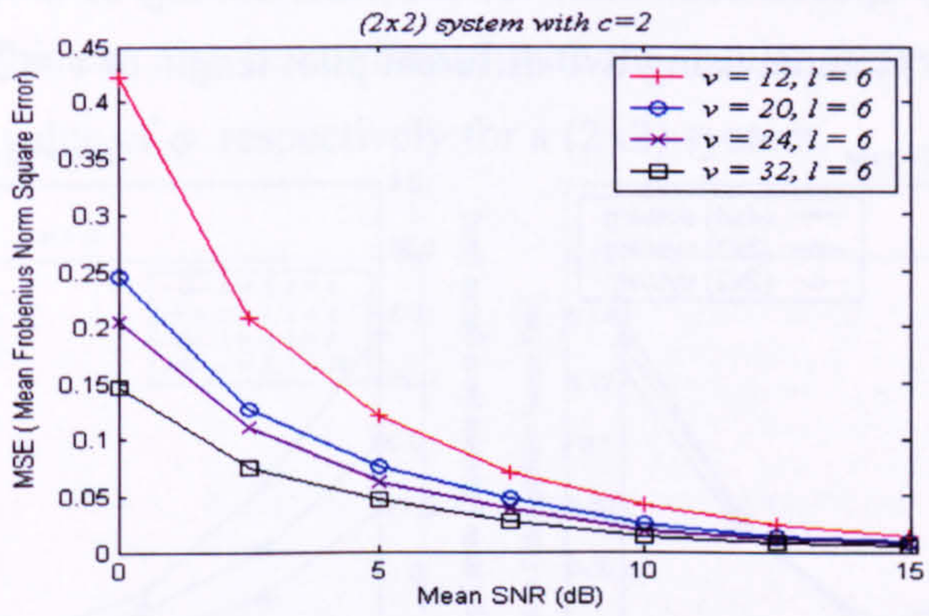

Figure 5.4.22: Performance of using different v in fractional estimation method

Similar to the previous block-invariant symbol-spaced model, the MSE also improves as the pilot length v increases accordingly, again indicating the trade-off between the pilot length and the achievable MSE. However, the overall performance is poorer as compared with figure 5.4.2. This is due to error propagation during the linear algebra process required at the end of the fractional estimation method as described in (4.106) & (4.107). Nevertheless, the results can be improved by averaging the channel estimates in the forward ascending process and the backward descending process in the algebra operation to smooth out the noise.

Figure 5.4.23 shows the performance of the proposed fractionally spaced estimator due to impact of reception diversity by increasing value of N = 2, 4, 6 & 8, for a fixed $M = 2$ system with C =2 & $\varphi = 3$ and pilot length v = 24 & 32, under block-invariant MIMO channel

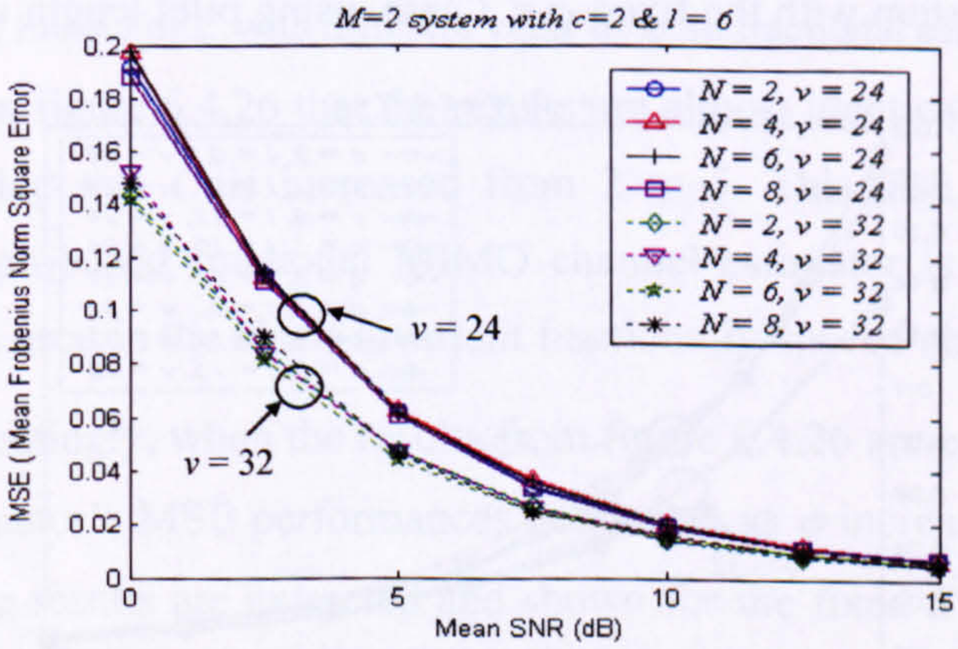

Figure 5.4.23: Impact of different N value in fractional estimation method

It can be seen in figure 5.4.23 that reception diversity has also no significant influence on the proposed fractional estimator. The results are identical in each case of pilot length v used, which are also same as the results obtained for the previous symbol-spaced model.

Next, figure 5.4.24 shows the impact of increasing the ($N\times M$) system order that has on the proposed fractionally-spaced estimator, for the same setting of $C = 2$ and $\varphi = 3$ in the fractionally-spaced delay channel using two different pilot length of $v = 24$ & 32.

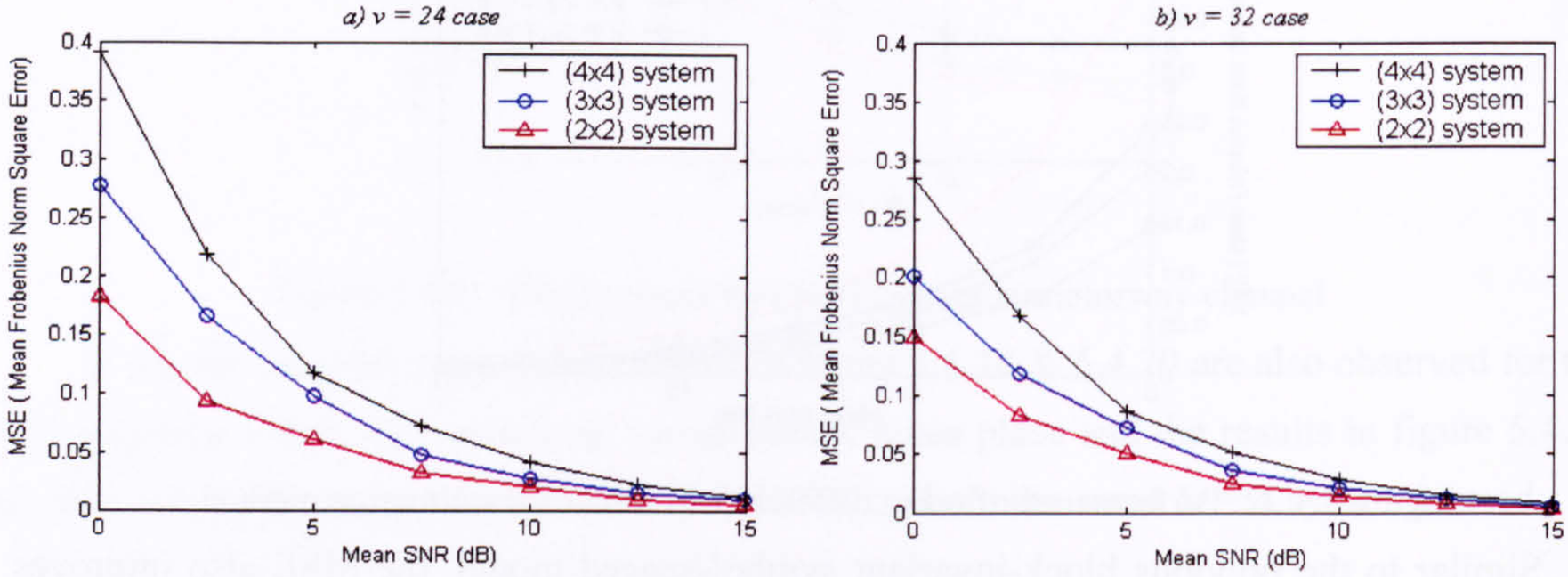

Figure 5.4.24: Impact of different M system in fractional estimation method

It can be seen that the results also exhibit similar performance trends as found in the symbol-spaced model shown earlier in figure 5.4.5 where a lower value of M demonstrates better error performance for both cases of $v = 24$ & 32. As ($N\times M$) increases, the performance gets poorer and the same explanation given for figure 5.4.5 can be applied here.

So far, the results have been presented for a fixed value of the fractional sampling rate, $C = 2$ and fixed total delay spread $\varphi = 3$ symbol periods. Next, the value of C is allowed to vary to assess the estimator's performance under fractionally-spaced case. (Note that the total number of paths, l, will also be altered accordingly stated for each value of C). Results are presented for a (2×2) system with the fixed $\varphi = 3$ case, using pilot length $v = 24$ and 32.

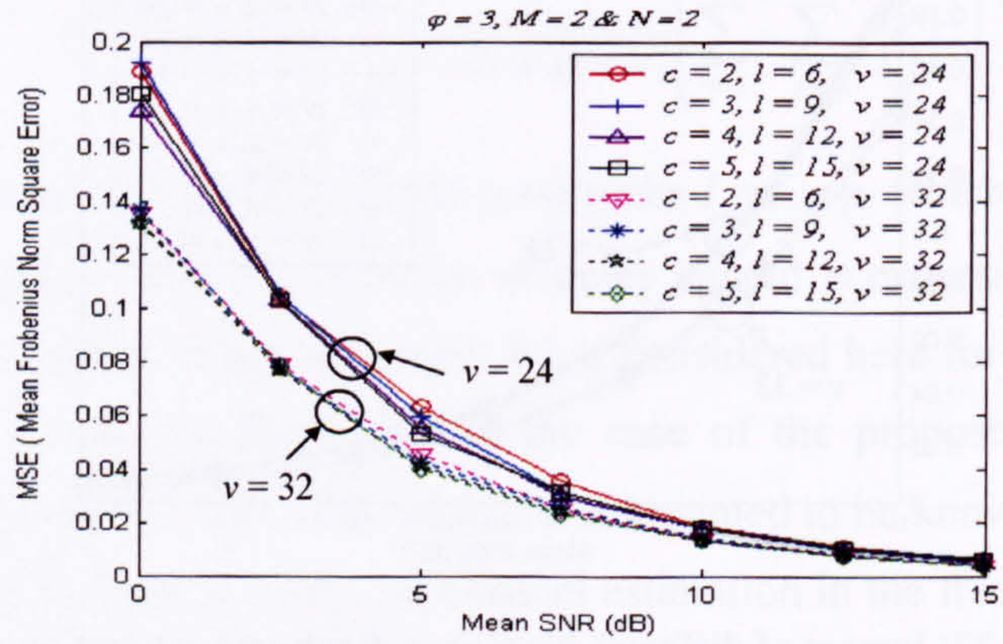

Figure 5.4.25: Impact of fractional sampling rate, C in fractional estimation method

It can be seen in figure 5.4.25 that the MSE performance stays relatively constant for each v case even when the fractional sampling rate, C increases from 2 to 5 for a fixed $\varphi = 3$ period. The results also show the impact of increasing the number of paths in the fractionally-spaced delay channel on the proposed estimator when the channel is invariant. The results are relatively consistent even l increases, which again demonstrate the ability of the proposed fractionally-spaced channel estimator to perform the channel estimation under fractionally-spaced delay model. This can also be confirmed with the results shown in the following figure 5.4.26 using different value of φ respectively for a (2×2) system.

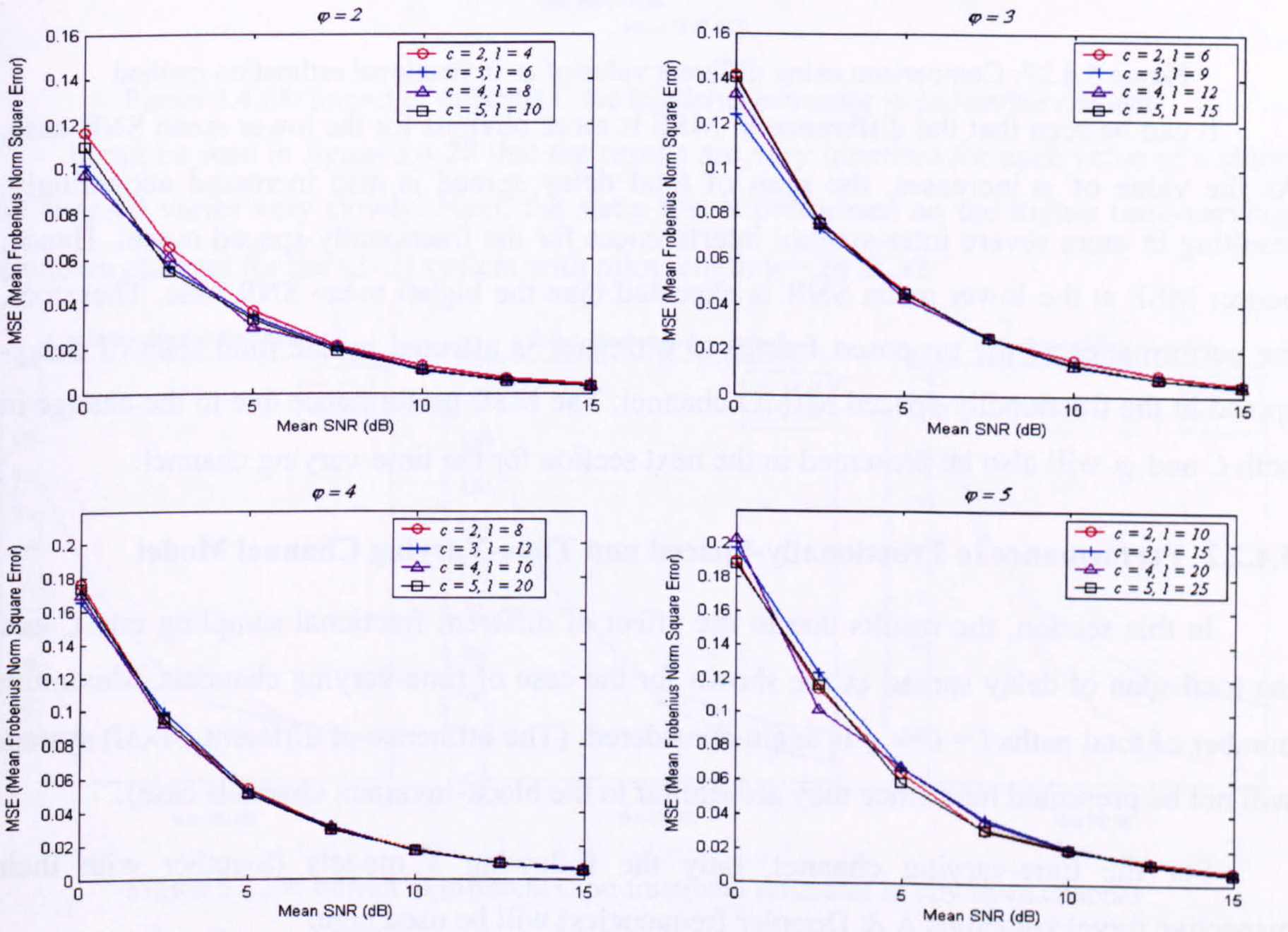

Figure 5.4.26: Impact of C with different value of φ in fractional estimation method

It can be seen in figure 5.4.26 that the results are almost identical for each value of φ as the fractional sampling rate C is increased from 2 to 5. This also demonstrates that the performance of the proposed fractional MIMO channel estimator is not influenced by the sampling rate c when used in the block-invariant fractionally-spaced channel model.

However, interestingly, when the results from figure 5.4.26 are compared closely, it can be seen that the estimator's MSE performances get poorer as φ increases from 2 to 5 for any fixed value of C. The results are extracted and shown for the fixed $C = 3$ case for the (2×2) system using pilot length of $v = 32$ in the following figure:

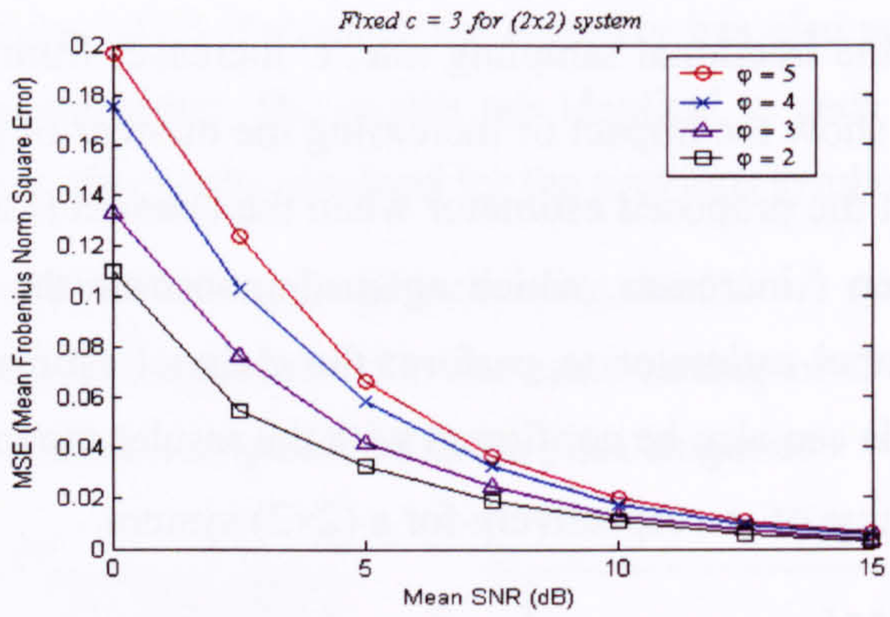

Figure 5.4.27: Comparison using different value of φ in fractional estimation method

It can be seen that the difference in MSE is more obvious for the lower mean SNR case. As the value of φ increases, the span of total delay spread is also increased accordingly, resulting in more severe inter-symbol interferences for the fractionally-spaced model. Hence, poorer MSE at the lower mean SNR is expected than the higher mean SNR case. Therefore, the performance of the proposed fractional estimator is affected by the total span of delay-spread in the fractionally-spaced MIMO channel. The MSE performance due to the change in both C and φ will also be presented in the next section for the time-varying channel.

5.4.2.2 Performance in Fractionally-Spaced and Time-Varying Channel Model

In this section, the results due to the effect of different fractional sampling rate C and the total span of delay spread φ, are shown for the case of time-varying channels. Maximum number of total paths $l = C \times \varphi$ is again considered. (The influence of different ($N \times M$) system will not be presented here since they are similar to the block-invariant channels case).

For the time-varying channel, only the following 3 models (together with their respective travel velocities Λ & Doppler frequencies) will be used here:

a) The pedestrian channel: $f_{dmax} = 6$ Hz, $\Lambda = 3$ km/hr $\cong 0.833$m/s.

b) The city/town channel: $f_{dmax} = 88$ Hz, $\Lambda = 45$ km/hr $\cong 28$ mph.

c) The motorway/highway channel: $f_{dmax} = 176$ Hz, $\Lambda = 90$ km/hr $\cong 56$ mph.

Again, the results are simulated at their maximum Doppler frequency f_{dmax} in each case using carrier frequency $f_c = 2.11$GHz with end-to-end data rate of $D_{total} = 480$Kbps. The data rate of individual transmit antenna D_{single} depends on the value of M where $D_{single} = D_{total} / M$.

First, the same test from figure 5.4.25 is used to assess the estimator's performance in the pedestrian channel for a (2×2) system with a fixed $\varphi = 3$ and increasing $c = 2$, 3 & 4. Results are shown for pilot length $v = 24$ and 32.

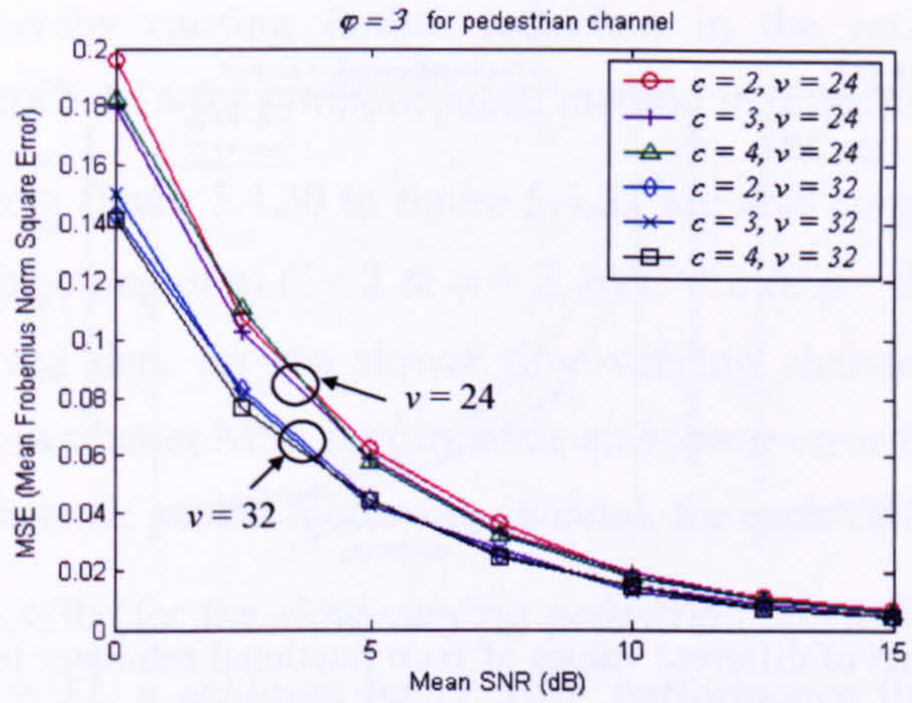

Figure 5.4.28: Impact of different C for fractional estimator in pedestrian channel

It can be seen in figure 5.4.28 that the results are very identical for each value of v since the channel varies very slowly. Next, the same test is performed on the higher time-varying city/town channel for the (2×2) system with pilot length $v = 24$ & 32.

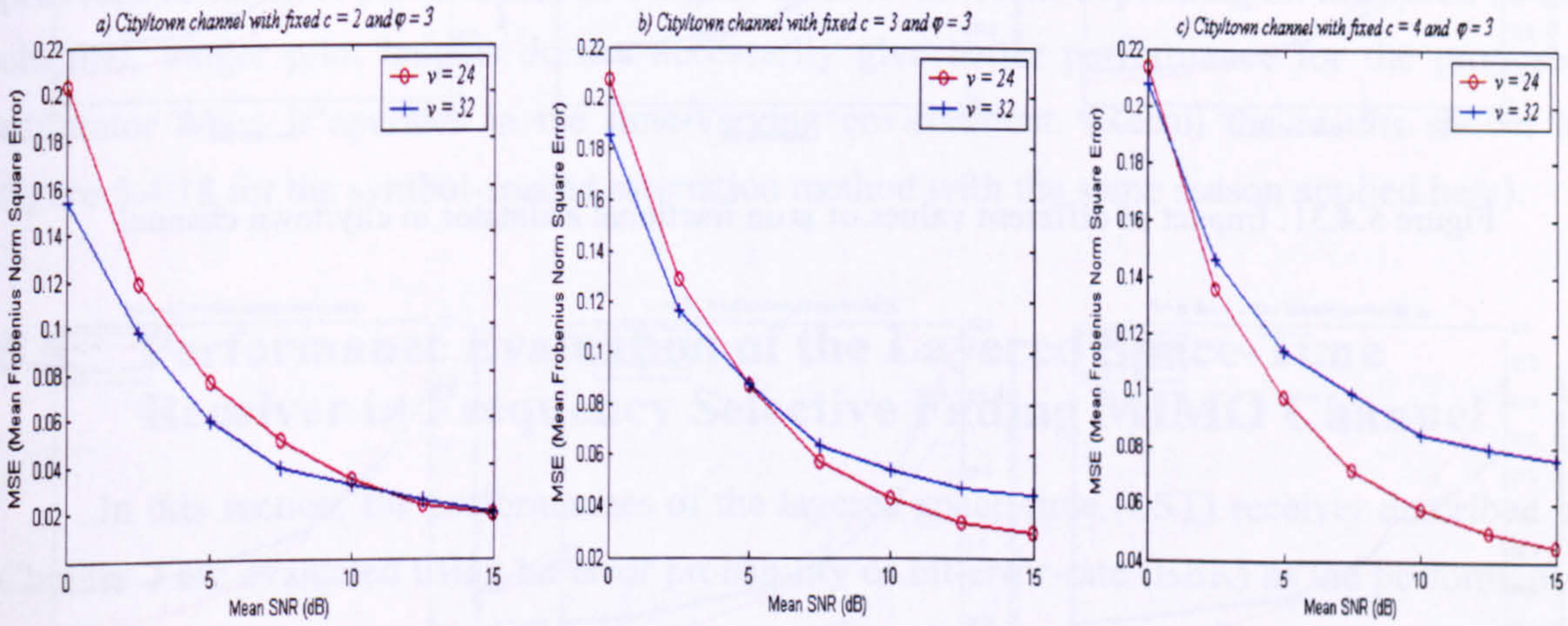

Figure 5.4.29: Impact of different C on fractional estimator in city/town channel

It can be observed that the value of C has an impact on the estimator's performance in the faster time-varying channel, depending on the pilot length v. The result for $v = 32$ case changes/degrades significantly as C increases from 2 to 4, whereas the result for $v = 24$ only vary slightly across all mean SNR. This again demonstrates that the optimum pilot length v must be chosen carefully in order to keep the good performance of the proposed estimator that operate under fast varying channel. If v is too long, time-variation during the training also increases, thereby further deteriorates the estimator performance.

Next, the effect of changing the total delay spread φ will be shown in the next set of figures for the 3 different time-varying channels. Results are shown for fixed value of $C = 2$ for a (2×2) system with $v = 24$ & 32.

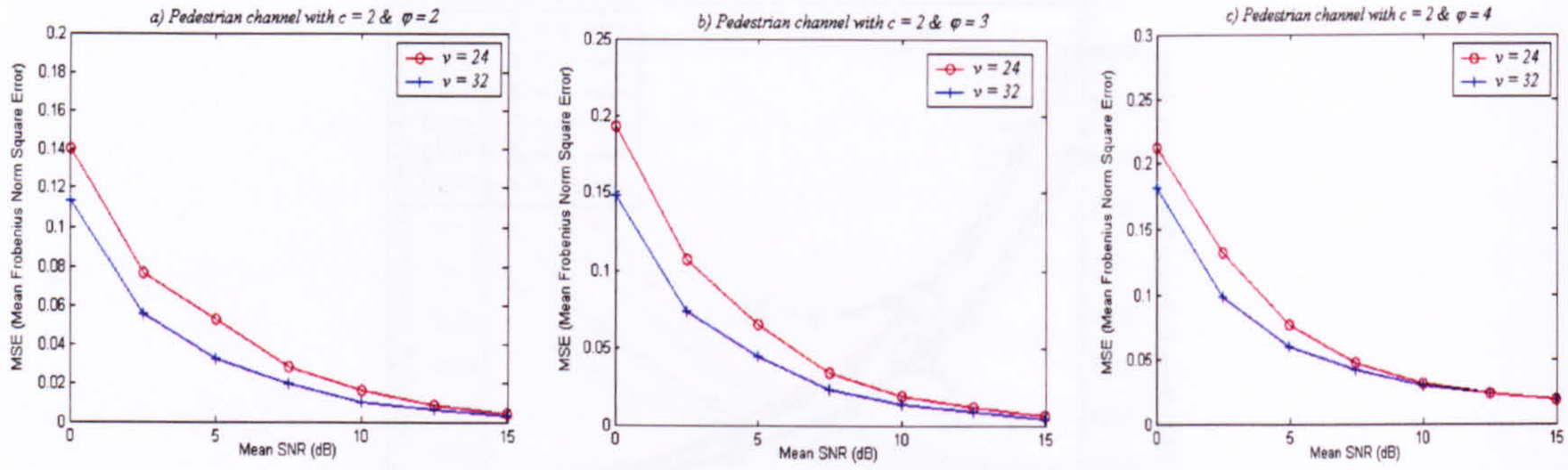

Figure 5.4.30: Impact of different values of φ on fractional estimator in pedestrian channel

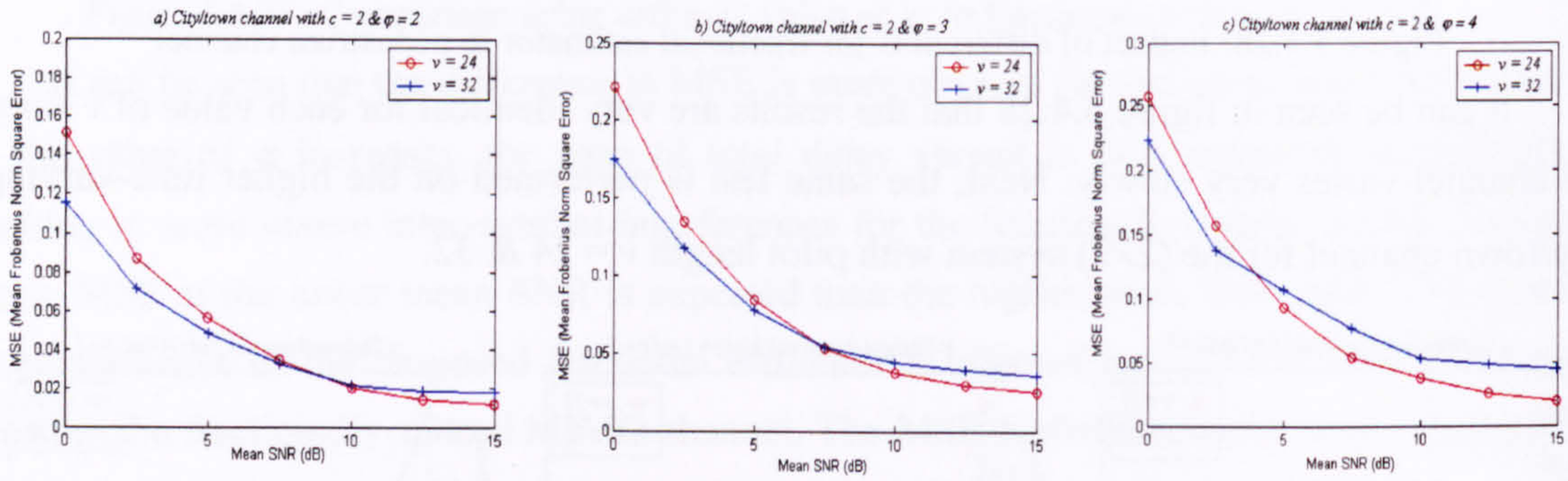

Figure 5.4.31: Impact of different values of φ on fractional estimator in city/town channel

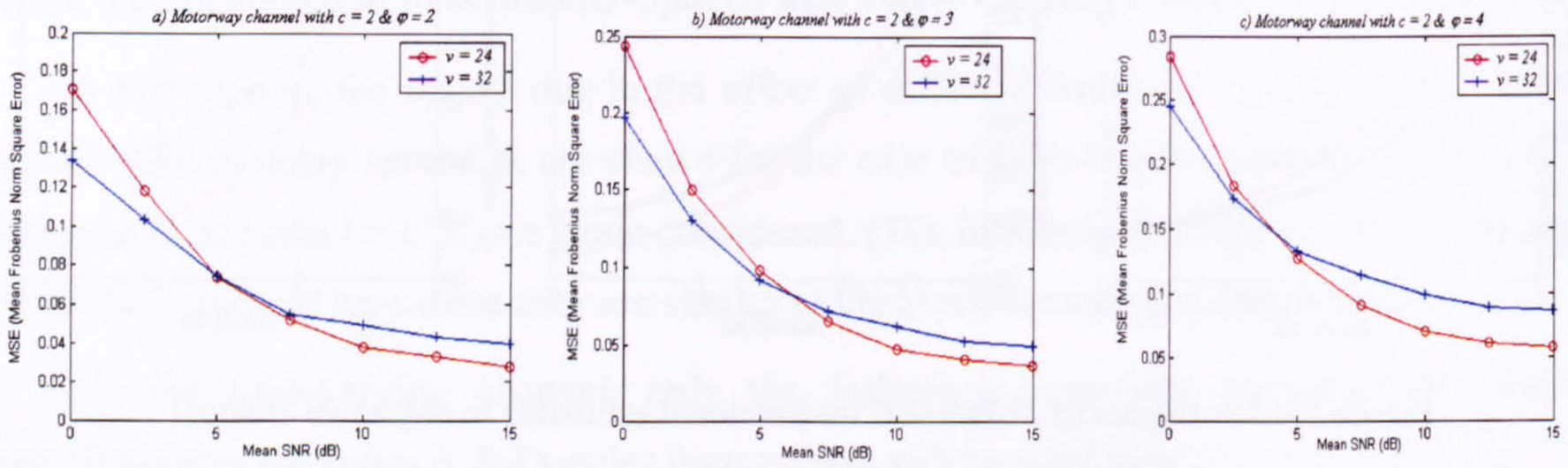

Figure 5.4.32: Impact of different values of φ on fractional estimator in motorway channel

Several observations can be made. First, it can be seen from the overall results that the error performance gets poorer as the total delay-spread φ increases. This is true for both cases of $v = 24$ & $v = 32$. The results show the degradation of the estimator's MSE performance when the frequency selectivity of the MIMO channel becomes more severe as the delay spread extends from $\varphi = 2$ to $\varphi = 4$ symbol periods. Also, the total number of paths l for each case of φ is different (total paths $l = C \times \varphi$, corresponding to $l = 4$, 6 and 8 respectively), allowing indirect assessment for the impact of fractionally-spaced paths l that has on the estimator's performance under time-varying fractionally spaced channel model. Similarly, increasing number of paths l means time-variation within the frequency selectivity also

increase accordingly, thereby causing further reduction in the estimator's performance. (Recall the results in figure 5.4.16 for symbol-spaced method in time-varying channels).

Next, the results from figure 5.4.30 to figure 5.4.32 are also compared across the time-varying channels for each setting of a) $C = 2$ & $\varphi = 2$, b) $C = 2$ & $\varphi = 3$ and c) $C = 2$ & $\varphi = 4$ respectively. It is observed that, for the slower time-varying channels; i.e. the pedestrian channel, the estimator shows better MSE performance and lower error floor as compared with the faster time-varying channel; i.e. the motorway channel, for each value of v.

Results of figure 6.4.30 (for the slow-varying pedestrian channel) show that by having longer pilot length of $v = 32$, it achieves better MSE performance than using shorter pilot length of $v = 24$, for each case of φ and all SNR values. However, for faster time-varying city/town and motorway channels, all results shown in figure 6.4.31 & 6.4.32 exhibit the 'switching' point on the MSE performance between the case of $v = 24$ & $v = 32$ where $v = 32$ case initially gives better error performance at a lower mean SNR level and then $v = 24$ case provides better error performance at a higher SNR level. Thus, depending on the speed of the channel, longer pilot lengths do not necessarily give better performance for the proposed estimator when it operates in the time-varying environment. (Recall the results shown in figure 5.4.18 for the symbol-spaced estimation method with the same reason applied here).

5.5 Performance Evaluation of the Layered Space-Time Receiver in Frequency Selective Fading MIMO Channel

In this section, the performances of the layered space-time (LST) receiver described in Chapter 2 are evaluated using bit error probability or bit-error-rate (BER) as the performance metric for assessment under different system configurations and parameter settings. The BER results are compared for the two cases: i) the perfect channel knowledge case (where the receiver is fed with the original coefficients that model the channel) and ii) the estimated channel case (where the estimates of channel coefficients obtained by the proposed MIMO-CE methods are used). The purpose is to assess the impact of the channel estimation errors that has on the system performance of the LST receiver under the frequency selective fading MIMO channel for both symbol-spaced initially and followed by fractionally-spaced model.

Results presented here are mostly employing the block-invariant channel model although some tests are performed using continuous time-varying channels. (Block invariant channel model means that the channel coefficients remain unchanged for each block of $M\times200$ column-vector symbols but then change to different set of coefficients and stay for the next block of $M\times200$ data symbols, and so on until all symbols are sent).

First, in figure 5.5.1, the BER performance for the LST receiver is shown for the different ($N\times M$) system configuration with and without the 'ordered successive interference cancellation' – OSIC scheme as described in Chapter 2. Results are plotted for the receiver's setting of feedforward equaliser's tap $K_f = 5$ and feedback equaliser's tap $K_b = 3$ in the MIMO channel where $(L+1) = 3$ paths are assumed in each CIR for symbol-space channel model.

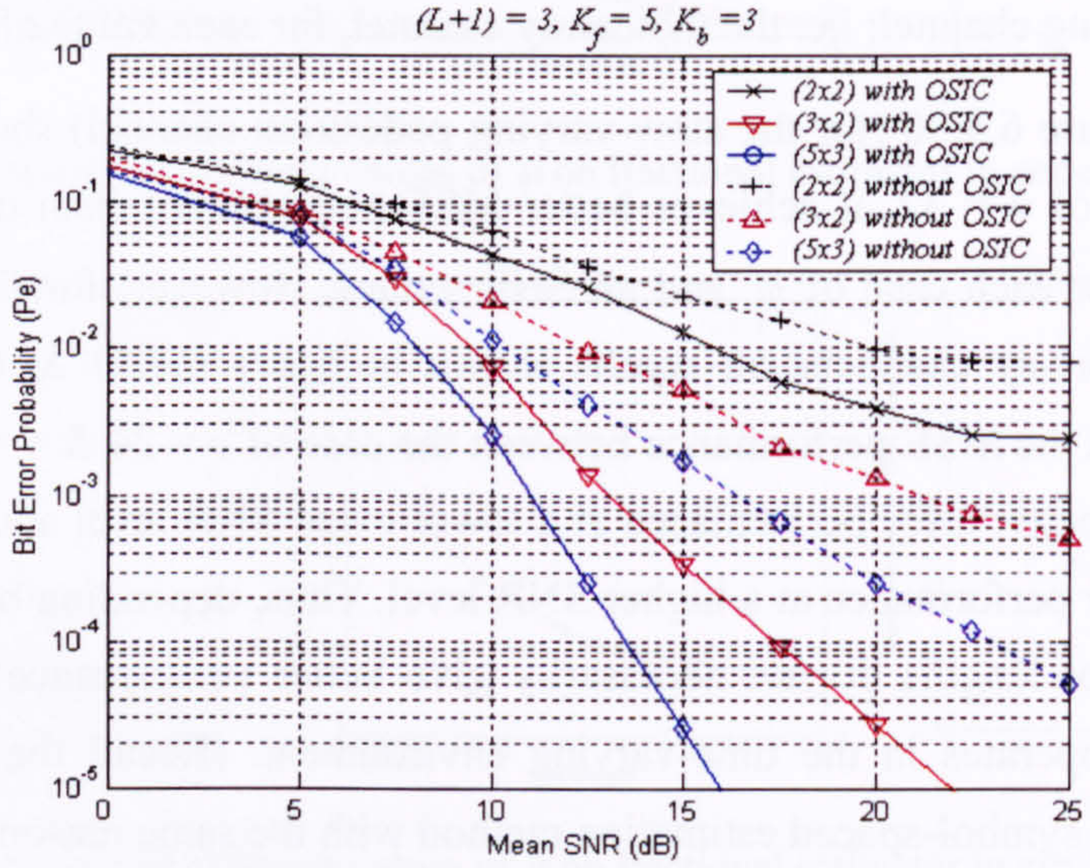

Figure 5.5.1: Bit error probability for layered space-time system

Several observations can be made from figure 5.5.1. First, it can be seen that the system with the OSIC scheme performs better than without OSIC scheme for all the configurations shown. This is also demonstrated by Lozano and Papadias [47] for their layered space-time receiver algorithm, showing how the MIMO-OSIC-DFE architecture is superior to the MIMO-DFE system without OSIC. The partial-connected version is used here for the MIMO-OSIC-DFE. Also, it can be observed that since the value of N is higher than the value of M, the BER performance also improves accordingly because of the added reception diversity.

The performance of the MIMO-OSIC-DFE can be further improved by increasing the number of feedforward taps K_f, for the same ($N\times M$) system configuration used in figure 5.5.1, with fixed setting of $(L+1) = 3$ and $K_b = 3$. It can be seen from figure 5.5.2 that the BER results of the LST system with the OSIC-DFE configuration improves as the number of feedforward taps K_f increases. It can also be seen in figure 5.5.2 that the rate of improvement in bit error probability diminishes as higher numbers for K_f taps are used progressively. This is because when the number of K_f taps in DFE is sufficient to represent and deal with the finite impulse response of the $(L+1) = 3$ taps channel in this case, any further increases in K_f taps beyond the sufficient value ($K_f = 7$ taps in this case), results in only minimal improvement of the system performance.

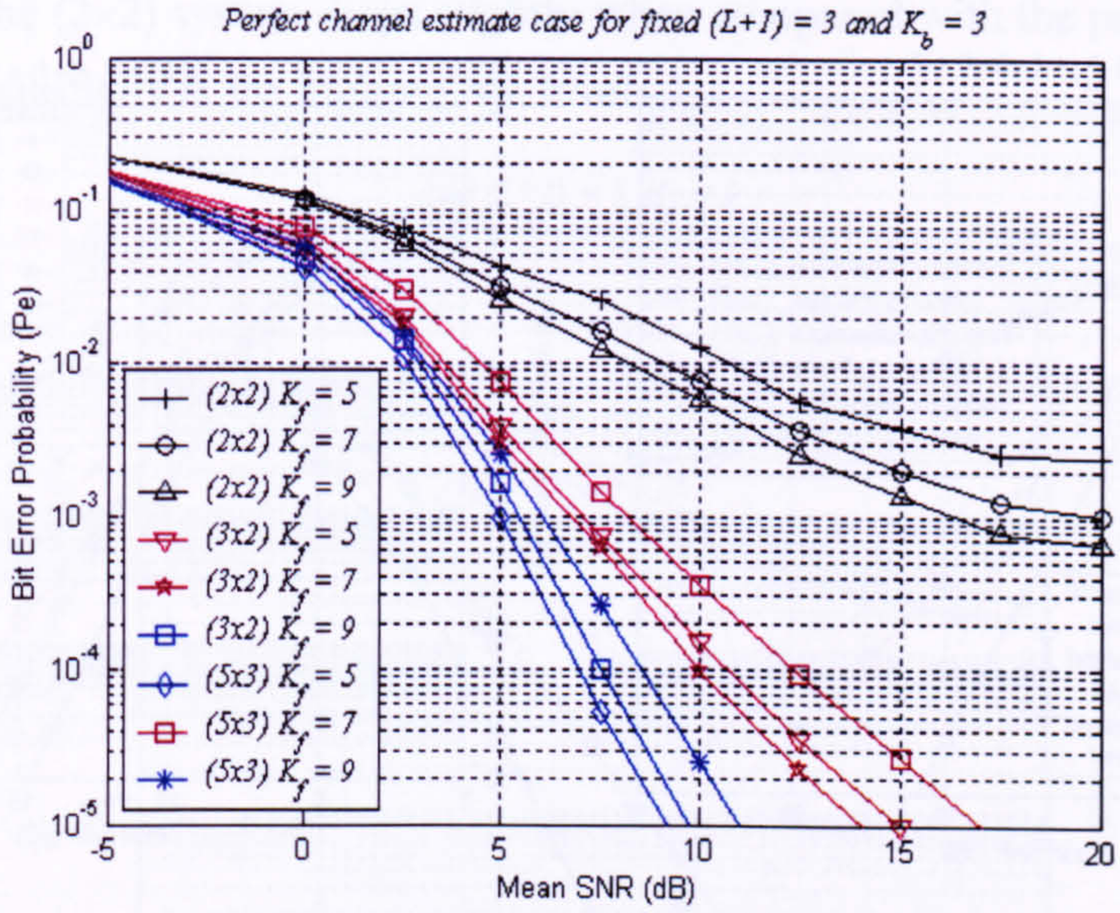

Figure 5.5.2: The effect of increasing number of feedforward taps in OSIC-DFE

Higher number of K_f taps also means that higher computational overhead is required to carry out both the MIMO equalisation and the OSIC process in the frequency-selective fading environment. Note that the performance due to the change in number of feedback K_b taps will not be discussed here since it involves the non-linear process that makes the analysis more difficult to be achieved due to the error propagation within the feedback section. Therefore, $K_b = 3$ will be kept throughout the subsequent analysis.

Next, the proposed MIMO-CE scheme is utilised to obtain the necessary channel coefficients using a pilot length $v = 24$. These channel coefficients will then be fed into the OSIC-DFE process of the LST receiver in order to assess the impact of the estimation error on the BER performance of the system. (The MIMO-OSIC-DFE receiver is described in Chapter 2 with the incorporation of the novel MIMO channel estimation scheme provided in Chapter 4). Results will be shown using the previous ($N \times M$) configurations with different values of K_f = 5,7 & 9 and K_b = 3 under a fixed (L+1) = 3 paths in each CIR of the MIMO channel. The results obtained using the proposed estimator are compares with the case where perfect channel estimates are assumed.

It can be seen from figure 5.5.3 that, for each value of K_f used, the proposed estimator demonstrates little degradation in BER performance of the LST receiver as compared to the case where perfect channel estimates are assumed. It is also seen that as the number of K_f increases, the BER performance for the estimated channel case also improves accordingly following the results of the perfect channel case. The results of the estimated channel case is also compared and shown in figure 5.5.3d.

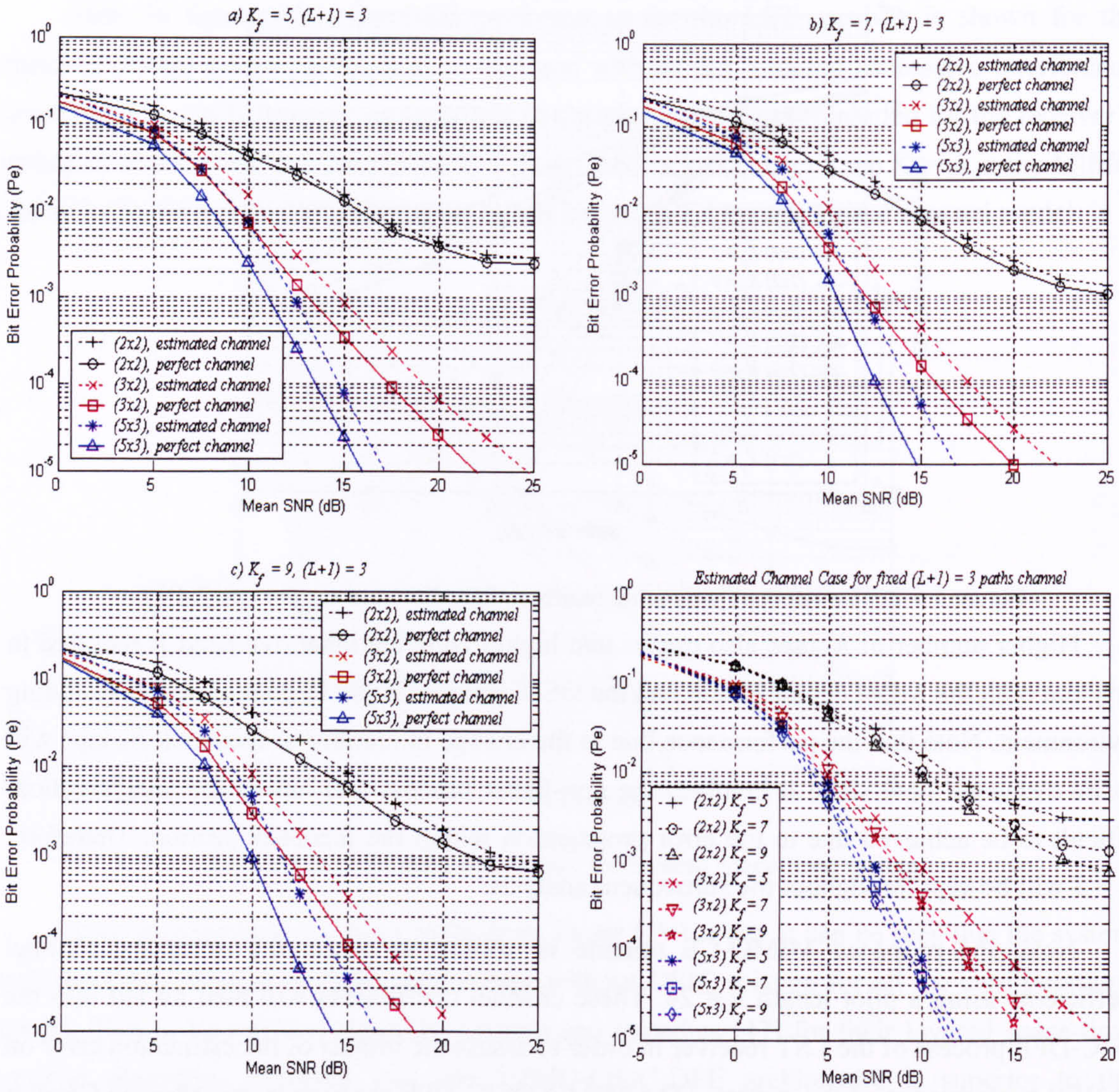

Figure 5.5.3: BER performance for different value of K_f using proposed MIMO-CE

In the following, different settings of (L+1) paths and K_f taps will be used to illustrate the BER performance for the same (N×M) system configurations: (2×2), (3×2) and (5×3). The impact of increasing the number of K_f taps setting relative to number of (L+1) paths will be evaluated for both the perfect channel case and the estimated channel case. Results will be provided for using fixed pilot length of v = 24.

First, the results are shown for the setting of K_f = 9 & K_b = 3, with (L+1) = 3 to 5 paths. It can be seen from figure 5.5.4 that the proposed MIMO-CE also results in little degradation in BER performance as compared to the perfect channel case. Interestingly, when comparing figure 5.5.4 with figure 5.5.3c (for both the estimated and perfect channel case), the results for the (3×2) system and the (5×3) system show improvement in its bit error probability performance as the number of (L+1) paths increase from 3 to 5. However, in contrary, the

performance for the (2×2) system drops slightly when compared with the previous case shown in figure 5.5.3c, especially at the higher SNR levels.

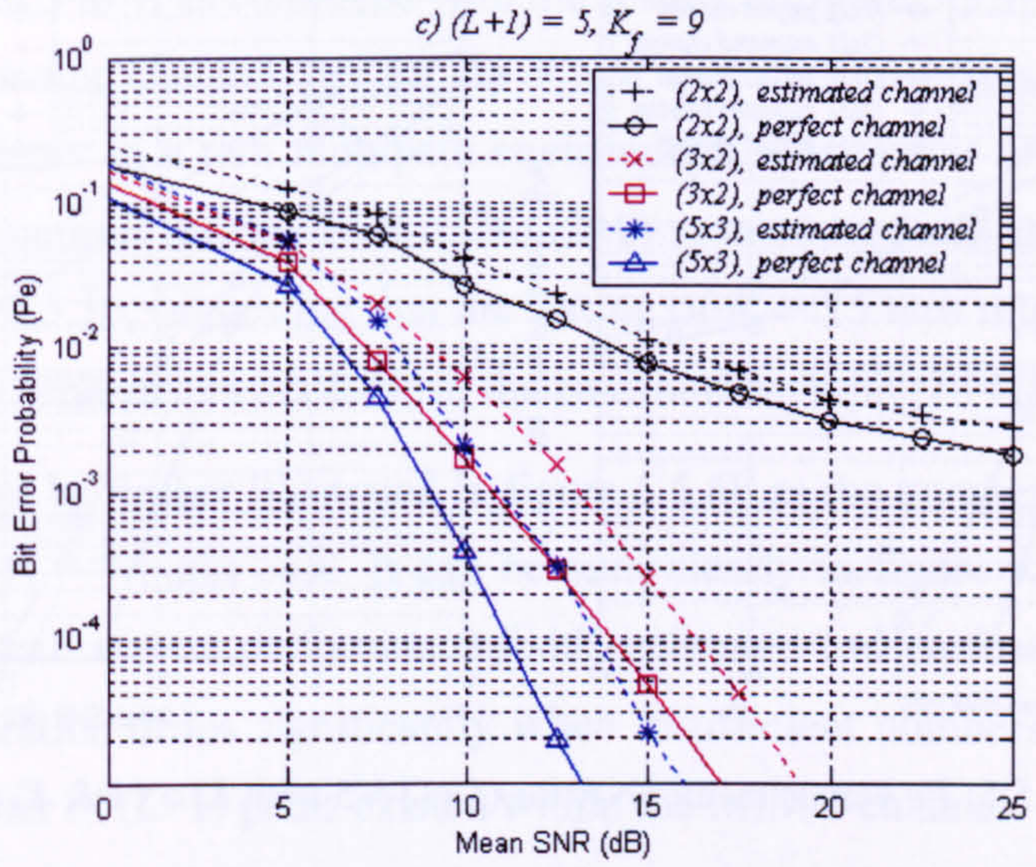

Figure 5.5.4: *Pe* versus mean SNR for $(L+1) = 5$, $K_f = 9$

Conventionally, the increase number of $(L+1)$ paths is responsible for providing the performance improvement by offering a "richer" scattering environment for the $(N\times M)$ system which has higher reception diversity; i.e. (3×2) system and (5×3) system, with diversity order greater than unity; i.e. $N/M > 1$. On the other hand, the results shown for the (2×2) system suggest that the number of K_f taps might be insufficient to cater the case with the increase number of $(L+1)$ paths in the $(N\times M)$ system with unity diversity order; $(N/M = 1)$.

Therefore, the bit error probability performance of a $(N\times M)$ layered space-time system is affected by: a) the number of $(L+1)$ paths existing within the CIR of the MIMO channel, b) the $(N\times M)$ configuration in terms of reception diversity order (or gain) expressed by the ratio of N/M and c) the number of feedforward K_f taps needed by OSIC-DFE in order to cater for the $(L+1)$ paths of the channel. To confirm these ideas, further combinations of $(L+1)$ and K_f settings were examined to find out which of this condition is more prioritising than the other.

In figure 5.5.5, the number of K_f taps is increased from $K_f = 9$ taps to $K_f = 11$ and 15 taps respectively for the same $(L+1) = 5$ setting as shown in figure 5.5.4. In comparison with figure 5.5.4, the overall results in figure 5.5.5a show a greater performance improvement for all the $(N\times M)$ configurations (especially for the $N > M$ case) as the number of K_f taps increases, which confirms the trend seen in figure 5.5.2. However, when both figure 5.5.5a and 5.5.5b are compared, it shows that the performance of the (2×2) system improves further as K_f taps increases from 11 to 15 but no significant performance improvement is observed for both (3×2) & (5×3) systems. (This applies to both perfect and estimated channel case).

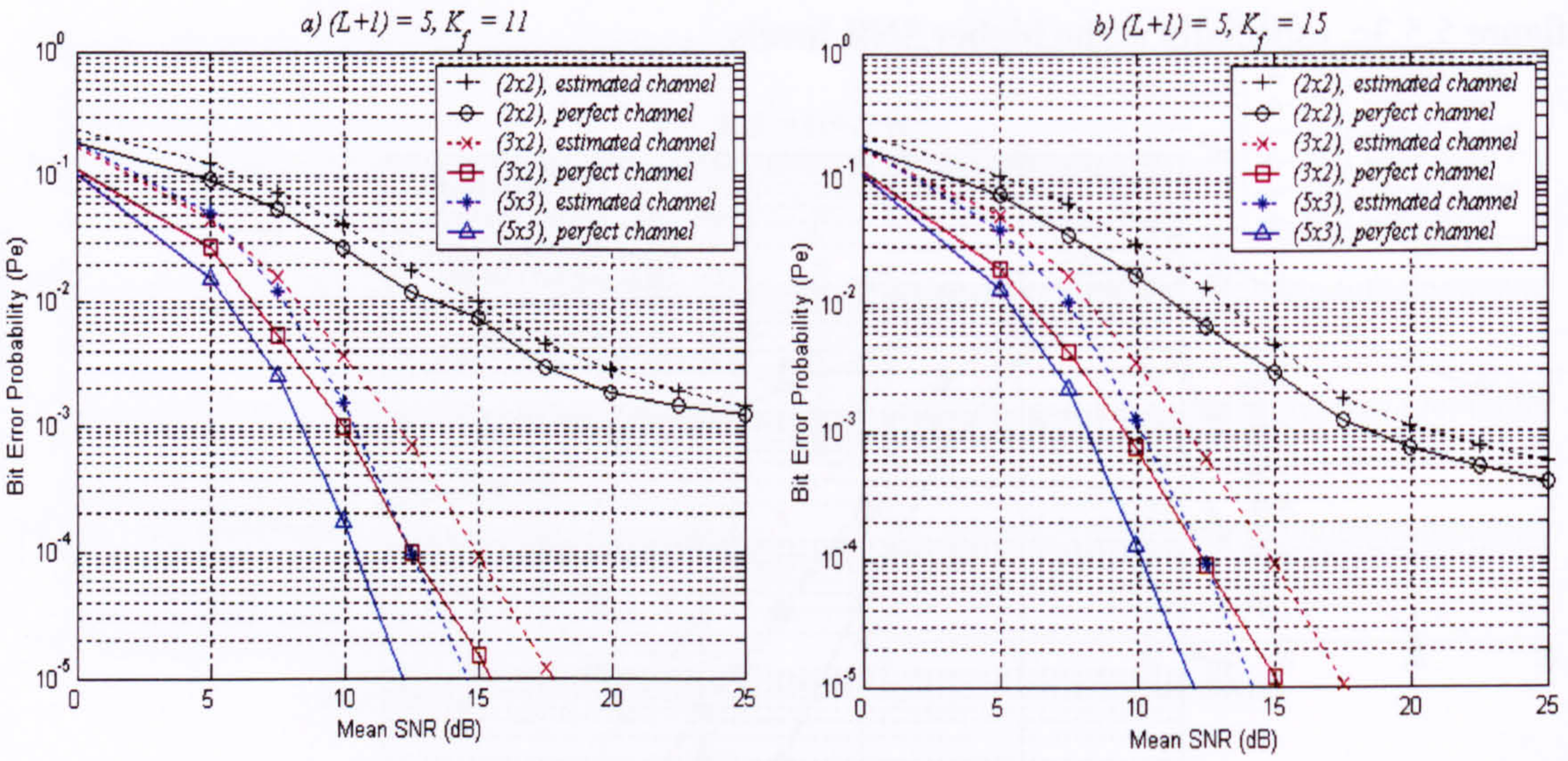

Figure 5.5.5: *Pe* versus mean SNR for $(L+1) = 5$ with $K_f = 11$ & $K_f = 15$

The results suggest that with the help of reception diversity gain in the $N > M$ systems, $K_f = 15$ taps might have already been sufficient to cater for $(L+1) = 5$ paths, whereas improvement can still be made for $N = M$ system if further number of K_f taps are used. This again demonstrates that the added reception diversity provides additional benefit to the LST receiver in 'counter-balancing' the number of K_f taps in the MIMO equaliser that is needed to sufficiently cater for certain number of $(L+1)$ paths in the frequency selective MIMO channel.

Next, in figure 5.5.6 the number $(L+1)$ paths is further increased from $(L+1) = 5$ paths to $(L+1) = 7$ path, to assess the system performance using the fixed setting of $K_f = 15$ & 9 taps in the OSIC-DFE of the space-time receiver.

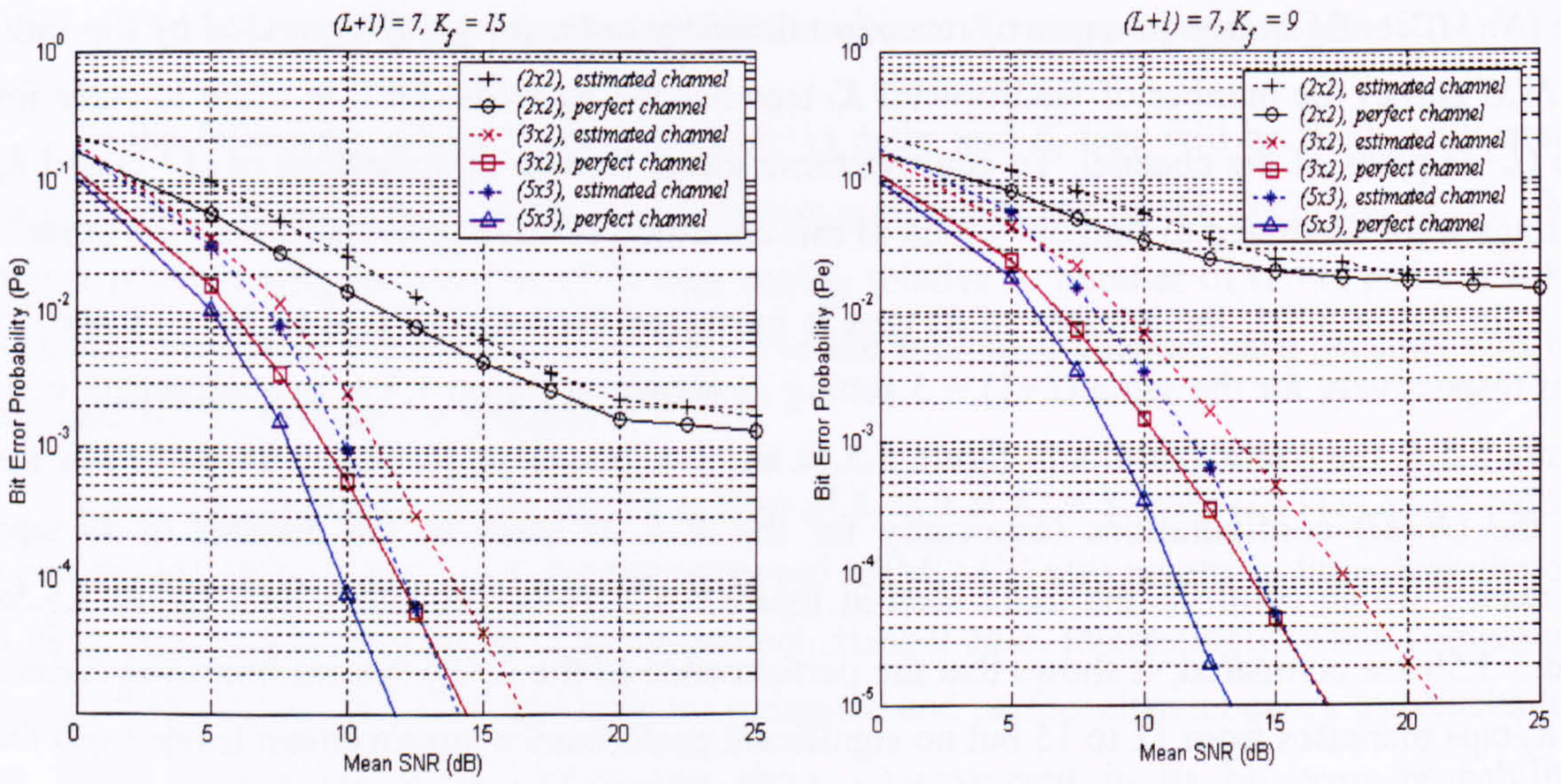

Figure 5.5.6: *Pe* versus mean SNR for $(L+1) = 7$ with $K_f = 15$ & $K_f = 9$

Several observations are obtained. First, for the case $K_f = 15$ in figure 5.5.6a, the BER performance for the (3×2) & (5×3) system is further improved when the number of $(L+1)$ paths increases from 5 to 7, as compared with the results in figure 5.5.5b, This is true for both the perfect and estimated channel case for the $N > M$ system. The results show that the MIMO system can work better in a rich multipath environment when paths are carefully exploited. However, it is also noticed that the BER of the (2×2) system degrades slightly as compared to the result in figure 5.5.5b, suggesting that the setting of $K_f = 15$ taps might be insufficient for the (2×2) system to achieve a better BER in the environment with $(L+1) = 7$ paths.

This effect can be further illustrated in figure 5.5.6b as the number of K_f taps is reduced to 9 taps w.r.t $(L+1) = 7$ paths case. It can be seen clearly in figure 5.5.6b (compared with 5.5.6a) that the overall system performance (both estimated and perfect channel case) for all the $(N\times M)$ configuration drops significantly when insufficient numbers of K_f taps are used relative to the number of $(L+1)$ paths existed within the MIMO channel.

The results from the previous figures can again be compared for the case of increasing $(L+1)$ paths at a fixed number of $K_f = 9$ taps in the perfect channel estimated case as follows:

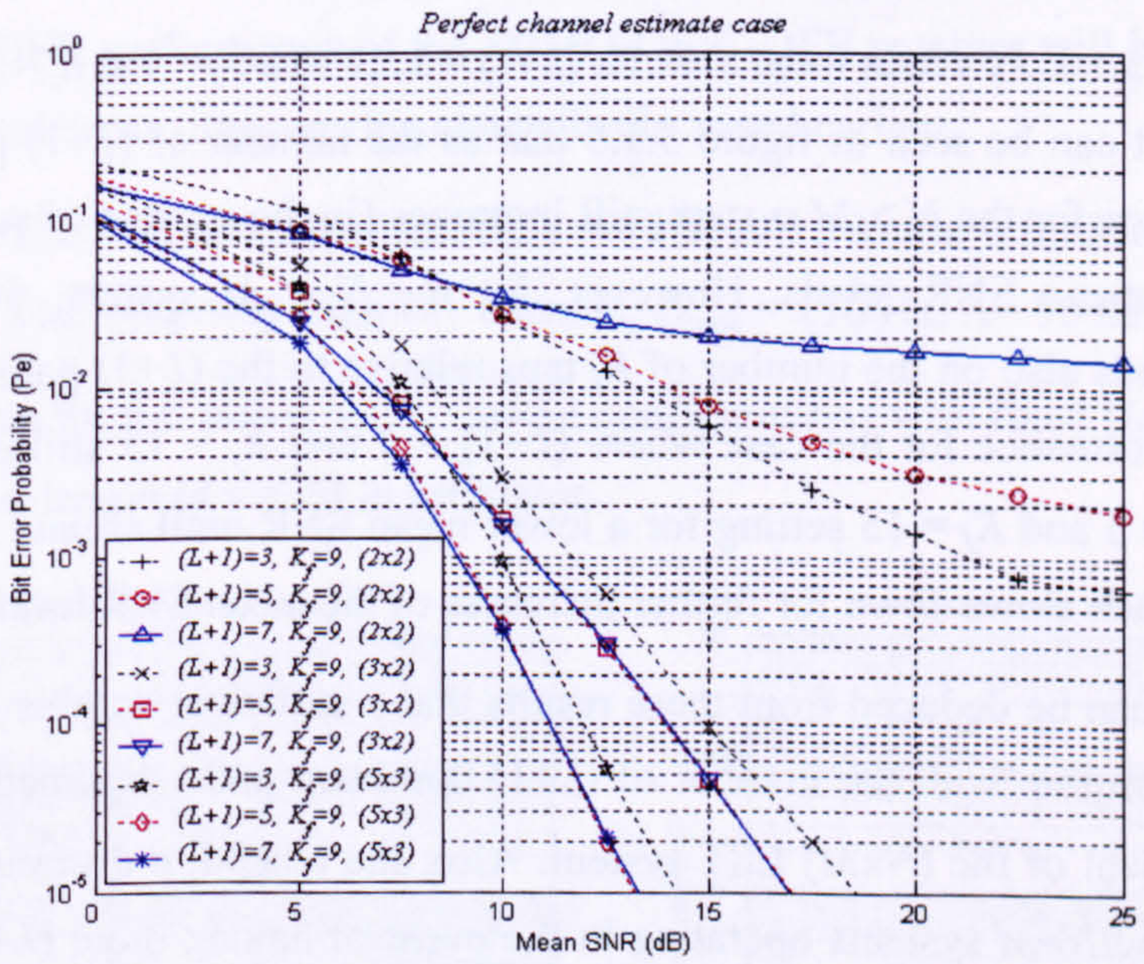

Figure 5.5.7: *Pe* versus mean SNR for $(L+1) = 3,5,7$ with fixed $K_f = 9$.

It can be seen in figure 5.5.7 that, as the number of $(L+1)$ paths for a fixed number of feedforward $K_f = 9$ taps increases, the performance deteriorates for the (2×2) system. However, as for the $N > M$ system, the results demonstrate slight performance improvement when $(L+1)$ is increased from 3 to 5 paths. Nevertheless, the improvement ceases for any further increases of $(L+1)$ paths due to an insufficient number of K_f taps used in MIMO equaliser.

Alternatively, the effect of increasing number of $(L+1)$ paths w.r.t the K_f setting can also be shown by comparing the previous results from figures 5.5.3, 5.5.5b and 5.5.6a for the perfect channel case with different combination of $(L+1)$ and K_f setting.

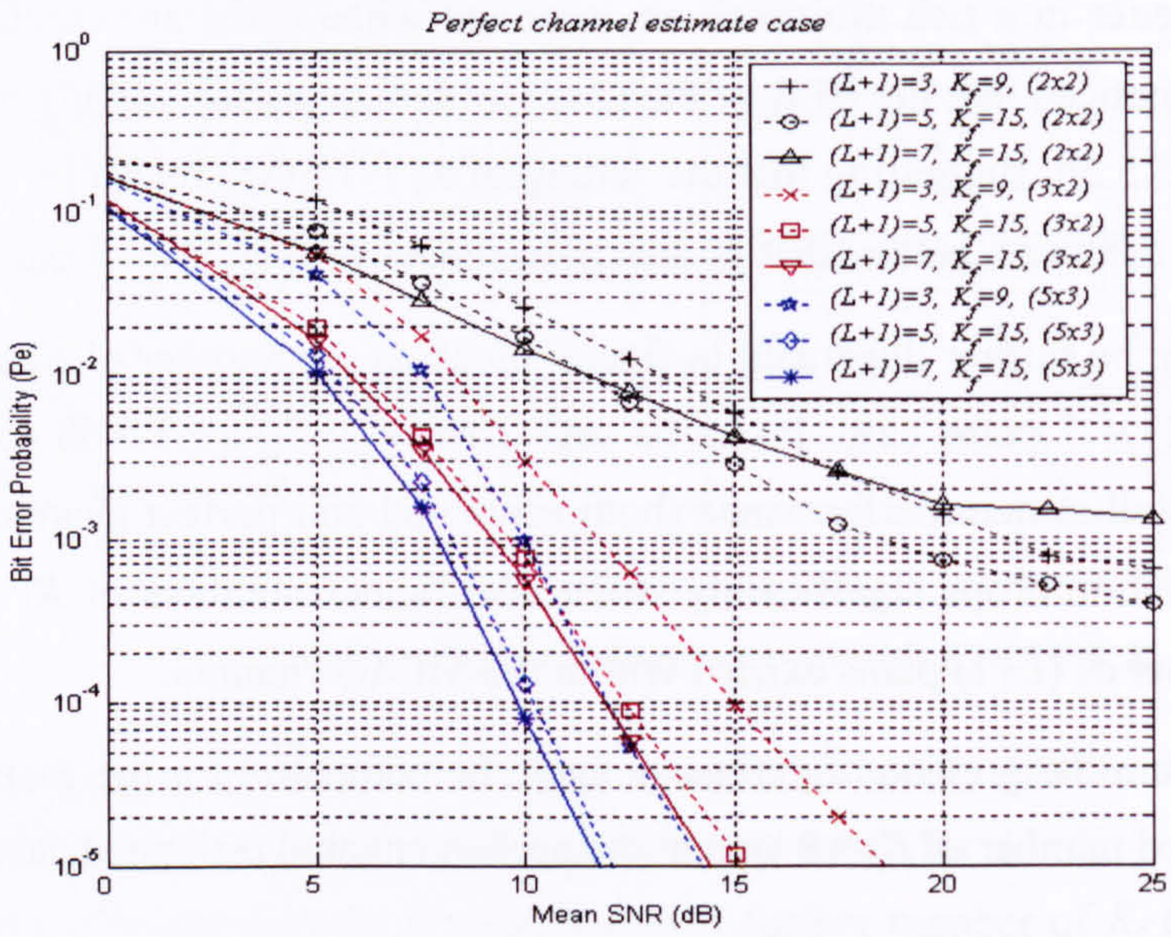

Figure 5.5.8: *Pe* versus mean SNR for $(L+1) = 3,5,7$ with $K_f = 9$ & $K_f = 15$

Once again, it can be seen in figure 5.5.8 that as the number of $(L+1)$ paths increases, the BER performance for the $N > M$ system still improves (in the present of sufficient K_f taps used), for all the mean SNR levels. However, for the $N = M$ system, the performance improvement depends also on the number of K_f taps relative to the $(L+1)$ paths. In particular, notice that the performance for the case where $(L+1) = 7$ and $K_f = 15$ still outperforms the case where $(L+1) = 5$ and $K_f = 15$ setting for a lower mean SNR until around 11~12 dB. The improvement rate then slows down for further increases of the mean SNR level.

Therefore, it can be deduced from these results that a sufficient number of K_f taps must be used to commensurate with the number of $(L+1)$ dominant paths assumed to exist in the operating environment of the $(N \times M)$ LST system. Also, the reception diversity does provide added benefit for the $N>M$ systems operating in the event of having more $(L+1)$ paths in the frequency selective fading MIMO channel.

The impact of increasing the pilot length v (used in the proposed MIMO channel estimation scheme) on the overall bit error probability performance is assessed in figure 5.5.9. The results are shown for $v = 20$ and $v = 32$ for the (3×2) and (5×3) system using a fixed setting for the number of feedforward $K_f = 5$ taps and feedback $K_b = 3$ taps in a MIMO channel that has $(L+1) = 3$ paths in each CIR. Results obtained using the proposed estimator are also compared with the case where perfect channel estimates are used.

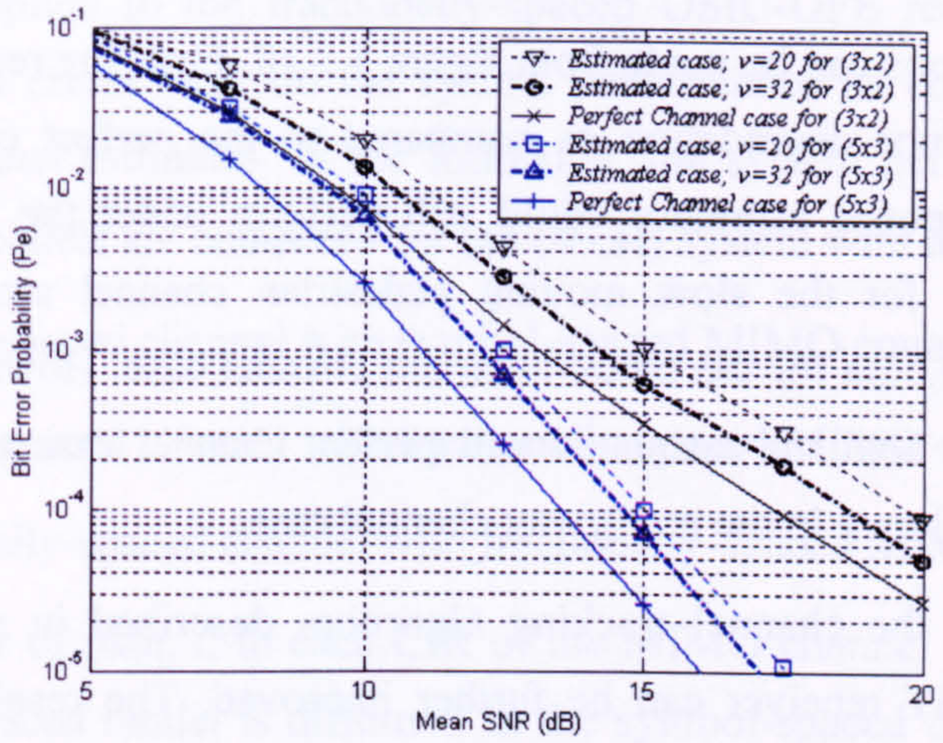

Figure 5.5.9: *Pe* versus mean SNR for different pilot length v used

It can be seen from figure 5.5.9 that as the pilot length v increases from $v = 20$ to 32, the BER performance of the LST receiver also improves accordingly. For the higher orders of v the results are much closer to the perfect channel estimate case. The results confirm the trend seen previously in the Section 5.4 for the block-invariant channel where the error performance of the estimator is improved by increasing the pilot length v during the estimation process.

Next, the BER performance of the MIMO-OSIC-DFE receiver will be evaluated for the two previous continuous time-varying channels discussed earlier:

- The pedestrian channel: $f_{dmax} = 6$ Hz, $\Lambda = 3$ km/hr $\cong 0.833$m/s.
- The motorway/highway channel: $f_{dmax} = 176$ Hz, $\Lambda = 90$ km/hr $\cong 56$ mph.

Results are shown for the same $(N \times M)$ system configurations with fixed $(L+1) = 3$, $K_f = 5$ and $K_b = 3$ using pilot length of $v = 24$ in estimator.

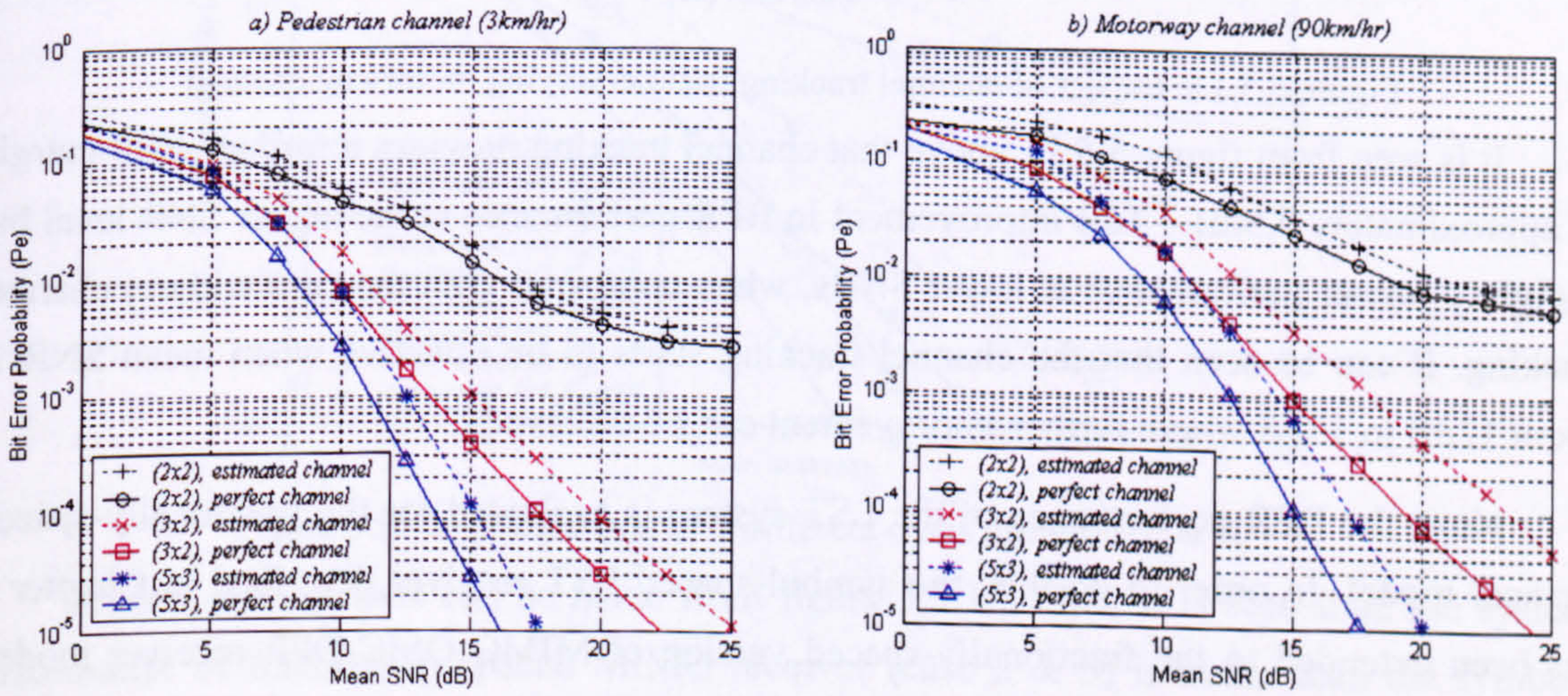

Figure 5.5.10: *Pe* versus mean SNR for 1) estimated channel case & 2) perfect channel case in different time-varying channels: a) pedestrian channel & b) motorway channel.

Several observations can be made from figure 5.5.10. First, the results for the estimated channel case show minor degradation as compared to the perfect channel estimate case indicating that the proposed estimator could still perform under the time-varying channel condition. The results for the slow moving pedestrian channel are almost identical as compared with figure 5.5.3a for the block-invariant channel case. However, the overall BER performance drops for both the estimated and perfect channel case as the velocity of the channel increases; i.e. shown in the motorway channel case.

With the use of the channel tracking algorithm described in section 4.5, the BER performance of the LST receiver can be further improved. The results are shown for the motorway channel for the two ($N\times M$) systems: the (3×2) system and the (5×3) system, using the fixed setting of $(L+1) = 3$, $K_f = 5$, $K_b = 3$ and pilot length of $v = 24$ in the estimator.

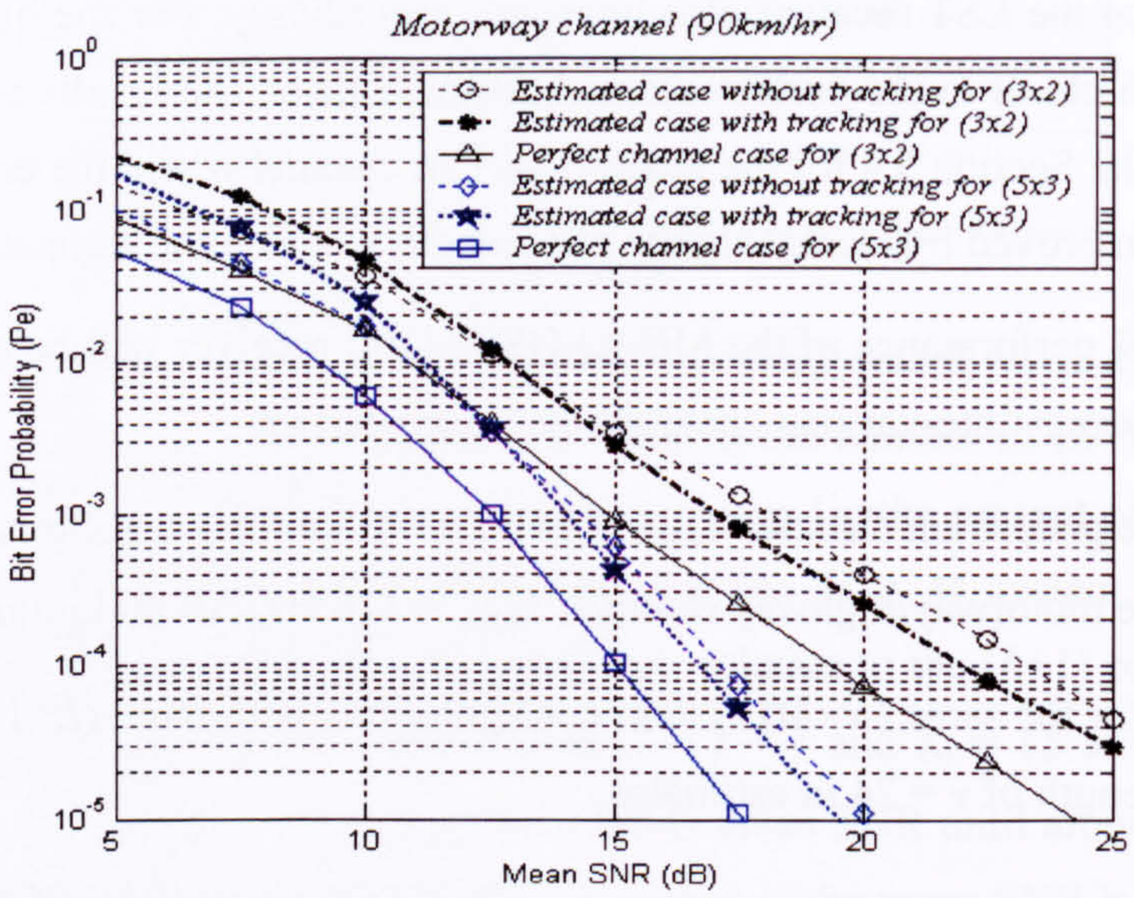

Figure 5.5.11: Impact of channel tracking in time-varying motorway channel

It is seen from figure 5.5.11 above that channel tracking provides a further small margin of approximately 0.5dB – 1dB improvement in BER performance at the higher SNR level but a slightly poorer performance at lower SNRs, when compared with the case without channel tracking. It can be seen that the channel tracking starts to be effective when mean SNR is about 12dB to 13dB where further improvement can be achieved.

Next, the BER performance of the LST system is evaluated for the fractionally-spaced channel model. In order to do this, the symbol-spaced LST receiver described in Chapter 2 has been extended to the fractionally-spaced version of MIMO-OSIC-DFE receiver model. The extension is straightforward and requires additional paths inserted within the fraction of a symbol period and the fractionally-spaced equaliser's tap-weights can be obtained using the same way as described in section 2.4. The proposed fractional channel estimator described in

section 4.4 is also applied to the fractionally-spaced OSIC-DFE receiver to evaluate the impact that estimation errors have on the system performance as compared with the case using the perfect channel estimates. In the following, the system performance for different channel and receiver models are compared for the ($N\times M$) system with the following set-up:

Case 1) Symbol-spaced channel with symbol-spaced MIMO equaliser.

Case 2) Symbol-spaced channel with fractionally-spaced MIMO equaliser.

Case 3) Fractionally-spaced channel with fractionally-spaced MIMO equaliser.

The total number of path, l, in each CIR of the MIMO channel for the symbol-spaced and the fractionally-spaced model is different. In the symbol-spaced channel, the number of path $l = (L+1) = \varphi$, whereas in fractionally-spaced channel, $l = c \times \varphi$ where φ is the total delay spread in symbol period and 'c' is the receiver's sampling rate. The total number of equaliser's feedforward tap K_f used in symbol-spaced equaliser is also different from the total number of taps K_{ff} used in fractionally-spaced equaliser, where $K_{ff} = c \times K_f$.

Unless otherwise stated, results are shown for overall delay-spread of $\varphi = 3$ symbol periods and $c = 2$ for the fractionally-spaced channel and equaliser with varying number of taps. The corresponding l for each case is also stated. (Again, uniform fractionally-spaced model in section 4.3 is considered here for maximum number of paths setting).

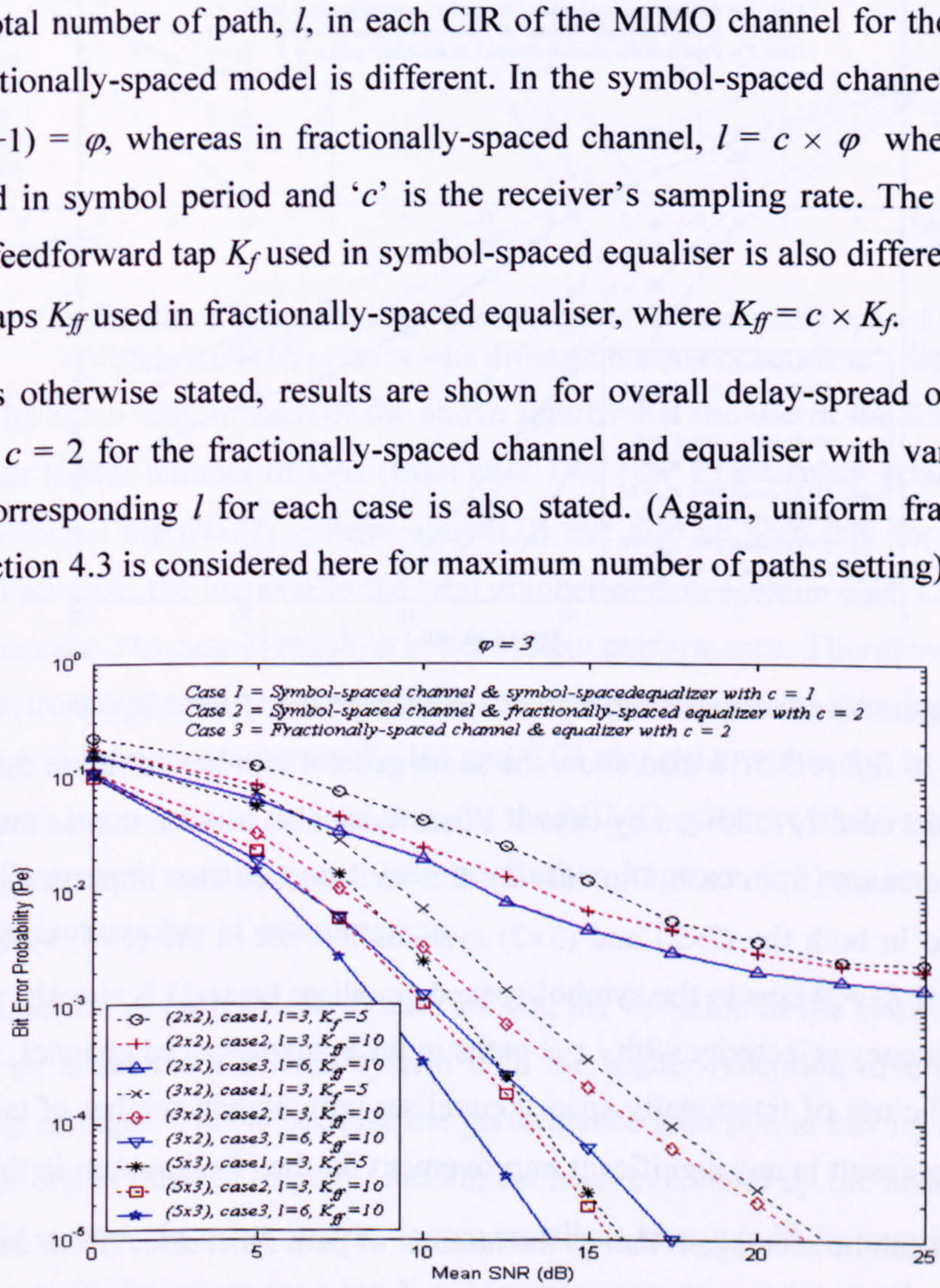

Figure 5.5.12: Comparison of 3 different cases using $\varphi = 3$ & $K_f = 5$.

Several observations can be made from figure 5.5.12. First, it is seen that, the system performance of fractionally-spaced MIMO receiver (case 2 & 3) is better than the symbol-spaced MIMO receiver (case 1) for all the ($N\times M$) configurations shown. Secondly, as the number of equaliser's tap increases (from case-1 to case 2), the system performance also

improves accordingly, showing that the fractionally-spaced equaliser is superior than the symbol-spaced equaliser. Thirdly, as the number of path l increases (from case 2 to case 3), the overall system performance also improves accordingly when sufficient equaliser's tap is used. This confirms the trends seen previously in figure 5.5.4 to figure 5.5.8.

Next, figure 5.5.13 shows the effect of increasing K_f and K_{ff} taps for the same ($N\times M$) systems in figure 5.5.12 to see the effect that has on the performance in each case 1 2 & 3.

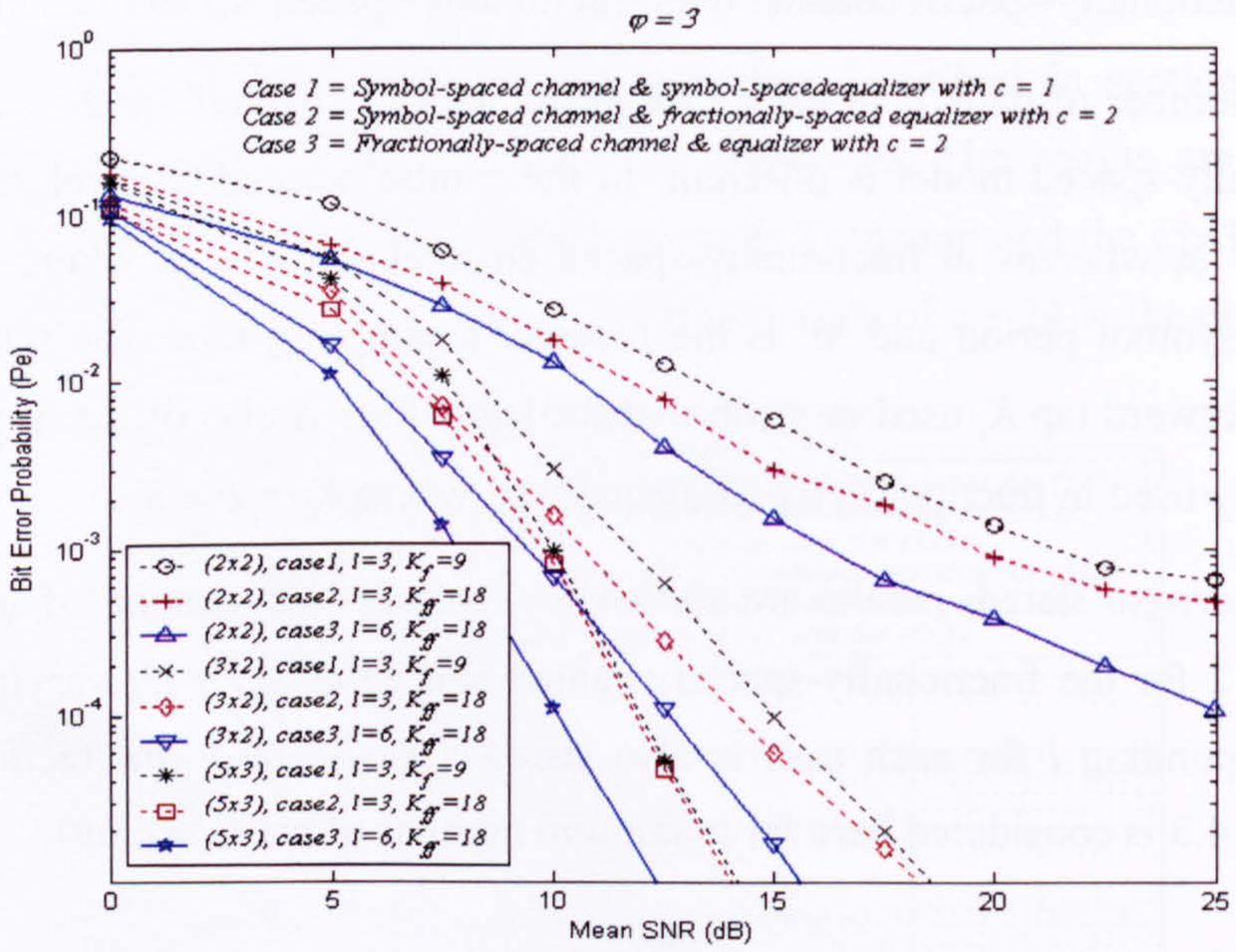

Figure 5.5.13: Comparison of 3 different cases using $\varphi = 3$ & $K_f = 9$.

The results in figure 5.5.13 also show the same general trend as in figure 5.5.12, where case 3 out-performs case 2, followed by case 1. First, it can also be seen that as the number of equaliser's tap increases (from case 1 to case 2), the performance also improves accordingly, which is observed in both the (2×2) and (3×2) systems but not in the (5×3) system. This is because, the use of $K_f = 9$ taps in the symbol-spaced equaliser (case-1) is already sufficient to deal with the frequency selectivity with $l = 3$ paths in the symbol-spaced channel, for a higher $N > M$ system. The use of fractionally-spaced equaliser with higher number of taps, $K_{ff} = 18$ (in case 2) will not result in any significant improvement for the (5×3) system in this case.

Secondly, it can be seen again that as the number of path l increases (from case 2 to case 3), the overall performance for all three systems also improves accordingly when sufficient number of equaliser's taps is used. This again confirms the trends seen from figure 5.5.3 to 5.5.8 for the symbol-spaced case. Certainly, different ($N\times M$) systems that have different N/M diversity gains that could contribute to different level of performance improvement for both the symbol-spaced and fractionally-spaced MIMO receivers.

The results in both figure 5.5.12 & 5.5.13 can again be compared for overall influence of the equaliser's tap with respect to the number of channel paths l on the system performance for each case of the ($N\times M$) system shown in the following figures:

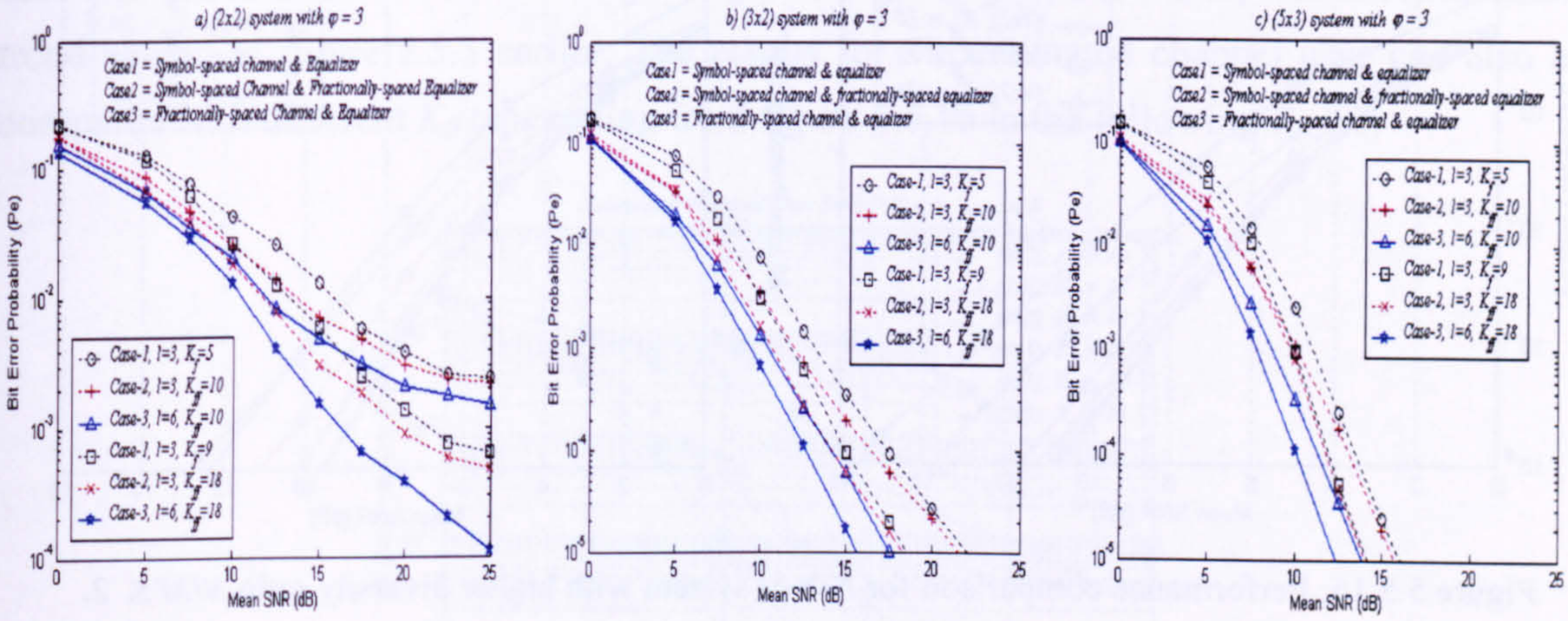

Figure 5.5.14: Performance comparison for symbol-spaced & fractionally-spaced MIMO receiver in different ($N\times M$) systems with different number of equaliser's tap

It can be again seen in each of the above figures that the use of the fractionally-spaced equaliser with higher number of taps (from case 1 to case 2) generally provides better BER performance for all the ($N\times M$) systems shown. It can also be seen that for the fractionally-spaced equaliser case, the increase in the total number of path l within each CIR of the MIMO channel (from case 2 to case 3) result in better system performance. Therefore, having 'richer' mulitpath environment tend to be beneficial for the MIMO systems provided that sufficient equaliser's tap is used to counteract the ISI and CCI that exist within the frequency selective MIMO channel. It can be also noticed that, for the MIMO system with $N = M$ setting, the use of fractionally-spaced equaliser can help to further improve the system performance by having a sufficient number of equaliser taps.

In comparison of each ($N\times M$) system shown, the variation in the system performance is observed to be lesser for a MIMO system with the higher reception diversity order as the number of tap changes. This is because the performance gain due to having more equaliser's tap as well as higher number of path l has almost been overcome by the added diversity gain in the $N > M$ system. In other words, lesser equaliser taps would be required to achieve a similar or better BER performance for $N > M$ system as compared with $N = M$ system. This can be further illustrated using the $N > M$ system with higher diversity order of, $N/M = 2$, to compare with cases of lower diversity order, $N/M < 2$, case; i.e. (4×2) versus (3×2) system and (6×3) versus (5×3) system for maximum number of path l=6, shown in next figure:

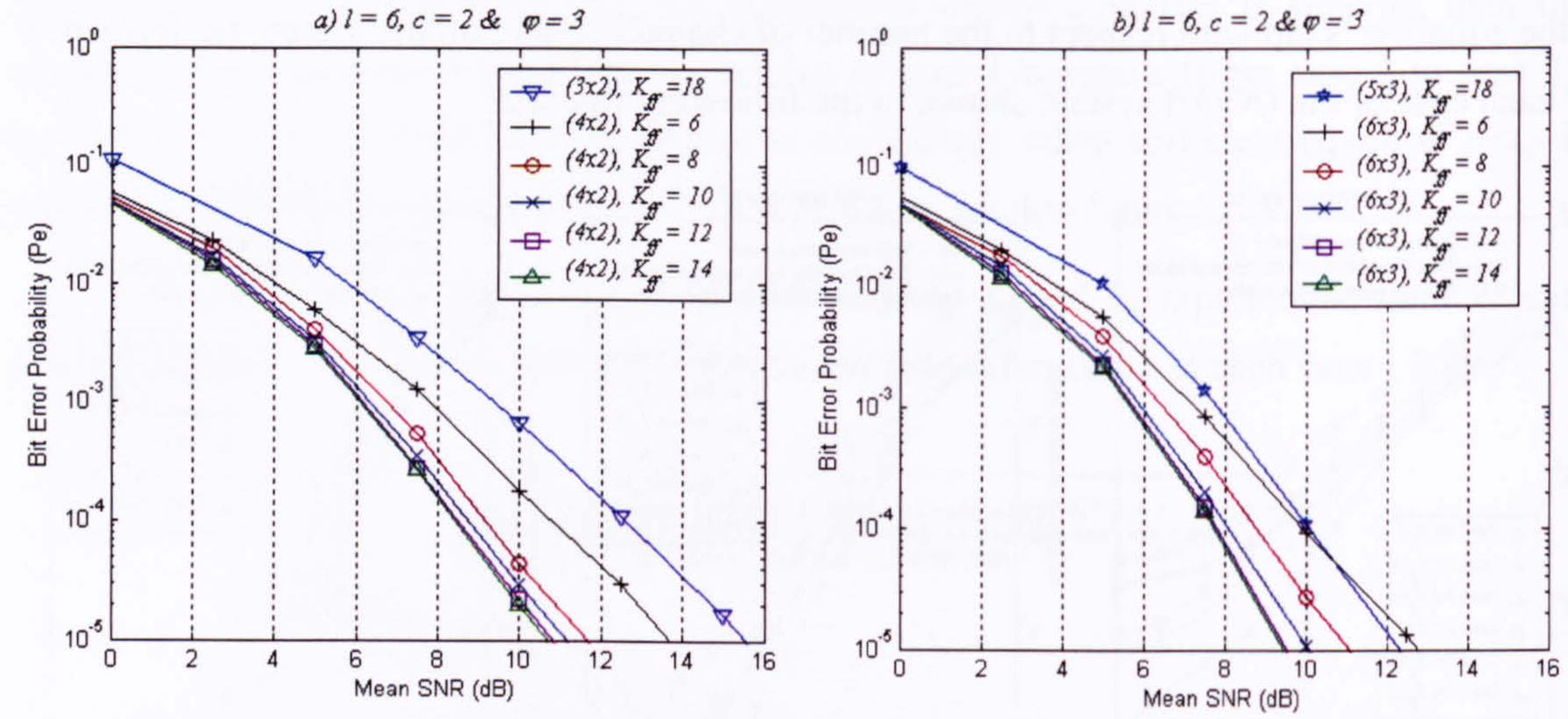

Figure 5.5.15: Performance comparison for $N > M$ system with higher diversity ratio $N/M \leq 2$.

It can be seen in figure 5.5.15 that the performance of the $N > M$ system with higher diversity order of $N/M = 2$; i.e. the (4×2) system and the (6×3) system, tends to perform better than the systems with a lower diversity ratio of $N/M < 2$; i.e. the (3×2) system and the (5×3) system respectively, even though fewer equaliser's tap is used. Also, as the number of K_{ff} taps (used in the fractionally-spaced equaliser) increases, the system performance also improves accordingly but with a diminishing rate.

Next, figure 5.5.16 shows the results using the proposed fractionally-spaced MIMO-CE method described in section 4.3.2 with the fractionally-spaced MIMO receiver to assess the impact of channel estimation error that has on the system performance. The results are also compared to the case where perfect channel estimate is assumed. Results are plotted for different (N×M) systems of case-3 (for fractionally-spaced channel & equaliser case).

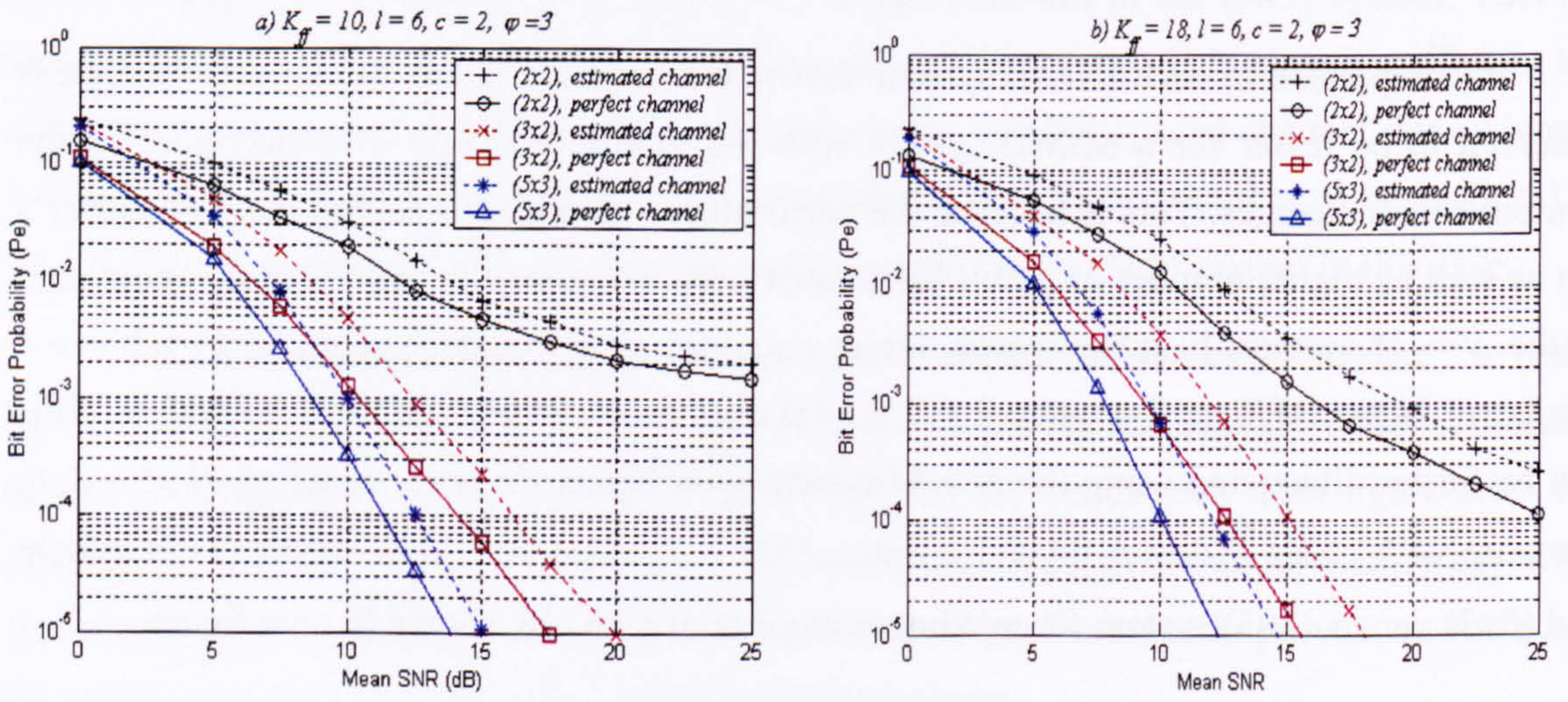

Figure 5.5.16: *Pe* versus mean SNR of the for φ = 3 with K_{ff} = 10 & 18 for different $N > M$ systems

It can be seen from figure 5.5.16 that the proposed estimator demonstrates consistent performance with a small degradation when compared with the perfect channel estimate case. Notice that the difference in the bit error probability performance between the perfect channel case and the estimated channel case get larger as higher K_{ff} taps are used, which confirms the trend shown in figure 5.5.3 earlier. The results for the estimated channel case can also be compared with different K_{ff} taps setting from figure 5.5.16 in the following figure:

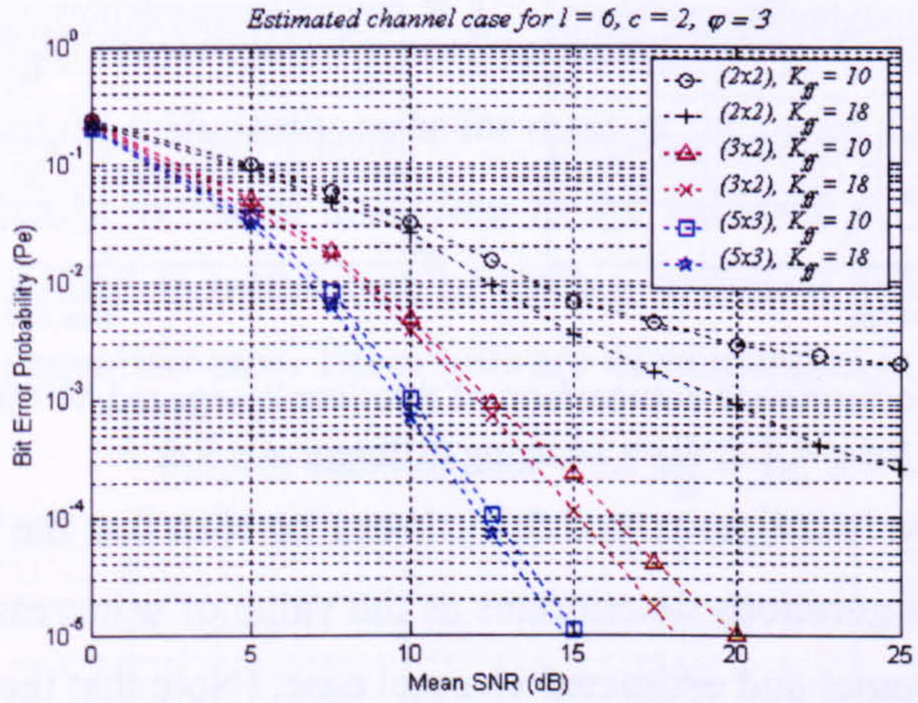

Figure 5.5.17: Comparison for the estimated channel case with different K_{ff} taps setting

It will be seen that the results for the estimated channel case also exhibit the same trend seen in case 3 of figure 5.5.14 where higher K_{ff} taps setting provide better performance in each ($N\times M$) system, particularly for the $N = M$ system. However, for the $N > M$ systems, there is only a marginal improvement in performance from $K_{ff} = 10$ to 18 taps setting. This could be due to the fact that a larger portion of the estimation error is generated for the higher $K_{ff} = 18$ taps setting when obtaining the weights for the equaliser. Nevertheless, the fact that the results of the $K_{ff} = 18$ taps setting is better than $K_{ff} = 10$ taps settings for the $N = M$ system, indirectly demonstrate the contribution to the performance advantage achieved by the $N > M$ system with added diversity gain in the layered spaced-time system (since the results using the perfect channel case also demonstrate the same trend as shown in case-3 of figure 5.5.14).

So far, the results presented for the fractionally-spaced channel and equaliser model are based on fixed value of c and φ. In the following, the value of c and φ are varied to assess the impact of these settings on the system performance of the layered space-time system. Results are shown for case 3 only where a fractionally-spaced model of the channel and equaliser are considered. Results are also plotted for both the estimated and perfect channel estimate case.

First, the effects of having different values of φ on the system performance are examined. The results are shown in figure 5.5.18 for the ($N\times M$) systems with the fixed setting of $c = 2$ & $K_{ff} = 14$ and $c = 2$ & $K_{ff} = 18$ settings and with various values of φ.

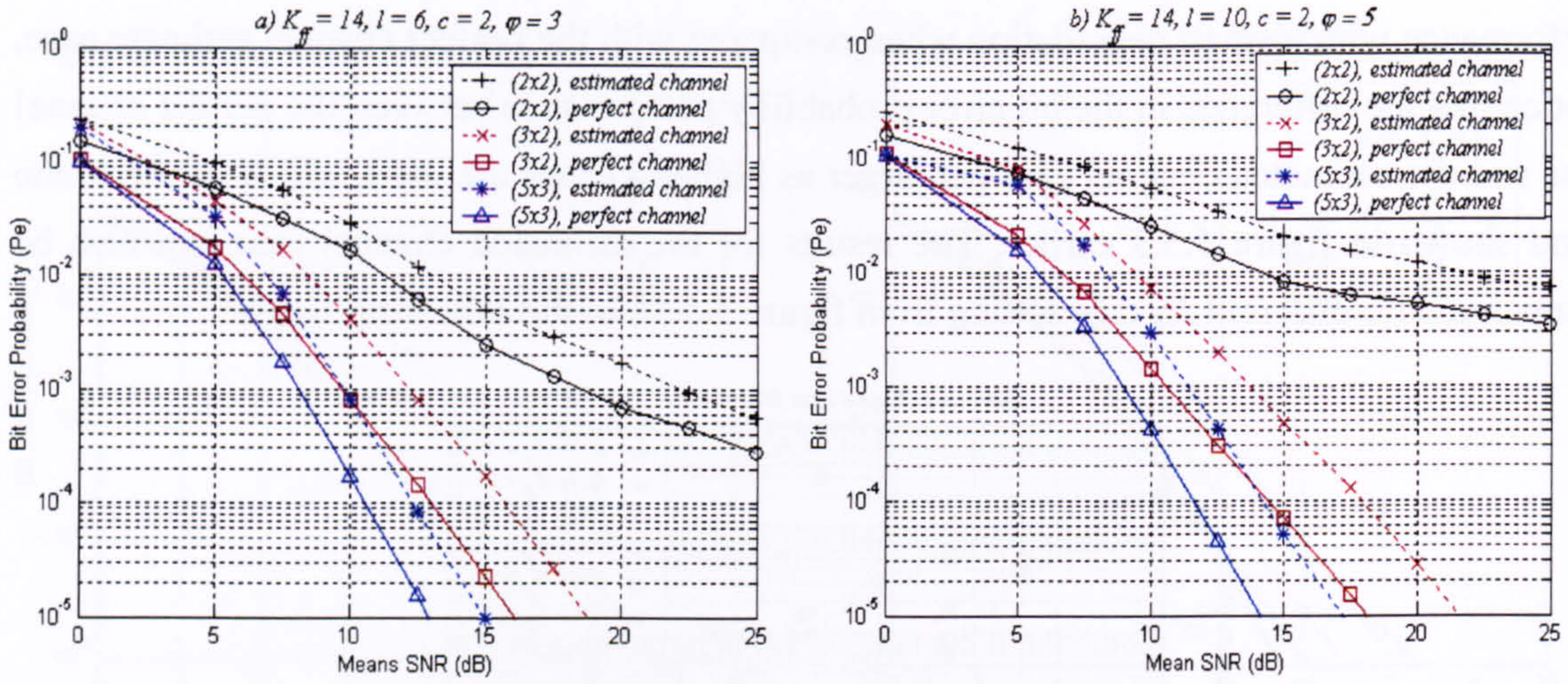

Figure 5.5.18: Performance comparison of fractionally-spaced MIMO receiver for $c = 2$ & $K_{ff} = 14$ using different $\varphi = 3$ & 5.

When comparing the two figures in 5.5.18, it can be seen that the system performance for all ($N \times M$) system configurations deteriorates as the value of φ increases from 3 to 5. This is true for both perfect channel and estimated channel case. (Note that the number of path l is: $l = 6$ for $\varphi = 3$, and $l = 10$ for $\varphi = 5$). The results also show the consistent performance of the proposed fractionally-spaced channel estimator for both cases of $\varphi = 3$ and $\varphi = 5$. The effect of φ that has on the system performance is shown more clearly by comparing the results for perfect channel case and estimated channel case separately in the following figure:

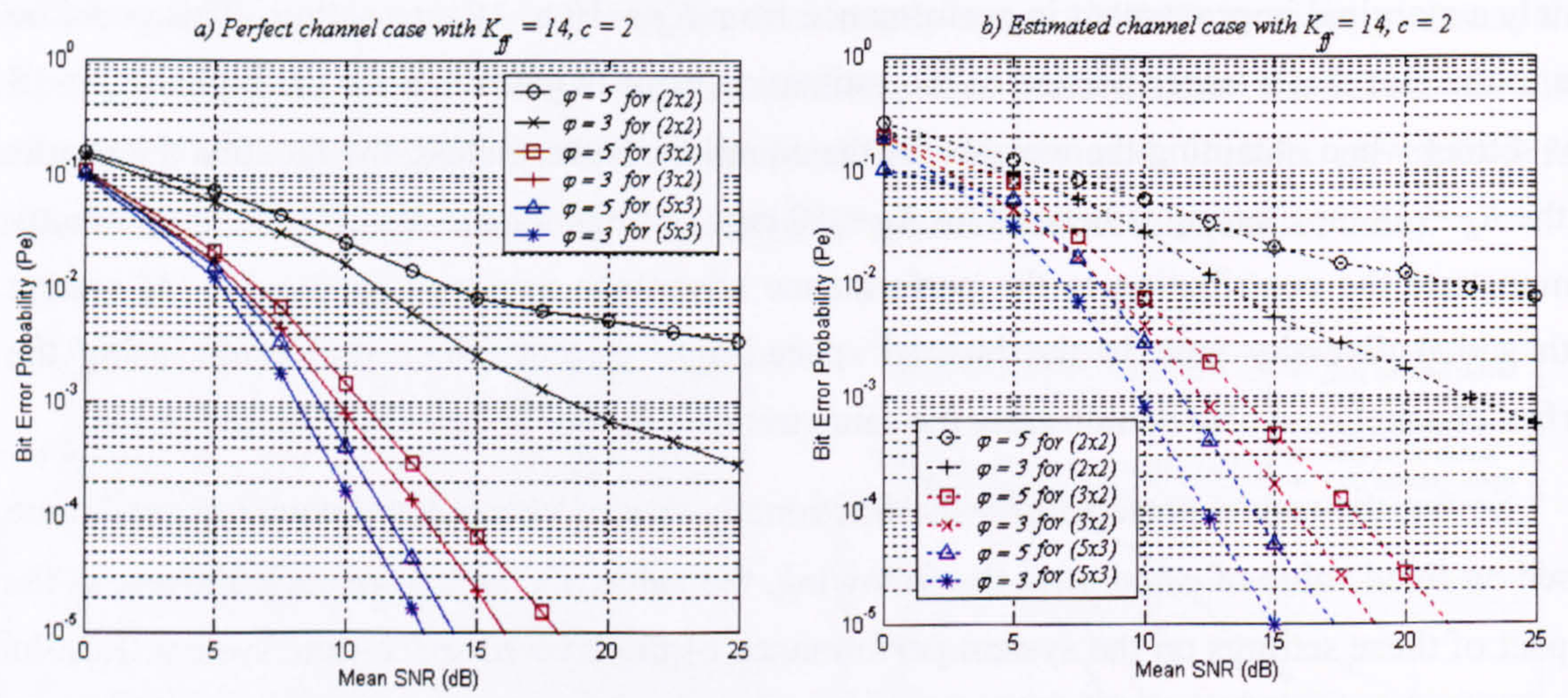

Figure 5.5.19: Performance comparison for both estimated channel & perfect channel case using $c = 2$ & $K_{ff} = 14$ with different $\varphi = 3$ & 5

It can be seen from figure 5.5.19a and 5.5.19b that as the value of φ increases (from 3 to 5), the BER performance for all the ($N \times M$) systems drops accordingly for the fixed setting of $K_{ff} = 14$ taps. This is because the receiver needs more equaliser taps to deal with the additional ISI as the delay spread lengthens from 3 symbol periods to 5 symbol periods. The $K_{ff} = 14$

taps might not be sufficient for the $\varphi = 5$ case since the corresponding total paths have been increased from the initial value of $l = 6$ (for $\varphi = 3$ case) to $l = 10$. The results also show the consistent performance of the proposed fractional channel estimator for the $\varphi = 5$ case.

Next, the results are shown for the fractionally-spaced channel and receiver model using the perfect channel case with $c = 2$ and $K_{ff} = 18$ for various values of φ, from 3 to 6. The corresponding number of path in each case can be obtained via the same equation: $l = \varphi \times c$, which is $l = 6$, 8, 10 & 12 respectively for corresponding value of φ. Larger setting of $K_{ff} = 18$ taps is deliberately used, to sufficiently cater for most of the cases where the number of path l is allowed to be gradually increased according to the value of φ. This allows the effect of increasing l to be examined from the case of having sufficient number of equaliser taps to insufficient number of equaliser taps. The results are demonstrated in the following figure:

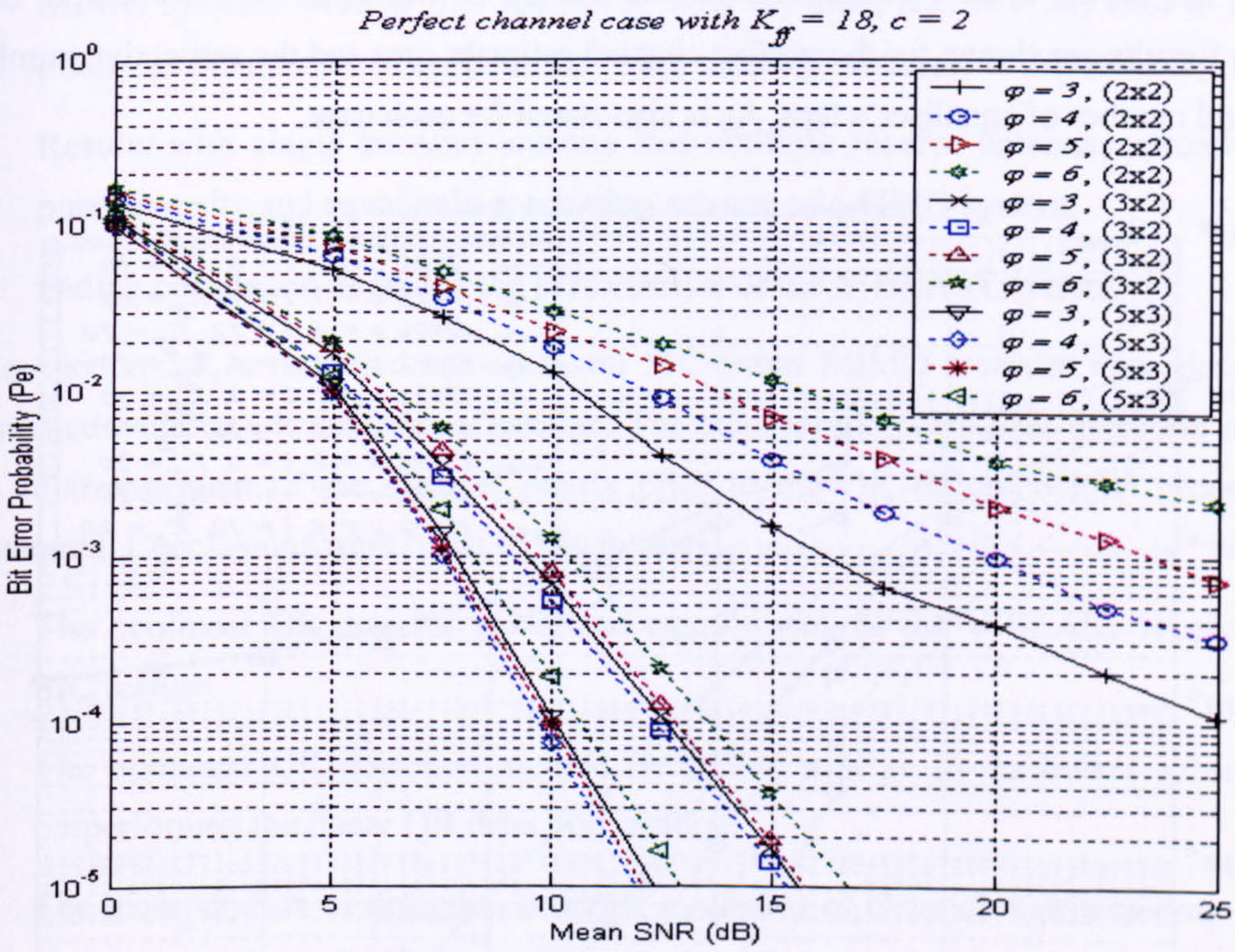

Figure 5.5.20: Performance for perfect channel case using $c = 2$ & $K_{ff} = 18$ with different $\varphi = 3,4,5$ & 6

Several observations can be made from figure 5.5.20. First, for the $N > M$ system, the results are almost identical as the value of φ increases from 3 to 6. However, when examine in greater detail, there are certain changes in the BER performance that depend on 1) the relative difference between the number of paths l to the available equaliser taps K_{ff} as φ changes and 2) the ($N \times M$) system configuration. For instance, as φ increases from 3 to 4, the available number of $K_{ff} = 18$ equaliser's taps in the $N > M$ system are still sufficient to cater for the total

path $l = 8$. However, as φ increases further to 5, the (3×2) system exhibit slight reduction in performance whereas the performance in (5×3) system still improve slightly. Nonetheless, as φ increases to 6, both (3×2) and (5×3) systems exhibit a reduction in performance, since the relative difference between l & K_{ff} reduces. In this case, $K_{ff} = 18$ equaliser's taps is no longer sufficient to accommodate for any additional paths as φ increases.

As for the $N = M$ system, the BER reduction is observed as φ increases from 3 to 6, indicates that $K_{ff} = 18$ equaliser's taps might not be even sufficient to deal with the increasing number of paths in the channel. This confirms all the previous findings for the importance of using sufficient equaliser's taps relative to the number of paths in the LST system.

Next, figure 5.5.21 shows the effect of having different fractional sampling rate $c = 2$, 3 & 4 that has on the system performance using a fixed setting of $\varphi = 3$ for different ($N \times M$) systems. Results are shown for the perfect channel estimate case and the respective number of paths l and number of equaliser's taps, K_{ff} is also stated for each case.

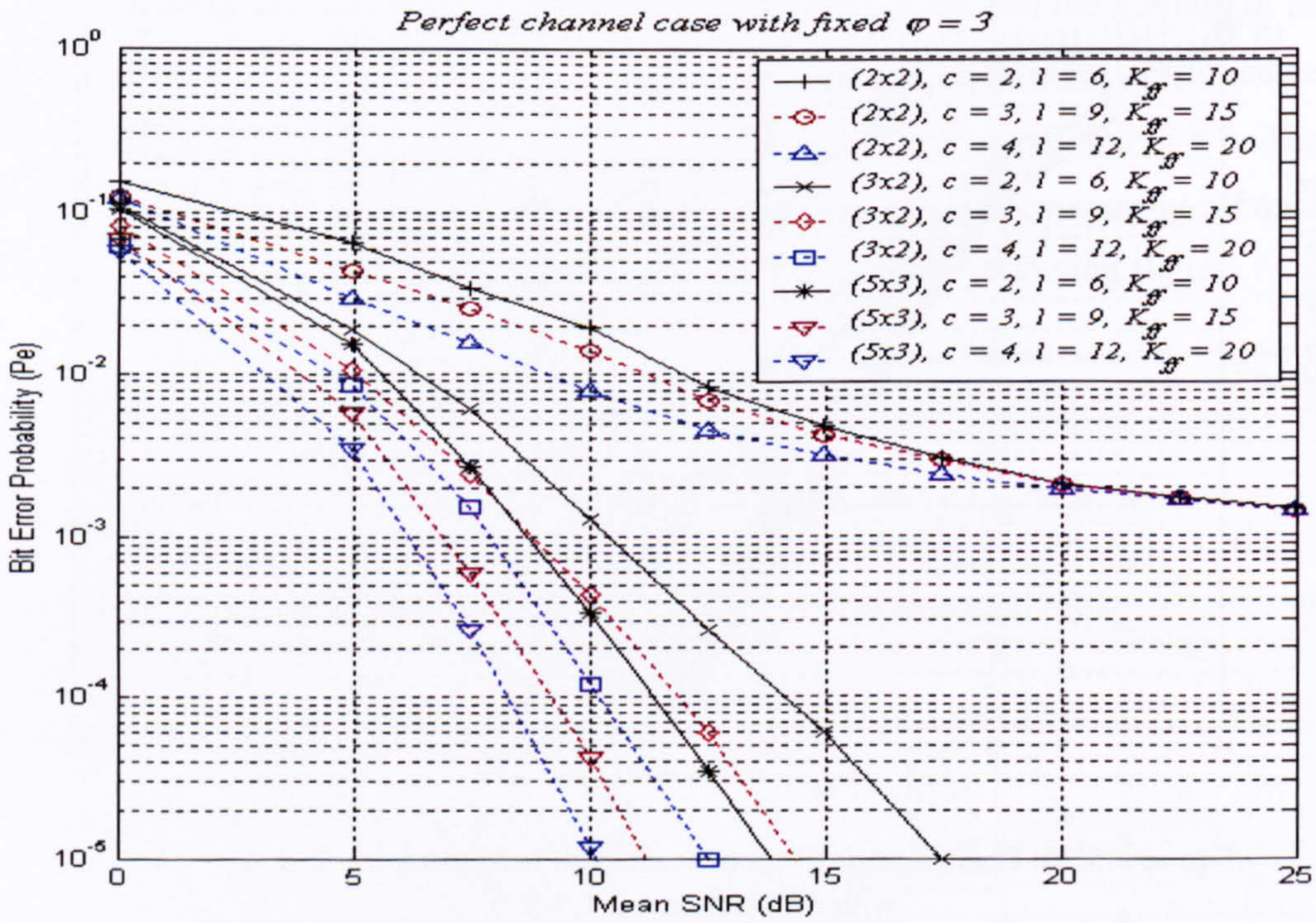

Figure 5.5.21: *Pe* versus mean SNR with different value of c

It can be observed from figure 5.5.21 that the bit error probability performance improves in general as c increases from 2 to 4. This is shown especially in the $N > M$ systems. The results further demonstrate that layered space-time system achieve better performance when operating in 'rich' multipath environment provided that each path exists within the channel is carefully exploited and estimated accurately.

5.6 Summary of Simulation Results

In section 5.1, the V-BLAST system (with M transmit antennas and N receive antennas) had been successfully implemented using four different detection algorithms, namely linear ZF, linear MMSE, nonlinear ZF and nonlinear MMSE. Results were obtained for various ($N \times M$) system configurations. Conclusions were observed as follows:

- Nonlinear detection methods (with symbol interference cancellation – SIC scheme) achieved better system performance as compared to the linear detection methods.
- MMSE technique was marginally better than the ZF technique.
- MIMO systems with higher reception diversity order (N/M) achieved better results than the one with lower diversity order.
- MIMO systems with no SIC feature & diversity gain, (i.e. $N = M$) tend to perform poorer as the number of antenna increases, although data rate is increased by M-fold.
- Results with single transmit antenna and multiple receive antennas resembled the pure diversity and equal gain combining scheme of a SIMO system.
- Fading correlation degraded the performance of the V-BLAST system

In section 5.2, a modified sub-optimum SIC-based MIMO receiver was successfully implemented with the QR detection algorithm. The incorporation of proper detection ordering by the re-arrangement of the channel matrix prior to the QR decomposition process was demonstrated. Conclusions were observed as follows:

- The nonlinear QR detector performed equally well as the V-BLAST receiver with SIC feature.
- The nonlinear QR detection method (with SIC scheme by backward substitution) outperformed the linear QR detection method.
- The incorporation of detection ordering by means of channel matrix re-arrangement demonstrated better performance than those with random detection ordering.

In section 5.3, various MIMO channel estimators catered for frequency-flat MIMO channel, namely the MIMO-LMS, MIMO-RLS and MIMO-PMI were successfully implemented. Performance of the estimators as well as the V-BLAST system was shown. Conclusions were observed as follows:

- MIMO-LMS was an unsuitable method since long time was needed for the estimator to converge to an acceptable solution.

- MIMO-RLS demonstrated adaptive channel estimation ability with very fast convergence and had good performance at higher SNR level.
- The forgetting factor in MIMO-RLS had influence on the estimator's performance. Lower forgetting factor results in more unstable condition of MIMO-RLS estimator.
- Different Doppler velocities at different SNR levels affected the performance of MIMO-PMI where trade-off between the pilot length & the MSE was demonstrated.
- For block-invariant or slow varying channel, increasing the pilot length would improve the estimator performance. For fast varying channel, an optimum pilot length was observed where estimator's performance would initially improve as pilot length increased until reaching an optimum value and later would gradually degraded (due to large variation in channel) for any further increase of pilot length.
- Both MIMO-RLS and MIMO-PMI estimators demonstrated little degradation in system performance as compared to the perfect channel estimates case.

In section 5.4, the novel frequency-selective MIMO-CE scheme using either ordinary Hadamard (OH) or the Paley-Hadamard (PH) matrix had been successfully implemented and incorporated into the MIMO-OSIC-DFE receiver. Performance of the proposed estimator had been carried out for both block-invariant and time-varying channel. Four types of time-varying channel with different Doppler velocities were used. Results were shown for both symbol-spaced model and fractionally-spaced model.

- In general, pilot length minimisation could be achieved by using the Paley-Hadamard matrix with no loss in estimator's performance. The performance of the proposed estimator was identical when using either OH or PH matrix to form the pilot matrix.
- In the block invariant, symbol-spaced model, the trade-off between pilot length and the MSE were shown where performance improved as the pilot length v increases. The estimator's performance was independent of the number of receive antennas N and the number of $(L+1)$ paths in each CIR. However, the performance degraded as the number of the transmit antennas M increased (due to the power reduction in each antenna since total transmit power had to be kept constant). Same performance results were shown for both cases of $N>M$ and $M>N$. The $M>N$ case demonstrated the ability of the proposed estimator to operate at the multiusers scenario.
- In the time-varying, symbol-spaced model, similar results from the MIMO-PMI estimator were observed where different Doppler velocities affected the proposed estimator's performance at different SNR levels. An optimum pilot length could be

observed in the fast varying channels where estimator's performance improved initially as pilot length increased until reaching the optimum value and later gradually degraded for any further increase of pilot length. N again was found to have no influence on the estimator's performance (for both $N>M$ and $M>N$ case) showing that no added advantages could be obtained in channel estimation with extra diversity order. Same as before, the estimator's performance degraded as M increased. Nevertheless, the number of $(L+1)$ paths had an impact on the estimator's performance especially in the fast varying channel where increasing value of $(L+1)$ paths caused further performance degradation since the estimator needed to deal with longer deviation within the varying-channel. It was also found that only minimal pilot length was needed when the estimator was operated at high SNR level but optimum pilot length resulted in minimum MSE at the nominal mean SNR levels.

- In the block-invariant fractionally-spaced model, the trade-off between pilot length and the MSE were again demonstrated where performance improved with increasing v. Similarly, N had no influence on the estimator's performance but the performance degraded as M increased. Also, the fractional sampling rate c and the total delay spread φ were of two crucial factors found. It was learned that for fixed value of φ, increasing c had no influence on estimator's performance but different value of φ itself had influence on the performance. Increasing φ resulted in poorer MSE due to the increase of ISI effect of the delay spread and error propagation during the estimation. The performance of the proposed fractional MIMO channel estimator was therefore affected by the total span of delay spread in the MIMO channel.

- In the time-varying fractionally-spaced model, for a fixed value of φ, increasing c had no influence on estimator's performance for slowly varying channel when optimum pilot length v was used. But when non-optimum pilot length has been used, the results show slight degradation in estimator's performance when operated in a faster time-varying channel for increasing value of c. Hence, the use of optimum pilot length was vital for proposed channel estimator to operate in fast time-varying channel. For a fixed value of c, increasing value of φ further degraded the estimator's performance especially for the fast varying channel even when optimum pilot length was used. This is because more severe time-variation within the frequency selectivity was introduced that might restrict the performance of the proposed estimator.

In section 5.5, the system performances of the MIMO-OSIC-DFE receiver that operated in frequency selective fading MIMO channel had been demonstrated for various system parameters and configuration. In particular, results were compared for the case of using the

channel estimates by the proposed MIMO channel estimator (symbol-spaced and fractionally-spaced type) and the perfect channel case. Both block-invariant and time-varying channels were used.

- System performance was better when order successive interference cancellation OSIC scheme is used as compared to those without OSIC for all configurations.
- For a fixed (L+1) paths, increasing the number of K_f taps in the DFE, improves the system performance in general. However, this also depended on two major factors: a) the relative number of K_f taps w.r.t the number of (L+1) paths and b) the diversity order of the systems. The bit error probability performance improved as the number of K_f taps in the DFE relative to the number of (L+1) paths increased. Also, the greater the diversity orders the better the bit error probability performance.
- For system with no diversity gain, N=M case, further increase of (L+1) paths caused degradation in system performance if the number of K_f taps were insufficient. Improvement in system performance only be observed when sufficient number of K_f taps was used.
- However, for the N>M system with higher reception diversity, increase of (L+1) paths further improved the system performance only until certain level and the system performance ceased to improve when the relative number of K_f taps w.r.t the number of (L+1) paths became closer.
- System performance achieved by the proposed MIMO-CE scheme demonstrated only slight degradation when compared to the perfect channel case.
- For the block-invariant system, it was shown that the higher the pilot length v used, the better the system performance.
- Faster time-varying channel results in further degradation of the system performance. This could be improved by the use of channel tracking, where channel tracking improves the system performance at high SNR but would worsen the performance at low SNR due to error propagation within the feedback mechanism.
- The use of fractionally-spaced equaliser could further improved the system performance when sufficient numbers of number of K_{ff} taps were used relative to the number of l paths.
- The system performance using the channel estimates obtained by the proposed fractional MIMO-CE scheme resulted in small degradation when compared to the perfect channel case.

Chapter 6

Conclusions

The focus of this thesis has been the design and development of suitable MIMO channel estimation scheme for *uncoded* MIMO wireless communications. The driver for this work has been the recognition of the importance of channel knowledge for the MIMO systems in order to fully achieve the quoted capacity. In the thesis, the channel estimation schemes have been focused on two layered space-time systems, namely: the V-BLAST receiver and its extended version, the MIMO-OSIC-DFE receivers. In the following, various research works that have been accomplished are summarised and suggestions for future research in the related areas of the MIMO systems, especially for the work of MIMO channel estimation are also discussed.

6.1 Summary of Research

Space-Time Receivers & Concepts – In Chapter 2, the essential background of the space-time processing (STP) technique [11] for the MIMO systems is provided. This chapter addressed the common problems in the typical MIMO systems such as CCI and ISI. Understanding the STP concept is vital for the subsequent introduction of BLAST receivers deploying with the successive interference cancellation (SIC) scheme. Arising from this preliminary study was a novel method that combines the V-BLAST detection method with the QR detection algorithm. As a result, sub-optimum but computational efficient SIC-based MIMO detector was successfully implemented, which incorporated proper detection ordering by the re-arrangement of the channel matrix prior to the QR decomposition process. Non-linear detection was then carried out by the triangularisation process, where each symbol was detected using only a single division of an appropriate channel coefficient in backward substitution. The recovered symbol and the associated channel paths are then subtracted to cancel its interference contribution to assist subsequent symbol detection. This proposed method was found to approximate the performance of the conventional V-BLAST receiver. The works are accomplished with the intention to verify the V-BLAST algorithm and confirm the understanding behind the space-time techniques used.

Adaptive and non-adaptive MIMO channel estimator (frequency-flat fading case) – In Chapter 3, due to the need for channel knowledge in the space-time receiver, the work regarding the MIMO channel estimators were carried out primarily for the case under frequency-flat fading MIMO channel condition. The objective was to estimate all $N \times M$ fading coefficients within the MIMO channel matrix. The initial approach was to consider the use of an adaptive algorithm such as the LMS and RLS algorithm to estimate the MIMO channel characteristic by means of training sequences. As a result, the MIMO-LMS and MIMO-RLS (or MEA-RLS) training-based algorithms were implemented. The latter approach was found to be more favourable due to the need for shorter training length for each antenna but at a higher cost of computational complexity.

In an attempt to reduce the computational burden a non-adaptive approach called the MIMO-PMI algorithm was subsequently implemented using orthogonal pilot training sequences to reduce the complexity of the matrix inversion process. The concept of using a set of orthogonal pilot sequence in a matrix was also proposed and introduced in Chapter 3. Similar channel estimation methods (derived for flat fading case) in [73, 83], had been followed through. The works reported in the thesis presented a more thorough investigation on the design of pilot symbols and possible extension of the pilot matrix to cater for different system configurations. The use of orthogonal sequences extracted from the Hadamard matrix was a major contribution to the development of the proposed MIMO-PMI algorithm. Results obtained were those which highlighted the trade-off between the length of the training sequence (or pilot length) and the channel estimation error, depending on the mobile speed of the channel. For a slow varying channel, the estimator's performance improves as the pilot length increases. For a fast varying channel, an optimum pilot length is observed where the MSE improves initially as pilot length increases until a certain value and then degraded (due to the variation in channel) for any further increases in pilot length. The proposed channel estimation approaches were successfully implemented in the V-BLAST receiver to allow performance evaluation of more practical case in the flat fading MIMO channel.

Novel MIMO channel estimation scheme (frequency-selective fading case) – In Chapter 4, the works on the channel estimation scheme (MIMO-PMI algorithm) in Chapter 3 was extended to deal with more realistic frequency-selective fading multipath model. The emphasis in this chapter was the incorporation of a suitable MIMO channel estimation scheme for MIMO-OISC-DFE receiver described in Chapter 2. The related problem of joint CCI and ISI was carefully studied and considered in the proposed MIMO channel estimation scheme. As a result, a novel training-based MIMO channel estimation scheme that could operate in frequency selective fading MIMO channels was successfully implemented for the uncoded layered space-time systems. The concept of the *concatenated* MIMO channel matrix was introduced to allow all $(L+1)$ delay paths to be considered and estimated simultaneously. The objective was to estimate all $M \times N \times (L+1)$ channel coefficients within each CIR of the frequency selective MIMO wireless channel.

Initially, the design of the pilot symbols was based on the use of orthogonal sequences extracted from the set of sequences contained in a Hadamard matrix are used for the construction of pilot matrix. The criteria for pilot matrix formulation was found to be independent of the number of receive antennas N but dependent on the number of transmit antennas M and the number of $(L+1)$ paths within the CIRs of the MIMO channel. It was also found later that the pilot sequence length could be minimised (and hence throughput increased) through the use of Paley's construction of the Hadamard matrix instead of the ordinary one. The comparison was presented in section 4.2.3.5. This later MIMO-CE method allows channel estimation to take place almost immediately after all the necessary received pilot symbols had been properly collected without introducing too much latency (the unnecessary time-gaps). This is done by using the unique combination of the orthogonal structure and the Toeplitz-like structure of the Paley-Hadamard matrix were. By exploiting the Toeplitz-like structure, the number of pilot symbols could be significantly reduced with no reduction on the estimator's performance. Concurrently, the orthogonal structure also allowed the estimation of the concatenated channel matrix to be carried out in a single matrix operation without the need of matrix inversion for the entire pilot matrix. The construction of the pilot matrix and the criteria for generating both ordinary and Paley's type of Hadamard matrix were also demonstrated for different system configurations and parameters. The trade-off between the length of the training sequence and the estimation error was once again shown for both the block-invariant and time-varying channel.

The proposed MIMO-CE method was also applied to the MIMO-OSIC-DFE receivers to demonstrate the BER results. A small reduction in the system performance due to channel estimation errors was observed as compared to the perfect channel estimates case. It was found that for both cases of the estimated channel and the perfect channel estimate, the system performance was dependent on two major factors: a) the relative number of K_f taps w.r.t the number of $(L+1)$ paths and b) the diversity order of the systems. The greater the diversity orders the better the system performance. The BER performance improved as the number of K_f taps in the receiver relative to the number of $(L+1)$ paths increases.

Novel fractionally-spaced MIMO-CE scheme – In Chapter 4, the fractionally-spaced channel delay model was also considered as an improvement model for the MIMO channel estimation in a frequency-selective fading MIMO channel case. This modification (from previous symbol-spaced model) allowed paths delays arrived at the receiver within a fraction of a symbol period to be estimated accordingly. In the proposed fractionally-spaced MIMO-CE scheme, only an additional orthogonal sequence per transmit antenna was added to cater for fractional estimation. Proper reconstruction of pilot matrix and the proper collection of the received pilot signals at the receiver were essential to the fractionally-spaced MIMO-CE scheme. The averaging process for the channel estimates obtained in the ascending and descending process of the algebra operation at the

end of the MIMO-CE process was necessary in order to smooth out the noise. The proposed fractionally spaced MIMO-CE scheme was also successfully implemented in the MIMO-OSIC-DFE receivers with fractionally-spaced equaliser's tap configuration to access performance evaluation of MIMO systems operate in more realistic channel condition.

Similar to the estimator's performance for the symbol-spaced block-invariant channel model, the MSE performance also improves accordingly as the pilot length v increases demonstrating the trade-off between the pilot length and the achievable MSE. It was also found that N had no influence on the estimator's performance but the performance degraded as M increases. The fractional sampling rate c and the total delay spans φ were two crucial parameters. It was learned that for fixed value of φ, increasing c had no influence on estimator's performance but different value of φ had influence on the estimator's performance. The performance of the proposed fractional MIMO channel estimator was found to be affected by the total span of delay spread in the MIMO channel. The estimator's performance degraded as the value ofφ increases due to the increase of ISI effect and error propagation during channel estimation.

In the time-varying fractionally-spaced model, for a fixed value of φ, increasing c had no influence on estimator's performance for a slow varying channel and when optimum pilot length v was chosen. But when non-optimum pilot length had been chosen, the results demonstrated slight degradation in estimator's performance when operated in a faster time-varying channel for increasing value of c. Therefore, the use of optimum pilot length was vital for proposed fraction channel estimation to operate in fast time-varying channel. For a fixed value of c, increasing value of φ further degraded the estimator's performance especially for the fast varying channel even when optimum pilot length was chosen. This was due to the fact that more severe frequency selectivity was introduced that could restrict the performance of the proposed estimator.

MIMO Channel Tracking – A channel tracking method was also presented to further improve the system performance of the MIMO-OSIC-DFE receiver under the influence of the time-varying channel (since the accuracy of the proposed MIMO-CE had been shown to be dependent upon the Doppler velocity of the channel). It was found that channel tracking improves the bit error performance for higher SNRs but slightly degraded the performance at lower SNR.

As an overall conclusion for this thesis, the corresponding channel interference problems such as co-channel interference and inter-symbol interference had been carefully considered for the design of suitable MIMO channel estimator for both flat-fading and frequency-selective MIMO channels. The V-BLAST receiver had been successfully extended to include various possible MIMO channel estimation schemes for flat fading MIMO channel by either adaptive or non-adaptive techniques in Chapter 3. (The flat-fading case is more straightforward since only spatial interference of CCI is present). In Chapter 4, a novel MIMO channel estimation scheme

(with channel tracking) had been successfully implemented and incorporated into the MIMO-OSIC-DFE receivers described in Chapter 2. The effects of frequency-selective fading channel had been considered by the proposed MIMO channel estimator to resolve the CCI and ISI problem while simultaneously obtaining the channel information. The performances of the proposed MIMO channel estimators, the system performance of the V-BLAST and MIMO-OSIC-DFE receivers were accessed in Chapter 5. These results have application to the practical design of space-time systems for high-capacity over frequency-selective fading MIMO channels.

6.2 Suggestions for Future Work

In this section, future work will be suggested subjectively for the proposed MIMO-CE schemes and possible related areas and then globally for other important fields in MIMO systems.

First, the proposed MIMO-CE schemes can be extended to include more efficient channel tracker in order to operate more effectively in the time-varying environment since estimation performance is affected greatly due to time variation of the channel. The channel tracking method provided in end of Chapter 4 only suggests a basic method to update the channel estimates adaptively. More advanced technique like Kalman estimator in [92] can be incorporated into the proposed MIMO-CE scheme to perform adaptive channel estimation of the time-varying MIMO channel. With the Kalman estimator, not only the variation of the channel can be tracked effectively but the Kalman filter also provides channel prediction capability which uses the autoregressive moving average technique to forecast the variation of the channel and makes proper adjustment of the estimate. The Kalman estimator can also be upgraded by considering non-uniform velocity or acceleration in channel variation as well as channel correlation.

Secondly, effective blind channel estimation algorithms [98, 99] such as subspace method can be combined with the novel fractionally-spaced MIMO-CE scheme to create a so-called semi-blind channel estimation method, which exploits the positive aspects of both techniques. The novel fractionally-spaced MIMO-CE scheme provides a readily fractionally-spaced structure, which can be used to further incorporate the blind technique, to fully utilise both the training information (known) as well as the unknown random data information. Although no training is needed, the blind techniques itself suffer from lack of robustness where channel must satisfy certain diversity conditions and the possibility of overestimation problems. On the other hand, the training-based method provides robust estimation but decreases bandwidth efficiency if longer training sequence is needed. Therefore, with the semi-blind technique, possible pitfalls of blind approach might be avoided while using fewer pilot symbols in the proposed estimator. Furthermore, exploiting the blind information in addition to the known symbol allows estimation of longer channel impulse responses than is possible with a certain training sequence length [101].

Thirdly, the proposed MIMO-CE scheme can be further tested and verified using the channels model proposed by industrial standards and real measurement of MIMO channel models. This includes the consideration of the channel models proposed by: a) IEEE 802.11n Working Group model [149-152] and b) the 3GPP/3GPP2 Technical Specification Group [153]. The 6 TGn channel models in [149] are developed preliminary for high throughput designed up to 500Mbit/s for indoor MIMO wireless local area networks (WLANs) applications [67, 151]. The real measurement models will also be helpful in order to access the true performance of the estimator in the real world environment if the suitable models of the MIMO channels measurement for different environment can be carried out or borrowed. Major works are carried out in [68-70]. This will be once for all useful for the complete analysis and performance evaluation of the practical MIMO systems under the influence of estimated channel information.

Fourthly, as for the MIMO-OSIC-DFE receiver itself, although different number K_f taps have been used in the simulation, the number of feedforward's taps and feedback's taps are set to be uniform for each stream and throughout all stages of detection. The decision delay parameter 'd' of the MIMO-DFE in section 2.6.3 is also fixed for the detection of each stream. Hence, it would be interesting to explore the use of different filter spans and decision delays at different stage in the detection process to examine the full functionality of the MIMO-OSIC-DFE. Another vital area is the synchronisation, which is assumed to be ideal in most of the research works of MIMO systems, can be a very good research topic in the future works of MIMO systems.

Fifthly, although the issue of fading correlation in the MIMO channel might limit the performance and capacity achievement of MIMO systems [56, 57], recent research in [60] has pointed out the possible utilisation and exploitation of the channel correlation information to bring further advantages instead of the disadvantages to the MIMO systems if channel knowledge is available at the transmitter. This could be a new exploration that might open up new directions for MIMO algorithms pre-coding technique and space-time coding that incorporates fading correlation nature. New joint decoding technique of channel estimation as well as data detection that takes into account of fading correlation in also a future work of the MIMO systems.

Lastly, the ultimate aim of MIMO systems is to allow high data rate transmission for the multi-users application of wireless communication application. Hence, MIMO-multiuser technique is also an important area of future research. Area related to this research includes MIMO-WCDMA or MIMO-CDMA techniques, MIMO-OFDM and adaptive modulation control, space-time coding and multiuser interference rejection techniques. The incorporation of MIMO systems to the current existing transmission standard e.g WCDMA-UMTS [142, 143], is also an essential research study that may up-lift the utilisation of multiple antennas in MIMO systems as the potential candidate for the future wireless communication systems.

References

[1] G. J. Foschini, "Layered space-time architecture for wireless communication in a fading environment when using multi-elemen antennas," *Bell Labs Tech. J.*, pp.41-59, Autumn, 1996.

[2] G. Raleigh, J. M Cioffi, "Spatio-temporal coding for wireless communication," *IEEE Trans. Commun.*, vol. 46, pp. 357-366, March 1998.

[3] G. J. Foschini, M. J. Gans, "On limit of wireless communications in a fading environment when using multiple antennas," *Wireless Pers. Commun.*, vol.6, pp. 311-335, Mar 1998.

[4] P. W. Wolniansky, G. J. Foschini, G. D. Golden, R. A. Valenzuela, "V-BLAST: An Architecture for Realizing Very High Data Rates Over the Rich-Scattering Wireless Channel", invited paper, *Proc. ISSSE-98*, Pisa, Italy, Sept. 29, 1998.

[5] H Holma, A Toskala, *W-CDMA for UMTS- Radio access for third generation mobile communications*, revised edition, John Wiley & Sons, 2001.

[6] http://www1/bell-labs.com/project/blast/press/ww_11_29.html

[7] M. A. Beach, D. P. McNamara, P. N. Fletcher, P. Karisson, "MIMO–A solution for advanced wireless access?," *11th International Conf. Antenna & Propagation*, no. 480, pp. 231-235, April 2001.

[8] D. Gesbert, M. Shafi, D. Shiu, P. J. Smith, A. Naguib, "From theory to practice: An overview of MIMO space-time coded wireless systems," *IEEE J. Select Areas Commun.*, vol.21, no.3, pp. 281-302, April 2003.

[9] I. E. Teletar, "Capacity if multi-antenna Gaussian channels," *AT&T Bell Laboratories, Tech. Memo.*, June 1995.

[10] B A Bjerke, J G Proakis, "Multiple transmit and receive antenna diversity techniques for wireless communications," IEEE Adaptive System for Signal Processing, Communications and Control symposium, AS-SPCC, pp. 70-75, 2000.

[11] A. J. Paulraj C. B. Papadias, "Space-time processing for wireless communications," *IEEE Signal Processing Mag.*, vol.14, no.5, pp. 49-83, Nov 1997.

[12] A. Paulraj, R. Nabar, D Gore, *Introduction to Space-Time Wireless Communications*, Cambridge Press, 2003.

[13] S. P. Applebaum, "Adaptive arrays," *IEEE Trans Antenna and Propagation*, AP-24, pp. 585-598, Sept 1976.

[14] B. Widrow, P. E. Mantey, L. J. Griffiths, B. B. Goode, "Adaptive antenna systems," *Proc. IEEE*, vol. 55, pp. 2143-2159, Dec 1967.

[15] W.F. Gabriel, "Adaptive arrays–an introduction," *Proc. IEEE*, 64: 239-272, Feb 1976

[16] J. Hudson, "Adaptive arrays principle," Peter Peregrinus Ltd., *IEE Electromagnetic Waves*, series 11, 1981.

[17] R.A. Monzingo, T.W. Miller, *Introduction to adaptive arrays*, Wiley, New York, 1980.

[18] J. H. Winters, "Optimum combining in digital mobile radio with co-channel interference," *IEEE J. Select Areas Commun.*, vol. SAC-2, pp. 528-539, 1984.

[19] J. H. Winters, "Optimum combining fir indoor radio systems with multiple users," *IEEE Trans. Commun.*, vol. COM-35, pp. 1222-1230, Nov 1987.

[20] B. D. Van Veen, K. M. Buckley, "Beamforming: A versatile approach to spatial filtering," IEEE ASSP Magazine, pp. 4-24, April, 1988.

[21] T. Shan, T Kailath, "Adaptive beamforming for coherent signals and interference," IEEE Trans. ASSP, vol. ASSP-33, pp. 527-536, June 1985.

[22] L. C. Godara, "Application of antenna arrays to mobile communications, Part I: Performance improvement, feasibility and system consideration," *Proc. IEEE*, vol.85, no. 7, pp. 1031-1060, July 1997.

[23] L. C. Godara, "Application of antenna arrays to mobile communications, Part II: Beam-forming and direction-of-arrival considerations," *Proc. IEEE*, vol.85, no. 8, pp. 1195-1245, Aug 1997.

[24] R Kohno, "Spatial and temporal communication theory using adaptive antenna array," *IEEE Personal Commun.*, vol. 5, no.1, pp. 28-35, Feb 1998.

[25] J. H. Winters, "Smart antennas for wireless systems," *IEEE Personal Commun.*, vol. 1, no.1, pp. 23-27, Feb 1998.

[26] M. A. Beach, P. Guemas, A. R. Nix, "Capacity and service extension for wireless networks using adaptive antennas," *Electron. Lett.*, vol.30, pp. 1813-1814, 1994.

[27] G. Tsoulos, M. Beach, J. McGeehan, "Wireless personal communications for the 21st century: European technological advances in adaptive antennas," *IEEE Commun. Magazine*, pp. 102-109, Sept 1997.

[28] S. C. Swales, M. A. Beach, D. J. Edwards, J. P. McGeehan, "The performance enhancement of multibeam adaptive base-station antennas for cellular land mobile radio systems," *IEEE Trans. Vehic. Tech.*, vol.39, no.1, pp. 56-67, Feb 1990.

[29] J. H. Winters, J. Salz, R. D. Gitlin, "The impact of antenna diversity on the capacity of wireless communication systems," IEEE Trans. Commun., vol. 42, no. 2/3/4, pp. 1740-1751, Feb/Mar/Apr 1994.

[30] Y. Wang, J. R. Cruz, "Adaptive antenna arrays for cellular CDMA communication systems," *IEEE Intem'l Conf. ASSP.*, pp. 1725-1728, May, 1995.

[31] J. S. Thompson, P. M. Grant, B Mulgrew, "Smart antenna arrays for CDMA systems," *IEEE Personal Commun.*, vol. 3, no. 5, pp. 16-25, 1996.

[32] A. F. Naguib, A. Paulraj, T Kailath, "Capacity improvement with base-station antenna arrays in cellular CDMA," *IEEE Trans. Vehic. Tech.*, vol.43, no.3, pp.691-698, 1994.

[33] J. C. Liberti, T. S. Rappaport, "Analysis of CDMA cellular radio systems employing adaptive antennas in mulitpath environments," *IEEE Vehic. Tech. Conf.*, pp.1076-1080, May 1996.

[34] G.J. Foschini, G.D. Golden, R.A. Valenzula, P.W. Wolniansky, "Simplified Processing for high spectral efficiency wireless communication employing multi-element arrays," *IEEE J. Select Areas Commun.*, vol.17, no.11, pp. 1841-1852, Nov 1999.

[35] G.L. Stüber, J.R Barry, S.W. McLaughlin, Y. Li, M.A. Ingram, T.G. Pratt, " Broadband MIMO-OFDM wireless communication," *Proc. IEEE*, vol. 92, no.2, pp. 271-294, 2004.

[36] R. J. Piechocki, P. N. Fletcher, A. Nix, N Canagarajah, J. McGeehan, "Performance of space-frequency techniques over measured channels in MIMO-OFDM systems," *IEE Tech. Seminar; MIMO Commun. System: From Concept to Implementation*, pp. 7/1-7/6, Savoy Place, London, Dec 2001.

[37] L. Giangaspero, L Agarossi, G. Paltenghi, S. Okamura, M. Okada, S. Komaki, "Co-channel interference cancellation based on MIMO OFDM systems," IEEE Wireless Commun. Magazine, pp. 8-17, Dec 2002.

[38] H. Bölcskei, M. Borgmann, A. Paulraj, "Impact of propagation environment on the performance of space-frequency coded MIMO-OFDM," *IEEE J. Select Areas Commun.*, vol.21, no.3, pp. 427-439, Apr 2003.

[39] R. S. Blum, Y. Li, J. H. Winters, Q. Yan, "Improved space-time coding for MIMO-OFDM wireless communications," IEEE Trans. Commun., vol. 49, no. 11, pp. 1873-1878, Nov 2001.

[40] N. Amitay, J. Salz, "Linear equalization theory in digital data transmission over dually polarized fading radio channels," *Bell Syst. Tech. J.*, vol.63, no.10, pp.2215-2259, 1984.

[41] J. Salz, "Digital transmission over cross-coupled linear channels," *Bell Syst. Tech. J.*, vol.64, no.6, July/Aug 1985.

[42] A. Dual-Hallen, "Equalizers for multiple-input multiple-output channels and PAM systems with cyclostationary input sequences," *IEEE J. Select Areas Commun.*, vol.10, pp. 630-639, Apr 1992.

[43] S. Verdu, *Multiuser Detection*, Cambridge University Press, UK, 1998.

[44] M. K. Varanasi, T. Guess, "Optimum decision feedback multiuser equalization with successive decoding achieves total capacity of the Gaussian multiple access channel," in *Proc. Asilomar Conf.*, Nov 1997.

[45] N. Al-Dhahir, A. H. Sayed, " The finite-length multi-input mulit-output MMSE DFE," *IEEE Trans. Signal Processing*, col. 48, no. 10, pp. 2921-2936, Oct 2000.

[46] C. Tidestav, M. Sternad, A. Ahlen, "Reuse within a cell–Interference rejection or multiuser detection?," *IEEE Trans. Commun.*, col. 47, pp. 1511-1522, Oct 1999

[47] A. Lozano, C Papadias, "Layered space-time receivers for frequency-selective wireless channels," *IEEE Trans. Commun.*, col. 50, no.1, pp. 65-73, Oct 2002.

[48] X. Zhu, R. D. Murch, "Layered space-time equalization of multiple-input multiple-output frequency selective channels," *IEEE* ICC 2002., pp. 330 – 334, vol.1, 2002.

[49] N. Al-Dhahir, C Fragouli, A. Stamoulis, W. Younis, R. Calderbank, "Space-time processing for broadband wireless access." *IEEE Commun. Magazine*, pp.136-142, Sept. 2002

[50] A. Naguib et all., "A space-time coding modem for high-data-rate wireless communications," *IEEE J. Select Areas Commun.*, pp. 1459-1477, Oct 1998.

[51] V. Tarokh, N. Seshadri, A. R. Calderbank, "Increasing data rate over wireless channel," *IEEE Signal Processing Magazine*, vol. 17, pp. 76-92, May 2000.

[52] S. M. Almouti, "A simple transmit diversity technique for wireless communications," *IEEE J. Select Areas Commun.*, vol.16, no.8, pp. 1451-1458, Oct 1998.

[53] V. Tarokh, N. Seshadri, A. R. Calderbank, "Space-time codes for high data rate wireless communications: Performance criterion and code construction," *IEEE Trans. Info. Theory*, pp. 744-765, Mar 1998.

[54] B. Vucetic, J. Yuan, *Performance limit of multiple-input multiple-output wireless communication systems space-time coding*, John Wiley & Sons, 2003.

[55] Lucent Technologies, http://mars.bell-labs.com

[56] D. Shiu, G. J. Foschini, M. J. Gans, J. M. Kahn, "Fading correlation and its effect on the capacity of multielement antenna systems," *IEEE Trans. Commun.*, vol. 48, no. 3, pp. 502-513, March 2000.

[57] S. Loyka, A. Kouki, "The impact of correlation on multi-antenna system performance: correlation matrix approach," *Proc. IEEE VTC*, pp. 533-537, Oct 2001.

[58] A. Abdi, M. Kaveh, "A space-time correlation model for multielement antenna systems in mobile fading channels," *IEEE J. Select Areas Commun.*, vol.20, no.3, pp. 550-560, Apr 2002.

[59] S. Loyka, J. Mosig, "Channel capacity of N-antenna BLAST architecture," *Electronics Letters*, vol. 36, no.7, pp. 660-661, March 2000.

[60] M. T. Ivriac, W. Utschick, J. A. Nossek, "Fading correlation in wireless MIMO communication systems," *IEEE J. Select Areas Commun.*, vol. 21, no. 5, pp. 819-828, June 2003.

[61] J. Salz, J. H. Winters, "Effect of fading correlations on adaptive arrays in digital mobile radio," IEEE Trans. Vehic. Tech., vol. 43, no. 4, pp. 1049-1057, Nov 1994.

[62] S. Loyka, "Channel capacity of two antenna BLAST architecture," *Electronics Letters*, vol. 35, no.17, pp. 1421-1422, Aug 1999.

[63] K. Yu, B. Ottersen, " Models for MIMO Propagation channels, a review," Wiley J. Wireless Commun. & Mobile Computing, vol.2, no.7, pp. 653-666, Nov 2002.

[64] M. Stege, J. Jelitto, M. Brozel, G. Fettweis, "A multiple-input multiple-output channel model for simulation of Tx and Rx-diversity wireless systems," in *Proc. IEEE VTC Fall*, vol. 2, pp. 833-839, 2000.

[65] T Klingenbrunn, P Mogensen, "Modelling frequency correlation of fast fading in frequency hopping GSM link Simulations," in *Proc. IEEE VTC'99*, pp. 2398-2402, 1999.

[66] J. P. Kermoal, L. Schumacher, K. I. Pedersen, P. E. Mogensen, F. Frederiksen, "A stochastic MIMO radio channel model with experimental validation," *IEEE J. Select Areas Commun.*, vol. 20, no. 6, pp. 1211-1226, Aug 2002.

[67] K. Yu, M. Bengtsson, B. Ottersten, D. McNamara, P. Karlsson, M. Beach, "Measurement analysis of NLOS indoor MIMO channels," in *Proc. IST Mobile Communication Summit*, pp. 277-282, Sept 2001.

[68] M. A. Beach, D. McNamara, P. Karlsson, "Development of a channel measurement system for multiple-input multiple-output (MIMO) applications," *in Proc. IST Mobile Communications Summit*, Galway, Eire, 1-4, pp. 497-501, 2000.

[69] C. C. Chong, C. M. Tan, D. I. Laurenson, S. McLaughlin, M. A. Beach, A. R. Nix, "A new statistical wideband spatio-temporal channel model for 5-GHz Band WLAN systems," *IEEE J. Select Areas Commun.*, vol. 21, no. 2, pp. 139-150, Feb 2003.

[70] M. A. Beach, B. Allen, P Karlsson, "Spatial channel characterization for smart antenna solutions in FDD wireless network," IEEE Trans. Antenna and Propagation, vol.52, no.1, pp. 252-262, Jan 2004.

[71] C. C. Martin, J. H. Winters, N. R. Sollenberger, "Multiple-input multiple-output (MIMO) radio channel measurements," *in Proc. IEEE Vehic. Tech.*, pp.774-779, 2000.

[72] M. A. Beach, C. M. Simmonds, P. Howard, P Darwood, "European smart antenna test-bed – Field trial results," *IEICE Trans. Vehic. Tech.*, vol. E84-B, no. 9, pp. 2348-2356, Sept 2001.

[73] B. Hassibi, B. M. Hochwald, "How much training is needed in multiple-antenna wireless link," *IEEE Trans. Information Theory*, vol. 49, no. 4, pp. 951-963, Apr 2003.

[74] C. Budianu, L. Tong, "Channel estimation for space-time orthogonal block codes," *IEEE Trans. Signal Processing*, vol. 50, no.10, pp. 2515-2528, Oct 2002.

[75] C. Fragouli, N. Al-Dhahir, W. Turin, "Training-based channel estimation for multiple-antenna broadband transmission," *IEEE. Trans. Wireless Commun.*, vol. 2, pp. 384-391, Mar 2003.

[76] A. F. Naguib, V. Tarokh, N, Seshadri, A. R. Calderbank, "Space-time coding modem for high data rate wireless communications," *IEEE J. Select Areas Commun.*, vol. 16, pp. 1459-1478, Oct 1998.

[77] R. M. Buehrer, N. A. Kumar, "The impact of channel estimation error on space-time block codes," in Proc. Vehic, Tech. Conf., vol. 3, pp. 1921-1925, Sept 2002.

[78] Y. Li, N. Seshadri, S. Ariyavisitakul, "Channel estimation for OFDM systems with transmit diversity in mobile wireless channels," *IEEE J. Select Areas Commun.*, vol. 17, no.3, pp. 461-471, Mar 1999.

[79] W. Bai, C. He, L. G. Jiang, X. X. Li, " Robust channel estimation in MIMO-OFDM systems," Electronic Letters, vol. 39, no.2, pp. 242-244, Jan 2003.

[80] Y Li, "Simplified channel estimation for OFDM systems with multiple transmit antennas," *IEEE Trans. on Wireless Communication*, vol. 1, no.1, pp 67-75, Jan 2002.

[81] I. Barhumi, G. Leus, M. Moonen, "Optimum training sequence for channel estimation in MIMO-OFDM systems in mobile wireless channels," in *Proc. International Zurich Seminar on Broadband Commun.*, pp. 44.1–44.6, Feb 2002.

[82] Y. Li, J. H. Winters, N. R. Sollenberger, "MIMO-OFDM for wireless communications: signal detection with enhance channel estimation," *IEEE Trans Commun.*, vol. 50, no.9, Sept 2002.

[83] T. L. Marzetta, "BLAST training: Estimating channel characteristics for high-capacity space-time wireless," in Proc. 37th *Annu. Allentown Conf. Communications, Control and Computing*, Sept 1999. [online]: http://mars.bell-labs.com

[84] Q. Sun, D. C. Donald, H. C. Huang, A. Lazano, "Estimation of continuous flat fading MIMO channels," *IEEE Trans. Wireless Commun.*, vol.1, no.4, pp. 549–553, Oct 2002.

[85] K. Lee, J. Chun, "On the interference nulling operation of the V-BLAST under channel estimation errors," *in Proc. Vehic. Tech.VTC-fall*, vol. 4, pp. 2131-2135, Sept 2002.

[86] S. T. Chung, A. Sutivong, "Practical considerations for Extended V-BLAST: Quantized parameter and imperfect channel estimation," *IEEE Wireless Communication and Networking Conf.*, vol. 2, pp. 682-686, Mar 2002.

[87] M. F. Siyau, P. Nobles, R. F. Ormondroyd, "Channel estimation for space-time systems using a multi-element array recursive least squares (MEA-RLS) algorithm," in *Proc. 4th International Symposium on Wireless Personal Multimedia Communication, WPMC'01*, pp. 1451-1456, vol.3, Sept, 2001.

[88] C. Cozzo, B. L. Hughes, "Joint channel estimation and data detection in space-time communications," *IEEE Trans. Commun.*, col. 51, no. 8, pp. 1266-1270, Aug 2003.

[89] C. Xu, T. Le-Ngoc, "Joint channel estimation and decoding of space-time block codes," in *Proc. Vehic. Tech. Conf. VTC-fall*, vol. 3, pp. 1540-1544, Sept 2002.

[90] K. Lo, Z. Chen, P. Alexander, B Vucetic, "Layered space time coding with joint iterative detection, channel estimation and decoding," *IEEE 7th Int. Symp. on Spread Spectrum Tech. & Appl.*, Prague, Czech Republic, Sep 2002.

[91] G. E. Bottomley, K. J. Molnar, "Adaptive channel estimation for multichannel MLSE receivers," *IEEE Commun. Letters*, vol. 3, no.2, pp. 40-42, Feb 1999.

[92] C. Komninakis, C. Fragouli, A. H. Sayed, R. D. Wessel, "Multi-input multi-output fading channel tracking and equalization using Kalman estimation," IEEE Trans. Signal Processing, no. 50, no. 5, pp. 1065-1076, May 2002.

[93] J. K. Tugnait, "Spatio-temporal signal processing for blind separation of multi-channel signals," in *Proc. of the SPIE Conf.*, pp. 88-103, 1996.

[94] A. J. van der Veen, S. Talwar, A. Paulraj, "A subspace approach to blind space-time signal processing for wireless communication systems," *IEEE Trans. Signal Processing*, vol. 45, no. 1, pp. 173-190, Jan 1997.

[95] L. Tong, S. Perreau, "Multichannel blind identification: From subspace to maximum likelihood methods," *IEEE Proc.*, vol. 86, no.10, pp. 1951-1568, Oct 1998.

[96] L. Perros-Meilhac, E. Moulines, K. Abed-Meraim, P. Chealier, P. Duhamel, "Blind identification of multipath channels: A parametric subspace approach," *IEEE Trans. Signal Processing*, vol. 49, no.7, pp. 1468-1480, July 2001.

[97] J. K. Tugnait, B. Huang, "On a whitening approaching to partial channel estimation and blind equalization of FIR/IIR multiple-input multiple-output channels," *IEEE Trans. Signal Processing*, vol.48, no.3, pp. 832-845, March 2000.

[98] C. B. Papadias, D. M. Slock, "Fractionally spaced equalization of linear polyphase channels and related blind techniques based on multichannel linear prediction," *IEEE Trans. Signal Processing*, vol.47, no.3, pp. 641-654, March 1999.

[99] G. B. Gainnakis, Y. Hua, P. Stoica, L. Tong, *Signal Processing Advances in Wireless & Mobile Communication: Volume.1: Trends in channel estimation and equalization*, Prentice Hall, 2001.

[100] P. A. Bello, "Characterization of randomly time-variant linear channel," *IEEE Trans. Commun. Systems.*, vol. CS-11, pp. 360-393, Dec 1963.

[101] E. de. Carvalho, D. T. M. Slock, "Blind and semiblind FIR multichannel estimation: (Global) Identifiability conditions," *IEEE Trans. Signal Processing*, vol. 52, no. 4, pp. 1053-1064, 2004.

[102] B. Farhang-Boroujeny, *Adaptive Filter Theory and Application*, John Wiley and Sons, 1998.

[103] L. R. Litwin, "Adaptive channel equalization for wireless communications," *IEEE Potential Magazine*, vol.18, no. 4, pp 9-12, Apr-May 1999.

[104] S. Haykin, *Adaptive Filter Theory*, 3rd edition, Prentice-Hall, 1996.

[105] L. R. Litwin "Blind channel equalization using constant modulus algorithm (CMA)," *IEEE Potential Magazine*, pp. 9-12, Oct-Nov 1999.

[106] H. Liu, G. Xu, L. Tong, T. Kailath, "Recent developments in blind channel equalization: From cyclostationarity to subspaces," *IEEE Signal Processing*, vol. 50, pp. 83-99, 1996.

[107] B. Windrow, S. D. Stearns, Adaptive Signal Processing, Prentice-Hall Signal Processing Series, 1985.

[108] S. R. Saunders, *Antennas and Propagation for Wireless Communication Systems*, John Wiley & Sons, 1999.

[109] R. Valenzuela, "Multiple Antennas Systems: A new wireless communication technology of extraordinary bandwidth efficiency for 3G and beyond," [online]: http://www.bell-labs.com/user/rav/Internet2.pdf

[110] J, Proakis, *Digital Communications*, McGraw-Hill, New York, 3rd Edition, 1995.

[111] J. D. Parson, *The Mobile Radio Propagation channel*, Pentech Press Publisher, 1992

[112] W. Jakes, *Microwave Mobile Communications*, Wiley, New York, 1974.

[113] T.S. Rappaport, *Wireless Communications: Principles & Practice*, Prentice-Hall, 1996.

[114] R. Steel, L. Hanzo, *Mobile Radio Communications*, John Wiley, 1998.

[115] E. Vanmarcke, *Random Fields: Analysis and Synthesis*. MIT Press, Cambridge, MA, 1983.

[116] G. H. Golub, C. F. Van Loan, *Matrix Computations*, North Oxford Academic Publishing Co. Ltd., 1983.

[117] G. Strang, *Linear algebra and its application*, 3rd edition, Saunders HBJ publishers, 1986.

[118] S.U.H. Qureshi, "Adaptive equalization," IEEE Proc., vol. 72, pp. 1349-1387, 1985.

[119] J. G. Proakis, "Adaptive equalization for TDMA digital mobile radio," *IEEE Trans. Vehic. Tech. Conf.*, vol. 40, no. 2, pp. 333-34, May 1991.

[120] H. V. Henderson, S. R. Searle, "The vec-permutation matrix, the vec operator and kronecker products: A review," Linear and Multilinear Algebra, vol. 9, pp. 271-288, 1981.

[121] D. Shiu, J. M. Kahn, "Layered space-time codes for wireless communications using multiple transmit antennas," in Proc. IEEE ICC., pp. 436-440, June 1999.

[122] R.L Cupo, G.D. Golden, C.C Martin, K.L. Sherman, N.R.Sollenberger, J.H. Winters, R.W. Wolniansky, "A four-element adaptive antenna array for IS-136 PCS based stations," in Proc. IEEE. Vehic. Tech. Conf., pp.1577-1581, May 1997.

[123] Lloyd N. Trefethen, David Bau, "Numerical Linear Algebra," *S.I.A.M*, 1997.

[124] C.Y. Yoon, R. Kohno, H. Imai, "A spread spectrum multi-access system with co-channel interference cancellation for multipath fading channels," *IEEE J. Select Areas Commun.*, vol. 11 pp. 1067-1075, Sept 1993.

[125] A. Hui, K. Letaief, "Successive interference cancellation for multiuser asynchronous DS/CDMA detectors in multipath fading links," *IEEE Trans. Commun.*, vol. 46, no. 3, Mar 1998.

[126] M. F. Siyau, P. Nobles, R. F. Ormondroyd, "Non-linear space-time systems using orthogonal triangularization by QR decomposition," in *Proc. IEE Colloquium on MIMO systems – from concept to implementation*, London, pp. 6/1-6/5, Dec 2001.

[127] W. Choi, R. Negi, J.M. Cioffi, "Combined ML and DFE decoding for V-BLAST system," *in Proc. IEEE ICC.*, vol. 3, pp. 1243-1248, 2000.

[128] B. Hassibi, "An efficient square-root algorithm for BLAST," *in Proc. IEEE ICASSP.*, vol. 2, pp. II737-II-740, 2000.

[129] K. Wong C. Tsui, R. S. Cheng, "A low complexity architecture of the V-BLAST system," in Proc. IEEE WCNC, vol.1, pp. 310-314, 2000.

[130] J. M. Cioffi, "When do I use an RLS adaptive filter", *Nineteeth Asilomar conference on Circuits, Systems and Computers*, pp. 636 – 639, 1985.

[131] J. R. Treichler, I. Fijalkow, C. R. Johnson JR., "Fractioanlly spaced Equalizers," *IEEE Signal Processing Magazine*, pp. 65-81, May 1996.

[132] N. J. A. Sloane, "A Library of Hadamard Matrices," [online]: http://www.research.att.com/~njas/hadamard/index.html.

[133] J. Seberry and M. Yamada, "Hadamard matrices, sequences and block designs," pp 431-560 of J. H. Dinitz & D. R. Stinson. Editor (1992), *Contemporary Design Theory: A Collection of Essays*, Wiley, New York.

[134] T. Ojanpera, R. Prasad, *Wideband CDMA for Third Generation Mobile Communication*, Artech House, 1998.

[135] 3GPP, TSG Services and System Aspect, "Service aspects; Service principle," 3G TS 22.101, release 1999.

[136] H. Huang, H. Viswanathan, G. J. Foschini, "Achieving high data rate in CDMA systems using BLAST techniques," *Global Telecommunication. Conf.*, vol. 5, pp. 2316-2320, 1999.

[137] A. M. Tehrani, R. Negi, J. Cioffi, "Space-time coding over a code division multiple access system," *IEEE WCNC.*, vol. 1, pp. 134–138, 1999.

[138] 3GPP, TSG Radio Access Network (RAN), Working Group 1 (WG1), "Spreading and modulation (FDD)", TS 25.213 (1999-4).

[139] K. Laird, N. Whinnett, S. Buljore, "A peak-to-average power reduction method for third Generation CDMA reverse links", *IEEE 49th VTC.*, vol. 1, pp. 551-555, 1999

[140] D. Gerakoulis, S. Ghassemzadeh, "Extended orthogonal code designs with applications in CDMA," *in Proc. 6th IEEE ISSSTA Conf.*, vol. 2, pp 657-661, 2000,

[141] B.N. Vejlgaard, P. Mogensen, J. B. Knudsen, "Downlink performance of channel estimation and tracking with high mobile speed in UMTS," *in Proc. 50th IEEE Vehic. Tech. Conf.-Fall*, vol. 2, pp 973 –977, 1999.

[142] S. L. Ling, M. F. Siyau, R. F. Ormondroyd, "Space-time UMTS uplink system for future generation mobile radio communication system," *European Wireless Conf.'02*, vol. 2, pp. 865-869, Florence, Italy, Feb 2002.

[143] S. L. Ling, M. F. Siyau, R. F. Ormondroyd, "Channel estimation of spactial-temporal UMTS uplink system for future generation mobile radio communication systems," *IEE 5th European Personal Mobile Commun. Conf. EPMCC'03*, pp. 71-75, Glasgow April 2003.

[144] M. F. Siyau, R. F. Ormondroyd, P. Nobles, "Estimation of time-varying channels for space-time system using a combined multi-element array pilot matrix inversion (MEA-PMI) and auto-tracking", *IEEE ICASSP'02 Conf.*, Florida, May 2002.

[145] M. F. Siyau, P. Nobles, R. F. Ormondroyd, "Channel estimation for layered space-time systems", *In Proc. IV IEEE Signal Processing Workshop on Signal Processing Advances in Wireless Communications* (*SPAWC'03*), W1.1, 615, Rome, June 2003.

[146] M. F. Siyau, P. Nobles, R. F. Ormondroyd, "Estimation of frequency selective wireless channels for layered space-time systems", In Proc. IEEE International Antenna and Propagation Symposium and USNC/CNC/URSI North America Radio Science Meting, URSI. C, session 29.8, Columbus, June 2003

[147] M. F. Siyau, P. Nobles, R. F. Ormondroyd, "Channel estimation for layered space-time systems in time-varying frequency selective wireless channels", *In Proc. 58th IEEE Vechi. Tech. Conf.* (*VTC'03-Fall*), Orlando, Oct, 2003.

[148] M. F. Siyau, R. F. Ormondroyd, P. Nobles, "Performance of a Layered Space-Time Cellular System used with Fractionally-Spaced Channel Estimation Operated in a Time-Varying, Frequency-Selective Wireless Channel," *In Proc. IEEE conference on Vehicular Technology* (*VTC-fall'04*), Los Angeles, USA, September 2004.

[149] V.Erceg, L. Schumachoer, P. Kyritsi, A Molisch, D. Baum, A. Gorokhov, C. Oestges, Q. Li, K Yu, N. Tal, B. Dijkstra, A. Jaganattam, C. Lanzi, V. Rhodes, J. Medbo, D. Michelson, M. Webster, E. Jocobsen, D. Cheung, C. Prettie, M. Ho, S. Howard, B. Bjerke, L. Jengx, H. Sampath, S. Catreux, S. Valle, A. Poloni, A. Forenza, R. Heath, "TGn channel models", *IEEE 802.11-03/940r4*, May 2004. http://www.802wirelesworld.com/.

[150] V. Erceg, L. Schumachoer, P. Kyritsi, A. Molisch, D. Baum, A. Gorokhov, "TGn channel models, " *IEEE P802.11 wireless LAN, IEEE 802.11-03/940r2*, January 2004.

[151] Kai Yu, "Mulitple-input multiple-output radio propagation channels: characteristics and models, " PhD Thesis, *http://www.diva-portal.org/diva/getDocument?urn_nbn_se_kth_diva-138-2__fulltext.pdf.*

[152] TGn Sync, "TGn sync proposed technical specifications, " *IEEE 802.11-04/998r0*, August 2004.

[153] Technical Sprecification Group Radio Access Network, "Spatial channel model for multiple input multiple output (MIMO) simulations (release 6, " Technical Report 3GPP TR25.996 V6.1.0, 3rd Generation Partnership Project, Septmenber 2003..

Appendix A

Research Publications

This appendix contains a copy of the published papers that correspond to the discussions of the major work in this thesis during the completion of this research project. The following list contains bibliographic details of each publication along with its page number in this thesis.

Channel Estimation for Layered Space-Time Systems in Time-Varying Frequency Selective Wireless Channels

M. F. SIYAU P. NOBLES R. F. ORMONDROYD

Communication and Wireless Networks Group, Cranfield University
Royal Military College of Science, Shrivenham, Swindon, SN6 8LA, United Kingdom
Tel: +44 (0) 1793 785722, email: v.siyau@rmcs.cranfield.ac.uk

***Abstract* - A novel training-based channel estimation scheme is presented for an uncoded layered space-time system that operates in a wideband frequency selective fading environment of a time-varying multiple-input multiple-output (MIMO) channel. The method uses a pilot matrix consisting of pilot symbols derived from the Paley-Hadamard matrix to estimate the MIMO channel impulse response. The orthogonality of the pilot matrix resolves both the inter-symbol interference and the co-channel interference of the wideband MIMO channel. The Toeplitz-like structure of the Paley-Hadamard matrix is exploited to minimise the length of the pilot sequence, reducing pilot symbol overhead. A decision feedback algorithm is used to track the time-varying MIMO channel. Results are presented which demonstrate the performance of the proposed MIMO channel estimator in a layered space-time system for different mobile velocities and system configurations.**

I. INTRODUCTION

Space-time techniques for multiple-input multiple-output (MIMO) channels potentially provide significant increases in capacity compared with traditional wireless communication systems for wireless channels that suffer from severe multipath propagation. This is achieved by properly exploiting the diversity that exists within this type of rich scattering channel environment between the multiple antennas at both the transmitter and receiver [1]. A number of MIMO approaches have been proposed for both narrowband and wideband channels. In particular, the Bell Laboratories layered space-time (BLAST) architecture has been presented for the narrowband flat-fading channel [2] and MIMO equalisation and interference cancellation approaches have recently been proposed for the wideband channel [3][4].

In order to achieve the quoted capacity gains for MIMO systems, the multiple channel impulse responses and their fading coefficients must be known or estimated. Thus far, existing MIMO channel estimation schemes have been limited to the narrowband case or cater specifically for coded space-time systems [5]-[8]. In this paper, we extend the order successive interference cancellation (OSIC) layered space-time receiver architecture described in [3] to incorporate a novel MIMO channel estimator for an uncoded layered space-time system that operates in a time-varying, wideband frequency-selective fading environment.

The proposed MIMO channel estimation scheme uses pilot symbols that are transmitted periodically from each transmit antenna to estimate the channel impulse response. The sequence of pilot symbols used for each antenna is unique and orthogonal to the pilot symbol sequences used for the other transmit antennas. They are generated from a pilot matrix obtained from Paley's construction of the Hadamard matrix [9]. This has two benefits. First, the use of the Hadamard pilot matrix allows the fading coefficients of *all* the individual channel impulse responses between each transmit and receive antenna to be estimated jointly in a single operation in the receiver for the wideband MIMO channel. Second, by exploiting the Toeplitz-like structure of the Paley form of the Hadamard matrix, the number of training symbols that are needed to estimate the channel impulse response is significantly reduced. In this paper, the method used to generate the pilot symbol sequences is presented.

The key to the proposed MIMO channel estimation scheme is the ability to extract from the received signals the orthogonal information contained within the pilot sequences. The estimated MIMO channel matrix is obtained by applying a single matrix operation to the received signal matrix. In addition, a decision feedback algorithm is employed to track the changes that occur in the time-varying MIMO channel between periodic transmission of the pilot sequences.

The paper is organised as follows. Section II briefly describes the space-time system and channel model. The proposed MIMO channel estimation scheme is introduced in Section III and the basic MIMO channel tracking in Section IV. Section V presents the simulation results. Conclusions are given in Section VI.

II. SPACE-TIME SYSTEM & CHANNEL MODEL

The basic space-time system and the MIMO channel model are outlined below. Unless otherwise stated, all notation and assumptions follow [3] for the class of MIMO equalisers described therein.

There are M transmit and N receive antennas where (N×M) signifies a particular system configuration. (L+1) indicates the number of finite symbol-spaced impulse response taps used for the simulated channel corresponding to time-varying delayed propagation paths. The sampled channel impulse response (CIR) from the m^{th} transmit antenna to n^{th} receive antenna is expressed as:

$$\mathbf{h}_{nm} = [h_{nm}(0) \quad h_{nm}(1) \quad \dots \quad h_{nm}(L)]^{\mathsf{T}} \tag{1}$$

where $[.]^{\mathsf{T}}$ is the transpose operation. Consequently, the channel matrix, $\mathbf{H}_m(k)$, comprises the multiple CIRs, $\mathbf{h}_{nm}$, between the m^{th} transmit antenna and all (n = 1 to N) receive antennas at time k, and is given by:

$$\mathbf{H}_m(k) = \begin{bmatrix} \mathbf{h}_{1m}^{\mathsf{T}} \\ \mathbf{h}_{2m}^{\mathsf{T}} \\ \vdots \\ \mathbf{h}_{Nm}^{\mathsf{T}} \end{bmatrix} = \begin{bmatrix} h_{1m}(0) & h_{1m}(1) & \cdots & h_{1m}(L) \\ h_{2m}(0) & h_{2m}(1) & \cdots & h_{2m}(L) \\ \vdots & \vdots & \vdots & \vdots \\ h_{Nm}(0) & h_{Nm}(1) & \cdots & h_{Nm}(L) \end{bmatrix} \text{ for } m=1 \text{ to } M \tag{2}$$

Each coefficient, h_{nm}, in (2) is generated as random complex components and all coefficients of the channel matrix are assumed to be uncorrelated and time-varying due to the effect of Doppler. The received signal vector, $\mathbf{x}$ at time k can be expressed as:

$$\mathbf{x}(k) = \sum_{m=1}^{M} \mathbf{H}_m(k)\,\mathbf{s}_m(k) + \mathbf{n}(k) \tag{3}$$

where $\mathbf{n}(k)$ is the additive white Gaussian noise (AWGN) vector and $\mathbf{s}_m(k)$ is the transmit vector for a sequence of L+1 symbols (i.e. from the current $(k)^{th}$ symbol back to the previous $(k\text{-}L)^{th}$ symbol) sent by the m^{th} transmit antenna:

$$\mathbf{s}_m(k) = \begin{bmatrix} s_m(k) & s_m(k-1) & \cdots & s_m(k-L) \end{bmatrix}^{\mathsf{T}} \tag{4}$$

The received signal vectors, $\mathbf{x}$, are collected at regular intervals and grouped into a received signal matrix as:

$$\mathbf{X}(k) = \begin{bmatrix} \mathbf{x}(k) & \mathbf{x}(k+1) & \cdots & \mathbf{x}(k+F) \end{bmatrix} \tag{5}$$

creating (F+1) N-dimensional symbols spanned by (F+1) memory slots in the channel estimator. Since the purpose of this paper is to present a channel estimation scheme, the MIMO equalisation and OSIC receiver model will not be further discussed here. ([3] has further details). However, we proceed to modify the representation in (3) in order to facilitate the channel estimation process described in the next Section.

We use $[Y \mid Z]$ to denote the concatenation of matrix or vector Y and Z and employ the same *vec*(.) operator in [3], expressed in the following:

$$vec\left(\begin{bmatrix} \mathbf{v}_1 & \mathbf{v}_2 & \cdots & \mathbf{v}_K \end{bmatrix}\right) = \begin{bmatrix} \mathbf{v}_1 \\ \vdots \\ \mathbf{v}_K \end{bmatrix} \tag{6}$$

By concatenating the channel matrices from $\mathbf{H}_1(k)$ to $\mathbf{H}_M(k)$ in (2) as:

$$\mathbf{H}_{1|M}(k) = \left[\mathbf{H}_1(k) \mid \cdots \mid \mathbf{H}_M(k)\right] \tag{7}$$

and applying the *vec*(.) operator to all the transmit vectors as:

$$s_{1|M}(k) = vec\left(\left[\mathbf{s}_1(k) \cdots \mathbf{s}_M(k)\right]\right) \tag{8}$$

the received signal vector, $\mathbf{x}(k)$, in (3) can be re-written as:

$$\mathbf{x}(k) = \mathbf{H}_{1|M}(k) \cdot s_{1|M}(k) + \mathbf{n}(k) \tag{9}$$

$$= \left[\mathbf{H}_1 \mid \cdots \mid \mathbf{H}_M\right] \cdot \left[\begin{array}{c} \mathbf{s}_1(k) \\ \vdots \\ \hline \mathbf{s}_M(k) \end{array}\right] + \mathbf{n}(k) \tag{10}$$

Note that the matrix representation in (10) allows proper partitioning (shown by the vertical and horizontal strokes) of the channel matrices and their associated transmit vectors, enabling matrix operations to take place referenced to each transmit antenna. Next, (10) can be extended for a collection of (F+1) non-adjacent $\mathbf{x}$ spaced by interval p as:

$$\mathbf{X}'(k) = \begin{bmatrix} \mathbf{x}(k) & \mathbf{x}(k+p) & \ldots & \mathbf{x}(k+Fp) \end{bmatrix} \tag{11}$$

Assuming $\mathbf{H}_{1|M}$ stays relatively constant throughout the intervals, the received signal matrix, $\mathbf{X}'(k)$ in (11) also corresponds to:

$$\mathbf{X}'(k) = \mathbf{H}_{1|M} \cdot S_F + \mathbf{N} \tag{12}$$

where $\mathbf{N}$ is a grouped matrix of AWGN vectors and S_F comprises a grouped matrix of transmitted $s_{1|M}(k)$ vectors:

$$S_F = \begin{bmatrix} s_{1|M}(k) \mid s_{1|M}(k+p) \mid \cdots \mid s_{1|M}(k+Fp) \end{bmatrix} \tag{13}$$

Formulating (5) as (11) allows (12) to be developed such that $\mathbf{X}'(k)$ comprises just the components of the received signal necessary for the proposed channel estimation scheme (described in the following section) in a format that enables the channel estimation process to be carried out as a single matrix operation.

III. Proposed MIMO Channel Estimation Scheme

Channel estimation is a vital component of space-time system design. For the case of the wideband MIMO-OSIC receivers described in [3], the channel information must be obtained in order to perform the MIMO equalisation process. This requires the estimation of the individual CIRs between each transmit and receive antenna.

In this paper, the proposed MIMO channel estimation scheme combines the following concepts to perform channel estimation in the wideband channel: 1) A pilot matrix transmitted as multiple sequences of pilot symbols is used to jointly estimate the CIRs, as opposed to using a series of individual pilot symbols and an adaptive algorithm [5]. 2) The orthogonal property of the Hadamard matrix is utilised where orthogonal sequences are assigned to individual transmit antennas in order to resolve both the inter-symbol interference (ISI) and the co-channel interference (CCI) of the multiple transmit and received signals. 3) The Toeplitz-like structure of the Paley matrix is exploited to reduce the number of pilot symbols that must be transmitted and thus maximise the effective data throughput.

A. Construction of the Pilot Matrix

The proposed MIMO channel estimation scheme exploits the orthogonal properties of the Hadamard matrix in order to jointly estimate the components of each CIR between each transmit and receive antenna and thus overcome ISI and CCI. The orthogonal property is as follows:

$$\mathbf{G}(v).\mathbf{G}(v)^{\mathsf{T}} = v.\mathbf{I} \tag{14}$$

where $\mathbf{G}(v)$ is the Hadamard matrix with order of v and $\mathbf{I}$ is the identity matrix. Note that $\mathbf{G}$ in (14) is a real matrix. If $\mathbf{G}$ is a complex matrix, then v becomes $2v$ and Hermitian transposition $[.]^{\mathsf{H}}$ replaces $[.]^{\mathsf{T}}$. The pilot matrix, S_F in (13), is chosen such that the orthogonal property in (14) is satisfied. The criteria to choose the order, v, for the pilot matrix, is determined such that:

$$v = (2^{\ell}) \geq M \times (L+1) \tag{15}$$

where ℓ is an integer that allows (15) to be satisfied.

By examining (9)-(13), assuming the channel stays relatively constant, it is possible to assign separate pilot sequences to each transmit antenna and individual path of each respective CIR. First, a Hadamard matrix is constructed based on the order v determined in (15) for the possible values of ℓ. Next, the formulation of the pilot matrix S_F can be obtained directly from this Hadamard matrix according to the number of transmit antennas (M) and the number of paths (L+1) in each CIR. Both parameters are assumed to be known *a priori*. Each row of S_F corresponds to an orthogonal row sequence of the Hadamard matrix. In general, any non-repeated rows can be chosen arbitrarily.

An example of the pilot matrix S_F (represented as real and imaginary matrices **A** and **B**) for the case of $M = 2$, $(L+1) = 3$ is shown below where the order v is chosen to be 8:

$$S_F = \mathbf{A} + j\mathbf{B} \tag{16}$$

where

$$\mathbf{A} = \mathbf{B} = \left[\begin{array}{cccccccc} +s & -s & +s & -s & +s & -s & +s & -s \\ +s & +s & -s & -s & +s & +s & -s & -s \\ +s & -s & -s & +s & +s & -s & -s & +s \end{array}\right] \text{Tx1}$$
$$\left[\begin{array}{cccccccc} +s & +s & +s & +s & -s & -s & -s & -s \\ +s & -s & +s & -s & -s & +s & -s & +s \\ +s & +s & -s & -s & -s & -s & +s & +s \end{array}\right] \text{Tx2}$$

In this example, six row sequences are taken directly from the Hadamard matrix to form **A** and **B**. The partition in the middle divides the pilot matrix into upper and lower regions for transmit antennas Tx1 and Tx2 respectively. For each transmit antenna, the transmitted pilot symbols are sent from consecutive column vectors from left to right in the order shown by the arrows. Thus, S_F contains all pilot symbols to be sent during the channel estimation process such that each column vector of (13) is represented by the corresponding column vector of (16). The use of the pilot matrix S_F thus allows a sequence of pilot symbols to be serially transmitted from each antenna that may then be reconstructed at the receiver into the matrix form shown above and used to jointly estimate the CIRs.

B. Obtaining the Estimate of the MIMO Channel Matrix

The multiple delayed components of $(L+1)$ transmitted symbols are contained within each received signal vector $\mathbf{x}(k)$, due to the multiple $(L+1)$ delayed paths, thus causing overlap of the components of the pilot matrix in successive received signal vectors. A receive signal matrix, $\mathbf{X}'(k)$, may be formed by selecting non-adjacent (p spaced) received signal vectors such that components from previous pilot symbols are not duplicated within any other entries of the matrix. Here, $p = L+1$ for the form of S_F used in (16). The estimate of the concatenated MIMO channel matrix, $\mathbf{H}_{1|M}$ can then be obtained by applying the Hermitian of S_F to the corresponding $\mathbf{X}'(k)$ as follows:

$$\hat{\mathbf{H}}_{1|M} = \frac{1}{(2v)s^2}\left\{\mathbf{X}'(k).S_F^{\mathsf{H}}\right\} \tag{17}$$

where s^2 is the energy per pilot symbol. $(.)^{\mathsf{H}}$ is the Hermitian operation. Each individual estimated CIR obtained by (17) as $\hat{\mathbf{H}}_{1|M} = \left[\hat{\mathbf{H}}_1 | \cdots | \hat{\mathbf{H}}_M\right]$ is subsequently used in the MIMO equalisation process of the OSIC receiver.

C. Minimising the Number of Transmitted Pilot Symbols

In this section, we demonstrate the use of the Paley-Hadamard matrix for the formulation of S_F in order to reduce the length of the pilot sequence. It is possible to exploit the repetition of pilot symbol components within the received signal, due to the multiple delayed paths, to reduce the length of the pilot sequence and thereby use *every* successive received signal vector (p=1) for the estimation process, rather than waiting for every pth received signal vector as before. This requires a Toeplitz-like matrix structure whilst maintaining the orthogonal property of (14). This requirement is fulfilled by selecting symbols in a particular order from a Hadamard matrix based on Paley's construction.

A.1

First, a Paley-Hadamard matrix of order v is chosen such that v is divisible by 4, $(v-1)$ is prime and where:

$$v > M \times (L+1) \tag{18}$$

An example of the Paley-Hadamard matrix for v=8 (with the Toeplitz-like structure diagonally shaded area) is shown below:

$$\mathbf{P} = \left[\begin{array}{cccccccc} +s & +s & +s & +s & +s & +s & +s & +s \\ -s & -s & -s & +s & -s & +s & +s & +s \\ +s & -s & -s & -s & +s & -s & +s & +s \\ +s & +s & -s & -s & -s & +s & -s & +s \\ -s & +s & +s & -s & -s & -s & +s & +s \\ +s & -s & +s & +s & -s & -s & -s & +s \\ +s & +s & -s & +s & +s & -s & -s & +s \\ -s & +s & -s & +s & -s & +s & -s & +s \end{array}\right] \tag{19}$$

Next, consider the same example where M=2 and $(L+1)$=3. Any three consecutive rows from matrix **P**, except the first row, can be chosen to comprise the pilot sequence for each transmit antenna. Rows 2 to 7 are selected from **P** and assigned to **A** & **B** in (16) to form the new S_F that is different from (16) The Toeplitz-like structure means that symbols are repeated in such a fashion that fewer symbols, in the correct order, may be transmitted whilst (14) remains satisfied. In this example, the 12 symbols, $s_m(a)$ to $s_m(l)$ that sequentially sent for each transmit antenna are shaded below.

	$s_{1\|M}(k)$	$s_{1\|M}(k+1)$	$s_{1\|M}(k+2)$	$s_{1\|M}(k+3)$	$s_{1\|M}(k+4)$	$s_{1\|M}(k+5)$	$s_{1\|M}(k+6)$	$s_{1\|M}(k+9)$	
1									
2	$s_1(c)$	$s_1(d)$	$s_1(e)$	$s_1(f)$	$s_1(g)$	$s_1(h)$	$s_1(i)$	$s_1(l)$	
3	$s_1(b)$	$s_1(c)$	$s_1(d)$	$s_1(e)$	$s_1(f)$	$s_1(g)$	$s_1(h)$	$s_1(k)$	Tx1
4	$s_1(a)$	$s_1(b)$	$s_1(c)$	$s_1(d)$	$s_1(e)$	$s_1(f)$	$s_1(g)$	$s_1(j)$	
5	$s_2(c)$	$s_2(d)$	$s_2(e)$	$s_2(f)$	$s_2(g)$	$s_2(h)$	$s_2(i)$	$s_2(l)$	
6	$s_2(b)$	$s_2(c)$	$s_2(d)$	$s_2(e)$	$s_2(f)$	$s_2(g)$	$s_2(h)$	$s_2(k)$	Tx2
7	$s_2(a)$	$s_2(b)$	$s_2(c)$	$s_2(d)$	$s_2(e)$	$s_2(f)$	$s_2(g)$	$s_2(j)$	
8									

Successive (p=1) received signal vectors, $\mathbf{x}$, may then be collected to form $\mathbf{X}'(k)$, except for those corresponding to $s_1(j)$, $s_1(k)$, $s_1(l)$, $s_2(j)$, $s_2(k)$, $s_2(l)$ from $s_{1|M}(k+9)$ which are taken at intervals of p=$(L+1)$ afterwards. Hence, the minimum number of pilot symbols that must be sent has been reduced from $Mv(L+1)$, required by the previous pilot matrix S_F in (16), to $M(v+2L)$ with no reduction in the proposed estimator's performance. To improve the channel estimation accuracy, v may be increased. This will be discussed in the Section V.

IV. Channel Tracking with Decision Feedback

The proposed MIMO channel estimator described above assumes that the channel remains constant during the period over which the pilot sequence is received. In a time-varying channel, however, the MIMO channel will be varying continuously with time, dependent on the Doppler velocity. This will affect the accuracy of the channel estimation process during reception of the pilot sequence, i.e. during the "training" periods, and subsequently the performance of the MIMO OSIC equalisation process during the "data delivery" periods. It is possible, however, to utilise the available data recovery information to perform channel tracking using a decision feedback algorithm during data delivery periods.

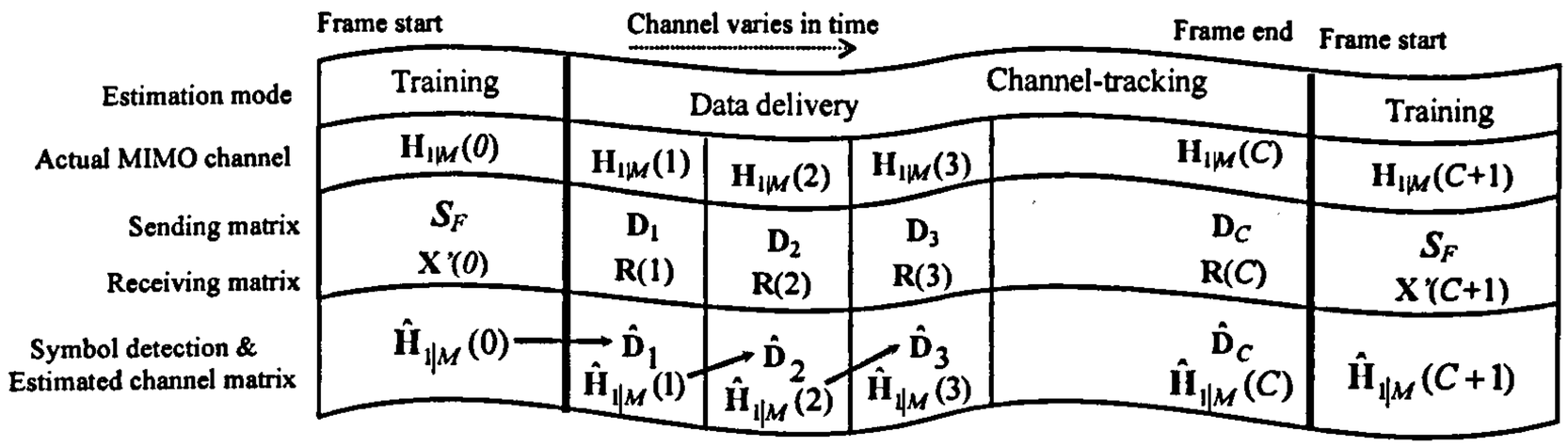

Figure.1: Overview of MIMO channel estimation and channel tracking process

Fig. 1 illustrates the entire process of channel estimation and tracking for a time-varying channel. During the training period, a pilot matrix S_F is transmitted to obtain an initial estimate of the MIMO channel $\hat{\mathbf{H}}_{1|M}(0)$ from the corresponding $\mathbf{X}'(0)$. During the data delivery period, the received data matrix $\mathbf{R}(k)$ can be expressed as:

$$\mathbf{R}(k) = \mathbf{H}_{1|M}(k)\,\mathbf{D}_k + \mathbf{N} \tag{20}$$

where (20) is equivalent to (12), i.e. $\mathbf{D}_k$ is equivalent to S_F in (13) and $\mathbf{R}(k)$ to $\mathbf{X}'(k)$ in (11). For each received signal matrix the previous channel estimate $\hat{\mathbf{H}}_{1|M}(k-1)$ is used for the MIMO OSIC equalisation and detection process to give the detected data matrix, $\hat{\mathbf{D}}_k$. In the decision feedback tracking process, $\mathbf{R}(k)$ and the detected data matrix, $\hat{\mathbf{D}}_k$, are then used to generate a new channel estimate, $\hat{\mathbf{H}}_{1|M}(k)$, as follows:

First the partial channel estimate, $\mathbf{F}_k$ is obtained by applying the Hermitian of the current detected data matrix, $\hat{\mathbf{D}}_k^{\mathsf{H}}$, to the corresponding received signal matrix, $\mathbf{R}(k)$ as follows:

$$\mathbf{F}_k = \mathbf{R}(k)\,\hat{\mathbf{D}}_k^{\mathsf{H}} = \left[\mathbf{H}_{1|M}(k)\,\mathbf{D}_k\right]\hat{\mathbf{D}}_k^{\mathsf{H}} + \mathbf{N}\,\hat{\mathbf{D}}_k^{\mathsf{H}} \tag{21}$$

The current channel estimate $\hat{\mathbf{H}}_{1|M}(k)$ can then be obtained by applying the following:

$$\hat{\mathbf{H}}_{1|M}(k) = \mathbf{F}_k\left[\hat{\mathbf{D}}_k\ \hat{\mathbf{D}}_k^{\mathsf{H}}\right]^{-1} \tag{22}$$

By multiplying $\hat{\mathbf{D}}_k$ & $\hat{\mathbf{D}}_k^{\mathsf{H}}$ together, the whole term can be reduced to a $(M(L+1)\times M(L+1))$ square matrix that is suitable for inversion. It is important to note that the inverse of $\left(\hat{\mathbf{D}}_k\hat{\mathbf{D}}_k^{\mathsf{H}}\right)$ must be non-singular. A pre-check for ill-conditioning might be required to ensure that this term is invertible.

V. Results and Discussion

The accuracy of the proposed MIMO channel estimator (during training period) may be given in terms of the mean square error (MSE), calculated as the mean Frobenius norm squared error of the channel estimate. The mean Frobenius norm squared error is a scalar measurement, which can be obtained as follows:

First, the error matrix of the MIMO channel estimates, e_{H} is obtained by taking the estimated concatenated MIMO channel matrix $\hat{\mathbf{H}}_{1|M}$ and subtracting from the actual concatenated MIMO channel matrix $\mathbf{H}_{1|M}$ expressed as follows:

$$e_{\mathrm{H}} = \mathbf{H}_{1|M} - \hat{\mathbf{H}}_{1|M} \tag{23}$$

Subsequently, the mean Frobenius norm squared error of e_{H} can be obtained as:

$$E\left\{\left\|e_{\mathrm{H}}\right\|_F^2\right\} = \frac{1}{(M\times(L+1)\times N)}\left[\sum_{i=1}^{N}\sum_{j=1}^{M\times(L+1)}\left|\varepsilon_{ij}\right|^2\right] \tag{24}$$

where ε_{ij} is the matrix element of e_{H}. and $E\{.\}$ is the expectation operator.

Fig. 2 and Fig. 3 show the accuracy of the proposed MIMO channel estimator for different SNR values, mobile velocities and system configurations without tracking obtained by simulation of an uncoded layered space-time system in a time-varying, frequency selective fading environment. The results are simulated for a maximum Doppler frequency of fd =176Hz (90km/hr) and fd = 88Hz (45km/hr) for two system configurations, (2×2) and (4×2), using carrier frequency of f_c = 2.1GHz with a data rate of 120kbps per transmit antenna. The frequency selective fading MIMO channel consists of $(L+1) = 3$ time-varying paths for each CIR.

Results are plotted for increasing pilot matrix order v from 8 to 84. Several observations can be made from the results. First, it can be seen that there is an optimal length of the pilot matrix with order v that produces the minimum error. This is more obvious for the 90km/hr channel in Fig. 2 than for the slower 45km/hr channel in Fig. 3 and for the lower SNR values of 5dB and 10dB. Increasing the matrix order v increases the number of pilot symbols and reduces the MSE, thereby improving the performance of the channel estimator. However, this is only true for order v from the minimum value of 8 to the optimum value around 20 to 30, after which any further increase of v degrades the channel estimator's performance. This is due to the channel variation during the training period, which is greater for a higher velocity, causing the estimation process to degrade. Estimator accuracy also increases with SNR. It has also been observed that increasing the number of antennas at the receiver from N=2 to N=4 demonstrates the improvement in performance that results from the added reception diversity.

Fig. 4 shows the bit error probability performance of a (3×2) & (5×3) MIMO OSIC partially connected layered space-time receiver (with K_f = 5 feedforward taps) for the case of 1) perfect channel estimates and 2) estimated channels with and without channel tracking. Results are presented for a 90km/hr time-varying channel with the previously given parameters. A matrix order v of 24 was used for the estimated channels.

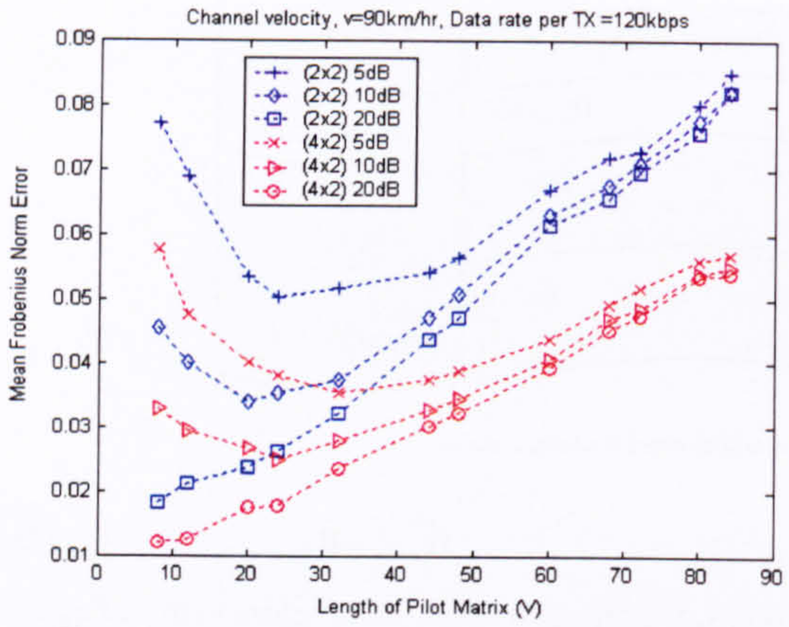

Figure 2: The error performance of the channel estimate versus the pilot length for different ($N\times M$) configurations and SNR values in a 90km/hr channel with (L+1) = 3 time-varying paths.

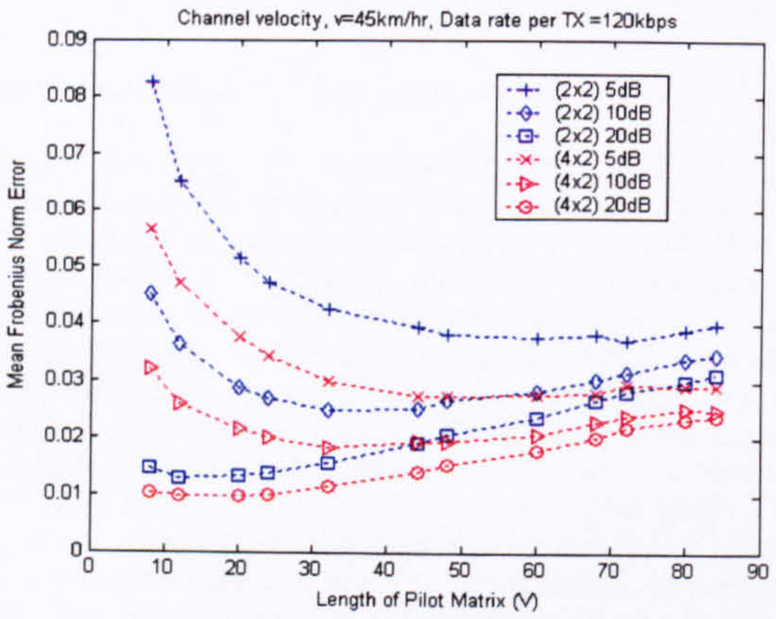

Figure 3: The error performance of the channel estimate versus the pilot length for different ($N\times M$) configurations and SNR values in a 45km/hr channel with (L+1) = 3 time-varying paths.

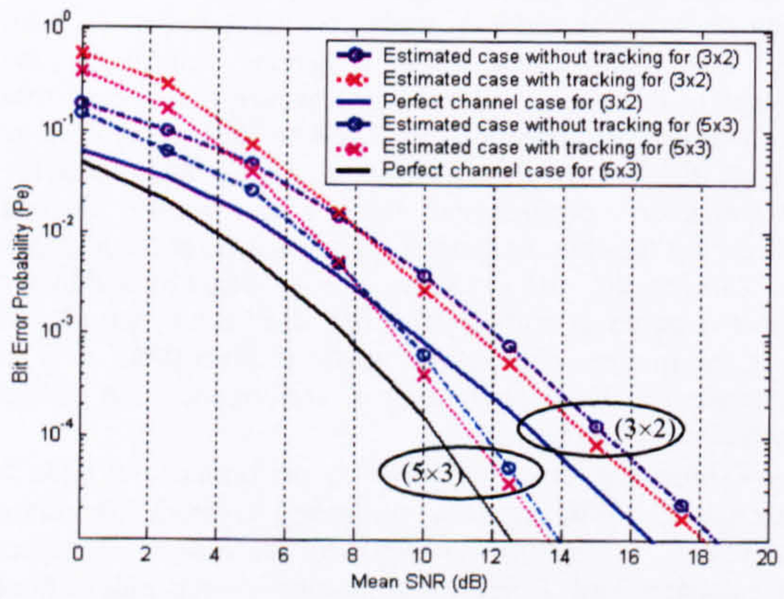

Figure 4: The bit error probability versus SNR for (3×2) and (5×3) system using perfect channel estimates and estimated channels with or without channel tracking in a 90km/hr channel with (L+1) = 3 time-varying paths using only K_f = 5 with optimum order v=24.

It is observed that the proposed MIMO channel estimation scheme results in only 2-3dB degradation in the bit error probability performance as compared to the perfect channel estimates case. The channel tracking provides about 0.5dB further improvement at the higher SNR case but worsens the bit error rate performance at lower SNR. This is due to error propagation within the decision feedback of the channel tracking process.

VI. Conclusions

A novel MIMO channel estimation scheme has been proposed for uncoded layered space-time systems operating in a time-varying, frequency selective fading channels. The Hadamard matrix has been used to construct the pilot matrix and the Toeplitz-like structure of the Paley-Hadamard matrix has been exploited to minimise the number of pilot symbols with no loss of estimator's performance. The accuracy of the proposed channel estimator has been shown to be dependent upon the Doppler velocity of the channel. Results for the bit error probability of an OSIC layered space-time system demonstrate a slight reduction in performance due to channel estimation errors as compared to the perfect channel estimates case. Channel tracking improves the bit error performance for higher SNR but degrades the performance at lower SNR. These results have application to the practical design of space-time systems for high-capacity over wideband MIMO channels.

References

[1] G. J. Foschini, "Layered Space-Time Architecture for Wireless Communication in Fading Environment When Using Multi-Element Antennas", *Bell Labs Tech Journal*, pp. 41-59, Autumn 1996.

[2] P. W. Wolniansky, G. J. Foschini, G. D. Golden, R. A. Valenzuela, "V-BLAST: An architecture for realizing very high data rates over the rich-scattering wireless channel," Proc. ISSSE-98, pp. 295-300, Sept., 1998.

[3] A. Lazono, C. Papadias, "Layered space-time receivers for frequency selective wireless channels," *IEEE Trans. On Communication*, pp. 65-73, vol. 50, No.1 Jan 2002.

[4] X. Zhu, R. D. Murch, "Layered space-time equalization of multiple-input multiple-output frequency selective channels," *IEEE* ICC 2002., pp. 330 – 334, vol.1, 2002.

[5] M. F. Siyau, P. Nobles, R. F. Ormondroyd, "Channel estimation for space-time systems using a multi-element array recursive least squares (MEA-RLS) algorithm," *4th International Symposium on WPCM'01*, pp. 1451-1456, vol.3, Sept, 2001.

[6] Q. Sun, C. Donald, H. C. Huang, A. Lazano, "Estimation of continuous flat fading MIMO channels," *IEEE* WCNC 2002., pp. 189–193, vol.1, 2002.

[7] C. Budianu, L Tong, "Channel estimation for space-time orthogonal block codes," *IEEE Trans. on Signal Processing*, pp. 2515-2528, vol. 50, No.10 Oct 2002.

[8] Y Li, "Simplified channel estimation for OFDM systems with multiple transmit antennas," *IEEE Trans. on Wireless Communication*, pp 67-75, vol.1, no.1, Jan 2002.

[9] J. Seberry and M. Yamada, "Hadamard matrices, sequences and block designs," pp 431-560 of J. H. Dinitz & D. R. Stinson. Editor (1992), Contemporary Design Theory: A Collection of Essays, Wiley, New York.

CHANNEL ESTIMATION FOR LAYERED SPACE-TIME SYSTEMS

M. F. SIYAU P. NOBLES R. F. ORMONDROYD

Communication and Wireless Networks Group, Cranfield University
Royal Military College of Science, Shrivenham, Swindon, SN6 8LA, UK
Tel: +44 (0) 1793 785722, email: v.siyau@rmcs.cranfield.ac.uk

ABSTRACT

Space-time techniques for multiple-input multiple-output (MIMO) systems potentially provide vast increases in capacity. In order to achieve the quoted capacity gains the MIMO channel impulse response (CIR) must be known or estimated. Thus far, existing MIMO channel estimation techniques have been limited to the narrowband case or cater specifically for coded space-time systems. In this paper, we present a novel training-based MIMO channel estimation scheme for an uncoded layered space-time system that operates in the wideband frequency-selective fading environment. The method uses a pilot matrix consisting of pilot symbols derived from the Paley-Hadamard matrix in order to jointly estimate the individual CIR of the MIMO channel. The orthogonal property of the pilot matrix is utilized to resolve both inter-symbol interference and inter-carrier interference of the multiple transmit and received signals. The Paley's Toeplitz structure is also exploited in order to minimise the length of the pilot sequence for a given length of CIR and thus maximise the effective data throughput. Results are presented which demonstrate the accuracy of the proposed channel estimation scheme and its performance in a layered space-time system.

1. INTRODUCTION

Space-time techniques [1] have recently received much interest for multiple-input multiple-output wireless systems due to the potential vast improvement in capacity. This is achieved by properly exploiting the multipath diversity within the rich scattering channel that exits between the multiple antennas at both the transmitter and receiver [2][3]. In particular, the Bell Laboratories layered space-time (BLAST) architecture has been proposed for the narrowband flat-fading channel [4] and MIMO equalisation approaches for the wideband channel [5][6].

For it to be effective in recovering the received symbols, the space-time receiver relies upon accurate channel estimation for both the narrowband and wideband cases. Perfect channel estimation has been assumed in [3]-[6] to demonstrate optimum performance. Thus far, existing MIMO channel estimation schemes are limited to either the narrowband case [7][8] or cater specifically for coded space-time systems [9].

In this paper, we extend the order-successive interference cancellation (OSIC) layered space-time receiver architecture described in [5] for uncoded systems by incorporating a MIMO channel estimation scheme into the receiver architecture. The proposed channel estimation scheme uses a pilot matrix consisting of pilot symbols derived from the Paley construction of the Hadamard matrix [10] in order to jointly estimate the individual CIR between each transmit and receive antenna for a MIMO channel in a frequency selective fading environment. Each transmit antenna sends a sequence of pilot symbols periodically spaced amongst the data. We demonstrate how to generate these sequences by exploiting the Toeplitz structure and the orthogonal properties of the Paley-Hadamard matrix in order to minimise the number of pilot symbols required for channel estimation.

The key to the proposed MIMO channel estimation scheme is the ability to extract the orthogonal information carried by the received signals corresponding to the pilot symbols sent by the transmitter.

The paper is organised as follows. Section 2 briefly describes the space-time system and channel model. The proposed MIMO channel estimation scheme is introduced in Section 3. Section 4 presents the simulation results. Conclusions are given in Section 5.

2. SPACE-TIME SYSTEM AND CHANNEL MODEL

With reference to [5], the space-time system model has been extended to the wideband case for MIMO frequency selective channels. Unless otherwise stated, all notation and assumptions follow [5] for the class of MIMO equalisers described therein. The basic space-time system and the MIMO channel model are outlined below.

There are M transmit and N receive antennas where $(M\times N)$ signifies the system configuration and $(L+1)$ indicates the number of finite symbol-spaced impulse response taps used for the simulated channel. The sampled channel impulse response (CIR) from the m^{th} transmit antenna to n^{th} receive antenna is expressed as:

$$\mathbf{h}_{nm} = \left[h_{nm}(0) \quad h_{nm}(1) \quad \cdots \quad h_{nm}(L)\right]^{\mathsf{T}} \tag{1}$$

where $[.]^{\mathsf{T}}$ is the transpose operation. The received signal vector, $\mathbf{x}$ at time (k) can be expressed as:

$$\mathbf{x}(k) = \sum_{m=1}^{M} \mathbf{H}_m \mathbf{s}_m(k) + \mathbf{n}(k) \tag{2}$$

where $\mathbf{n}(k)$ is the additive white Gaussian noise (AWGN) vector and $\mathbf{s}_m(k)$ is the transmit vector for a sequence of $L+1$ symbols

(i.e. from the current $(k)^{th}$ symbol back to the previous $(k\text{-}L)^{th}$ symbol) sent by the m^{th} transmit antenna:

$$\mathbf{s}_m(k) = \left[s_m(k) \quad s_m(k-1) \quad \cdots \quad s_m(k-L) \right]^{\mathsf{T}} \quad (3)$$

$\mathbf{H}_m$ in (2) represents the channel matrix with respect to the m^{th} transmit antenna, specifying the individual CIR, $\mathbf{h}_{nm}$, between the m^{th} transmit antenna and all (n = 1 to N) receive antennas:

$$\mathbf{H}_m = \begin{bmatrix} \mathbf{h}_{1m}^{\mathsf{T}} \\ \mathbf{h}_{2m}^{\mathsf{T}} \\ \vdots \\ \mathbf{h}_{Nm}^{\mathsf{T}} \end{bmatrix} = \begin{bmatrix} h_{1m}(0) & h_{1m}(1) & \cdots & h_{1m}(L) \\ h_{2m}(0) & h_{2m}(1) & \cdots & h_{2m}(L) \\ \vdots & \vdots & \vdots & \vdots \\ h_{Nm}(0) & h_{Nm}(1) & \cdots & h_{Nm}(L) \end{bmatrix} \quad (4)$$

where m = 1 to M. Note that each fading coefficient h_{nm} is represented by random complex components and all coefficients of the channel matrix are assumed to be totally uncorrelated. The receive signal vectors $\mathbf{x}$ can be grouped as:

$$\mathbf{X}(k) = \left[\mathbf{x}(k) \quad \mathbf{x}(k+1) \quad \cdots \quad \mathbf{x}(k+F) \right] \quad (5)$$

creating (F+1) N-dimensional symbols spanned by (F+1) memory slots in the channel estimator. Since the purpose of this paper is to present a channel estimation scheme, the MIMO equalisation and OSIC receiver model will not be further discussed here. ([5] has further details). However, we proceed to modify the representation in (2) in order to facilitate the channel estimation process described in the next Section.

We use $[\boldsymbol{Y} \mid \boldsymbol{Z}]$ to denote the concatenation of matrix or vector $\boldsymbol{Y}$ and $\boldsymbol{Z}$ and employ the same *vec*(.) operator in [5], expressed in the following:

$$vec\left(\left[\mathbf{v}_1 \; \mathbf{v}_2 \cdots \mathbf{v}_K\right]\right) = \begin{bmatrix} \mathbf{v}_1 \\ \vdots \\ \mathbf{v}_K \end{bmatrix} \quad (6)$$

By concatenating the channel matrices from $\mathbf{H}_1$ to $\mathbf{H}_M$ in (4) as $\mathbf{H}_{1|M} = \left[\mathbf{H}_1 \mid \cdots \mid \mathbf{H}_M\right]$ and applying the *vec*(.) operator to all the transmit vectors as $\boldsymbol{s}_{1|M}(k) = vec\left(\left[\mathbf{s}_1(k) \cdots \mathbf{s}_M(k)\right]\right)$, the received signal vector, $\mathbf{x}(k)$, in (2) can be re-written as:

$$\mathbf{x}(k) = \mathbf{H}_{1|M} \cdot \boldsymbol{s}_{1|M}(k) + \mathbf{n}(k) \quad (7)$$

$$= \left[\mathbf{H}_1 \mid \cdots \mid \mathbf{H}_M \right] \cdot \begin{bmatrix} \mathbf{s}_1(k) \\ \hline \vdots \\ \hline \mathbf{s}_M(k) \end{bmatrix} + \mathbf{n}(k) \quad (8)$$

Note that the matrix representation in (8) allows proper partitioning (shown by the vertical and horizontal strokes) of the channel matrices and their respective transmit vectors, enabling matrix operations to take place referenced to each transmit antenna. Thus, the grouping of $\mathbf{x}$ by the interval p can be expressed as:

$$\mathbf{X}(k') = \left[\mathbf{x}(k) \quad \mathbf{x}(k+p) \quad \ldots \quad \mathbf{x}(k+Fp)\right] \quad (9)$$

Assuming $\mathbf{H}_{1|M}$ stays relatively constant throughout the interval, the received signal matrix, $\mathbf{X}(k')$ in (9) also corresponds to:

$$\mathbf{X}(k') = \mathbf{H}_{1|M} \cdot \boldsymbol{S}_F + \mathbf{N} \quad (10)$$

where $\boldsymbol{S}_F$ is the grouped matrix of the transmit vectors:

$$\boldsymbol{S}_F = \left[\; \boldsymbol{s}_{1|M}(k) \mid \boldsymbol{s}_{1|M}(k+1) \mid \cdots \mid \boldsymbol{s}_{1|M}(k+F) \; \right] \quad (11)$$

$\mathbf{N}$ in (10) is the grouped matrix of the AWGN vectors containing $\mathbf{n}(k)$ to $\mathbf{n}(k+F)$ respectively. Note that the p parameter allows us to group the non-adjacent received signal vectors. When p = 1, (9) is equivalent to (5). However, this also leads to a change in the corresponding $\boldsymbol{s}_{1|M}$ so that $\boldsymbol{S}_F$, has a Toeplitz structure. This will be further explained in Section 3.3.

3. MIMO CHANNEL ESTIMATION SCHEME

Channel estimation is a vital component of space-time system design. For the case of the wideband OSIC receivers described in [5], the channel information must be obtained in order to perform the equalisation process that attempts to counteract the inter-symbol interference due to the frequency selective channel. This requires the estimation of the individual CIRs between each transmit and receive antenna.

In this paper, the channel is assumed to stay relatively constant over the duration of a data packet. The proposed MIMO channel estimation scheme combines the following concepts to perform channel estimation in the wideband channel: 1) A pilot matrix transmitted as a sequence of pilot symbols is used to jointly estimate the CIRs, as opposed to using a series of individual pilot symbols and an adaptive algorithm [8]. 2) The orthogonal property of the Hadamard matrix is utilised where each sequence of the pilot symbols is constructed to be orthogonal with respect to one another and assigned to individual transmit antennas in order to resolve both the inter-symbol interference (ISI) and the inter-carrier interference (ICI) of the multiple transmit and received signals as well as to extract the channel information carried by these orthogonal pilot symbols. 3) The Toeplitz structure of the Paley-Hadamard matrix is exploited to reduce the number of pilot symbols that must be transmitted and thus maximise the effective data throughput.

3.1. Construction of the Pilot Matrix

The proposed MIMO channel estimation scheme exploits the orthogonal properties of the Hadamard matrix in order to jointly estimate the CIR between each transmit and receive antenna. The orthogonal property is as follows:

$$\mathbf{G}(v).\mathbf{G}(v)^{\mathsf{T}} = v.\mathbf{I} \quad (12)$$

where $\mathbf{G}(v)$ is the Hadamard matrix with order of v and $\mathbf{I}$ is the identity matrix. Note that $\mathbf{G}$ in (12) is a real matrix. If $\mathbf{G}$ is a complex matrix, then v becomes $2v$ and Hermitian transposition '^{H}' replaces '^{T}'. The pilot matrix, $\boldsymbol{S}_F$ in (11), is chosen such that the orthogonal property in (12) is satisfied. The criteria to choose the order, v, for the pilot matrix, is determined such that:

$$v = (2^{\ell}) \geq M \times (L+1) \quad (13)$$

where ℓ is an integer that allows (13) to be satisfied.

By examining (7)-(11), it is possible to assign separate sequences of pilot symbols to each transmit antenna. First, an arbitrary Hadamard matrix is constructed based on the order v determined in (13) for the possible values of ℓ. Next, the formulation of the pilot matrix $\boldsymbol{S}_F$ is obtained directly from this Hadamard matrix according to the number of transmit antennas (M) and the number of paths (L+1) in each CIR. Both parameters are assumed to be known *a priori*. Each row of $\boldsymbol{S}_F$ corresponds to a chosen row sequence of the Hadamard matrix. In general, any non-repeated rows can be chosen arbitrary. However, in the case of the Paley-Hadamard construction, considered later,

specific arrangements of rows have to be chosen in order to form the required Toeplitz structure.

An example of the pilot matrix $\boldsymbol{S}_F$ (represented as real and imaginary matrices **A** and **B**) for the case of $M = 2$, $(L+1) = 3$ is shown below where the order v is chosen to be 8:

$$\boldsymbol{S}_F = \mathbf{A} + j\mathbf{B} \tag{14}$$

where

$$\mathbf{A} = \mathbf{B} = \left[\begin{array}{cccccccc} +s & -s & +s & -s & +s & -s & +s & -s \\ +s & +s & -s & -s & +s & +s & -s & -s \\ +s & -s & -s & +s & +s & -s & -s & +s \\ \hline +s & +s & +s & +s & -s & -s & -s & -s \\ +s & -s & +s & -s & -s & +s & -s & +s \\ +s & +s & -s & -s & -s & -s & +s & +s \end{array}\right] \begin{array}{l} \\ \\ \\ \text{Tx1} \\ \\ \\ \text{Tx2} \end{array}$$

In this example, the partition in the middle divides the pilot matrix into upper and lower regions for transmit antennas Tx1 and Tx2 respectively. For each transmit antenna, the transmitted pilot symbols are sent from consecutive column vectors from left to right in the order shown by the arrows. Thus, $\boldsymbol{S}_F$ contains all pilot symbols to be sent during the channel estimation process such that each column vector of (11) is represented by the corresponding column vector of (14). The use of the pilot matrix $\boldsymbol{S}_F$ thus allows a sequence of pilot symbols to be serially transmitted from each antenna that may then be reconstructed at the receiver into the matrix form shown above and used to jointly estimate the CIRs.

3.2. Obtaining the estimate of the channel matrix

By grouping the respective received vectors **x** with the interval p, where $p = L+1$ for the form of $\boldsymbol{S}_F$ used in (14), the estimate of the concatenated MIMO channel matrix, $\mathbf{H}_{1|M}$ can be obtained by applying the Hermitian of $\boldsymbol{S}_F$ to the corresponding $\mathbf{X}(k')$ as follows:

$$\hat{\mathbf{H}}_{1|M} = \frac{1}{(2v).s^2}\left\{\mathbf{X}(k').\boldsymbol{S}_F{}^{\mathsf{H}}\right\} \tag{15}$$

where s^2 is the energy per pilot symbol. $(.)^{\mathsf{H}}$ is the Hermitian operation. Each individual estimated CIR obtained by (15) as $\hat{\mathbf{H}}_{1|M} = \left[\hat{\mathbf{H}}_1 \,|\cdots|\, \hat{\mathbf{H}}_M\right]$ is subsequently used in the MIMO equalisation process of the OSIC receiver.

It is worth noting that due to the embedded orthogonal structure, the formulation of the pilot matrix $\boldsymbol{S}_F$ provides the means to concurrently segregate and resolve the composition of the multiple received signals, not only in terms of each transmitted pilot sequence with their respective transmit antenna, but also the individual $(L+1)$ multipaths in each CIRs. Hence, the problems of ISI and ICI during the training of the channel can be dealt directly by the use of pilot matrix $\boldsymbol{S}_F$ and the received signal matrix $\mathbf{X}(k')$ through (15). The key here is the ability to extract the useful orthogonal information carried by the received signals corresponding to the pilot sequences sent by each antenna in order to carry out the MIMO channel estimation.

3.3. Minimising the number of transmitted pilot symbols

It is important to ensure the proper grouping of the received training vector, $\mathbf{X}(k')$ in (9), at the correct 'p' interval, and the proper assignment of the pilot symbols in $\boldsymbol{S}_F$, across all the transmit antenna in order to jointly estimate all the CIRs in the MIMO frequency selective channel. In this section, we demonstrate the use of Paley's construction of the Hadamard matrix [10] to reduce the length of the transmitted sequence of pilot symbols. This is achieved by reducing the interval p to 1 such that the consecutive received training vectors, **x**, can be grouped together as $\mathbf{X}(k)$, as expressed in (5) (except for the last column vector). Such a pilot matrix requires the Toeplitz structure, while maintaining the orthogonal property in (12). This requirement is fulfilled by the Hadamard matrix based on Paley's construction [10] which combines the orthogonal structure and the Toeplitz structure together. However, this also requires the formation of the pilot matrix, $\boldsymbol{S}_F$ to be altered in order to fulfil (5) which subsequently leads to the alteration in the corresponding $\boldsymbol{s}_{1|M}(k)$ to $\boldsymbol{s}_{1|M}(k+F)$. The order v used for the construction of the Paley-Hadamard matrix and the pilot matrix formulation is also different for the proposed MIMO channel estimation scheme and is outlined below:

First, a Paley-Hadamard matrix of order v is chosen such that v is divisible by 4, $(v\text{-}1)$ is prime and where:

$$v > M \times (L+1) \tag{16}$$

An example of the Paley-Hadamard matrix for v=8 is shown below:

$$\mathbf{P} = \left[\begin{array}{cccccccc} +s & +s & +s & +s & +s & +s & +s & +s \\ -s & -s & -s & +s & -s & +s & +s & +s \\ +s & -s & -s & -s & +s & -s & +s & +s \\ +s & +s & -s & -s & -s & +s & -s & +s \\ \hline -s & +s & +s & -s & -s & -s & +s & +s \\ +s & -s & +s & +s & -s & -s & -s & +s \\ -s & +s & -s & +s & +s & -s & -s & +s \\ -s & -s & +s & -s & +s & +s & -s & +s \end{array}\right] \tag{17}$$

Next, consider the same example where M=2 and $(L+1)$=3. Any three consecutive rows from this matrix, except the first, can be chosen to comprise the sequence of pilot symbols for each transmit antenna. In this example, rows 2 to 7 are selected to form the different pilot matrix $\boldsymbol{S}_F$ as compared to the one in (14), but with the same matrix dimension. The Toeplitz structure means that symbols are repeated in such a fashion that fewer symbols, in the correct order, may be transmitted whilst (12) remains satisfied. In this example, the 12 symbols, $s_m(a)$ to $s_m(l)$, for each transmit antenna as chosen from (17), are shaded below.

	$\boldsymbol{s}_{1M}(k)$	$\boldsymbol{s}_{1M}(k+1)$	$\boldsymbol{s}_{1M}(k+2)$	$\boldsymbol{s}_{1M}(k+3)$	$\boldsymbol{s}_{1M}(k+4)$	$\boldsymbol{s}_{1M}(k+5)$	$\boldsymbol{s}_{1M}(k+6)$	$\boldsymbol{s}_{1M}(k+7)$	
1									
2	$s_1(c)$	$s_1(d)$	$s_1(e)$	$s_1(f)$	$s_1(g)$	$s_1(h)$	$s_1(i)$	$s_1(l)$	
3	$s_1(b)$	$s_1(c)$	$s_1(d)$	$s_1(e)$	$s_1(f)$	$s_1(g)$	$s_1(h)$	$s_1(k)$	Tx1
4	$s_1(a)$	$s_1(b)$	$s_1(c)$	$s_1(d)$	$s_1(e)$	$s_1(f)$	$s_1(g)$	$s_1(j)$	
5	$s_2(c)$	$s_2(d)$	$s_2(e)$	$s_2(f)$	$s_2(g)$	$s_2(h)$	$s_2(i)$	$s_2(l)$	
6	$s_2(b)$	$s_2(c)$	$s_2(d)$	$s_2(e)$	$s_2(f)$	$s_2(g)$	$s_2(h)$	$s_2(k)$	Tx2
7	$s_2(a)$	$s_2(b)$	$s_2(c)$	$s_2(d)$	$s_2(e)$	$s_2(f)$	$s_2(g)$	$s_2(j)$	
8									

The 12 symbols are sequentially sent from each transmit antenna and the respective received signal vector **x** are to be carefully

grouped such that the time gap in between these vectors **x** is minimised with p=1 where consecutive received signal vectors can be utilised. Only the last column vector of $\mathbf{X}(k')$ has to be taken at $(L+1)$ interval later that corresponds to $\boldsymbol{s}_{1|M}(k+7)$ with the transmit symbols $s_m(j)$ to $s_m(l)$ shown in the example case above. Hence, the minimum number of pilot symbols that must be transmitted has been reduced from $M(vL)$ (required by the previous pilot matrix $\boldsymbol{S}_F$ in (14)), to $M(v+2L)$ from the shaded symbols above, with no reduction in performance. Again, the key is to extract these useful orthogonal information carried by the pilot received signals in order to carry out the MIMO channel estimation with the optimum number of pilot symbols. To improve the channel estimation accuracy, v may be increased. This will be discussed in the next Section.

4. RESULTS AND DISCUSSION

The performance of the proposed MIMO channel estimator for an uncoded space-time system is shown in figure 1 using the mean square error (MSE) (which is the mean Frobenius norm squared error of the channel estimate) as the performance metric. The mean Frobenius norm squared error is a scalar measurement of the proposed MIMO channel estimator's performance, which can be obtained as follows:

First, the error matrix of the MIMO channel estimation, $\boldsymbol{e}_{\mathrm{H}}$ is obtained by taking the estimated concatenated MIMO channel matrix $\hat{\mathbf{H}}_{1|M}$ and subtracted from the actual concatenated MIMO channel matrix $\mathbf{H}_{1/M}$ and is expressed as follows:

$$\boldsymbol{e}_{\mathrm{H}} = \mathbf{H}_{1|M} - \hat{\mathbf{H}}_{1|M} \tag{18}$$

Subsequently, the mean Frobenius norm squared error of $\boldsymbol{e}_{\mathrm{H}}$ can be obtained as:

$$E\left\{\left\|\boldsymbol{e}_{\mathrm{H}}\right\|_F^2\right\} = \frac{1}{(M\times(L+1)\times N)}\left[\sum_{i=1}^{N}\sum_{j=1}^{M\times(L+1)}\left|\varepsilon_{ij}\right|^2\right] \tag{19}$$

where ε_{ij} is the matrix element of $\boldsymbol{e}_{\mathrm{H}}$. and $E\{.\}$ is the expectation operator.

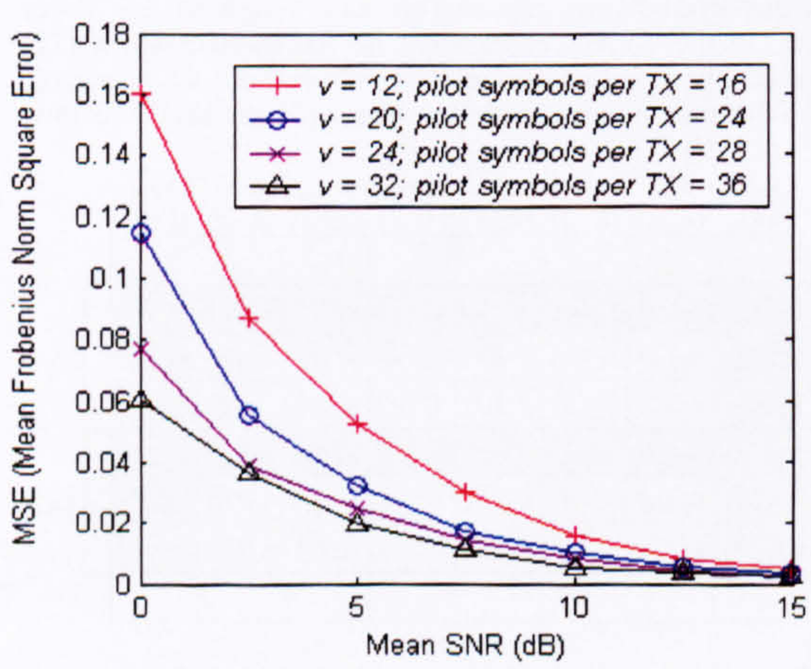

Figure 1: The channel estimate MSE versus mean SNR for different pilot matrix order, v. M=2, N=3 and $(L+1)$=3.

In figure 1, the MSE is plotted against mean SNR for increasing matrix order, v, for a layered space-time system with M=2, N=3 and $(L+1)$=3. The minimum number of pilot symbols that may be transmitted in this case is 12, corresponding to v=8. Results for pilot matrix orders v=12, 20, 24 and 32 are shown in the figure. The corresponding number of pilot symbols sent per transmit antenna is also stated. Increasing the matrix order increases the number of pilot symbols transmitted and reduces the MSE, thereby improving the performance of the channel estimator. The results demonstrate the consistency of the channel estimation performance and the trade-off between the length of the sequence of pilot symbols and the channel estimation error.

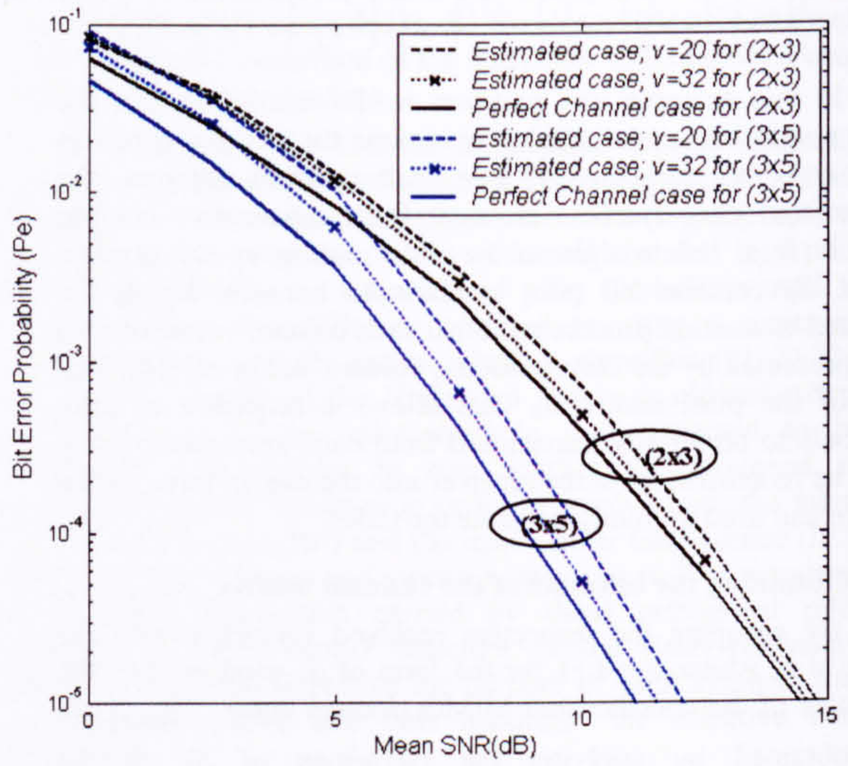

Figure 2: The bit error probability versus SNR for system configurations (2×3) and (3×5) using perfect channel estimates and estimated channels for different pilot matrix order, v, where $(L+1)$ = 3, Kf=5 and Kb=3.

The impact of the channel estimation error on the bit error probability, Pe, performance of an OSIC layered space-time receiver was investigated for a system comprising Kf feedforward and Kb feedback taps in the partially connected version of the MIMO equaliser from [5]. Figure 2 compares the performance of the proposed channel estimation scheme with the case where perfect channel estimates are assumed. Pe versus SNR for system configurations (2×3) and (3×5) is shown for pilot matrix orders of v=20 and v=32. The proposed channel estimation scheme results in a small degradation in the bit error probability performance as compared to the case where perfect channel estimation is assumed.

It can also be observed that for higher orders of v the results are much closer to the perfect channel estimate case. This result confirms the trend seen in figure 1, where the performance is improved by increasing the number of pilot symbols sent during the channel estimation process. It is worth noting that the decision-feedback equaliser (DFE) structure of the MIMO equaliser in the OSIC layered space-time system means that error propagation is likely to have a disproportionate impact on the bit error performance despite the accuracy of the channel estimation process.

5. CONCLUSIONS

A novel MIMO channel estimation scheme has been proposed for uncoded layered space-time systems operating in frequency selective fading channels. The Hadamard matrix has been used to construct sequences of pilot symbols that are transmitted from the multiple antennas of the MIMO system. By choosing a sequence that exploits the Toeplitz structure of the Paley-Hadamard matrix the number of pilot symbols may be significantly reduced with no impact on the performance of the channel estimation scheme. Results for the bit error probability of an OSIC MIMO-DFE layered space-time system demonstrate a slight reduction in performance due to channel estimation errors as compared to the case where perfect channel estimates are assumed. These results have application to the practical design of space-time systems for high-capacity wireless data transmission over frequency selective channels.

REFERENCES

[1] C. B. Papadias, A. J. Paulraj, "Space-time processing for wireless communications," *IEEE Signal Processing Magazine*, pp. 49-83, vol. 14, Issue. 6, Nov 1997.

[2] G. J. Foschini, "Layered Space-Time Architecture for Wireless Communication in Fading Environment When Using Multi-Element Antennas", *Bell Labs Tech Journal*, pp. 41-59, Autumn 1996.

[3] B. A. Bjerke, J. G. Proakis, "Multiple transmit and receive antenna diversity techniques for wireless communications", Adaptive System for Signal Processing, Communications and Control symposium, AS-SPCC, IEEE 2000.

[4] P. W. Wolniansky, G. J. Foschini, G. D. Golden, R. A. Valenzuela, "V-BLAST: An Architecture for Realizing Very High Data Rates Over the Rich-Scattering Wireless Channel," Proc. ISSSE-98, pp. 295-300, Sept., 1998.

[5] A. Lazono, C. Papadias, "Layered space-time receivers for frequency selective wireless channels," *IEEE Trans. On Communication*, pp. 65-73, vol. 50, No.1 Jan 2002.

[6] X. Zhu, R. D. Murch, "Layered space-time equalization of multiple-input multiple-output frequency selective channels," *IEEE* ICC 2002., pp. 330 – 334, vol.1, 2002.

[7] Q. Sun, C. Donald, H. C. Huang, A. Lazano, "Estimation of continuous flat fading MIMO channels," *IEEE* WCNC 2002., pp. 189–193, vol.1, 2002.

[8] M. F. Siyau, P. Nobles, R. F. Ormondroyd, "Channel estimation for space-time systems using a multi-element array recursive least squares (MEA-RLS) algorithm," *4th International Symposium on WPCM'01*, pp. 1451-1456, vol.3, Sept, 2001.

[9] C. Budianu, L Tong, "Channel estimation for space-time orthogonal block codes," *IEEE Trans. on Signal Processing*, pp. 2515-2528, vol. 50, No.10 Oct 2002.

[10] J. Seberry and M. Yamada, "Hadamard matrices, sequences and block designs," pp 431-560 of J. H. Dinitz & D. R. Stinson. Editor (1992), Contemporary Design Theory: A Collection of Essays, Wiley, New York.

NON-LINEAR DETECTION FOR SPACE-TIME SYSTEMS USING ORTHOGONAL TRIANGULARIZATION BY QR DECOMPOSITION

M F Siyau, P Nobles, R F Ormondroyd

Abstract

A new non-linear symbol detection algorithm is proposed that uses an orthogonal triangularization method to reduce the complexity of the detection process. First, the optimum symbol detection order is obtained based on the post-detection SNR, using criteria such as zero-forcing or minimum mean square error, as in V-BLAST. This order is then used to rearrange the columns of the channel matrix. The new algorithm then applies QR decomposition to this rearranged channel matrix. The resulting triangular properties allow the sequence of symbols to be recovered by simple backward substitution with symbol cancellation. The proposed method equals the performance of V-BLAST. Results are presented for various system configurations that demonstrate the importance of rearranging the channel matrix using the proposed method as compared to random ordering.

Introduction

Space-time communication techniques promise significant increases in the capacity of wireless systems that operate in rich scattering environments [1]. MIMO systems, such as V-BLAST [2], employ multiple antennas at both the transmitter and receiver to exploit multipath diversity. Recently, there have been a number of developments to the V-BLAST method. In [3], an efficient square-root algorithm for the nulling and cancellation step has been proposed to reduce the computational complexity. In [4], a new decoding algorithm based on the joint maximum likelihood and decision feedback equalization method for V-BLAST has been proposed for performing symbol detection. Both [3] and [4] partially adopt the concept of QR decomposition for the space-time channel matrix. In [5], a low complexity V-BLAST architecture is proposed where Gram-Schmitt Orthogonalization (GSO) is applied to the channel matrix in order to find the weights. Here, we present a simpler concept for the non-linear space-time symbol detection using orthogonal triangularization structure achieved by QR decomposition.

Space-Time Model and Detection Algorithm

In the space-time model of Fig. 1, there are M parallel transmitters and N parallel receivers. The incoming data stream A is split into M parallel streams of symbols mapped to the chosen modulation scheme. They are then transmitted simultaneously as the column vector $\boldsymbol{a} = [a_1, a_2, \cdots, a_M]^T$ into the space-time channel $\mathbf{H}$ with the matrix dimension $(N \times M)$. The power radiated by each transmitter is proportional to $1/M$ in order to maintain a constant total transmit power as the number of transmitting antennas changes. We assume a Rayleigh flat-fading channel model. The elements of the received signal vector $\boldsymbol{r} = [r_1, r_2, \cdots, r_N]^T$ are the distorted versions of the transmitted symbols at each receiving antenna, where:

$$\boldsymbol{r} = \mathbf{H}\boldsymbol{a} + \boldsymbol{n} \tag{1}$$

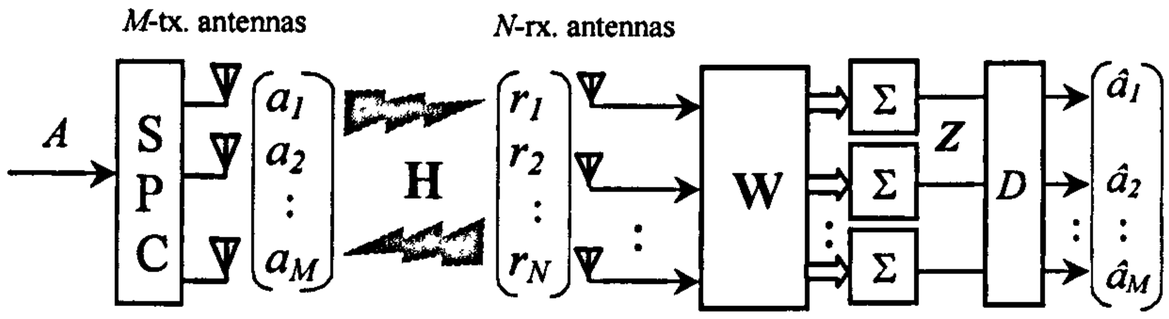

Fig.1: Space-time communication system model with symbol detection block.

Communication and Wireless Networks Group, Cranfield University, Royal Military College of Science, Shrivenham, Swindon, SN6 8LA, UK. Tel: +44 1793 785722, email: v.siyau@rmcs.cranfield.ac.uk

Here, $\boldsymbol{n}$ is the i.i.d. additive white Gaussian noise vector. The received signal vector is processed by weighting each element of $\boldsymbol{r}$ with the elements of the weighting matrix, **W**. The weights, ω_{ij} in **W** are obtained according to one of two possible criteria: Zero-Forcing (ZF) or Minimum Mean Square Error (MMSE) [6]. The weighted signals are combined to form $\boldsymbol{Z} = [z_1, z_2, \cdots, z_M]^{\mathsf{T}}$. Each element in vector $\boldsymbol{Z}$ can be expressed as:

$$z_i = \sum_{j=1}^{N} \omega_{ij} r_j \tag{2}$$

Using the zero forcing criterion as an example, estimates of the symbol vector, $\hat{\boldsymbol{a}} = [\hat{a}_1, \cdots, \hat{a}_M]^{\mathsf{T}}$ are recovered by applying the inverse of **H** to, $\boldsymbol{r}$, assuming that the fading coefficients in **H** are perfectly known by the receiver and each element in the received vector $\boldsymbol{r}$ is totally uncorrelated. The process is represented as follows:

$$\mathbf{W} = \mathbf{H}^{+} \tag{3a}$$
$$\boldsymbol{Z} = \mathbf{W}\boldsymbol{r} \tag{3b}$$
$$\hat{\boldsymbol{a}} = D(\boldsymbol{Z}) \tag{3c}$$

where D is the 'slicing' operator that decides upon the symbol estimate, according to the decision threshold for the modulation scheme employed. The $^{+}$ sign denotes the pseudo-inverse operation and is applied for the case when $N \geq M$. In practice, the channel coefficients must be estimated by some method [7].

V-BLAST Nonlinear Detection and Symbol Cancellation

The symbol detection algorithm of (3) is a linear process where all symbols in the transmitted vector $\boldsymbol{a}$ can be resolved simultaneously, assuming perfect symbol synchronization. However, superior performance can be obtained if nonlinear detection methods, such as symbol cancellation, are used. The nonlinear detection method resolves each symbol by treating the already-detected symbol components of vector $\boldsymbol{a}$ as symbol interference and they are subsequently eliminated from the received signal vector $\boldsymbol{r}$ one at a time [2]. The V-BLAST process can be separated into two parts; namely a) the optimum ordering process and b) the symbol detection process, as follows:

a) The optimum ordering process:

Initialization

$$i \leftarrow 1 \tag{4a}$$
$$\mathbf{G}_1 = \mathbf{H}^{+} \tag{4b}$$
$$\mathrm{v}_1 = \arg\min_{j} \left\| (\mathbf{G}_1)_j \right\|^2 \tag{4c}$$

Recursion

$$\mathbf{G}_{i+1} = \left\{ Z(\mathbf{H})_{\mathrm{v}_i} \right\}^{+} \tag{4d}$$
$$\mathrm{v}_{i+1} = \arg\min_{j \notin \{\mathrm{v}_1 \cdots \mathrm{v}_i\}} \left\| (\mathbf{G}_{i+1})_j \right\|^2 \tag{4e}$$
$$i \leftarrow i+1 \tag{4f}$$

b) The symbol detection process:

Initialization

$$i \leftarrow 1 \tag{5a}$$

Recursion

$$\mathbf{w}_{\mathrm{v}_i} = (\mathbf{G}_i)_{\mathrm{v}_i} \tag{5b}$$
$$\hat{a}_{\mathrm{v}_i} = D(\mathbf{w}_{\mathrm{v}_i}^{\mathsf{T}} \boldsymbol{r}_i) \tag{5c}$$
$$\boldsymbol{r}_{i+1} = \boldsymbol{r}_i - \hat{a}_{\mathrm{v}_i} (\mathbf{H})_{\mathrm{v}_i} \tag{5d}$$
$$i \leftarrow i+1 \tag{5e}$$

where v_i is the order in which the subsequent symbol detection will be carried out and is determined by the post-detection SNR, as described in [2]. The 'Z' operator in (4*d*) sets the respective column of **H** to zero according to the value of 'v_i'. The same 'D' operator from (3*c*) is used in (5c). The values of the matrix **G** are stored following each iteration of the ordering process and may subsequently be used in the symbol detection process. On completion of the optimum detection ordering process (4*a*)-(4*f*), the detection ordering set is obtained and written as:

$$\Re_{VBLAST} = \{\mathrm{v}_1, \mathrm{v}_2, \cdots, \mathrm{v}_M\} \tag{6}$$

The order in (6) may be obtained by other methods that avoid the pseudo-inverse process [3]. In this paper, we assume that we have been able to obtain the optimum ordering and the paper concentrates on the symbol detection process described in the next section.

Nonlinear QR Detection Algorithm

The method makes use of the orthogonal triangularization process [8,9] to resolve each symbol iteratively by symbol cancellation. First, the order obtained in (6) is used to rearrange the columns of the channel matrix. The algorithm then

applies QR decomposition to this rearranged channel matrix, $\mathbf{H}_{new}$. The resulting triangular properties allow the sequence of transmitted symbols to be recovered by simple backward substitution with cancellation. It is important, therefore, that the best estimates of the symbols are used first. The process is described in the following section.

Channel Matrix Rearrangement

The ordering set obtained by the ordering process can be expressed as:

$$\Re = \{ s_1, s_2, \cdots, s_M \} \tag{7}$$

This is simply a restatement of (6) for the general case. Once the ordering is obtained, the rearrangement from $\mathbf{H}$ to $\mathbf{H}_{new}$ can be accomplished by rearranging columns using the following procedure:

$$\begin{aligned}
&\underline{\textit{Initializa tion}} \\
&i \leftarrow 1 && (8a)\\
&b \leftarrow M && (8b)\\
&\underline{\textit{Recursion}} \\
&(\mathbf{H}_{new})_b = (\mathbf{H})_{s_i} && (8c)\\
&i \leftarrow i+1 && (8d)\\
&b \leftarrow b-1 && (8e)
\end{aligned}$$

The nomenclature of equation (8*c*) implies that the s_i^{th} column of $\mathbf{H}$ is selected and replaces the b^{th} column of $\mathbf{H}_{new}$ for all M columns.

Orthogonal Triangularization by QR decomposition

The reordered channel matrix, $\mathbf{H}_{new}$, can be decomposed into the orthonormal matrix, $\mathbf{Q}_{new}$, and upper triangular matrix, $\mathbf{R}_{new}$, as follows:

$$\mathbf{H}_{new} = \mathbf{Q}_{new} \begin{bmatrix} \mathbf{R}_{new} \\ \boldsymbol{O} \end{bmatrix} \tag{9}$$

where $\boldsymbol{O}$ is the zero matrix. To illustrate the method adopted we assume the noise free condition. Hence, from (1), the received vector can be written as:

$$\boldsymbol{r} = \mathbf{Q}_{new} \begin{bmatrix} \mathbf{R}_{new} \\ \boldsymbol{O} \end{bmatrix} \boldsymbol{a}_{new} \tag{10}$$

A property of an orthogonal matrix is that $\mathbf{Q}^{\mathsf{T}} = \mathbf{Q}^{-1}$ and $\mathbf{Q}^{\mathsf{T}}\mathbf{Q} = 1$, therefore, (10) can be re-written as follows:

$$\mathbf{Q}_{new}^{\mathsf{T}} \boldsymbol{r} = \boldsymbol{x} = \begin{bmatrix} \mathbf{R}_{new} \\ \boldsymbol{O} \end{bmatrix} \boldsymbol{a}_{new} \tag{11}$$

where $\boldsymbol{x}$ denotes the 'orthogonalized' receive vector and its elements q_i can be expressed as: $\boldsymbol{x} = [q_1, q_2, \cdots, q_N]^{\mathsf{T}}$. Estimates of the symbol elements of vector $\boldsymbol{a}$ are then recovered by a non-linear process that includes backward substitution into the upper triangular matrix $\mathbf{R}_{new}$ in (11) with symbol cancellation.

Nonlinear QR Symbol Detection Process

Having rearranged $\mathbf{H}$ to give $\mathbf{H}_{new}$, we now apply QR decomposition to obtain $\mathbf{Q}_{new}$ and $\mathbf{R}_{new}$. At the receiver, the symbol elements in the original transmitted vector $\boldsymbol{a}$ are 'rearranged' so that the received vector $\boldsymbol{r}$ remains the same. The $\mathbf{R}_{new}$ obtained from $\mathbf{H}_{new}$ can be expressed as:

$$\begin{aligned}
\mathbf{R}_{new} &= \begin{bmatrix} R_1 & R_2 & \cdots & R_M \end{bmatrix} \\
&= \begin{bmatrix} \gamma_{11} & \gamma_{12} & \cdots & \gamma_{1M} \\ 0 & \gamma_{22} & \cdots & \gamma_{2M} \\ \vdots & 0 & \ddots & \vdots \\ 0 & \cdots & 0 & \gamma_{MM} \end{bmatrix}
\end{aligned} \tag{12}$$

where R_i is the i^{th} column vector in $\mathbf{R}_{new}$ and γ_{nm} are the elements in $\mathbf{R}_{new}$. The rearrangement of the columns of $\mathbf{H}$ is determined by the detection ordering set, $\Re$, such that the first element of $\Re$ corresponds to the last column of $\mathbf{H}_{new}$, etc.

For example, in a (3×3) system, if $\Re = \{2,1,3\}$, then $\mathbf{H}$ is rearranged such that $\mathbf{H}_{new} = [H_3, H_1, H_2]$ where H_i denotes the columns of $\mathbf{H}$. Once the 'orthogonalized' receive vector, $\boldsymbol{x}$, in (11) is obtained, the symbol estimates of the transmit vector, $\hat{\boldsymbol{a}}_{new} = [\hat{a}_3, \hat{a}_1, \hat{a}_2]^T$, can be detected by either backward substitution, which is equivalent to linear detection, or the following non-linear approach with symbol cancellation. It is worth noting that QR decomposition applied to $\mathbf{H}_{new}$ is only carried out once and the columns of $\mathbf{R}_{new}$ are used in the following algorithm:

Initializa tion

$$j \leftarrow M \qquad (13a)$$

$$k = 1 \qquad (13b)$$

Recursion

$$\hat{a}_j = D\left(\frac{q_j^k}{\gamma_{jj}}\right) \qquad (13c)$$

$$\boldsymbol{x}^{k+1} = \boldsymbol{x}^k - \hat{a}_j R_j \qquad (13d)$$

$$j \leftarrow j-1 \qquad (13e)$$

$$k = k+1 \qquad (13f)$$

where 'D' is the same decision operator mentioned in (3c). 'k' is the recursion index. It can be noticed that (13c) resolves each symbol estimate sequentially in a backward manner and (13d) performs the symbol cancellation of the already detected component a_j from the orthogonalized received vector $\boldsymbol{x}$.

Methods of performing QR decomposition

The QR decomposition can be performed by several methods as mentioned in [10]. For the results presented in this paper, the QR decomposition used Householder's method since it is numerically more stable than the Gram-Schmidt Orthogonalization (GSO) process [8]. The number of computational 'flops' required is also less for the Householder QR factorization as compared to the classical or modified GSO method [8].

Results and Discussion

The performance results of the space-time system were obtained by computer simulation using the proposed QR detection algorithm for both linear and nonlinear detection algorithms. It is assumed that the channel is time varying. However, the fading coefficients are assumed to be relatively constant over a 'block' of symbols and change prior to the next 'block'. For the results described in this paper, a 'block' comprises 100 vectors, $\boldsymbol{a}$, where each vector comprises M QPSK symbols. Perfect channel estimation is also assumed.

Fig. 2 shows the bit error probability performance of the space-time system for both linear and nonlinear QR detection algorithms using either the ZF or MMSE criterion for two example systems with configuration of (3×3) and (6×4). It is shown in Fig. 2 that the (6×4) system has better performance than the (3×3) system in all cases. This is due to the fact that higher multipath diversity is achieved by the multi-antenna arrangement. The result of non-linear detection is equivalent to the performance of V-BLAST.

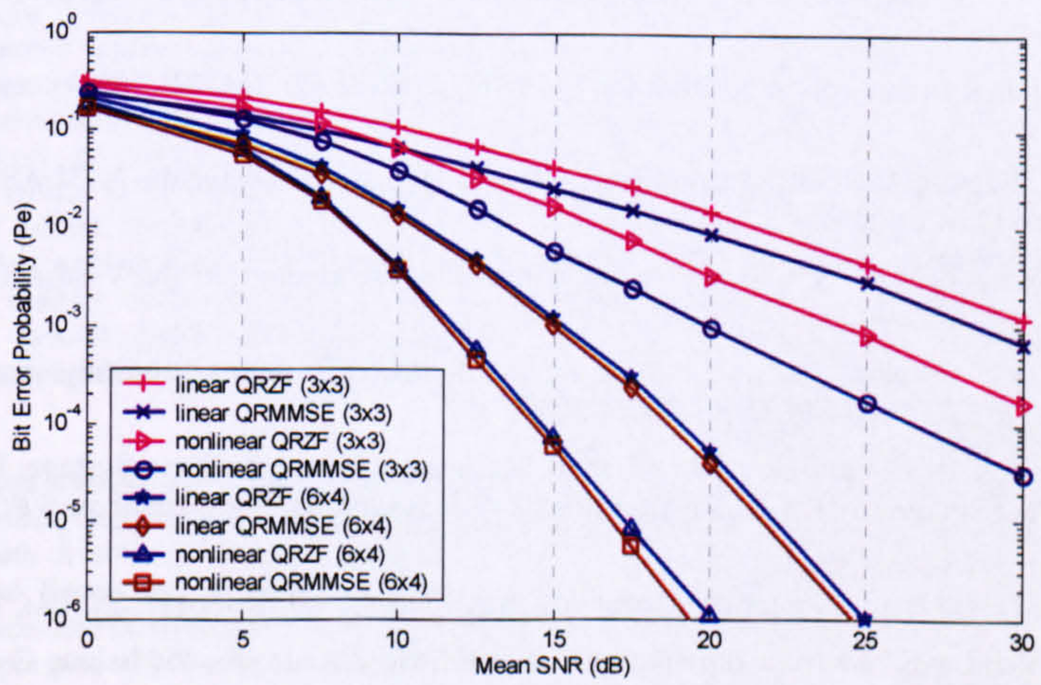

Fig. 2. System performance for the (6×4) & (3×3) system configuration for both linear and nonlinear QR detection using either ZF or MMSE criteria

It can also be observed that the nonlinear detection process performs better than the linear detection process for both systems due to the optimum ordering process and symbol cancellation technique used in the detection algorithm.

In Fig. 3, we demonstrate the importance of the rearranging the channel matrix **H** into $\mathbf{H}_{\mathbf{new}}$ for the non-linear QRMMSE algorithm. The bit error probability is considerably reduced when the correct order is chosen.

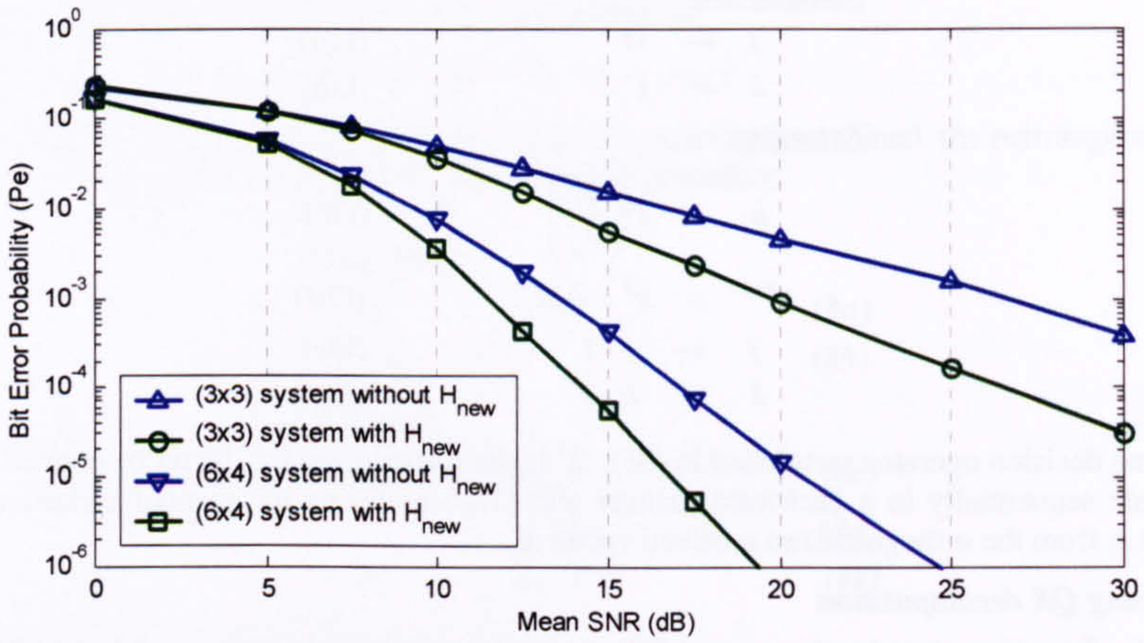

Fig. 3. System performance using nonlinear QRMMSE detection a) with the rearranged channel matrix $\mathbf{H}_{new}$ & b) without the rearranged channel matrix $\mathbf{H}_{new}$ for the (3×3) & (6×4) system.

Conclusions

In this paper, the nonlinear QR symbol detection algorithm has been successfully implemented for the space-time system in the flat-fading Rayleigh environment. It is found that the proposed method equals the performance of V-BLAST. The paper has also shown the importance of obtaining the correct symbol detection order.

References

[1] G. G. Raleigh, J. M Cioffi, "Spatio-temporal coding for wireless communication," *Communications, IEEE Trans. on*, Vol. 46, Issue: 3, March 1998.

[2] P. W. Wolniansky, G. J. Foschini, G. D. Golden, R. A. Valenzuela, "V-BLAST: An Architecture for Realizing Very High Data Rates Over the Rich-Scattering Wireless Channel," Invited paper, *Proc. ISSSE-98*, Pisa, Italy, Sept. 29, 1998.

[3] B. Hassibi, "An efficient square-root algorithm for BLAST," *2000 IEEE ICASSP '00. Proceedings*, vol.2, pp II737-II740, 2000.

[4] Won-Joon Choi; R. Negi, J. M. Cioffi, "Combined ML and DFE decoding for the V-BLAST system," *2000 IEEE ICC*, vol.3 pp. 1243 –1248, 2000

[5] K. W. Wong, Chi-Ying Tsui; R. S. Cheng, "A low complexity architecture of the V-BLAST system." *2000 IEEE WCNC*, vol.1, pp 310-314, 2000.

[6] B. A. Bjerke, J. G. Proakis, "Multiple transmit and receive antenna diversity techniques for wireless communications," *IEEE 2000 AS-SPCC*, pp 70-75, 2000.

[7] M. F. Siyau, P. Nobles, R. F. Ormondroyd," Channel Estimation for Space-Time Systems Using a Multi-Element Array Recursive Least Squares (MEA-RLS) Algorithm," *4th International Symposium on WPCM'01*, Denmark, Sept, 2001.

[8] Lloyd N. Trefethen, David Bau, "Numerical Linear Algebra," ISBN:0-89871-361-7, *S.I.A.M*, 1997.

[9] G. H. Golub, C. F. Van Loan. "Matrix Computations," North Oxford Academic Publishing Co. Ltd., 1983.

[10] L. J. Mason, "Detection of digital signals with antenna arrays using estimation," Canadian Conference on Electrical and Computer Engineering, pp. 380-383, vol.1, Conference Proceedings, Halifax, NS, Canada, 1994.

Channel Estimation for Space-Time Systems Using a Multi-Element Array Recursive Least Squares (MEA-RLS) Algorithm

M. F. Siyau *P. Nobles* *R. F. Ormondroyd*

Communication and Wireless Networks Group, Cranfield University
Royal Military College of Science, Shrivenham, Swindon, SN6 8LA, UK
Tel: +44 1793 785722, email: v.siyau@rmcs.cranfield.ac.uk

Abstract

Space-time communication techniques promise significant increases in the capacity of wireless systems that operate in rich scattering environments. However, exploitation of this type of environment requires accurate channel estimation. A novel uncoded space-time system that applies the concept of the recursive least squares algorithm to an adaptive spatial multi-element array structure is proposed for realizing channel estimation in a space-time system. The bit-error probability performance of this multi-element array recursive least squares (MEA-RLS) algorithm is investigated for different configura-tions of multiple transmitting and receiving antennas. Both linear and non-linear symbol detection methods are used and in each case, zero-forcing and minimum mean square error criteria are considered to evaluate the results. These results are compared with the case where perfect channel estimates are assumed.

Key words

Space-time system, channel estimation, MEA-RLS.

1. Introduction

The multi-layered space-time architecture for wireless communication is of increasing interest due to the need for higher data rates to support future generation personal wireless multimedia systems. Space-time techniques promise to provide a very high capacity compared with conventional wireless communication systems by exploiting the multipath diversity between multiple antennas at the transmitter and receiver [1-4]. This capacity improvement relies upon the spatial diversity brought about by a rich scattering environment, but it requires accurate channel estimation. So far, the issue of channel estimation has received little attention, despite being critical to the performance of space-time systems. In most papers, perfect knowledge of the channel is assumed [3,5,6] without further discussion of the effects that imperfect channel estimation has on system performance. However, general issues concerning channel estimation techniques for space-time systems are described in [7].

Space-time systems require accurate knowledge of the channel between multiple transmitting and receiving antennas in order to maximize the multipath diversity. Consequently, accurate channel estimation is vital. Recent work in the area of channel estimation for *coded* space-time systems has been carried out in [8-11] for different types of space-time system. The authors in [8] examine the impact of three types of channel estimator on data detection for reduced rank channels and show that although the maximum likelihood detector provides the best channel estimate, the overall bit error rate using this method is worse than if sub-space methods had been used. The use of joint channel estimation and data detection for the case of coded space-time systems is examined in [9-11]. In [9] particularly, the channel is subjected to fast fading and the authors apply the sub-optimal iterative receiver based on the expectation-maximization (EM) algorithm to estimate the channel for various space-time schemes. The EM algorithm is also used in [10] for channel estimation in conjunction with the hidden Markov model (HMM) method for symbol detection. However, the method proposed in [10] relies specifically on the knowledge of the coding scheme. In [11], decision feedback is used iteratively together with coded information in the training sequence to estimate the channel state information. In this paper, however, the effect of channel estimation for *uncoded* space-time systems is considered. A simple space-time array structure based on the recursive least-squares (RLS) algorithm is used that does not employ any special space-time codes. Therefore, the channel estimation process is achieved with less complexity.

The RLS algorithm [12-14] may be used to perform channel estimation with a reasonably fast convergence rate. Traditionally, the algorithm is implemented using an adaptive transversal structure for the single-input single-output (SISO) channel. In this paper, we develop a novel space-time system that applies the concept of the RLS algorithm to a multi-element array (MEA) structure in order to estimate the fading coefficients between M-transmitting antennas and N-receiving antennas for the multiple-input multiple-output (MIMO) channel. This MEA-RLS channel estimation algorithm makes use of a sequence of 'training vectors' to estimate the channel characteristics during a burst period. Following the training sequence, data is sent and it is assumed that the channel characteristics remain unchanged until the next training sequence is sent. One of the aims of this paper is to compare the performance of a space-time system using the MEA-RLS channel estimation algorithm with a system where the channel is assumed to be known perfectly. Section 2 describes the space-time system model and different symbol detection algorithms for linear and non-linear methods. Section 3 presents the MEA-RLS channel estimation algorithm. Results and discussions of the performance of different system configurations using MEA-RLS channel estimation, compared to the ideal channel case, are given in Section 4. Conclusions are presented in Section 5.

2. System Model

Fig. 1 shows the architecture for the space-time communication system used in this paper. The system consists of M parallel transmitting antennas and N parallel receiving antennas operating in a co-channel bandwidth. The system configuration is defined in terms of an ($N\times M$) matrix. The incoming data stream, S, is split into M-parallel sub-streams and these are mapped into a vector of symbols $\boldsymbol{a} = [a_1, a_2, \cdots, a_M]^{\mathsf{T}}$ according to the QPSK modulation scheme. The symbol vector is transmitted over a Rayleigh flat-fading channel, $\mathbf{H}$, with matrix dimension ($N\times M$), where the signals are distorted and superimposed at each receiving antenna. The received signal vector, $\boldsymbol{r} = [r_1, r_2, \cdots, r_N]^{\mathsf{T}}$, can be represented by:

$$\boldsymbol{r} = \mathbf{H}\boldsymbol{a} + \boldsymbol{n} \tag{1}$$

where $\boldsymbol{n}$ is the i.i.d. additive white Gaussian noise (AWGN) vector. Note that all elements in the above matrix and vectors are complex. It is assumed that the total power radiated by each transmitter antenna element is proportional to $1/M$ in order to provide a constant power to the receiver as the number of transmitter antenna elements changes [3,15]. In common with others, the free space loss of the channel is normalized to unity and each sub-stream is pre-multiplied with a factor of $\sqrt{\rho/M}$, where ρ is the expected signal to noise ratio at the receiver.

For the typical space-time system, the ($N\times M$) channel matrix, $\mathbf{H}$, can be represented as $\mathbf{H} = [\boldsymbol{u}_1\ \boldsymbol{u}_2 \cdots \boldsymbol{u}_M]$, where the i^{th} vector element, $\boldsymbol{u}_i = [h_{1i}, h_{2i}, \cdots, h_{Ni}]^{\mathsf{T}}$ specifies the complex fading coefficients from the i^{th} transmitting antenna element to the N receiving antenna elements in the space-time system and h_{ji} is the individual fading coefficient between the i^{th} transmitting antenna element and j^{th} receiving antenna element. All coefficients of the channel matrix are assumed to be uncorrelated with zero mean and unit variance [16,17]. The elements of the channel matrix can be represented by random complex components whose real and imaginary parts are normally distributed:

$$h_{ji} = \text{Normal}(0,1/\sqrt{2}) + \text{j.Normal}(0,1/\sqrt{2}) \tag{2}$$

where $|h_{ji}|^2$ is a chi-squared χ^2 variate. Referring to Fig. 1, the received signal vector is processed by weighting each element of $\boldsymbol{r}$ with the vector element of the weighting matrix, $\mathbf{W}$, where perfect symbol synchronization is assumed. The weights in $\mathbf{W}$ are obtained according to one of two possible criteria: Zero-Forcing (ZF) or Minimum Mean Square Error (MMSE) [3,18]. The weighted signals are combined to form $\boldsymbol{Y} = [y_1, y_2, \cdots, y_M]^{\mathsf{T}}$ and then quantised according to the QPSK decision threshold in order to yield the estimates of the transmitted symbols, $\hat{\boldsymbol{a}}$. Each element in vector $\boldsymbol{Y}$ can be expressed as:

$$y_i = w_{i1}r_1 + w_{i2}r_2 + \cdots + w_{iN}r_N \tag{3}$$

where i is in range 1 to M. The quantization process is denoted as Q(.) in Fig. 1.

2.1. Symbol Detection Algorithms

The weighting matrix, $\mathbf{W}$, is obtained from the channel matrix, $\mathbf{H}$, using either the ZF or MMSE criterion, as shown in (4) and (5) respectively:

a) ZF:
$$\mathbf{W}_{ZF} = \mathbf{H}^{+}; \qquad \hat{\boldsymbol{a}}_{ZF} = \mathrm{Q}(\mathbf{W}_{ZF}\boldsymbol{r}) \tag{4}$$

b) MMSE:
$$\mathbf{B} = [\boldsymbol{w}_1\ \boldsymbol{w}_2 \cdots \boldsymbol{w}_M]$$
$$\boldsymbol{w}_d = \mathbf{R}_{\boldsymbol{uu}}^{-1}\boldsymbol{u}_d \quad \text{for } 1 \le d \le M$$
$$\mathbf{W}_{MSE} = \mathbf{B}^{\mathsf{H}} \qquad \hat{\boldsymbol{a}}_{MSE} = \mathrm{Q}(\mathbf{W}_{MSE}\boldsymbol{r}) \tag{5}$$

where $^{+}$ denotes the Moore-Penrose pseudo-inverse [19] and the subscript $^{\mathsf{H}}$ is the Hermitian operator. An alternative way to achieve the pseudo-inverse is by the method of singular value decomposition [20]. The pseudo-inverse method is used when the channel matrix is not square (i.e. $N \neq M$) although it can still be applied to the case where ($N = M$). The corresponding symbol estimates, $\hat{\boldsymbol{a}}$, for each criterion can then be obtained, as shown above. In (5), $\mathbf{R}_{\boldsymbol{uu}}^{-1}$ is the inverse of the covariance matrix of the channel vector fading coefficients and $\boldsymbol{u}_d$ is the

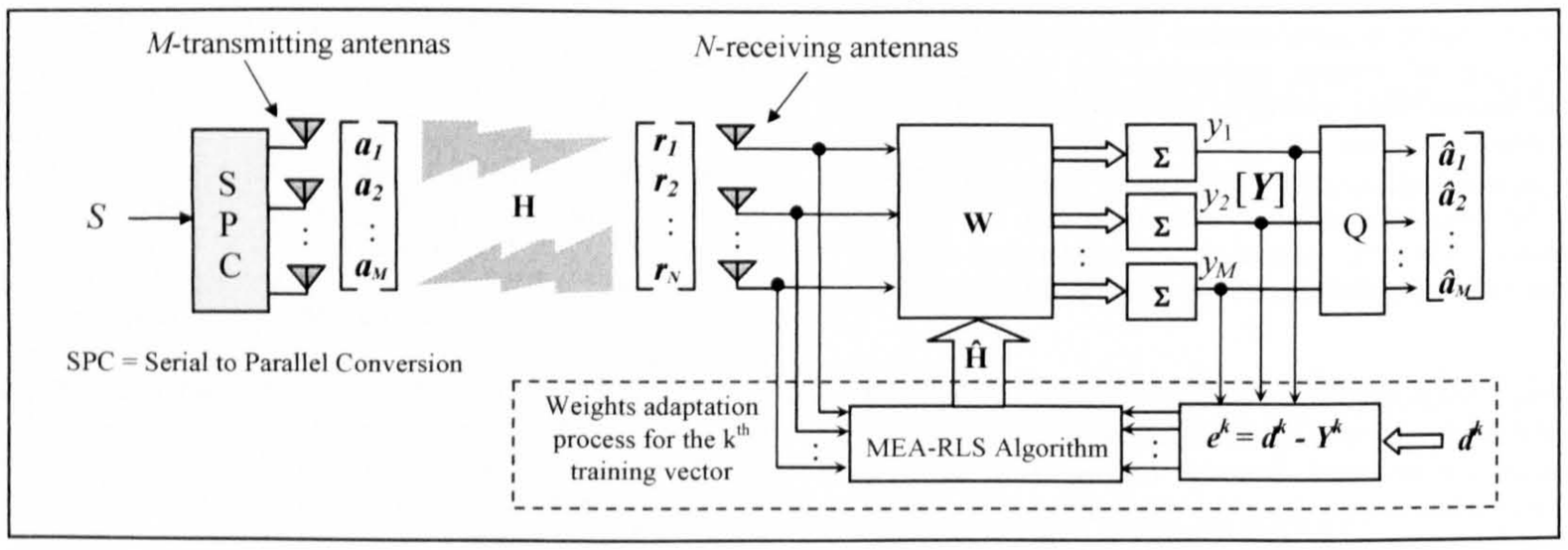

Figure-1 Space-time communication system incorporating the MEA-RLS channel estimation block

desired fading vector for the d[th] transmitting element. $\mathbf{R}_{\boldsymbol{uu}}$ can be resolved from the received signal vector $\boldsymbol{r}$, assuming the transmitted symbols and each propagation vector $\boldsymbol{u}$ in channel matrix $\mathbf{H}$ are uncorrelated. It can be written as $\mathbf{R}_{\boldsymbol{uu}} = \boldsymbol{u}_d \boldsymbol{u}_d^{\mathsf{T}} + \sigma^2 \mathbf{I}$, where σ^2 is variance of the noise and $\mathbf{I}$ is the identity matrix. Note that the vector elements of $\mathbf{W}_{MSE}$ are obtained by Wiener solution [12].

2.2. Linear and Non-linear Detection

The ZF and MMSE algorithms may be implemented using linear or non-linear methods. For the linear method, the detection process is accomplished in a single-step for all symbols arriving at the receiver at a particular time, whereas the non-linear method solves for each received symbol in an iterative manner using symbol interference cancellation [3]. The linear detection method resolves all symbols simultaneously and (4) and (5) can be applied directly. However, non-linear detection resolves each symbol by treating the already-detected symbol components of vector $\boldsymbol{a}$ as symbol interference and they are subsequently eliminated from the received signal vector $\boldsymbol{r}$ one at a time, according to the optimum detection ordering process [3].

3. MEA-RLS Channel Estimation

Equations (4) and (5) assume that the channel matrix is known perfectly. In practice, the channel matrix must be estimated using noisy measurements and this invariably worsens the symbol estimates. In this paper, the channel estimation process is carried out prior to symbol detection and the estimated channel matrix, $\hat{\mathbf{H}}$, is used for the symbol recovery process in conjunction with the symbol detection criterion chosen. Consequently, $\hat{\mathbf{H}}$ replaces $\mathbf{H}$ in (4) and $\boldsymbol{u}_d$ is replaced by $\hat{\boldsymbol{u}}_d = \left[\hat{h}_{1d}, \hat{h}_{2d}, \cdots, \hat{h}_{Nd}\right]^{\mathsf{T}}$ in (5) together with a corresponding change to $\mathbf{R}_{\boldsymbol{uu}}$.

In this paper, the channel is estimated using the MEA-RLS adaptation process. It is implemented using a training sequence known *a priori* to the receiver. The training sequence is actually transmitted as a sequence of vectors, $\boldsymbol{d}^k = \left[q_1^k, q_2^k, \cdots, q_M^k\right]^{\mathsf{T}}$ with element, q_i^k, of the training vector representing the k[th] training symbol transmitted by the i[th] transmitter element. It is assumed that the channel is time varying. However, the fading coefficients are assumed to be constant over a block of symbols. The block of symbols comprise the training sequence (where the MEA-RLS estimation process is carried out) followed by the data. The channel coefficients are then assumed to change prior to the next block. Once the MEA-RLS algorithm has been used to estimate the channel coefficients, the process is then switched to actual data detection using the estimates of $\hat{\mathbf{H}}$ that are valid for that block.

The choice of the number of training vectors is important. Too little training will result in poor bit error probability performance due to poor channel estimates, whereas too much training may result in an unnecessarily costly overhead and reduced efficiency in the overall utilization of the bandwidth. In this paper, the number of training vectors used per block was determined on the basis of minimizing the mean absolute squared error of the channel estimate. This was further reinforced by checking the impact of the number of training vectors on the bit error probability. This is described in greater detail in Section 4.

Referring to Fig. 1, for the ideal channel, the expected vector response of the channel estimator to the k[th] training vector is $\boldsymbol{d}^k$. In fading conditions, the actual vector response of the combiner output is $\boldsymbol{Y}^k$. The error vector, $\boldsymbol{e}^k$, between the actual and expected vector responses is:

$$\boldsymbol{e}^k = \boldsymbol{d}^k - \boldsymbol{Y}^k \tag{6}$$

This error vector is the innovation needed for correcting and updating weights during the training process using the MEA-RLS channel estimation algorithm. The process is as follows:

For convenience, let $\hat{\mathbf{C}}^k$ represent the pseudo-inverse of the estimated channel matrix $\hat{\mathbf{H}}$ after the k[th] training vector and $\mathbf{P} = \mathbf{R}_{\boldsymbol{rr}}^{-1}$. During training, the weights of $\hat{\mathbf{C}}^k$ from the MEA-RLS algorithm are updated by applying the adaptation formula in the following procedure:

$$\boldsymbol{g}^k = \frac{\mathbf{P}^{k-1}\boldsymbol{r}^k}{\left[\gamma + \left(\boldsymbol{r}^k\right)^{\mathsf{H}} \mathbf{P}^{k-1}\boldsymbol{r}^k\right]} \tag{7}$$

$$\hat{\mathbf{C}}^{k+1} = \hat{\mathbf{C}}^k + \boldsymbol{e}^k \left(\boldsymbol{g}^k\right)^{\mathsf{H}} \tag{8}$$

$$\mathbf{P}^k = \frac{1}{\gamma}\left[\mathbf{P}^{k-1} - \boldsymbol{g}^k \left(\boldsymbol{r}^k\right)^{\mathsf{H}} \mathbf{P}^{k-1}\right] \tag{9}$$

$\mathbf{R}_{\boldsymbol{rr}}$ is the covariance matrix of the received signal vector, $\boldsymbol{r}$, $\boldsymbol{g}^k$ is the gain vector at the k[th] training vector that determines the contribution of the error vector, $\boldsymbol{e}^k$, in the update of $\hat{\mathbf{C}}^k$ to $\hat{\mathbf{C}}^{k+1}$. The superscript $^{\mathsf{H}}$ denotes the Hermitian operation, the $^{+}$ operator is the pseudo-inverse and γ is the forgetting factor.

The MEA-RLS algorithm is first initialized by setting all the elements of $\hat{\mathbf{C}} = [\hat{\mathbf{c}}_1, \hat{\mathbf{c}}_2, \ldots, \hat{\mathbf{c}}_M]^{\mathsf{T}}$ to 0 and setting the inverse of the covariance matrix of received signal vector, $\mathbf{P}$ to the identity matrix, $\mathbf{I}$. The algorithm is then carried out in a recursive manner from equation (6) to (9) for each training vector in the sequence until the end of the training sequence. This method results in faster convergence of the estimator and the actual matrix inversion process is avoided by this recursive solution [12]. Finally, the estimated channel matrix is obtained when the final training vector $k = K$ has been received.

$$\hat{\mathbf{H}} = \left(\hat{\mathbf{C}}^K\right)^{+} \tag{10}$$

The estimated channel matrix $\hat{\mathbf{H}}$ consists of estimates of the fading vector $\hat{\mathbf{u}}$, related as $\hat{\mathbf{H}} = [\hat{\mathbf{u}}_1\ \hat{\mathbf{u}}_2 \ldots\ \hat{\mathbf{u}}_M]$. Note that during the inversion process, the column vectors of $\hat{\mathbf{H}}$ correspond to

the row vectors of $\hat{\mathbf{C}}$; $[\hat{\mathbf{c}}_1, \hat{\mathbf{c}}_2, \ldots, \hat{\mathbf{c}}_M]^T \Leftrightarrow [\hat{\mathbf{u}}_1\ \hat{\mathbf{u}}_2 \ldots\ \hat{\mathbf{u}}_M]$. After the channel estimation process, $\hat{\mathbf{H}}$ is used in equations (4) and (5) for symbol detection.

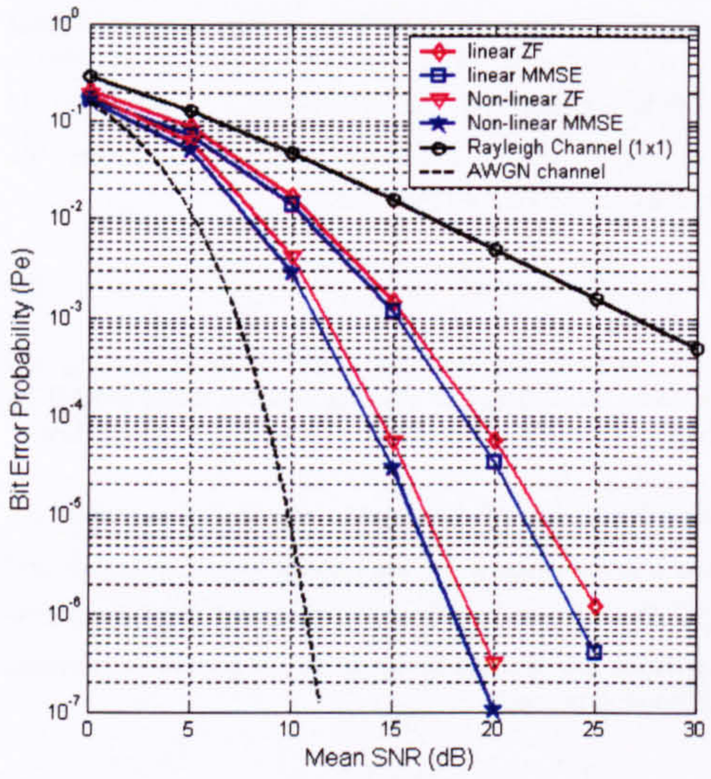

Figure-2: System performance for a (6×4) system using a perfect channel estimate with various combinations of symbol detection algorithm

A measure of the effectiveness of the MEA-RLS algorithm is contained in the absolute error squared, $\left|\varepsilon_i^k\right|^2$ at each step, k, of the training sequence, where $\varepsilon_i^k = q_i^k - y_i^k$ is the error in the response of the i[th] transmitting element for the k[th] training symbol and $\boldsymbol{e}^k = \left[\varepsilon_1^k, \varepsilon_2^k, \cdots, \varepsilon_M^k\right]^T$. In the interests of clarity, in the results that follow, the mean absolute square error, $\frac{1}{M}\sum_{i=1}^{M}\left|\varepsilon_i^k\right|^2$, is shown rather than plotting each curve of $\left|\varepsilon_i^k\right|^2$ individually.

4. Results and Discussions

The performance of the MEA-RLS channel estimation algorithm in the uncoded space-time system of Fig. 1 was obtained by computer simulation. For the results described in this paper, the block comprises 125×M symbols (i.e. 125 vectors of length M). Within each block, 25 training vectors of length M symbols are used for training the MEA-RLS channel estimation algorithm and the remaining 100×M symbols are the actual data. The justification for the choice of training sequence length will be given in the results. The forgetting factor γ is nominally set to 0.98. In the results that follow, the effect of γ is not examined explicitly, however, results have been obtained for a wide range of γ.

Fig. 2 shows the bit error probability performance of ZF and MMSE algorithms for both linear and non-linear detection for an example system where there are 6 receiving elements and 4 transmitting elements (i.e. a (6×4) configuration). In this figure, perfect channel estimation is assumed. The lower and upper bounding curves of this figure represent: a) the additive white Gaussian noise (AWGN) case and b) the conventional SISO Rayleigh fading channel case. These two cases define the best and the worst channel scenarios respectively.

Two observations are drawn from the results in Fig.2. First, it can be seen that, irrespective of whether linear or non-linear detection is used, the MMSE algorithms achieve a lower bit error probability than the ZF algorithms. This is due, in part, to the noise enhancement process of the ZF algorithm near channel nulls and that the MMSE solution provides an optimum way of resolving the signal in a minimum mean square error sense by the Wiener solution. Second, the iterative non-linear symbol detection method performs better than the one-step linear detection method due to the optimum detection ordering process explained in [3]. Note that non-linear detection reduces the required mean SNR to achieve a given bit error probability by several dB. Our results are consistent with those achieved for the space-time system described in [3,18].

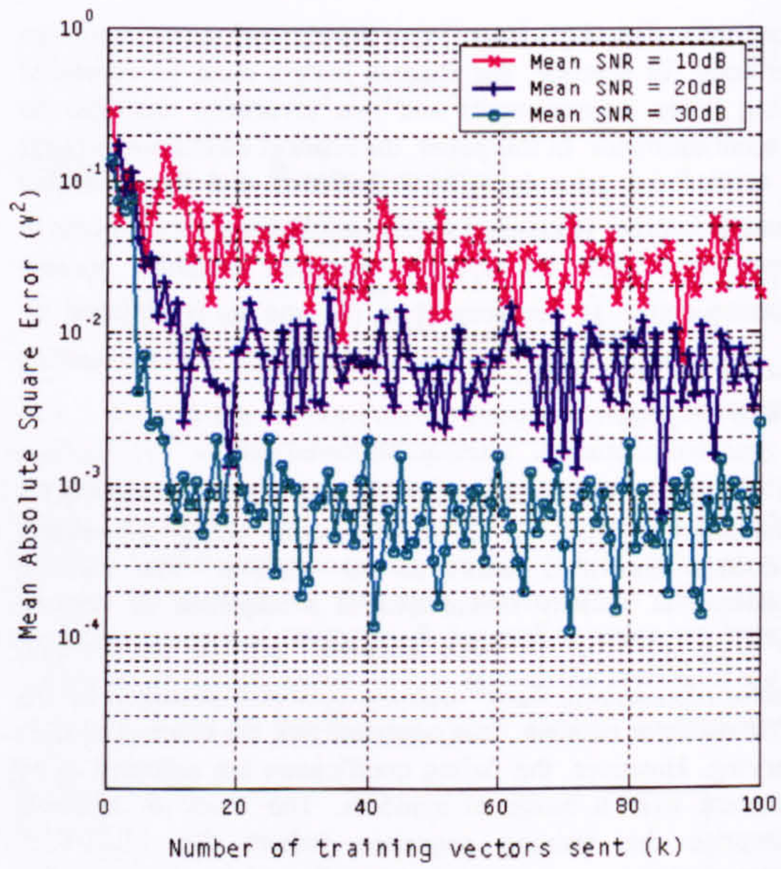

Figure-3: Convergence of the mean absolute square error of the MEA-RLS channel estimation algorithm with training for different mean SNRs for a (6x4) non-linear space-time system

Fig. 3 illustrates the performance of the MEA-RLS channel estimator for mean SNRs from 10dB to 30dB in terms of the evolution of its mean absolute square error as training vectors are passed through the system. For a forgetting factor of 0.98, the mean absolute square error falls to an error 'floor' within about 20-25 training vectors, depending on SNR. Using further training vectors achieves no further accuracy in the channel estimate. For a mean SNR of 30dB, the error 'floor' is

about 1×10^{-3} V^2 but this rises to about 3×10^{-2} at a mean SNR of 10dB. These observations have been used to set the length of the training sequence at 25 vectors. Small variations in forgetting factor from the nominal value of 0.98 have been observed to have little effect on either the convergence or the error floor. The stability issues of using the RLS algorithm in general are discussed in [12-14] and Cioffi [21] has discussed the applicability of the RLS algorithm at high and low SNR situations.

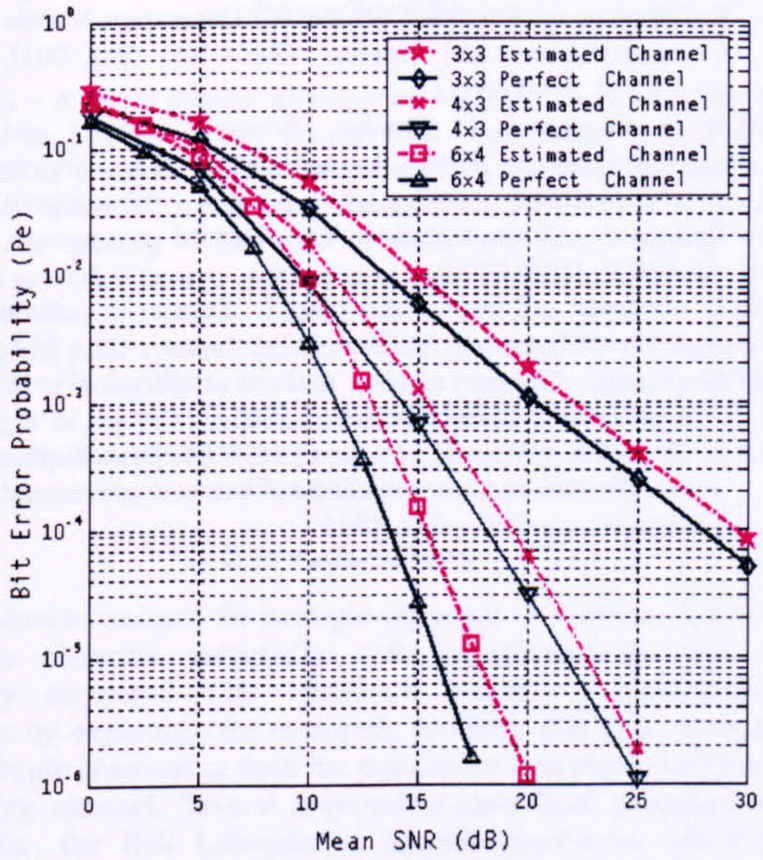

Figure-4: System performance of various ($N\times M$) non-linear MMSE configurations for the case of (i) perfect channel estimation, (ii) estimated channel using the MEA-RLS algorithm.

The error in the channel estimate after training has an impact on the probability of errors occurring in the data. This is shown in Fig. 4, where the bit error probability obtained for a perfect channel estimate is compared with that obtained using the MEA-RLS channel estimation algorithm. In this figure, the algorithm has been implemented for different transmitter (M) and receiver (N) configurations, where $N \geq M$. Note that results are only shown for the case where non-linear MMSE detection is used as it has been ascertained from Fig. 2 that this configuration provides the best performance for the MEA-RLS system in a fading channel when perfect channel estimation is assumed.

Over the range of values chosen for M and N, Fig. 4 shows that the (6×4) system gives the best performance followed subsequently by the (4×3) system and (3×3) system respectively. This is due to the fact that multipath diversity is achieved by the multi-element adaptive spatial array arrangement in conjunction with the combining method. The higher the number of receiving elements relative to the number of transmitting elements, the better the channel diversity that may be achieved by the space-time system. The spatial-temporal array arrangement not only allows the system to effectively resolve the effect of multiple simultaneous transmissions between the transmitter and the receiver as the receiving element increases but also effectively allows the capacity in terms of data rates to be increased in proportion to the number of transmitting elements.

The results show quite clearly that the MEA-RLS channel estimation algorithm results in only a small degradation in the bit error probability performance for all systems tested. However, a configuration such as the (6×4) system, which has a very good performance when the channel is perfectly estimated is degraded slightly more when the there are channel estimation errors than a configuration such as the (4×3) system. In this situation, the (6×4) system is not able to exploit the diversity gain fully because of the channel estimation errors.

5. Conclusions

In this paper, the MEA-RLS channel estimation algorithm has been developed for use with an uncoded space-time communication system. The MEA-RLS algorithm exploits the temporal and spatial diversity of the MIMO channel to provide an implementation that uses a simple adaptive array structure. This structure is of significantly reduced complexity compared to decoders suggested for joint channel estimation and symbol detection for coded space-time systems. The performance of the MEA-RLS algorithm has been assessed in a flat-fading Rayleigh MIMO channel and it has been found to converge with very few training vectors in mean SNRs of 10-30dB. The paper has shown that when the MEA-RLS algorithm is used there is little degradation in the bit error probability compared with the assumption of a perfect channel estimate.

6. References

[1] G. J. Foschini, "Layered Space-Time Architecture for Wireless Communication in Fading Environment When Using Multi-Element Antennas", Bell Labs Tech Journal, pp 41-59, Autumn 1996,.

[2] G. G. Raleigh, J. M Cioffi, "Spatio-temporal coding for wireless communication", Communications, IEEE Transactions on, Vol. 46 Issue: 3 March 1998.

[3] P. W. Wolniansky, G. J. Foschini, G. D. Golden, R. A. Valenzuela, "V-BLAST: An Architecture for Realizing Very High Data Rates Over the Rich-Scattering Wireless Channel", invited paper, *Proc. ISSSE-98*, Pisa, Italy, Sept. 29, 1998.

[4] D. D. N. Bevan, R. Tanner, C. R. Ward, "Space-Time Coding for Capacity Enhancement in Future-Generation Wireless Communications ", IEE Colloquium on Capacity and Range Enhancement Techniques for the 3rd Generation Mobile Communications and Beyond (Ref. No. 2000/003), 2000.

[5] F. R. Farrokhi, A. Lozano, G. J. Foschini, R. A. Valenzuela, "Spectral efficiency of wireless systems with multiple transmit and receive antennas", The 11th IEEE International Symposium on Personal, Indoor and Mobile Radio Communications, vol.1, pp 373-377, PIMRC 2000.

[6] F. R. Farrokhi, G. J. Foschini, A. Lozano, R. A. Valenzuela, "Link-optimal space-time processing with multiple transmit and receive antennas", IEEE

Communications Letters, Volume: 5 Issue: 3, pp 85- 87, March 2001.

[7] A. J. Paulraj, B. C. Ng, "Space-Time Modems for Wireless Personal Communications", IEEE Personal Communications Magazine, pp.36-48, Feb 1998.

[8] E. Lindskog, C. Tidestav, "Reduced rank channel estimation", IEEE 49th Vehicular Technology Conference, VTC, Vol.2, pp 1126-1130, May 1999.

[9] C. Cozzo, B. L. Hughes, "Joint channel estimation and data symbol detection in space-time communications", IEEE International Conference on Communications, ICC, vol.1, pp 287-291, June 2000.

[10] S. Perreau, L. B. White, "Channel estimation and symbol detection for space-time codes in mobility conditions", International Zurich Seminar on Broadband Communications Proceedings, pp 105-108, Feb 2000.

[11] A. Grant, "Joint decoding and channel estimation for space-time codes", IEEE VTS Fall 52nd Vehicular Technology Conference, VTC, vol.1, pp.416-420, Sept 2000.

[12] Simon Haykin. "Adaptive Filter Theory" 3rd –edition, Prentice-Hall, 1996.

[13] B. Farhang-Boroujeny, "Adaptive Filter Theory and Application", John Wiley and Sons, 1998.

[14] Loius R. Litwin, Jr, "Adaptive channel equalization for wireless communications", IEEE Potentials, Vol.18, Issue: 4, pp 9-12 Apr-May 1999

[15] T. L. Marzetta, B. M. Hochwald, B. Hassibi, "Space-time Autocoding", Bell Labs Technical Memorandum, 1999.(http://mars.bell-labs.com.)

[16] J. G. Foschini, M. J. Gans, "On limits of wireless communications in a fading environment when using multiple antennas", Wireless personal communication, vol.6, pp.311-335, 1998.

[17] A. G. Burr, "Space-time coding in 3rd generation and beyond", IEE Collouium on Capacity and Range Enhancement Techniques for the 3rd Generation Mobile Communications and Beyond (Ref. No. 2000/003), pp.7/1-7/8, 2000.

[18] B. A. Bjerke, J. G. Proakis, "Multiple transmit and receive antenna diversity techniques for wireless communications", Adaptive System for Signal Processing, Communications and Control symposium, AS-SPCC, IEEE 2000.

[19] R. Bronson, "Matrix Operations", Schaum's outline series in mathematics, McGraw-Hill company, US, 1989.

[20] G. Strang, "Linear algebra and its application", 3rd edition, Saunders HBJ publishers, 1986.

[21] J. M. Cioffi, "When Do I Use an RLS Adaptive Filter", Nineteeth Asilomar conference on Circuits, Systems and Computers, pp. 636 – 639, 1985.

Performance of a Layered Space-Time Cellular System used with a Fractionally-Spaced Channel Estimator Operated in a Time-Varying, Frequency-Selective Wireless Channel

M. F. Siyau R. F. Ormondroyd P. Nobles

Communication and Wireless Networks Group, Cranfield University
Royal Military College of Science, Shrivenham, Swindon, SN6 8LA, United Kingdom
v.siyau@cranfield.ac.uk, r.f.ormondroyd@cranfield.ac.uk, p.nobles@cranfield.ac.uk

***Abstract* – A novel fractionally-spaced MIMO channel estimation scheme is presented for the layered space-time system that operates in a time-varying, frequency selective, fading channel. The new method estimates delay-spreads of several symbols, where the spacing of the echo arrivals is within fractions of a symbol period. The new method uses pilot symbols to estimate the channel characteristics. These are generated from a Paley-Hadamard pilot symbol matrix whose orthogonal and Toeplitz-like structure is able to resolve interference as well as minimise the length of the pilot sequence. Results of the performance of the fractionally-spaced MIMO channel estimator in a layered space-time system are presented for different channel scenarios.**

I. Introduction

Space-time techniques for multiple-input multiple-output (MIMO) wireless channels potentially offer significant increases in capacity compared with traditional wireless communication systems by exploiting the multipath diversity that exits between the multiple antennas at both the transmitter and receiver [1] in a scattering channel. Several approaches have been proposed. In particular, the Bell Laboratories layered space-time (BLAST) architecture has been presented for the narrowband flat-fading channel [2] and MIMO equalisation with interference cancellation examined for the wideband frequency selective channel [3][4].

In order to achieve the quoted capacity gains of MIMO systems, the multiple channel impulse responses (CIRs) and their fading coefficients must be known or estimated. Most MIMO channel estimation schemes have been limited to the narrowband flat-fading case or use coded space-time systems e.g. space-time block coded systems or MIMO-OFDM systems [5]-[7]. In [8], the authors have proposed a MIMO channel estimation scheme to cater for the frequency selective MIMO channel with the assumption that the principle echoes of the channel impulse are symbol spaced. In this paper, the work in [8] is extended to incorporate a novel fractionally-spaced MIMO channel estimator within the order-successive interference cancellation (OSIC) layered space-time receiver [3] that operates in a time-varying, frequency-selective fading environment. The new method estimates multipath delay-spreads of many symbols, where the spacing of the echo arrivals is within fractions of a symbol period. As a result, the layered space-time receiver is able to handle more realistic MIMO channel scenarios than those presented in [8].

II. Background of Proposed MIMO-CE Scheme

The MIMO channel estimation scheme presented in [8] uses a pilot matrix, which consists of pilot symbols that are periodically transmitted in short blocks within frames of data from each transmit antenna, to jointly estimate the fading coefficients of the individual CIRs between the multiple transmit and receive antennas. This is in contrast to using a series of individual pilot symbols and an adaptive algorithm [9].

The pilot symbol sequences used for each transmit antenna are mutually orthogonal and are extracted from the Paley-Hadamard matrix [10], which is both orthogonal and Toeplitz-like. This has two benefits. First, by using orthogonal pilot sequences, the fading coefficients of *all* the individual CIRs between each transmit and receive antenna can be estimated jointly in a single operation and both the inter-symbol interference (ISI) and the co-channel interference (CCI) of the wideband MIMO signals can be resolved [8]. Secondly, by exploiting the Toeplitz-like structure of the Paley-Hadamard matrix, the number of training symbols can be reduced significantly, thus maximising the effective data throughput [8]. The key to the proposed MIMO channel estimator is the ability to extract the orthogonal information carried by the received signals corresponding to the pilot sequences sent by each transmitter. Details of the symbol-spaced MIMO channel estimator and the construction of the pilot matrix are given in [8]. Here, only the essential differences needed to explain the fractionally-spaced channel estimator are presented.

III. Fractionally Spaced MIMO Channel Estimator

In the symbol-spaced channel estimator [8], the delay-spread is modelled by the taps of the FIR channel model where the spacing between the taps is τ and $1/\tau$ is the symbol rate. However this does not represent a realistic channel model, where the main multipath echoes may arrive or be separated by less than a symbol period. For this case, a more representative channel model is required where the tap delays of the FIR filter are fractionally spaced with a delay, τ/C, where C is the over-sampling factor, which is generally an integer. This requires that an over-sampling process is used in both the channel estimator and the receiver that matches that used in the channel model. To do this, two important parameters must be known *a priori*: (i) the total span of the delay spread, φ, in terms of symbol periods within each CIR and (ii) the over-sampling rate, C, required to model the fractional delay paths. By defining these two parameters, the fractionally-spaced MIMO channel estimator can be obtained in terms of an extension to the symbol-spaced MIMO channel estimator.

A. Fractionally-spaced MIMO Channel Estimator Algorithm

The basic space-time system and the MIMO channel model are outlined below. There are M transmit and N receive antennas where (N×M) signifies a particular MIMO system configuration.

The fractionally-spaced CIR from the m^{th} transmit antenna to the n^{th} receive antenna can be defined as:

$$\mathbf{h}'_{nm} = \left[h^1_{nm}(0) \cdots h^C_{nm}(0) \quad \ldots \quad h^1_{nm}(L) \cdots h^C_{nm}(L)\right]^{\mathsf{T}} \qquad (1)$$

where $h^i_{nm}(k)$ specifies the i^{th} sample of the channel coefficient within the k^{th} symbol period and the overall duration of the CIR is $\varphi = (L+1)$ symbols. Thus, the total number of fractionally-spaced impulse response taps used for the simulated channel between transmitter m and receiver n is $(C\times\varphi)$. To illustrate the nomenclature, consider the following example, which consists of four delay paths with uneven spacing between each path:

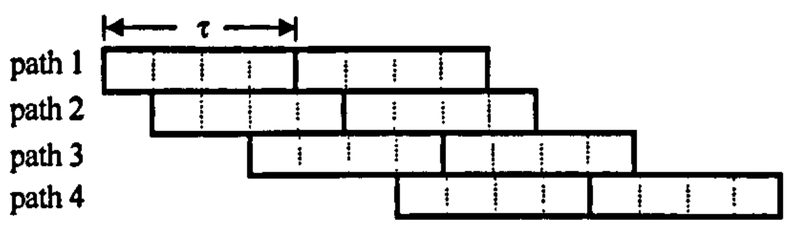

In this example, the total span of the delay spread is φ=2 symbols (which may be shortened by using trailing zeros) and the over-sampling factor is C=4. For this case, up to eight equally spaced multipaths can be accommodated, however, in this example there are four unequally spaced paths that are represented by the fractionally-spaced sampled CIR as:

$$\mathbf{h}'_{nm} = \left[h^1_{nm}(0) \;\; h^2_{nm}(0) \;\; 0 \;\; h^4_{nm}(0) \;\; 0 \;\; 0 \;\; h^3_{nm}(1) \;\; 0\right] \qquad (2)$$

Note that in this case, the unequal delays between each path are obtained by inserting zero coefficient values in the CIR vector, as appropriate. From the fractional CIR $\mathbf{h}'_{nm}$ in (1), the basic fractional channel matrix $\mathbf{H}'_m$ of dimension $(N\times(L+1)C)$ with respect to the m^{th} transmit antenna can be defined as:

$$\mathbf{H}'_m = \begin{bmatrix} \mathbf{h}'^{\mathsf{T}}_{1m} \\ \vdots \\ \mathbf{h}'^{\mathsf{T}}_{Nm} \end{bmatrix} = \begin{bmatrix} h^1_{1m}(0)\ldots h^C_{1m}(0) & \cdots & h^1_{1m}(L)\ldots h^C_{1m}(L) \\ & \vdots & \\ h^1_{Nm}(0)\ldots h^C_{Nm}(0) & \cdots & h^1_{Nm}(L)\ldots h^C_{Nm}(L) \end{bmatrix} \qquad (3)$$

Although not indicated in (3) in order to simplify the notation, all the channel coefficients in the channel matrix are slowly time varying due to the effect of Doppler.

At some fraction of a symbol, k within the r^{th} symbol, the received signal vector $\mathbf{x}'(r-k)$ of dimension $(N\times1)$ containing signal samples at each of the N receivers due to all M transmitters can be expressed as:

$$\mathbf{x}'(r-k) = \sqrt{\rho/M}\sum_{m=1}^{M}\mathbf{H}'_m\,\mathbf{s}'_m(r-k) + \mathbf{n}'(r-k) \qquad (4)$$

where $k = g/C$, defined for $g = 0, 1,\ldots, (C\text{-}1)$. For example, if C=4, k takes the values, 0, 1/4, 1/2, 3/4. ρ is the expected signal to noise ratio at each receiver, $\mathbf{n}'(r-k)$ is the over-sampled AWGN vector and $\mathbf{s}'_m(r-k)$ is the over-sampled transmit vector from the m^{th} transmitter corresponding to $\mathbf{x}'(r-k)$ at the time of sampling and can be expressed as follows:

$$\mathbf{s}'_m(r-k) = \left[s_m\left(r-\frac{g}{C}\right) \;\; s_m\left(r-\frac{g+1}{C}\right) \;\cdots\; s_m\left(r-\frac{g+(L+1)C-1}{C}\right)\right]^{\mathsf{T}} \qquad (5)$$

where, because the received samples are fractionally-spaced and the transmitted symbols are symbol-spaced, $s_m\left(r-(g+i)/C\right)$ are the duplicated samples of the transmitted pilot symbol, $s_m(r-j)$, where j is the integer part of $(g+i)/C$. During channel estimation, the symbols transmitted by each transmitter are pilot symbols and these are generated according to a Paley-Hadamard matrix, described in the next section.

B. Construction of the pilot matrix $\mathbf{S}_F$ at the transmitter

The ultimate goal of the proposed fractional MIMO channel estimator is to be able to estimate all the complex fading coefficients within each basic fractional channel matrix, $\mathbf{H}'_m$ in (3) for all the M transmitters. The basic concatenated fractional channel matrix can be expressed as follows:

$$\mathbf{H}'_{1|M} = \left[\,\mathbf{H}'_1 \,\middle|\, \cdots \,\middle|\, \mathbf{H}'_M\,\right] \qquad (6)$$

At the transmitter, a pilot matrix, $\mathbf{S}_F$ (for the fractional case) is constructed based on the Paley-Hadamard matrix of order v which is obtained according to the following criteria:

$$v \;>\; M\times(\varphi+1) \qquad (7)$$

where v must be divisible by 4 and $(v\text{-}1)$ is prime. This matrix represents the pilot sequences to be transmitted by all M transmitters. It is important to note that the criteria in (7) is slightly different from the symbol-spaced method in [8]. The extra '+1' term in (7) is needed to transmit an additional row of sequences per transmit antenna in order to provide the essential format of the block-Toeplitz channel matrix $\bar{\mathbf{H}}'_m$ shown in (10) and the formulation of $\bar{\mathbf{H}}'_{1|M}$ shown in (9).

Next, assuming that the total delay-spread, φ, is known *a priori* or can be predicted, $M\times(\varphi+1)$ rows of consecutive non-repeated orthogonal sequences (except for the first row), are extracted from this v-ordered Paley-Hadamard matrix to form the required $\mathbf{S}_F$. Once $\mathbf{S}_F$ is constructed, $(\varphi+1)$ consecutive rows of orthogonal sequences are then assigned to each transmit antenna and launched sequentially in the same manner described in [8].

C. Matrix Expressions for fractionally-spaced MIMO-CE method

In order to perform MIMO channel estimation for the fractional case, each fractional $\mathbf{x}'(r-k)$ has to be grouped properly so that the received signal matrix $\mathbf{X}'$ contains the following matrix format that allows channel estimation to take place in a similar way to that described in [8]:

$$\mathbf{X}' \;=\; \sqrt{\rho/M}\,\bar{\mathbf{H}}'_{1|M}\,.\,\mathbf{S}'_F \;+\; \mathbf{N}' \qquad (8)$$

where $\mathbf{N}'$ is the AWGN noise matrix in the fractional case. $\bar{\mathbf{H}}'_{1|M}$ is the extended version of the concatenated channel matrix that cascades the block-Toeplitz channel matrices from $\bar{\mathbf{H}}'_1$ to $\bar{\mathbf{H}}'_M$ as:

$$\bar{\mathbf{H}}'_{1|M} = \left[\,\bar{\mathbf{H}}'_1 \,\middle|\, \cdots \,\middle|\, \bar{\mathbf{H}}'_M\,\right] \qquad (9)$$

where the individual $\bar{\mathbf{H}}'_m$ in (9) have been formed from the basic fractional channel matrix $\mathbf{H}'_m$ from (3) using:

$$\bar{\mathbf{H}}'_m = \begin{bmatrix} \mathbf{H}'_m & \mathbf{0} & \dots & \mathbf{0} \\ \mathbf{0} & \mathbf{H}'_m & \mathbf{0} & \dots \mathbf{0} \\ \vdots & & \ddots & \vdots \\ \mathbf{0} & \dots & \mathbf{0} & \mathbf{H}'_m \end{bmatrix} \quad (10)$$

D. The proper grouping of the received signal samples

Upon receiving each fractionally-sampled signal at the receiver, each received signal vector $x'(r-k)$ in (4) is buffered and then grouped into a received signal matrix $\mathbf{X}'$ so that the necessary format of $\bar{\mathbf{H}}'_{1|M}$ and $\mathbf{S}'_F$ in (10) and (15) respectively can be achieved. This is achieved in the following steps:

First, the $((C+1)\times N)$ dimension received symbols' matrix spanned from the previous $(r-1)^{th}$ sample to the next $(r)^{th}$ sample can be gathered as:

$$Z(r) = \left[x'(r) \ \cdots \ x'\left(r-\frac{t}{C}\right) \ \cdots \ x'(r-1) \right]; \ 1 \le t \le C-1 \quad (11)$$

Note that $Z(r)$ also contains all the 'in-between' fractional received signal samples taken at $(r-t/C)$ where t is an integer taking values from 1 to $(C-1)$ and $C \ge 2$. Next, the *vec*(.) operator:

$$vec\left(\left[\mathbf{a}_1 \ \cdots \ \mathbf{a}_\alpha\right]\right) = \begin{bmatrix} \mathbf{a}_1 \\ \vdots \\ \mathbf{a}_\alpha \end{bmatrix} \quad (12)$$

defined in [8] is used to define $\mathbf{z}(r) = vec(Z(r))$ and $\mathbf{X}'$ can be obtained by grouping the corresponding $\mathbf{z}(r)$ at different time instants as follows:

$$\mathbf{X}' = \left[\mathbf{z}(r) \ \ \mathbf{z}(r+1) \ \cdots \ \mathbf{z}(r+q) \ \ \mathbf{z}(r+(L+1)+q) \right] \quad (13)$$

where parameter q can be obtained from the value of matrix order v in (7) as follows:

$$q = v-2 \quad (14)$$

E. Reconstruction of the pilot matrix $\mathbf{S}'_F$ at the receiver

Once $\mathbf{X}'$ is formed, $\mathbf{S}'_F$ is reconstructed at the channel estimator such that each row of the original orthogonal sequence of pilot symbols in $\mathbf{S}_F$ is duplicated according to the required amount of over-sampling, C, in the format expected by the receiver (expressed in fractional samples of the pilot symbols). This format consists of a set of individual fractional concatenated transmit vectors $\bar{s}'_{1|M}(k)$ cascaded as follows:

$$\mathbf{S}_F = \left[\bar{s}'_{1|M}(r) \,|\, \bar{s}'_{1|M}(r+1) \,|\, \cdots \,|\, \bar{s}'_{1|M}(r+q) \,|\, \bar{s}'_{1|M}(r+(L+1)+q) \right] \quad (15)$$

where the individual $\bar{s}'_{1|M}(k)$ in (15) can be obtained using the *vec*(.) operator from (12) as follows:

$$\bar{s}'_{1|M}(r-k) = vec\left(\left[\bar{s}'_1(r-k) \ \cdots \ \bar{s}'_M(r-k)\right]\right) \quad (16)$$

where each $\bar{s}'_m(r-k)$ in (16) is the extended version of the transmit vector from (5) that can be expressed as:

$$\bar{s}'_m(r-k) = \left[s_m\left(r-\frac{g}{C}\right) \ s_m\left(r-\frac{g+1}{C}\right) \ \cdots \ s_m\left(r-\frac{g+(L+1)C-1+(L+1)}{C}\right) \right]^T \quad (17)$$

F. Obtaining the fractional channel estimates

Once $\mathbf{X}'$ and $\mathbf{S}'_F$ have been formed, the fractional channel estimates can be obtained according to the following steps:

First, the partial estimated channel matrix **J** is obtained as follows:

$$\mathbf{J} = f\left\{ \mathbf{X}' . \mathbf{S}'^{\mathsf{H}}_F \right\} = f\left\{ \left(\bar{\mathbf{H}}'_{1|M} . \mathbf{S}'_F \right) \mathbf{S}'^{\mathsf{H}}_F \right\} \quad (18)$$

The multiplication of $\mathbf{S}'_F$ and its Hermitian in (18) produces a unique weighted block-identity matrix $\breve{\mathbf{I}}$:

$$\mathbf{S}'_F . \mathbf{S}'^{\mathsf{H}}_F = 2v\,\breve{\mathbf{I}} \quad (19)$$

where $\breve{\mathbf{I}} = \begin{bmatrix} \mathbf{A} & \mathbf{0} & \cdots & \mathbf{0} \\ \mathbf{0} & \mathbf{A} & \mathbf{0} & \vdots \\ \vdots & \mathbf{0} & \ddots & \mathbf{0} \\ \mathbf{0} & \cdots & \mathbf{0} & \mathbf{A} \end{bmatrix}$ and $\mathbf{A} = \begin{bmatrix} 1 & \cdots & 1 \\ \vdots & \ddots & \vdots \\ 1 & \cdots & 1 \end{bmatrix}$

A is the $(C\times C)$ all-ones square matrix and **0** is the $(C\times C)$ all-zeros square matrix. Again, v is the matrix order known *a priori* at the receiver. Substituting (19) into (18) leads to the following:

$$\mathbf{J} = f\left\{ \bar{\mathbf{H}}'_{1|M} . 2v . \breve{\mathbf{I}} \right\} \quad (20)$$

where f is the correction factor with the following value:

$$f = 2v\sqrt{M/\rho} \quad (21)$$

It can seen from (20) that the matrix **J** ultimately comprises of $\bar{\mathbf{H}}'_{1|M}$ and $\breve{\mathbf{I}}$, which contains all the information of the fractional channel estimates. However, since $\breve{\mathbf{I}}$ is non-invertible, the channel estimates cannot be obtained directly. Fortunately, both $\bar{\mathbf{H}}'_{1|M}$ and $\breve{\mathbf{I}}$ have a matrix structure that contains necessary zeros shown in (10) and (19) respectively that allows each individual basic fractional channel matrix $\mathbf{H}'_m$ contained in $\bar{\mathbf{H}}'_{1|M}$ to be conveniently extracted through an appropriate linear arithmetic operation. This is illustrated using only the first block-Toeplitz channel matrix $\bar{\mathbf{H}}'_1$ in (9) with N=2, φ=2 and C=2. Let the basic fractional channel matrix be:

$$\mathbf{H}'_1 = \begin{bmatrix} \mathbf{h}'^{\mathsf{T}}_{1m} \\ \mathbf{h}'^{\mathsf{T}}_{2m} \end{bmatrix} = \begin{bmatrix} a & c & e & g \\ b & d & f & h \end{bmatrix} \quad (22)$$

The expansion of the linear operation $(\bar{\mathbf{H}}'_1 . \breve{\mathbf{I}}_1)$ is shown as:

$$\bar{\mathbf{H}}'_1 \cdot \breve{\mathbf{I}}_1 = \begin{bmatrix} a & c & e & g & 0 & 0 \\ b & d & f & h & 0 & 0 \\ 0 & a & c & e & g & 0 \\ 0 & b & d & f & h & 0 \\ a & c & e & g & 0 & 0 \\ b & d & f & h & 0 & 0 \end{bmatrix} \begin{bmatrix} 1 & 1 & 0 & 0 & 0 & 0 \\ 1 & 1 & 0 & 0 & 0 & 0 \\ 0 & 0 & 1 & 1 & 0 & 0 \\ 0 & 0 & 1 & 1 & 0 & 0 \\ 0 & 0 & 0 & 0 & 1 & 1 \\ 0 & 0 & 0 & 0 & 1 & 1 \end{bmatrix}$$

$$= \begin{bmatrix} a+c & a+c & e+g & e+g & 0 & 0 \\ b+d & b+d & f+h & f+h & 0 & 0 \\ a & a & c+e & c+e & g & g \\ b & b & d+f & d+f & h & h \\ 0 & 0 & a+c & a+c & e+g & e+g \\ 0 & 0 & b+d & b+d & f+h & f+h \end{bmatrix} \quad (23)$$

By resolving (23) in either ascending or descending order of the alphabets, all the channel coefficients in the fractional model can be retrieved accordingly. Our aim is to estimate all the fractional fading coefficients from 'a' to 'h' in each $\mathbf{H}'_m$. Once all the coefficients have been estimated, the estimated basic fractional channel matrix, $\hat{\mathbf{H}}'_m$ for $m = 1$ to M, can be cascaded as follows:

$$\hat{\mathbf{H}}'_{1|M} = \left[\hat{\mathbf{H}}'_1 \,\middle|\, \cdots \,\middle|\, \hat{\mathbf{H}}'_M \right] \quad (24)$$

IV. Results and Discussion

The performance of the fractionally-spaced MIMO channel estimation scheme has been assessed using the mean Frobenius norm squared error of the MIMO channel estimates as a metric. It is calculated using the following steps:

First, the error matrix of the MIMO channel estimates, $\boldsymbol{e}_{\mathrm{H}}$ is obtained by taking the difference between the estimated fractional concatenated MIMO channel matrix, $\hat{\mathbf{H}}'_{1|M}$, given by (24) and the actual fractional concatenated MIMO channel matrix $\mathbf{H}'_{1|M}$ defined in (6):

$$\boldsymbol{e}_{\mathrm{H}} = \mathbf{H}'_{1|M} - \hat{\mathbf{H}}'_{1|M} \quad (25)$$

Subsequently, the mean Frobenius norm squared error of $\boldsymbol{e}_{\mathrm{H}}$ is obtained using:

$$E\left[\left\| \boldsymbol{e}_{\mathrm{H}} \right\|_F^2 \right] = \frac{1}{(M \times l \times N)} \left[\sum_{i=1}^{N} \sum_{j=1}^{M \times l} \left| \varepsilon_{ij} \right|^2 \right] \quad (26)$$

where ε_{ij} is an element of $\boldsymbol{e}_{\mathrm{H}}$, $E[.]$ is the expectation operator and l represents the actual number of paths used in the channel model. In the results presented here, the multipath channel is assumed to consist of $l = C \times \varphi$ equal loss paths so that if C=3 and φ=4, l=12 paths, each separated by ¼ symbol period.

Results are presented here for a (2×2) MIMO system for two types of Rayleigh frequency-selective, time-varying, channels. The first is a pedestrian channel where the handset velocity is 3km/hr, which corresponds to a maximum Doppler frequency of f_d=6Hz at the carrier frequency of f_c=2.11GHz. The second channel type is a city/town channel where the mobile velocity is 45km/hr, corresponding to a maximum Doppler frequency of f_d=88Hz. The data rate is assumed to be 120kb/s per transmit antenna (i.e. a total of 240kb/s for the (2×2) case).

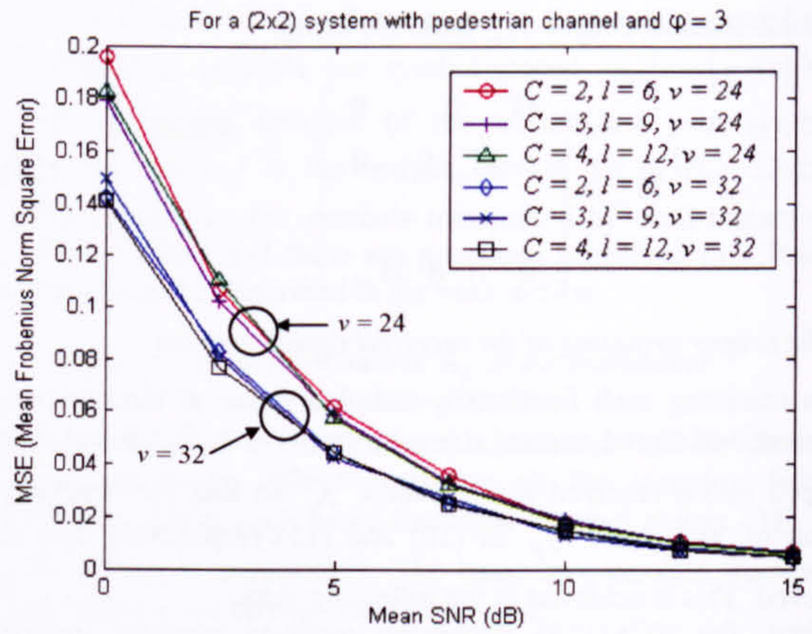

Figure 1: MSE performance of channel estimate versus Mean SNR for the pedestrian channel using different pilot lengths (v =24 & 32) in different channel scenarios with fixed φ=3 and increasing C.

Figure 1 shows the MSE performance of the proposed fractionally-spaced MIMO channel estimator as a function of the SNR over the pedestrian channel. In this figure, two pilot sequence lengths, v=24 and v=32, have been used for different numbers of paths ranging from C=2, φ=3 (i.e. l = 6 paths each with a ½ symbol delay spacing) to C=4, φ=3 (i.e. l = 12 paths each with a ¼ symbol delay spacing). In this figure, the delay spread, φ, remains constant at 3 symbols. It is clear from this result, that the longer pilot sequence (v =32) provides more accurate channel estimation at pedestrian velocities because the channel is only slowly varying relative to the duration of the pilot sequence used to estimate the channel. The estimator accuracy also increases with improving mean SNR, as expected. For each pilot sequence length, the estimator performance is largely independent of the number of paths, l, and the spacing between the delay paths given by C.

However, this is not the case when the channel is more rapidly time varying, as shown in Fig. 2 for the city/town channel. The same values for C and φ as used for Fig. 1 are used here.

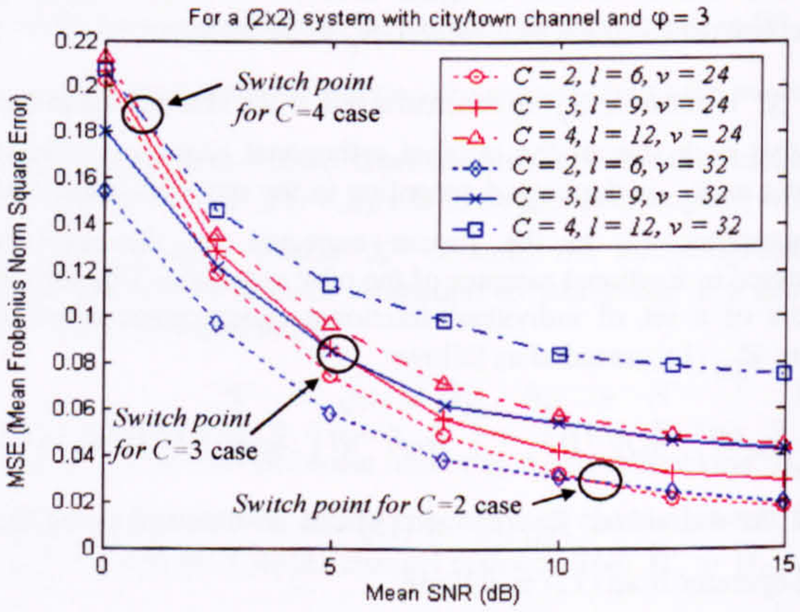

Figure 2: MSE performance of channel estimate versus Mean SNR for the city/town channel using different pilot lengths (v=24 & 32) in different channel scenarios with fixed φ=3 and increasing C.

First, it is observed that the MSE is slightly larger for the city/town channel than the pedestrian channel and it is very much dependent upon the number of multipaths, l, for both v=24 and v=32. The spread in the MSE characteristics for different values of C and l is much wider for the v=32 case than for the v=24 case. Furthermore, it is no longer guaranteed that the longer pilot sequence (v=32) will obtain the best channel estimate for all values of C and l (especially at high values of SNR), as was the case for Fig. 1. This is because, at higher mean SNRs, a pilot length of v=24 is sufficient to provide an adequate channel estimate before the channel characteristics change due to the Doppler effect, even at this higher handset velocity. However, at this velocity, the channel characteristics have certainly changed during the longer pilot length, v=32, at the assumed data rate of 120kb/s per transmit antenna and it is the change in characteristics during the estimation process that worsens the estimate.

In Fig. 2, three 'switch over' points are shown where the estimator performance for the shorter (v=24) pilot sequence outperforms the longer (v=32) pilot sequence. Consequently when C=2, which corresponding to l=6 multipaths, the shorter pilot sequence begins to outperform the longer pilot sequence at a mean SNR≈11dB whereas for C=3, corresponding to l=9 multipaths, the shorter pilot sequence begins to outperform the longer sequence at a mean SNR≈5dB.

Figures 3 and 4 assess the impact of different values of delay spread, φ, on the estimator performance for a fixed over-sampling factor, C=2 (corresponding to a spacing of the multipaths of ½ symbol period) for pedestrian and city/town channels respectively. Figure 3 shows that for the slowly varying pedestrian channel (particularly at low values of SNR) the longer the delay spread the worse the MSE performance of the estimator and that by using longer pilot sequences the estimate is improved. This is to be expected because as the delay spread increases the total number of paths included in the channel model increases linearly with φ.

For the more rapid city/town channel, shown in Fig. 4, a slightly different result is observed whereby a pilot length of v=24 provides much better MSE performance at higher mean SNRs than for v=32. This is particularly noticeable for the case of φ=4. Once again, the reason is due to the rapid time-variation of the channel characteristics due to the effect of Doppler.

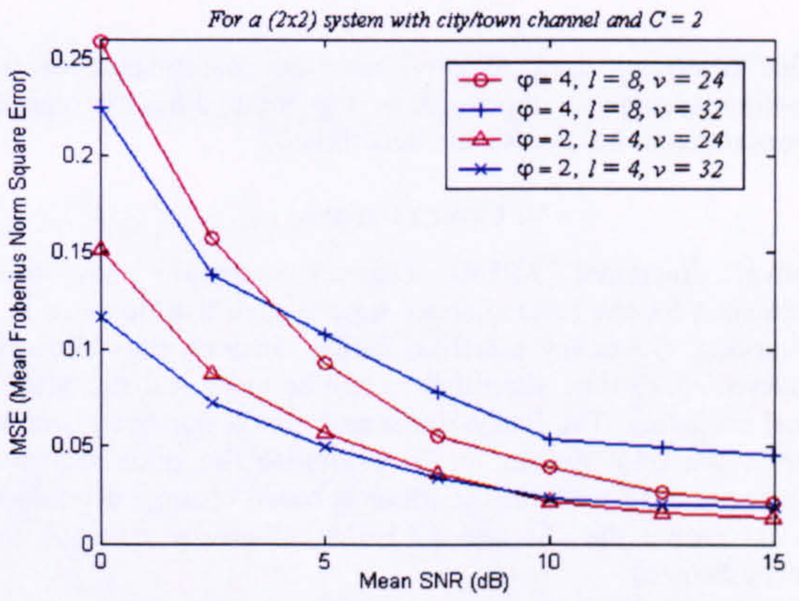

Figure 4: MSE performance of channel estimate versus Mean SNR for the city/town channel using different pilot lengths (v=24 & 32) in different channel scenarios with fixed C =2 and increasing φ.

Figure 5 shows the bit error rate performance of the MIMO system when employing the fractional MIMO channel estimator. A number of different situations are compared in this figure. Case 1 shows a non-fractionally spaced estimator used with an idealised non-fractionally spaced channel with 3 paths. It uses a K_f=9 tap equaliser in the receiver. Case 2 shows a fractionally spaced channel estimator used with a non-fractionally spaced channel having 3 paths. It uses a K_{ff}=18 tap equaliser. Case 3 shows a fractionally spaced estimator used with a fractionally spaced channel. In this case, the number of paths is 6 and the number of equalisers taps is 18. The graphs are plotted for (2x2), (3x2) and (5x3) MIMO systems, showing the effect of increasing diversity as the number of receiver antennas is increased from 2 to 5. In each case, the use of the proposed fractionally spaced estimator and equaliser performs considerably better than the non-fractionally spaced estimator and equaliser. Note also that the performance of the MIMO system is invariably better when the fractionally-spaced estimator and equaliser are used with the fractionally spaced channel even though it has twice as many equal-loss paths.

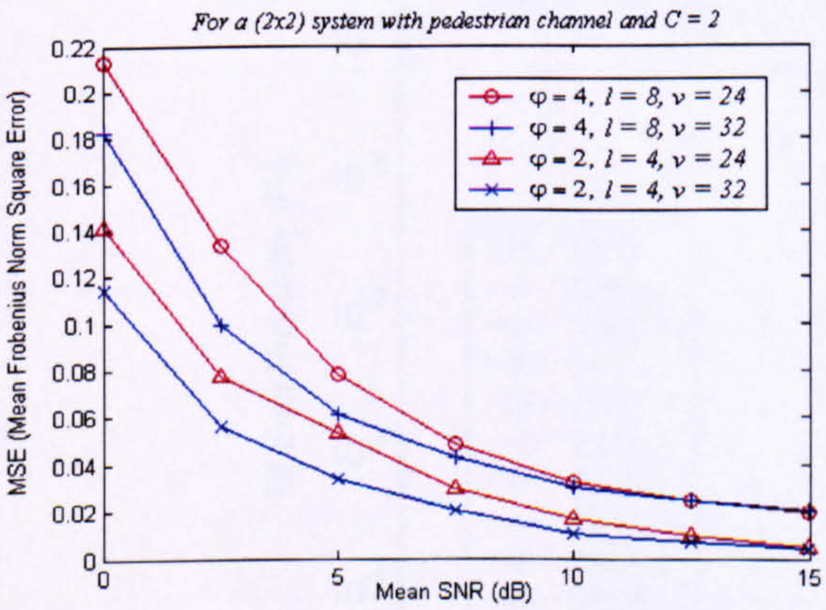

Figure 3: MSE performance of channel estimate versus Mean SNR for the pedestrian channel using different pilot lengths (v=24 & 32) in different channel scenarios with fixed C =2 and increasing φ.

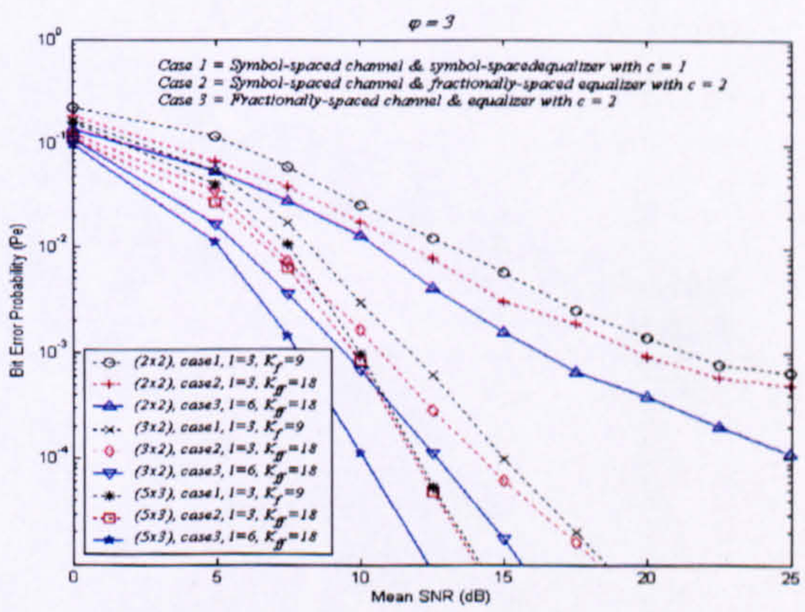

Figure 5: Bit error probability of different (N×M) configurations when deploying the proposed symbol spaced and fractionally spaced MIMO channel estimators, as indicated

This illustrates, quite clearly how the performance of the space-time system is improved as the multipath environment becomes much more diverse and decorrelated.

V. Conclusions

A novel fractional MIMO channel estimator has been implemented for the layered space-time system that operates in a time-varying, frequency selective fading channel; thus allowing the layered space-time algorithm to handle more realistic MIMO channel scenarios. The Paley-Hadamard matrix has been used to construct the pilot matrix to: (i) minimise the pilot sequence length required to perform the training based channel estimation and (ii) resolve the ISI and CCI that otherwise corrupts the channel estimates.

The accuracy of the proposed channel estimator has been shown to be dependent upon the Doppler velocity of the channel. Longer pilot sequence lengths (e.g. v=32) only give better MSE performance in slowly time-varying pedestrian channels. For the city/town channel, the MSE performance of the estimator depends on the number of paths l, the total span of the delay spread φ and the minimum spacing between each delay path, τ/C. At high SNRs, the shorter pilot sequence can outperform the longer pilot sequence length due to the rapid variability of the channel.

Results for the bit error probability of an OSIC layered space-time system show that the use of the proposed fractionally spaced channel estimator and equaliser performs considerably better than the symbol spaced channel estimator and equaliser.

References

[1] G. J. Foschini, "Layered Space-Time Architecture for Wireless Communication in Fading Environment When Using Multi-Element Antennas", *Bell Labs Tech Journal*, pp. 41-59, 1996.

[2] P. W. Wolniansky, G. J. Foschini, G. D. Golden, R. A. Valenzuela, "V-BLAST: An Architecture for Realizing Very High Data Rates Over the Rich-Scattering Wireless Channel," Proc. ISSSE-98, pp. 295-300, Sept., 1998.

[3] A. Lazono, C. Papadias, "Layered space-time receivers for frequency selective wireless channels," *IEEE Trans. On Communication*, pp. 65-73, vol. 50, No.1 Jan 2002.

[4] X. Zhu, R. D. Murch, "Layered space-time equalization of multiple-input multiple-output frequency selective channels," *IEEE* ICC 2002., pp. 330 – 334, vol.1, 2002.

[5] Q. Sun, C. Donald, H. C. Huang, A. Lazano, "Estimation of continuous flat fading MIMO channels," *IEEE* WCNC 2002., pp. 189–193, vol.1, 2002.

[6] C. Budianu, L Tong, "Channel estimation for space-time orthogonal block codes," *IEEE Trans. on Signal Processing*, pp. 2515-2528, vol. 50, No.10 Oct 2002.

[7] Y Li, "Simplified channel estimation for OFMD systems with multiple transmit antennas," *IEEE Trans. on Wireless Communication*, pp 67-75, vol.1, no.1, Jan 2002.

[8] M F Siyau, P Nobles and R. F. Ormondroyd, "Channel estimation for layered space-time systems in time-varying, frequency-selective, wireless channels", *Proc. IEEE VTC Fall 2004*, vol.2, pp. 1258-1262, October 2004.

[9] M. F. Siyau, P. Nobles, R. F. Ormondroyd, "Channel estimation for space-time systems using a multi-element array recursive least squares (MEA-RLS) algorithm," *4th International Symposium on WPMC'01*, pp. 1451-1456, vol.3, Sept, 2001.

[10] J. Seberry and M. Yamada, "Hadamard matrices, sequences and block designs," pp 431-560 of J. H. Dinitz & D. R. Stinson. Editor (1992), Contemporary Design Theory: A Collection of Essays, Wiley, New York.

Appendix B1

The following results show the performance of V-BLAST system achieved by different detection algorithms in the various ($N \times M$) MIMO systems operated in flat fading MIMO channel.

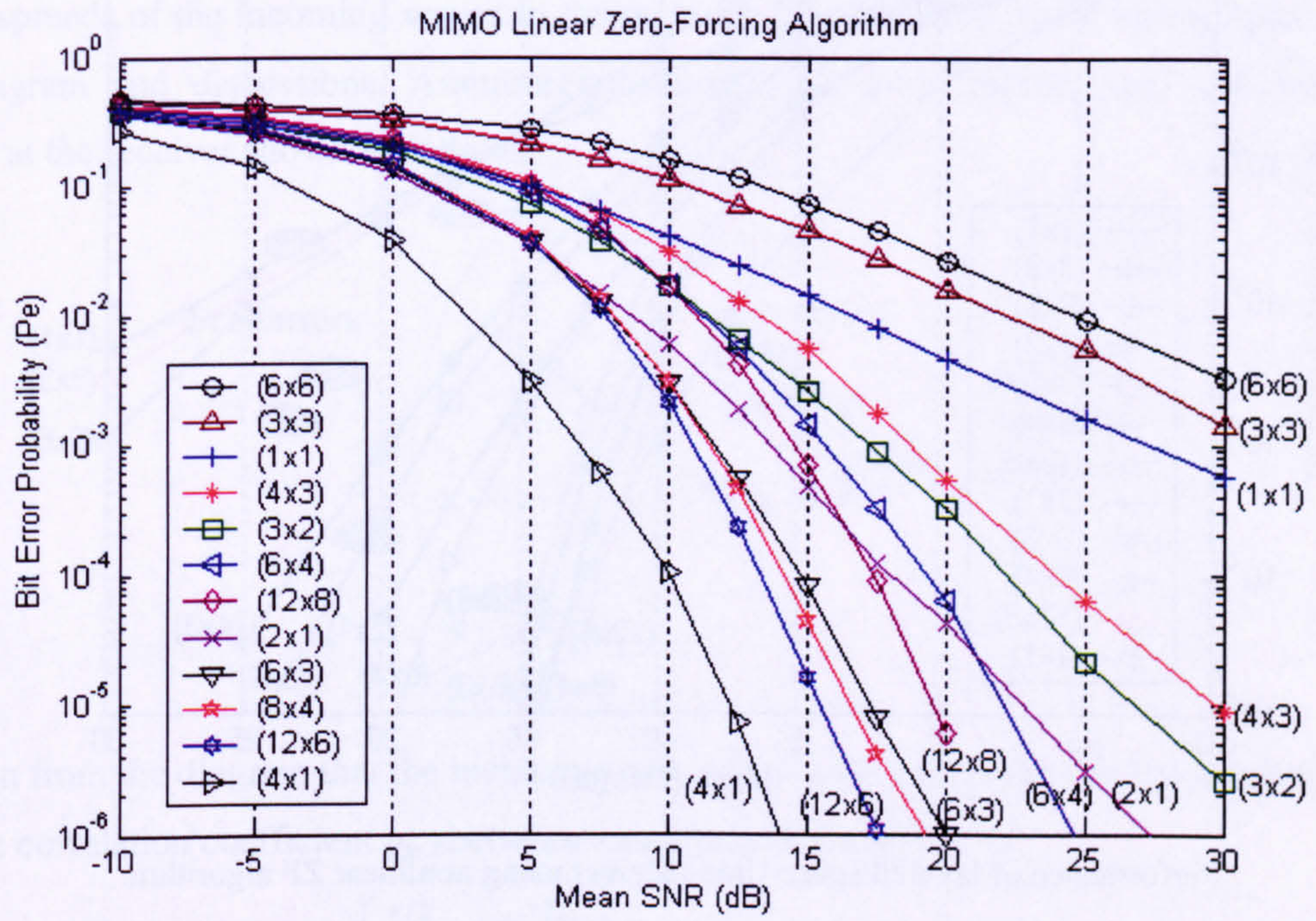

Performance of layered space-time receiver using linear ZF algorithm.

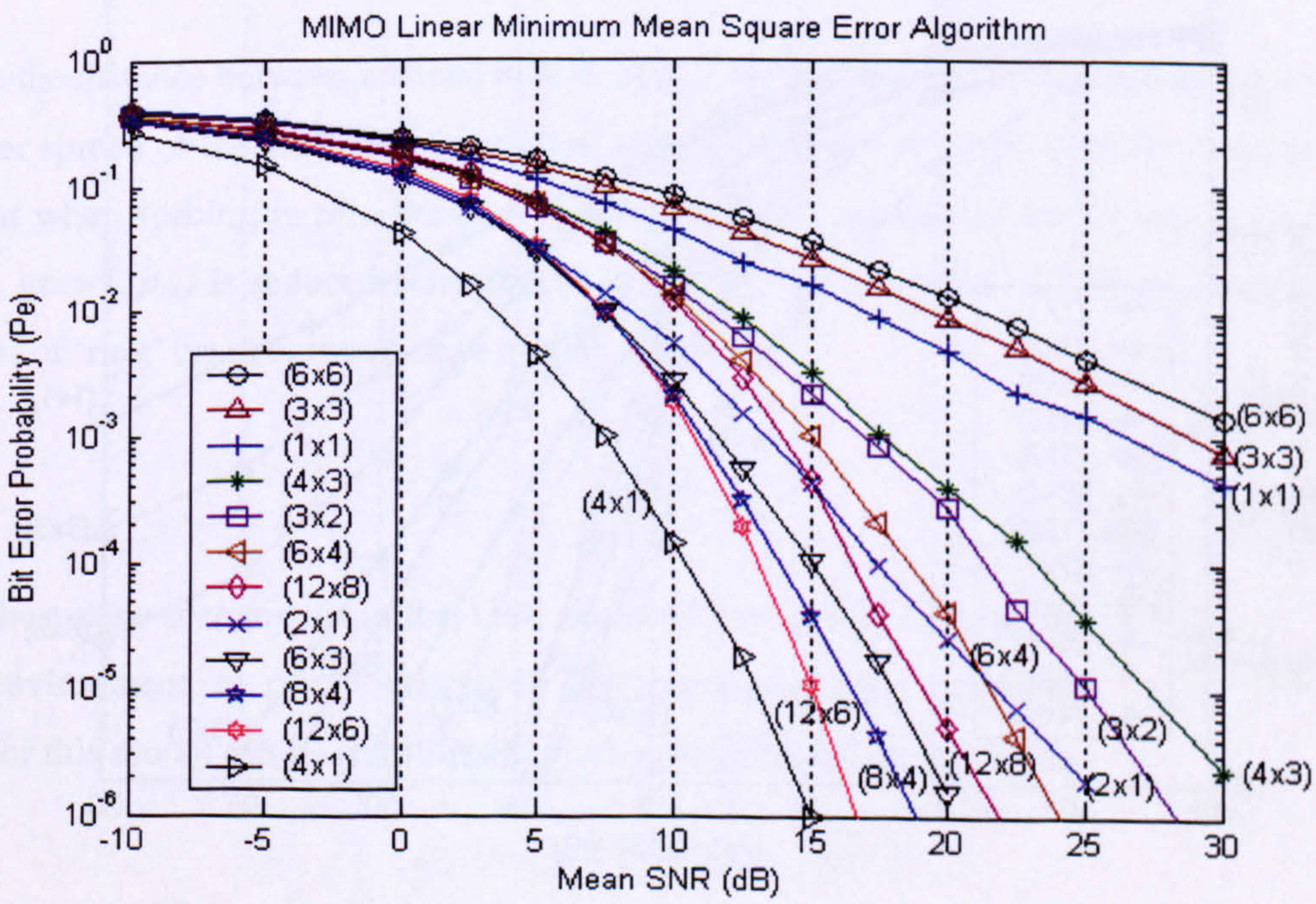

Performance of layered space-time receiver using linear MMSE algorithm.

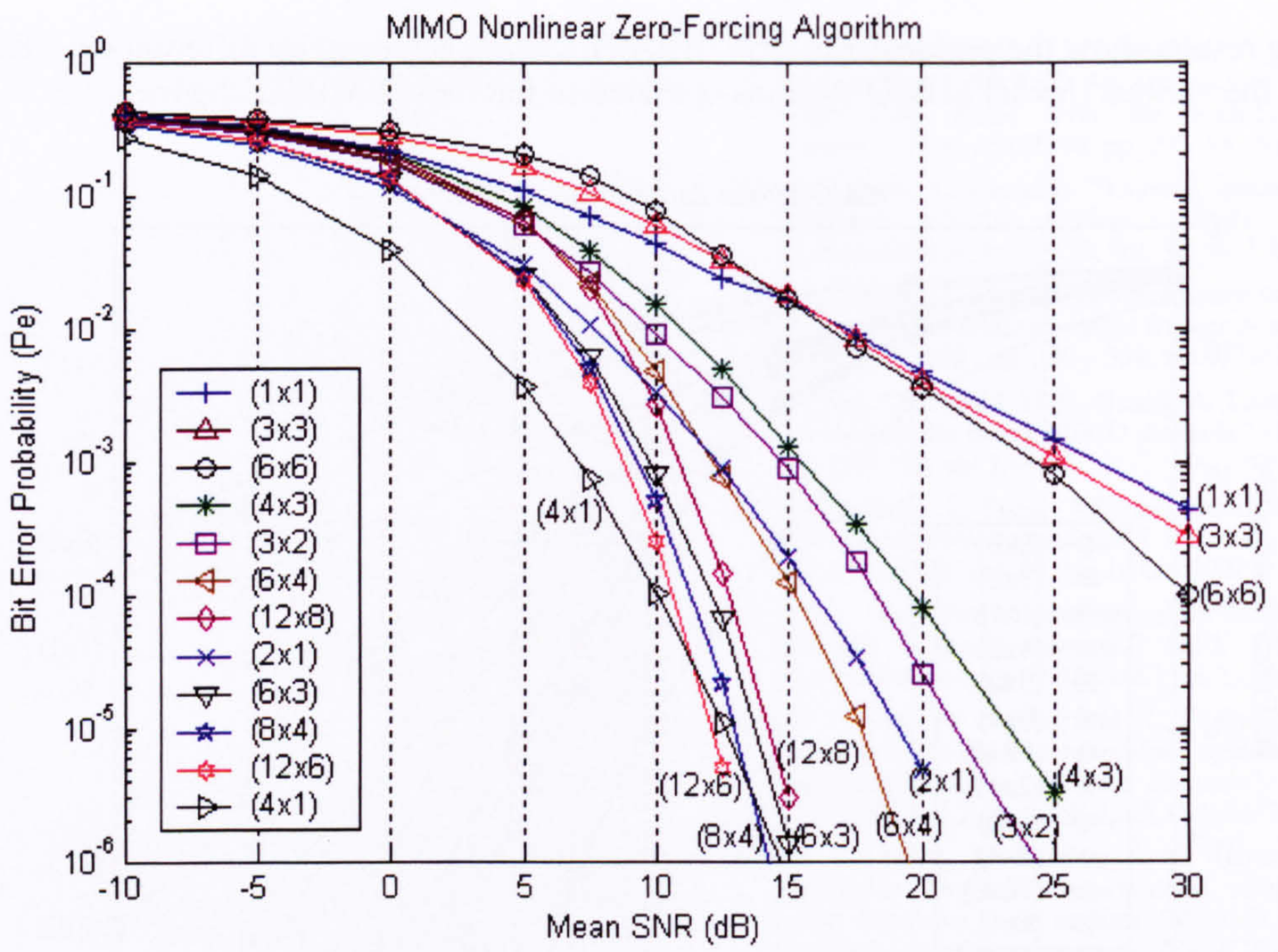

Performance of layered space-time receiver using nonlinear ZF algorithm.

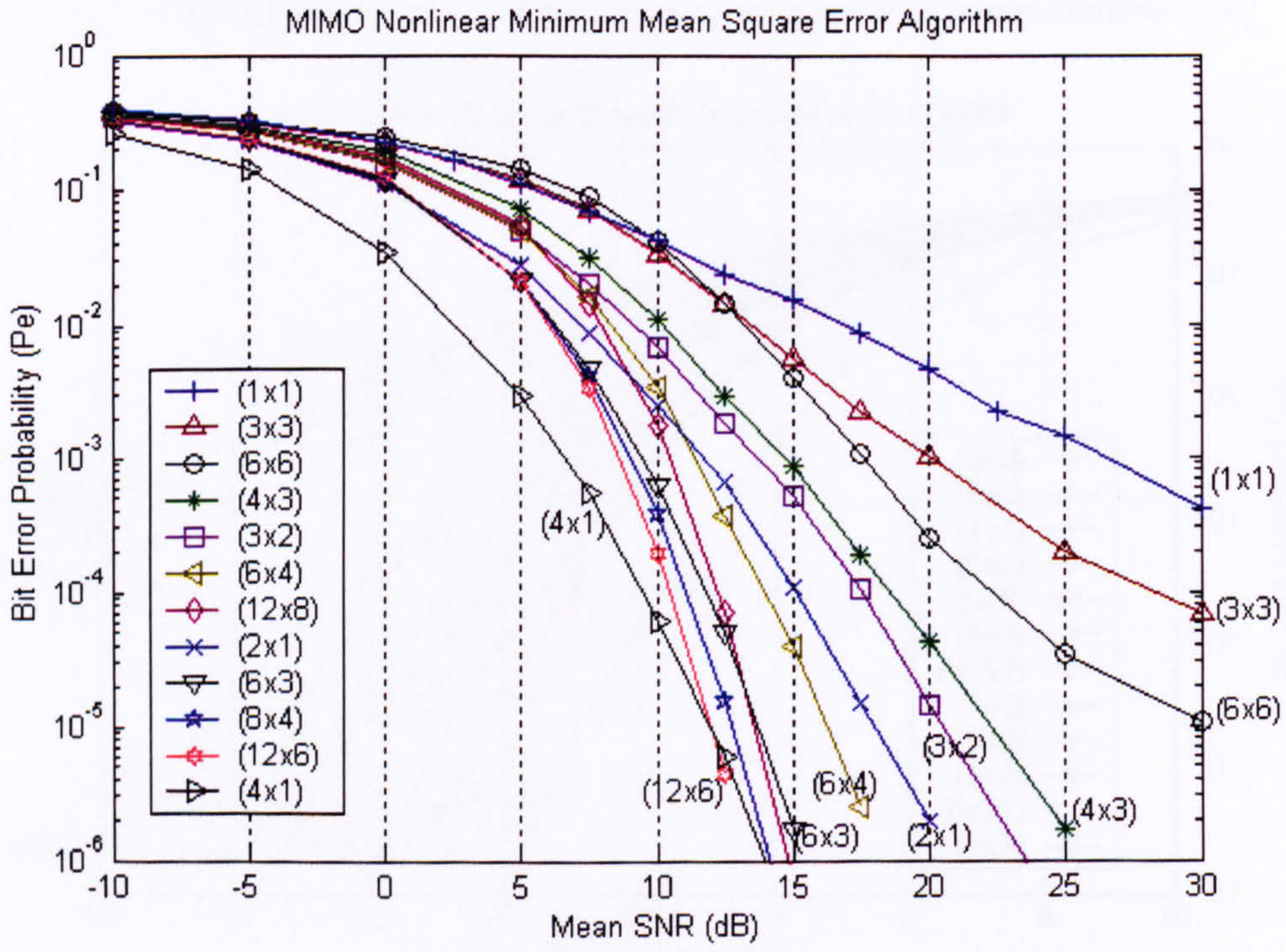

Performance of layered space-time receiver using nonlinear MMSE algorithm.

Appendix B2 – Spatial correlated channel model for MIMO system

As mention in Section 5.1 for results related the spatial correlation channel, where spatial correlation depends on: the distance between each antenna's spacing, the number & distribution of the scatterrers and the angular spreads of the incoming waves to the receiver. These can be made clearer with the following physical diagram and discussions. Assuming uniform linear array model with equi-distant antenna separation d at the receiver shown as follows:

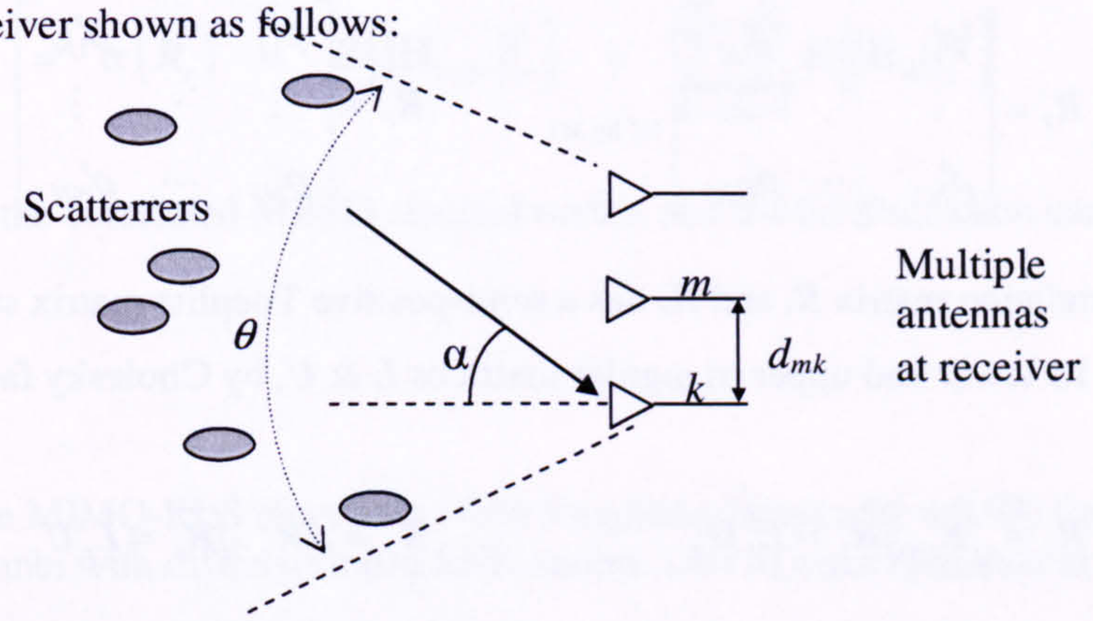

It can be seen from the diagram that the incident wave arrives with and angle α to the respective receive antenna. The correlation coefficient $\rho_{m,k}$ between antenna m & k is given by:

$$\rho_{m,k} = \begin{cases} \int_{-\theta/2}^{\theta/2} e^{-j2\pi \frac{d_{mk}}{\lambda} \sin\alpha} p(\theta) d(\alpha), & m \neq k \\ 1, & m = k \end{cases}$$

where d_{mk} is the distance between antenna m & k, $p(\theta)$ is the probability distribution of the scatterers and θ is the angular spread of the scatterers distributed around the receiver. First, it can be seen from the above equation that when spacing is zero between two antenna, the correlation coefficient $\rho_{m,k}$ is unity. As the distance d_{mk} grows, $\rho_{m,k}$ is reduced accordingly. Secondly, for a uniform distributed angular spread of θ (Lee's model of 'ring' case) between -π to π, $p(\theta)$ is given as:

$$p(\theta) = \frac{1}{2\pi}$$

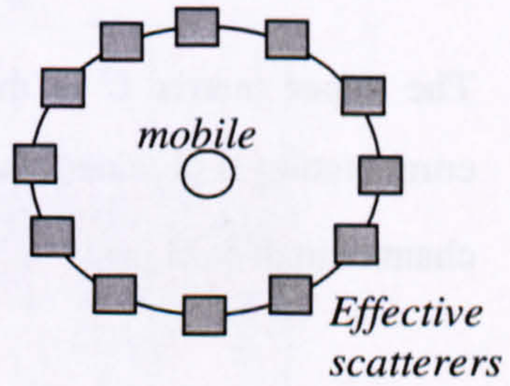

This is the best case scenario from the view point of low spatial correlation since the environment is richly scattered. The corresponding correlation coefficient for this model can be simplified according to Jakes model [112] as:

$$\rho_{m,k} = J_o\left(2\pi \frac{d_{mk}}{\lambda}\right), \qquad m \neq k$$

where J_o is the zeroth order Bessel function. To achieve zero correlation in this case, the antenna's spacing must be at least $d_{mk} = \lambda/2$, since $J_o(\pi) \cong 0$.

Generation of correlated MIMO channel matrix

In the MIMO systems, the spatial correlation can be incorporated into the channel matrix by first defining the respective correlation matrix at both the transmitter (denoted as $\boldsymbol{R}_t$) and at the receiver (denoted as $\boldsymbol{R}_r$). Each correlation matrix consists of respective set of correlation coefficients ρ_{ij}^t & ρ_{ij}^r expressed as follows:

$$\boldsymbol{R}_t = \begin{bmatrix} \rho_{11}^t & \cdots & \rho_{1M}^t \\ \vdots & \ddots & \vdots \\ \rho_{M1}^t & \cdots & \rho_{MM}^t \end{bmatrix}_{(M \text{ by } M)} \qquad \boldsymbol{R}_r = \begin{bmatrix} \rho_{11}^r & \cdots & \rho_{1N}^r \\ \vdots & \ddots & \vdots \\ \rho_{N1}^r & \cdots & \rho_{NN}^r \end{bmatrix}_{(N \text{ by } N)}$$

The corresponding correlation matrix $\boldsymbol{R}_t$ and $\boldsymbol{R}_r$ has a semi-positive Toeplitz matrix structure, which can also be factorized into its lower and upper triangular matrices $\boldsymbol{L}$ & $\boldsymbol{U}$, by Cholesky factorization [116, 117] as:

$$\boldsymbol{R}_t = \sqrt{\boldsymbol{R}_t} \cdot \sqrt{\boldsymbol{R}_t} = \boldsymbol{L}_t \boldsymbol{U}_t \qquad \boldsymbol{R}_r = \sqrt{\boldsymbol{R}_r} \cdot \sqrt{\boldsymbol{R}_r} = \boldsymbol{L}_r \boldsymbol{U}_r$$

where

$$\boldsymbol{L}_t \text{ or } \boldsymbol{L}_r = \begin{bmatrix} 1 & 0 & 0 & 0 & \cdots & 0 \\ \alpha & \beta & 0 & \ddots & \vdots & \vdots \\ \alpha^2 & \alpha\beta & \beta & 0 & \ddots & \vdots \\ \alpha^3 & \alpha^2\beta & \alpha\beta & \beta & 0 & 0 \\ \vdots & \vdots & \vdots & \ddots & \ddots & 0 \\ \alpha^{k-1} & \alpha^{k-1} & \alpha^{k-1} & \cdots & \alpha\beta & \beta \end{bmatrix}; \quad \text{and} \quad \alpha = \rho, \quad \beta = \sqrt{1-\rho^2}$$

Note that k is the respective size of the matrix: $k=M$ for $\boldsymbol{R}_t$ & $k=N$ for $\boldsymbol{R}_r$ and the respective identical correlation coefficients ρ_{ij}^t & ρ_{ij}^r also applied accordingly to both α and β terms. In the simulation results, the transmit correlation coefficient is made equivalent to the receive correlation coefficient as $\rho_{ij}^t = \rho_{ij}^r$ for all $\boldsymbol{L}$ and $\boldsymbol{U}$ matrices where uniform correlation coefficient is assumed.

The upper matrix $\boldsymbol{U}$ is the transpose of the lower matrix $\boldsymbol{L}$ in this case. Once each pair of the LU combination is obtained, the correlated MIMO channel $\mathbf{H}_{corr}$ can be obtained from its uncorrelated MIMO channel matrix $\mathbf{H}_w$ as:

$$\mathbf{H}_{corr} = \boldsymbol{L}_r \mathbf{H}_w \boldsymbol{U}_t \quad or \quad \sqrt{\boldsymbol{R}_r}\, \mathbf{H}_w \sqrt{\boldsymbol{R}_t}$$

In fact, in general, the fading correlation (for complex value case) can also be modeled as:

$$\mathbf{H}_{corr} = \frac{1}{\sqrt{\text{tr}(\boldsymbol{R}_t)}} \boldsymbol{R}_r^{1/2} \mathbf{G}\, \boldsymbol{R}_t^{1/2}$$

where $\boldsymbol{R}_r = E\{\mathbf{H}_{corr}\mathbf{H}_{corr}^{\mathrm{H}}\}$ is the $N\times N$ receive correlation matrix and $\boldsymbol{R}_t = E\{\mathbf{H}_{corr}^{\mathrm{H}}.\mathbf{H}_{corr}\}$ is the $M\times M$ transmit correlation matrix, while $\mathbf{G}$ is the random matrix with independent, zero mean, unit variance complex entries. $\mathbf{G}$ is also assumed to be drawn from a complex Gaussian distribution leading to correlated Rayleigh fading. Also note that the channel's total power is given as:

$$\mathrm{tr}(\boldsymbol{R}_t) = \mathrm{tr}(\boldsymbol{R}_t) = E\left\{\|\mathbf{H}_{corr}\|_F^2\right\} = \sum_{m=1}^{M}\sum_{n=1}^{N} E\left\{|\mathbf{H}_{nm}|^2\right\}$$

Further details of how the correlated MIMO channel matrix and useful discussion can be found in [12, 54, 63-67, 112]

Appendix B3

The performance of the MIMO-RLS algorithm (with forgetting factor of $\gamma = 0.98$) for a (4×4) system in flat fading MIMO channel with different mean SNR values. (All M error elements in that $\mathbf{e}(n)$ are shown).

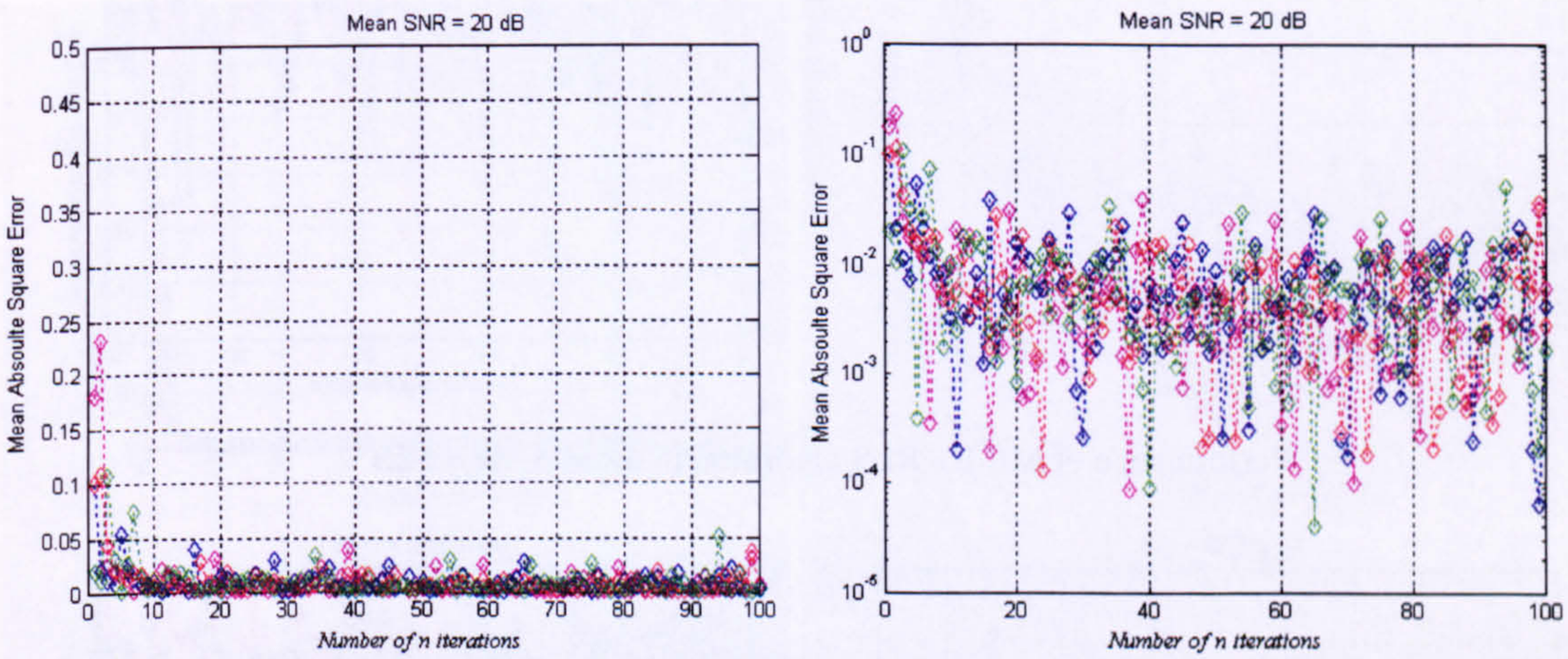

Performance of MIMO-RLS algorithm in mean SNR = 15dB

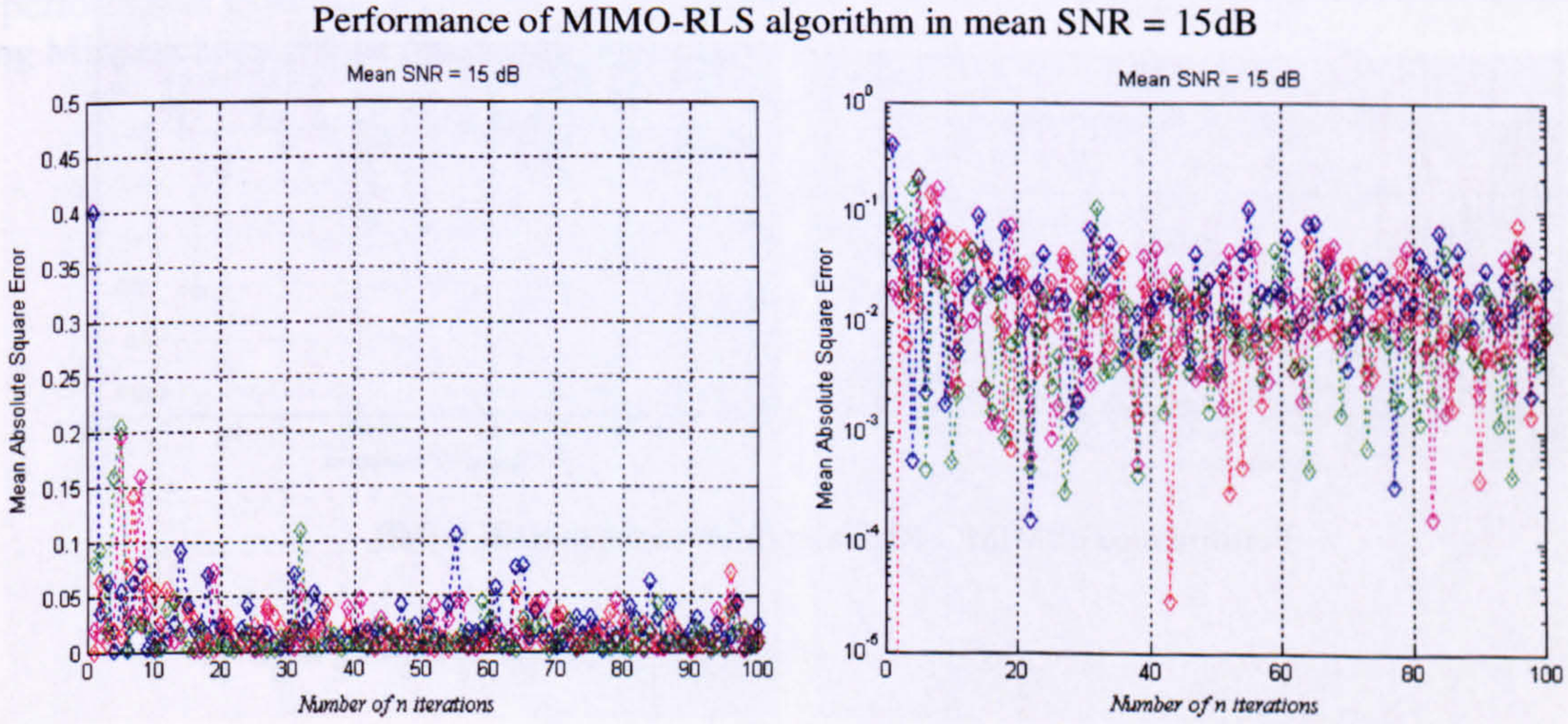

Performance of MIMO-RLS algorithm in mean SNR = 15dB

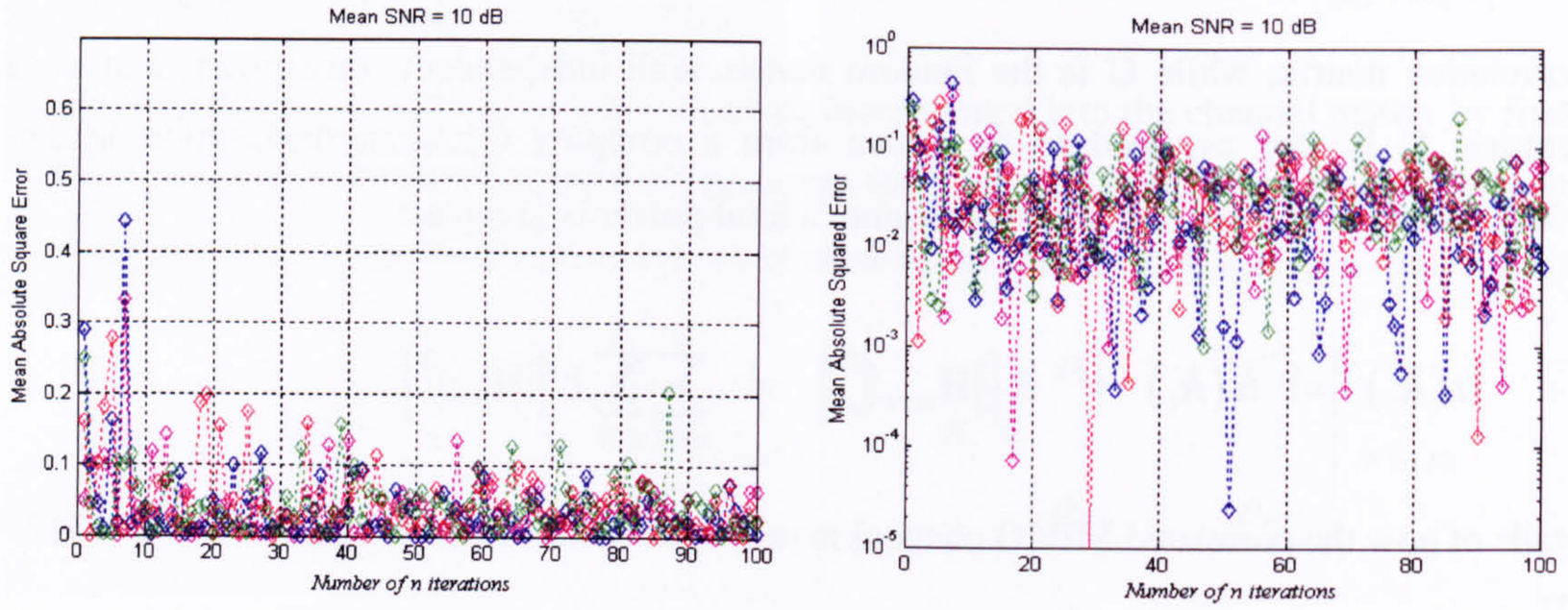

Performance of MIMO-RLS algorithm in mean SNR = 10dB

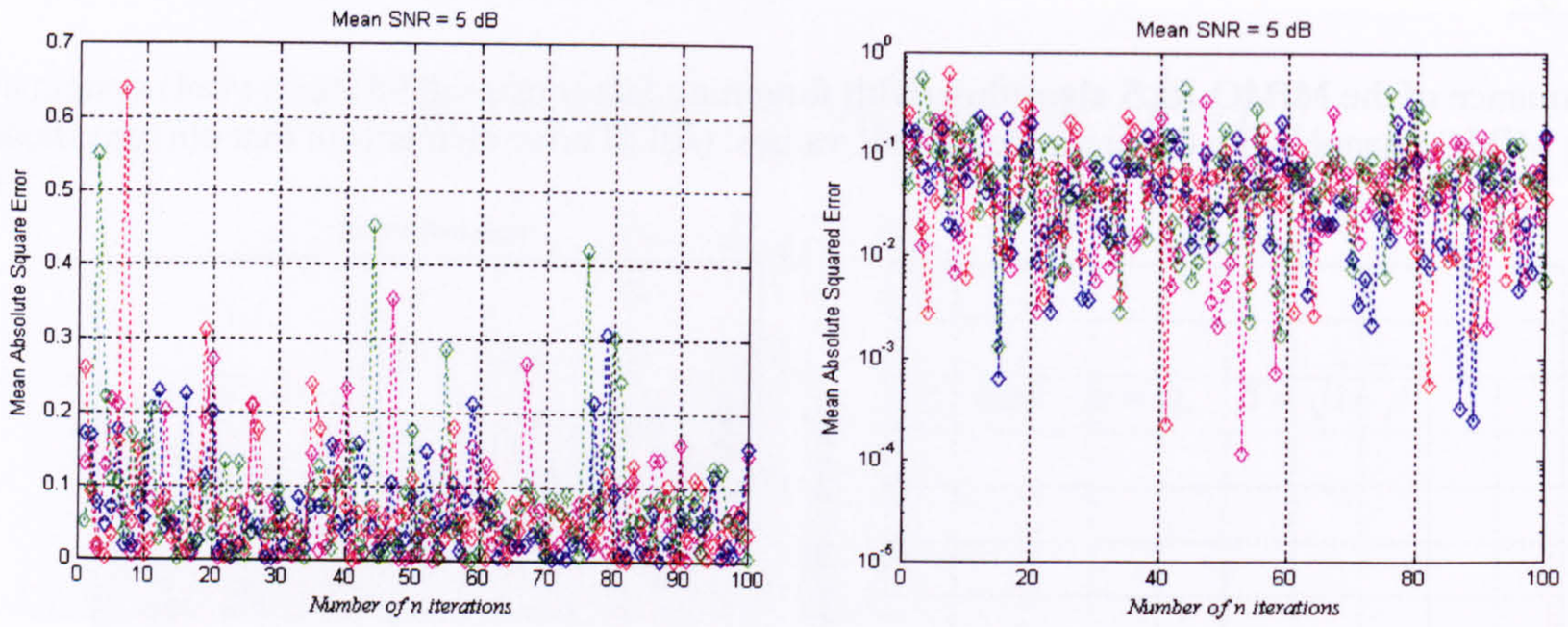

Performance of MIMO-RLS algorithm in mean SNR = 5dB

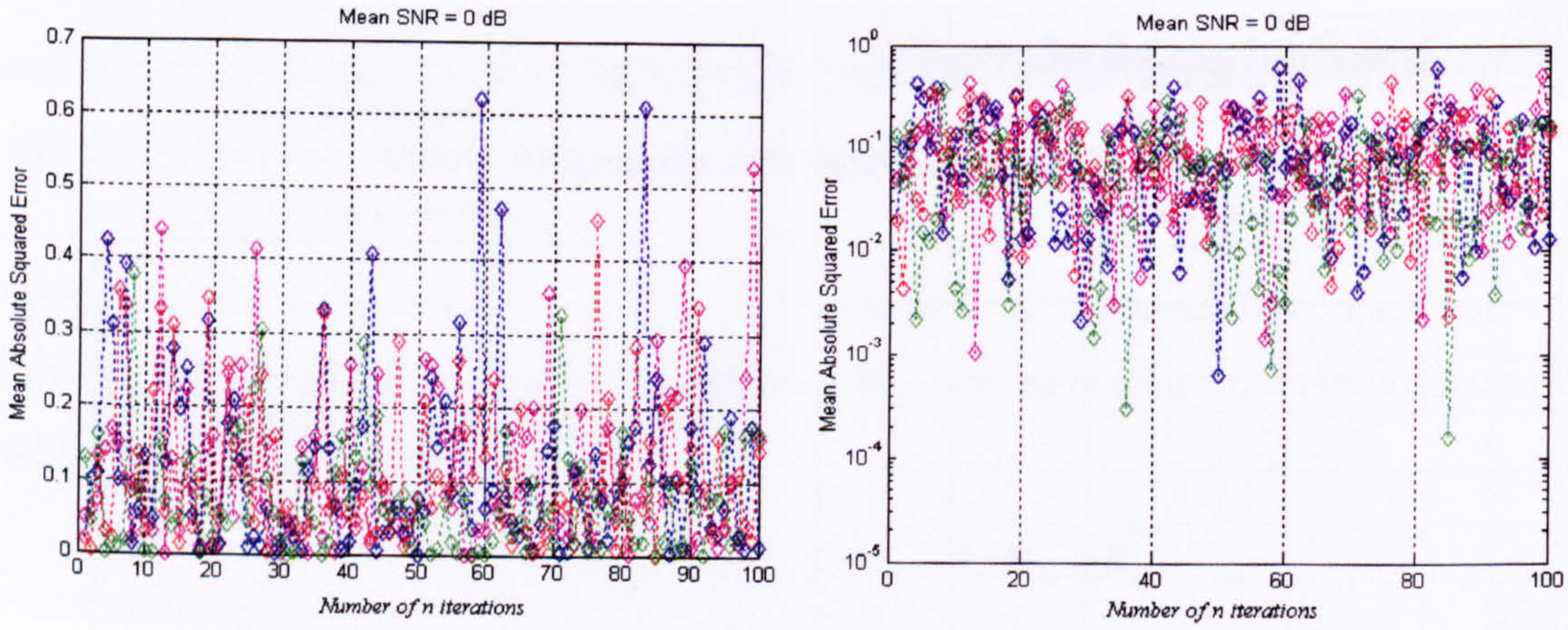

Performance of MIMO-RLS algorithm in mean SNR = 0dB

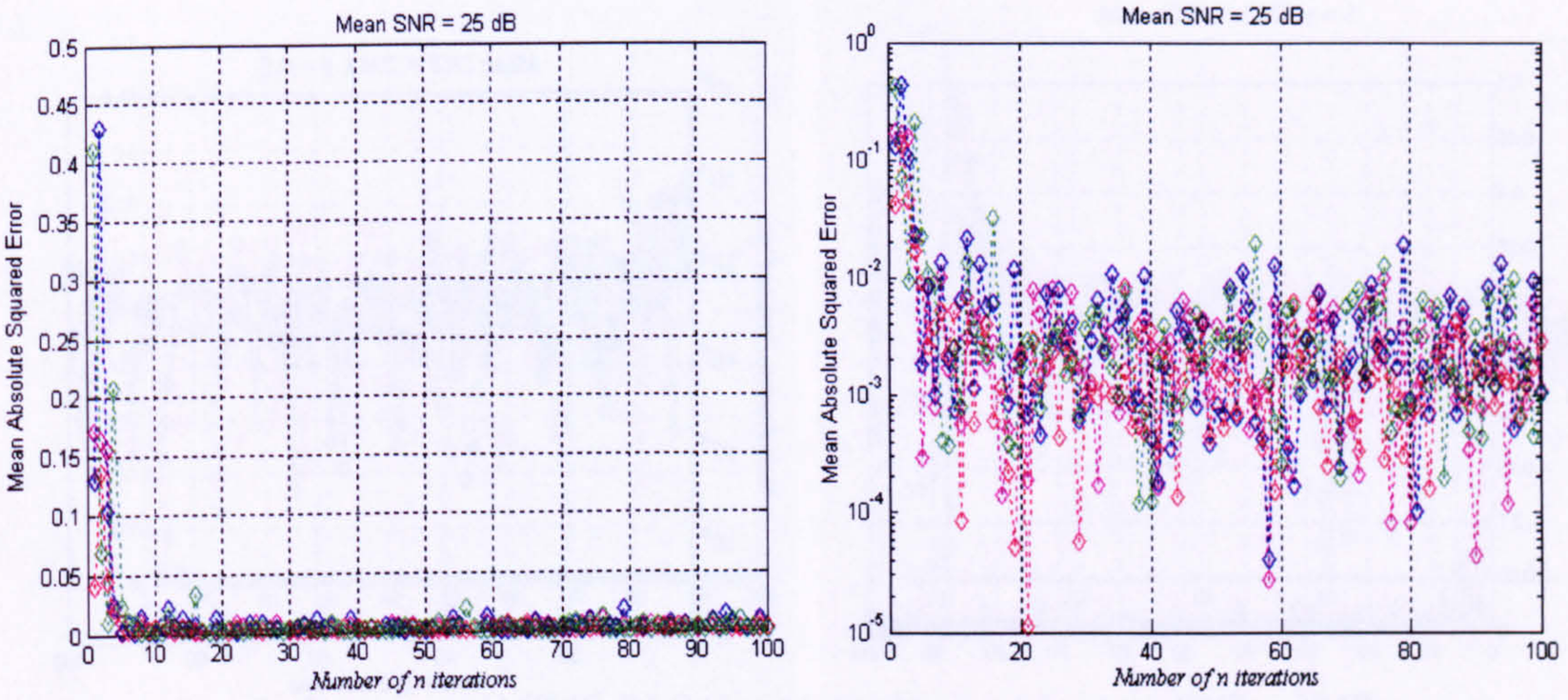

Performance of MIMO-RLS algorithm in mean SNR = 25dB

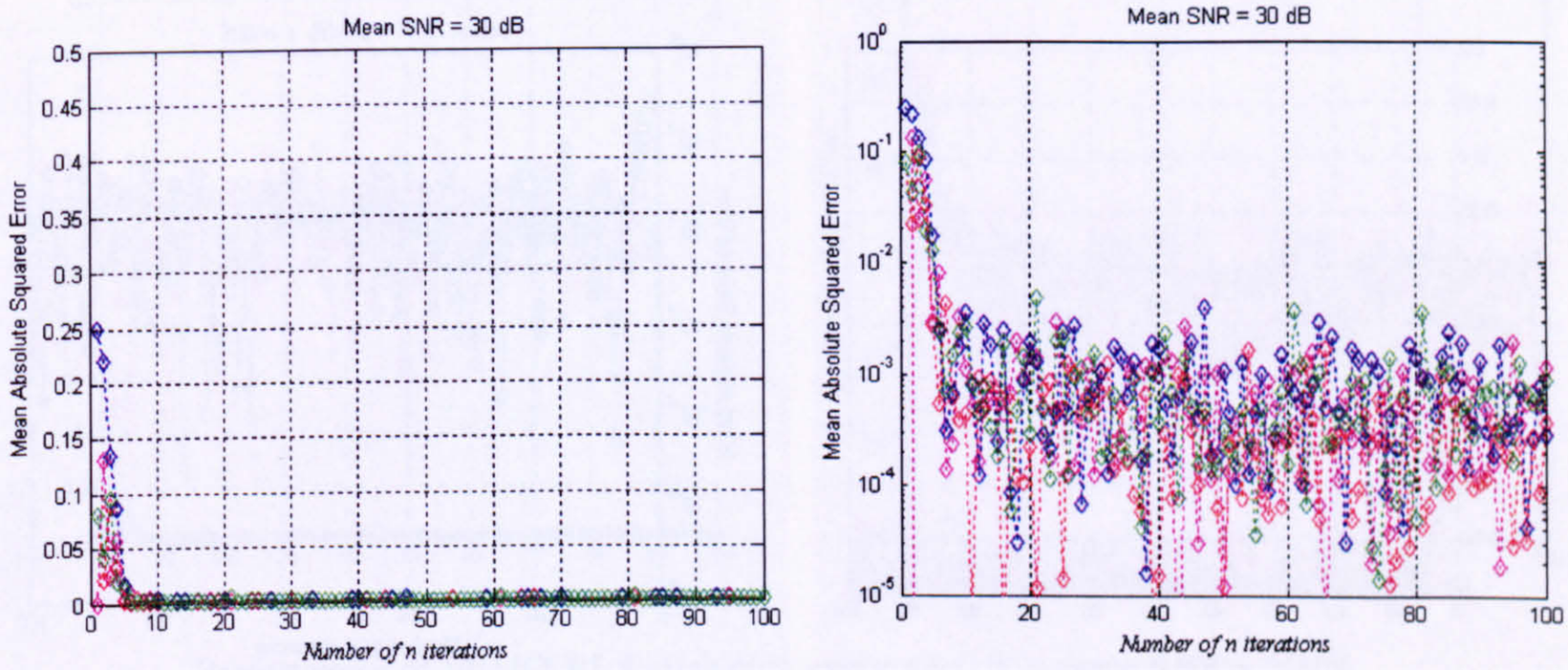

Performance of MIMO-RLS algorithm in mean SNR = 30dB

The performance of the MIMO-RLS algorithm with different forgetting factor for a (6×4) system in flat fading MIMO channel with fixed mean SNR = 20dB & 30 dB.

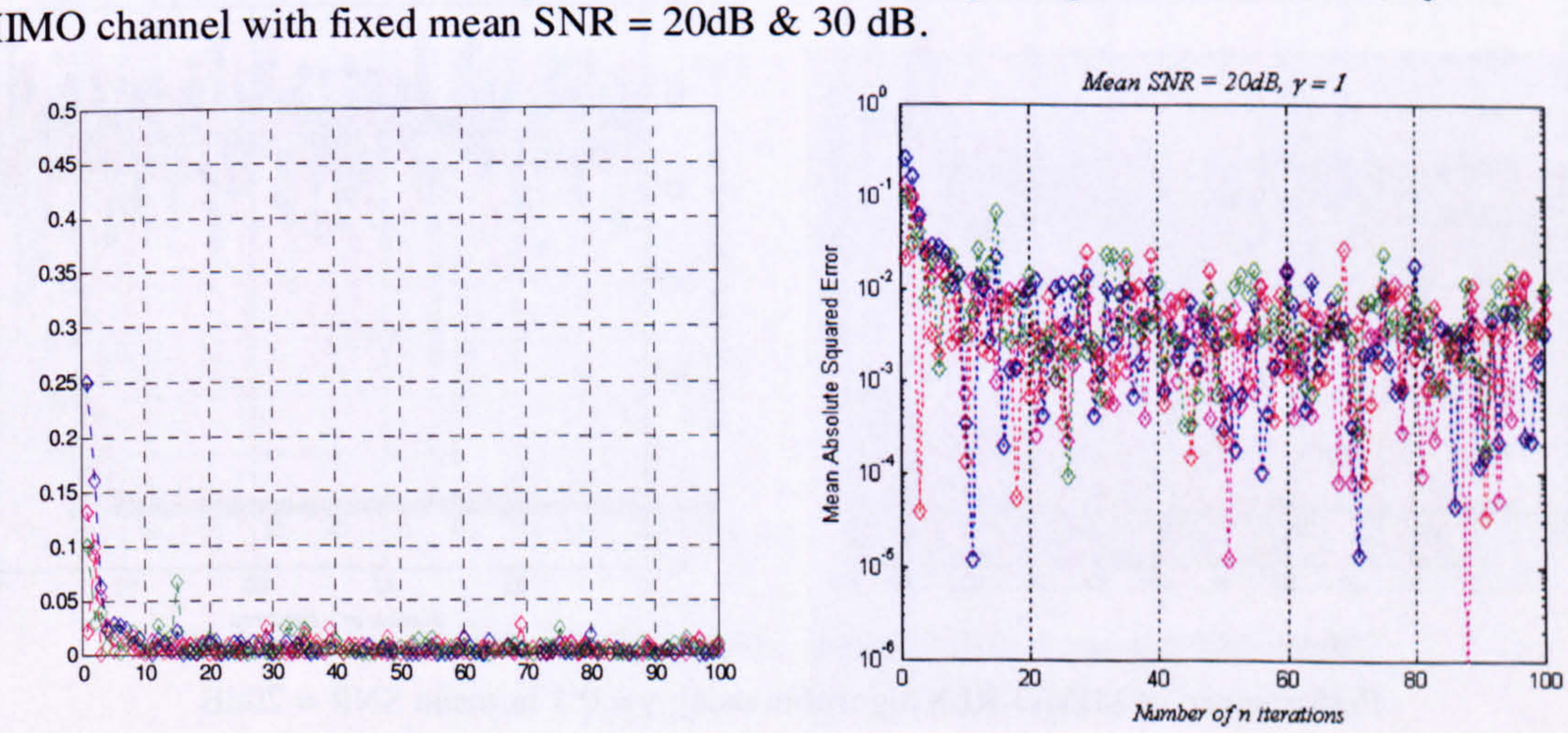

Performance of MIMO-RLS algorithm using $\gamma = 1$ in mean SNR = 20dB

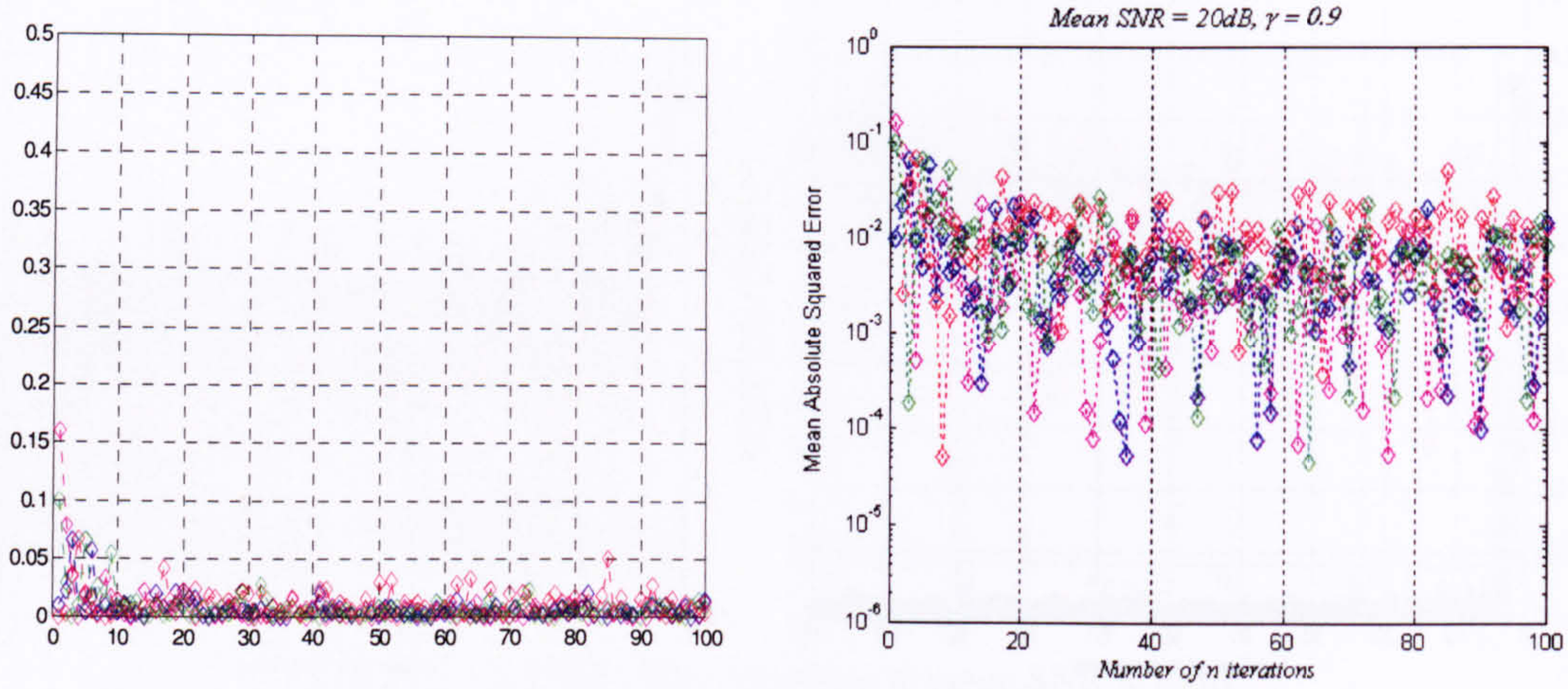

Performance of MIMO-RLS algorithm using $\gamma = 0.9$ in mean SNR = 20dB

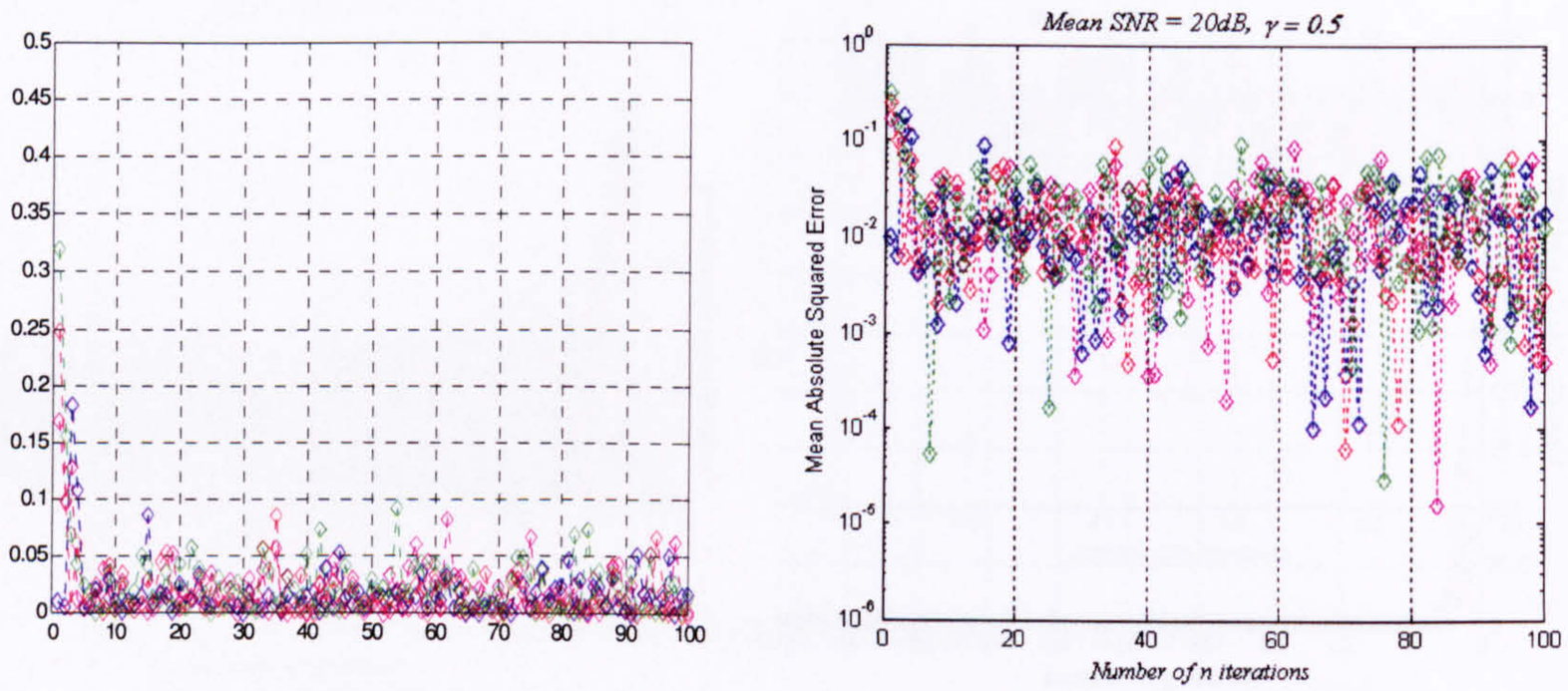

Performance of MIMO-RLS algorithm using $\gamma = 0.5$ in mean SNR = 20dB

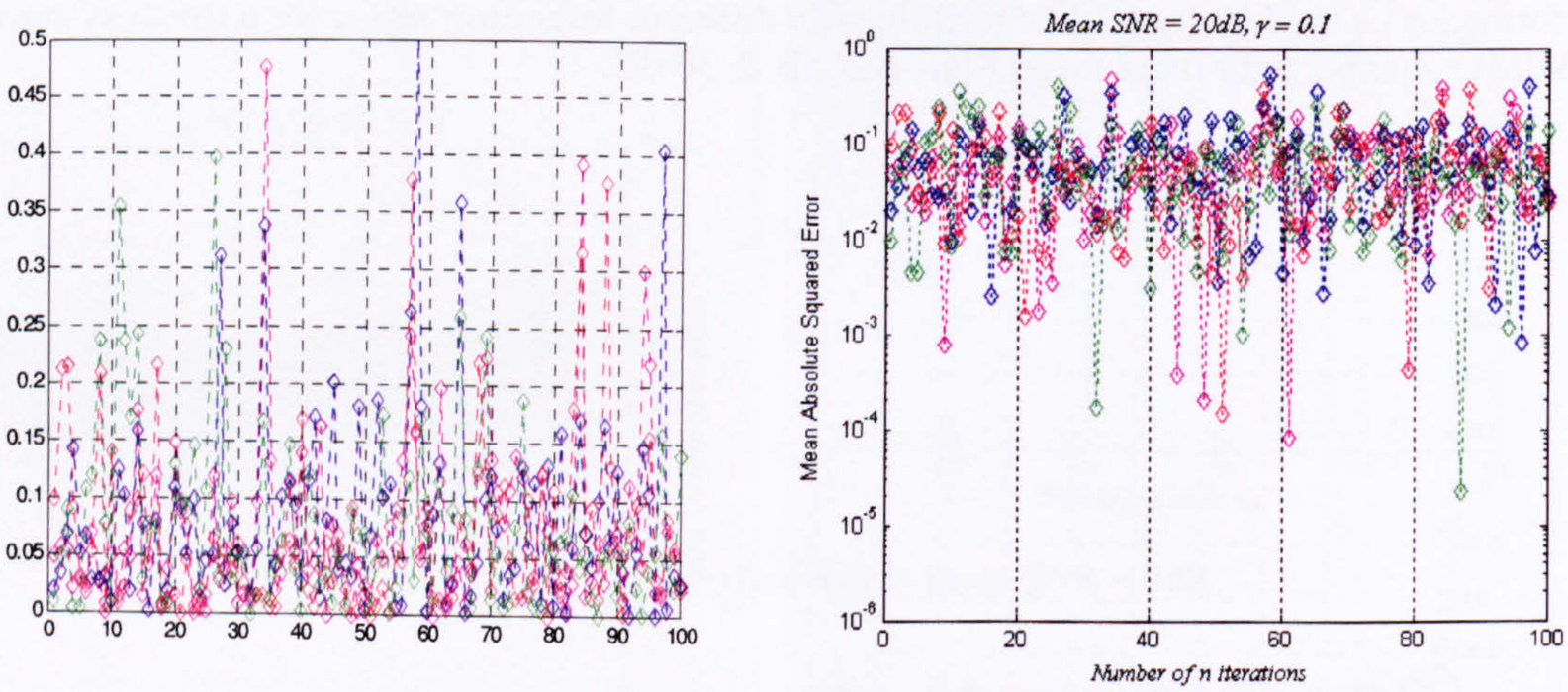

Performance of MIMO-RLS algorithm using $\gamma = 0.1$ in mean SNR = 20dB

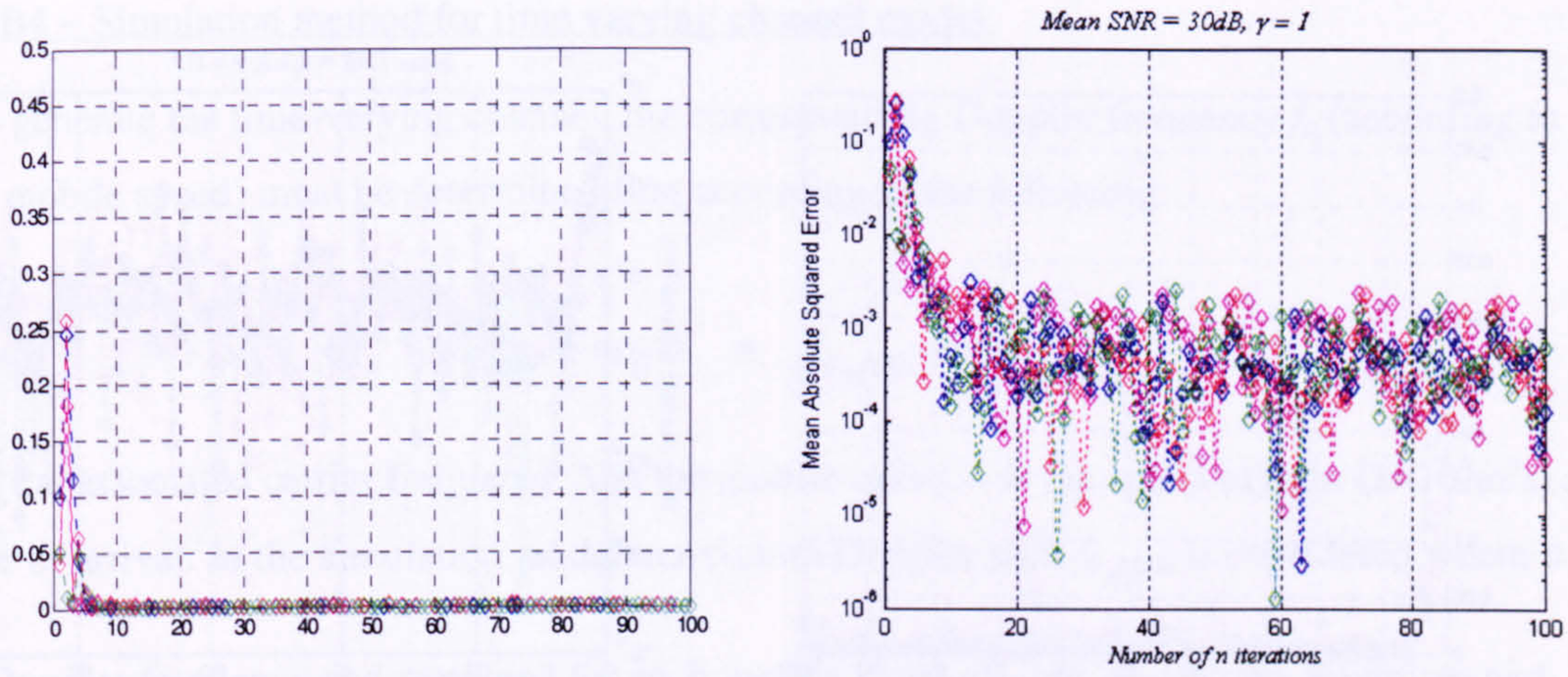

Performance of MIMO-RLS algorithm using $\gamma = 1$ in mean SNR = 30dB

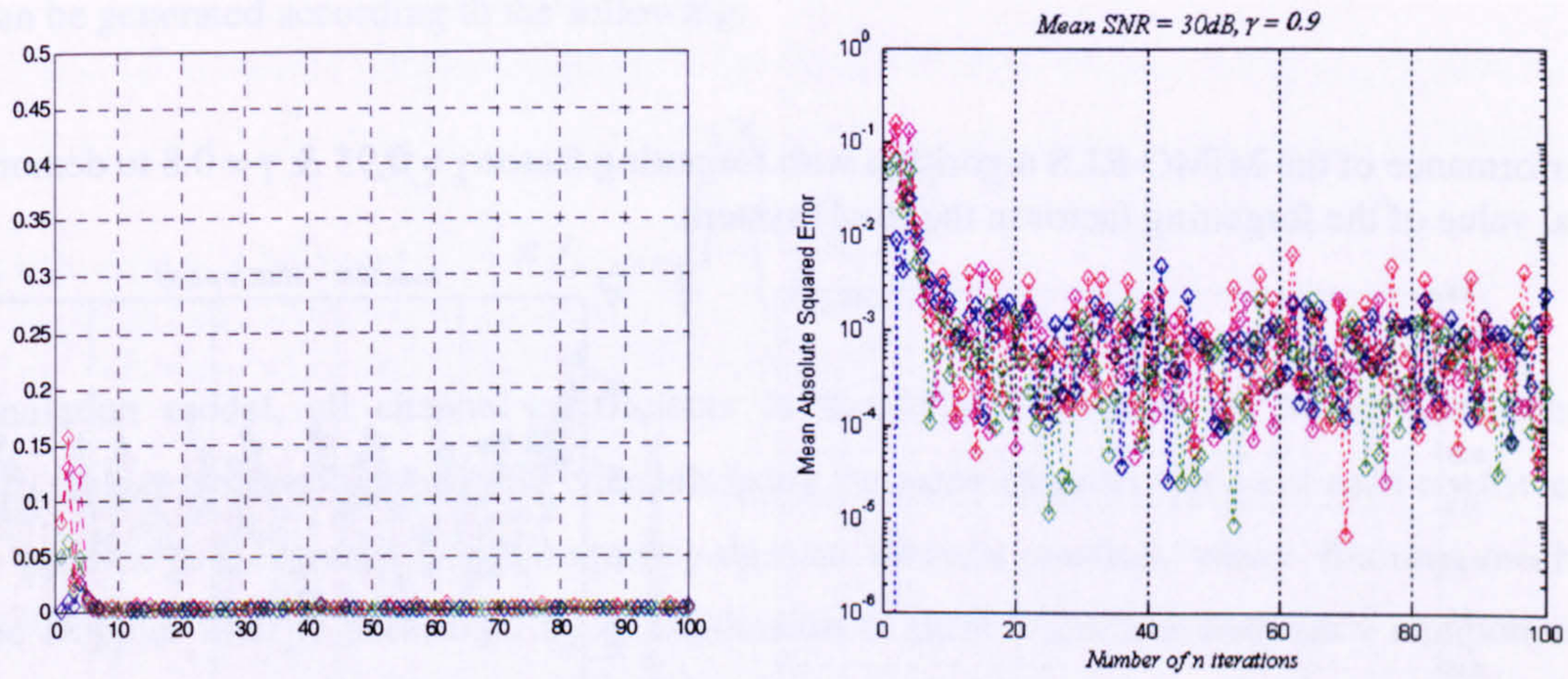

Performance of MIMO-RLS algorithm using $\gamma = 0.9$ in mean SNR = 30dB

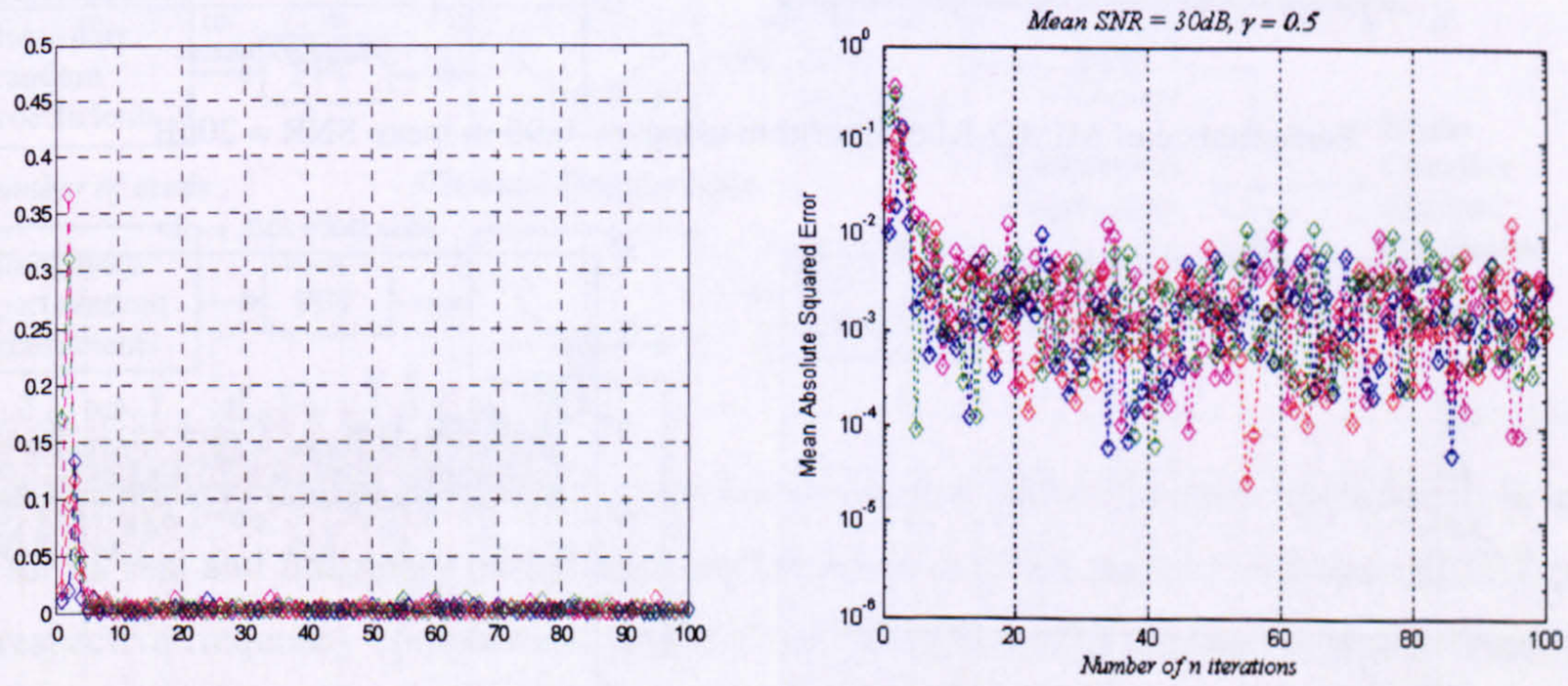

Performance of MIMO-RLS algorithm using $\gamma = 0.5$ in mean SNR = 30dB

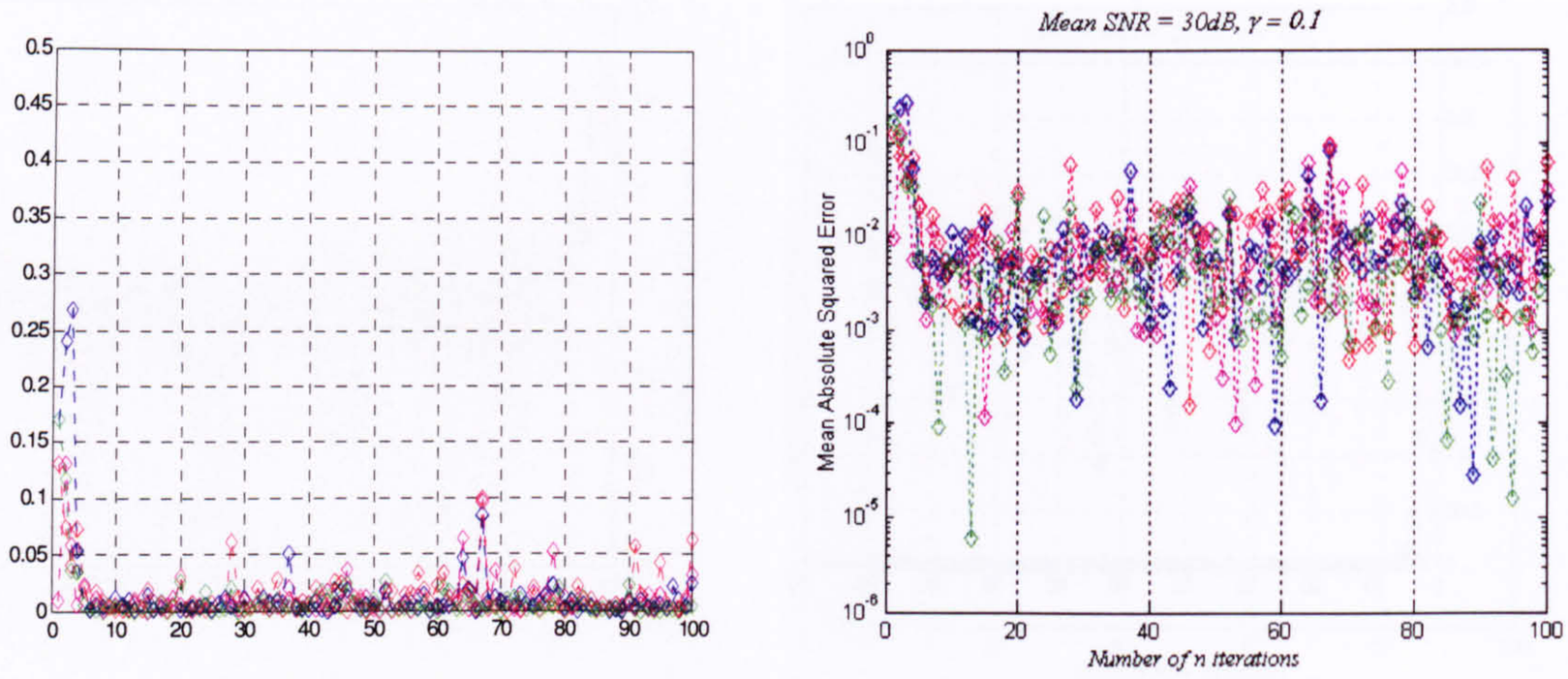

Performance of MIMO-RLS algorithm using $\gamma = 0.1$ in mean SNR = 30dB

The performance of the MIMO-RLS algorithm with forgetting factor $\gamma = 0.95$ & $\gamma = 0.8$ to demonstrate the nominal value of the forgetting factor in the (6×4) system.

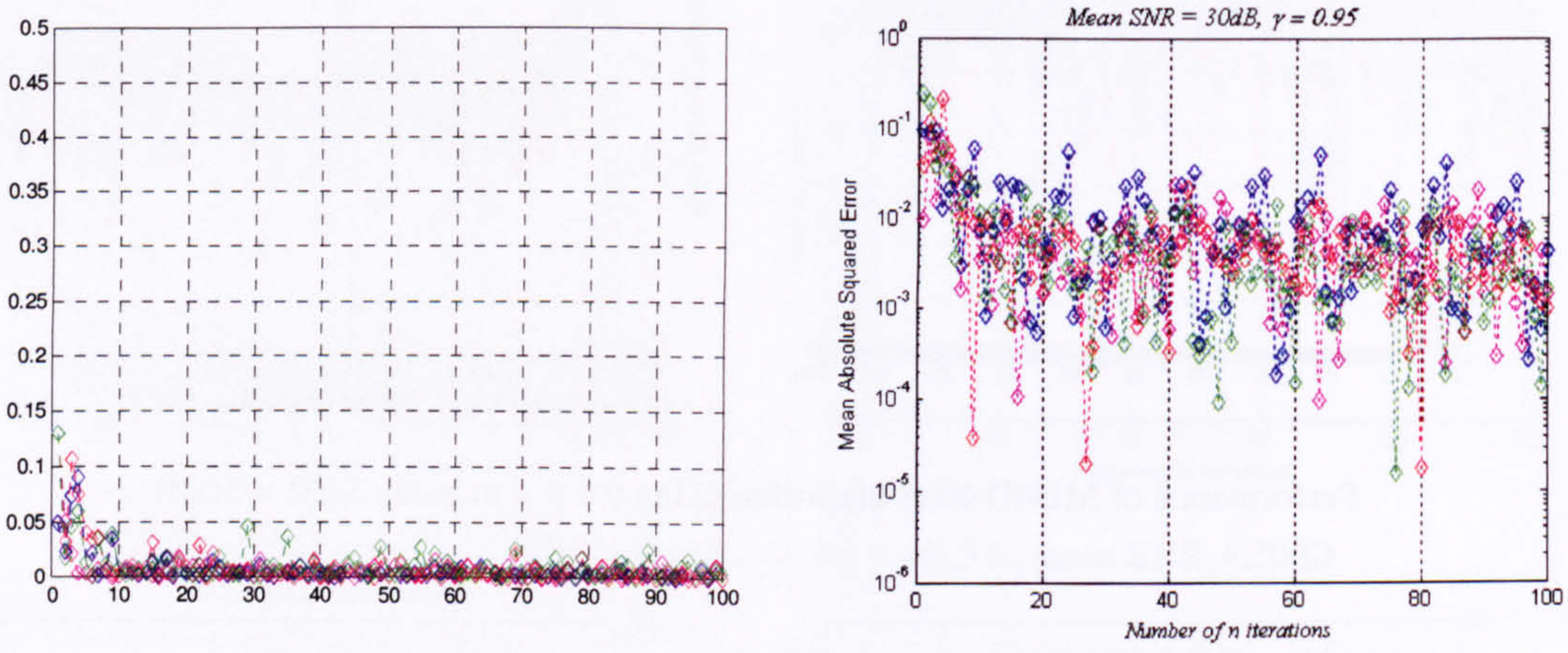

Performance of MIMO-RLS algorithm using $\gamma = 0.95$ in mean SNR = 20dB

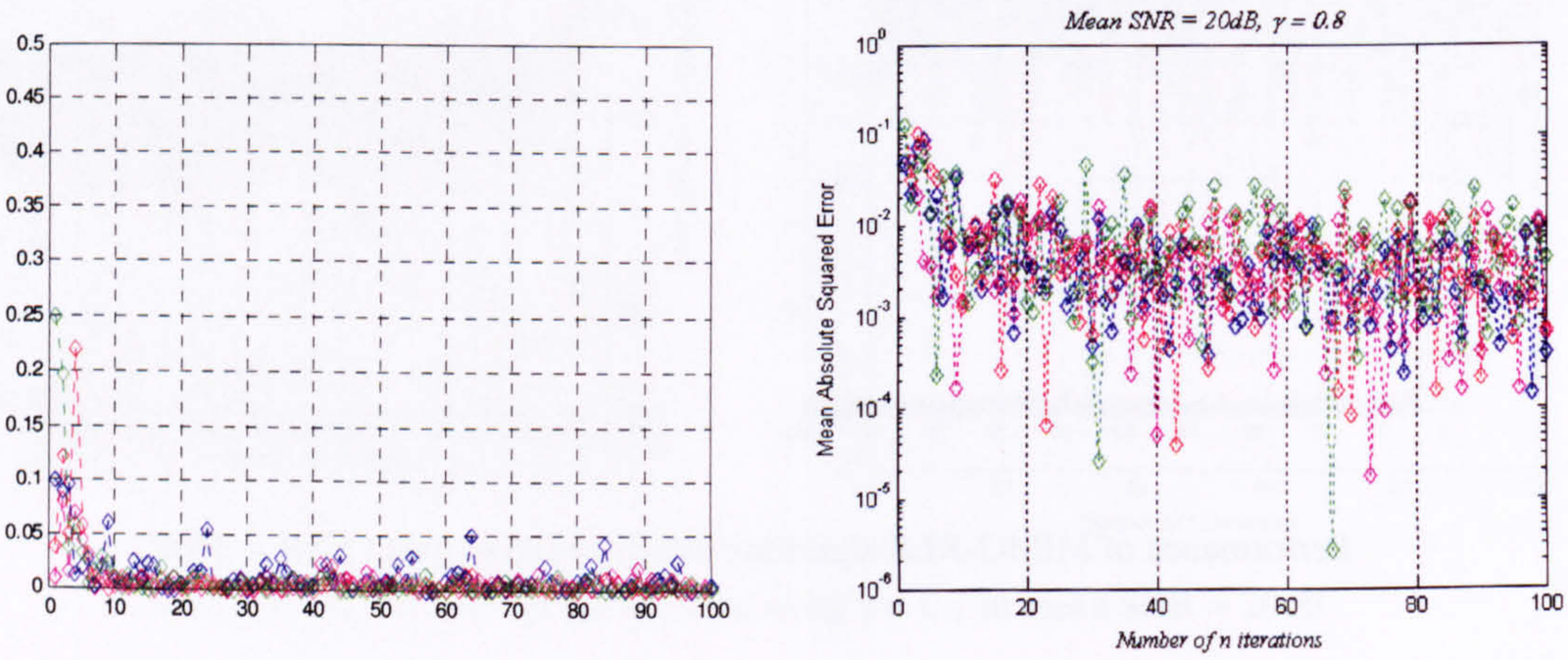

Performance of MIMO-RLS algorithm using $\gamma = 0.8$ in mean SNR = 20dB

Appendix B4 – Simulation method for time varying channel model

In order to generate the time-varying channel, the corresponding Doppler frequency f_d (according to individual mobile speed) must be determined first according to the following:

$$f_d = f_C \frac{\Lambda}{c} \cos\alpha = f_{d\_MAX} \cos\alpha$$

where f_c is the associated carrier frequency Λ is the mobile speed, c is the speed of light (3×10^8m/s) and α is the angle of arrival. In the simulation model, maximum Doppler shift f_{d_MAX} is considered where $\alpha = 0$.

Once the Doppler frequency is determined for each mobile channels (e.g. pedestrian, city/town and motorway/highway channels), individual Doppler filter with classical bath-tub spectrum (in frequency-domain) can be generated according to the following:

$$S(f) = \frac{1.5}{\pi f_{d\_MAX} \sqrt{1-\left(\frac{f}{f_{d\_MAX}}\right)^2}}$$

In the simulation model, all channel coefficients in the MIMO channel are varied simultaneously according to their respective time-varying channels using the same Doppler filter and each coefficient that is varying in time is generated using frequency-domain discrete method, where filtering mechanism through the Doppler filter is performed by multiplication of their respective frequency component. The general diagram of time-varying channel simulation is shown as follows:

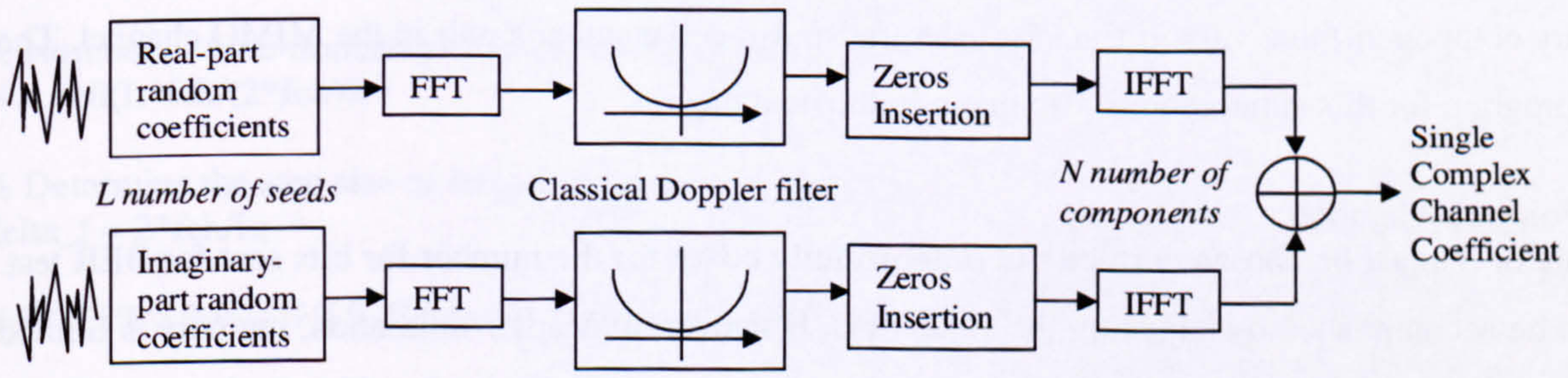

First, for each complex channel coefficient, L number of random seeds (Gaussian distributed) is initially generated for its real and imaginary part. These random seeds are then transformed through FFT process into their respective frequency components, which is later filtered by the classical Doppler filer (with the same length of L) by multiplication process in the frequency domains.

In order to process for actual symbol transmission rate e.g. 480Kbps, the channel sampling rate f_{ch} must be taken into account for consideration of realistic model of time-varying channel. This is achieved by zeros-insertion process where bins of zero seeds are inserted in-between the frequency components of the Doppler filter's output before transformed back into time-domain with N number of components through the IFFT process. The following diagram shows the rationale behind the process described above:

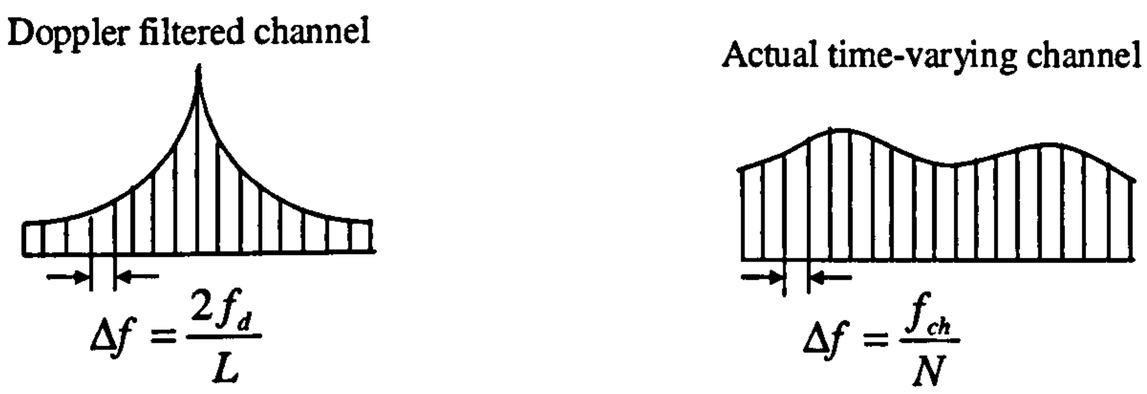

It can be seen from the above that the step size is the smallest representation of sample in each case. Since they are both equivalent, the actual number of samples N that completely represent the time-domain varying channel can be achieved as follows:

$$\Delta f = \frac{2f_d}{L} = \frac{f_{ch}}{N}$$

Hence,
$$\therefore N = \frac{f_{ch}}{2f_d} \times L$$

Note that the actually number of necessary zeros to be inserted in-between the frequency components of the Doppler filter's output is (N-L). Once the IFFT process is carried-out, the time-varying channel components in time domain is added together to form the complex channel coefficients (both real & imaginary component) that vary in time for each transmit-receive antenna pair in the MIMO channel. The matlab program for this simulation is also given in the next page.

Simulation Consideration:

The value of N must be chosen correctly in order to fully cover for the number for bits sent for BER test. This can be accomplished by adjusting the value of L. However, in Matlab simulation, memory is limited to the generation of N if greater transmission rate f_s is to be considered. For instant if f_{ch} is chosen to be the same f_s as 160Kbps and L is chosen to be 1024, for the slowly varying channel with f_d = 7Hz, the N is found to be approximately 11.7×10^6 samples, which is very heavy for the subsequent IFFT process. This will indeed cause insufficient memory problem in Matlab.

One solution is to slow down the channel sampling rate f_{ch} and then use point-interpolation method to match up with the actual data transmission rate f_s. In this way, number of N components can be reduced

until suitable size for the IFFT process. The number of interpolation point p that must be filled in between the simulated samples can be found using the following:

$$p = \frac{f_s}{f_{ch}}$$

Hence, the channel sampling rate f_{ch} and the value of N must be considered carefully during the simulation such that IFFT can still be perform within a reasonable amount of time while number of interpolation points p to be filled later between the samples are not too large to invalidate the actual time-variation of the intended mobile channel.

Matlab Program for Doppler Channel Generation

```
% Doppler Rayleigh channel by Virginia Tech.      %function r = rayleigh(fch,fd,L)

clear all;

% General parameter for MIMO
i = 3;          %Number of Transmit antenna
j = 4;          %Number of Receive antenna
Y = i*j;        %Total Number of paths involved
im = sqrt(-1); %imaginary term
v=1/sqrt(2);   %factor to achieve unit variance

%Parameters for Doppler channel
fd = 235;       %Doppler frequency according to various mobile speed.
fch = 480000;  %Channel sampling rate
L = 2048;       %Number bins to represent Doppler filter

% Number of time-domain points after IFFT process (ceil for smoothing)
N = ceil(L*fch/(2*fch));

% Determine the step size of frequency spacings of signal after FFT process
delta_f = 2*fch/L;

%%%%%%%%%%% Begin Random Input Generation %%%%%%%%%%%%%%%%%%

%time domain input
I_input_time = v*randn(Y,L);       % Generating random coefficients for
Q_input_time = v*randn(Y,L);       % complex MIMO channel (flat-freq)
H_in = I_input_time + (Q_input_time*im);   %MIMO channel before Doppler

%frequency transform (FFT process)
for a = 1:Y
        I_input_freq = fft(I_input_time(a,:));
        Q_input_freq = fft(Q_input_time(a,:));
end;
```

```
%**************************Generating Doppler Filter*******************************
% filter's DC component
   SEZ(1) = 1.5/(pi*fch);
   gain = SEZ(1);                %Gain of Doppler filter
% generate frequency component of the Doppler filter between 0 < f < fch
for j=2:L/2
        f(j) = (j-1)*delta_f;
        SEZ(j) = gain/sqrt(1-(f(j)/fch)^2);
        SEZ(L-j+2) = SEZ(j);
end
% to cater middle point where f=fch (since actual value is infinity)
k=2;
p=polyfit(f(L/2-k:L/2),SEZ(L/2-k:L/2),k);
SEZ(L/2+1) = polyval(p,f(L/2)+delta_f);
%************************************************************************

% Doppler filtering operation (Multiplication in frequency domain)
for a = 1:Y
        I_output_freq(a,:) = I_input_freq(a,:).*sqrt(SEZ);
        Q_output_freq(a,:) = Q_input_freq(a,:).*sqrt(SEZ);
end;

% Taking inverse IFFT process
for a = 1:Y
        I_temp = [I_output_freq(a,1:L/2) zeros(1,N-L) I_output_freq(a,(L/2)+1:L)];
        I_time = ifft(a,I_temp);
        Q_temp = [Q_output_freq(a,1:L/2) zeros(1,N-L) Q_output_freq(a,(L/2)+1:L)];
        Q_time = ifft(a,Q_temp);
end;

% back to real and imaginary term for the time-varying MIMO channel.
for a = 1:Y
        I_output_time(a,:) = real(I_time(a,:))-imag(Q_time(a,:));
        Q_output_time(a,:) = imag(I_time(a,:))+real(Q_time(a,:));
        % Doppler channel
        H_doppler(a,:) = I_output_time(a,:) + (Q_output_time(a,:)*im);
        rms(a,1) = sqrt(mean(H_doppler(a,:).*conj(H_doppler(a,:))));
        H_doppler(a,:) = H_doppler(a,:)/rms(a,1);
end;
```

Appendix B4

The performance of MIMO-PMI estimator in (3×3) system under three different of mobile time-varying flat fading channels, for different mean SNR values at 5dB, 10dB and 20dB respectively

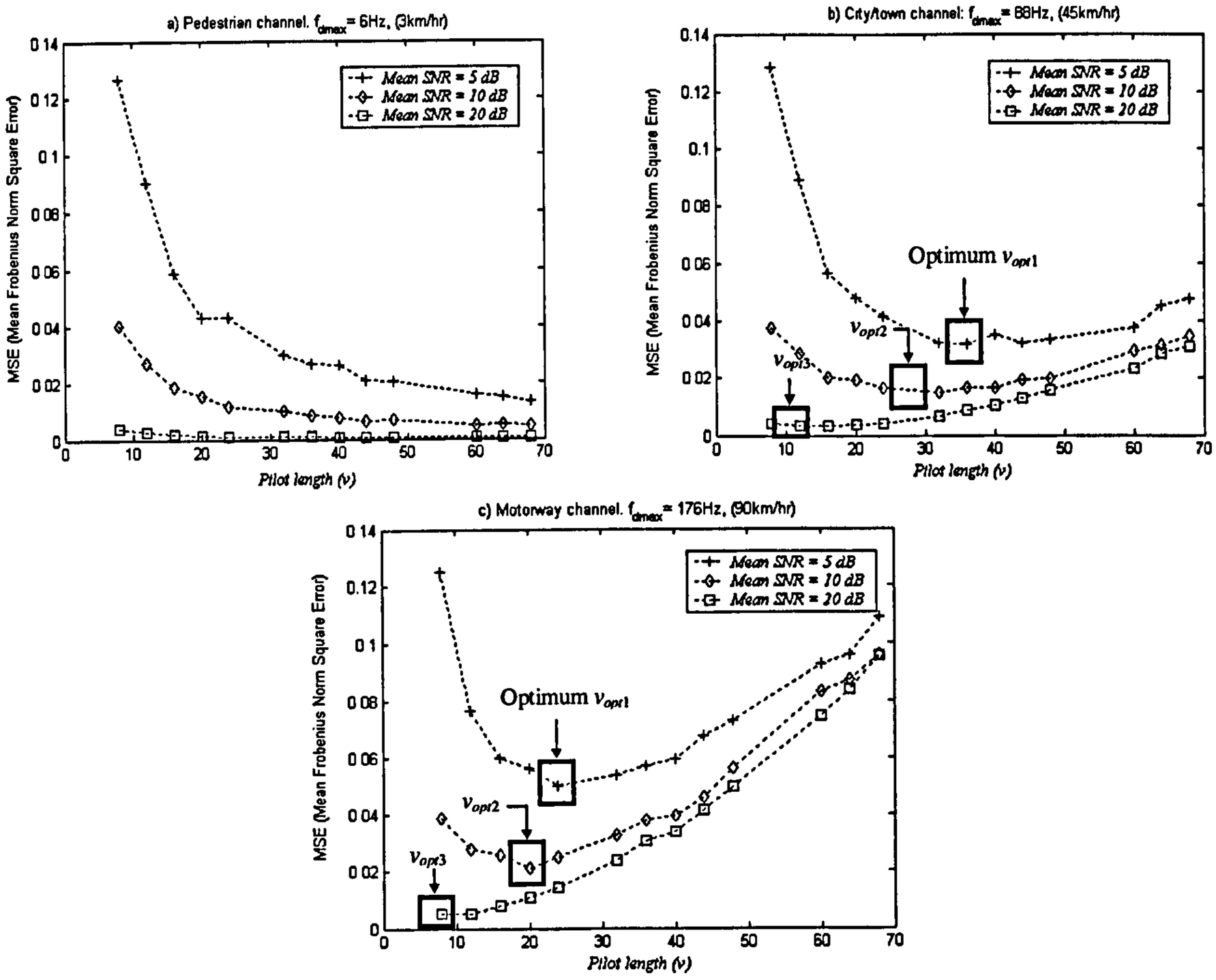

Performance of MIMO-PMI estimator for (3×3) system in different time-varying channels

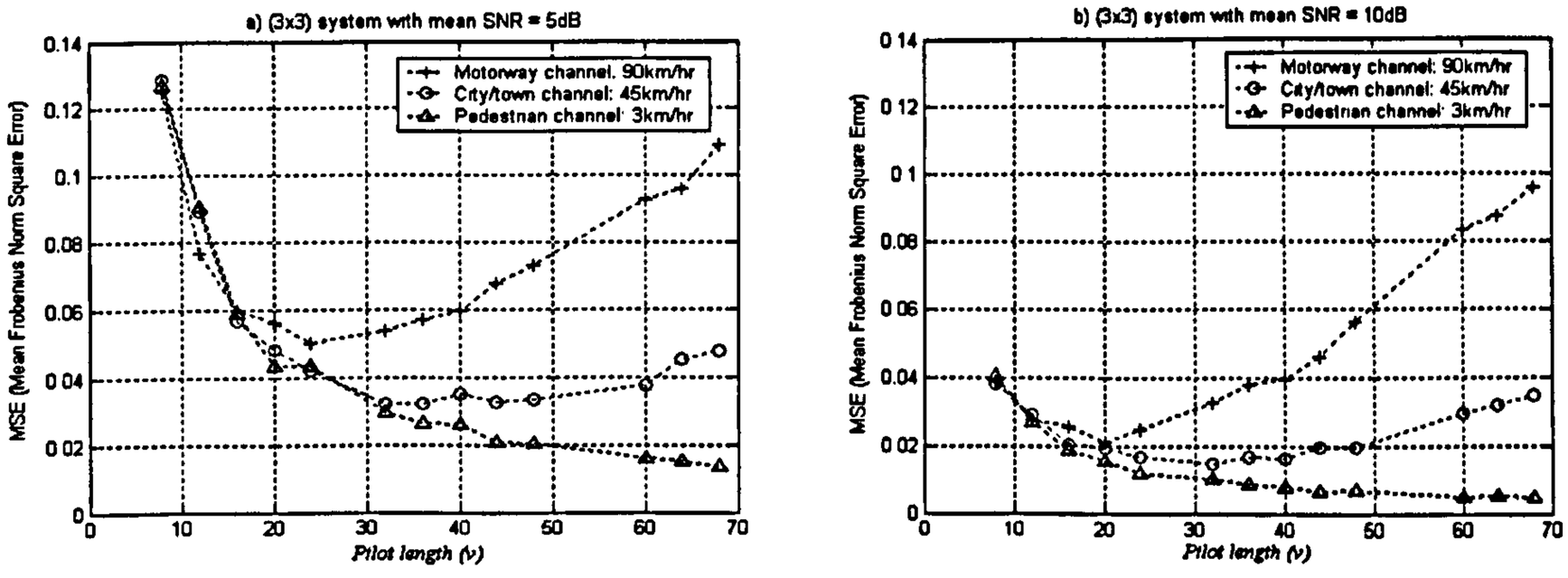

Performance of MIMO-PMI estimator for different mobile speed in (3×3) system with SNR = 5 & 10dB.

```
%*************************Generating Doppler Filter*****************************
% filter's DC component
   SEZ(1) = 1.5/(pi*fch);
   gain = SEZ(1);              %Gain of Doppler filter
% generate frequency component of the Doppler filter between 0 < f < fch
for j=2:L/2
        f(j) = (j-1)*delta_f;
        SEZ(j) = gain/sqrt(1-(f(j)/fch)^2);
        SEZ(L-j+2) = SEZ(j);
end
% to cater middle point where f=fch (since actual value is infinity)
k=2;
p=polyfit(f(L/2-k:L/2),SEZ(L/2-k:L/2),k);
SEZ(L/2+1) = polyval(p,f(L/2)+delta_f);
%*********************************************************************************

% Doppler filtering operation (Multiplication in frequency domain)
for a = 1:Y
        I_output_freq(a,:) = I_input_freq(a,:).*sqrt(SEZ);
        Q_output_freq(a,:) = Q_input_freq(a,:).*sqrt(SEZ);
end;

% Taking inverse IFFT process
for a = 1:Y
        I_temp = [I_output_freq(a,1:L/2) zeros(1,N-L) I_output_freq(a,(L/2)+1:L)];
        I_time = ifft(a,I_temp);
        Q_temp = [Q_output_freq(a,1:L/2) zeros(1,N-L) Q_output_freq(a,(L/2)+1:L)];
        Q_time = ifft(a,Q_temp);
end;

% back to real and imaginary term for the time-varying MIMO channel.
for a = 1:Y
        I_output_time(a,:) = real(I_time(a,:))-imag(Q_time(a,:));
        Q_output_time(a,:) = imag(I_time(a,:))+real(Q_time(a,:));
        % Doppler channel
        H_doppler(a,:) = I_output_time(a,:) + (Q_output_time(a,:)*im);
        rms(a,1) = sqrt(mean(H_doppler(a,:).*conj(H_doppler(a,:))));
        H_doppler(a,:) = H_doppler(a,:)/rms(a,1);
end;
```

Appendix B4

The performance of MIMO-PMI estimator in (3×3) system under three different of mobile time-varying flat fading channels, for different mean SNR values at 5dB, 10dB and 20dB respectively

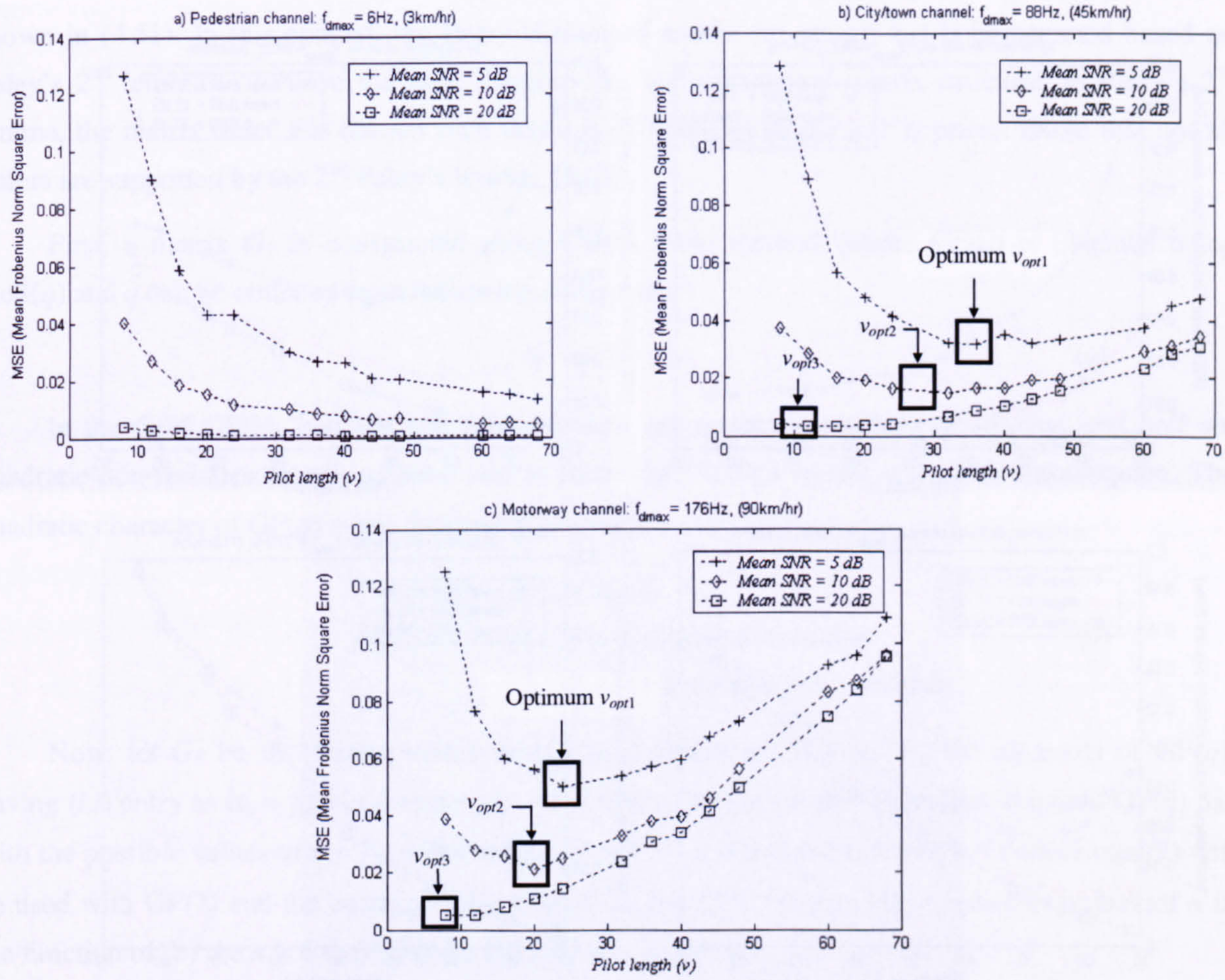

Performance of MIMO-PMI estimator for (3×3) system in different time-varying channels

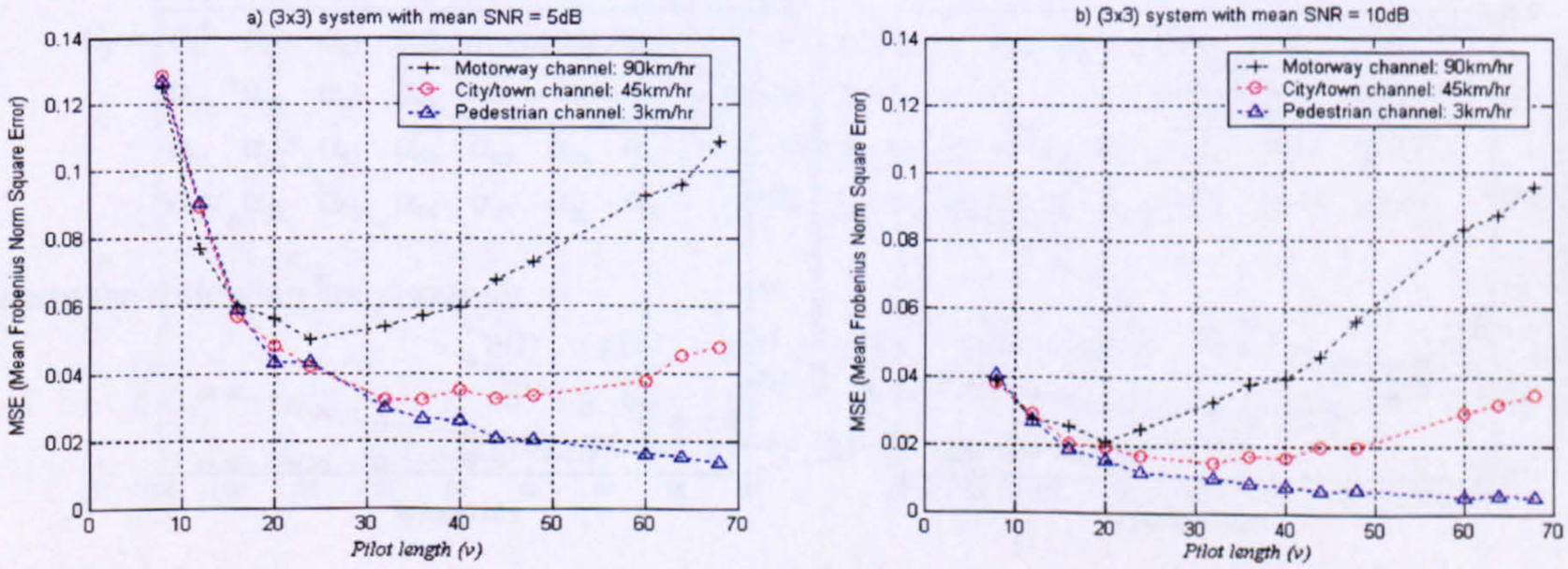

Performance of MIMO-PMI estimator for different mobile speed in (3×3) system with SNR = 5 & 10dB.

Appendix B5

Performance of $(N\times M) = (3\times3)$ MIMO-OSIC system with fixed $(L+1) = 3$ under various frequency selective time-varying channels with increasing pilot length v from 12 to 84.

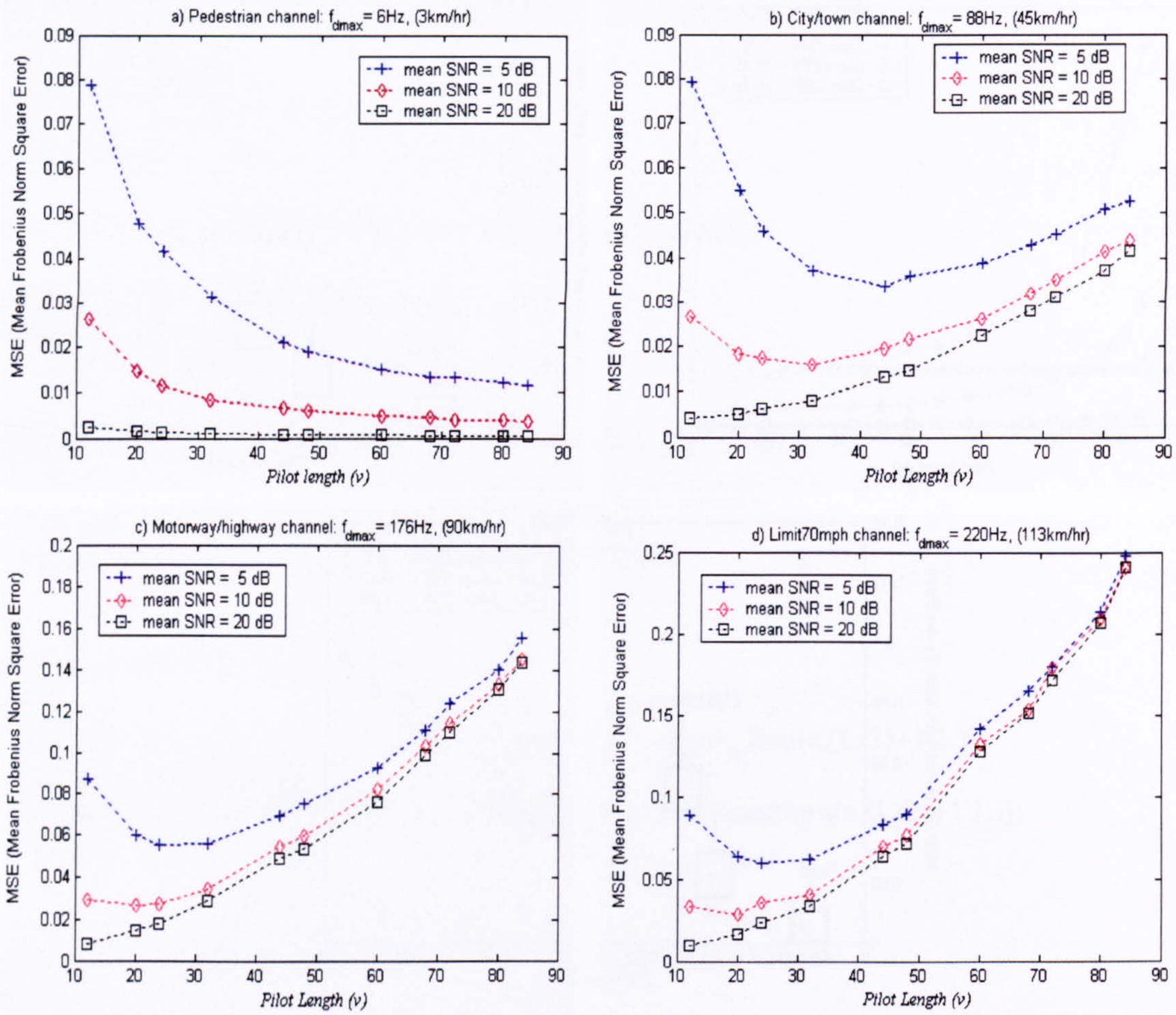

Estimator's performance for a (3×3) system with $(L+1) = 3$ in different time-varying channels

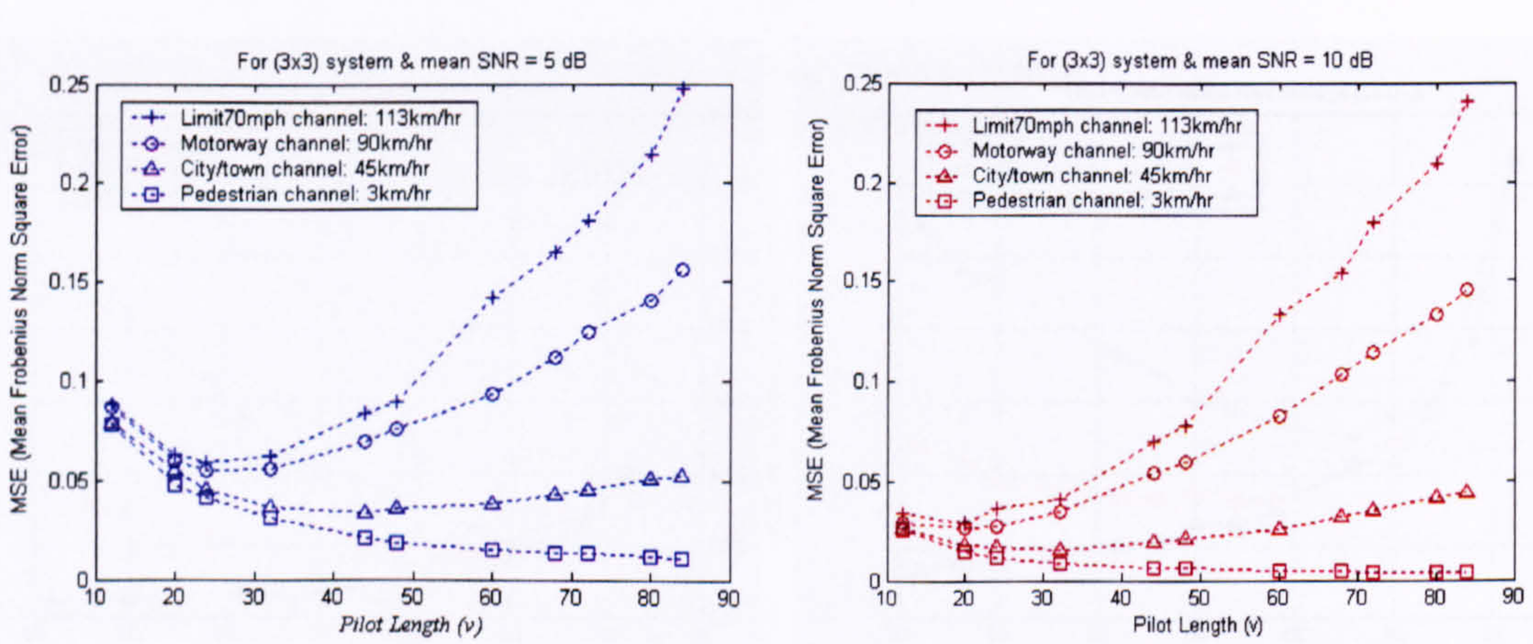

Estimator's performance for a (3×3) system in different mobile channels & mean SNR.

Appendix C1 - Formulation of the Paley-Hadamard Matrix

Here, the construction of the Paley-Hadamard matrix will be briefly outlined using example shown in (4.51). In this context, the Paley-Hadamard matrix (to design $\mathbf{S}_F$) is constructed based on Paley's 2nd lemma to achieve the joint Toeplitz-like and orthogonal matrix structure. In Paley's 2nd lemma, the matrix order v is chosen such that v is divisible by 4 and $v-1$ is prime. (Note that not all orders are supported by the 2nd Paley's lemma. [132]).

First, a matrix $\boldsymbol{G}_F$ is constructed using Galois Field method, where GF(q) is obtained using mod(q) and q can be obtained from the matrix order v as:

$$q = v-1 \qquad \text{(a)}$$

In the field GF(q), half the non-zero elements are quadratic residues or squares, and half are quadratic non-residues or non-squares; and in particular, +1 is a square and –1 is a non-square. The quadratic character of GF(q) is the function χ given by:

$$\chi(n)\begin{cases} = & 0 & \text{if } n=0 \\ & +1 & \text{if } n \text{ is a quadratic residue} \\ & -1 & \text{if } n \text{ is a quadratic non}-\text{residue} \end{cases} \qquad \text{(b)}$$

Now, let $\boldsymbol{G}_F$ be the matrix whose rows and columns are indexed by the elements of GF(q), having (i,j) entry as $\alpha_{ij} = \chi(j-i)$, where $\chi(j-i)$ is related to $\chi(n)$ in (b). Therefore, the field GF(q) has with the possible values of $n = j-i$. For instant, if order $v = 8$ is chosen, then $q = 7$, where mod(7) will be used with GF(7) and the corresponding matrix $\boldsymbol{G}_F$ has (7×7) entries. Thus, possible values of n in the function of (b) are $n = 0$ to 6 with the field shown as follows:

$$\boldsymbol{G}_F = \begin{bmatrix} \alpha_{11} & \alpha_{12} & \alpha_{13} & \alpha_{14} & \alpha_{15} & \alpha_{16} & \alpha_{17} \\ \alpha_{21} & \alpha_{22} & \alpha_{23} & \alpha_{24} & \alpha_{25} & \alpha_{26} & \alpha_{27} \\ \alpha_{31} & \alpha_{32} & \alpha_{33} & \alpha_{34} & \alpha_{35} & \alpha_{36} & \alpha_{37} \\ \alpha_{41} & \alpha_{42} & \alpha_{43} & \alpha_{44} & \alpha_{45} & \alpha_{46} & \alpha_{47} \\ \alpha_{51} & \alpha_{52} & \alpha_{53} & \alpha_{54} & \alpha_{55} & \alpha_{56} & \alpha_{57} \\ \alpha_{61} & \alpha_{62} & \alpha_{63} & \alpha_{64} & \alpha_{65} & \alpha_{66} & \alpha_{67} \\ \alpha_{71} & \alpha_{72} & \alpha_{73} & \alpha_{74} & \alpha_{75} & \alpha_{76} & \alpha_{77} \end{bmatrix} \equiv \begin{bmatrix} \chi(0) & \chi(1) & \chi(2) & \chi(3) & \chi(4) & \chi(5) & \chi(6) \\ \chi(-1) & \chi(0) & \chi(1) & \chi(2) & \chi(3) & \chi(4) & \chi(5) \\ \chi(-2) & \chi(-1) & \chi(0) & \chi(1) & \chi(2) & \chi(3) & \chi(4) \\ \chi(-3) & \chi(-2) & \chi(-1) & \chi(0) & \chi(1) & \chi(2) & \chi(3) \\ \chi(-4) & \chi(-3) & \chi(-2) & \chi(-1) & \chi(0) & \chi(1) & \chi(2) \\ \chi(-5) & \chi(-4) & \chi(-3) & \chi(-2) & \chi(-1) & \chi(0) & \chi(1) \\ \chi(-6) & \chi(-5) & \chi(-4) & \chi(-3) & \chi(-2) & \chi(-1) & \chi(0) \end{bmatrix} \qquad \text{(c)}$$

where the following are also true:

$$\begin{array}{cccccc} \chi(1) & \chi(2) & \chi(3) & \chi(4) & \chi(5) & \chi(6) \\ \Updownarrow & \Updownarrow & \Updownarrow & \Updownarrow & \Updownarrow & \Updownarrow \\ \chi(-6) & \chi(-5) & \chi(-4) & \chi(-3) & \chi(-2) & \chi(-1) \end{array} \qquad \text{(d)}$$

Next, the quadratic residues need to be determined with the possible n values as follows:

Let	n	=	1	2	3	4	5	6
and	n^2	=	1	4	9	16	25	36
mod(7)		=	1	4	2	2	4	1

Therefore, the quadratic residue are sited within those $\chi(n)$ with n = 1,2 and 4. In contrary, the quadratic non-residue are sited in the rest of $\chi(n)$ (except n = 0) which corresponds to value of n = 3,5 and 6. Using (b) the quadratic character of GF(7) can be obtained as:

$$\begin{array}{cccccc} \chi(1) & \chi(2) & \chi(3) & \chi(4) & \chi(5) & \chi(6) \\ \Updownarrow & \Updownarrow & \Updownarrow & \Updownarrow & \Updownarrow & \Updownarrow \\ +1 & +1 & -1 & +1 & -1 & -1 \end{array} \qquad \text{(e)}$$

Next, using (c) to (e), G_F (with full-Toeplitz structure) is obtained as:

$$G_F = \begin{bmatrix} 0 & +1 & +1 & -1 & +1 & -1 & -1 \\ -1 & 0 & +1 & +1 & -1 & +1 & -1 \\ -1 & -1 & 0 & +1 & +1 & -1 & +1 \\ +1 & -1 & -1 & 0 & +1 & +1 & -1 \\ -1 & +1 & -1 & -1 & 0 & +1 & +1 \\ +1 & -1 & +1 & -1 & -1 & 0 & +1 \\ +1 & +1 & -1 & +1 & -1 & -1 & 0 \end{bmatrix} \qquad \text{(f)}$$

Consequently, the Paley-Hadamard matrix **P** can be obtained by replacing the diagonal zeros in (f) by −1s and border matrix G_F with a row and column of +1s shown as follows:

$$\mathbf{P} = \begin{bmatrix} +1 & +1 & \cdots & +1 \\ +1 & & & \\ \vdots & & G_F & \\ +1 & & & \end{bmatrix} = \begin{bmatrix} +1 & +1 & +1 & +1 & +1 & +1 & +1 & +1 \\ +1 & -1 & +1 & +1 & -1 & +1 & -1 & -1 \\ +1 & -1 & -1 & +1 & +1 & -1 & +1 & -1 \\ +1 & -1 & -1 & -1 & +1 & +1 & -1 & +1 \\ +1 & +1 & -1 & -1 & -1 & +1 & +1 & -1 \\ +1 & -1 & +1 & -1 & -1 & -1 & +1 & +1 \\ +1 & +1 & -1 & +1 & -1 & -1 & -1 & +1 \\ +1 & +1 & +1 & -1 & +1 & -1 & -1 & -1 \end{bmatrix} \qquad \text{(g)}$$

Note that **P** has the so-called Toeplitz-like structure (which is distinguished from the full-Toeplitz structure in G_F itself), where G_F is semi-encapsulated by the borders of +1s at its 1st row and 1st column. Providentially, this Toeplitz-like structure in **P** also provides an orthogonal structure that is suitable for more efficient formulation of the pilot matrix discussed subsequently.

Appendix C2 – MIMO Channel Models

Consider a MIMO system with M transmit antenna and N receive antenna. In general, the MIMO channel can be modelled using the following channel matrix **H** as:

$$\mathbf{H}(\tau,t)=\begin{bmatrix} h_{1,1}(\tau,t) & h_{1,2}(\tau,t) & \cdots & h_{1,M}(\tau,t) \\ h_{2,1}(\tau,t) & h_{2,2}(\tau,t) & \cdots & h_{2,M}(\tau,t) \\ \vdots & \vdots & \ddots & \vdots \\ h_{N,1}(\tau,t) & h_{N,2}(\tau,t) & \cdots & h_{N,M}(\tau,t) \end{bmatrix} \qquad \text{(a)}$$

where $h_{n,m}(\tau,t)$ is the individual complex fading coefficient from m^{th} transmit antenna to n^{th} receive antenna within the MIMO channel (where m = 1 to M & n = 1 to N). Each coefficient is generated by stochastic/statistical method using independent identical distributed or Gaussian random seeds. Each coefficient is assumed to be Rayleigh faded with non light-of-sight channel condition. All coefficients are assumed to be uncorrected. Note that 't' in (a) represent the time-index for each coefficient to be varied in time (according to the Doppler channel in Appendix-B2) whereas 'τ' is the delay-index to represent individual delay instant within a channel impulse response (CIR) of each sub-channel between each transmit-receive pair.

In flat fading channel condition, the delay-index 'τ' can be omitted since the delay between each path is assumed to be insignificant and the resultant fading condition can be modelled by only a single path for each sub-channel. Therefore, the flat fading MIMO channel only consists of (N×M) fading coefficients as shown in (a) with delay-index 'τ' omitted. However, in the frequency selective fading condition, delay-index 'τ' become useful whereby (L+1) significant paths that arrived at different delay instant (for each CIR of each sub-channel) can be effectively described. Hence, depending on the number of significant paths within each CIR, the frequency selective MIMO channel may consists of (L+1) multiple copies of (N×M) channel matrix described in (a) according to individual value of 'τ'.

An alternative way to model the frequency-selective MIMO channel is shown in section 2.6.1 where channel matrix is expressed with respect to each m^{th} transmit antenna rather than each delay-index 'τ'. This is shown again in the following:

$$\mathbf{H}_m=\begin{bmatrix} \mathbf{h}_{1m}^{\mathsf{T}} \\ \mathbf{h}_{2m}^{\mathsf{T}} \\ \vdots \\ \mathbf{h}_{Nm}^{\mathsf{T}} \end{bmatrix}=\begin{bmatrix} h_{1m}(0) & h_{1m}(1) & \cdots & h_{1m}(L) \\ h_{2m}(0) & h_{2m}(1) & \cdots & h_{2m}(L) \\ \vdots & \vdots & \vdots & \vdots \\ h_{Nm}(0) & h_{Nm}(1) & \cdots & h_{Nm}(L) \end{bmatrix}, \quad m=1,2,\ldots,M. \qquad \text{(b)}$$

where $\mathbf{h}_{nm}$ is the sampled CIR from the m^{th} transmit antenna to n^{th} receive antenna expressed as:

$$\mathbf{h}_{nm}=\begin{bmatrix} h_{nm}(0) & h_{nm}(1) & \cdots & h_{nm}(L) \end{bmatrix}^{\mathsf{T}} \qquad \text{(c)}$$

The interaction of the transmitted signals and respective associated paths $h_{nm}(k)$ in the frequency selective fading condition can also be modelled using the FIR tap-delay-line (TDL) filter model as follows:

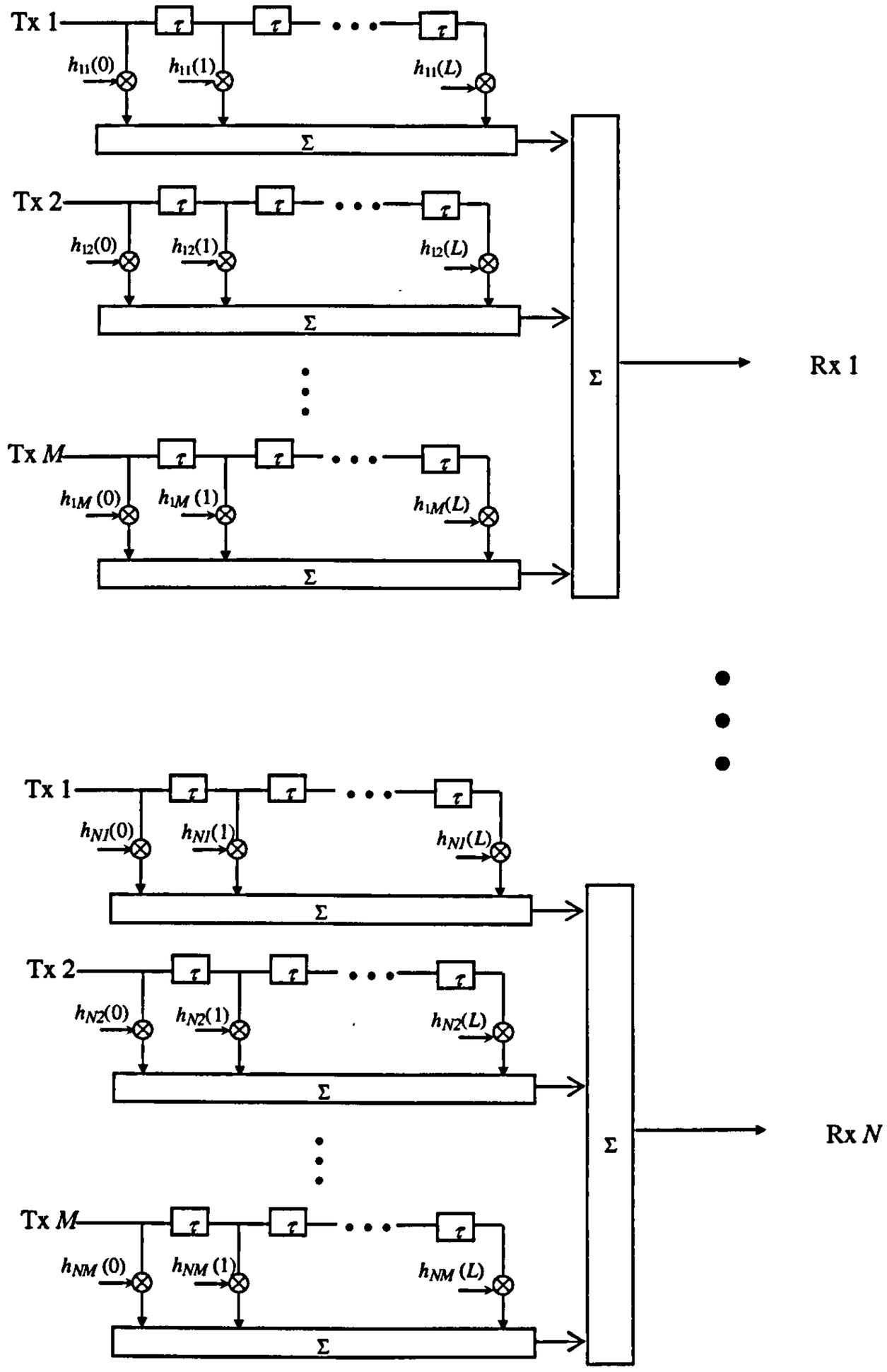

Note that M rows of FIR TDL filters are summed together at each n^{th} receive antenna and there are N banks of such TDL filters that model the signal received at individual receive antenna at respective time.